Hellenic Republic
National and Kapodistrian University of Athens
Department of Geology and Geoenvironment
Sector of Geophysics and Geothermal

A Non-Extensive Statistical Physics view to the temporal properties of aftershocks related to major subduction zone earthquakes worldwide

Supervisor: Dr. Filippos Vallianatos

Thesis presented

by

Eleni-Apostolia Anyfanti

for the bachelor's degree of Geology and Geoenvironment

Academic Year: 2020-2021

Eleni-Apostolia Anyfanti 2021

ABSTRACT

Large subduction zone earthquakes generate aftershock sequences which last over an extended period of time and affect wide spatial areas. Modeling aftershock sequences of large subduction zone earthquakes is of considerable importance for seismic-hazard assessments and earthquake risk mitigation.

In this work, we analyze the statistical properties of the temporal evolution of aftershock sequences that followed recent large subduction zone earthquakes worldwide from January 1976 to October 2020. We analyzed 44 aftershock sequences generated by mainshocks of M 7.0 and above and with focal depths less than 70km. To model their temporal behavior, we estimate the parameters of the modified Omori law. Their temporal scaling properties are further studied by looking into the probability distribution of the interevent times between the successive aftershocks, in terms of Non-Extensive Statistical Physics (NESP), a generalized statistical mechanics framework that characterizes complex systems with finite degrees of freedom, long-range interactions and self-organized criticality. In addition, the statistical parameter qM estimated, which is related to the frequency-magnitude distribution and could be used as an auxiliary factor to characterize the physical condition of the seismic region because its changes are related with the release rate of the energy. We also demonstrate the applicability of NESP in the cumulative distribution functions of interevent times and the presence of a crossover behavior from power-law ($q \neq 1$) to exponential ($q=1$) scaling for greater interevent times. Furthermore, most of the estimated q-values that characterize the observed distributions are close to 1.76, suggesting a system with low degrees of freedom. A discussion of the observed crossover behavior in terms of superstatistics is further provided.

KEYWORDS

Subduction Zone
Megathrust Earthquake
Earthquake Catalog
Aftershock Sequences
Interevent Times
Gutenberg-Richter Law
Omori Law
Non-Extensive Statistical Physics (NESP)
Probability Distribution
Complex System
Tsallis Entropy

Acknowledgements

First and foremost, I would like to thank my supervisor Dr. Filippos Vallianatos, because without his assistance and expertise I would not have been able to complete this thesis. He was always by my side, with his technical skills and experience, to assist me in answering the issues that came from the study and drawing the appropriate conclusions. I am looking forward to future collaborations with him since his consistency, ingenuity, critical and innovative thinking, discretion and understanding contributed to a pleasant working atmosphere which made the whole procedure fruitful.

A special thanks to Dr. Giorgos Michas who has helped me understand some concepts of the programming language of MATLAB and provide me with the necessary knowledge and the ability to analyze the results of MATLAB and to Dr. Kyriaki Pavlou who helped me with the ZMAP and advised me on how to utilize it effectively.

Of course, I couldn't have denied the help of my friends, each of whom provided me with patient advice and guidance throughout the research process.

Last but not least, the consistent support and encouragement of my family during this effort is precious. They always support me with love and understanding. They are an inspiration to me for a brilliant success and a bright future.

Table of Contents

List of Figures…….. 8

1. Introduction……29

1.1 Motivation…… 30

1.2 Description of the Problem……... 31

2. Basic Concepts and Theory……... 32

2.1 Subduction Zone…….. 33

2.2 Seismotectonic Regime…… 34

2.3 Aftershock Sequences…….. 35

3. Applied Methodology……. 38

3.1 Empirical Laws for Aftershock Sequences…….. 39

3.1.1 The Gutenberg-Richter Law…… 39

3.1.2 Modified Omori Law…….. 42

3.2 Non-Extensive Statistical Physics…… 44

3.2.1 NESP Distribution Law and Interevent Times…… 44

3.2.2 NESP Distribution Law for Earthquake Magnitude…… 48

3.3 A Superstatistical View…… 50

4. Data Analysis and Results……. 52

4.1 Earthquake Catalogs…… 53

4.2 Analysis of Each Aftershock Sequence..……. 55

4.2.1 The 1976 Kermadec Island Earthquake Mw 8.0 (New Zealand)…… 56

4.2.2 The 1977 Waingapu, Indonesia Earthquake (Mw=8.3)…….. 63

4.2.3 The 1986 Kermadec Island, New Zealand Earthquake (Mw=7.7)……. 67

4.2.4 The 1994 Shikotan, Russia Earthquake (Mw=8.3)……. 71

4.2.5 The 1995 Panguna, Papua New Guinea Earthquake (Mw=7.7)……. 75

4.2.6 The 1995 Kuril'sk, Russia Earthquake (Mw=7.9)……. 78

4.2.7 The 2000 Bengkulu, Indonesia Earthquake (Mw=7.9)…… 82

4.2.8 The 2000 Rabaul, Papua New Guinea Earthquake (Mw=8.0)……. 86

4.2.9 The 2001 Atico, Peru Earthquake (Mw=8.4)…….. 90

4.2.10 The 2003 Kushiro, Japan Earthquake (Mw=8.3)…….. 94

4.2.11 The 2004 Sumatra-Andaman Islands Earthquake (Mw=9.0)…… 98

4.2.12 The 2005 Singkil, Indonesia Earthquake (Mw=8.6)…… 102

4.2.13 The 2006 Pangai, Tonga Earthquake (Mw=8.0)……. 105

4.2.14 The 2006 Singaparna, Indonesia Earthquake (Mw=7.7)……. 109

4.2.15 The 2007 Gizo, Solomon Island Earthquake (Mw=8.1)……. 113

4.2.16 The 2007 Bengkulu, Indonesia Earthquake (Mw=8.4)…… 117

4.2.17 The 2009 Sarangani, Philippines Earthquake (Mw=7.2)……. 120

4.2.18 The 2009 Matavai, Samoa Earthquake (Mw=8.1)…….. 123

4.2.19 The 2009 Sola, Vanuatu Earthquake (Mw=7.8)……. 127

4.2.20 The 2010 Quirihue, Chile Earthquake (Mw=8.8)…… 131

4.2.21 The 2011 Great Tohuko, Japan Earthquake (Mw=9.1)…….. 135

4.2.22 The 2011 Kermadec Islands, New Zealand Earthquake (Mw=7.6)……. 138

4.2.23 The 2012 West Coast of Northern Sumatra Earthquake (Mw=8.6)…… 142

4.2.24 The 2013 Atka, Alaska Earthquake (Mw=7.0)…… 146

4.2.25 The 2014 Kirakira, Solomon Islands Earthquake (Mw=7.6)…….. 150

4.2.26 The 2014 Panguna, Papua New Guinea Earthquake (Mw=7.5)…….. 154

4.2.27 The 2014 Ternate, Indonesia Earthquake (Mw=7.1)…….. 158

4.2.28 The 2015 Kokopo, Papua New Guinea Earthquake (Mw=7.5)…… 162

4.2.29 The 2015 Bharatpur, Nepal Earthquake (Mw=7.8)……. 166

4.2.30 The 2015 Illapel, Chile Earthquake (Mw=8.3)…… 170

4.2.31 The 2016 South Sandwich Islands Earthquake (Mw=7.2)…….. 174

4.2.32 The 2016 Gisborne, New Zealand Earthquake (Mw=7.0)…….. 178

4.2.33 The 2016 Amberley, New Zealand Earthquake (Mw=7.8)……. 182

4.2.34 The 2016 Kirakira, Solomon Islands Earthquake (Mw=7.8)……... 186

4.2.35 The 2017 Chiapas, Mexico Earthquake (Mw=8.2)…….. 189

4.2.36 The 2017 Alabja, Iraq Earthquake (Mw=7.3)…….. 193

4.2.37 The 2018 Chiniak, Alaska Earthquake (Mw=7.9)…….. 197

4.2.38 The 2018 Tadine, New Caledonia Earthquake (Mw=7.5)……... 200

4.2.39 The 2018 Uts'-Kamchatsk Staryy, Russia Earthquake (Mw=7.3)……... 203

4.2.40 The 2019 Kokopo, Papua New Guinea Earthquake (Mw=7.6)…… 207

4.2.41 The 2019 Kermadec Islands, New Zealand Earthquake (Mw=7.3)……. 211

4.2.42 The 2019 Ternate, Indonesia Earthquake (Mw=7.1)…… 215

4.2.43 The 2020 Kermadec Islands, New Zealand Earthquake (Mw=7.4)…….. 218

4.2.44 The 2020 Sand Point, Alaska Earthquake (Mw=7.6)…… 222

5. Discussion and Conclusions……. 226

Bibliography……. 229

List of Figures

Figure 1. Geographical location of 44 subduction-zone earthquakes. The event indexes provided in Table 1 correspond to the index numbers displayed in this figure……... 55

Figure 2. (a) The Guttenberg-Richter distribution using maximum likelihood method with the best combination of maximum curvature M_c 95% and M_c 90% probability. The red star shows the magnitude of the mainshock M_w 8.0. **(b)** The best model (1) of the estimated curve of the modified Omori formula (dashed line) applied to the aftershock data and the observed cumulative number of aftershocks (solid line) based on the AIC. **(c)** The model 4 of the estimated curve of the modified Omori formula (dashed line) applied to the aftershock data and the observed cumulative number of aftershocks (solid line), with the lowest RMS= 2.8…….. 58

Figure 3. The magnitude-time pattern versus the logarithm of time of the mainshock M_w 8.0……... 59

Figure 4. Frequency-magnitude distribution. The bold red line represents the model of equation (26) for qM= 1.42, while the other two lines present the corresponding 95% confidence intervals…… 59

Figure 5. The cumulative distribution function of the interevent times. The red line is the Q-exponential fitting with q = 1.78……... 60

Figure 6. The Q-logarithmic function of the P(>T) as a function of the interevent times where the dashed line is the fitting with q= 1.78. The deviation from the linearity suggests Tc values close to 400,000 s…….. 61

Figure 7. The evolution of interevent time T as a function of time t since the main event. The Tc value is indicated by the dashed line (see text)…….. 62

Figure 8. (a) The Guttenberg-Richter distribution using maximum likelihood method with the best combination of maximum curvature M_c 95% and M_c 90% probability. The red star shows the magnitude of the mainshock M_w 8.3. **(b)** The Guttenberg-Richter distribution using the manual method……. 63

Figure 9. The best model (1) of the estimated curve of the modified Omori formula (dashed line) applied to the aftershock data and the observed cumulative number of aftershocks (solid line) based on the AIC with RMS=4.32…….. 64

Figure 10. The magnitude-time pattern versus the logarithm of time of the mainshock M_w 8.3……. 64

Figure 11. Frequency-magnitude distribution. The bold red line represents the model of equation (26) for qM= 1.31, while the other two lines present the corresponding 95% confidence intervals…… 66

Figure 12. (a) The cumulative distribution function of the interevent times. The red line is the Q-exponential fitting with q = 1.68. **(b)** The Q-logarithmic function of the P(>T) as a function of the interevent times where the dashed line is the fitting with q=1.68. The deviation from the linearity suggests Tc values close to 750,000 s. **(c)** The evolution of interevent time T as a function of time t since the main event. The Tc value is indicated by the dashed line……. 67

Figure 13. (a) The Guttenberg-Richter distribution using maximum likelihood method with the best combination of maximum curvature M_c 95% and M_c 90% probability. The red star shows the magnitude of the mainshock M_w 7.7. **(b)** The Guttenberg-Richter distribution using the manual method……. 68

Figure 14. (a) The best model (1) of the estimated curve of the modified Omori formula (dashed line) applied to the aftershock data and the observed cumulative number of aftershocks (solid line) based on the AIC. **(b)** The model 4 of the estimated curve of the modified Omori formula (dashed line) applied to the aftershock data and the observed cumulative number of aftershocks (solid line), with the lowest RMS= 4.98.

Figure 15. The magnitude-time pattern versus the logarithm of time of the mainshock M_w 7.7……. 69

Figure 16. Frequency-magnitude distribution. The bold red line represents the model of equation (26) for qM= 1.32, while the other two lines present the corresponding 95% confidence intervals…… 69

Figure 17. (a) The cumulative distribution function of the interevent times. The red line is the Q-exponential fitting with q = 1.74. **(b)** The Q-logarithmic function of the P(>T) as a function of the interevent times where the dashed line is the fitting with q=1.74. The deviation from the linearity suggests Tc values close to 75,000 s. **(c)** The evolution of interevent time T as a function of time t since the main event. The Tc value is indicated by the dashed line…….. 70

Figure 18. The Guttenberg-Richter distribution using maximum likelihood method with the best combination of maximum curvature M_c 95% and M_c 90% probability. The red star shows the magnitude of the mainshock M_w 8.3……. 71

Figure 19. (a) The best model (4) of the estimated curve of the modified Omori formula (dashed line) applied to the aftershock data and the observed cumulative number of aftershocks (solid line) based on the AIC. **(b)** The model 1 of the estimated curve of the modified Omori formula (dashed line) applied to the aftershock data and the observed cumulative number of aftershocks (solid line), with the lowest RMS= 4.76…… 72

Figure 20. The magnitude-time pattern versus the logarithm of time of the mainshock M_w 8.3……. 72

Figure 21. Frequency-magnitude distribution. The bold red line represents the model of equation (26) for qM= 1.46, while the other two lines present the corresponding 95% confidence intervals…… 73

Figure 22. (a) The cumulative distribution function of the interevent times. The red line is the Q-exponential fitting with q = 1.72. **(b)** The Q-logarithmic function of the P(>T) as a function of the interevent times where the dashed line is the fitting with q=1.72. The deviation from the linearity suggests Tc values close to 200,000 s. **(c)** The evolution of interevent time T as a function of time t since the main event. The Tc value is indicated by the dashed line…….. 73

Figure 23. The Guttenberg-Richter distribution using maximum likelihood method with the best combination of maximum curvature M_c 95% and M_c 90% probability. The red star shows the magnitude of the mainshock M_w 7.7……. 74

Figure 24. The best model (1) of the estimated curve of the modified Omori formula (dashed line) applied to the aftershock data and the observed cumulative number of aftershocks (solid line) based on the AIC with RMS=1.05…….. 75

Figure 25. The magnitude-time pattern versus the logarithm of time of the mainshock M_w 7.7……. 75

Figure 26. Frequency-magnitude distribution. The bold red line represents the model of equation (26) for qM= 1.55, while the other two lines present the corresponding 95% confidence intervals…… 76

Figure 27. (a) The cumulative distribution function of the interevent times. The red line is the Q-exponential fitting with q = 1.77. **(b)** The Q-logarithmic function of the P(>T) as a function of the interevent times where the dashed line is the fitting with q=1.77. The deviation from the linearity suggests Tc values close to 50,000 s. **(c)** The evolution of interevent time T as a function of time t since the main event. The Tc value is indicated by the dashed line……. 76

Figure 28. The Guttenberg-Richter distribution using maximum likelihood method with the best combination of maximum curvature M_c 95% and M_c 90% probability. The red star shows the magnitude of the mainshock M_w 7.9……. 77

Figure 29. (a) The best model (4) of the estimated curve of the modified Omori formula (dashed line) applied to the aftershock data and the observed cumulative number of aftershocks (solid line) based on the AIC. **(b)** The model 1 of the estimated curve of the modified Omori formula (dashed line) applied to the aftershock data and the observed cumulative number of aftershocks (solid line), with the lowest RMS= 6.56…… 78

Figure 30. The magnitude-time pattern versus the logarithm of time of the mainshock M_w 7.9……. 79

Figure 31. Frequency-magnitude distribution. The bold red line represents the model of equation (26) for qM= 1.43, while the other two lines present the corresponding 95% confidence intervals…… 79

Figure 32. (a) The cumulative distribution function of the interevent times. The red line is the Q-exponential fitting with q = 1.83. **(b)** The Q-logarithmic function of the P(>T) as a function of the interevent times where the dashed line is the fitting with q=1.83. The deviation from the linearity

suggests Tc values close to 200,000 s. **(c)** The evolution of interevent time T as a function of time t since the main event. The Tc value is indicated by the dashed line……. 80

Figure 33. The Guttenberg-Richter distribution using maximum likelihood method with the best combination of maximum curvature M_c 95% and M_c 90% probability. The red star shows the magnitude of the mainshock M_w 7.9……. 81

Figure 34. (a) The best model (3) of the estimated curve of the modified Omori formula (dashed line) applied to the aftershock data and the observed cumulative number of aftershocks (solid line) based on the AIC. **(b)** The model 4 of the estimated curve of the modified Omori formula (dashed line) applied to the aftershock data and the observed cumulative number of aftershocks (solid line), with the lowest RMS= 2.35…… 82

Figure 35. The magnitude-time pattern versus the logarithm of time of the mainshock M_w 7.9……. 83

Figure 36. Frequency-magnitude distribution. The bold red line represents the model of equation (26) for qM= 1.38, while the other two lines present the corresponding 95% confidence intervals…… 83

Figure 37. (a) The cumulative distribution function of the interevent times. The red line is the Q-exponential fitting with q = 1.82. **(b)** The Q-logarithmic function of the P(>T) as a function of the interevent times where the dashed line is the fitting with q=1.82. The deviation from the linearity suggests Tc values close to 400,000 s. **(c)** The evolution of interevent time T as a function of time t since the main event. The Tc value is indicated by the dashed line…….. 84

Figure 38. The Guttenberg-Richter distribution using maximum likelihood method with the best combination of maximum curvature M_c 95% and M_c 90% probability. The red star shows the magnitude of the mainshock M_w 8.0……. 85

Figure 39. (a) The best model (3) of the estimated curve of the modified Omori formula (dashed line) applied to the aftershock data and the observed cumulative number of aftershocks (solid line) based on the AIC. **(b)** The model 2 of the estimated curve of the modified Omori formula (dashed line) applied to the aftershock data and the observed cumulative number of aftershocks (solid line), with the lowest RMS= 18.08…….. 86

Figure 40. The magnitude-time pattern versus the logarithm of time of the mainshock M_w 8.0……. 87

Figure 41. Frequency-magnitude distribution. The bold red line represents the model of equation (26) for qM= 1.38, while the other two lines present the corresponding 95% confidence intervals…… 87

Figure 42. (a) The cumulative distribution function of the interevent times. The red line is the Q-exponential fitting with q = 1.69. **(b)** The Q-logarithmic function of the P(>T) as a function of the interevent times where the dashed line is the fitting with q=1.69. The deviation from the linearity suggests Tc values close to 20,000 s. **(c)** The evolution of interevent time T as a function of time t since the main event. The Tc value is indicated by the dashed line…….. 88

Figure 43. The Guttenberg-Richter distribution using maximum likelihood method with the best combination of maximum curvature M_c 95% and M_c 90% probability. The red star shows the magnitude of the mainshock M_w 8.4……. 89

Figure 44. (a) The best model (4) of the estimated curve of the modified Omori formula (dashed line) applied to the aftershock data and the observed cumulative number of aftershocks (solid line) based on the AIC. **(b)** The model 2 of the estimated curve of the modified Omori formula (dashed line) applied to the aftershock data and the observed cumulative number of aftershocks (solid line), with the lowest RMS= 3.86…… 90

Figure 45. The magnitude-time pattern versus the logarithm of time of the mainshock M_w 8.4……. 91

Figure 46. Frequency-magnitude distribution. The bold red line represents the model of equation (26) for qM= 1.42, while the other two lines present the corresponding 95% confidence intervals…… 91

Figure 47. (a) The cumulative distribution function of the interevent times. The red line is the Q-exponential fitting with q = 1.80. **(b)** The Q-logarithmic function of the P(>T) as a function of the interevent times where the dashed line is the fitting with q=1.80. The deviation from the linearity suggests Tc values close to 40,000 s. **(c)** The evolution of interevent time T as a function of time t since the main event. The Tc value is indicated by the dashed line……. 92

Figure 48. The Guttenberg-Richter distribution using maximum likelihood method with the best combination of maximum curvature M_c 95% and M_c 90% probability. The red star shows the magnitude of the mainshock M_w 8.3……. 93

Figure 49. (a) The best model (1) of the estimated curve of the modified Omori formula (dashed line) applied to the aftershock data and the observed cumulative number of aftershocks (solid line) based on the AIC. **(b)** The model 3 of the estimated curve of the modified Omori formula (dashed line) applied to the aftershock data and the observed cumulative number of aftershocks (solid line), with the lowest RMS= 3.18…… 94

Figure 50. The magnitude-time pattern versus the logarithm of time of the mainshock M_w 8.3……. 95

Figure 51. Frequency-magnitude distribution. The bold red line represents the model of equation (26) for qM= 1.53, while the other two lines present the corresponding 95% confidence intervals…… 96

Figure 52. (a) The cumulative distribution function of the interevent times. The red line is the Q-exponential fitting with q = 1.78. **(b)** The Q-logarithmic function of the P(>T) as a function of the interevent times where the dashed line is the fitting with q=1.78. The deviation from the linearity suggests Tc values close to 700,000 s. **(c)** The evolution of interevent time T as a function of time t since the main event. The Tc value is indicated by the dashed line…….. 97

Figure 53. The Guttenberg-Richter distribution using maximum likelihood method with the best combination of maximum curvature M_c 95% and M_c 90% probability. The red star shows the magnitude of the mainshock M_w 9.0……. 98

Figure 54. (a) The best model (3) of the estimated curve of the modified Omori formula (dashed line) applied to the aftershock data and the observed cumulative number of aftershocks (solid line) based on the AIC. **(b)** The model 1 of the estimated curve of the modified Omori formula (dashed line) applied to the aftershock data and the observed cumulative number of aftershocks (solid line), with the lowest RMS= 2.41…… 99

Figure 55. The magnitude-time pattern versus the logarithm of time of the mainshock M_w 9.0……. 99

Figure 56. Frequency-magnitude distribution. The bold red line represents the model of equation (26) for qM= 1.47, while the other two lines present the corresponding 95% confidence intervals…….. 100

Figure 57. (a) The cumulative distribution function of the interevent times. The red line is the Q-exponential fitting with q = 1.69. **(b)** The Q-logarithmic function of the P(>T) as a function of the interevent times where the dashed line is the fitting with q=1.69. The deviation from the linearity suggests Tc values close to 400,000 s. **(c)** The evolution of interevent time T as a function of time t since the main event. The Tc value is indicated by the dashed line…… 101

Figure 58. The Guttenberg-Richter distribution using maximum likelihood method with the best combination of maximum curvature M_c 95% and M_c 90% probability. The red star shows the magnitude of the mainshock M_w 8.6……. 102

Figure 59. The best model (1) of the estimated curve of the modified Omori formula (dashed line) applied to the aftershock data and the observed cumulative number of aftershocks (solid line) based on the AIC with RMS=4.83…… 102

Figure 60. The magnitude-time pattern versus the logarithm of time of the mainshock M_w 8.6…... 103

Figure 61. Frequency-magnitude distribution. The bold red line represents the model of equation (26) for qM= 1.45, while the other two lines present the corresponding 95% confidence intervals…….. 103

Figure 62. (a) The cumulative distribution function of the interevent times. The red line is the Q-exponential fitting with q = 1.83. **(b)** The Q-logarithmic function of the P(>T) as a function of the interevent times where the dashed line is the fitting with q=1.83. The deviation from the linearity suggests Tc values close to 175,000 s. **(c)** The evolution of interevent time T as a function of time t since the main event. The Tc value is indicated by the dashed line…… 104

Figure 63. (a) The Guttenberg-Richter distribution using maximum likelihood method with the best combination of maximum curvature M_c 95% and M_c 90% probability. The red star shows the magnitude of the mainshock M_w 8.0. **(b)** The Guttenberg-Richter distribution using the manual method……... 105

Figure 64. (a) The best model (1) of the estimated curve of the modified Omori formula (dashed line) applied to the aftershock data and the observed cumulative number of aftershocks (solid line) based on the AIC. **(b)** The model 3 of the estimated curve of the modified Omori formula (dashed line) applied to the aftershock data and the observed cumulative number of aftershocks (solid line), with the lowest RMS= 3.79…….. 106

Figure 65. The magnitude-time pattern versus the logarithm of time of the mainshock M_w 8.0…... 107

Figure 66. Frequency-magnitude distribution. The bold red line represents the model of equation (26) for qM= 1.27, while the other two lines present the corresponding 95% confidence intervals…….. 107

Figure 67. (a) The cumulative distribution function of the interevent times. The red line is the Q-exponential fitting with q = 1.75. **(b)** The Q-logarithmic function of the P(>T) as a function of the interevent times where the dashed line is the fitting with q=1.75. The deviation from the linearity suggests Tc values close to 300,000 s. **(c)** The evolution of interevent time T as a function of time t since the main event. The Tc value is indicated by the dashed line……..... 108

Figure 68. (a) The Guttenberg-Richter distribution using maximum likelihood method with the best combination of maximum curvature M_c 95% and M_c 90% probability. The red star shows the magnitude of the mainshock M_w 7.7. **(b)** The Guttenberg-Richter distribution using the manual method……... 109

Figure 69. (a) The best model (1) of the estimated curve of the modified Omori formula (dashed line) applied to the aftershock data and the observed cumulative number of aftershocks (solid line) based on the AIC. **(b)** The model 4 of the estimated curve of the modified Omori formula (dashed line) applied to the aftershock data and the observed cumulative number of aftershocks (solid line), with the lowest RMS= 2.75…….. 110

Figure 70. The magnitude-time pattern versus the logarithm of time of the mainshock M_w 7.7…... 111

Figure 71. Frequency-magnitude distribution. The bold red line represents the model of equation (26) for qM= 1.06, while the other two lines present the corresponding 95% confidence intervals…….. 111

Figure 72. (a) The cumulative distribution function of the interevent times. The red line is the Q-exponential fitting with q = 1.67. **(b)** The Q-logarithmic function of the P(>T) as a function of the interevent times where the dashed line is the fitting with q=1.67. The deviation from the linearity suggests Tc values close to 15,000 s. **(c)** The evolution of interevent time T as a function of time t since the main event. The Tc value is indicated by the dashed line…… 112

Figure 73. (a) The Guttenberg-Richter distribution using maximum likelihood method with the best combination of maximum curvature M_c 95% and M_c 90% probability. The red star shows the magnitude of the mainshock M_w 8.1. **(b)** The Guttenberg-Richter distribution using the manual method……... 113

Figure 74. The best model (1) of the estimated curve of the modified Omori formula (dashed line) applied to the aftershock data and the observed cumulative number of aftershocks (solid line) based on the AIC with RMS= 5.06……... 114

Figure 75. The magnitude-time pattern versus the logarithm of time of the mainshock M_w 8.1….. 114

Figure 76. Frequency-magnitude distribution. The bold red line represents the model of equation (26) for qM= 1.42, while the other two lines present the corresponding 95% confidence intervals…….. 115

Figure 77. (a) The cumulative distribution function of the interevent times. The red line is the Q-exponential fitting with q = 1.80. **(b)** The Q-logarithmic function of the P(>T) as a function of the interevent times where the dashed line is the fitting with q=1.80. The deviation from the linearity suggests Tc values close to 800,000 s. **(c)** The evolution of interevent time T as a function of time t since the main event. The Tc value is indicated by the dashed line…… 116

Figure 78. The Guttenberg-Richter distribution using maximum likelihood method with the best combination of maximum curvature M_c 95% and M_c 90% probability. The red star shows the magnitude of the mainshock M_w 8.4……... 117

Figure 79. The best model (1) of the estimated curve of the modified Omori formula (dashed line) applied to the aftershock data and the observed cumulative number of aftershocks (solid line) based on the AIC with RMS=3.79…… 117

Figure 80. The magnitude-time pattern versus the logarithm of time of the mainshock M_w 8.4…... 118

Figure 81. Frequency-magnitude distribution. The bold red line represents the model of equation (26) for qM= 1.58, while the other two lines present the corresponding 95% confidence intervals…….. 118

Figure 82. (a) The cumulative distribution function of the interevent times. The red line is the Q-exponential fitting with q = 1.83. **(b)** The Q-logarithmic function of the P(>T) as a function of the interevent times where the dashed line is the fitting with q=1.83. The deviation from the linearity suggests Tc values close to 150,000 s. **(c)** The evolution of interevent time T as a function of time t since the main event. The Tc value is indicated by the dashed line…… 119

Figure 83. The Guttenberg-Richter distribution using maximum likelihood method with the best combination of maximum curvature M_c 95% and M_c 90% probability. The red star shows the magnitude of the mainshock M_w 7.2……... 120

Figure 84. The best model (4) of the estimated curve of the modified Omori formula (dashed line) applied to the aftershock data and the observed cumulative number of aftershocks (solid line) based on the AIC with RMS= 2.29……... 120

Figure 85. The magnitude-time pattern versus the logarithm of time of the mainshock M_w 7.2…... 121

Figure 86. Frequency-magnitude distribution. The bold red line represents the model of equation (26) for qM= 1.48, while the other two lines present the corresponding 95% confidence intervals…….. 121

Figure 87. (a) The cumulative distribution function of the interevent times. The red line is the Q-exponential fitting with q = 1.80. **(b)** The Q-logarithmic function of the P(>T) as a function of the interevent times where the dashed line is the fitting with q=1.80. The deviation from the linearity suggests Tc values close to 1,500,000 s. **(c)** The evolution of interevent time T as a function of time t since the main event. The Tc value is indicated by the dashed line…… 122

Figure 88. (a) The Guttenberg-Richter distribution using maximum likelihood method with the best combination of maximum curvature M_c 95% and M_c 90% probability. The red star shows the magnitude of the mainshock M_w 8.1. **(b)** The Guttenberg-Richter distribution using the manual method……... 123

Figure 89. The best model (1) of the estimated curve of the modified Omori formula (dashed line) applied to the aftershock data and the observed cumulative number of aftershocks (solid line) based on the AIC with RMS= 7.04……... 124

Figure 90. The magnitude-time pattern versus the logarithm of time of the mainshock M_w 8.1….. 124

Figure 91. Frequency-magnitude distribution. The bold red line represents the model of equation (26) for qM= 1.23, while the other two lines present the corresponding 95% confidence intervals…….. 125

Figure 92. (a) The cumulative distribution function of the interevent times. The red line is the Q-exponential fitting with q = 1.83. **(b)** The Q-logarithmic function of the P(>T) as a function of the interevent times where the dashed line is the fitting with q=1.83. The deviation from the linearity suggests Tc values close to 150,000 s. **(c)** The evolution of interevent time T as a function of time t since the main event. The Tc value is indicated by the dashed line…… 126

Figure 93. The Guttenberg-Richter distribution using maximum likelihood method with the best combination of maximum curvature M_c 95% and M_c 90% probability. The red star shows the magnitude of the mainshock M_w 7.8……... 127

Figure 94. (a) The best model (1) of the estimated curve of the modified Omori formula (dashed line) applied to the aftershock data and the observed cumulative number of aftershocks (solid line) based on the AIC. **(b)** The model 4 of the estimated curve of the modified Omori formula (dashed line) applied to the aftershock data and the observed cumulative number of aftershocks (solid line), with the lowest RMS= 2.97…….. 128

Figure 95. The magnitude-time pattern versus the logarithm of time of the mainshock M_w 7.8…... 128

Figure 96. Frequency-magnitude distribution. The bold red line represents the model of equation (26) for qM= 1.56, while the other two lines present the corresponding 95% confidence intervals…….. 129

Figure 97. (a) The cumulative distribution function of the interevent times. The red line is the Q-exponential fitting with q = 1.80. **(b)** The Q-logarithmic function of the P(>T) as a function of the interevent times where the dashed line is the fitting with q=1.80. The deviation from the linearity suggests Tc values close to 400,000 s. **(c)** The evolution of interevent time T as a function of time t since the main event. The Tc value is indicated by the dashed line…… 130

Figure 98. The Guttenberg-Richter distribution using maximum likelihood method with the best combination of maximum curvature M_c 95% and M_c 90% probability. The red star shows the magnitude of the mainshock M_w 8.8……... 131

Figure 99. (a) The best model (1) of the estimated curve of the modified Omori formula (dashed line) applied to the aftershock data and the observed cumulative number of aftershocks (solid line) based on the AIC. **(b)** The model 4 of the estimated curve of the modified Omori formula (dashed line) applied to the aftershock data and the observed cumulative number of aftershocks (solid line), with the lowest RMS= 3.64…….. 132

Figure 100. The magnitude-time pattern versus the logarithm of time of the mainshock M_w 8.8…. 132

Figure 101. Frequency-magnitude distribution. The bold red line represents the model of equation (26) for qM= 1.50, while the other two lines present the corresponding 95% confidence intervals... 133

Figure 102. (a) The cumulative distribution function of the interevent times. The red line is the Q-exponential fitting with q = 1.67. **(b)** The Q-logarithmic function of the P(>T) as a function of the interevent times where the dashed line is the fitting with q=1.67. The deviation from the linearity suggests Tc values close to 1,000,000 s. **(c)** The evolution of interevent time T as a function of time t since the main event. The Tc value is indicated by the dashed line…… 134

Figure 103. The Guttenberg-Richter distribution using maximum likelihood method with the best combination of maximum curvature M_c 95% and M_c 90% probability. The red star shows the magnitude of the mainshock M_w 9.1……... 135

Figure 104. The best model (1) of the estimated curve of the modified Omori formula (dashed line) applied to the aftershock data and the observed cumulative number of aftershocks (solid line) based on the AIC with RMS= 6.53……... 135

Figure 105. The magnitude-time pattern versus the logarithm of time of the mainshock M_w 9.1…. 136

Figure 106. Frequency-magnitude distribution. The bold red line represents the model of equation (26) for qM= 1.51, while the other two lines present the corresponding 95% confidence intervals... 136

Figure 107. (a) The cumulative distribution function of the interevent times. The red line is the Q-exponential fitting with q = 1.67. **(b)** The Q-logarithmic function of the P(>T) as a function of the interevent times where the dashed line is the fitting with q=1.67. The deviation from the linearity

suggests Tc values close to 300,000 s. **(c)** The evolution of interevent time T as a function of time t since the main event. The Tc value is indicated by the dashed line…… 137

Figure 108. The Guttenberg-Richter distribution using maximum likelihood method with the best combination of maximum curvature M_c 95% and M_c 90% probability. The red star shows the magnitude of the mainshock M_w 7.6……... 138

Figure 109. (a) The best model (1) of the estimated curve of the modified Omori formula (dashed line) applied to the aftershock data and the observed cumulative number of aftershocks (solid line) based on the AIC. **(b)** The model 3 of the estimated curve of the modified Omori formula (dashed line) applied to the aftershock data and the observed cumulative number of aftershocks (solid line), with the lowest RMS= 3.9…… 139

Figure 110. The magnitude-time pattern versus the logarithm of time of the mainshock M_w 7.6…. 139

Figure 111. Frequency-magnitude distribution. The bold red line represents the model of equation (26) for qM= 1.51, while the other two lines present the corresponding 95% confidence intervals... 140

Figure 112. (a) The cumulative distribution function of the interevent times. The red line is the Q-exponential fitting with q = 1.74. **(b)** The Q-logarithmic function of the P(>T) as a function of the interevent times where the dashed line is the fitting with q=1.74. The deviation from the linearity suggests Tc values close to 500,000 s. **(c)** The evolution of interevent time T as a function of time t since the main event. The Tc value is indicated by the dashed line…… 141

Figure 113. (a) The Guttenberg-Richter distribution using maximum likelihood method with the best combination of maximum curvature M_c 95% and M_c 90% probability. The red star shows the magnitude of the mainshock M_w 8.6. **(b)** The Guttenberg-Richter distribution using the manual method……... 142

Figure 114. (a) The best model (1) of the estimated curve of the modified Omori formula (dashed line) applied to the aftershock data and the observed cumulative number of aftershocks (solid line) based on the AIC. **(b)** The model 4 of the estimated curve of the modified Omori formula (dashed line) applied to the aftershock data and the observed cumulative number of aftershocks (solid line), with the lowest RMS= 3.71……. 143

Figure 115. The magnitude-time pattern versus the logarithm of time of the mainshock M_w 8.6…. 144

Figure 116. Frequency-magnitude distribution. The bold red line represents the model of equation (26) for qM= 1.30, while the other two lines present the corresponding 95% confidence intervals….144

Figure 117. (a) The cumulative distribution function of the interevent times. The red line is the Q-exponential fitting with q = 1.83. **(b)** The Q-logarithmic function of the P(>T) as a function of the interevent times where the dashed line is the fitting with q=1.83. The deviation from the linearity

suggests Tc values close to 250,000 s. **(c)** The evolution of interevent time T as a function of time t since the main event. The Tc value is indicated by the dashed line…….. 145

Figure 118. (a) The Guttenberg-Richter distribution using maximum likelihood method with the best combination of maximum curvature M_c 95% and M_c 90% probability. The red star shows the magnitude of the mainshock M_w 7.0. **(b)** The Guttenberg-Richter distribution using the manual method……... 146

Figure 119. The best model (3) of the estimated curve of the modified Omori formula (dashed line) applied to the aftershock data and the observed cumulative number of aftershocks (solid line) based on the AIC with the lowest RMS= 3.68…….. 147

Figure 120. The magnitude-time pattern versus the logarithm of time of the mainshock M_w 7.0…. 147

Figure 121. Frequency-magnitude distribution. The bold red line represents the model of equation (26) for qM= 1.50, while the other two lines present the corresponding 95% confidence intervals... 148

Figure 122. (a) The cumulative distribution function of the interevent times. The red line is the Q-exponential fitting with q = 1.77. **(b)** The Q-logarithmic function of the P(>T) as a function of the interevent times where the dashed line is the fitting with q=1.77. The deviation from the linearity suggests Tc values close to 1,000,000 s. **(c)** The evolution of interevent time T as a function of time t since the main event. The Tc value is indicated by the dashed line…… 149

Figure 123. (a) The Guttenberg-Richter distribution using maximum likelihood method with the best combination of maximum curvature M_c 95% and M_c 90% probability. The red star shows the magnitude of the mainshock M_w 7.6. **(b)** The Guttenberg-Richter distribution using the manual method……... 150

Figure 124. The best model (1) of the estimated curve of the modified Omori formula (dashed line) applied to the aftershock data and the observed cumulative number of aftershocks (solid line) based on the AIC with RMS= 6.52…….. 151

Figure 125. The magnitude-time pattern versus the logarithm of time of the mainshock M_w 7.6…. 151

Figure 126. Frequency-magnitude distribution. The bold red line represents the model of equation (26) for qM= 1.55, while the other two lines present the corresponding 95% confidence intervals... 152

Figure 127. (a) The cumulative distribution function of the interevent times. The red line is the Q-exponential fitting with q = 1.74. **(b)** The Q-logarithmic function of the P(>T) as a function of the interevent times where the dashed line is the fitting with q=1.74. The deviation from the linearity suggests Tc values close to 1,000,000 s. **(c)** The evolution of interevent time T as a function of time t since the main event. The Tc value is indicated by the dashed line…… 153

Figure 128. (a) The Guttenberg-Richter distribution using maximum likelihood method with the best combination of maximum curvature M_c 95% and M_c 90% probability. The red star shows the magnitude of the mainshock M_w 7.5. **(b)** The Guttenberg-Richter distribution using the manual method……... 154

Figure 129. The best model (4) of the estimated curve of the modified Omori formula (dashed line) applied to the aftershock data and the observed cumulative number of aftershocks (solid line) based on the AIC with RMS= 4.72…….. 155

Figure 130. The magnitude-time pattern versus the logarithm of time of the mainshock M_w 7.5…. 155

Figure 131. Frequency-magnitude distribution. The bold red line represents the model of equation (26) for qM= 1.21, while the other two lines present the corresponding 95% confidence intervals... 156

Figure 132. (a) The cumulative distribution function of the interevent times. The red line is the Q-exponential fitting with q = 1.78. **(b)** The Q-logarithmic function of the P(>T) as a function of the interevent times where the dashed line is the fitting with q=1.78. The deviation from the linearity suggests Tc values close to 1,000,000 s. **(c)** The evolution of interevent time T as a function of time t since the main event. The Tc value is indicated by the dashed line…… 157

Figure 133. (a) The Guttenberg-Richter distribution using maximum likelihood method with the best combination of maximum curvature M_c 95% and M_c 90% probability. The red star shows the magnitude of the mainshock M_w 7.1. **(b)** The Guttenberg-Richter distribution using the manual method……... 158

Figure 134. (a) The best model (4) of the estimated curve of the modified Omori formula (dashed line) applied to the aftershock data and the observed cumulative number of aftershocks (solid line) based on the AIC. **(b)** The model 1 of the estimated curve of the modified Omori formula (dashed line) applied to the aftershock data and the observed cumulative number of aftershocks (solid line), with the lowest RMS= 4.46……. 159

Figure 135. The magnitude-time pattern versus the logarithm of time of the mainshock M_w 7.1…. 160

Figure 136. Frequency-magnitude distribution. The bold red line represents the model of equation (26) for qM= 1.55, while the other two lines present the corresponding 95% confidence intervals... 160

Figure 137. (a) The cumulative distribution function of the interevent times. The red line is the Q-exponential fitting with q = 1.77. **(b)** The Q-logarithmic function of the P(>T) as a function of the interevent times where the dashed line is the fitting with q=1.77. The deviation from the linearity suggests Tc values close to 1,000,000 s. **(c)** The evolution of interevent time T as a function of time t since the main event. The Tc value is indicated by the dashed line…… 161

Figure 138. (a) The Guttenberg-Richter distribution using maximum likelihood method with the best combination of maximum curvature M_c 95% and M_c 90% probability. The red star shows the

magnitude of the mainshock M_w 7.5. **(b)** The Guttenberg-Richter distribution using the manual method……... 162

Figure 139. The best model (1) of the estimated curve of the modified Omori formula (dashed line) applied to the aftershock data and the observed cumulative number of aftershocks (solid line) based on the AIC with RMS= 3.14…….. 163

Figure 140. The magnitude-time pattern versus the logarithm of time of the mainshock M_w 7.5…. 163

Figure 141. Frequency-magnitude distribution. The bold red line represents the model of equation (26) for qM= 1.56, while the other two lines present the corresponding 95% confidence intervals... 164

Figure 142. (a) The cumulative distribution function of the interevent times. The red line is the Q-exponential fitting with q = 1.71. **(b)** The Q-logarithmic function of the P(>T) as a function of the interevent times where the dashed line is the fitting with q=1.71. The deviation from the linearity suggests Tc values close to 1,000,000 s. **(c)** The evolution of interevent time T as a function of time t since the main event. The Tc value is indicated by the dashed line…… 165

Figure 143. (a) The Guttenberg-Richter distribution using maximum likelihood method with the best combination of maximum curvature M_c 95% and M_c 90% probability. The red star shows the magnitude of the mainshock M_w 7.8. **(b)** The Guttenberg-Richter distribution using the manual method……... 166

Figure 144. (a) The best model (2) of the estimated curve of the modified Omori formula (dashed line) applied to the aftershock data and the observed cumulative number of aftershocks (solid line) based on the AIC. **(b)** The model 4 of the estimated curve of the modified Omori formula (dashed line) applied to the aftershock data and the observed cumulative number of aftershocks (solid line), with the lowest RMS= 2.21…….. 167

Figure 145. The magnitude-time pattern versus the logarithm of time of the mainshock M_w 7.8…. 168

Figure 146. Frequency-magnitude distribution. The bold red line represents the model of equation (26) for qM= 1.54, while the other two lines present the corresponding 95% confidence intervals... 168

Figure 147. (a) The cumulative distribution function of the interevent times. The red line is the Q-exponential fitting with q = 1.71. **(b)** The Q-logarithmic function of the P(>T) as a function of the interevent times where the dashed line is the fitting with q=1.71. The deviation from the linearity suggests Tc values close to 2,500,000 s. **(c)** The evolution of interevent time T as a function of time t since the main event. The Tc value is indicated by the dashed line…… 169

Figure 148. The Guttenberg-Richter distribution using maximum likelihood method with the best combination of maximum curvature M_c 95% and M_c 90% probability. The red star shows the magnitude of the mainshock M_w 8.3…….. 170

Figure 149. (a) The best model (1) of the estimated curve of the modified Omori formula (dashed line) applied to the aftershock data and the observed cumulative number of aftershocks (solid line) based on the AIC. **(b)** The model 4 of the estimated curve of the modified Omori formula (dashed line) applied to the aftershock data and the observed cumulative number of aftershocks (solid line), with the lowest RMS= 2.07…….. 171

Figure 150. The magnitude-time pattern versus the logarithm of time of the mainshock M_w 8.3…. 171

Figure 151. Frequency-magnitude distribution. The bold red line represents the model of equation (26) for qM= 1.50, while the other two lines present the corresponding 95% confidence intervals... 172

Figure 152. (a) The cumulative distribution function of the interevent times. The red line is the Q-exponential fitting with q = 1.78. **(b)** The Q-logarithmic function of the P(>T) as a function of the interevent times where the dashed line is the fitting with q=1.78. The deviation from the linearity suggests Tc values close to 500,000 s. **(c)** The evolution of interevent time T as a function of time t since the main event. The Tc value is indicated by the dashed line…… 173

Figure 153. (a) The Guttenberg-Richter distribution using maximum likelihood method with the best combination of maximum curvature M_c 95% and M_c 90% probability. The red star shows the magnitude of the mainshock M_w 7.2. **(b)** The Guttenberg-Richter distribution using the manual method……... 174

Figure 154. The best model (2) of the estimated curve of the modified Omori formula (dashed line) applied to the aftershock data and the observed cumulative number of aftershocks (solid line) based on the AIC with RMS= 1.4……. 175

Figure 155. The magnitude-time pattern versus the logarithm of time of the mainshock M_w 7.2…. 175

Figure 156. Frequency-magnitude distribution. The bold red line represents the model of equation (26) for qM= 1.41, while the other two lines present the corresponding 95% confidence intervals... 176

Figure 157. (a) The cumulative distribution function of the interevent times. The red line is the Q-exponential fitting with q = 1.78. **(b)** The Q-logarithmic function of the P(>T) as a function of the interevent times where the dashed line is the fitting with q=1.78. The deviation from the linearity suggests Tc values close to 700,000 s. **(c)** The evolution of interevent time T as a function of time t since the main event. The Tc value is indicated by the dashed line……... 177

Figure 158. (a) The Guttenberg-Richter distribution using maximum likelihood method with the best combination of maximum curvature M_c 95% and M_c 90% probability. The red star shows the magnitude of the mainshock M_w 7.0. **(b)** The Guttenberg-Richter distribution using the manual method……... 178

Figure 159. The best model (1) of the estimated curve of the modified Omori formula (dashed line) applied to the aftershock data and the observed cumulative number of aftershocks (solid line) based on the AIC with RMS= 3.49……... 179

Figure 160. The magnitude-time pattern versus the logarithm of time of the mainshock M_w 7.0…. 179

Figure 161. Frequency-magnitude distribution. The bold red line represents the model of equation (26) for qM= 1.25, while the other two lines present the corresponding 95% confidence intervals... 180

Figure 162. (a) The cumulative distribution function of the interevent times. The red line is the Q-exponential fitting with q = 1.74. **(b)** The Q-logarithmic function of the P(>T) as a function of the interevent times where the dashed line is the fitting with q=1.74. The deviation from the linearity suggests Tc values close to 250,000 s. **(c)** The evolution of interevent time T as a function of time t since the main event. The Tc value is indicated by the dashed line…… 181

Figure 163. The Guttenberg-Richter distribution using maximum likelihood method with the best combination of maximum curvature M_c 95% and M_c 90% probability. The red star shows the magnitude of the mainshock M_w 7.8…….. 182

Figure 164. (a) The best model (3) of the estimated curve of the modified Omori formula (dashed line) applied to the aftershock data and the observed cumulative number of aftershocks (solid line) based on the AIC. **(b)** The model 4 of the estimated curve of the modified Omori formula (dashed line) applied to the aftershock data and the observed cumulative number of aftershocks (solid line), with the lowest RMS= 4.1……..... 183

Figure 165. The magnitude-time pattern versus the logarithm of time of the mainshock M_w 7.8…. 183

Figure 166. Frequency-magnitude distribution. The bold red line represents the model of equation (26) for qM= 1.47, while the other two lines present the corresponding 95% confidence intervals... 184

Figure 167. (a) The cumulative distribution function of the interevent times. The red line is the Q-exponential fitting with q = 1.73. **(b)** The Q-logarithmic function of the P(>T) as a function of the interevent times where the dashed line is the fitting with q=1.73. The deviation from the linearity suggests Tc values close to 2,000,000 s. **(c)** The evolution of interevent time T as a function of time t since the main event. The Tc value is indicated by the dashed line……... 185

Figure 168. The Guttenberg-Richter distribution using maximum likelihood method with the best combination of maximum curvature M_c 95% and M_c 90% probability. The red star shows the magnitude of the mainshock M_w 7.8……... 186

Figure 169. The best model (1) of the estimated curve of the modified Omori formula (dashed line) applied to the aftershock data and the observed cumulative number of aftershocks (solid line) based on the AIC with RMS= 1.83…….. 186

Figure 170. The magnitude-time pattern versus the logarithm of time of the mainshock M_w 7.8…. 187

Figure 171. Frequency-magnitude distribution. The bold red line represents the model of equation (26) for qM= 1.51, while the other two lines present the corresponding 95% confidence intervals... 187

Figure 172. (a) The cumulative distribution function of the interevent times. The red line is the Q-exponential fitting with q = 1.71. **(b)** The Q-logarithmic function of the P(>T) as a function of the interevent times where the dashed line is the fitting with q=1.71. The deviation from the linearity suggests Tc values close to 10,000,000 s. **(c)** The evolution of interevent time T as a function of time t since the main event. The Tc value is indicated by the dashed line……. 188

Figure 173. The Guttenberg-Richter distribution using maximum likelihood method with the best combination of maximum curvature M_c 95% and M_c 90% probability. The red star shows the magnitude of the mainshock M_w 8.2…….. 189

Figure 174. (a) The best model (1) of the estimated curve of the modified Omori formula (dashed line) applied to the aftershock data and the observed cumulative number of aftershocks (solid line) based on the AIC. **(b)** The model 4 of the estimated curve of the modified Omori formula (dashed line) applied to the aftershock data and the observed cumulative number of aftershocks (solid line), with the lowest RMS= 3.25…….. 190

Figure 175. The magnitude-time pattern versus the logarithm of time of the mainshock M_w 8.2…. 190

Figure 176. Frequency-magnitude distribution. The bold red line represents the model of equation (26) for qM= 1.31, while the other two lines present the corresponding 95% confidence intervals... 191

Figure 177. (a) The cumulative distribution function of the interevent times. The red line is the Q-exponential fitting with q = 1.74. **(b)** The Q-logarithmic function of the P(>T) as a function of the interevent times where the dashed line is the fitting with q=1.74. The deviation from the linearity suggests Tc values close to 400,000 s. **(c)** The evolution of interevent time T as a function of time t since the main event. The Tc value is indicated by the dashed line……... 192

Figure 178. The Guttenberg-Richter distribution using maximum likelihood method with the best combination of maximum curvature M_c 95% and M_c 90% probability. The red star shows the magnitude of the mainshock M_w 7.3……. 193

Figure 179. (a) The best model (1) of the estimated curve of the modified Omori formula (dashed line) applied to the aftershock data and the observed cumulative number of aftershocks (solid line) based on the AIC. **(b)** The model 4 of the estimated curve of the modified Omori formula (dashed line) applied to the aftershock data and the observed cumulative number of aftershocks (solid line), with the lowest RMS= 2.21…….. 194

Figure 180. The magnitude-time pattern versus the logarithm of time of the mainshock M_w 7.3…. 194

Figure 181. Frequency-magnitude distribution. The bold red line represents the model of equation (26) for qM= 1.44, while the other two lines present the corresponding 95% confidence intervals.. 195

Figure 182. (a) The cumulative distribution function of the interevent times. The red line is the Q-exponential fitting with q = 1.80. **(b)** The Q-logarithmic function of the P(>T) as a function of the interevent times where the dashed line is the fitting with q=1.80. The deviation from the linearity suggests Tc values close to 150,000 s. **(c)** The evolution of interevent time T as a function of time t since the main event. The Tc value is indicated by the dashed line…… 196

Figure 183. The Guttenberg-Richter distribution using maximum likelihood method with the best combination of maximum curvature M_c 95% and M_c 90% probability. The red star shows the magnitude of the mainshock M_w 7.9…….. 197

Figure 184. The best model (1) of the estimated curve of the modified Omori formula (dashed line) applied to the aftershock data and the observed cumulative number of aftershocks (solid line) based on the AIC with RMS= 7.41…….. 197

Figure 185. The magnitude-time pattern versus the logarithm of time of the mainshock M_w 7.9…. 198

Figure 186. Frequency-magnitude distribution. The bold red line represents the model of equation (26) for qM= 1.03, while the other two lines present the corresponding 95% confidence intervals... 198

Figure 187. (a) The cumulative distribution function of the interevent times. The red line is the Q-exponential fitting with q = 1.80. **(b)** The Q-logarithmic function of the P(>T) as a function of the interevent times where the dashed line is the fitting with q=1.80. The deviation from the linearity suggests Tc values close to 300,000 s. **(c)** The evolution of interevent time T as a function of time t since the main event. The Tc value is indicated by the dashed line…… 199

Figure 188. The Guttenberg-Richter distribution using maximum likelihood method with the best combination of maximum curvature M_c 95% and M_c 90% probability. The red star shows the magnitude of the mainshock M_w 7.5…….. 200

Figure 189. The best model (3) of the estimated curve of the modified Omori formula (dashed line) applied to the aftershock data and the observed cumulative number of aftershocks (solid line) based on the AIC with RMS= 3.4……. 200

Figure 190. The magnitude-time pattern versus the logarithm of time of the mainshock M_w 7.5…. 201

Figure 191. Frequency-magnitude distribution. The bold red line represents the model of equation (26) for qM= 1.52, while the other two lines present the corresponding 95% confidence intervals... 201

Figure 192. (a) The cumulative distribution function of the interevent times. The red line is the Q-exponential fitting with q = 1.78. **(b)** The Q-logarithmic function of the P(>T) as a function of the interevent times where the dashed line is the fitting with q=1.78. The deviation from the linearity

suggests Tc values close to 1,000,000 s. **(c)** The evolution of interevent time T as a function of time t since the main event. The Tc value is indicated by the dashed line…… 202

Figure 193. The Guttenberg-Richter distribution using maximum likelihood method with the best combination of maximum curvature M_c 95% and M_c 90% probability. The red star shows the magnitude of the mainshock M_w 7.3……... 203

Figure 194. (a) The best model (1) of the estimated curve of the modified Omori formula (dashed line) applied to the aftershock data and the observed cumulative number of aftershocks (solid line) based on the AIC. **(b)** The model 4 of the estimated curve of the modified Omori formula (dashed line) applied to the aftershock data and the observed cumulative number of aftershocks (solid line), with the lowest RMS= 5.02…….. 204

Figure 195. The magnitude-time pattern versus the logarithm of time of the mainshock M_w 7.3…. 204

Figure 196. Frequency-magnitude distribution. The bold red line represents the model of equation (26) for qM= 1.42, while the other two lines present the corresponding 95% confidence intervals... 205

Figure 197. (a) The cumulative distribution function of the interevent times. The red line is the Q-exponential fitting with q = 1.78. **(b)** The Q-logarithmic function of the P(>T) as a function of the interevent times where the dashed line is the fitting with q=1.78. The deviation from the linearity suggests Tc values close to 750,000 s. **(c)** The evolution of interevent time T as a function of time t since the main event. The Tc value is indicated by the dashed line……... 206

Figure 198. The Guttenberg-Richter distribution using maximum likelihood method with the best combination of maximum curvature M_c 95% and M_c 90% probability. The red star shows the magnitude of the mainshock M_w 7.6……... 207

Figure 199. (a) The best model (1) of the estimated curve of the modified Omori formula (dashed line) applied to the aftershock data and the observed cumulative number of aftershocks (solid line) based on the AIC. **(b)** The model 2 of the estimated curve of the modified Omori formula (dashed line) applied to the aftershock data and the observed cumulative number of aftershocks (solid line), with the lowest RMS= 9.59…….. 208

Figure 200. The magnitude-time pattern versus the logarithm of time of the mainshock M_w 7.6…. 208

Figure 201. Frequency-magnitude distribution. The bold red line represents the model of equation (26) for qM= 1.30, while the other two lines present the corresponding 95% confidence intervals... 209

Figure 202. (a) The cumulative distribution function of the interevent times. The red line is the Q-exponential fitting with q = 1.87. **(b)** The Q-logarithmic function of the P(>T) as a function of the interevent times where the dashed line is the fitting with q=1.87. The deviation from the linearity suggests Tc values close to 500,000 s. **(c)** The evolution of interevent time T as a function of time t since the main event. The Tc value is indicated by the dashed line…… 210

Figure 203. The Guttenberg-Richter distribution using maximum likelihood method with the best combination of maximum curvature M_c 95% and M_c 90% probability. The red star shows the magnitude of the mainshock M_w 7.3…….. 211

Figure 204. (a) The best model (1) of the estimated curve of the modified Omori formula (dashed line) applied to the aftershock data and the observed cumulative number of aftershocks (solid line) based on the AIC. **(b)** The model 4 of the estimated curve of the modified Omori formula (dashed line) applied to the aftershock data and the observed cumulative number of aftershocks (solid line), with the lowest RMS= 4.13…….. 212

Figure 205. The magnitude-time pattern versus the logarithm of time of the mainshock M_w 7.3…. 212

Figure 206. Frequency-magnitude distribution. The bold red line represents the model of equation (26) for qM= 1.43, while the other two lines present the corresponding 95% confidence intervals... 213

Figure 207. (a) The cumulative distribution function of the interevent times. The red line is the Q-exponential fitting with q = 1.75. **(b)** The Q-logarithmic function of the P(>T) as a function of the interevent times where the dashed line is the fitting with q=1.75. The deviation from the linearity suggests Tc values close to 400,000 s. **(c)** The evolution of interevent time T as a function of time t since the main event. The Tc value is indicated by the dashed line…… 214

Figure 208. The Guttenberg-Richter distribution using maximum likelihood method with the best combination of maximum curvature M_c 95% and M_c 90% probability. The red star shows the magnitude of the mainshock M_w 7.1…….. 215

Figure 209. The best model (4) of the estimated curve of the modified Omori formula (dashed line) applied to the aftershock data and the observed cumulative number of aftershocks (solid line) based on the AIC with RMS= 3.18……... 215

Figure 210. The magnitude-time pattern versus the logarithm of time of the mainshock M_w 7.1…. 216

Figure 211. Frequency-magnitude distribution. The bold red line represents the model of equation (26) for qM= 1.37, while the other two lines present the corresponding 95% confidence intervals... 216

Figure 212. (a) The cumulative distribution function of the interevent times. The red line is the Q-exponential fitting with q = 1.74. **(b)** The Q-logarithmic function of the P(>T) as a function of the interevent times where the dashed line is the fitting with q=1.74. The deviation from the linearity suggests Tc values close to 250,000 s. **(c)** The evolution of interevent time T as a function of time t since the main event. The Tc value is indicated by the dashed line…… 217

Figure 213. The Guttenberg-Richter distribution using maximum likelihood method with the best combination of maximum curvature M_c 95% and M_c 90% probability. The red star shows the magnitude of the mainshock M_w 7.4……... 218

Figure 214. (a) The best model (1) of the estimated curve of the modified Omori formula (dashed line) applied to the aftershock data and the observed cumulative number of aftershocks (solid line) based on the AIC. **(b)** The model 4 of the estimated curve of the modified Omori formula (dashed line) applied to the aftershock data and the observed cumulative number of aftershocks (solid line), with the lowest RMS= 4.76…….. 219

Figure 215. The magnitude-time pattern versus the logarithm of time of the mainshock M_w 7.4…. 219

Figure 216. Frequency-magnitude distribution. The bold red line represents the model of equation (26) for qM= 1.17, while the other two lines present the corresponding 95% confidence intervals... 220

Figure 217. (a) The cumulative distribution function of the interevent times. The red line is the Q-exponential fitting with q = 1.72. **(b)** The Q-logarithmic function of the P(>T) as a function of the interevent times where the dashed line is the fitting with q=1.72. The deviation from the linearity suggests Tc values close to 100,000 s. **(c)** The evolution of interevent time T as a function of time t since the main event. The Tc value is indicated by the dashed line…… 221

Figure 218. (a) The Guttenberg-Richter distribution using maximum likelihood method with the best combination of maximum curvature M_c 95% and M_c 90% probability. The red star shows the magnitude of the mainshock M_w 7.6. **(b)** The Guttenberg-Richter distribution using the manual method……... 222

Figure 219. The best model (1) of the estimated curve of the modified Omori formula (dashed line) applied to the aftershock data and the observed cumulative number of aftershocks (solid line) based on the AIC with RMS= 2.21……... 223

Figure 220. The magnitude-time pattern versus the logarithm of time of the mainshock M_w 7.6…. 223

Figure 221. Frequency-magnitude distribution. The bold red line represents the model of equation (26) for qM= 1.43, while the other two lines present the corresponding 95% confidence intervals... 224

Figure 222. (a) The cumulative distribution function of the interevent times. The red line is the Q-exponential fitting with q = 1.71. **(b)** The Q-logarithmic function of the P(>T) as a function of the interevent times where the dashed line is the fitting with q=1.71. The deviation from the linearity suggests Tc values close to 40,000 s. **(c)** The evolution of interevent time T as a function of time t since the main event. The Tc value is indicated by the dashed line…… 225

Chapter 1

INTRODUCTION

1.1 Motivation

Megathrust subduction faults are generally accepted to be the source of the world's largest earthquakes that have ever recorded in human history. These megathrust earthquakes occur at catastrophic convergent boundaries, when one tectonic plate is pushed beneath another by slip along the thrust fault that connects them. These interplate earthquakes are the most destructive on the world, with magnitudes exceeding 9.0 Mw and it is well-known that events with a magnitude of 9.0 or greater have been megathrust earthquakes since 1900. Moreover, these major events are almost exclusively found in tectonic subduction zones and are frequently linked to the Pacific and Indian Oceans, where they are also responsible for most of the volcanism related with the Pacific Ring of Fire. In addition, megathrust earthquakes that occur in these subduction zones cause deformation of the ocean floor, producing a substantial series of tsunami waves and generating long periods of severe shaking and ground motion, lasting up to 5 minutes.

Instead of the natural disasters that a megathrust earthquake causes, it can even result in economic and human losses, injuries, structural damage, cultural consequences, and even population migrations. For instance, on March 27, 1964, at 5:36 p.m., the Mw 9.2 Alaskan earthquake, commonly known as the Good Friday earthquake, struck when the Pacific Plate lurched northward underneath the North American Plate. This earthquake, which lasted four minutes and thirty seconds, is still the largest in North American history and the world's second most violent earthquake (the first one is the Mw 9.5 Great Chilean Earthquake, 1960). The nine hundred and seventy kilometer long fault burst all at once, shifting up to eighteen meters and releasing five hundred years of built-up tension. As a result, landslides, cracks and other soil failures destroyed many cities and caused extensive property damage. However, the most devastating consequence was the nine deaths caused by the earthquake itself and another one hundred and twenty two deaths from the incoming tsunami all over the word. That's because this subduction zone earthquake triggered two types of tsunamis. In addition to the tectonic tsunami, there were around twenty minor and local tsunamis because of which caused the biggest damage. Tsunami waves have been seen in more than twenty nations, including Peru, New Zealand, Papua New Guinea, Japan, and Mexico, with the exception of Alaska, where the largest tsunami of fifty seven meters was generated. Similar earthquakes occur frequently in subduction zones and have devastating effects on humanity, as demonstrated by the earthquakes in Chile in 2010, Sumatra in 2004, and Tohoku in 2011.

1.2 Description of the problem

Estimating the seismic hazard of subduction zone earthquakes and subsequent aftershocks is one of the difficulties of subduction zone earthquake research. Even in distant regions away from the mainshock fault zone, aftershock sequences after megathrust earthquakes can raise the degree of seismic danger.

For this reason, the parameters of several empirical statistical laws used to describe the occurrence of aftershock sequences are analyzed in this dissertation. Especially, the aftershock sequences of major subduction zone earthquakes with magnitudes larger than 7.0 between 1976 and 2020 were studied for this purpose, emphasizing the time and magnitude distributions based on the science of complex systems. Moreover, in terms of Non-Extensive Statistical Physics, the temporal scaling features of the aftershock sequences are investigated further, by looking at the probability distribution of the interevent times between subsequent aftershocks. In particular, in this study, the non-extensive parameter q_{Time} is estimated, which is associated with the interevent time distribution, and the statistical parameter $q_{Magnitude}$ is calculated, which is related to the frequency-magnitude distribution and could be used as an auxiliary factor to characterize the physical condition of the seismic region because $q_{Magnitude}$ parameter changes are related with the release rate of the energy. Eventually, it will be ascertained that the models utilized matched the observed distributions well enough, suggesting that Non-Extensive Statistical Physics may be used to investigate phenomena with scale-free nature and long-range memory effects.

Chapter 2

BASIC CONCEPTS AND THEORY

2.1 Subduction Zone

Subduction is a crucial mechanism that affects the Earth's dynamics on a first-order level. Many writers believe that the sinking of the cool lithosphere into the Earth's mantle is the primary source of energy for plate driving forces. It also affects the mantle's temperature and chemical structure, causes arc volcanism, and is responsible for the majority of seismic energy released on Earth. But first of all, we have to describe what the so-called subduction zone is and the relation between subduction and tectonic plates[1].

It is generally accepted that the lithosphere of the Earth, which comprises the crust and upper mantle, is made up of tectonic plates, which move slowly over time. The tectonic plate boundaries can be divided into three categories, the convergent, the divergent and the transform boundaries. First of all, when two tectonic plates move apart from each other, they form a diverging border. Earthquakes are prevalent at these borders where magma rises to the surface from the Earth's mantle, solidifying to form new oceanic crust. The divergent plate boundaries include the known Mid-Atlantic Ridge and the Pacific Ring of Fire. Concerning the transform plate boundary, it is formed by two plates moving past one other. The San Andreas fault zone, which stretches underwater, host one of the most well-known transform plate borders. As the plates grind along, the rocks at the boundary are crushed, forming a valley fault system or an underwater canyon where earthquakes occur often. Moreover, at transform margins, crust is not generated or destroyed but it is only cracked and shattered. The third category of the plate boundaries it is the convergent boundary which is formed when two plates come together. The collision of the plates can force one or both plates' edges to buckle up into mountain ranges, or one of the plates to bend down into a deep undersea trench. Parallel to convergent plate boundaries, a chain of volcanoes typically arises, and major earthquakes occur frequently[2].

The convergent or consuming plate margins are located where adjacent plates move towards each other, and this movement is accompanied by the pushing up of one upon the other, which then sinks below it. The cause of the sinking is due to the larger density of the oceanic lithosphere than of the asthenosphere, caused by the cooling of the oceanic crust, and to the plasticity of the asthenosphere. These margins are also called as subduction zones, and they are classified as oceanic or subcontinental,

[1] Serge Lallemand and Francesca Funiciello (Eds.), Fronties in Earth Sciences, *Subduction Zone Geodynamics*, Springer-Verlag Berlin Heidelberg: Berlin, 2009.
[2] See the "NOAA Ocean Exploration - What are the different types of tectonic boundaries?", retrieved on 15 June 2021, https://oceanexplorer.noaa.gov/facts/plate-boundaries.html .

depending on whether the riding plate's crust is oceanic or continental just above the convergence boundary. The crust of the riding or subcontinental plate is almost always oceanic and for those cases where it is continental, a collision zone is formed, which leads to the formation of an orogenetic zone and subsidence cannot generally be continued long, as the continental crust is less dense and therefore cannot participate in the subsidence. Oceanic subduction zones are bounded by a trench (i.e., a linear morphological degradation at the ocean floor) where the submerged plate curves and rises toward the Earth's mantle, as well as by a series of volcanic arcs on the riding plate, called volcanic arc, island arc, or oceanic island arc. The converging margins of the subcontinents are also bounded by an oceanic trench and an arcuate chain of volcanoes that develop in the pushed continental crust. These margins are called continental arcs or Andean-style continental margins, after the current corresponding Andean geotectonic framework[3].

2.2 Seismotectonic Regime

On the surface of the earth, the boundaries of the plates where a convergence takes place are determined by a seismic zone which is very different from the one that defines the boundaries of the divergence. The energy released in the subduction zone is much greater than that released in the divergence and earthquakes are not only shallow (0-100km) but also intermediate and deep (100-700km). In addition, the release of water from the sinking plate is a crucial part that distinguishes subduction zones from other areas. Seismogenesis, melting, and viscosity decrease occur as a result of this process, which improves mantle flow. Concerning the geometric location of subduction zones' seismic epicenters, this defines a sloping zone with respect to the horizontal plane, whose intersection with the earth's surface coincides with the oceanic trenches of the active continental margins. This zone is called the "Wadati-Benioff" zone, in honor of the American seismologist Hugo Benioff, who was the first to observe that earthquakes gradually progressed deeper from the trenches towards the inner part of the continents, and the Japanese seismologist Kiyoo Wadati, who was engaged in research into methods of comparing earthquake magnitudes. From the beginning of the subduction zone in the oceanic trench to a depth of about 300 km, the intense friction between the descending and riding plates causes cracks along the upper fracture section of the plate, resulting in shallow or intermediate earthquakes. These seismic events generally represent the major seismic zones in the subduction zones.

[3] Spyridon P. Lekkas, Stylianos G. Lozios and Emmanuel N. Skourtsos, *Introduction to Geodynamics*, National and Kapodistrian University of Athens, Department of Geology and Geoenvironment, Department of Dynamics, Tectonics & Applied Geology, Second Edition, Athens, December 2006.

As the subsidence process proceeds, seismic activity continues inside the crumbling part of the descending plate because it has not remained inside the Earth long enough to heat up and "soften". The plate eventually sinks to about 700 km below the surface, where it is heated to such an extent that it is plastically deformed as a whole, resulting in earthquakes at depths greater than 700 km which are rarely observed[4].

Many processes and dangers are caused by the sinking of cold lithosphere into the mantle, including arc volcanism caused by thermal and chemical alteration of the mantle, as well as the release of huge amounts of seismic energy. During subduction, earthquakes can occur both within the downgoing and overriding plates, as well as along the interface between the two plates[5]. The magnitude of earthquakes varies considerably, depending on the type of the boundaries which produce them. Almost all major earthquakes occur along convergence or transform boundaries. Earthquakes at plate divergences typically have small magnitudes because stress-induced rocks tend to fracture before high deformation energy is accumulated. Approximately 80% of the world's seismic energy is released each year along the Pacific coast, as the Pacific Basin's oceanic plates sink beneath their adjacent plates, almost along the entire perimeter of the Pacific Ocean. The majority of the remaining 20% of global seismic energy is released along the Alpine-Himalayan system's collision zone, primarily in Greece, Turkey, Iran, India, and Pakistan in the Himalayan zone, as well as southern China and Myanmar[6].

2.3 Aftershock Sequences

One of the basic principles of plate tectonics is that tectonic contact between oceanic and continental lithosphere causes shallow large earthquakes in plate borders and the deeper mantle[7]. This connection of surfaces between overthrusting and underthrusting plates in subduction zones, namely the megathrust faults, host the largest earthquakes on Earth, along with a variety of smaller events that contribute to plate convergence the point at which the oceanic lithosphere dips into the underlying mantle. Subduction zones are notorious for this downward movement of the subducting plate which causes extremely large earthquakes, with magnitudes up to M_w 7, and are thus investigated by scientists

[4] Supra Note 1.
[5] Elenora van Rijsingen, *Subduction interface roughness and megathrust earthquakes*: *Insights from natural data and analogue models*, Université Montpellier; Università degli studi Roma Tre, 2018.
[6] Supra Note 3.
[7] L.I. Lobkovsky, V.I. Kerchman, B.V. Baranov and E.I. Pristavakina, *Analysis of Seismotectonic Processes in Subduction Zones from the Standpoint of a Keayboard Model of Great Earthquakes*, Tectonophysics, Volume 199, Issues 2-4, December 1991.

because those large megathrust earthquakes occurring at subduction zones can release enormous amounts of energy and have catastrophic consequences over vast geographic regions. The spatial extent affected by a single large event can be much greater than for events in the Earth's crust. The recent M_w 9.1 Tohoku earthquake on 11 March 2011 and the M_w 9.3 Sumatra earthquake on 26 December 2004, which occurred in highly populated areas and inflicted horrific human and economic losses, demonstrate the enormous impact of such disasters on populations. As a result, a better understanding of the geographic and temporal incidence of such catastrophic occurrences is crucial because these megathrust earthquakes regularly cause both significant damage and loss of life and that is the reason why understanding the rupture characteristics of megathrust episodes is critical for earthquake rupture physics and earthquake early warning systems[8].

It is widely acknowledged that a major earthquake is followed by more aftershocks, minor earthquakes that strike in the same general location days to years after a big occurrence or a mainshock and it takes longer for seismic activity to settle back to normal levels. Not only the mainshock of the megathrust earthquake can affect multiple infrastructures in a city, but also the induced aftershocks along the subduction zone can impact many facilities in a metropolis. As a result, emergency preparedness and planning must take into account the effects of aftershocks on susceptible sectors of society and infrastructure[9]. This may be accomplished by estimating the parameters of various well-established empirical laws for aftershock sequences that may be predicted after major mainshocks in a particular seismogenic location and there are hundreds to thousands of instrumentally measurable aftershocks that can be occurred after major earthquakes, which diminish in magnitude and frequency over time according to empirical laws[10].

Concerning the aftershock sequences, there are three types of aftershocks that may occur, depending on the mainshock parameters and the geotechnical characteristics of the area. The first type referring to aftershocks that are generated on the fault surface, where the mainshock's hypocenter is nucleated and the rupture propagates. This group often includes aftershocks that occur within 24 to 48 hours of the mainshock, but it is confirmed that on the rupture surface of the mainshock that had a significant slip, a few aftershocks were found (Mendoza and Hartzell, 1988). The second type of aftershock occurs on the main fault, but on the external side of the ruptured section created by the initial displacement of

[8] Supra Note 5.
[9] Lizhong Zhang, *Spatiotemporal Seismic Hazard and Risk Assessment of Global M9.0 Megathrust Earthquake Sequences*, University of Bristol, March 2020.
[10] Susan L. Bilek and Thorne Lay, *Subduction Zone Megathrust Earthquakes*, The Geological Society of America, Geosphere, Volume 14, Number 4, 2018.

the mainshock. On the other hand, when the mainshock causes aftershocks at great distances, on faults different than the one that generated the mainshock, these aftershocks are classified as the third kind of aftershock sequences (Kisslinger, 1996)[11].

[11] Armick Ivanian, *Studies of Aftershock Sequences of Large Subduction Zone Earthquakes*, The University of Western Ontario, School of Graduate and Postgraduate Studies, 2012.

Chapter 3

APPLIED METHODOLOGY

3.1 Empirical Laws for Aftershock Sequences

In order to estimate the factors that affect the seismicity of different tectonic settings, some important laws may be applied to the aftershock sequences after the mainshock which will be thoroughly explained in this chapter.

3.1.1 The Gutenberg-Richter Law

In Gutenberg-Richter research, earthquakes include strain-release events on major active faults in a variety of tectonic zones all over the world. The risk and expense of these faults, as well as their periodic ruptures, necessitated a scientific effort to better understand and predict big earthquakes. The urge to accomplish the search resulted in the G-R power-law scaling based on the interpretation of earthquake catalogues. If the catalog numbers of minor earthquake magnitudes did not follow the G-R relation established by major earthquake magnitudes, it was assumed that there was a problem with observing the small events rather than the lack of small occurrences caused by natural physical processes[12]. The classic frequency – magnitude (F-M) distribution of Gutenberg-Richter (1944) is generally used to assess earthquake danger over time in terms of regional statistical characteristics of earthquake occurrence and recurrence[13]. The Gutenberg–Richter law states that earthquake magnitudes are distributed exponentially[14] and the probability N≥ m of events with magnitudes greater than or equal to m is given as follows (Gutenberg and Richter 1944):

$$\log_{10} N(m) = a - bm \tag{1}$$

[12] P. Leary, P. Marlin and Tero Saarno, *A Physical Basis for Gutenberg-Richter Fractal Scaling*, Proceeding, 45th Workshop on Geothermal Reservoir Engineering Stanford University, California, February 2020.

[13] Tzanis A., Vallianatos F. and Efstathiou A. (2013), *Multidimensional earthquake frequency distributions consistent with Non-Extensive statistical physics: The interdependence of magnitude, interevent time and interevent distance in North California*, Bulletin of the Geological Society of Greece, Volume XLVII, No3, 1326-1337, doi: https://doi.org/10.12681/bgsg.10914.

[14] C. Godano, E. Lippiello and L. de Arcangelis, *Variability of the b valuein the Gutenberg-Richter distribution*, Geophysical Journal International, June 2014.

where α and b are the so-called G-R α and b parameters or values[15] with b characterized as a scaling parameter while α as a constant[16] that relies on the seismicity rate and the duration of the observation time and it is the logarithm of the total number of earthquakes of magnitude N≥ m[17].

Earthquake self-similarity is thought to be expressed by the G-R law and the logarithmic connection between earthquake magnitude and energy released results in a power-law distribution for earthquake energy (Kanamori & Anderson 1975), indicating the absence of a typical scale in earthquake occurrence[18].

Concerning the b value, the estimation of which is critical for determining the chance of an earthquake occurring, varies by location, but in most cases typically ranges from 0.8 to 1.2 (Frohlich and Davis, 1993; Turcotte and Shcherbakov, 2007)[19]. There are several factors that affect the b-value such as the pore pressure fluctuations, the fault heterogeneity (Mogi, 1962) and the stress level imposed on rocks (Scholz, 1968)[20]. For instance, an area with a lower b-value has received higher shear stress after a mainshock, whereas a place with a higher b-value has experienced lower shear stress and areas that have already been exposed to earthquakes and are more fractured also exhibit higher b-values (Ito and Enescu, 2002). In addition, depending on the tectonic regime of the region, normal faulting earthquakes produce the highest b-values because the load of the materials above the fault zone is equal to the highest main stress, whereas strike-slip faults and thrust faults produce the middle and smallest b-values (Schorlemmer et al, 2005). Ultimately, the lower b-values in the aftershock sequences indicate that there are more aftershocks with high magnitude, while on the other hand, higher b-values are explained by a greater proportion of aftershocks with smaller magnitude (Bender, 1983)[21].

The numerous uses of b-value in seismology, especially in the field of seismic hazard analysis, demonstrate the importance of the accurately calculating of it to get relevant and trustworthy results[22]. Apart from the magnitude interval size, the lack of occurrences within particular magnitude intervals,

---

[15] Serge A. Shapiro, *Fluid-Induced Seismicity*, Earth Science Department, Freie Universität Berlin, Cambridge Uneversity Press, United Kingdom, 2015.
[16] Supra Note 13.
[17] F. A. Nava, V. H. Márquez-Ramírez, F. R. Zúñiga, L. Ávila-Barrientos and C. B. Quinteros, Gutenberg-Richter b-values maximum likelihood estimation and sample size, Springer Science and Business Media Dordrecht, June 2016.
[18] Supra Note 13.
[19] Robert Shcherbakov, Donald L. Turcotte and John B. Rundle, *Aftershock Statistics*, Pure and Applied Geophysics, Birkhäuser Verlag, Basel, 2005.
[20] Warner Marzocchi and Laura Sandri, *A review and new insights on the estimation of the b-value and its uncertainty*, Istituto Nazionale di Geofisica e Vulcanologia, Bologna, Italy, Annals of Geophysics, Vol. 46, N. 6, December 2003.
[21] Supra Note 11.
[22] Supra note 16.

and the size variation of the sample data set (Bender, 1983), multiple b-values can be calculated for the same data set of earthquakes due to the diversity of fitting methodologies[23]. The most typical approach for estimating the b-value is the maximum likelihood estimate method, which was proposed for the first time by both Aki and Utsu in 1965 and is the most commonly used method today.

The G-R law that relates the number of earthquakes above a given magnitude $N(m)$ to the magnitude m indicates that magnitudes are distributed as an exponential function as

$$f(M) = \beta e^{-\beta(m-m_c)}, \quad m \geq m_c \tag{2}$$

where $\beta = b/\log_{10}(e)$ [24] so Aki (1965) demonstrated that the maximum likelihood estimate of b is based on the premise of this magnitude distribution and is given as follows:

$$b = \frac{\log_{10}(e)}{\bar{m}-m_c} \tag{3}$$

where $\bar{m}$ is the average magnitude greater than or equal to m_c and m_c is the minimum magnitude in the given sample, the completeness magnitude[25]. Because of spatial and temporal differences in seismic event observation and various sensitivity in the seismograph arrays, the value of m_c is generally greater than the actual threshold of magnitude detection. These are frequently the main causes of earthquake catalogs' small event incompleteness[26].

A more applicable equation than (3) formed using the rounded magnitudes to some δm (typically δm=0.1) resulting the exact minimum magnitude to be $m_c - \delta m/2$. The new equation developed as[27]

$$b = \frac{\log_{10}(e)}{\bar{m}-(m_c-\delta m/2)} \tag{4}$$

In comparison to Aki and Utsu's equation, this one offers accurate b-values for big magnitude interval data sets.

---

[23] Bernice Bender, *Maximum Likelihood Estimation of b Values for Magnitude Grouped Data*, Bulletin of the Seismological Society of America, Vol 73, No 3, June 1983.
[24] Yosihiko Ogata and Ken'ichiro Yamashina, *Unbiased Estimate for b-Value of Magnitude Frequency*, J. Phys. Earth, 34, The Univeristy of Tokyo, Japan, 1986.
[25] Keiiti Aki, *Maximum Likelihood Estimate of b in the Formula logN= a -bm and its Confidence Limits*, Bulletin of the Earthquake Research Institute, Vol 43, March 1965.
[26] Andrzej Kijko and Asie Smit, *Estimation of the Frequency-Magnitude Gutenberg-Richter b-Value without Making Assumptions on Levels of Completeness*, Seismological Research Letters, Vol. 88, N. 2A, March/April 2017.
[27] Supra Note 19.

3.1.2 Modified Omori Law

Aftershocks are the most physical sign of the global relaxation process triggered by sudden changes in the level of tension in the vicinity of seismic ruptures. This study involves the analysis of the aftershocks sequences in regard to Omori's law, one of the few basic empirical laws in seismology. It outlines how aftershock activity decreases over time and has been widely utilized as a key for analyzing aftershocks, in both its original and modified forms[28].

Until Omori first experimentally discovered in 1894 that aftershocks decrease as about 1/t, the fundamental physical process driving aftershocks of major earthquakes has remained unknown[29]. Omori documented the number of earthquakes generated by the Mw 8.0 Nobi earthquake at Honshu, Japan on the 18 October 1891 and he offered the first quantitative description of an aftershock decay rate. He demonstrated that at time t, the frequency of aftershocks per unit time interval N(t) is well described by

$$N(t) = K(t + c)^{-1} \tag{5}$$

where K and c are constants. Omori used the letter h instead of the letter c, but c has been more widely used in recent years. It's also typical to estimate t from the mainshock's origin time, but Omori's writings utilized a different time origin, with t =0, t= 1, and … corresponding to the first, second, and … unit time intervals, respectively. According to the Omori formula, often known as the hyperbolic law, aftershock activity of corresponding earthquakes decreased more or less consistently[30].
Later, Utsu (1961) adapted the hyperbolic behavior observed by Omori into the so-called modified Omori law to more precisely reflect the diversity of aftershock decay rates that had been subsequently recorded[31]. In this study, we use the modified version of Omori's law (Omori 1894; Utsu 1961) to investigate the temporal decay of aftershock activity as follows:

$$R(t, M) = \frac{dN}{dt} = \frac{1}{\tau\left(1+\frac{t}{c}\right)^{p}} \tag{6}$$

[28] Jiancang Zhuang, *Statistical modeling of seismicity patterns before and after the Cape Palliser earthquake*, Centre for Analysis and Prediction State Seismological Bureau Beijing, China, 2000.
[29] Stephen A. Miller, *Aftershocks are fluid-driven and decay rates controlled by permeability dynamics*, Nature Communications, 2020.
[30] Tokuji Utsu, Yosihiko Ogata and Ritsuko S. Matsu'ra, *The Centenary of the Omori Formula for a Decay Law of Aftershock Activity*, Institute of Statistical Mathematics, Minato-ku, Tokyo 106, Japan, J. Phys. Earth, Vol 43, No 1, 1995.
[31] M. Holschneider, C. Narteau, P. Shebalin, Z. Peng and D. Schorlemmer, *Bayesian analysis of the modified Omori law*, Journal of Geophysical Research, vol. 17, B06317, 2012, doi:10.1029/2011JB009054.

where $R(t, M) = \frac{dN}{dt}$ is the rate of occurrence of aftershocks with magnitude greater than M, τ and c are characteristic times and depend on the total number of the aftershocks sequence above a given cutoff[32], while the estimation of them is accomplished with the maximum likelihood method using the occurrence times of individual shocks (Ogata, 1983 and 1999). In addition, t is the time since the triggering shock occurrence that is the mainshock and p is the power law exponent[33]. The modified Omori's law expresses the temporal correlation in the sequence of aftershocks, which are thought to be the pattern of a complicated relaxation process occurring following the mainshock. Moreover, we utilize the total number of aftershocks N(t) for a given period t with magnitude greater than M, as determined by integrating $R(t, M)$, to examine Omori's scaling.

$$N(t) = \begin{cases} \frac{c}{\tau(p-1)}\left[1 - (1 + \frac{t}{c})^{1-p}\right] & for\ \ p \neq 1 \\ \frac{c}{\tau}\ln\left(1 + \frac{t}{c}\right) & for\ \ p = 1 \end{cases} \tag{7}$$

If Omori's law applies equally at all time scales, the total number of aftershocks is finite only if p >1[34]. The most significant is the p-value, which specifies the mode of aftershock decay as a function of time and frequency (Nanjo et al., 1998). It is considered that aftershock sequences with a high p-value decay quickly, while those with a low p-value decay slowly and according to several studies, the p-value for distinct aftershock sequences varies between 0.5 and 1.8 (Utsu et al., 1995; Olsson, 1999; Wiemer and Katsumata, 1999; Enescu and Ito, 2002; Polat et al., 2002; Bayrak and Öztürk, 2004)[35]. These changes in p might be linked to variations of material characteristics or fault heterogeneity, variations in the state of stress, temperature, pore fluid flow which can lead to a fault's weakening and reduction of shear strength (Nur and Booker, 1971) and changes in the seismic cycle. However, it is still unclear which of these conditions is more connected to the p-value[36].

---

[32] Filippos Vallianatos and Kyriaki Pavlou, *Scaling properties of the Mw 7.0 Samos (Greece), 2020 aftershock sequence*, Acta Geophysica, Institute of Geophysics, April 2021.
[33] A. Schmid and J.-R. Grasso, *Omori law for eruption foreshocks and aftershocks*, Journal of Geophysical Research, vol 117, B07302, 2012, doi:10.1029/2011JB008975.
[34] Supra Note 29.
[35] Serkan Öztürk and Şakir Şahin, *A statistical space-time0magnitude analysis on the aftershocks occurrence of the July 21th, 2017 Mw=6.5 Bodrum-Kos, Turkey, earthquake*, Joyrnal of Asian Earth Sciences, October 2018, doi:10.1016/j.jseaes.2018.10.008.
[36] Paul Nyffenegger and Cliff Frohlich, *Recommendations for Determining p Values for Aftershock Sequences and Catalogs*, Bulletin of the Seismological Society of America, Vol.88, No.5, October 1998.

3.2 Non-Extensive Statistical Physics

One of the primary areas of seismological studies connected to earthquake generating mechanisms has long been the statistical properties of the occurrence of aftershocks. Significant efforts have been made to promote the research of the origins of earth dynamics from the perspectives of fractal geometry, non-equilibrium thermodynamics, chaos and complexity physics (Beck and Schlogl, 1993; Turcotte et al., 2000; Tsallis, 2012; Keilis-Borok, Soloviev, 2003 and Tsallis, 2001, 2009). An extensive study of a catastrophic earthquake typically involves distributions of aftershocks in time, magnitude and space. The goal of this study is to investigate the behavior of aftershocks related to major subduction zone earthquakes worldwide, using a non-extensive statistical physics (NESP) (Tsallis, 1988, 1999, 2001, 2009) extension of Boltzmann–Gibbs (BG) statistical physics, based on the analysis of distributions of aftershocks sequences in time and magnitude. The NESP method, as proposed by Tsallis entropy (Tsallis, 2001), has the benefit of being able to represent the spatiotemporal evolution of seismicity using the universal principle of entropy[37]. The idea of non-extensivity was introduced recently in the statistical explanation of earthquake occurrence because if the frequency distributions of the relevant parameters display the characteristics anticipated of non-extensive systems, then the system generating these distributions is very certainly universally non-extensive[38]. It will be demonstrated that time series have high fluctuations and probability distributions with "fat" tails, which may be precisely represented by the q-Gaussian distribution developed inside the NESP framework which provides a coherent theoretical framework for deriving the collective characteristics of earthquakes based on the notion of entropy[39].

3.2.1 NESP Distribution Law and Interevent Times

The time delayed between successive events over a magnitude threshold across a particular region is a measure of temporal dynamics and this parameter is referred to as interevent time. This time, in addition to energy release rates indicated by the magnitude M, is a measure of the temporal and understanding the earthquake frequency – interevent time (F-T) distribution statistics is critical to comprehending the seismogenetic system. Power-law behavior and long tails are common features of

[37] F. Vallianatos, V. Karakostas and E. Papadimitriou, *A Non-Extensive Statistical Plhsics View in the Spatiotemporal Properties of the 2003 (Mw6.2) Lefkada, Ionian Island Greece, Aftershock Sequence*, Pure and Applied Geophysics, doi:10.1007/s00024-013-0706-6.
[38] Supra Note 13.
[39] Filippos Vallianatos and Georgios Michas, *Complexity of Fracturing in Terms of Non-Extensive Statistical Physics: From Earthquake Faults to Arctic Sea Ice Fracturing*, Entropy, October 2020, doi:10.3390/e22111194.

empirical F-T distributions, which have been examined using traditional statistical models with tails that are causally related to power-laws[40].

As detailed below, a quick overview of the theory's basic concepts is essential in order to allow discussion of its relevance to earthquakes. The theory's foundation is an extension of BG statistics that allows for the analysis of systems with long-range interactions and long-term memory. The BG statistical physics has limited application for such systems, necessitating its generalization to account for all length scale interactions among the system's constituents, resulting in wide distributions with power-law asymptotic behavior[41]. In order to study the distribution of interevent times in the aftershocks sequence, we utilized this modified version of BG statistical physics known NESP (Tsallis 2009; Vallianatos et al. 2016 and Chelidze et al. 2018). This estimation which is based on Tsallis' generalized expression of entropy, may be used to characterize complex systems with finite degrees of freedom, self-organized criticality, and non-Markovian processes (Telesca 2012; Tsallis 2009; Vallianatos et al 2016; Vallianatos et al 2018)[42]. Hereupon, is the expression of the non-extensive Tsallis entropy Sq (Tsallis 1988) in terms of a fundamental seismic parameter's probability distribution p(X), where in this case X is the interevent time T, the interval between events[43]:

$$S_q = k_B \frac{1-\sum p^q(X)}{q-1} \tag{8}$$

where k_B is the Boltzmann constant and the q is the so-called entropic index which is the degree of non-additivity[44]. For the specific situation of q = 1 then $S_q = S_{BG}$, the BG entropy is obtained.

$$S_{BG} = -k \frac{1}{q-1} \left[1 - \int p(X) \ln\big(p(X)\big) dX\right] \tag{9}$$

Despite the fact that S_q and S_{BG} have many similarities, such as non-negativity, expansibility, and concavity, there is a major difference between the two entropies. The BG entropy is additive, meaning that the entropy of a coupled system is equal to the sum of the entropies of its constituent components,

[40] Supra Note 13.
[41] Alejandro Ramírez-Rojas, Leonardo Di G. Sigalotti, Elsa Leticia Flores Márquez and Otto Rendón, *Time Series Analysis in Seismology*, Practical Applications, Elsevier, 2019.
[42] Supra note 32.
[43] Supra Note 37
[44] Chris G. Antonopoulos, George Michas, Filippos Vallianatos and Tassos Bountis, *Evidence of q-exponential statistics in Greek seismicity*, Physica A, 2014

whereas the Tsallis entropy S_q (with q= 1) is non-additive[45]. The Tsallis entropy applies the required conditions for any two probabilistically independent systems, A and B:

$$S_q(A+B) = S_q(A) + S_q(B) + \frac{(q-1)}{k_B} S_q(A) S_q(B) \tag{10}$$

Non-extensive statistical physics has this as a fundamental principle. Particularly, q < 1 correspond to superadditivity, q > 1 correspond to subadditivity and finally, the right-hand side of Eq (9) disappears when q = 1, so it corresponds to additivity-extensivity characteristic[46].

If X is a physical parameter that characterizes the system, the probability distribution of X, p(X) is determined using the Lagrange multipliers approach by maximizing of entropy under suitable constraints (Tsallis et al. 1998, Lyra and Tsallis 1998, Tsallis 1999). The first constraint is the normalization condition

$$\int_0^\infty p(X)dX = 1 \tag{11}$$

and the second one is the generalized expectation value X_q which is defined as

$$X_q = \langle X \rangle_q = \int_0^\infty X P_q\,(X) dX \tag{12}$$

where $P_q(X) = \frac{p^q(X)}{\int_0^\infty p^q(X)dX}$ is the escort probability distribution (Tsallis, 2009)[47].

When q→1, $P_q(x) \rightarrow p(x)$, the q-expectation value becomes the standard expectation. The maximizing of the functional is based on the previous constraints and the approach of Lagrange multipliers[48]

$$\Phi_q = S_q - a \int_0^{x_{max}} p(X)dX - \beta X_q \tag{13}$$

where a and β represent the Lagrange multipliers and we lead to the probability distribution function

[45] Filippos Vallianatos, Giorgos Michas, Giorgos Papadakis and Peter Sammonds, *A Non-Extensive Statistical Physics View to the Spatiotemporal Properties of the June 1995, Aigion Earthquake (M6.2) Aftershock Sequence (West Corinth Rift, Greece)*, Acta Geophysica, vol. 60, no. 3, June 2012, doi:10.2478/s11600-012-0011-2.
[46] Supra Note 41.
[47] Supra Note 37.
[48] Supra Note 41.

$$p(X) = \frac{[1-(1-q)\beta_q X]^{\frac{1}{1-q}}}{z_q} = \frac{exp_q(-\beta_q X)}{z_q} \quad (14)$$

where z_q is the q-partition function

$$z_q = \int_0^{x_{max}} exp_q\left(-\beta_q X\right)dX \quad (15)$$

where $\beta_q = \frac{\beta}{c_q+(1-q)\beta X_q}$ (16) and $c_q = \int_0^{x_{max}} p^q\,(X)dX$ (17)

and the Q-exponential function is defined as

$$exp_q(X) = [1 + (1-q)X]^{\frac{1}{1-q}} \quad (18)$$

that is applicable when $1 + (1-q)X \geq 0$ while in all other cases it is

$$exp_q(X) = 0 \quad (19)$$

It is to be noted that if q→1, the Q-exponential function leads to the ordinary exponential, if q>1 has a long power tail and exhibit an asymptomatic power-law behavior and in contrast if 0<q<1 a cut-off appears at $x_c = 1/[(1-q)\beta_q]$[49].

The cumulative distribution function P (> T) = N (> T)/No of the interevent times is estimated using the acquired probability function in Eq. (14), where N(> T) is the number of interevent times with a value larger than T and No is the total number. The cumulative distribution function was calculated using the p(T) distribution as follows[50]:

$$P(>T) = exp_Q(-T/T^*) \quad (20)$$

which is a mathematically q-exponential function with $T^* = T_q Q$ and $q = 2 - (1/Q)$.

The inverse function of the Q-exponential is called Q-logarithm and defined as

$$ln_Q(x) = \frac{x^{1-Q}-1}{1-Q} \quad (21)$$

[49] Supra Note 41.
[50] Supra Note 32.

Abe and Suzuki (2003) argued that the cumulative distribution function F(> x) can be better derived by integrating the escort probability Pq(x) rather than p(x) in the context of the Tsallis theory (2009)

$$F(> X) = \int_0^\infty P_q\,(X)dX = exp_q(-\frac{X}{X_0}) \tag{22}$$

where $P_q(X)$ is the escort probability associated with p(x) and X_0 is a positive scaling parameter for q>1 and is defined by

$$X_0 = (1-q)\langle X\rangle_q + \frac{1}{\beta_q} \tag{23}$$

Another common instance is when we use equation (12) to impose the mean value of the squared variable X^2, which gives us the q-mean value X_q^2. In this example, optimizing S_q under normalization restrictions (equation (11)) and the q-mean value X_q^2 gives:

$$p(X) = \left(1/Z_q\right)[1-\beta(1-q)X^2]^{1/(1-q)} \tag{24}$$

where $\beta = [(3-q)X^2]^{-1}$. The q-Gaussian distribution is the name given to the latter equation. The q-Gaussian converges to the conventional Gaussian distribution in the limit of q→1, but for q > 1 it decays asymptotically as a power-law, $|X|^{-2/(q-1)}$[51].

3.2.2 NESP Distribution Law for Earthquake Magnitude

Sotolongo-Costa and Posadas created a broad physical model for the earthquake generating process in 2004, known as the fragment-asperity model for earthquake magnitudes, starting from the base and included the G-R relation as a special instance, in order to explain the earthquake generation mechanism and specifically, local breaking and movement of asperities and fragments between fault planes are the causes of earthquake energy release in this model. Fragment displacement is considerably more common than asperity breaking, thus it is reasonable to believe that most earthquakes are caused by fragment displacement. Large fragments are more difficult to release than the small ones, so the released energy is believed to be proportional to the size of the obstructing particles. This indicates that the size distribution of the fragments across the plates can be reflected in the energy distribution of earthquakes caused by this process. Long-range interactions arise among all parts of the fragmented piece as a result of the severe fractioning of the material. As a result, deriving

[51] Supra Note 39.

the size distribution function of the fragments would necessitate the use of non-extensive statistical physics[52]. As already mentioned, Tsallis (1988) suggested NESP as a potential generalization of BG statistical physics and it offers a coherent theoretical framework for analyzing complicated dynamical systems with fractal features and long-range correlations (Tsallis, 2009)[53]. Silva et al. (2006) updated the fragment-asperity model and developed an energy distribution function that can be used to calculate the relative number of earthquakes as a function of magnitude.

The cumulative distribution in terms of the earthquake magnitude can be obtained considering Telesca's (2011) relationship between magnitude and released relative energy as

$$M = \frac{2}{3}\log(E) \tag{25}$$

In 2012 Telesca proposed a modified function based on the non-extensive statistical physics theory, taking into account the threshold magnitude M_c in a seismic region, which relates the cumulative number of earthquakes with the magnitude, normalized by the total number of earthquakes

$$\log\left(\frac{N(>M)}{N}\right) = \frac{2-q_M}{1-q_M}\log\left(\frac{1-\left(\frac{1-q_M}{2-q_M}\right)\left(\frac{10^M}{A^{2/3}}\right)}{1-\left(\frac{1-q_M}{2-q_M}\right)\left(\frac{10^{M_c}}{A^{2/3}}\right)}\right) \tag{26}$$

where M is the earthquake magnitude, M_c is the threshold, A is proportional to the volumetric energy density and q_M is the entropic index[54].

In compared to the Gutenberg–Richter scaling, the fragment-asperity model gives a reasonable explanation of recorded earthquake magnitudes over a larger range of scales, although it may be obtained as a special case for values over a certain threshold magnitude[55], for the value of b which is the NESP generalization of the b value in G-R law[56]

$$b = \frac{(2-q_M)}{(q_M-1)} \tag{27}$$

---

[52] Supra Note 41.
[53] Michas G., Papadakis G., Vallianatos F., *A Non-Extensive approach in investigating Greek seismicity, Bulletin of the Geological Society of Greece*, Volume XLVII, No3, 2016, doi: https://doi.org/10.12681/bgsg.10973.
[54] Giorgos Papadakis, Filippos Vallianatos and Peter Sammonds, *A Nonextensive Statistical Physics Analysis of the 1995 Kobe, Japan Earthquake*, Pure and Appled Geophysics, 2014, doi:10.1007/s00024-014-0876-x.
[55] Supra Note 41.
[56] Tamaz Chelidze, Filippos Vallianatos and Luciano Telesca, Andreas Tzanis and Angeliki Efstathiou, *Complexity of Seismic Time Series: Are Seismogenetic Systems Random or Organized? A Treatise of Their Statistical Nature Based on the Seismicity of the North-Northeast Pacific Rim*, Elsevier, 2018.

The non-extensive parameter q_M in the fragment-asperity model framework notifies us about the magnitude of interactions between fault planes and fragments (Matcharashvili et al. 2011; Papadakis et al. 2013; Telesca 2010; Valverde-Esparza et al. 2012). As a result, a rise in q_M shows that a seismic area's physical condition is moving away from equilibrium[57].

3.3 A Superstatistical View

Non-extensive statistical mechanics formalism can be thought of as an embedding of conventional statistical mechanics within a wide framework and a superposition of various statistics can also adequately describe the system's statistical characteristics[58]. The underlying concept of the previous thought is that if the Shannon entropy is substituted with more general entropy measurements, certain systems that do not obey standard statistical mechanics can nonetheless obey a comparable formalism. Tsallis entropies, which depend on a real parameter q and decrease to the Shannon entropy for $q \to 1$, are great prospects for these more general entropy measurements. Generalizations of the canonical distributions, represented as q-exponentials, are known as Tsallis distributions for general q. These generalized statistics are called superstatistics and with them we have a supplementary method to understanding non-extensive statistical mechanics' dynamical reasons (Beck and Cohen, 2003; Beck 2009) while as already mentioned, these superstatistics are also subdivided into Tsallis statistics. For instance, studying a system that is forced out of equilibrium and has spatiotemporal variations in an intensive parameter such as a function of the flow's changing energy dissipation, inverse temperature, or chemical potential, ordinary statistical mechanics such as ordinary Boltzmann factors $e^{-\beta E}$, where E is an effective energy in each field, describes the system locally where is nearly constant. A spatiotemporal average over the fluctuations is used to characterize the system in the longer term. As a result, a superposition of two statistics, those of β and that of $e^{-\beta E}$ is obtained and thus the term "superstatistics"[59].

The occurrence of geomagnetic reversals has recently been studied using a superstatistical model (Vallianatos, 2011) and therefore we use the latter method to create a superstatistical approach to the interevent timings of our earthquake sequences, assuming a basic model where the local distribution is supplied by a Poisson process $p(T|\beta) = \beta e^{-\beta T}$ (Beck, 2009). The conditional probability density to observe the interevent time T when the parameter has a particular value is denoted by the equation

[57] Supra Note 54.
[58] Denis Nikolaevich Sob'yanin, *Generalization of the Beck-Cohen superstatistics*, November 2011.
[59] C. Beck, *Superstatistics: theory and applications*, Continum Mech. Thermodyn, 2004, doi:10.1007/s00161-003-0145-1.

$p(T|\beta)$ and by making the parameter a random variable, this exponential model becomes superstatistical. We may get the marginal distributions of interevent times if is distributed with probability density f(β) and fluctuates on a long-time scale[60].

$$p(T) = \int_0^\infty f(\beta) p\,(T|\beta) d\beta = \int_0^\infty f(\beta) \beta e^{-\beta T}\, d\beta \tag{28}$$

There may be n distinct Gaussian random variables Xi, i = 1, ..., n, that have additive effects on the dynamics of the positive random variable, when create a basic model for the distribution of f (β), (Beck 2009). It can also be assumed a simple model that $\beta = \sum_{i=1}^{n} x_i^2$, where $\langle x_i \rangle = 0$ and $\langle x_1^2 \rangle \neq 0$. In this case, the probability density of β is given by a x^2-distribution with n degrees of freedom:

$$f(\beta) = \frac{1}{\Gamma(n/2)} \left(\frac{n}{2\beta_0}\right)^{n/2} \beta^{\frac{n}{2}-1} exp\left(-\frac{n\beta}{2\beta_0}\right) \tag{29}$$

The average value of β is given by $\langle \beta \rangle = n\langle X_i^2 \rangle = \int_0^\infty \beta f(\beta) d\beta = \beta_0$ and the variance by $\langle \beta \rangle^2 - \beta_0^2 = (2/n)\beta_0^2$. The integral (28) is easily evaluated (Beck, 2009) and one obtains $p(T) \approx C(1 + B(q-1)T)^{1/(1-q)}$, which is exactly the result obtained in the frame of NESP, where $q = 1 + 2/(n+2)$ and $B = 2\beta_0/(2 - q)$[61].

From the above it is recognized that we can calculate the degrees of freedom that are influencing the value of β by $n = \frac{2}{q-1} - 2$ that describe the temporal evolution of earthquake aftershock seismicity by using the q_T value of the interevent times calculated for each earthquake sequence from our q-statistics fit and taking into account the fluctuation of q_T due to its sensitivity to the data set used each time[62].

[60] F. Vallianatos, P. Benson, P. Meredith, P. Sammonds, *Experimental evidence of a non-extensive statistical physics behavior of fracture in triaxially deformed Etna basalt using acoustic emissions*, A Letters Jernal Exploring the Fronties of Physics, March 2012, doi:10.1209/0295-5075/97/58002.
[61] Filippos Vallianatos, Ioannis Koutalonis, Georgios Chatzopoulos, *Evidence of Tsallis entropy signature on medicane induced ambient seismic signals*, Physica A: Statistical Mechanics and its Applications, Volume 520, 2019, doi: https://doi.org/10.1016/j.physa.2018.12.045.
[62] Supra Note 45.

Chapter 4

DATA ANALYSIS AND RESULTS

4.1 Earthquake Catalogs

In this study, we analyze the statistical properties of the temporal evolution of aftershock sequences that followed recent large subduction zone earthquakes worldwide. The analyzed earthquakes occurred in different subduction zones all around the edge of the Pacific Ocean, Canada, Alaska, Russia, Indonesia and Japan. We use 44 aftershock sequences generated by mainshocks of *M* 7.0 and above, with focal depths less than 70km and the duration of the available data is from January 1976 to October 2020. The information that we used is provided by the United States Geological Survey (USGS) catalog which included various magnitude scales such as moment magnitude, body-wave magnitude and surface magnitude.

It is commonly accepted that the most significant parameter which characterize an earthquake is its size, a measure that is directly associated with the amount of energy released. There are various magnitude scales that describe the size of an earthquake but the primary issue it that, except for M_w, all the other magnitude scales do not react consistently throughout magnitude ranges and display saturation effects at various levels for major earthquakes. These restrictions may cause earthquake magnitudes to be underestimated or overestimated. On the contrary, the moment magnitude (Kanamori and Hanks, 1977, 1979) which is defined by

$$M_w = \frac{2}{3} log M_0 - 10.7 \tag{30}$$

where M_0 is the seismic moment, is sufficiently reliable due to the fact that this scale determined by the fault size and the dislocation. In addition, the robustness of this scale estimation is ensured by the fact that seismic moment estimation is based on spectral amplitudes. The moment magnitude is exactly proportional to the logarithm of seismic moment thus it does not saturate, resulting in consistent behavior across all magnitude ranges[63,64] .

For the aforementioned reasons, in the next table we have converted all the magnitudes provided by USGS catalog to moment magnitudes (M_w) using Scordilis' formulas which estimate the moment magnitude based on other magnitude scales.

[63] E.M. Scordilis, *Emprirical global relations converting Ms and mb to moment magnitude*, Journal of Seismology, January 2006, doi:10.1007/s10950-006-9012-4.
[64] See Ranjit Das, H. R. Wason and M. L. Sharma, *Global regression relation for conversion of surface wave and body wave magnitudes to moment magnitude*, Nat Hazards, 2011, doi:10.1007/s11069-011-9796-6.

Table 1

The list of the used Mainshocks

Event Index	Date	Epicenter	Depth (km)	Mainshock Magnitude (Mw)
1	14/01/76	-28.43, -177.66	33.00	8.0
2	19/08/77	-11.14, 118.23	23.30	8.3
3	20/10/86	-27.93, -176.07	50.40	7.7
4	04/10/94	43.60, 147.63	68.20	8.3
5	16/08/95	-5.51, 153.64	45.60	7.7
6	03/12/95	44.82, 150.17	25.90	7.9
7	04/06/00	-4.73, 101.94	43.90	7.9
8	16/11/00	-4.56, 152.79	24.00	8.0
9	23/06/01	-17.28, -72.71	29.60	8.4
10	25/09/03	42.21, 143.84	28.20	8.3
11	26/12/04	3.09, 94.26	28.60	9.0
12	28/03/05	1.67, 97.07	25.80	8.6
13	03/05/06	-22.41, -177.31	67.80	8.0
14	17/07/06	-9.28, 107.78	20.00	7.7
15	01/04/07	-7.79, 156.34	14.10	8.1
16	12/09/07	-3.78, 100.99	24.40	8.5
17	11/02/09	3.92, 126.81	23.90	7.2
18	29/09/09	-15.13, -171.97	12.00	8.1
19	07/10/09	-11.86, 166.01	41.70	7.8
20	27/02/10	-35.98, -73.15	23.20	8.8
21	11/03/11	37.52, 143.05	20.20	9.1
22	06/07/11	-29.22, -175.83	32.50	7.6
23	11/04/12	2.35, 92.82	45.60	8.6
24	30/08/13	51.54, -175.23	29.00	7.0
25	12/04/14	-11.35, 162.24	27.30	7.6
26	19/04/14	-6.64, 154.67	43.40	7.5
27	15/11/14	1.98, 126.37	45.00	7.1
28	29/03/15	-5.18, 152.59	37.60	7.5
29	25/04/15	28.23, 84.73	8.20	7.8
30	16/09/15	-31.57, -71.67	22.40	8.3
31	28/05/16	-56.24, -26.94	68.00	7.2
32	01/09/16	-37.36, 179.15	19.00	7.0
33	13/11/16	-42.74, 173.05	15.10	7.8
34	08/12/16	-10.68, 161.33	40.00	7.8
35	08/09/17	15.02, -93.90	47.40	8.2
36	12/11/17	34.91, 45.96	19.00	7.3
37	23/01/18	56.00, -149.17	14.10	7.9
38	05/12/18	-21.95, 169.43	10.00	7.5
39	20/12/18	55.10, 164.70	16.60	7.3
40	14/05/19	-4.05, 152.60	10.00	7.6
41	15/06/19	-30.64, -178.10	46.00	7.3
42	14/11/19	1.62, 126.42	33.00	7.1
43	18/06/20	-33.29, -177.86	10.00	7.4
44	19/10/20	54.60, -159.62	29.10	7.6

In order to create the catalog of the aftershock sequence of each earthquake, a suitable elliptical region was selected for each mainshock based on the distribution of aftershocks to designate a probable aftershock zone of each mainshock and all probable aftershocks that occurred within two years of the mainshock were evaluated and studied in each of these zones. We choose to analyze the catalogs with totally up to 100 events so as to extract better results and to get a reasonable estimation of the required parameters. Once the catalogs have been finalized, the GR relationship was plotted to estimate the magnitude of aftershock sequence completeness. More precisely, to verify the catalog's completeness, the cutoff magnitude Mc was calculated for each sequence based on the frequency– magnitude distribution. Ultimately, the final list of the selected earthquakes includes 44 occurrences, as presented above[65].

4.2 Analysis of Each Aftershock Sequence

Hereafter, the results of the mainshock-aftershock sequences processing as well as the estimated parameters will be presented and described. The entire statistical analysis is based on the theory examined in Chapter 3.

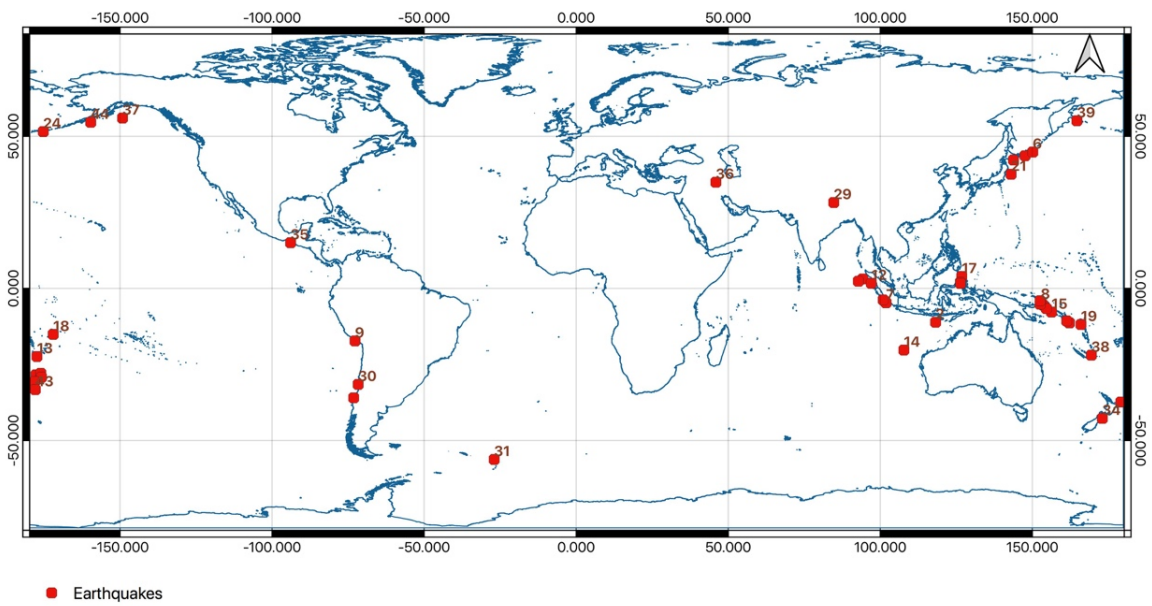

Figure 1. Geographical location of 44 subduction-zone earthquakes. The event indexes provided in Table 1 correspond to the index numbers displayed in this figure.

[65] Robert Shcherbakov, Katsuichiro Goda, Armick Ivanian and Gail M. Atkinson, *Aftershock Statistics of Major Subduction Earthquakes*, Bulletin of the Seismological Society of America, Vol. 103, No. 6, December 2013, doi:10.1785/0120120337.

4.2.1 The 1976 Kermadec Island Earthquake M_w 8.0 (New Zealand)

The statistical analysis of the aftershock sequence started with the plot of the cumulative number of aftershocks $N(>M_w)$ with magnitude greater than M_w as a function of magnitude, where the GR frequency magnitude scaling proposed by Gutenberg and Richter (1954) as $logN(>Mw) = a - bM_w$. We work with the ZMAP software in order to perform the statistical analysis of the detected catalog. Using maximum likelihood estimation and the optimum combination of maximum curvature with M_c 95% and M_c 90% probability, the a and b values were retrieved, as well as the completeness magnitude M_c upon which b= 1.31, a= 9.08 and M_c= 5.4 (Fig. 2a).

In respect to the temporal decay of the aftershock activity, it was used the modified version of Omori's law (Omori 1894; Utsu 1961) as it has already described on Chapter 3 (function (6)). Using the observed data from the period of each earthquake, the maximum likelihood method is used to fit the statistical parameters of four different models of Omori law of aftershock decay to the aftershock sequences of each earthquake.[66] The goodness-of-fit is examined for the Akaike Information Criterion (AIC) (Akaike, 1974; Ogata, 1983) model to the observed data by applying a Kolmogorov-Smirnov (KS) Test.[67] In AIC models with various forms and parameters are compared by obtaining the statistic for each

$$AIC = -2logL + 2k \tag{31}$$

where L denotes the likelihood and k signifies the total number of fitted parameters for the model under consideration.[68] The AIC has a minimum value for the best-fitting parameters of each model and the AIC may be used to evaluate models with different numbers of parameters. It was chosen because it preserves all of the temporal information available in the aftershock sequence and is a common statistical approach for fitting aftershock decays that incorporates significant measures. Moreover, it is only used to compare various fits to the same set of data and only the disparities in AIC's can be interpreted in a significant way.[69] Nonetheless, there are some cases when the suggested model based

[66] Prasanta Chingtham, Babita Sharma, Sumer Chopra and Pareshnath SinghaRoy, *Statistical analysis of aftershock sequences related with two major Nepal earthquakes: April 25, 2015, M_w 7.8, and May 12, 2015, M_w 7.2*, Annals of Geophysics, doi:10.4401/ag-7025.
[67] Prasanta Chingtham, Babita Sharma, Sumer Chopra and Pareshnath SinghaRoy, *Statistical analysis of aftershock sequences related with two major Nepal earthquakes: April 25, 2015, Mw 7.8 and May 12, 2015, Mw 7.2*, Annals of Geophysics, 59, 5, 2016, S0540; doi:10.4401/ag-7025.
[68] Supra Note 27.
[69] Susanna J. Gross and Carl Kisslinger, *Tests of Models of Aftershock Rate Decay, Bulletin of the Seismological Society of America*, Vol. 84, No. 5, October 1994.

on the AIC has a higher RMS than another model, thus we give the results of both models in these cases. In reality, the model with the lowest RMS has a better fit between the observed aftershock activity and the forecasted curve.

The forecasted curve of aftershock activity is plotted using the simple modified Omori model throughout the forecasted period of 47 days. Parameter K defines the sequence's production, c adjusts for missing earthquakes in the catalog, and p determines how fast the activity returns to the constant background intensity and normally, these figures are converted to days. The normal range for p is 0.6 to 2.5. Higher p values are associated with earthquake swarms, as seen in geothermal and volcanic areas while, superimposed aftershock sequences have been linked to lower p values, as the decay would be slower than predicted.[70]

Figure 2b presents the model proposed by the AIC with p= 1.17, c= 0.124 and k= 10 while figure 2c presents the model 4 of modified Omori law, with the lowest RMS and p1= 1.66, p2=1.36, c1=0.382, c2=5, k1=16.1 and k2= 10.

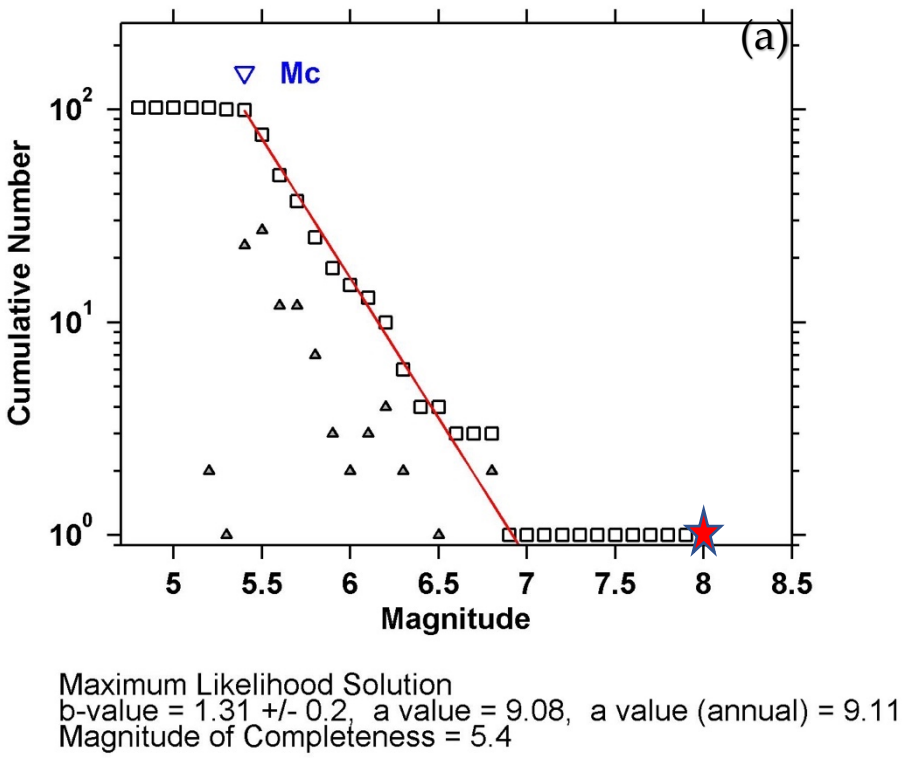

[70] Brendan Sullivan, lecture of "Earthquake Physics", *Basic Statistical Seismology Tutorial*, Website link: http://geophysics.eas.gatech.edu/people/bsullivan/tutorial/StatisticalSeismology.htm#part1_1

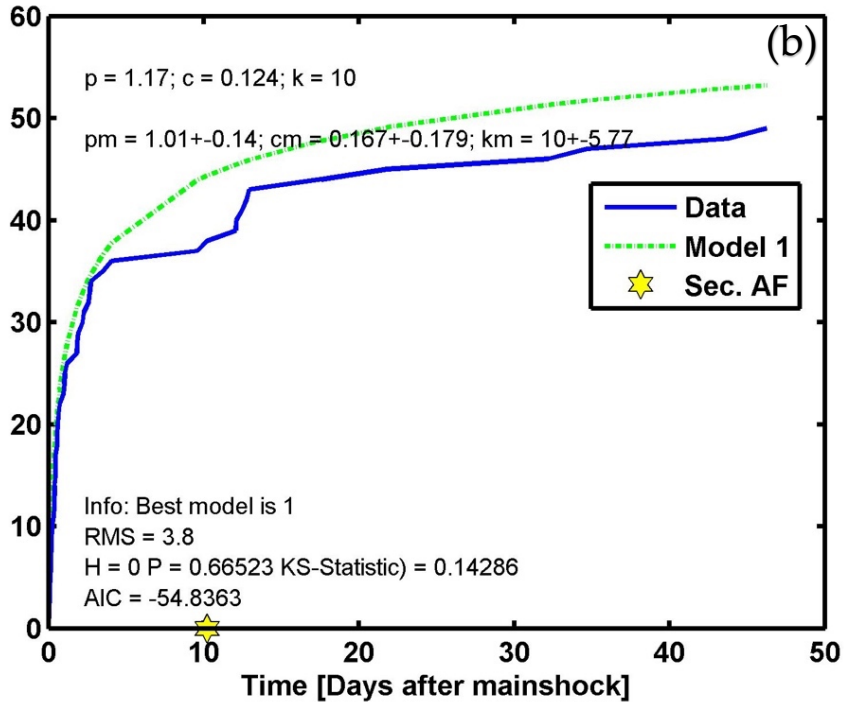

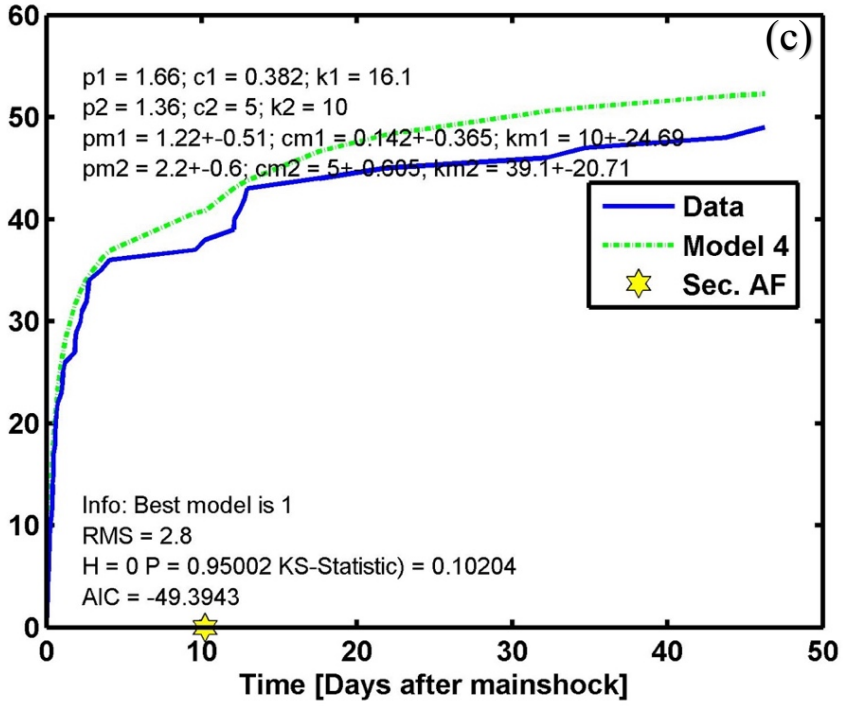

Figure 2. (a) The Guttenberg-Richter distribution using maximum likelihood method with the best combination of maximum curvature M_c 95% and M_c 90% probability. The red star shows the magnitude of the mainshock M_w 8.0. **(b)** The best model (1) of the estimated curve of the modified Omori formula (dashed line) applied to the aftershock data and the observed cumulative number of aftershocks (solid line) based on the AIC. **(c)** The model 4 of the estimated curve of the modified Omori formula (dashed line) applied to the aftershock data and the observed cumulative number of aftershocks (solid line), with the lowest RMS= 2.8.

Subsequently, plotting the aftershock magnitude versus the logarithm of time after the mainshock reveals the magnitude-time structure of the aftershock sequence (Utsu et al. 1995) (Fig. 3) where we indirectly observe the reduction of energy release after the occurrence of the mainshock. In fact, earthquakes do not exceed the magnitude of the Mw 7.0.

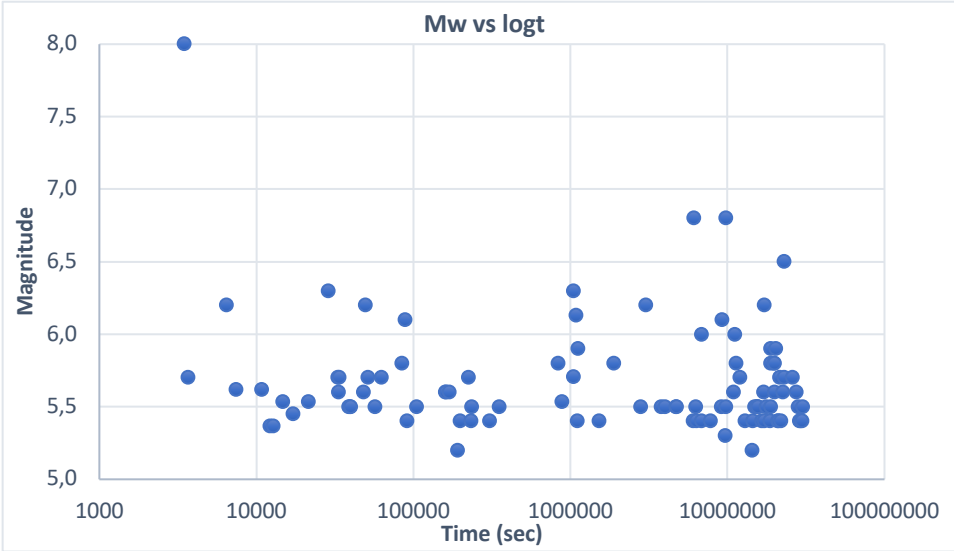

Figure 3. The magnitude-time pattern versus the logarithm of time of the mainshock M_w 8.0.

The figure below shows the application of the fragment-asperity model to this earthquake activity which can effectively represent the frequency-magnitude distribution of earthquakes across a wider range of scales. Furthermore, q_M temporal fluctuations in regional seismicity have been utilized as a proxy for tectonic instability and proximity to larger earthquakes. For this earthquake it is estimated a q_M= 1.42 with ci= 1.37-1.47.

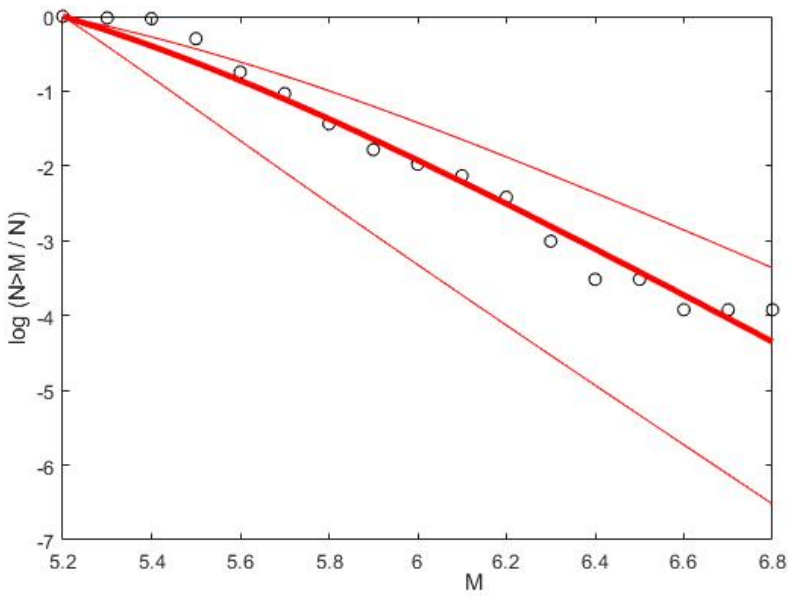

Figure 4. Frequency-magnitude distribution. The bold red line represents the model of equation (26) for qM= 1.42, while the other two lines present the corresponding 95% confidence intervals.

Figure 5 shows a typical Q-exponential (see function 18) pattern in the log–log plot of the cumulative distribution function, P(>T) of the aftershocks interevent times and reveals that for large values of T ($T > T_c$, where T_c is the critical interevent time), there is a deviation from the Q-exponential. Furthermore, q = 1.78 is obtained by fitting Q-exponential to the observed data up to a value near to T_c.

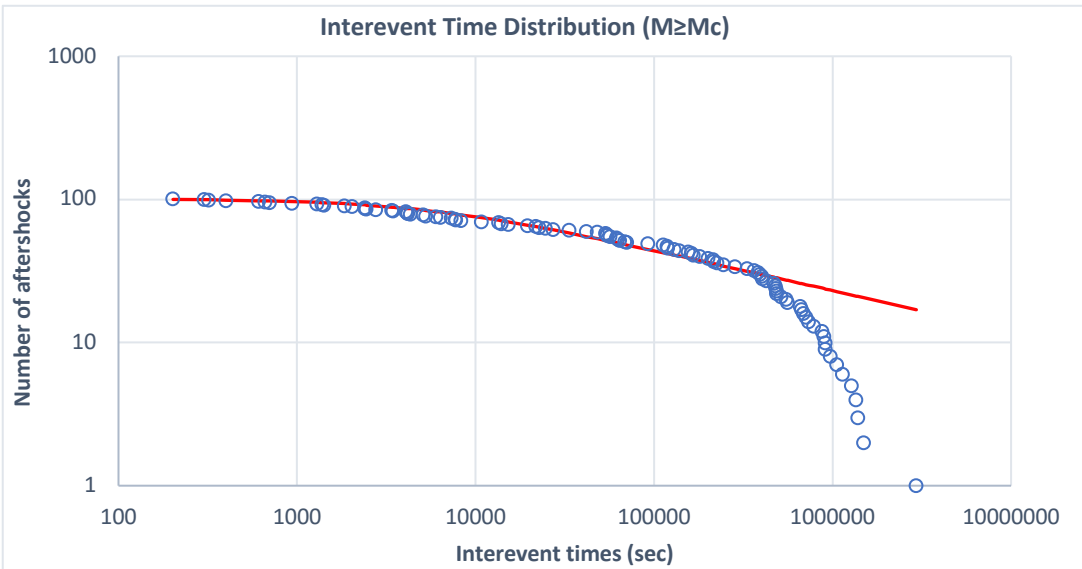

Figure 5. The cumulative distribution function of the interevent times. The red line is the Q-exponential fitting with q = 1.78.

The Q-logarithm (see function 21) implies that the expression $ln_Q P(>T) = -\frac{1}{T^*}T$ is linear with T with slope -1/T* when the Q, that describes the distribution of interevent time intervals, is introduced (Vallianatos 2011). The figure 6 presents the $ln_Q P(>T)$ as a function of interevent time T for q = 1.78 and it is estimated that T_c has a value of 400,000 s based on the deviation from expected linearity. Furthermore, the observed deviation from the Q-exponential might be described as adding two aftershock sequence mechanisms. The first mechanism, regulated by Tsallis entropy, is dominant for interevent time $T < T_c$, whereas the second, characterized by an exponential function and it is evident for $T > T_c$. The generalized probability distribution related with the first mechanism (for $T<T_c$) is given by the equation 14 and may be derived by solving the nonlinear differential equation in the context of the non-extensive statistical physics approach by $\frac{dp}{dT} = -\beta p^q$. To incorporate a crossover from anomalous ($q\neq1$) to normal (q=1) statistical mechanics while extending the interevent time duration T, this differential equation solution is utilized to generalize the anomalous equilibrium distribution. The differential equation is considered as

$$\frac{dp}{dT} = -\beta_1 p_i - (\beta_q - \beta_1)p^q \tag{32}$$

whose solution is

$$p(T) = C\left[1 - \frac{\beta_q}{\beta_1} + \frac{\beta_q}{\beta_1} e^{(q-1)\beta_1 T}\right]^{1/1-Q} \tag{33}$$

where C is a normalization factor and p(T) decreases monotonically with increasing p(T) for positive βq and β1. As a result, in the case where (q-1)β_1 = 1, equation (33) is approximated as q-exponential, p(T) $p(T) \approx Cexp_q(-T/T_q)$, where $T_q = 1/\beta_q$, whereas for (q-1)β_1 > > 1, the asymptotic behavior of the probability distribution is $p(T) \propto \left(\frac{\beta_1}{\beta_q}\right)^{1/(q-1)} e^{-\beta_1 T}$, an exponential function, where Tc = 1/(q-1)β_1 is the crossover point between the non-additive and additive behavior.[71]

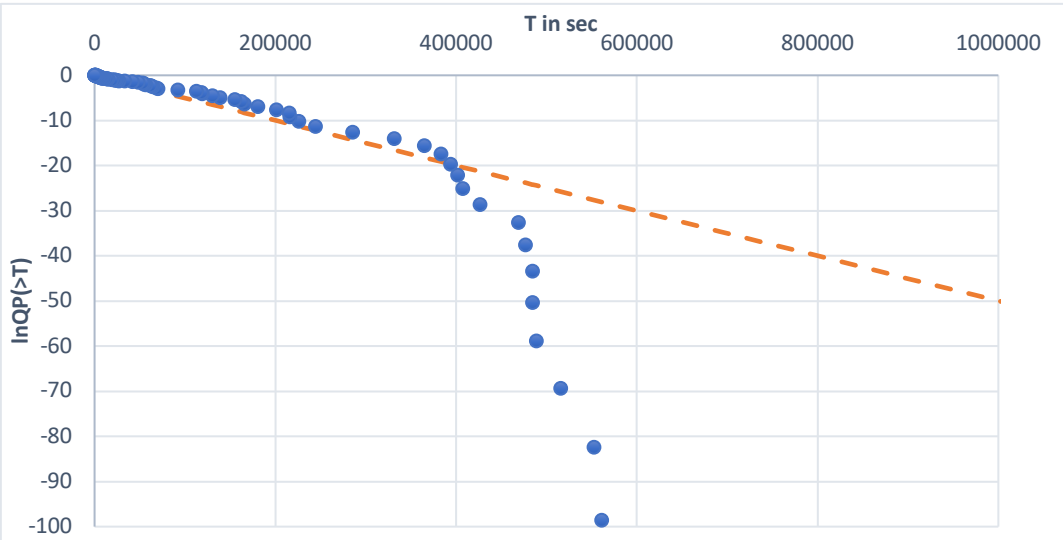

Figure 6. The Q-logarithmic function of the P(>T) as a function of the interevent times where the dashed line is the fitting with q= 1.78. The deviation from the linearity suggests Tc values close to 400,000 s.

As it is already described on chapter 3.4, the superstatistical model generates a q-exponential distribution of interevent times for T< Tc via a simple mechanism, namely a χ^2-distributed allocated parameter β of the local Poisson process, and may be used to explain the interevent time distribution in the aftershock sequence. By using the observed distribution and the q-value q= 1.78 obtained from our q-statistics fits, it is calculated a n= 0.6 implying that the number of degrees of freedom impacting the value of β is incredibly law. To mention that that the observed exponential functions are associated with a notable high number of degrees of freedom when T > Tc.

[71] Supra Note 32.

The figure 7 plots the development of interevent time T as a function of time since the main event. The Tc value indicates that in the early aftershock period, the majority of interevent times have a T value lower than Tc, implying that the Tsallis entropic mechanism is prevalent in the main part of the aftershock evolution, while the characteristics of aftershock sequences, such as finite degree of freedom and long-range memory, which are associated with a non-extensive statistical physics description, become less prominent as time passes and the BG statistical physics is recovered[72].

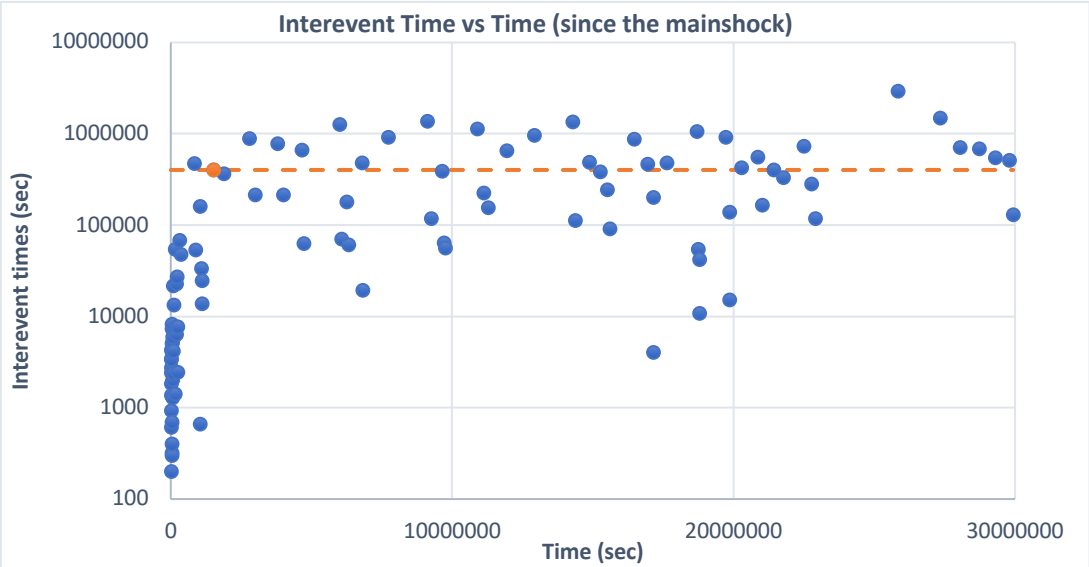

Figure 7. The evolution of interevent time T as a function of time t since the main event. The Tc value is indicated by the dashed line (see text).

The aforementioned earthquake's statistical analysis and processing was carried out also in the seismic sequences of the following major earthquakes of the subduction zone, with the respective diagrams and results being provided further below.

[72] Supra Note 32.

4.2.2 The 1977 Waingapu Earthquake M_w=8.3 (Indonesia)

Figure 8a presents Guttenberg-Richter distribution using maximum likelihood solution. However, as it can be observed, the fit of the red line was influenced by the great magnitude of the earthquake thus the manual method is used (8b) where the fitting can be controlled. The estimated parameters are Mc=5.3 and b=1.33 with a standard deviation of 0.05.

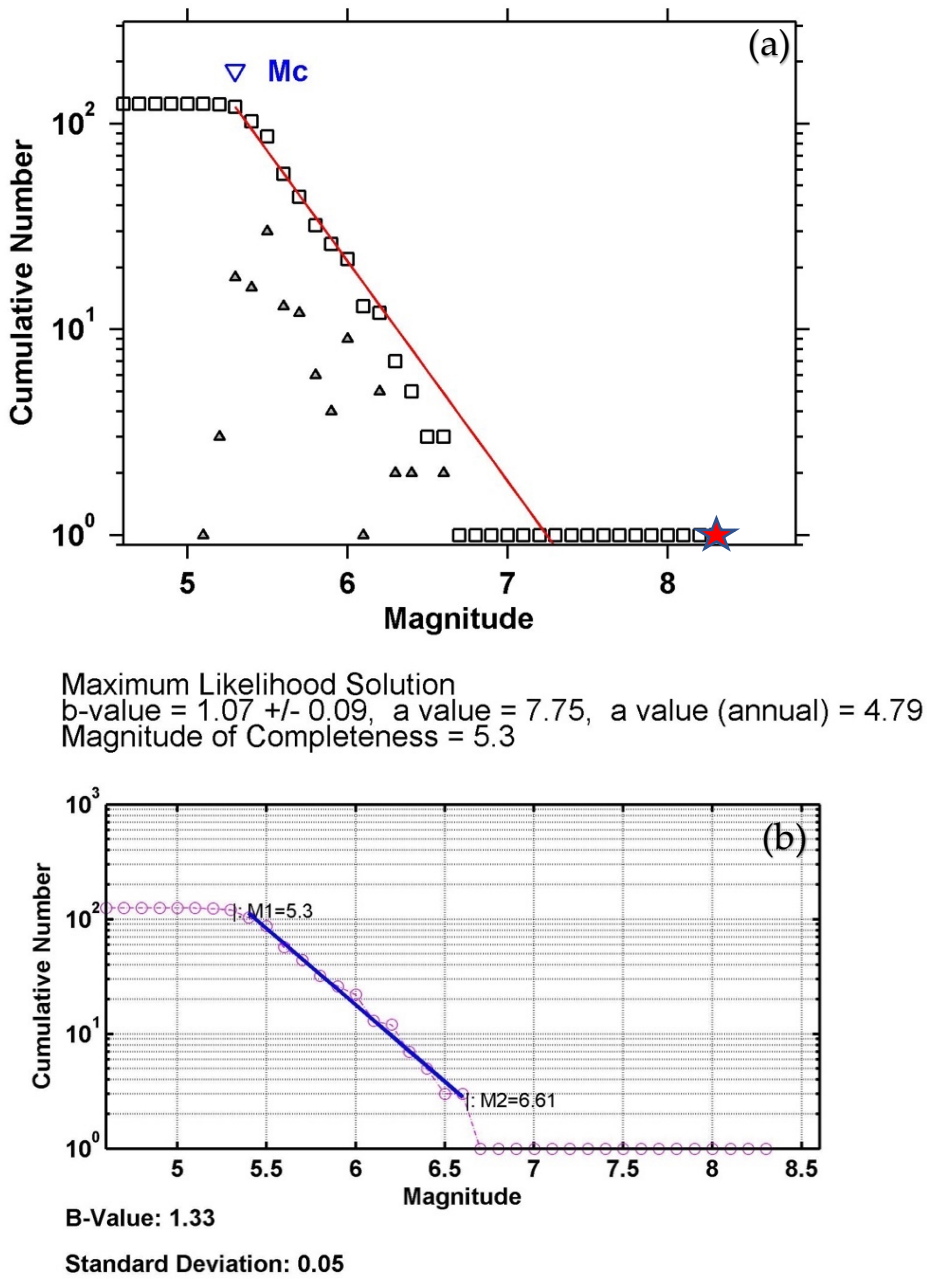

Figure 8. (a) The Guttenberg-Richter distribution using maximum likelihood method with the best combination of maximum curvature M_c 95% and M_c 90% probability. The red star shows the magnitude of the mainshock M_w 8.3. **(b)** The Guttenberg-Richter distribution using the manual method.

The figure below presents the model proposed by the AIC with p= 0.78, c= 0.18 and k= 12.6. In this case, the best model proposed by the AIC is identified with the model with the lowest RMS.

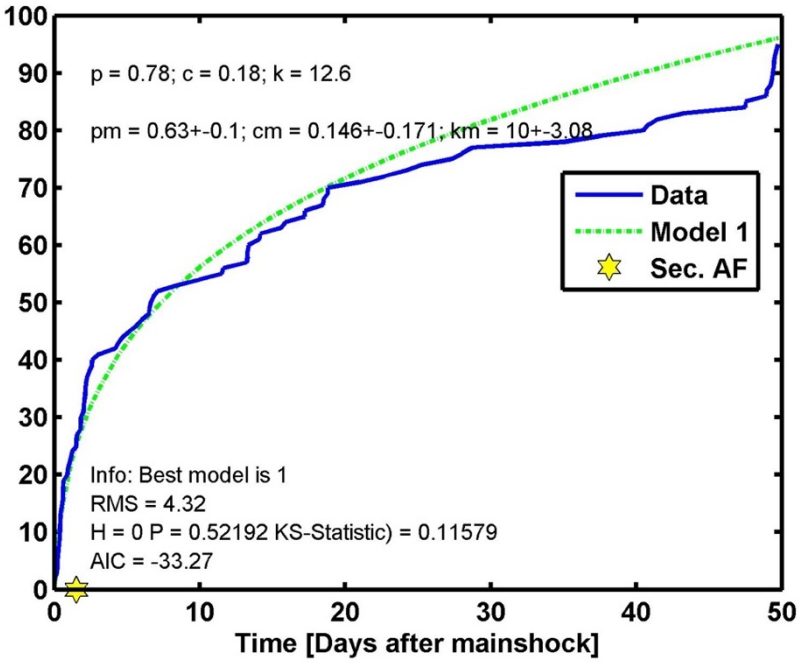

Figure 9. The best model (1) of the estimated curve of the modified Omori formula (dashed line) applied to the aftershock data and the observed cumulative number of aftershocks (solid line) based on the AIC with RMS=4.32.

Following, the plot of the aftershock magnitude versus the logarithm of time after the mainshock which reveals the magnitude-time structure of the aftershock sequence (Utsu et al. 1995).

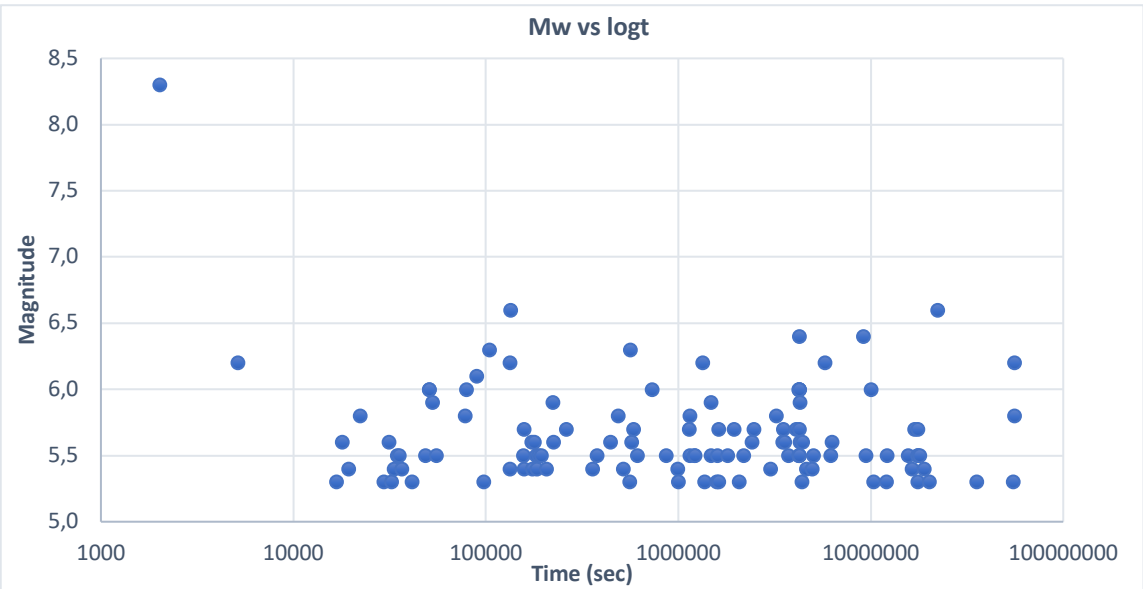

Figure 10. The magnitude-time pattern versus the logarithm of time of the mainshock M_w 8.3.

Using the frequency-magnitude distribution for this earthquake, it is estimated a q_M= 1.31 with ci= 1.27-1.35.

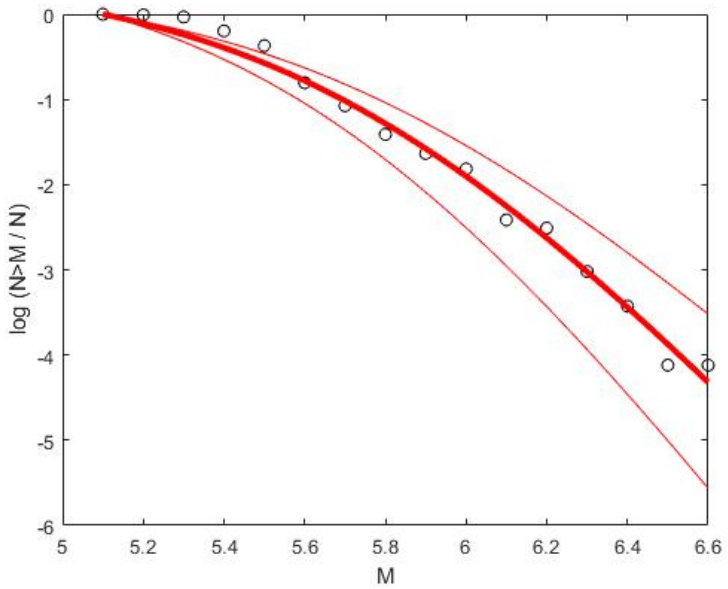

Figure 11. Frequency-magnitude distribution. The bold red line represents the model of equation (26) for qM= 1.31, while the other two lines present the corresponding 95% confidence intervals.

Figure 12a shows the typical Q-exponential pattern of the cumulative distribution function, P(>T) of the aftershocks interevent times. By fitting the Q-exponential to the observed data up to a value near to T_c, a q=1.68 is obtained and 12b presents the Q-logarithmic function of the P(>T) as a function of the interevent times.

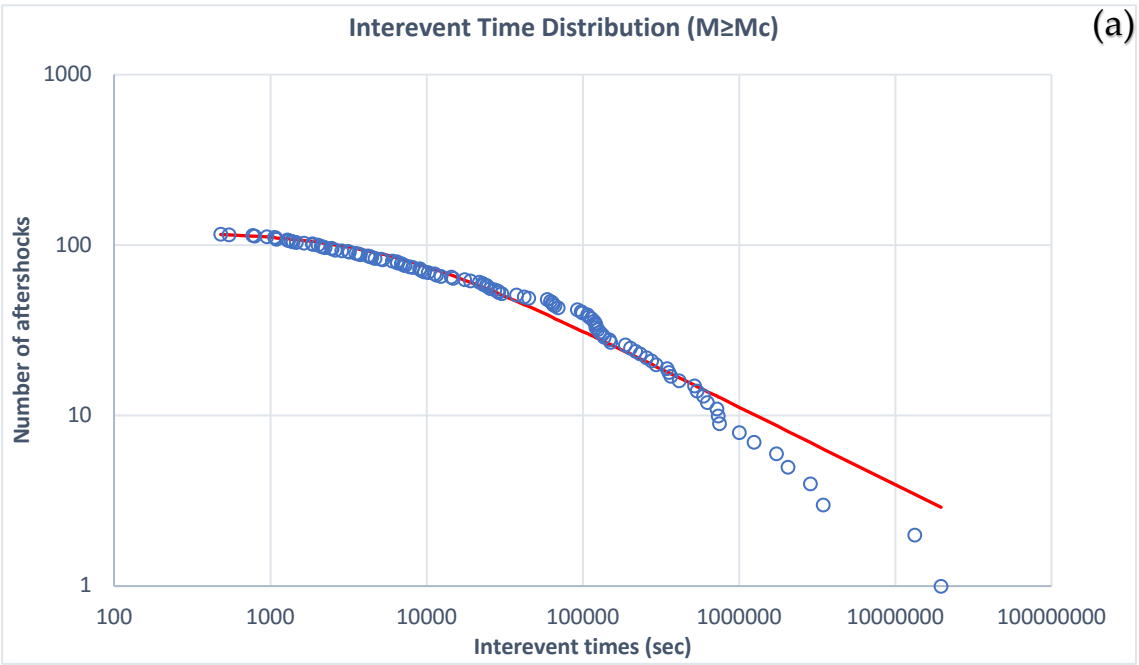

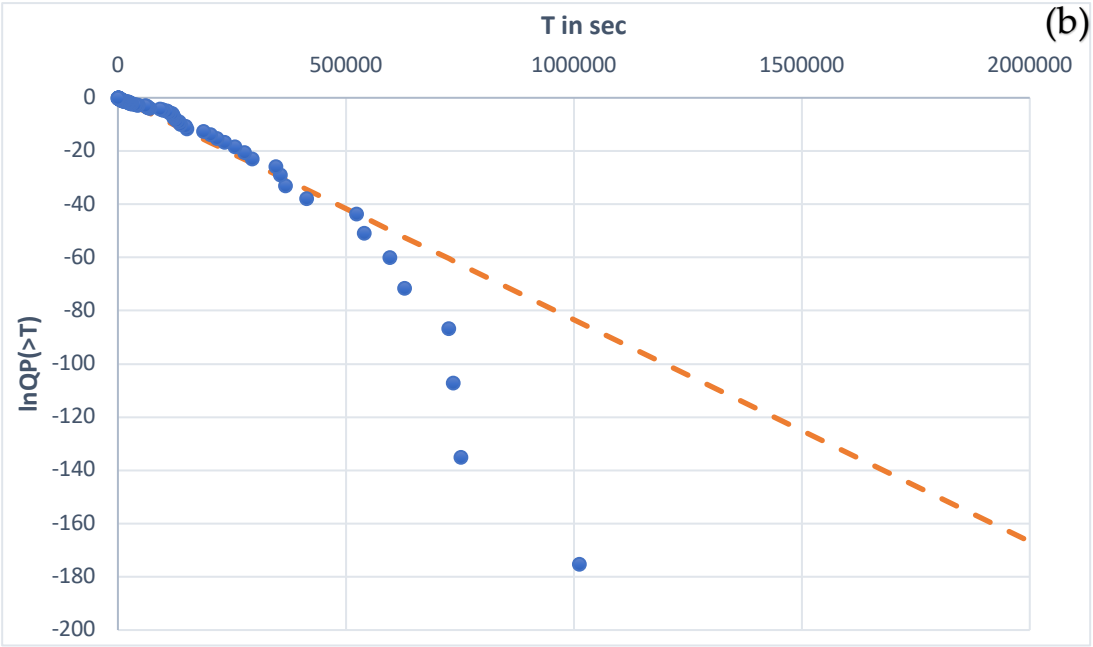

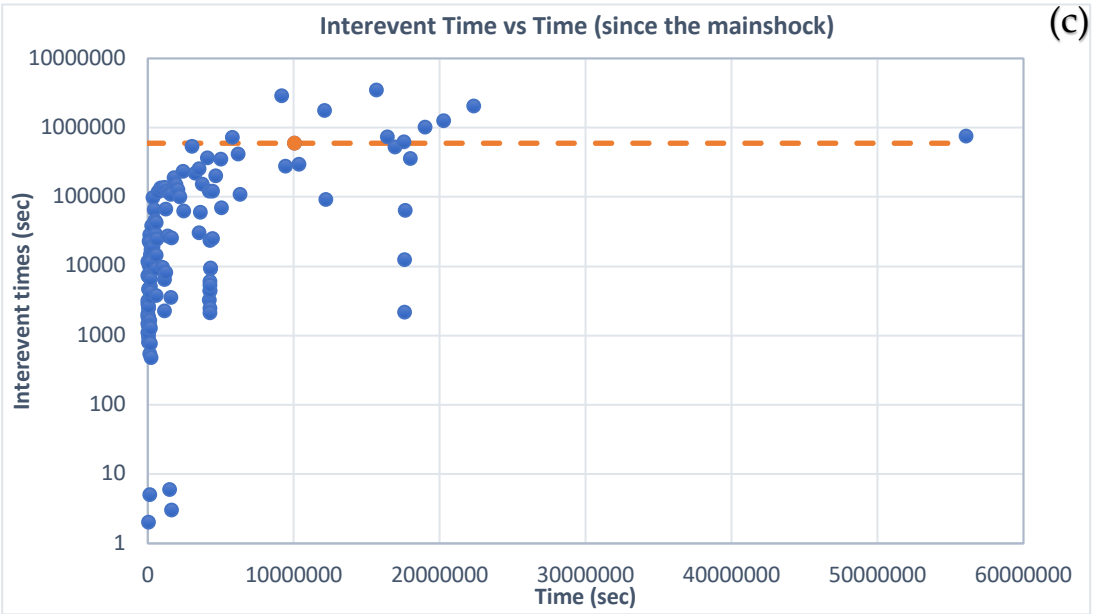

Figure 12. (a) The cumulative distribution function of the interevent times. The red line is the Q-exponential fitting with q = 1.68. **(b)** The Q-logarithmic function of the P(>T) as a function of the interevent times where the dashed line is the fitting with q=1.68. The deviation from the linearity suggests Tc values close to 750,000 s. **(c)** The evolution of interevent time T as a function of time t since the main event. The Tc value is indicated by the dashed line.

4.2.3 The 1986 Kermadec Island Earthquake M_w=7.7 (New Zealand)

Figure 13a presents Guttenberg-Richter distribution using maximum likelihood solution. However, as it can be observed, the fit of the red line was influenced by the great magnitude of the earthquake thus the manual method is used (8b) where the fitting can be controlled. The estimated parameters are Mc=5.2 and b=1.41 with a standard deviation of 0.04.

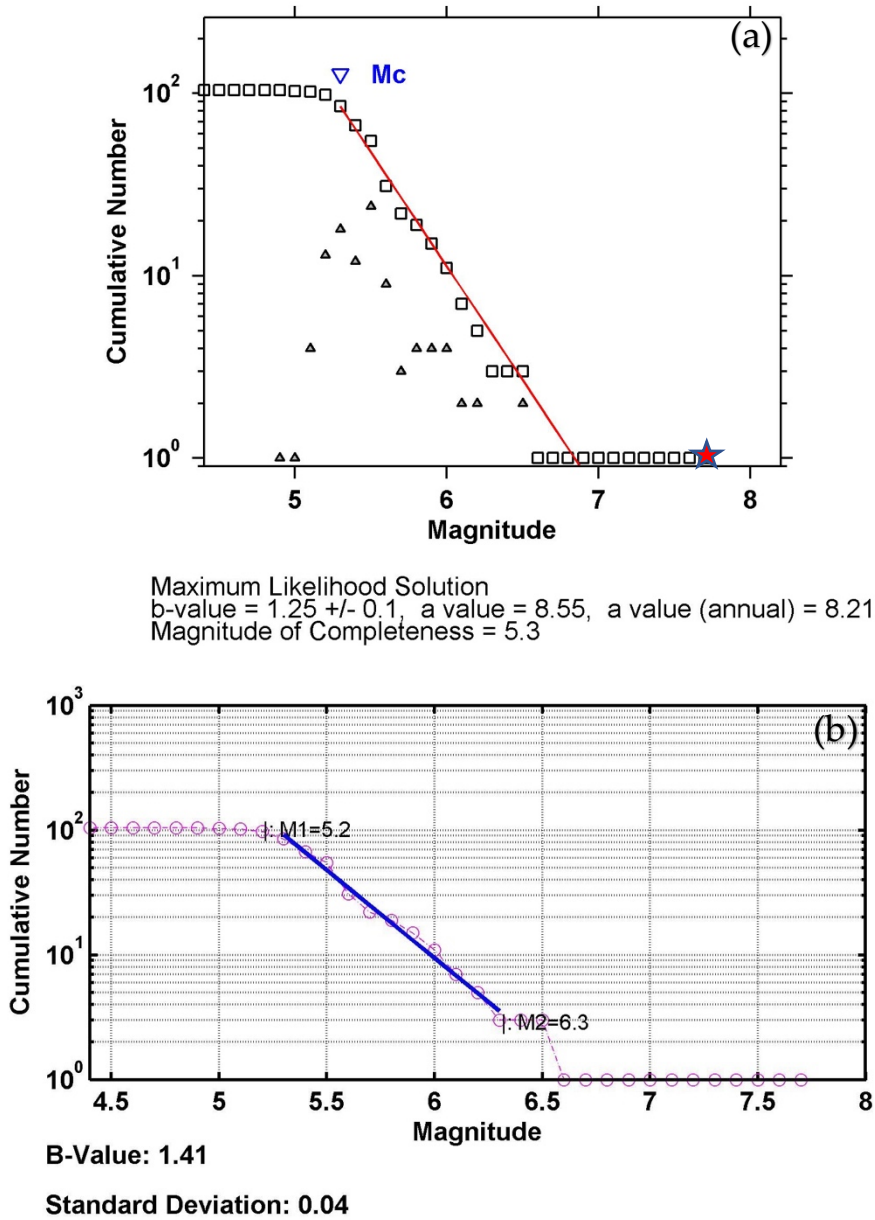

Figure 13. (a) The Guttenberg-Richter distribution using maximum likelihood method with the best combination of maximum curvature M_c 95% and M_c 90% probability. The red star shows the magnitude of the mainshock M_w 7.7. **(b)** The Guttenberg-Richter distribution using the manual method.

Figure 14a presents the model proposed by the AIC with p= 0.96, c= 0.026 and k= 11.3 while figure 14b presents the model 4 of modified Omori law, with the lowest RMS and p1= 1.18, p2=1.27, c1=0.111, c2=5, k1=13.5 and k2= 10.

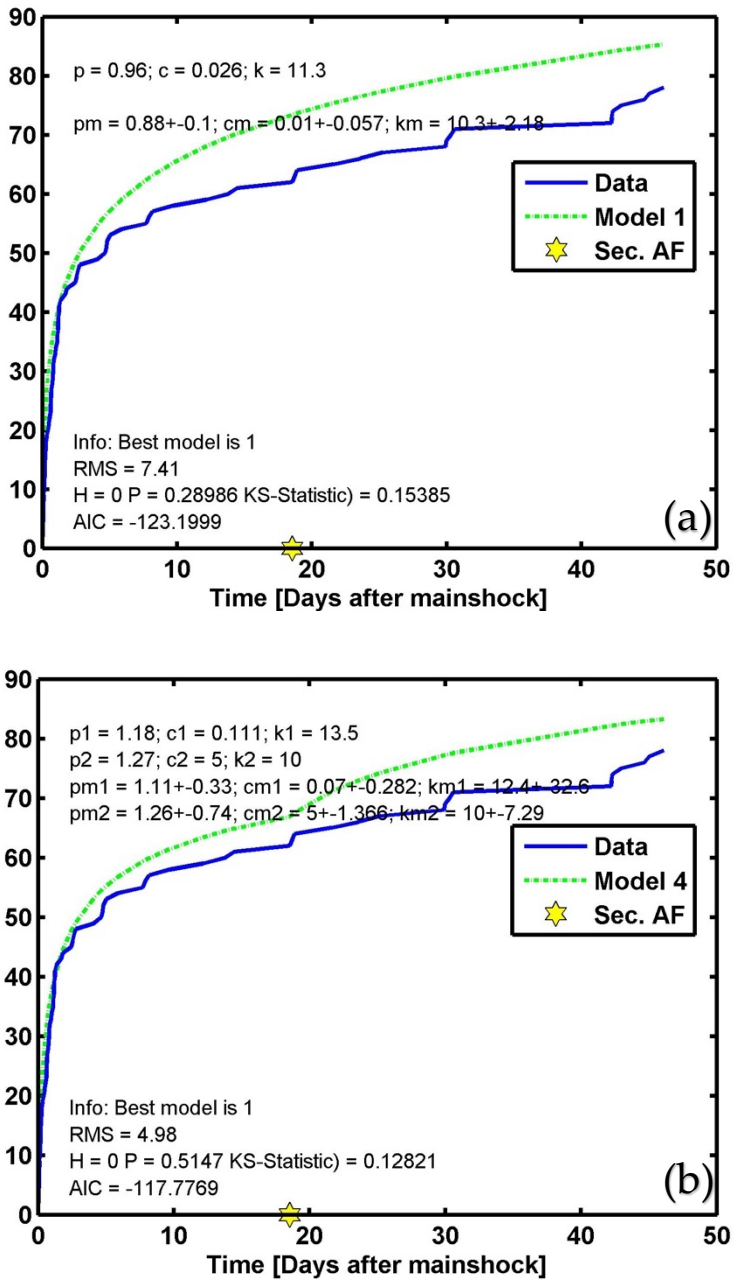

Figure 14. (a) The best model (1) of the estimated curve of the modified Omori formula (dashed line) applied to the aftershock data and the observed cumulative number of aftershocks (solid line) based on the AIC. **(b)** The model 4 of the estimated curve of the modified Omori formula (dashed line) applied to the aftershock data and the observed cumulative number of aftershocks (solid line), with the lowest RMS= 4.98.

Here the magnitude-time form of the aftershock sequence is available.

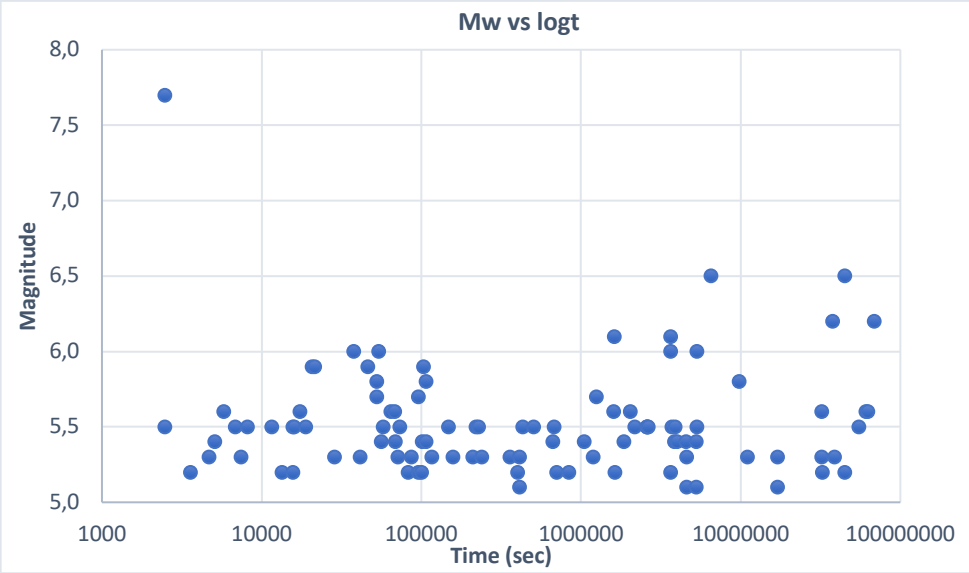

Figure 15. The magnitude-time pattern versus the logarithm of time of the mainshock M_w 7.7.

By the frequency-magnitude distribution for this earthquake, it is estimated a q_M= 1.32 with ci= 1.26-1.38.

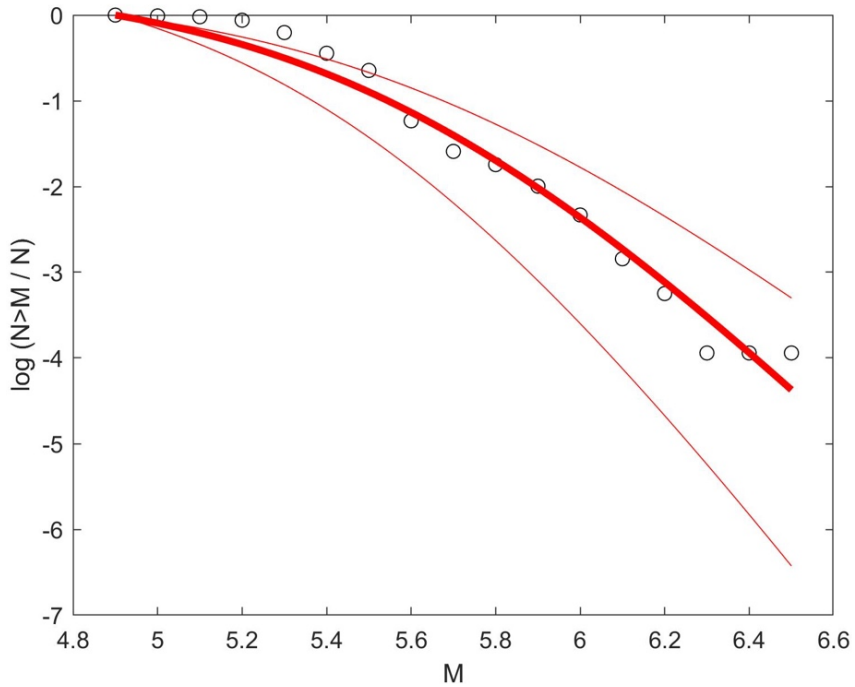

Figure 16. Frequency-magnitude distribution. The bold red line represents the model of equation (26) for qM= 1.32, while the other two lines present the corresponding 95% confidence intervals.

Figure 17a shows the typical Q-exponential pattern of the cumulative distribution function, P(>T) of the aftershocks interevent times. By fitting the Q-exponential to the observed data up to a value near to T_c, a q=1.74 is obtained and 17b presents the Q-logarithmic function of the P(>T) as a function of the interevent times.

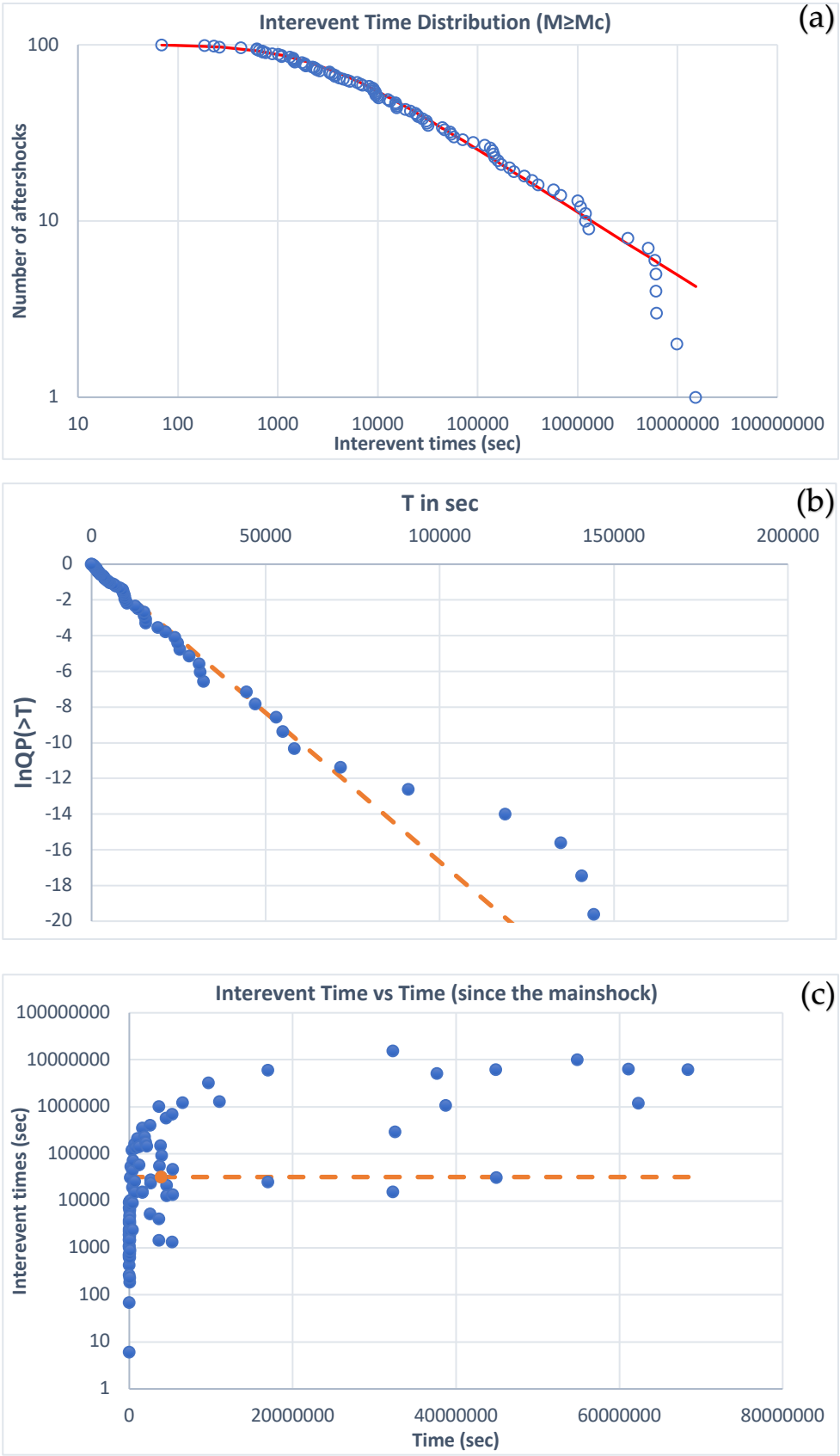

Figure 17. (a) The cumulative distribution function of the interevent times. The red line is the Q-exponential fitting with q = 1.74. **(b)** The Q-logarithmic function of the P(>T) as a function of the interevent times where the dashed line is the fitting with q=1.74. The deviation from the linearity suggests Tc values close to 75,000 s. **(c)** The evolution of interevent time T as a function of time t since the main event. The Tc value is indicated by the dashed line.

4.2.4 The 1994 Shikotan Earthquake M_w=8.3 (Russia)

The figure below shows Guttenberg-Richter distribution. The estimated parameters are Mc=5.2, b=1.35 and a=9.32.

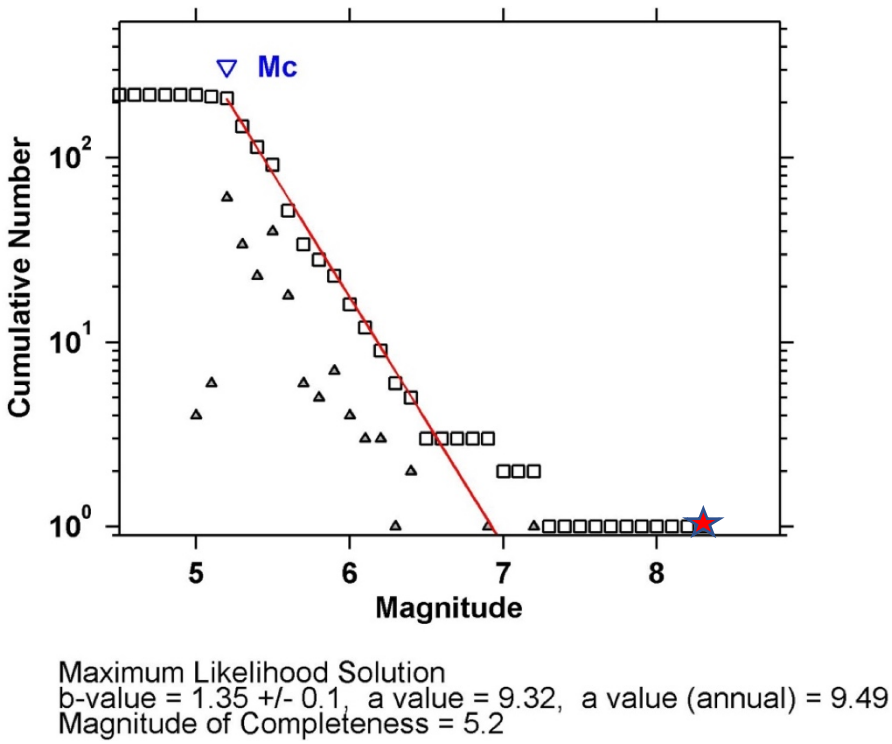

Figure 18. The Guttenberg-Richter distribution using maximum likelihood method with the best combination of maximum curvature M_c 95% and M_c 90% probability. The red star shows the magnitude of the mainshock M_w 8.3.

Next figure (19a) presents the model proposed by the AIC with p1= 1.19, p2=2.7, c1=0.146, c2=0.588, k1=35.8 and k2= 10, while (19b) presents the model with the lowest RMS and p= 1.18, c= 0.166 and k= 39.4.

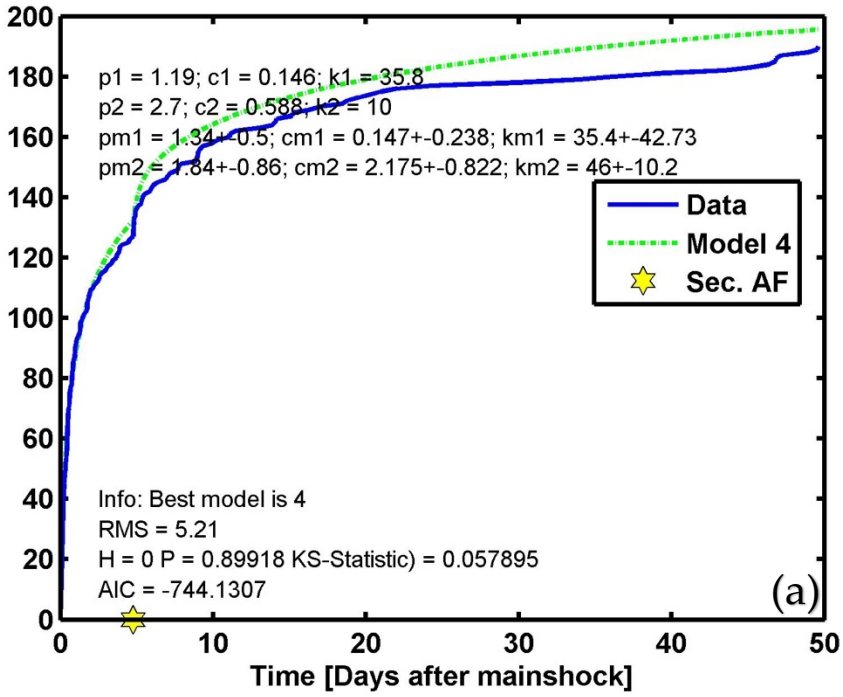

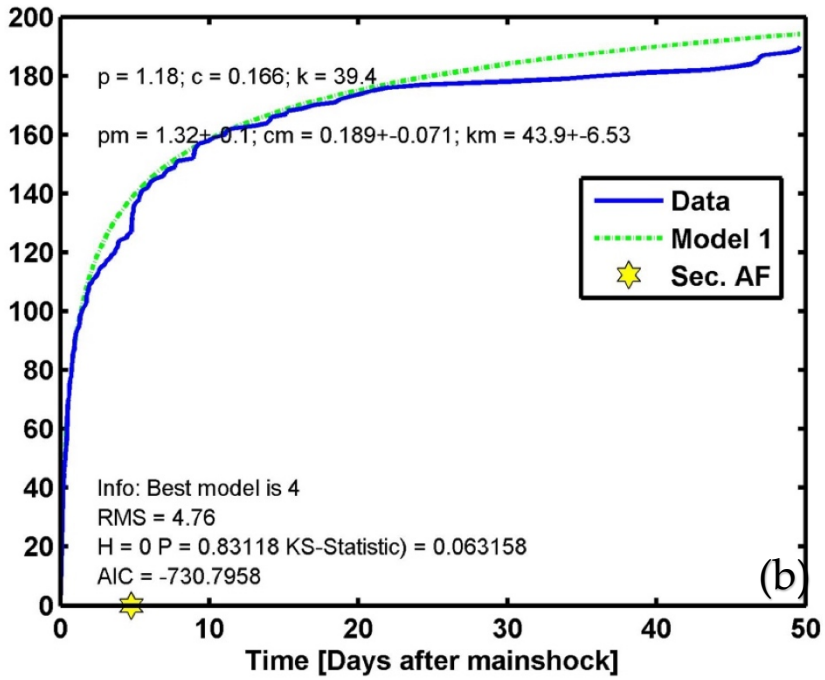

Figure 19. (a) The best model (4) of the estimated curve of the modified Omori formula (dashed line) applied to the aftershock data and the observed cumulative number of aftershocks (solid line) based on the AIC. **(b)** The model 1 of the estimated curve of the modified Omori formula (dashed line) applied to the aftershock data and the observed cumulative number of aftershocks (solid line), with the lowest RMS= 4.76.

Here is the magnitude-time form of the aftershock sequence.

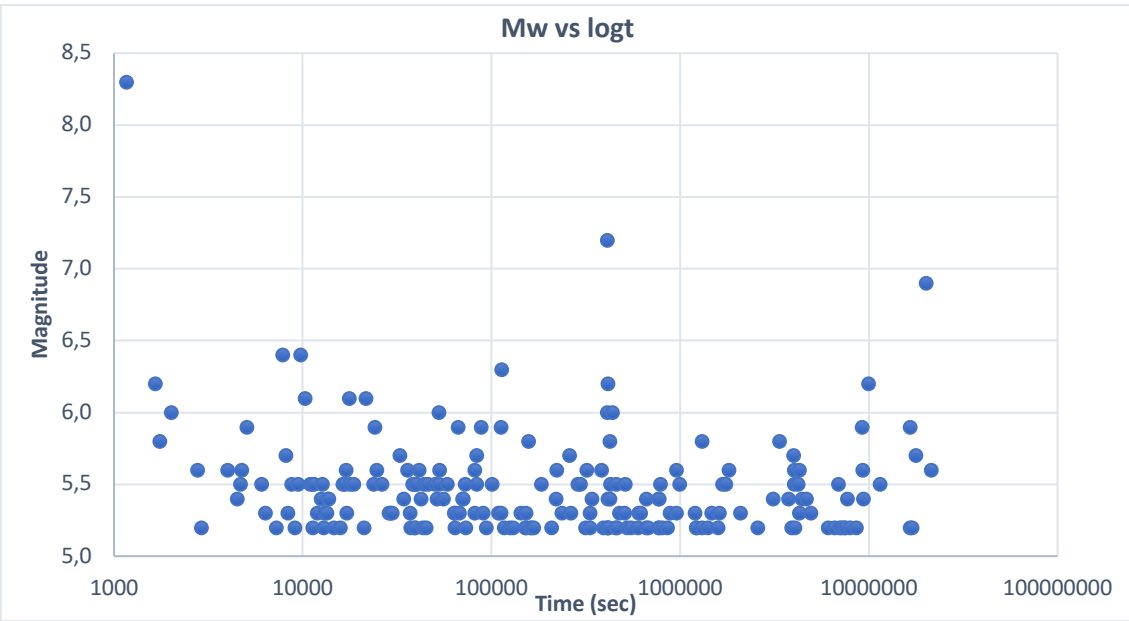

Figure 20. The magnitude-time pattern versus the logarithm of time of the mainshock M_w 8.3.

By the frequency-magnitude distribution for this earthquake, it is estimated a q_M= 1.46 with ci= 1.42-1.49.

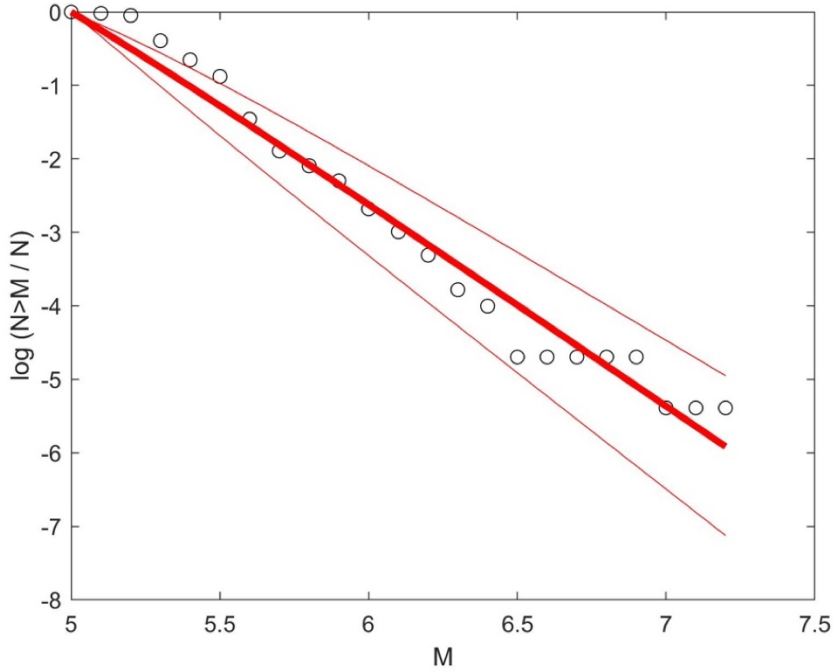

Figure 21. Frequency-magnitude distribution. The bold red line represents the model of equation (26) for qM= 1.46, while the other two lines present the corresponding 95% confidence intervals.

Figure 22 shows the typical Q-exponential pattern and Q-logarithmic function of the cumulative distribution function, P(>T) of the aftershocks interevent times and a q=1.72 is obtained.

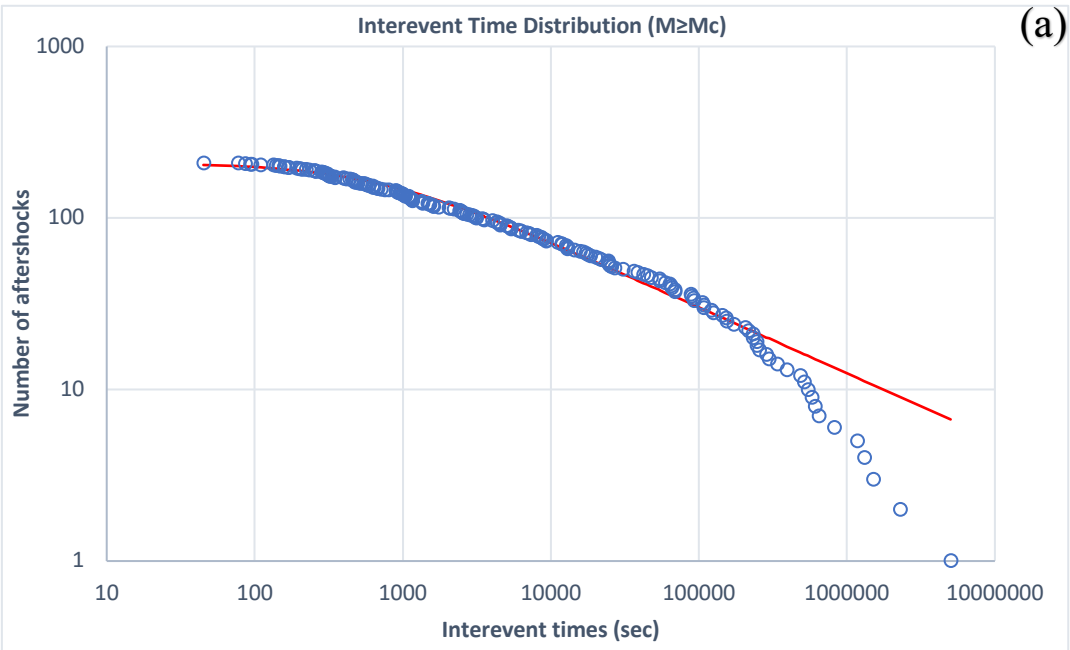

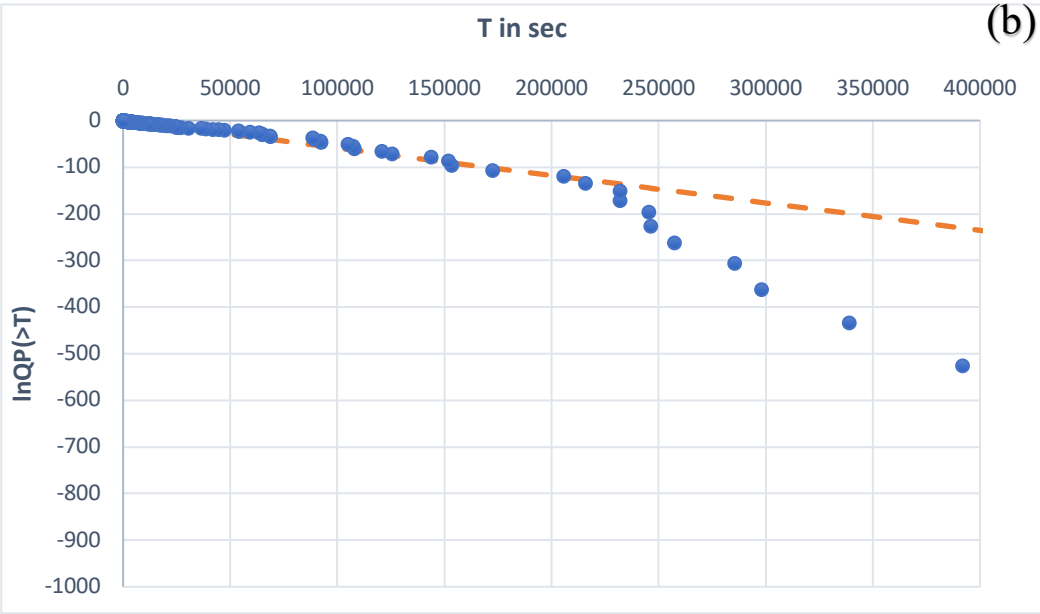

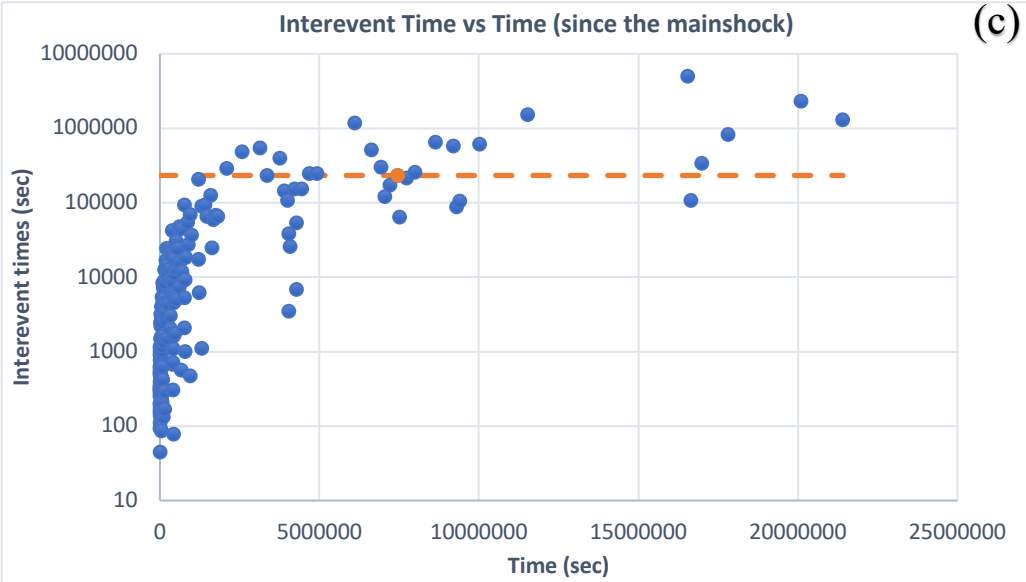

Figure 22. (a) The cumulative distribution function of the interevent times. The red line is the Q-exponential fitting with q = 1.72. **(b)** The Q-logarithmic function of the P(>T) as a function of the interevent times where the dashed line is the fitting with q=1.72. The deviation from the linearity suggests Tc values close to 200,000 s. **(c)** The evolution of interevent time T as a function of time t since the main event. The Tc value is indicated by the dashed line.

4.2.5 The 1995 Panguna Earthquake M_w=7.7 (Papua New Guinea)

The figure below shows Guttenberg-Richter distribution. The estimated parameters are Mc=5.2, b=0.97 and a=7.01.

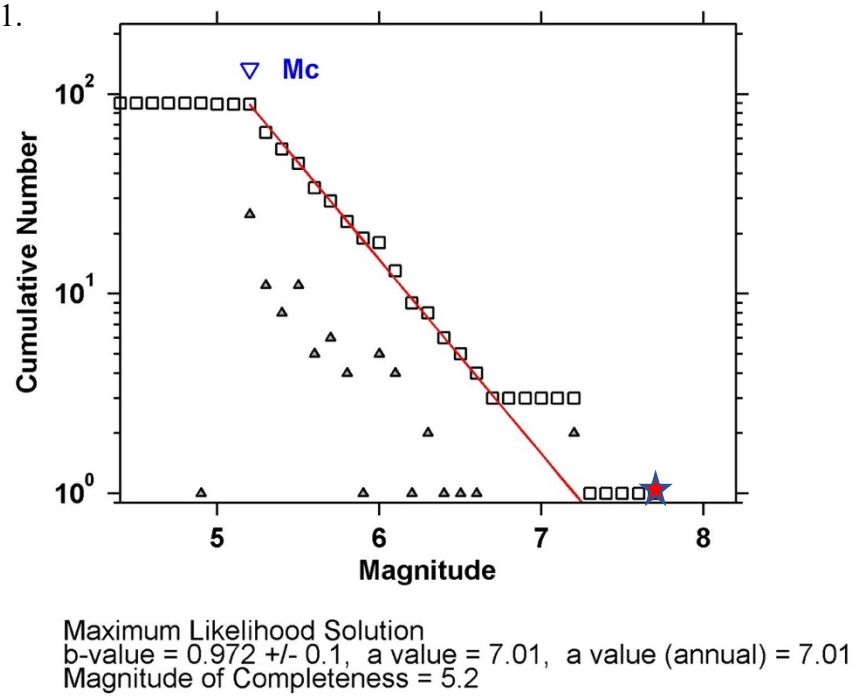

Figure 23. The Guttenberg-Richter distribution using maximum likelihood method with the best combination of maximum curvature M_c 95% and M_c 90% probability. The red star shows the magnitude of the mainshock M_w 7.7.

Next figure presents the model proposed by the AIC with p= 1.31, c= 0.32 and k= 11.7.

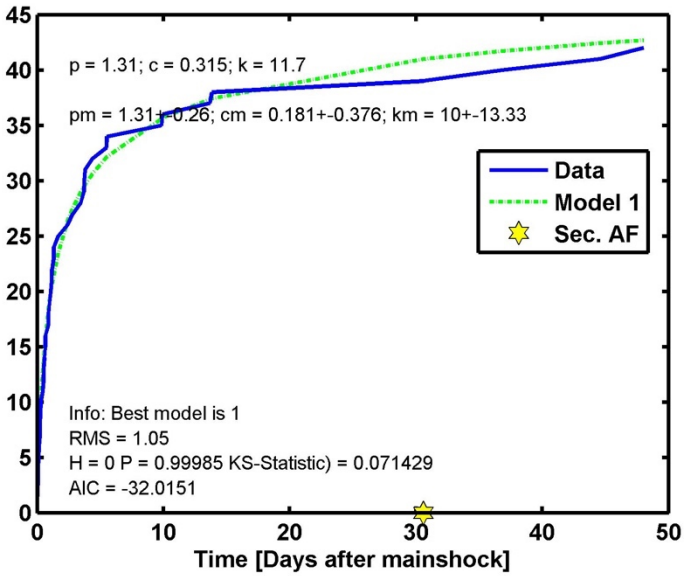

Figure 24. The best model (1) of the estimated curve of the modified Omori formula (dashed line) applied to the aftershock data and the observed cumulative number of aftershocks (solid line) based on the AIC with RMS=1.05.

Here is the magnitude-time form of the aftershock sequence.

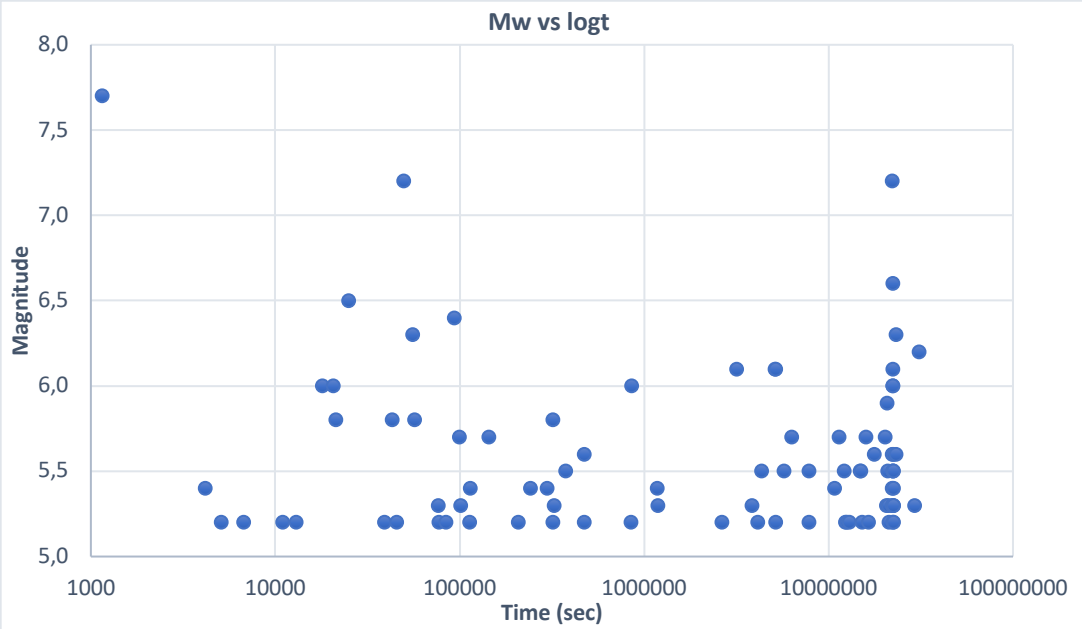

Figure 25. The magnitude-time pattern versus the logarithm of time of the mainshock M_w 7.7.

By the frequency-magnitude distribution for this earthquake, it is estimated a q_M= 1.55 with ci= 1.53-1.58.

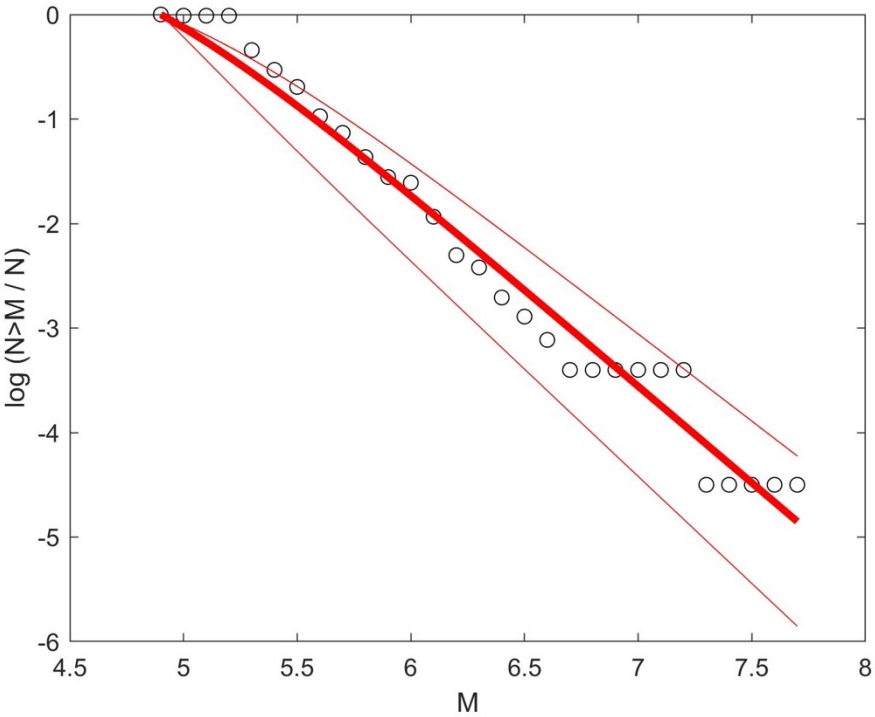

Figure 26. Frequency-magnitude distribution. The bold red line represents the model of equation (26) for qM= 1.55, while the other two lines present the corresponding 95% confidence intervals.

Figure 27 shows the typical Q-exponential pattern and Q-logarithmic function of the cumulative distribution function, P(>T) of the aftershocks interevent times and a q=1.77 is obtained.

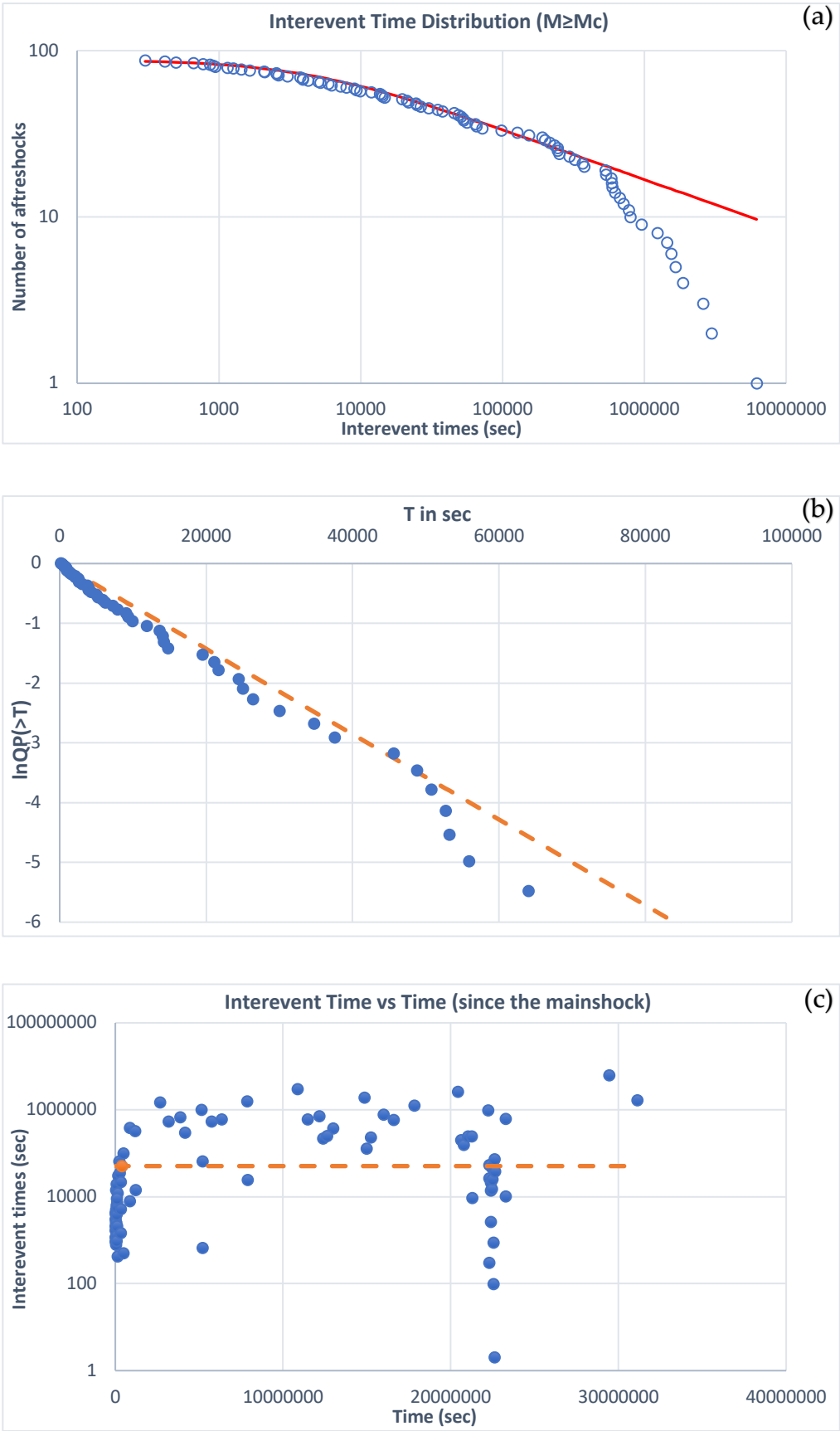

Figure 27. (a) The cumulative distribution function of the interevent times. The red line is the Q-exponential fitting with q = 1.77. **(b)** The Q-logarithmic function of the P(>T) as a function of the interevent times where the dashed line is the fitting with q=1.77. The deviation from the linearity suggests Tc values close to 50,000 s. **(c)** The evolution of interevent time T as a function of time t since the main event. The Tc value is indicated by the dashed line.

4.2.6 The 1995 Kuril'sk Earthquake M_w=7.9 (Russia)

The figure below shows Guttenberg-Richter distribution. The estimated parameters are Mc=5.2, b=1.19 and a=8.33.

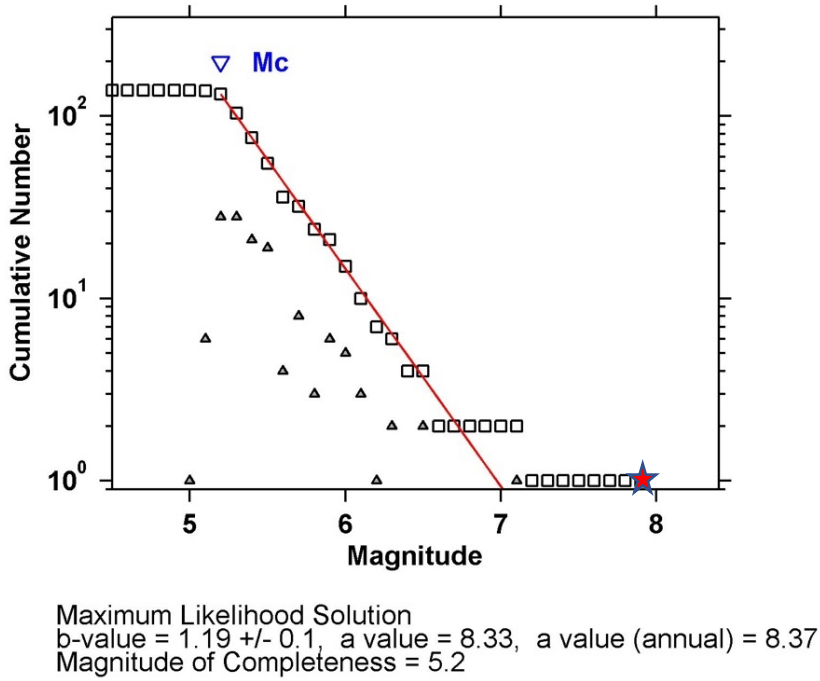

Figure 28. The Guttenberg-Richter distribution using maximum likelihood method with the best combination of maximum curvature M_c 95% and M_c 90% probability. The red star shows the magnitude of the mainshock M_w 7.9.

Next figure (29a) presents the model proposed by the AIC with p1= 1.1, p2=2.7, c1=0.01, c2=0.852, k1=10 and k2= 10, while (29b) presents the model with the lowest RMS and p= 1.06, c= 0.01 and k= 10.5.

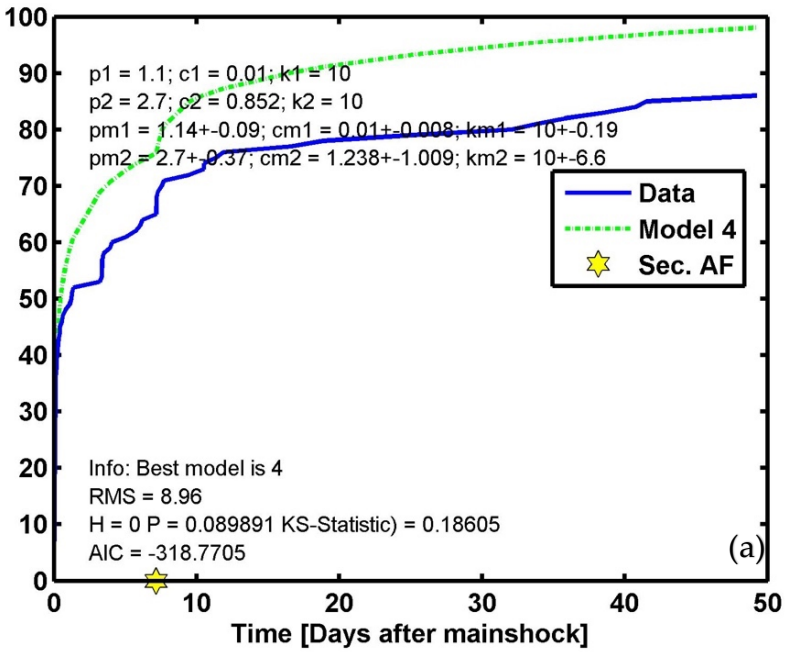

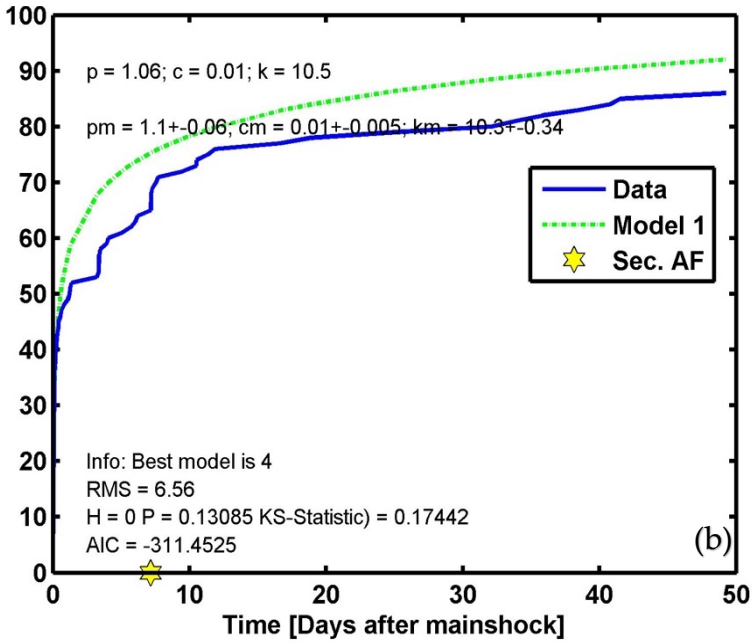

Figure 29. (a) The best model (4) of the estimated curve of the modified Omori formula (dashed line) applied to the aftershock data and the observed cumulative number of aftershocks (solid line) based on the AIC. **(b)** The model 1 of the estimated curve of the modified Omori formula (dashed line) applied to the aftershock data and the observed cumulative number of aftershocks (solid line), with the lowest RMS= 6.56.

Here is the magnitude-time form of the aftershock sequence.

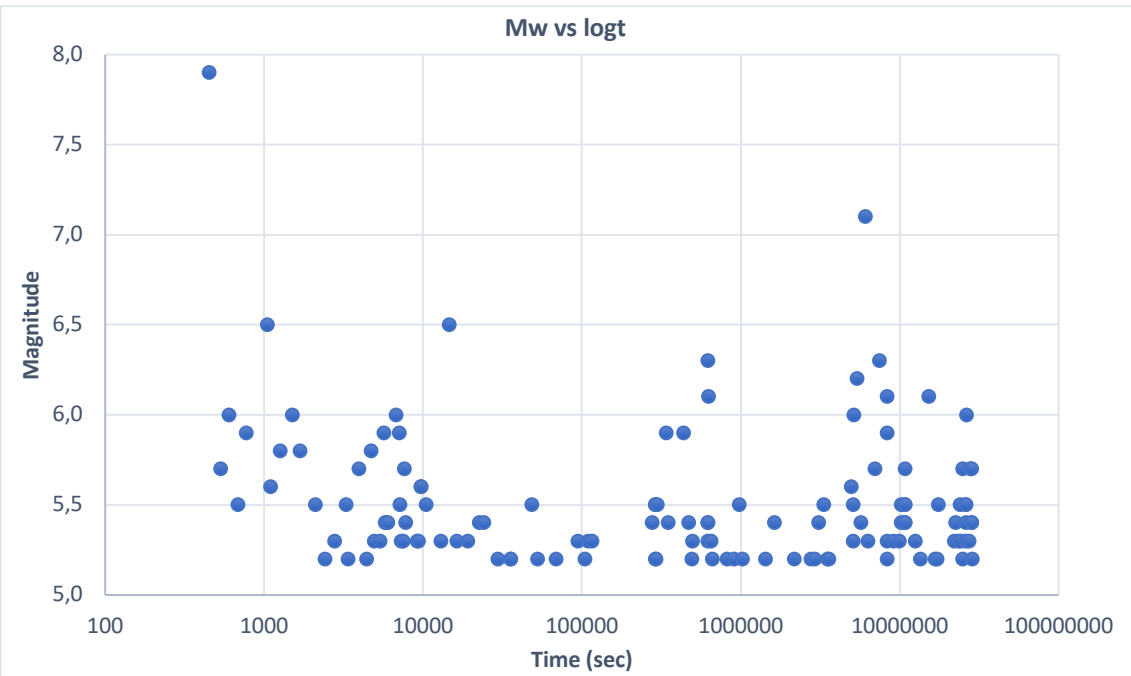

Figure 30. The magnitude-time pattern versus the logarithm of time of the mainshock M_w 7.9.

By the frequency-magnitude distribution for this earthquake, it is estimated a q_M= 1.43 with ci= 1.40-1.47.

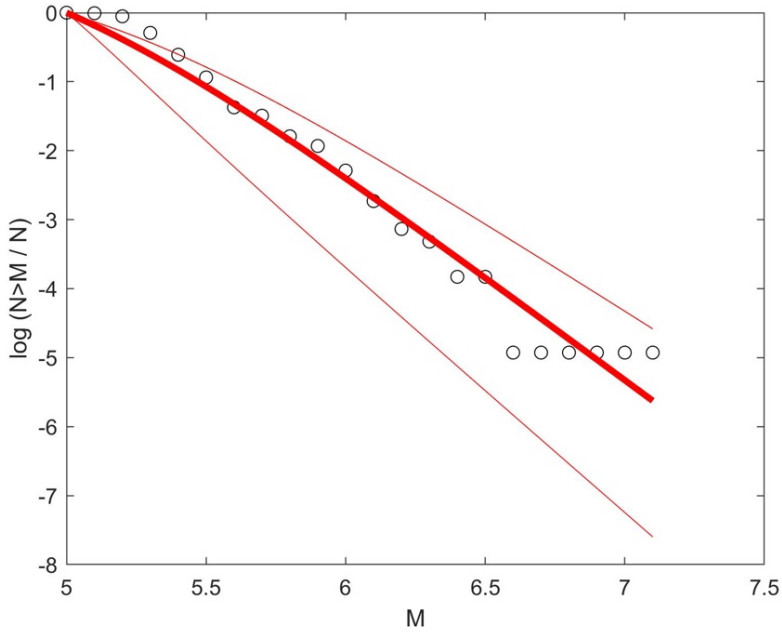

Figure 31. Frequency-magnitude distribution. The bold red line represents the model of equation (26) for qM= 1.43, while the other two lines present the corresponding 95% confidence intervals.

Figure 32 shows the typical Q-exponential pattern and Q-logarithmic function of the cumulative distribution function, P(>T) of the aftershocks interevent times and a q=1.83 is obtained.

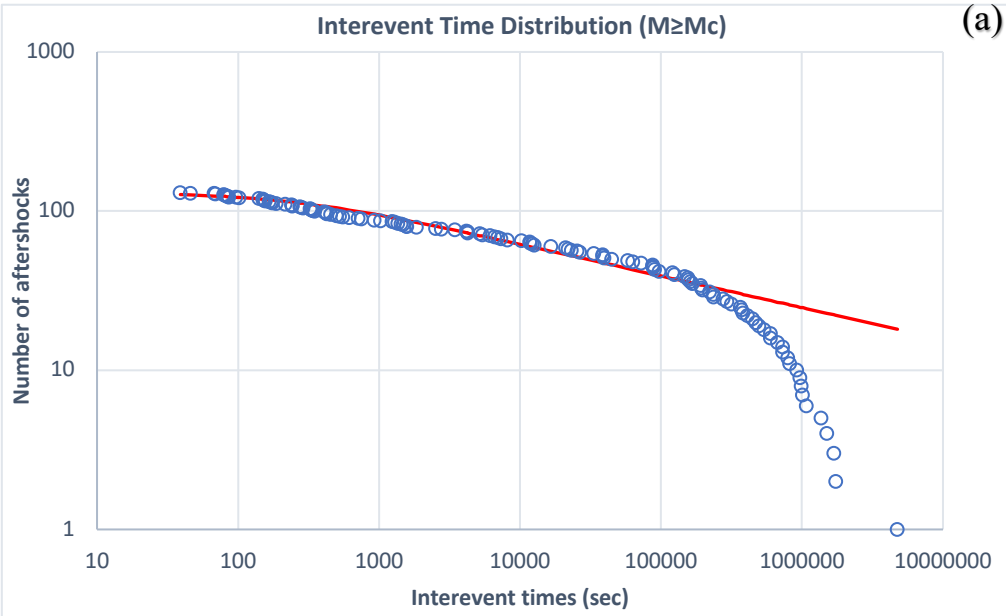

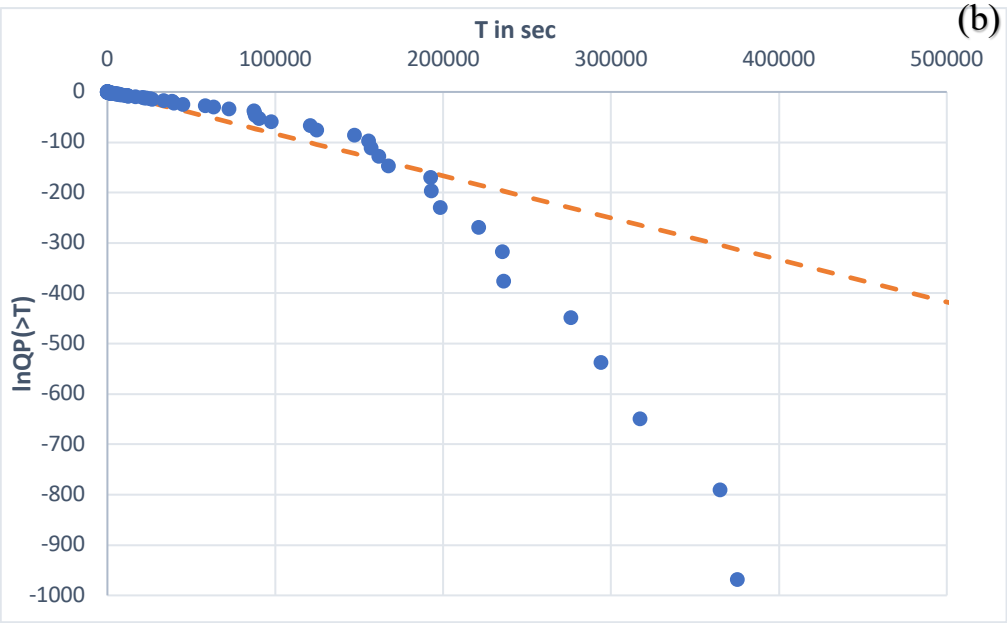

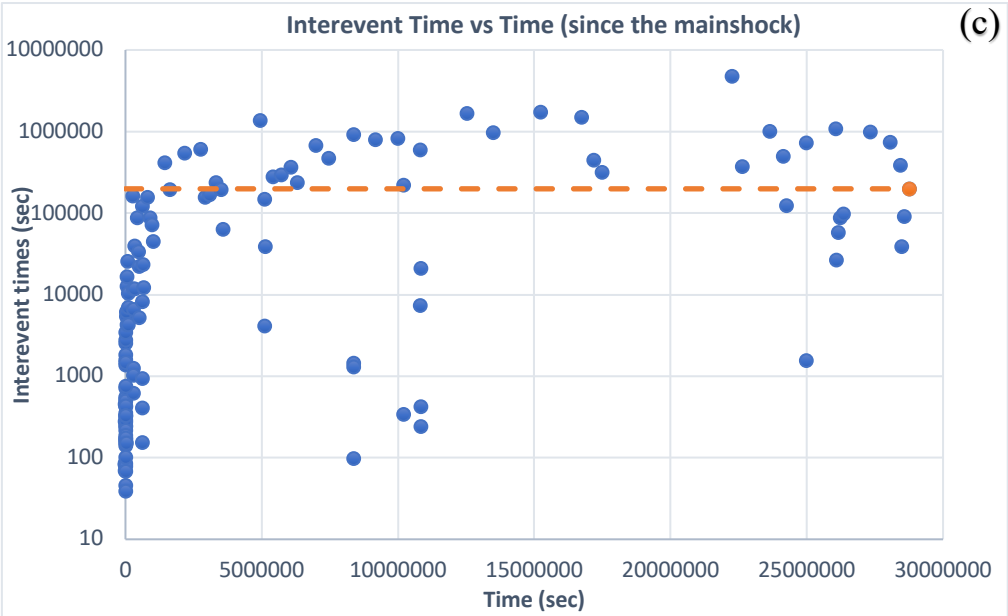

Figure 32. (a) The cumulative distribution function of the interevent times. The red line is the Q-exponential fitting with q = 1.83. **(b)** The Q-logarithmic function of the P(>T) as a function of the interevent times where the dashed line is the fitting with q=1.83. The deviation from the linearity suggests Tc values close to 200,000 s. **(c)** The evolution of interevent time T as a function of time t since the main event. The Tc value is indicated by the dashed line.

4.2.7 The 2000 Bengkulu Earthquake M_w=7.9 (Indonesia)

The figure below shows Guttenberg-Richter distribution. The estimated parameters are Mc=5.2, b=1.49 and a=9.92.

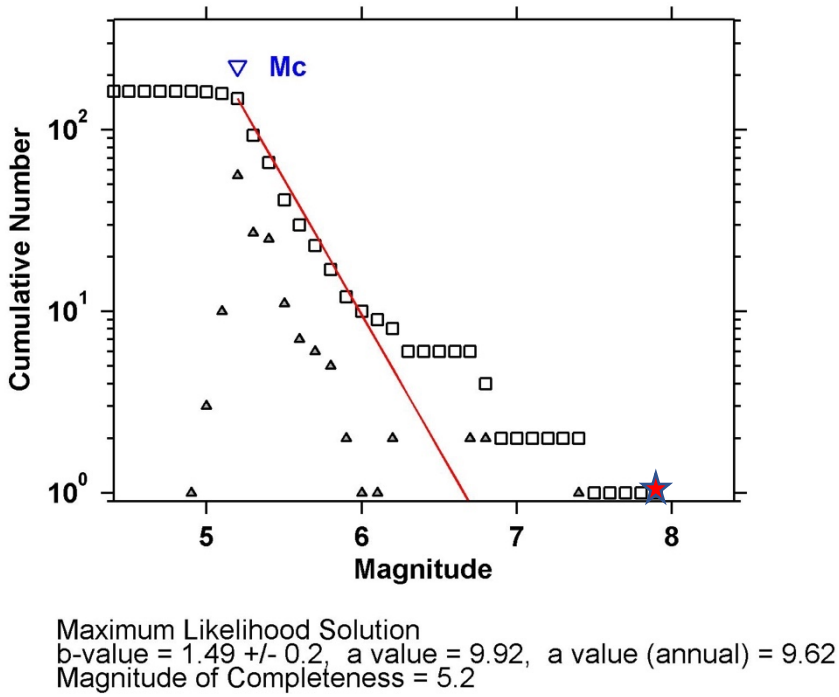

Figure 33. The Guttenberg-Richter distribution using maximum likelihood method with the best combination of maximum curvature M_c 95% and M_c 90% probability. The red star shows the magnitude of the mainshock M_w 7.9.

Next figure (34a) presents the model proposed by the AIC with p1=2.7, p2=0.95, c=0.727, k1=43.3 and k2=10 while (34b) presents the model with the lowest RMS and p1= 2.7, p2=0.95, c1=0.714, c2=0.808, k1=42 and k2= 10.

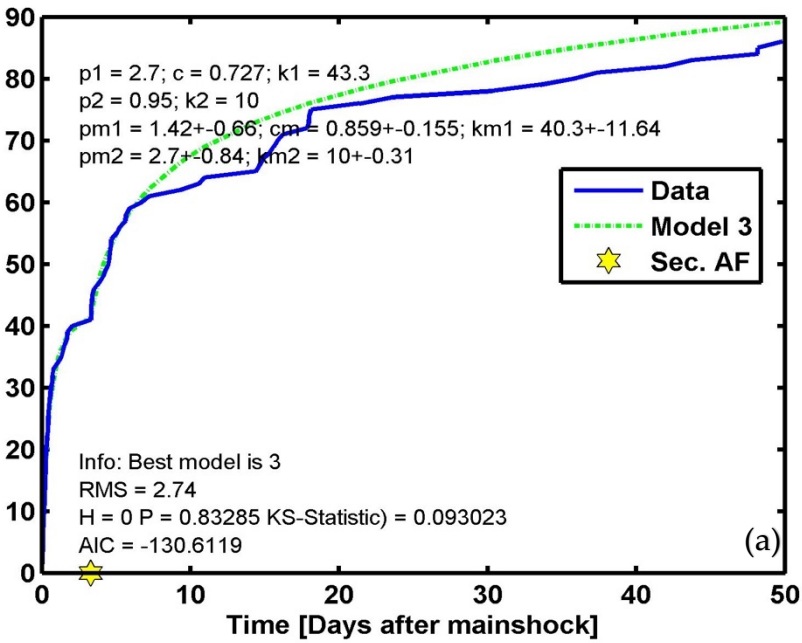

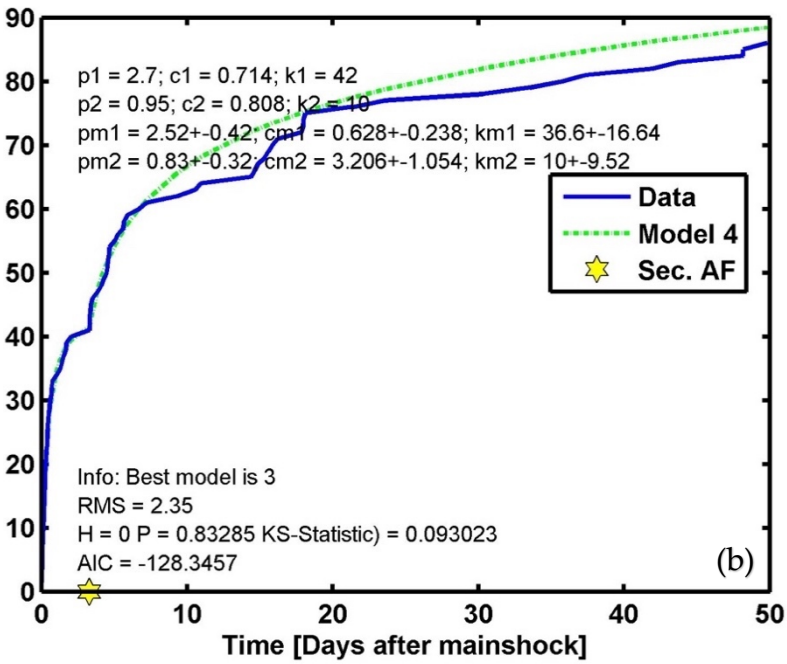

Figure 34. (a) The best model (3) of the estimated curve of the modified Omori formula (dashed line) applied to the aftershock data and the observed cumulative number of aftershocks (solid line) based on the AIC. **(b)** The model 4 of the estimated curve of the modified Omori formula (dashed line) applied to the aftershock data and the observed cumulative number of aftershocks (solid line), with the lowest RMS= 2.35.

Here is the magnitude-time form of the aftershock sequence.

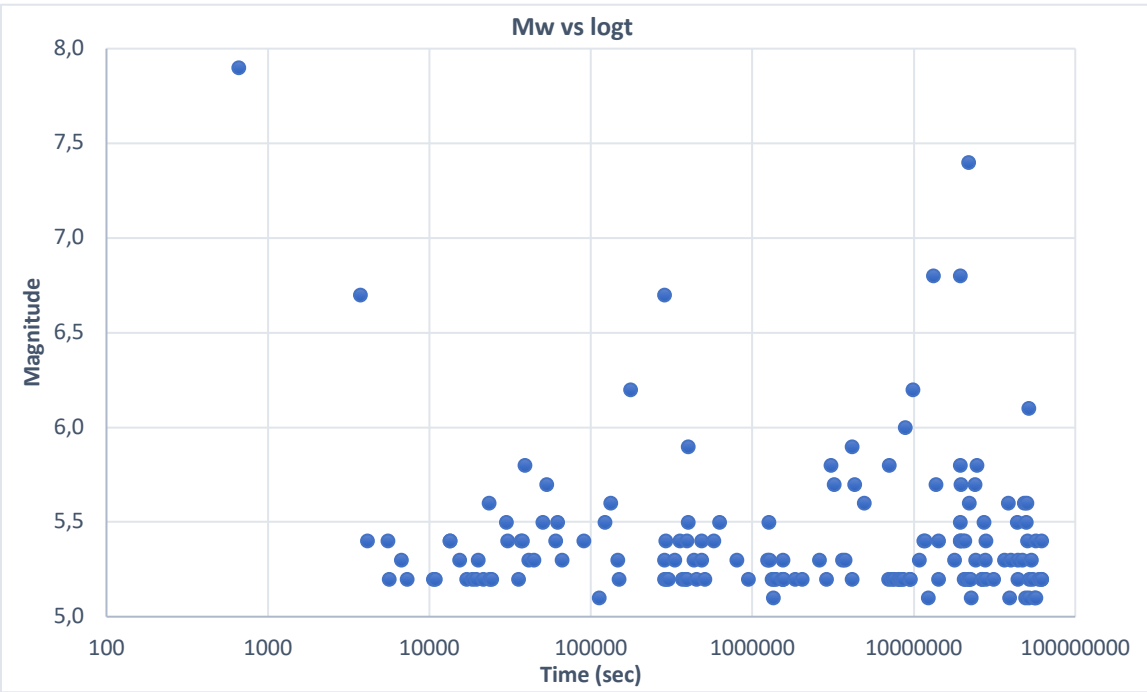

Figure 35. The magnitude-time pattern versus the logarithm of time of the mainshock M_w 7.9.

By the frequency-magnitude distribution for this earthquake, it is estimated a q_M= 1.38 with ci= 1.34-1.42.

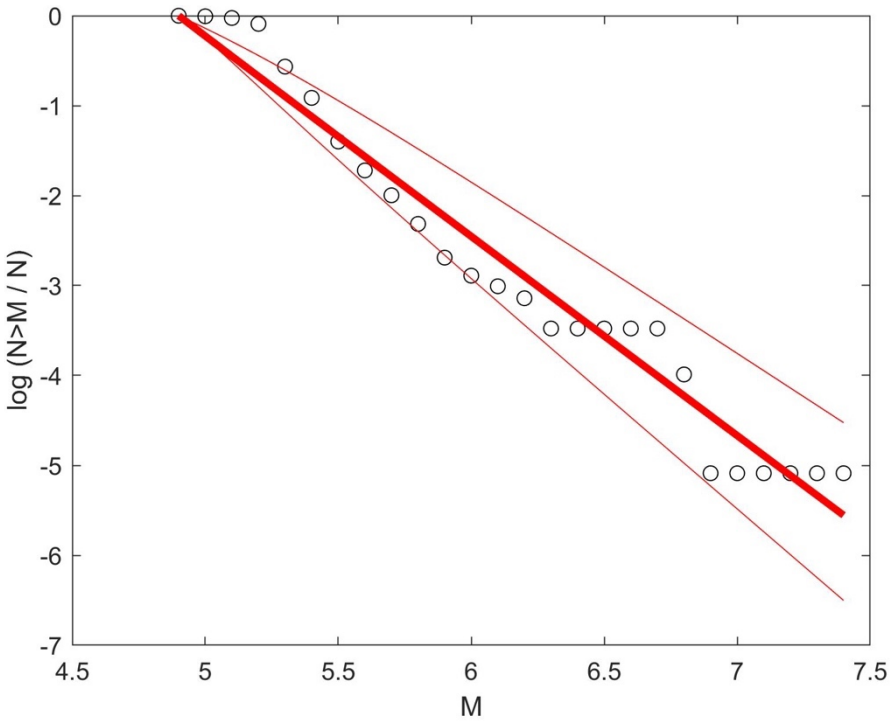

Figure 36. Frequency-magnitude distribution. The bold red line represents the model of equation (26) for qM= 1.38, while the other two lines present the corresponding 95% confidence intervals.

Figure 37 shows the typical Q-exponential pattern and Q-logarithmic function of the cumulative distribution function, P(>T) of the aftershocks interevent times and a q=1.82 is obtained.

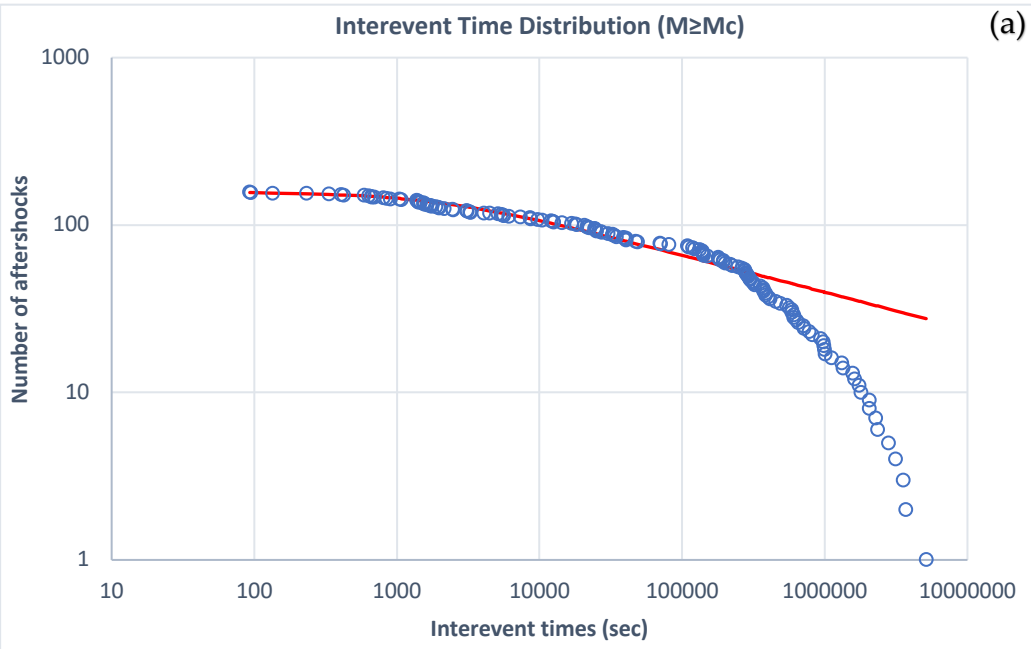

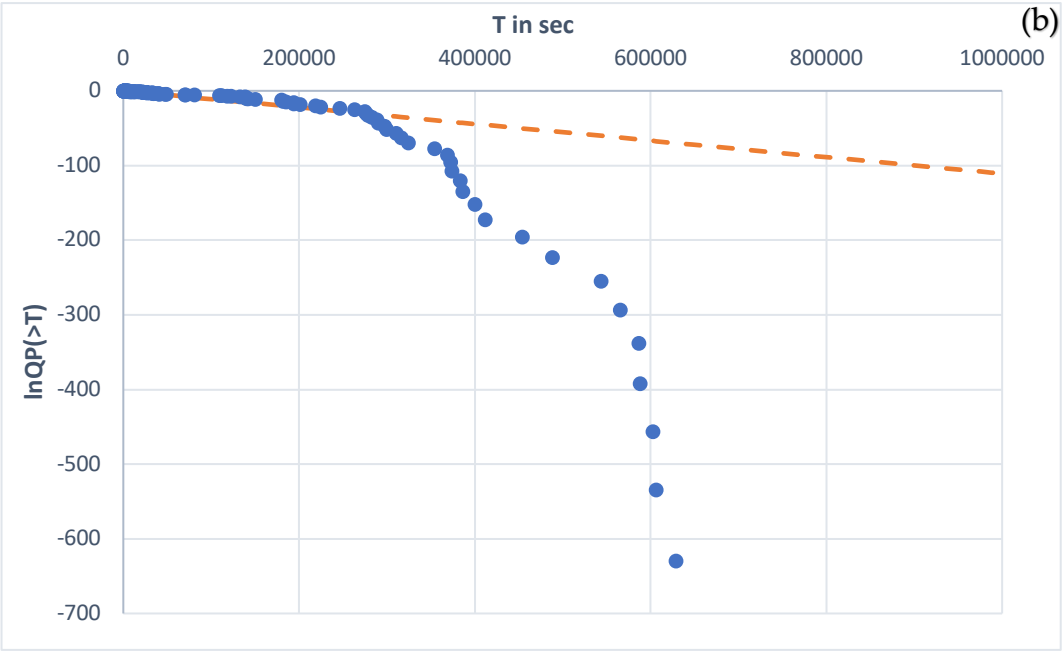

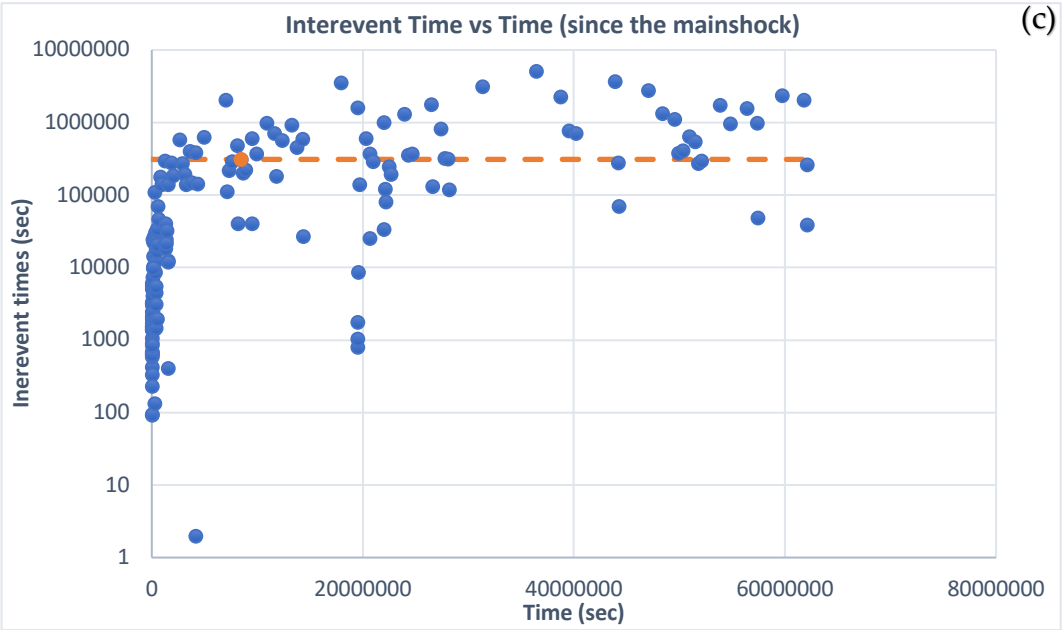

Figure 37. (a) The cumulative distribution function of the interevent times. The red line is the Q-exponential fitting with q = 1.82. **(b)** The Q-logarithmic function of the P(>T) as a function of the interevent times where the dashed line is the fitting with q=1.82. The deviation from the linearity suggests Tc values close to 400,000 s. **(c)** The evolution of interevent time T as a function of time t since the main event. The Tc value is indicated by the dashed line.

4.2.8 The 2000 Rabaul Earthquake M_w=8.0 (Papua New Guinea)

The figure below shows Guttenberg-Richter distribution. The estimated parameters are Mc=5.5, b=1.32 and a=9.17.

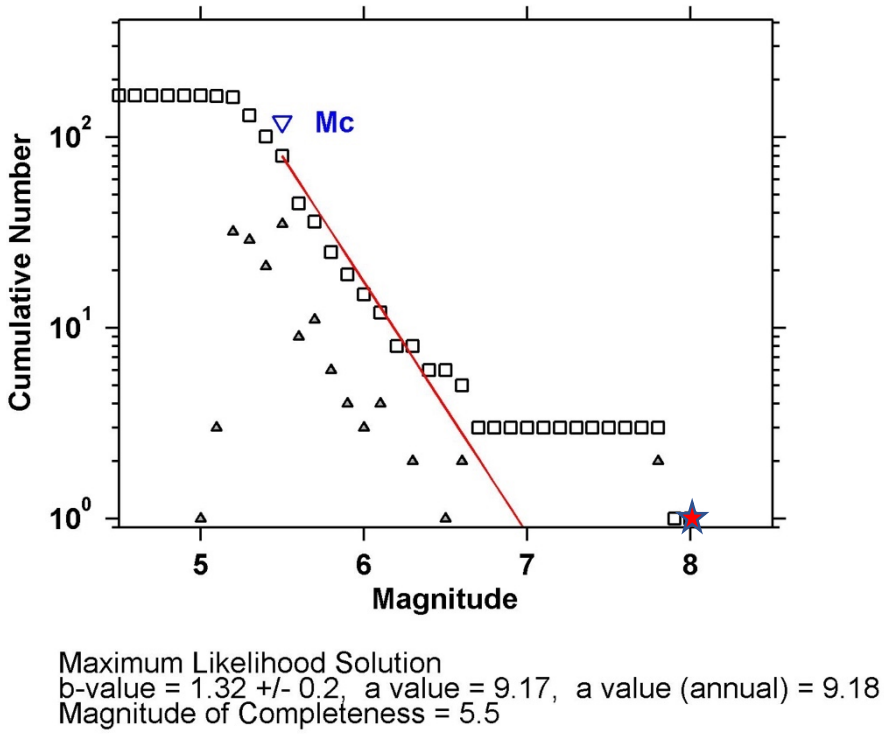

Figure 38. The Guttenberg-Richter distribution using maximum likelihood method with the best combination of maximum curvature M_c 95% and M_c 90% probability. The red star shows the magnitude of the mainshock M_w 8.0.

Next figure (39a) presents the model proposed by the AIC with p1= 2.7, p2=1.03, c1=0.568, k1= 64.9 and k2=15.8 while (39b) presents the model with the lowest RMS and p1= 1.45, c=0.364, k1=41.6 and k2= 10.

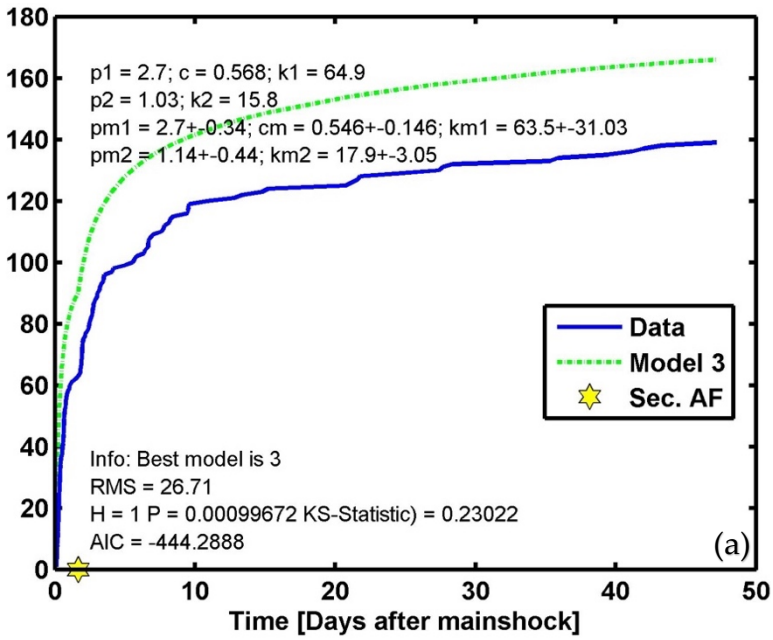

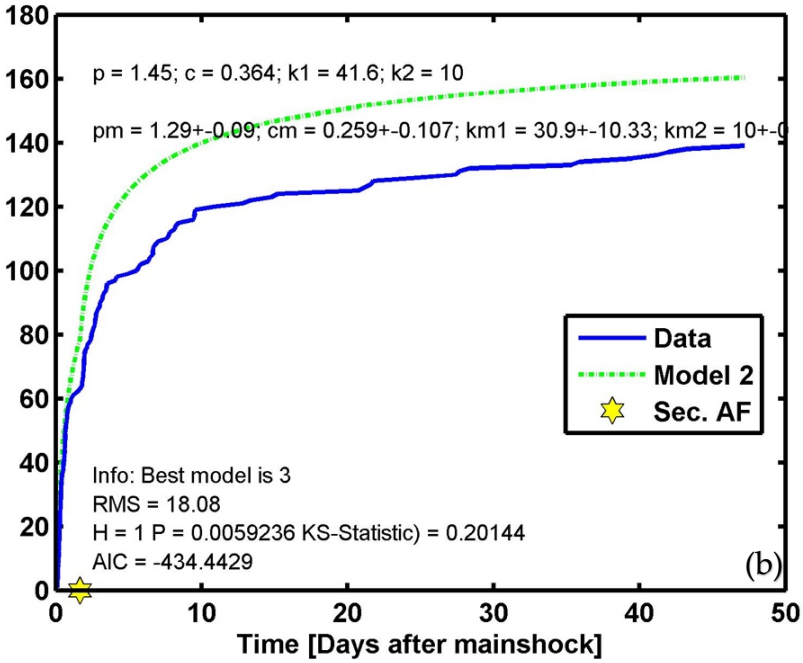

Figure 39. (a) The best model (3) of the estimated curve of the modified Omori formula (dashed line) applied to the aftershock data and the observed cumulative number of aftershocks (solid line) based on the AIC. **(b)** The model 2 of the estimated curve of the modified Omori formula (dashed line) applied to the aftershock data and the observed cumulative number of aftershocks (solid line), with the lowest RMS= 18.08.

Here is the magnitude-time form of the aftershock sequence.

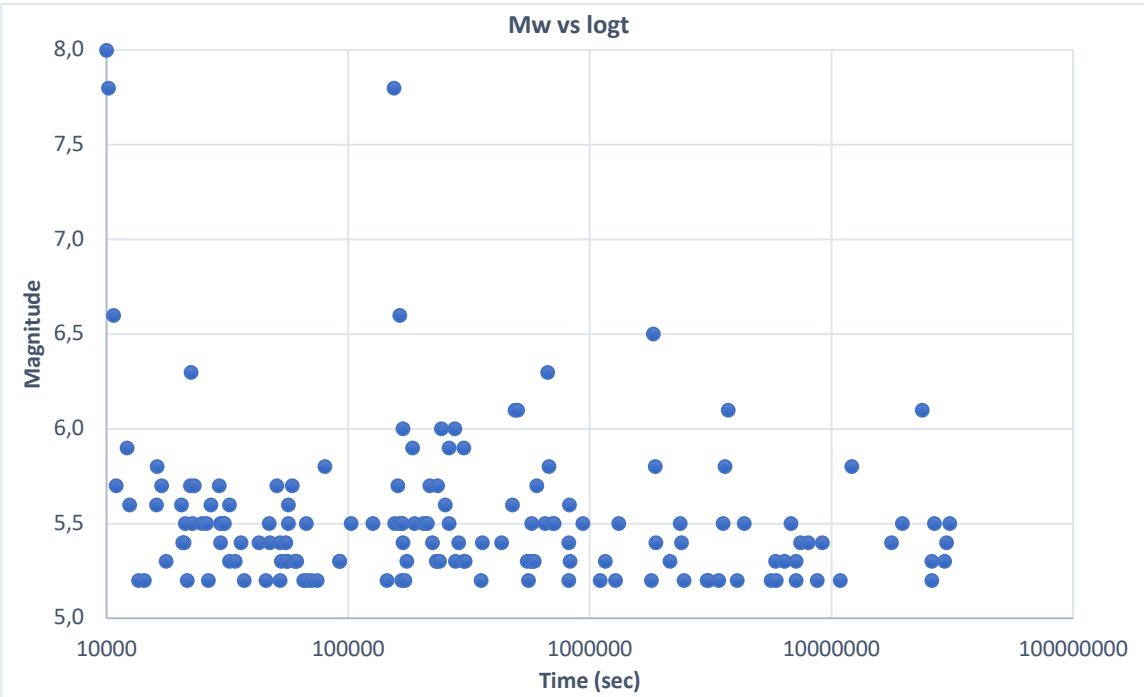

Figure 40. The magnitude-time pattern versus the logarithm of time of the mainshock M_w 8.0.

By the frequency-magnitude distribution for this earthquake, it is estimated a q_M= 1.38 with ci= 1.34-1.42.

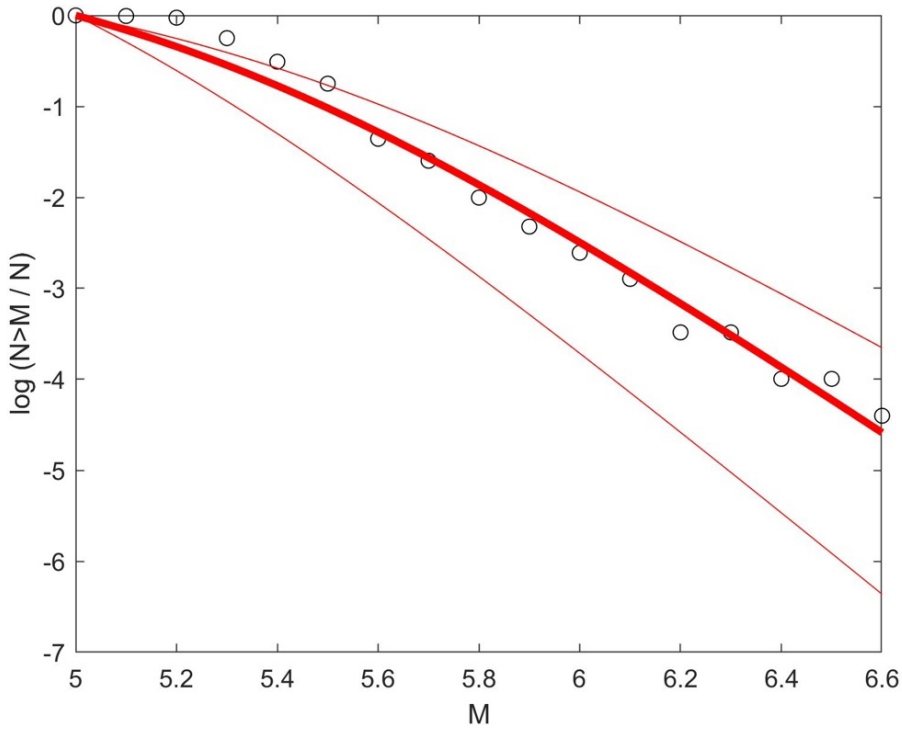

Figure 41. Frequency-magnitude distribution. The bold red line represents the model of equation (26) for qM= 1.38, while the other two lines present the corresponding 95% confidence intervals.

Figure 42 shows the typical Q-exponential pattern and Q-logarithmic function of the cumulative distribution function, P(>T) of the aftershocks interevent times and a q=1.69 is obtained.

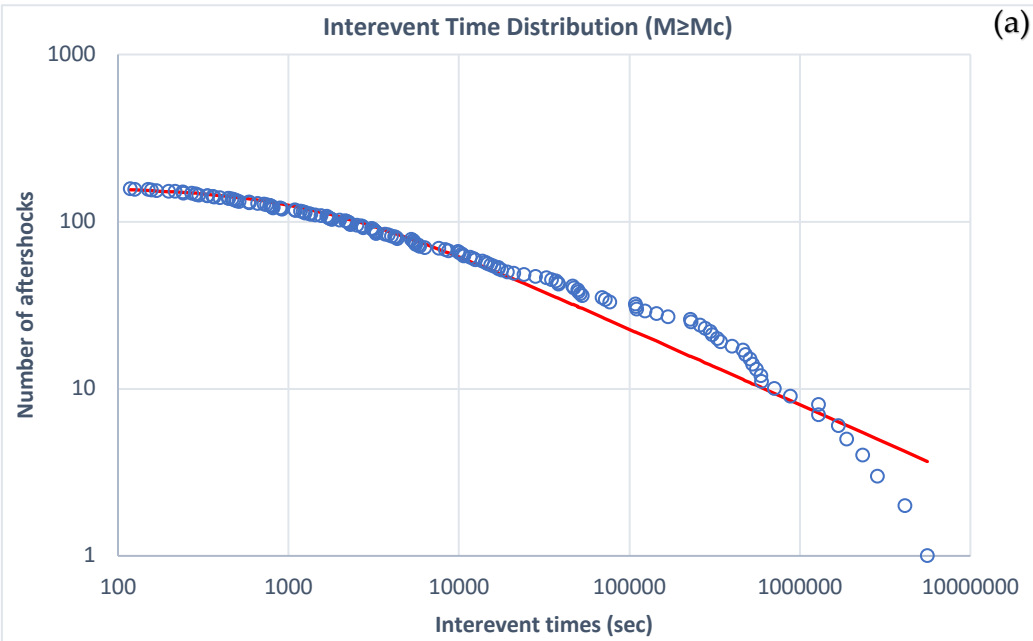

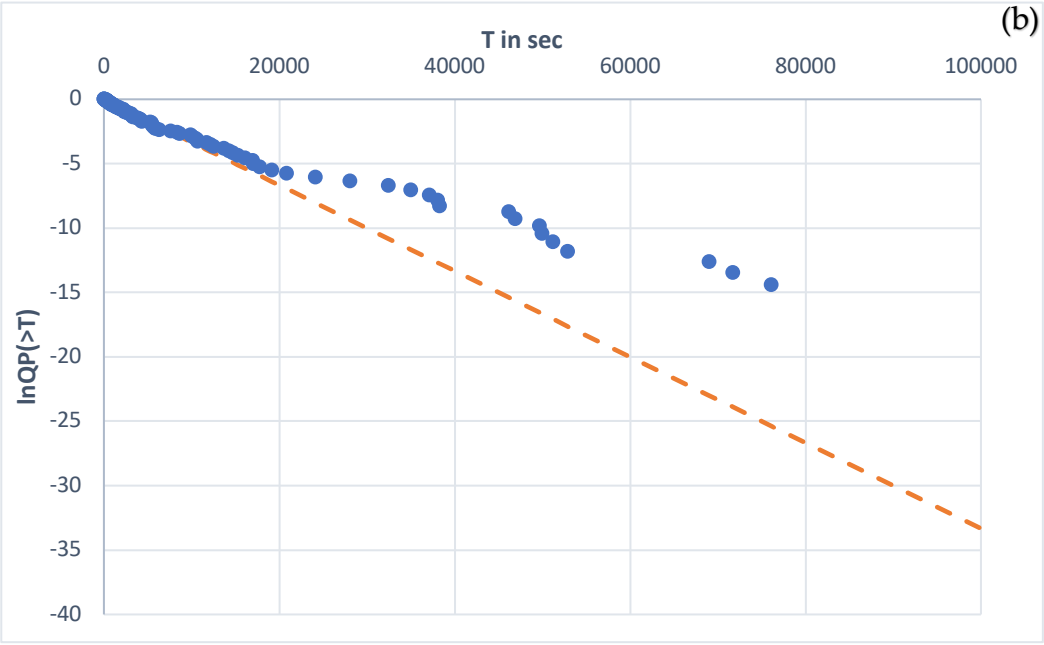

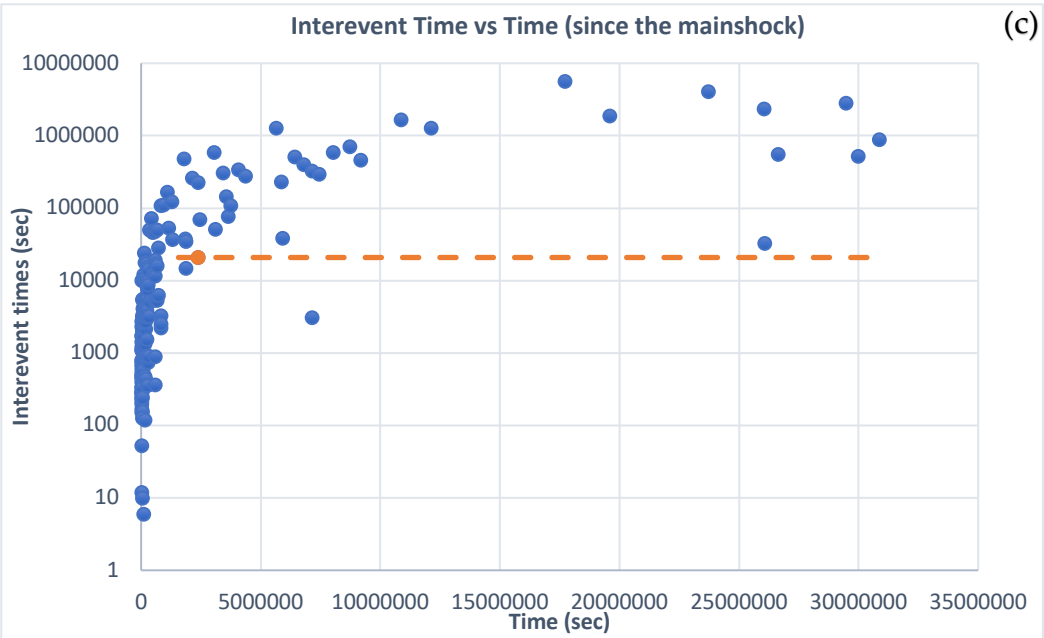

Figure 42. (a) The cumulative distribution function of the interevent times. The red line is the Q-exponential fitting with q = 1.69. **(b)** The Q-logarithmic function of the P(>T) as a function of the interevent times where the dashed line is the fitting with q=1.69. The deviation from the linearity suggests Tc values close to 20,000 s. **(c)** The evolution of interevent time T as a function of time t since the main event. The Tc value is indicated by the dashed line.

4.2.9 The 2001 Atico Earthquake M_w=8.4 (Peru)

The figure below shows Guttenberg-Richter distribution. The estimated parameters are Mc=5.2, b=1.41 and a=9.38.

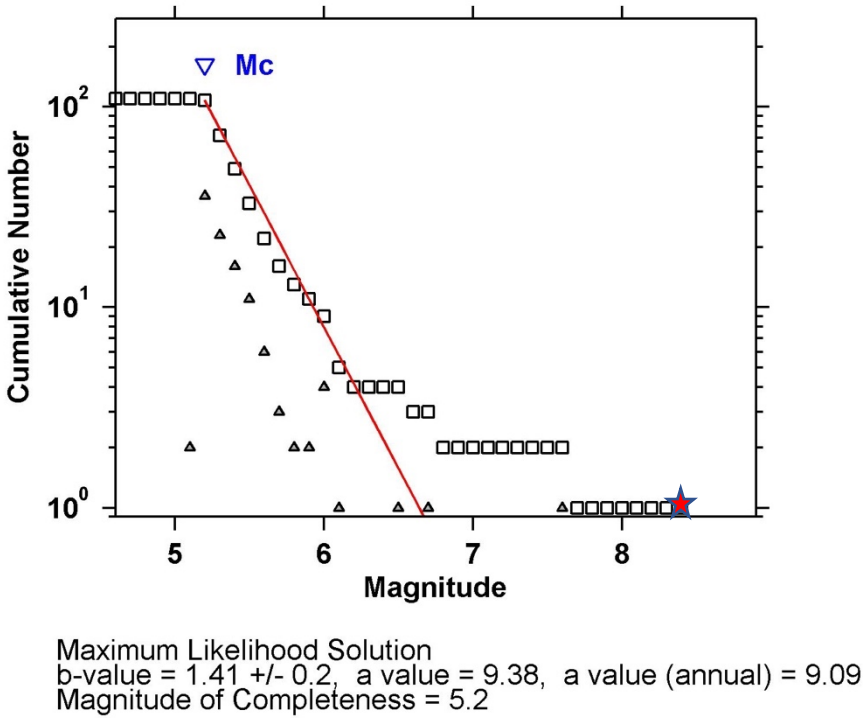

Figure 43. The Guttenberg-Richter distribution using maximum likelihood method with the best combination of maximum curvature M_c 95% and M_c 90% probability. The red star shows the magnitude of the mainshock M_w 8.4.

Next figure (44a) presents the model proposed by the AIC with p1= 1.39, p2=2.7 c1= 0.134, c2=0.645 and k1= 16.6, k2=10 while (44b) presents the model with the lowest RMS and p= 1.96, c=0.545, k1=43.6 and k2= 10.

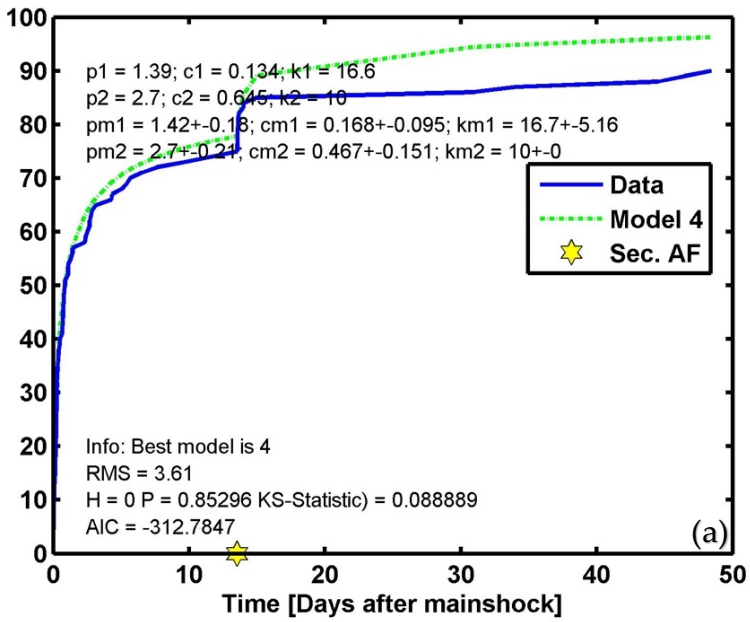

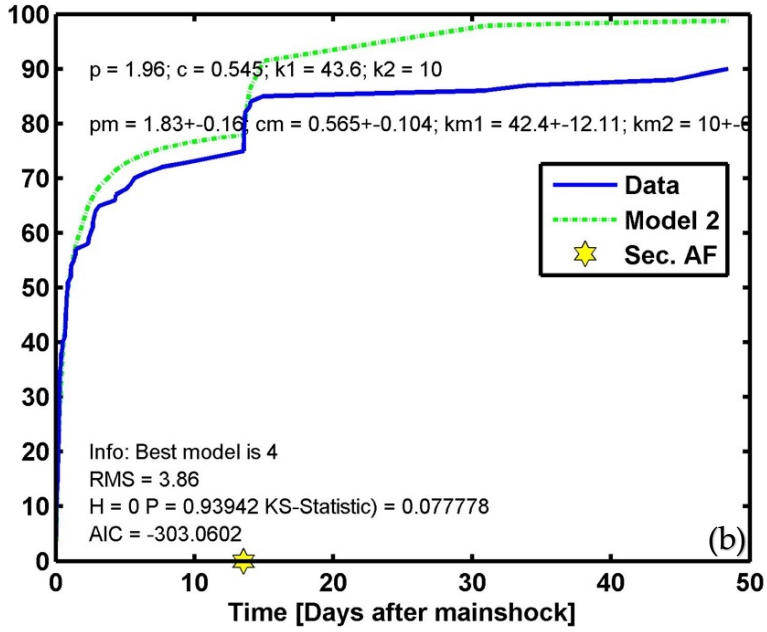

Figure 44. (a) The best model (4) of the estimated curve of the modified Omori formula (dashed line) applied to the aftershock data and the observed cumulative number of aftershocks (solid line) based on the AIC. **(b)** The model 2 of the estimated curve of the modified Omori formula (dashed line) applied to the aftershock data and the observed cumulative number of aftershocks (solid line), with the lowest RMS= 3.86.

Here is the magnitude-time form of the aftershock sequence.

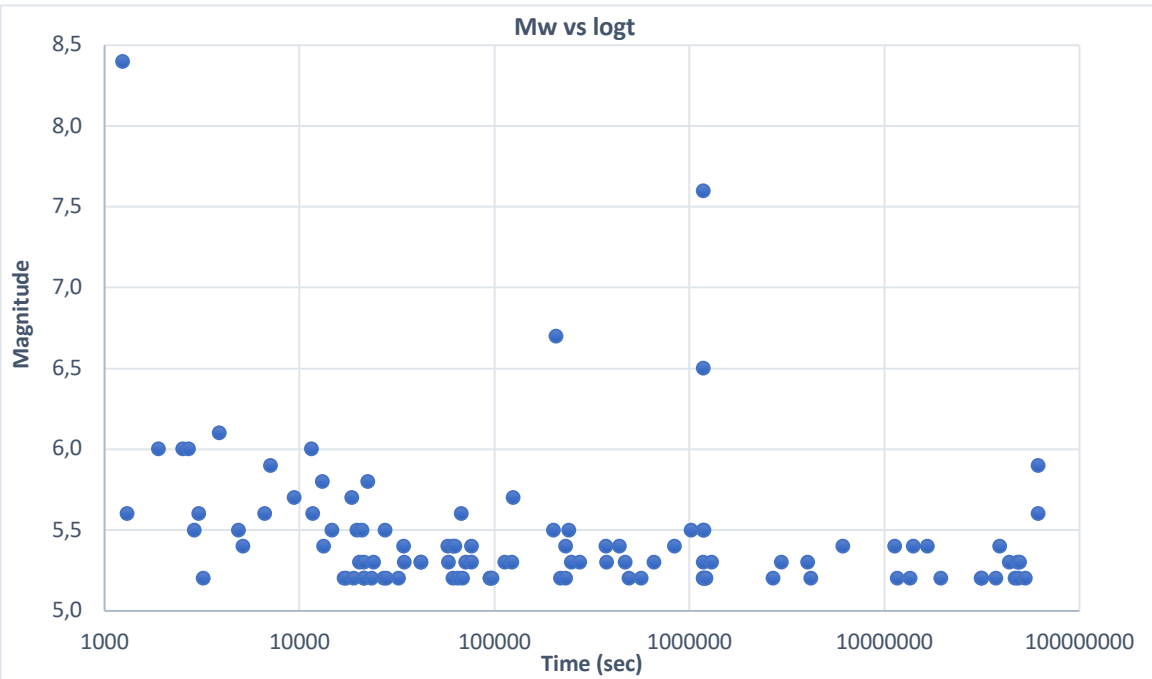

Figure 45. The magnitude-time pattern versus the logarithm of time of the mainshock M_w 8.4.

By the frequency-magnitude distribution for this earthquake, it is estimated a q_M= 1.42 with ci= 1.38-1.47.

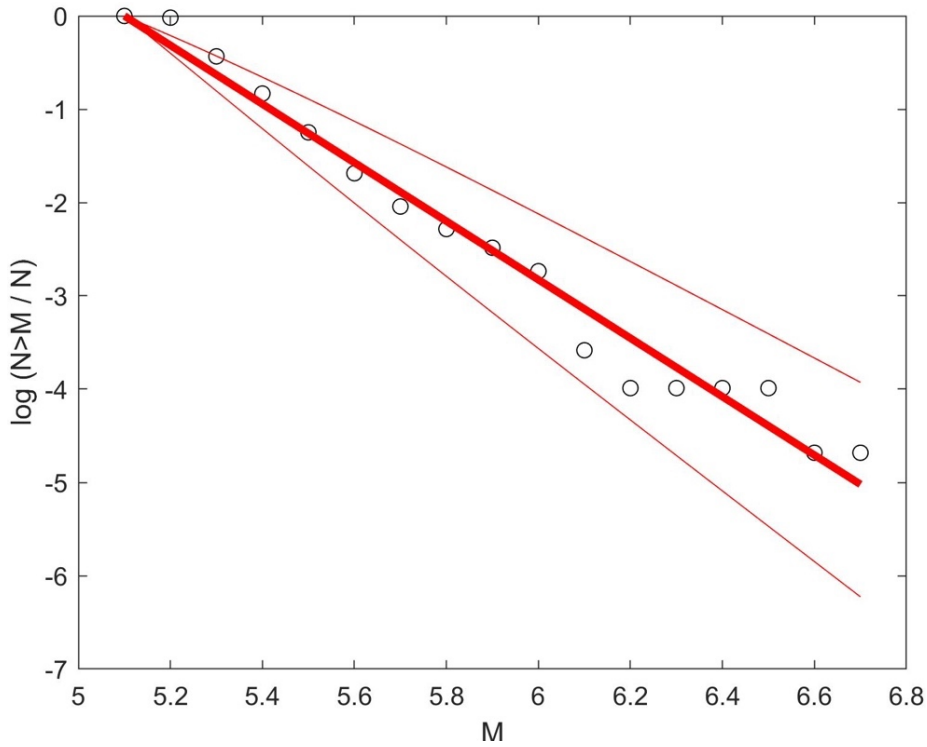

Figure 46. Frequency-magnitude distribution. The bold red line represents the model of equation (26) for qM= 1.42, while the other two lines present the corresponding 95% confidence intervals.

Figure 47 shows the typical Q-exponential pattern and Q-logarithmic function of the cumulative distribution function, P(>T) of the aftershocks interevent times and a q=1.80 is obtained.

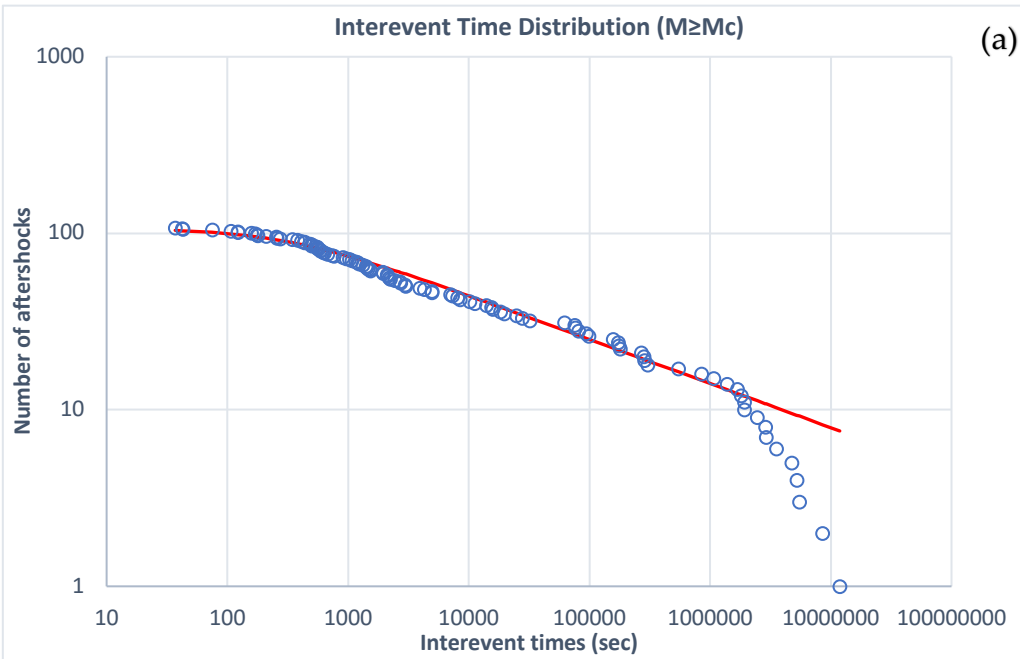

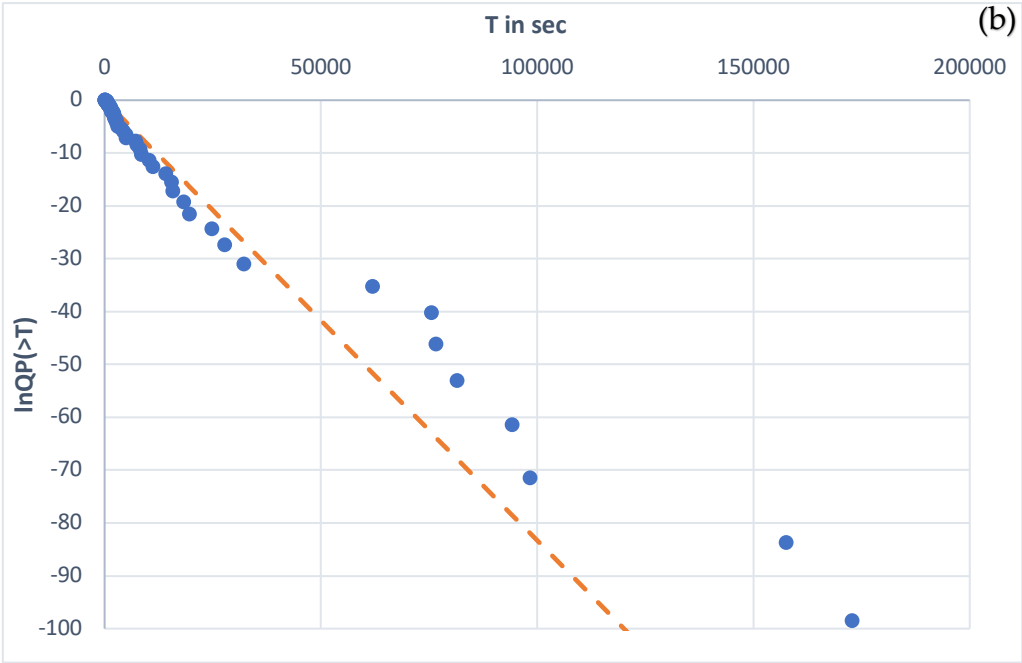

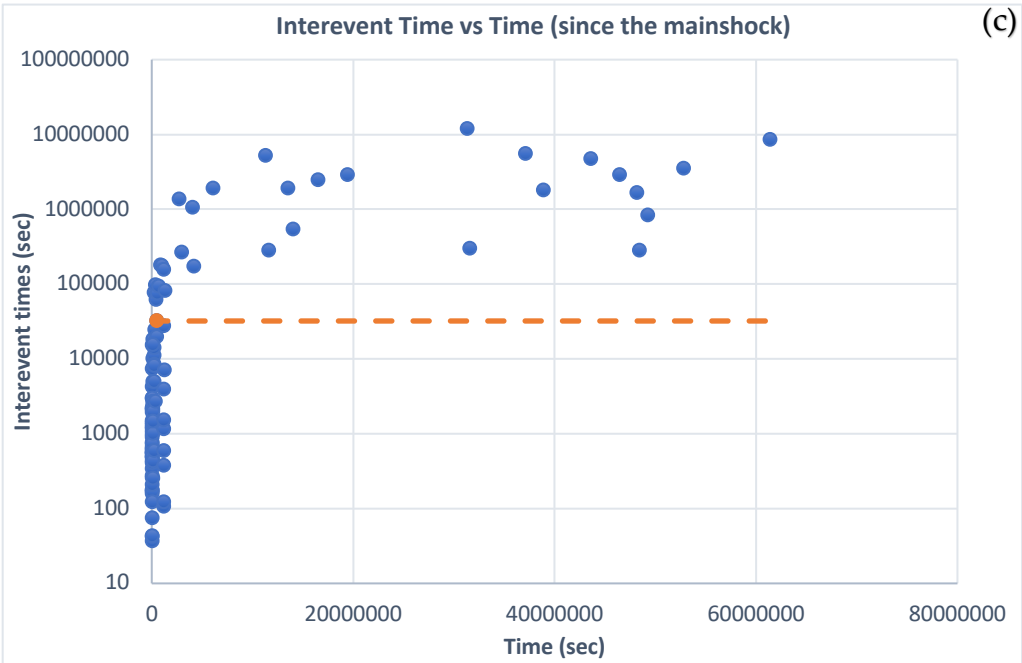

Figure 47. (a) The cumulative distribution function of the interevent times. The red line is the Q-exponential fitting with q = 1.80. **(b)** The Q-logarithmic function of the P(>T) as a function of the interevent times where the dashed line is the fitting with q=1.80. The deviation from the linearity suggests Tc values close to 40,000 s. **(c)** The evolution of interevent time T as a function of time t since the main event. The Tc value is indicated by the dashed line.

4.2.10 The 2003 Kushiro Earthquake M_w=8.3 (Japan)

The figure below shows Guttenberg-Richter distribution. The estimated parameters are Mc=5.1, b=0.87 and a=6.41.

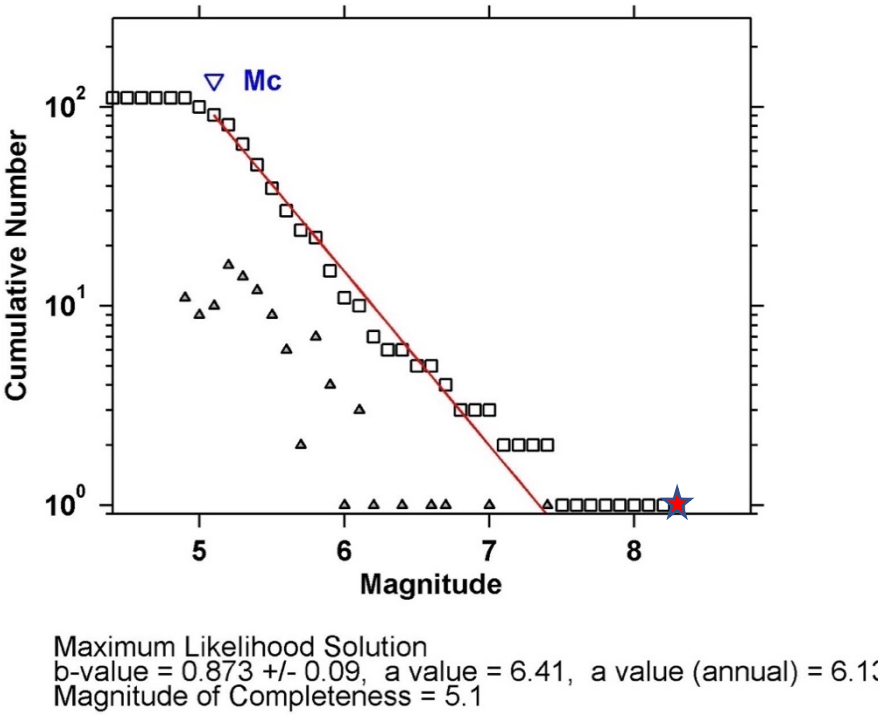

Figure 48. The Guttenberg-Richter distribution using maximum likelihood method with the best combination of maximum curvature M_c 95% and M_c 90% probability. The red star shows the magnitude of the mainshock M_w 8.3.

Next figure (49a) presents the model proposed by the AIC with p= 0.92, c= 0.063 and k= 10 while (49b) presents the model with the lowest RMS and p1= 1.33, p2=2.63, c=1.052, k1=26.3 and k2= 10.

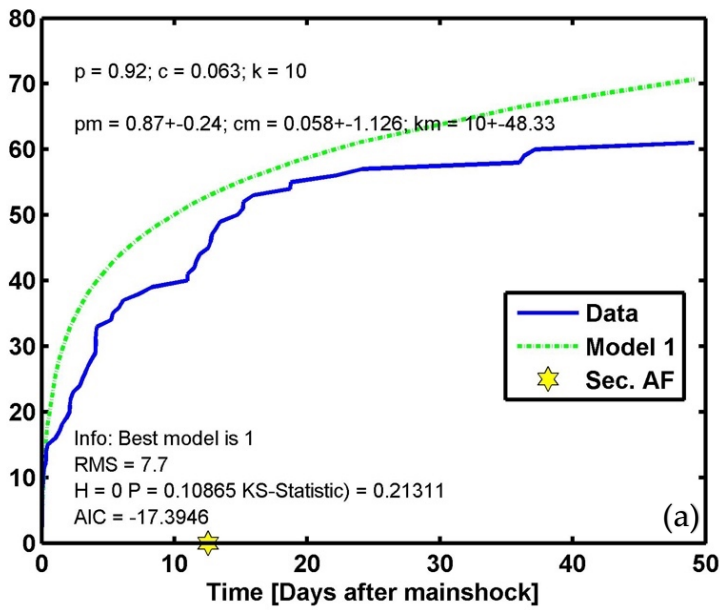

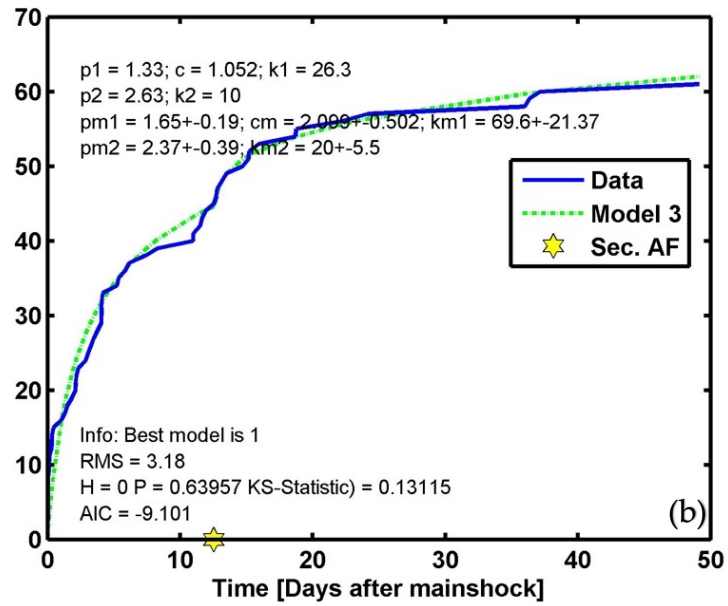

Figure 49. (a) The best model (1) of the estimated curve of the modified Omori formula (dashed line) applied to the aftershock data and the observed cumulative number of aftershocks (solid line) based on the AIC. **(b)** The model 3 of the estimated curve of the modified Omori formula (dashed line) applied to the aftershock data and the observed cumulative number of aftershocks (solid line), with the lowest RMS= 3.18.

Here is the magnitude-time form of the aftershock sequence.

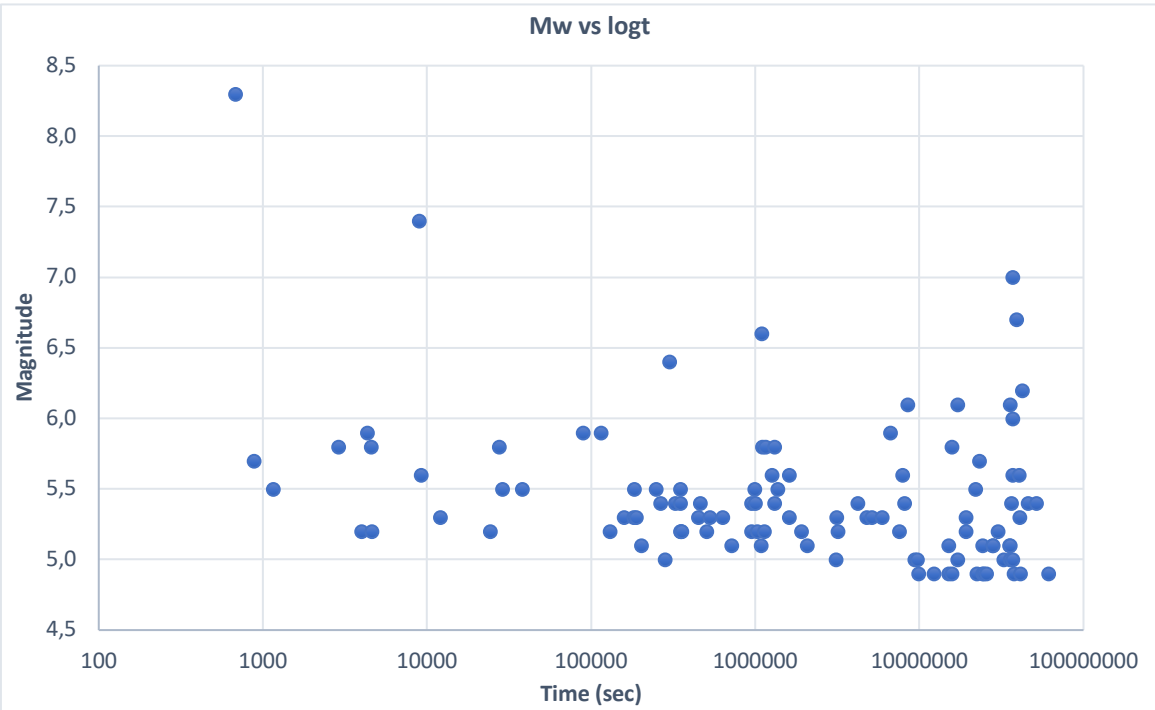

Figure 50. The magnitude-time pattern versus the logarithm of time of the mainshock M_w 8.3.

By the frequency-magnitude distribution for this earthquake, it is estimated a q_M= 1.53 with ci= 1.51-1.55.

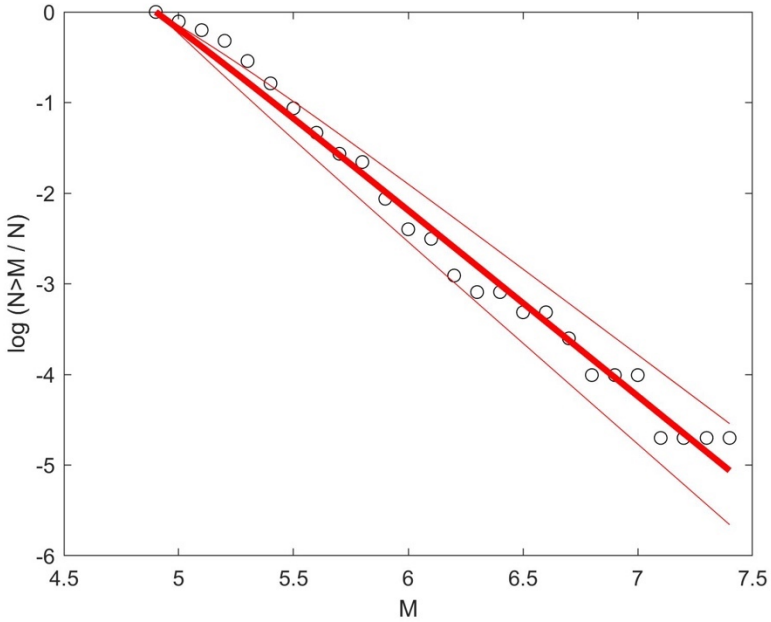

Figure 51. Frequency-magnitude distribution. The bold red line represents the model of equation (26) for qM= 1.53, while the other two lines present the corresponding 95% confidence intervals.

Figure 52 shows the typical Q-exponential pattern and Q-logarithmic function of the cumulative distribution function, P(>T) of the aftershocks interevent times and a q=1.78 is obtained.

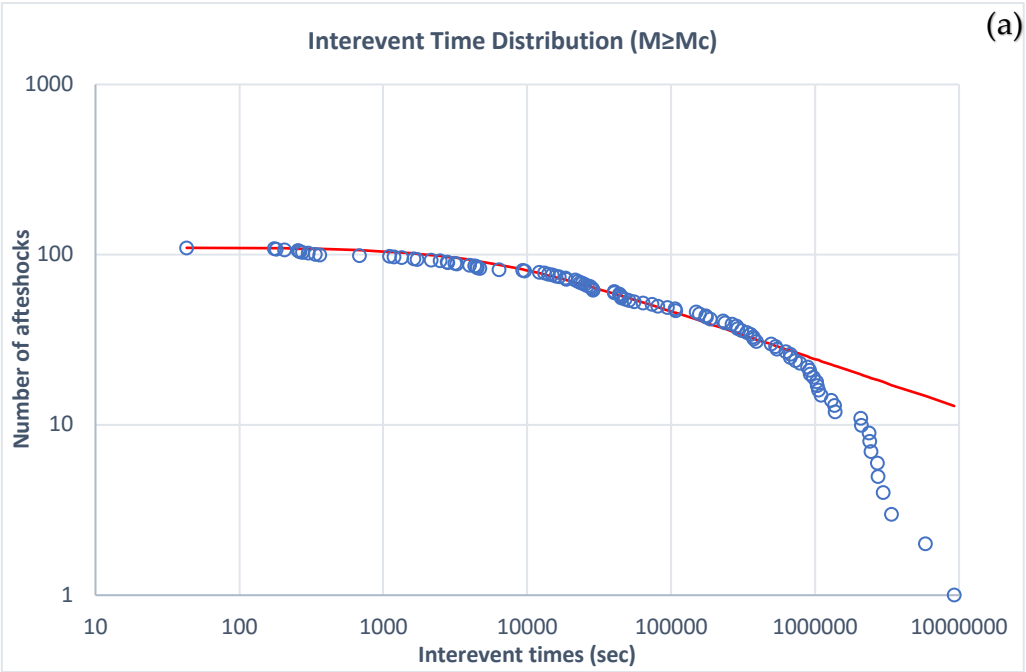

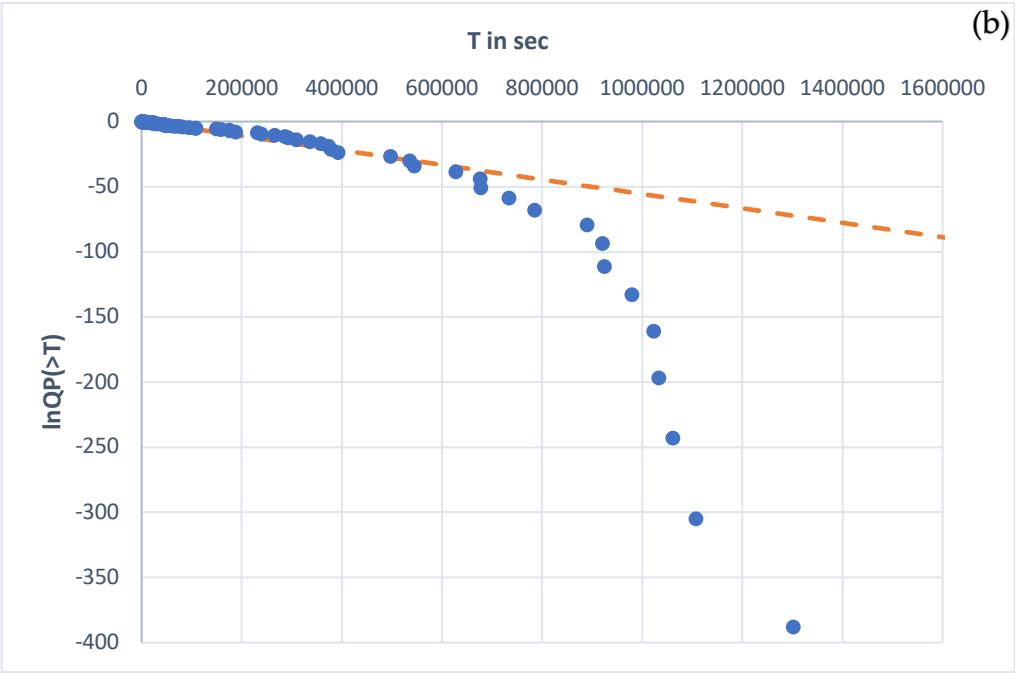

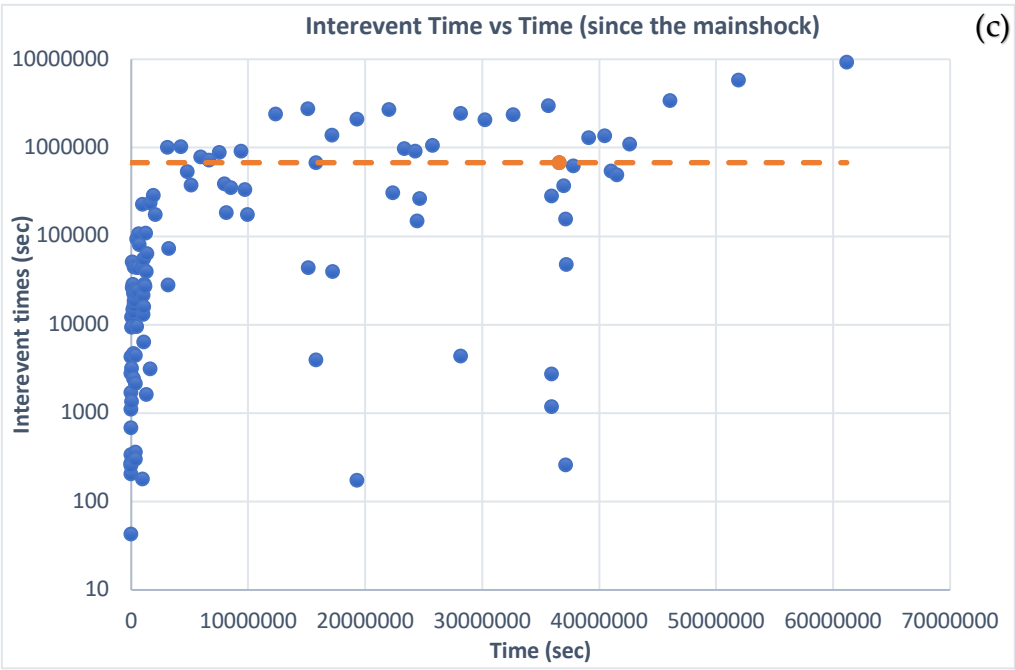

Figure 52. (a) The cumulative distribution function of the interevent times. The red line is the Q-exponential fitting with q = 1.78. **(b)** The Q-logarithmic function of the P(>T) as a function of the interevent times where the dashed line is the fitting with q=1.78. The deviation from the linearity suggests Tc values close to 700,000 s. **(c)** The evolution of interevent time T as a function of time t since the main event. The Tc value is indicated by the dashed line.

4.2.11 The 2004 Sumatra-Andaman Islands Earthquake M_w=9.0

The figure below shows Guttenberg-Richter distribution. The estimated parameters are Mc=5.1, b=1.21 and a=8.65.

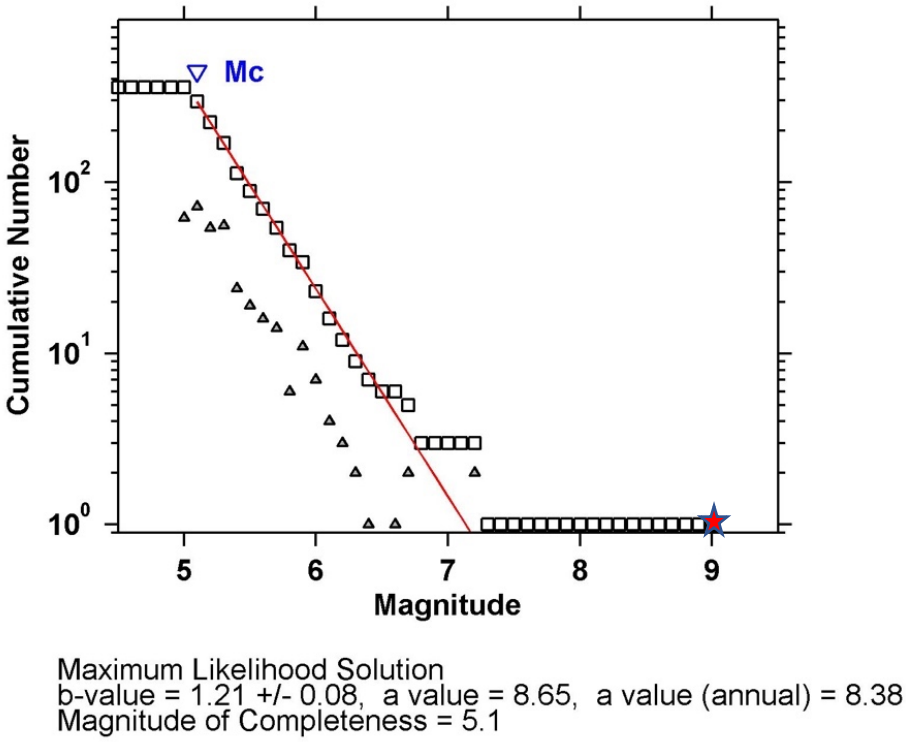

Figure 53. The Guttenberg-Richter distribution using maximum likelihood method with the best combination of maximum curvature M_c 95% and M_c 90% probability. The red star shows the magnitude of the mainshock M_w 9.0.

Next figure (54a) presents the model proposed by the AIC with p1= 2.7, p2=0.95, c= 0.727, k1=43.4 and k2= 10 while (54b) presents the model with the lowest RMS and p= 1, c=0.116 and k= 14.3.

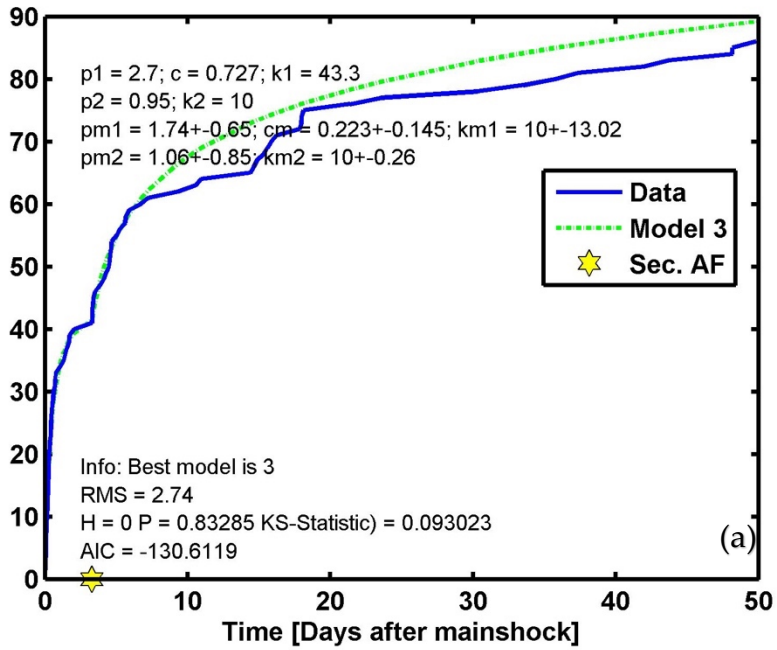

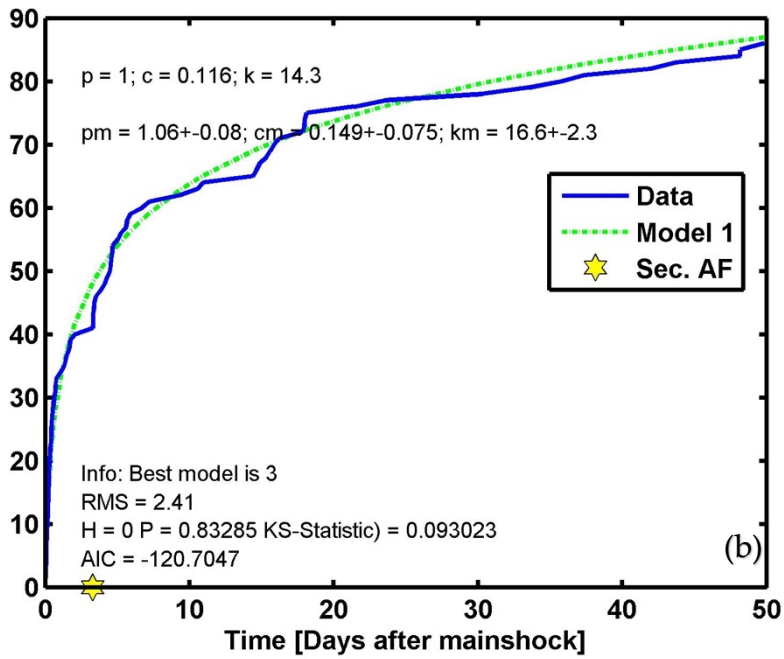

Figure 54. (a) The best model (3) of the estimated curve of the modified Omori formula (dashed line) applied to the aftershock data and the observed cumulative number of aftershocks (solid line) based on the AIC. **(b)** The model 1 of the estimated curve of the modified Omori formula (dashed line) applied to the aftershock data and the observed cumulative number of aftershocks (solid line), with the lowest RMS= 2.41.

Here is the magnitude-time form of the aftershock sequence.

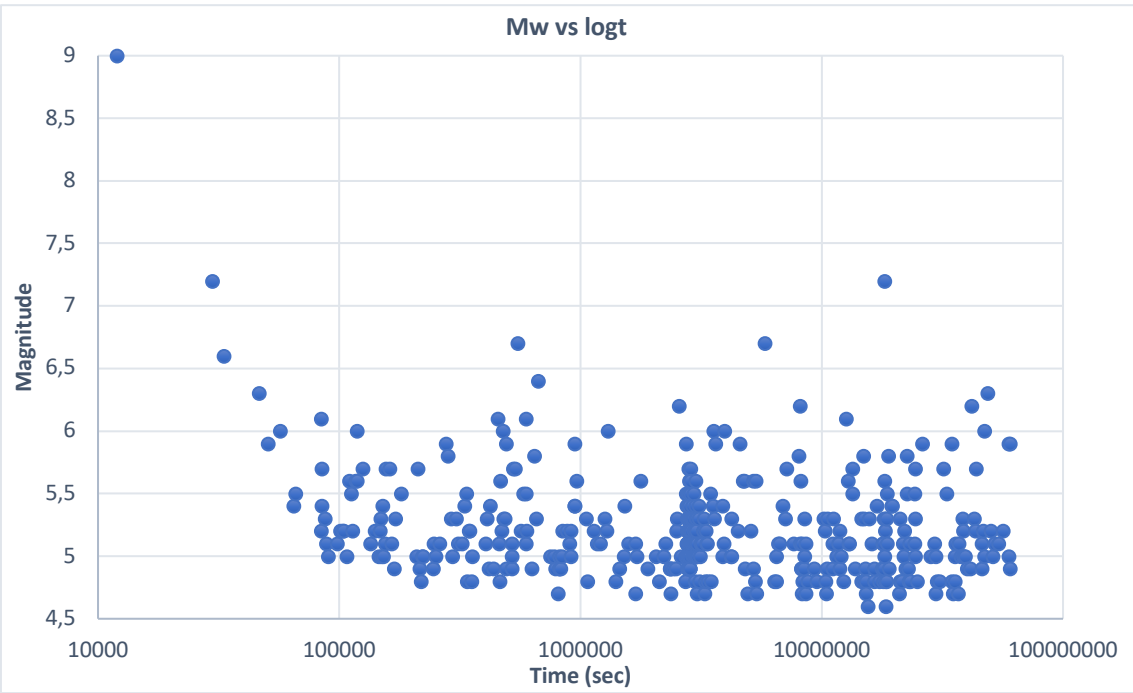

Figure 55. The magnitude-time pattern versus the logarithm of time of the mainshock M_w 9.0.

By the frequency-magnitude distribution for this earthquake, it is estimated a q_M= 1.47 with ci= 1.44-1.49.

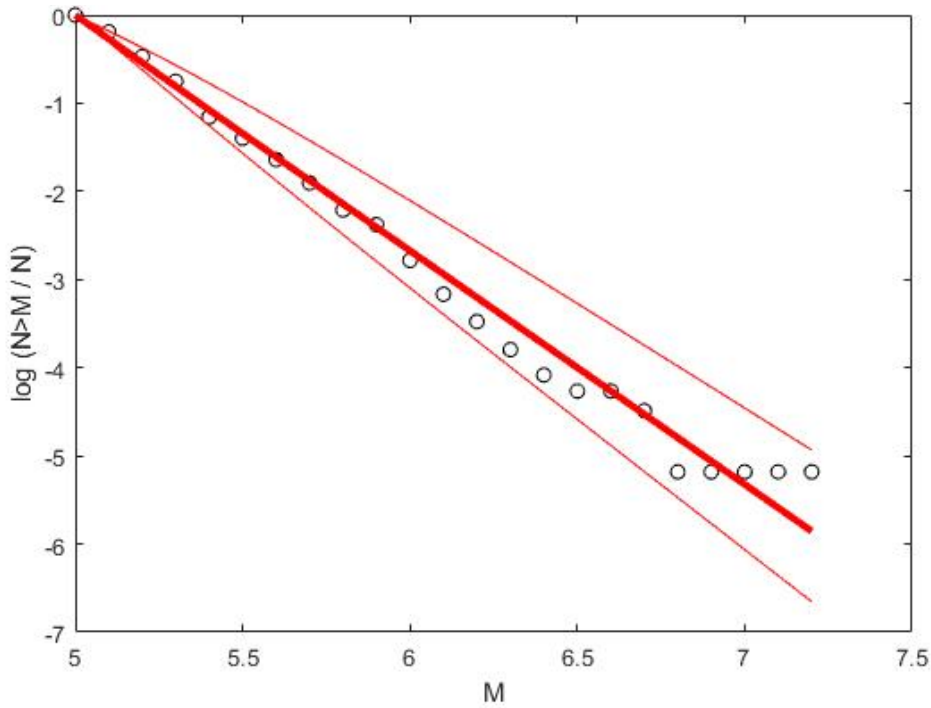

Figure 56. Frequency-magnitude distribution. The bold red line represents the model of equation (26) for qM= 1.47, while the other two lines present the corresponding 95% confidence intervals.

Figure 57 shows the typical Q-exponential pattern and Q-logarithmic function of the cumulative distribution function, P(>T) of the aftershocks interevent times and a q=1.69 is obtained.

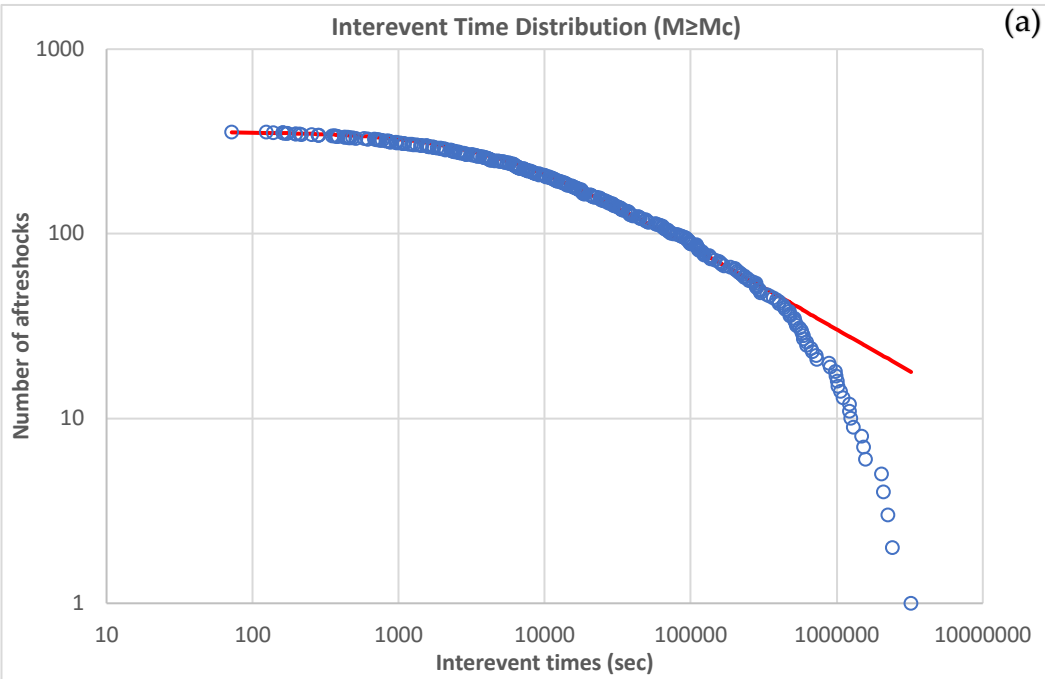

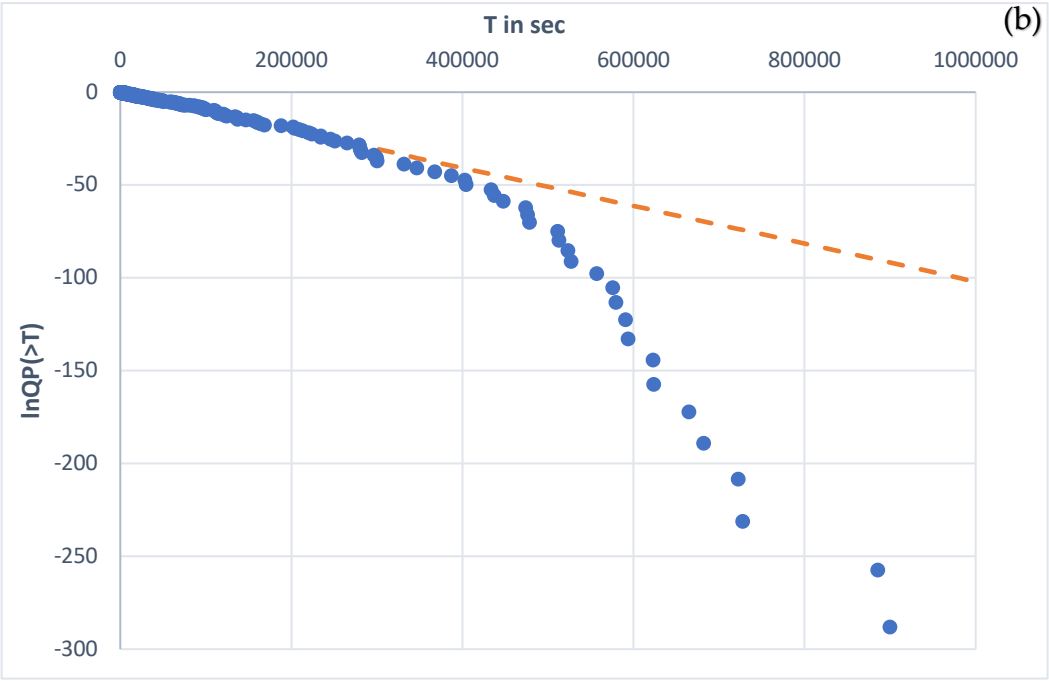

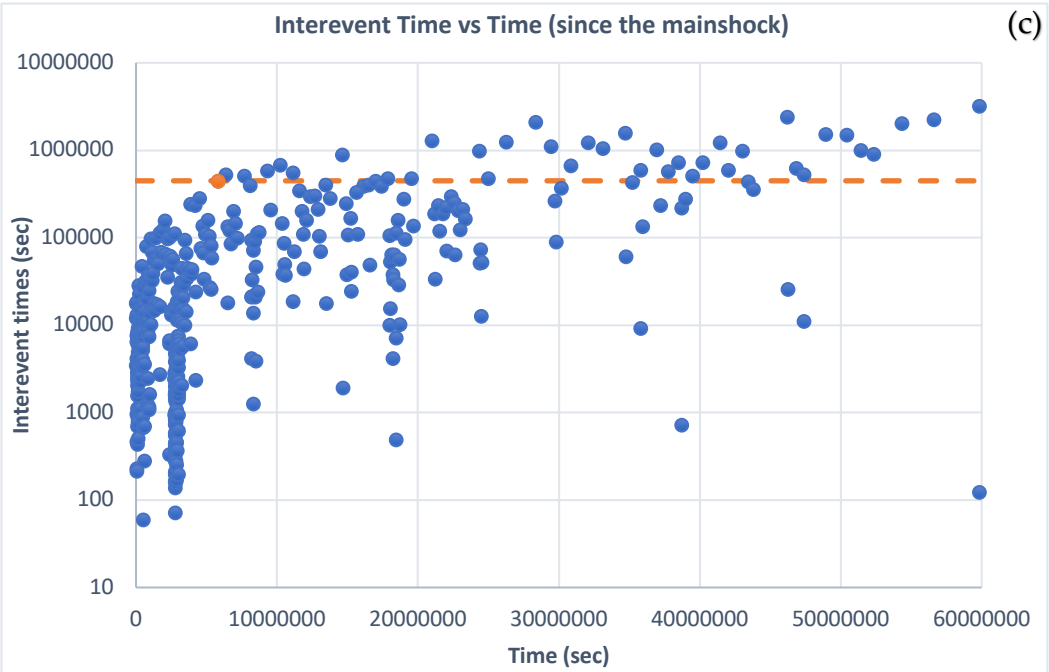

Figure 57. (a) The cumulative distribution function of the interevent times. The red line is the Q-exponential fitting with q = 1.69. **(b)** The Q-logarithmic function of the P(>T) as a function of the interevent times where the dashed line is the fitting with q=1.69. The deviation from the linearity suggests Tc values close to 400,000 s. **(c)** The evolution of interevent time T as a function of time t since the main event. The Tc value is indicated by the dashed line.

4.2.12 The 2005 Singkil Earthquake M_w=8.6 (Indonesia)

The figure below shows Guttenberg-Richter distribution. The estimated parameters are Mc=5.1 and b=1.09 and a=7.77.

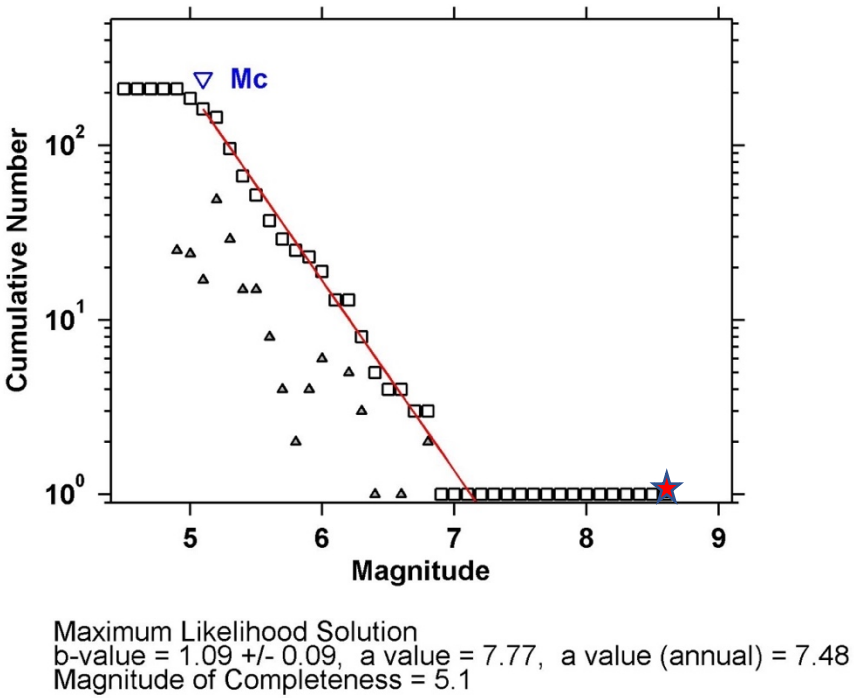

Figure 58. The Guttenberg-Richter distribution using maximum likelihood method with the best combination of maximum curvature M_c 95% and M_c 90% probability. The red star shows the magnitude of the mainshock M_w 8.6.

Next figure presents the model proposed by the AIC with p= 0.88, c= 0.01 and k= 14.3.

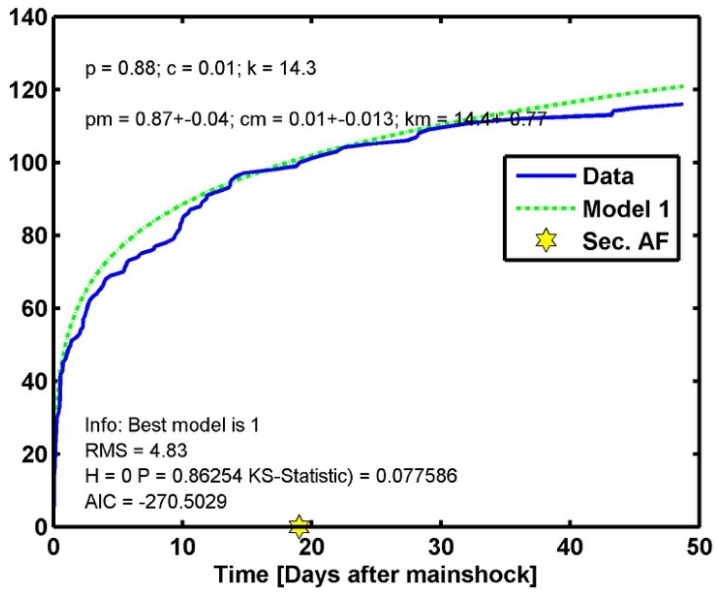

Figure 59. The best model (1) of the estimated curve of the modified Omori formula (dashed line) applied to the aftershock data and the observed cumulative number of aftershocks (solid line) based on the AIC with RMS=4.83.

Here is the magnitude-time form of the aftershock sequence.

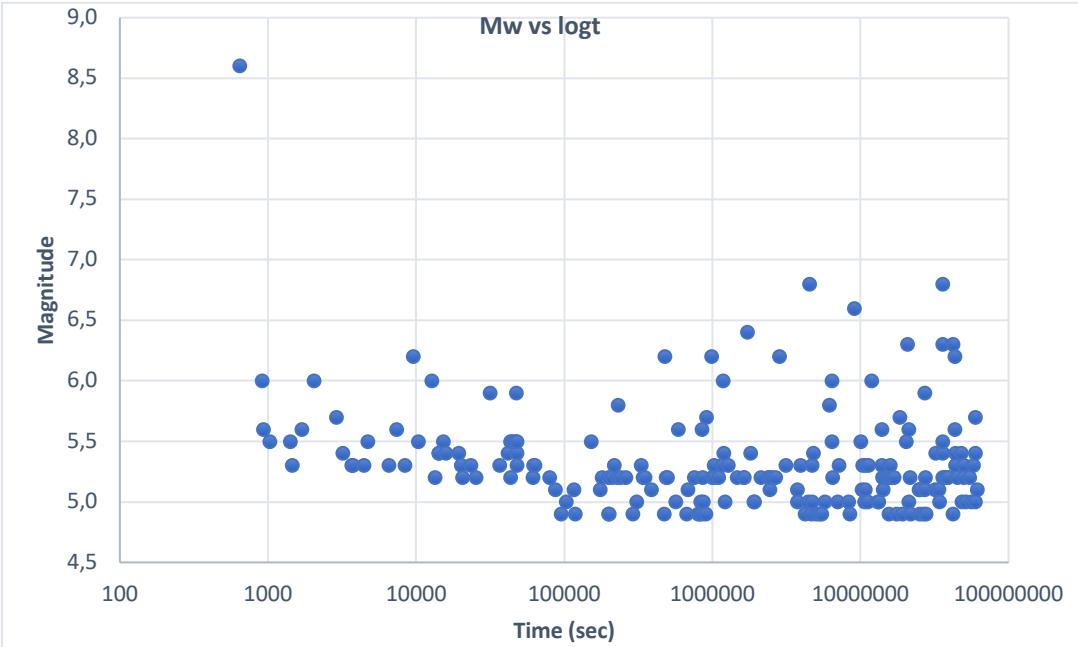

Figure 60. The magnitude-time pattern versus the logarithm of time of the mainshock M_w 8.6.

By the frequency-magnitude distribution for this earthquake, it is estimated a q_M= 1.45 with ci= 1.43-1.48.

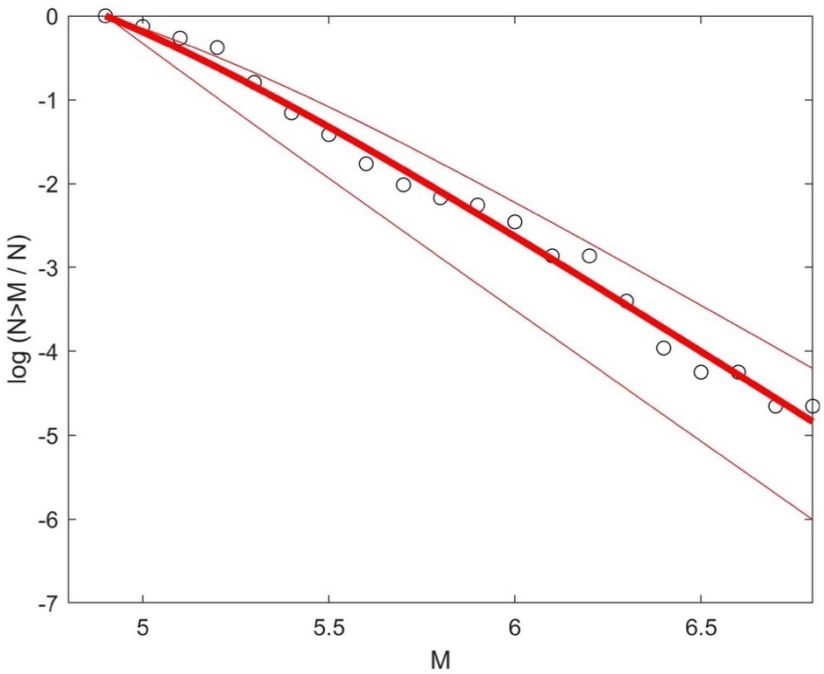

Figure 61. Frequency-magnitude distribution. The bold red line represents the model of equation (26) for qM= 1.45, while the other two lines present the corresponding 95% confidence intervals.

Figure 62 shows the typical Q-exponential pattern and Q-logarithmic function of the cumulative distribution function, P(>T) of the aftershocks interevent times and a q=1.83 is obtained.

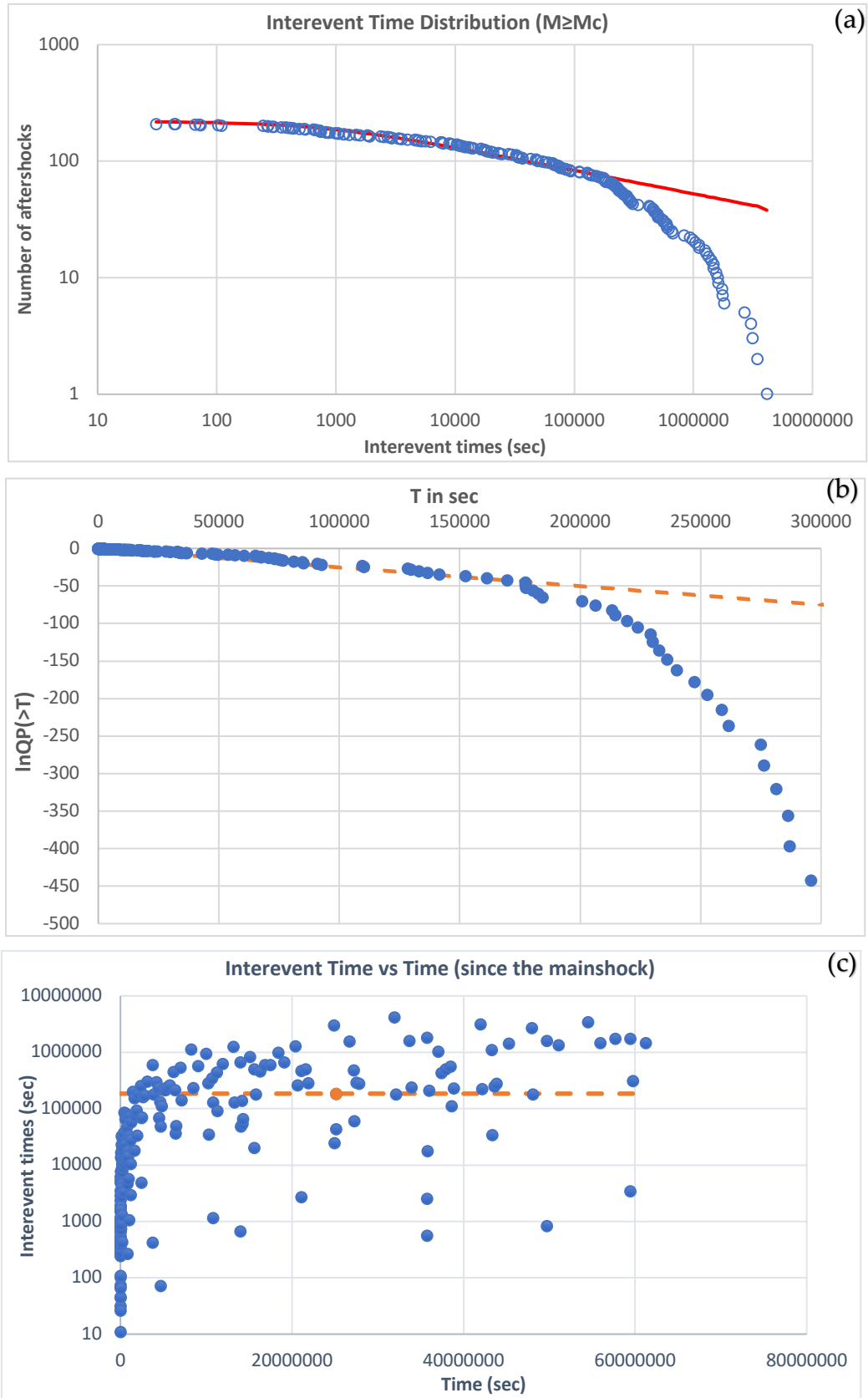

Figure 62. (a) The cumulative distribution function of the interevent times. The red line is the Q-exponential fitting with q = 1.83. **(b)** The Q-logarithmic function of the P(>T) as a function of the interevent times where the dashed line is the fitting with q=1.83. The deviation from the linearity suggests Tc values close to 175,000 s. **(c)** The evolution of interevent time T as a function of time t since the main event. The Tc value is indicated by the dashed line.

4.2.13 The 2006 Pangai Earthquake M_w=8.0 (Tonga)

The figure below shows Guttenberg-Richter distribution. The estimated parameters are Mc=5.0 and b=1.41 with a standard deviation of 0.07.

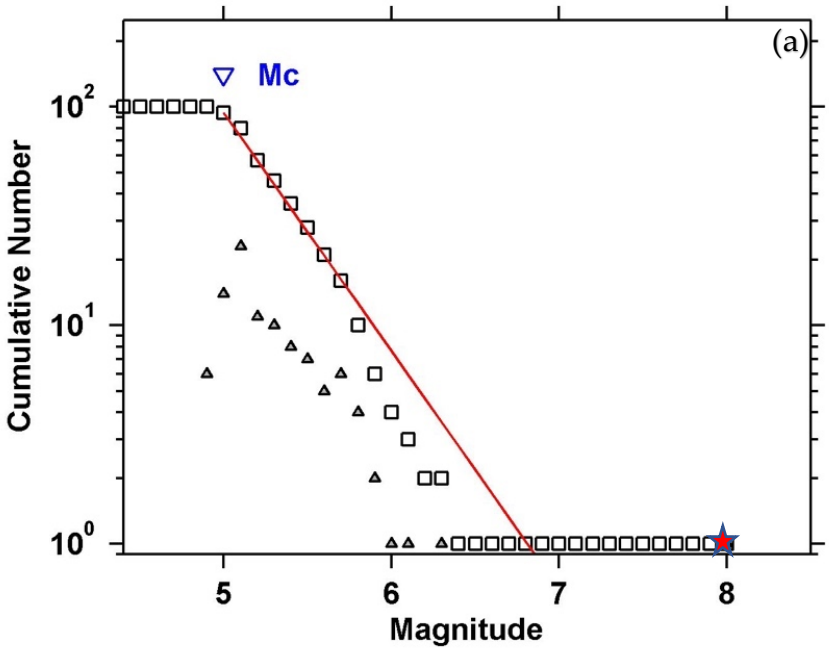

Maximum Likelihood Solution
b-value = 1.09 +/- 0.1, a value = 7.42, a value (annual) = 7.13
Magnitude of Completeness = 5

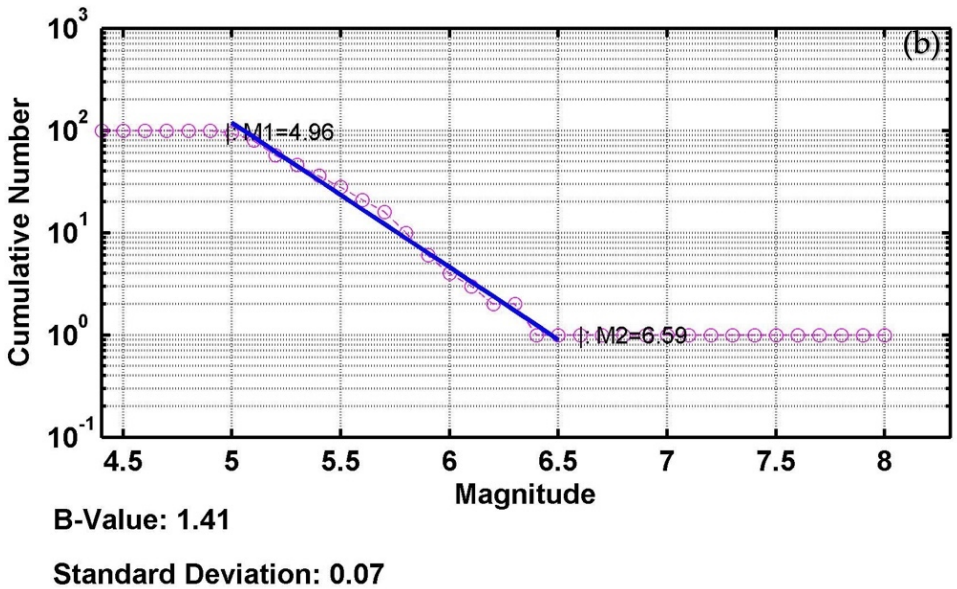

Figure 63. (a) The Guttenberg-Richter distribution using maximum likelihood method with the best combination of maximum curvature M_c 95% and M_c 90% probability. The red star shows the magnitude of the mainshock M_w 8.0. **(b)** The Guttenberg-Richter distribution using the manual method.

Next figure (64a) presents the model proposed by the AIC with p= 0.93, c= 1.98 and k= 10 while (64b) presents the model with the lowest RMS and p1= 0.91, p2=2.7, c=2.9, k1=10 and k2= 10.

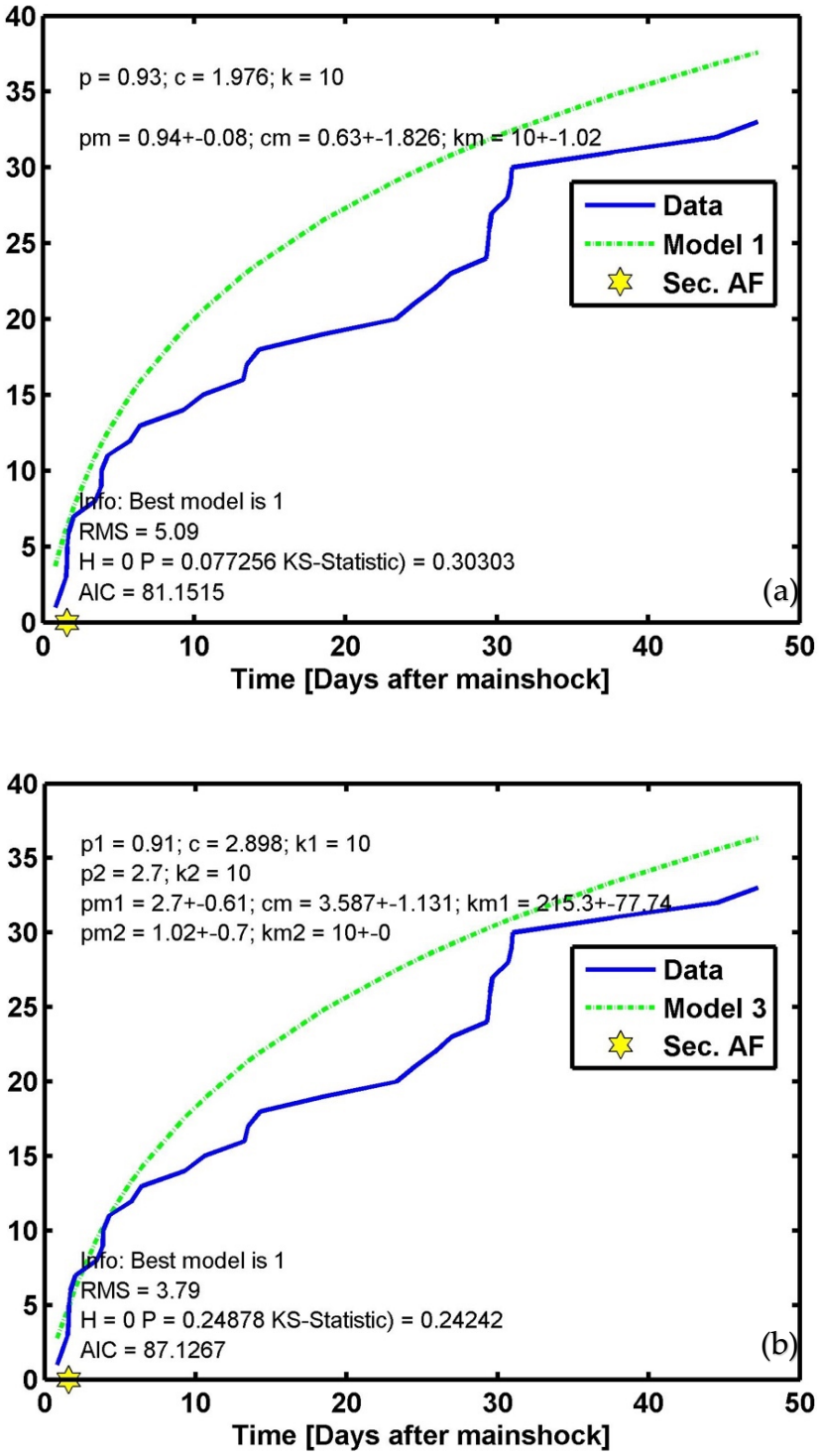

Figure 64. (a) The best model (1) of the estimated curve of the modified Omori formula (dashed line) applied to the aftershock data and the observed cumulative number of aftershocks (solid line) based on the AIC. **(b)** The model 3 of the estimated curve of the modified Omori formula (dashed line) applied to the aftershock data and the observed cumulative number of aftershocks (solid line), with the lowest RMS= 3.79.

Here is the magnitude-time form of the aftershock sequence.

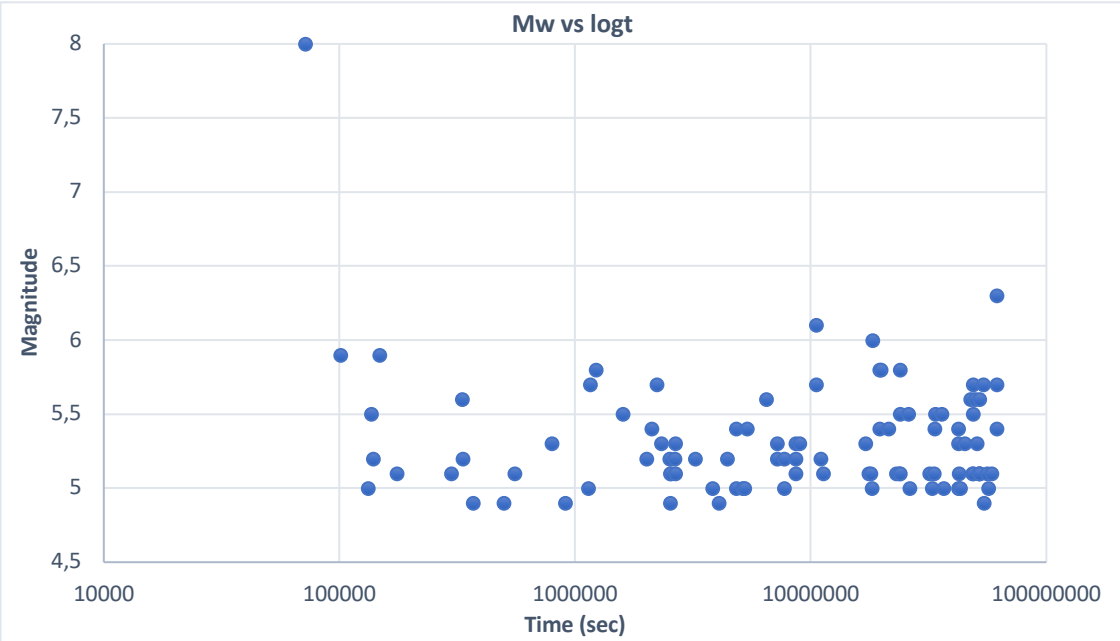

Figure 65. The magnitude-time pattern versus the logarithm of time of the mainshock M_w 8.0.

By the frequency-magnitude distribution for this earthquake, it is estimated a q_M= 1.27 with ci= 1.24-1.31.

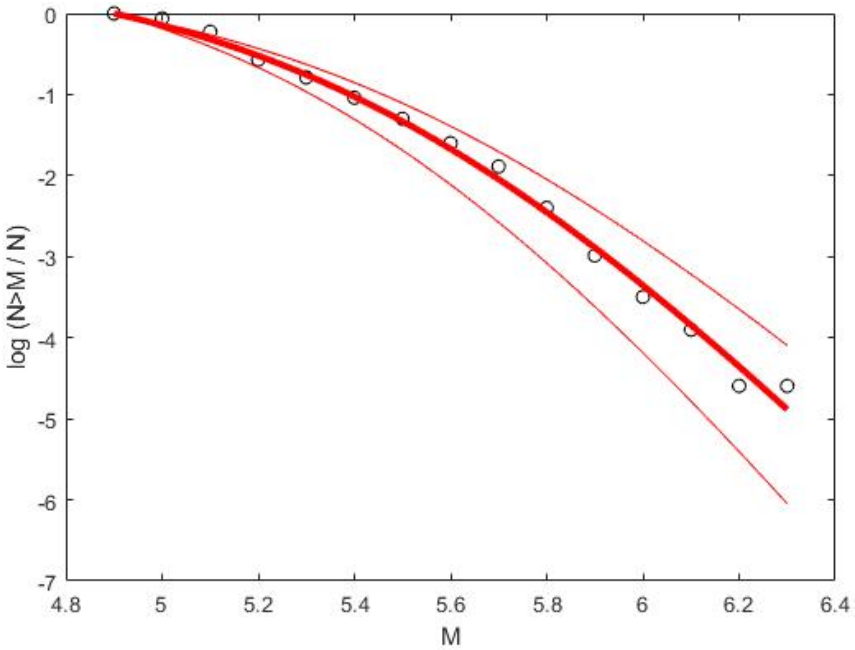

Figure 66. Frequency-magnitude distribution. The bold red line represents the model of equation (26) for qM= 1.27, while the other two lines present the corresponding 95% confidence intervals.

Figure 67 shows the typical Q-exponential pattern and Q-logarithmic function of the cumulative distribution function, P(>T) of the aftershocks interevent times and a q=1.75 is obtained.

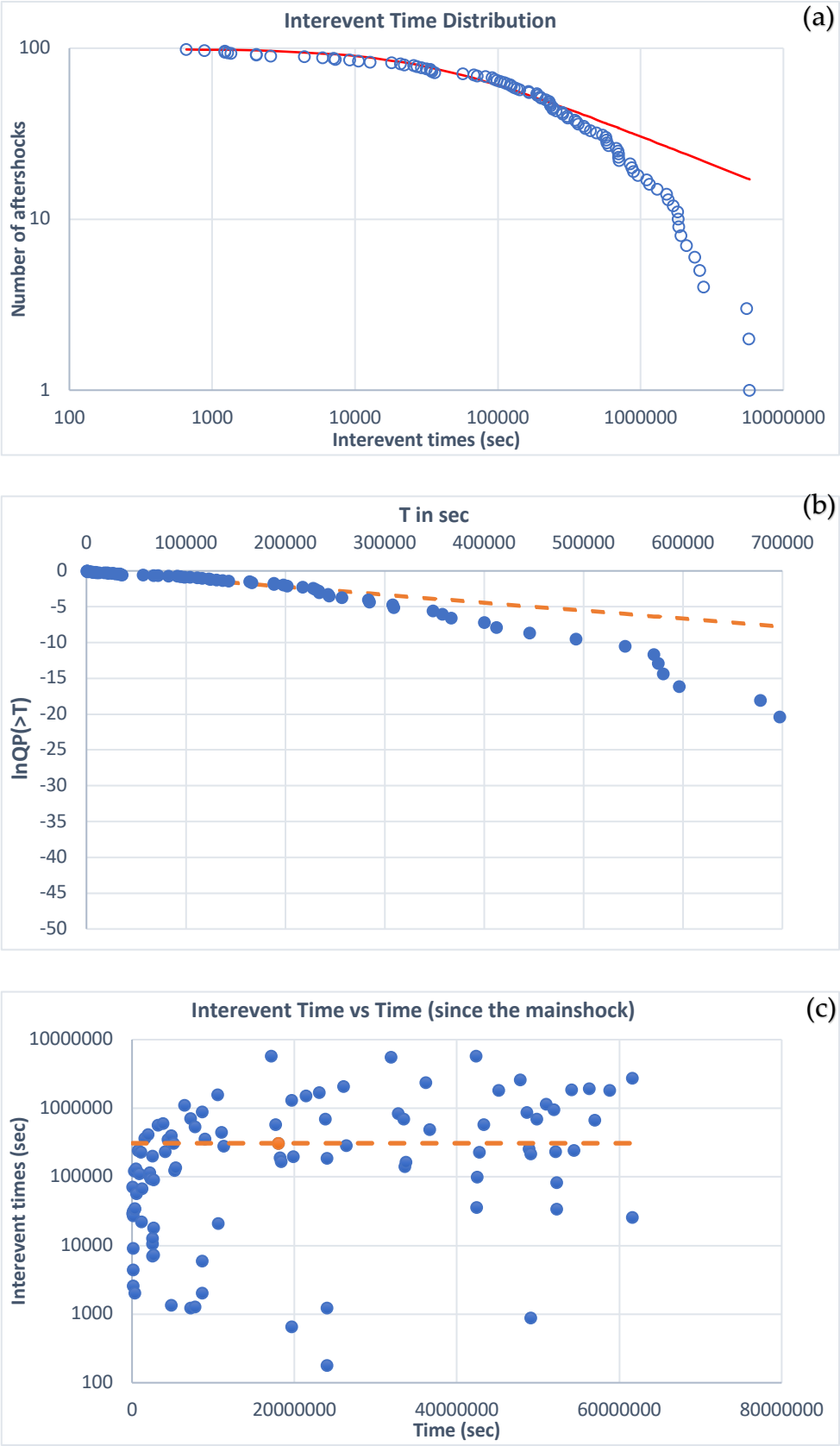

Figure 67. (a) The cumulative distribution function of the interevent times. The red line is the Q-exponential fitting with q = 1.75. **(b)** The Q-logarithmic function of the P(>T) as a function of the interevent times where the dashed line is the fitting with q=1.75. The deviation from the linearity suggests Tc values close to 300,000 s. **(c)** The evolution of interevent time T as a function of time t since the main event. The Tc value is indicated by the dashed line.

4.2.14 The 2006 Singaparna Earthquake M_w=7.7 (Indonesia)

The figure below shows Guttenberg-Richter distribution. The estimated parameters are Mc=5.2 and b=2.02 with a standard deviation of 0.08.

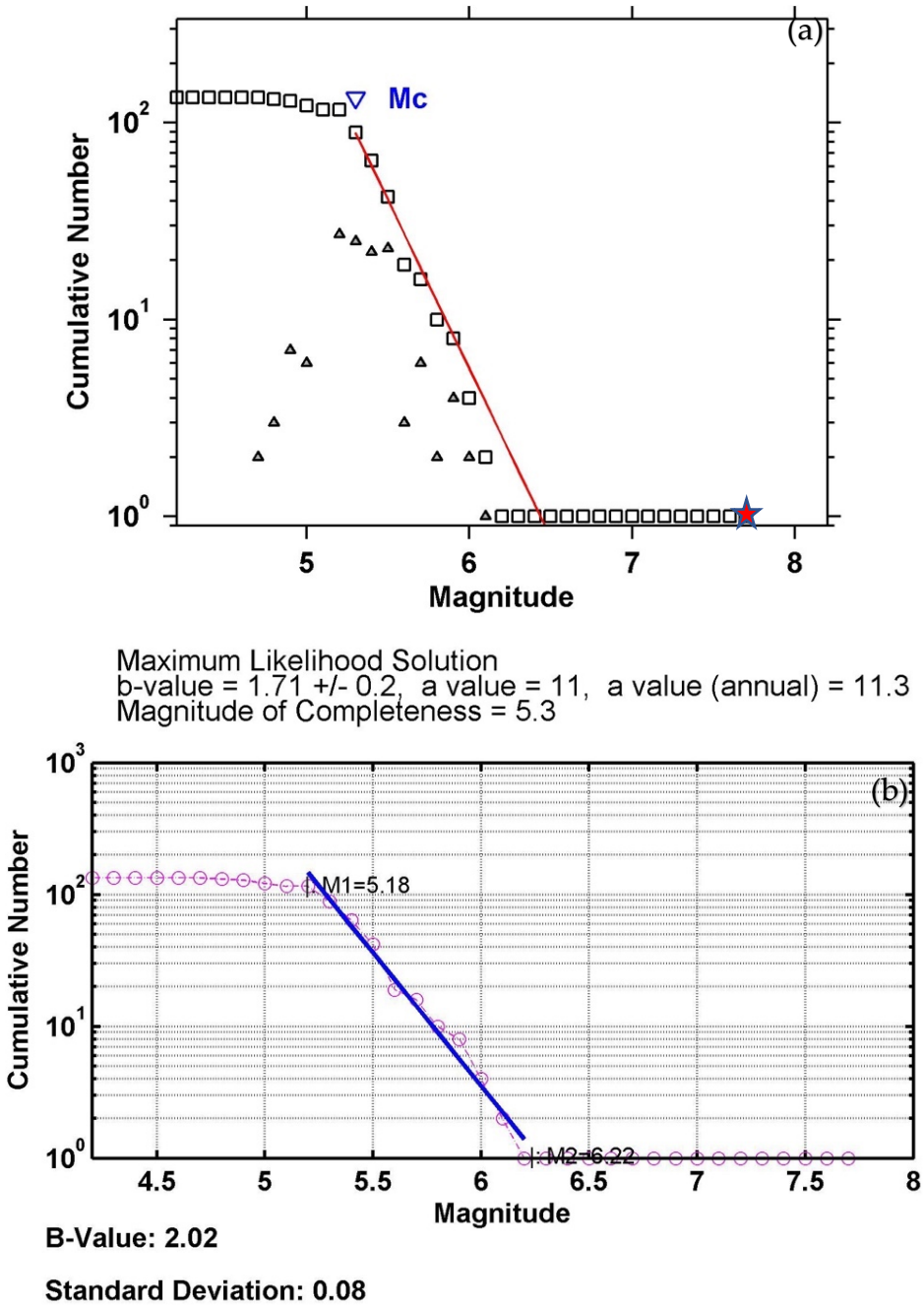

Figure 68. (a) The Guttenberg-Richter distribution using maximum likelihood method with the best combination of maximum curvature M_c 95% and M_c 90% probability. The red star shows the magnitude of the mainshock M_w 7.7. **(b)** The Guttenberg-Richter distribution using the manual method.

Next figure (69a) presents the model proposed by the AIC with p= 1.31, c= 0.205 and k= 30.2 while (69b) presents the model with the lowest RMS and p1= 2.5, p2=1.12, c1=0.689, c2=3.839, k1=81.2 and k2= 10.4.

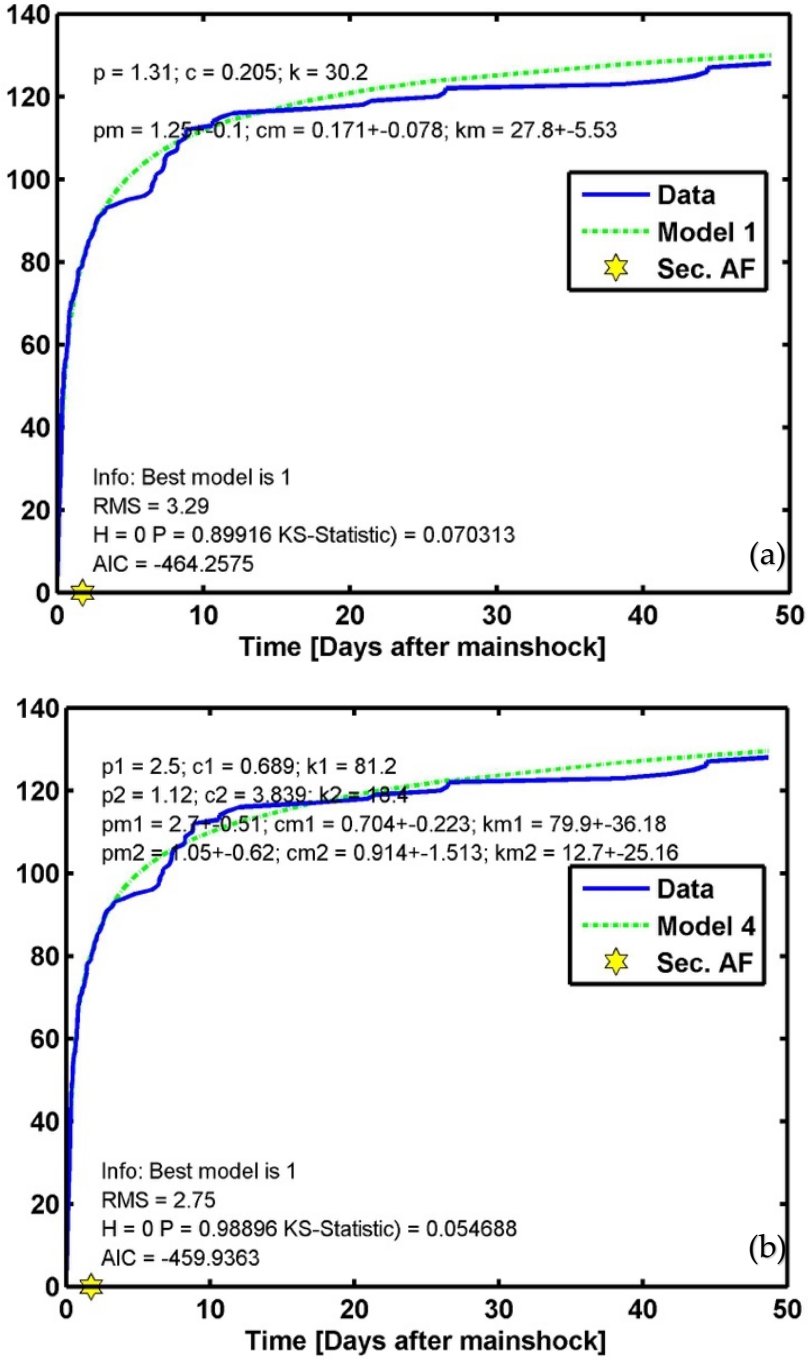

Figure 69. (a) The best model (1) of the estimated curve of the modified Omori formula (dashed line) applied to the aftershock data and the observed cumulative number of aftershocks (solid line) based on the AIC. **(b)** The model 4 of the estimated curve of the modified Omori formula (dashed line) applied to the aftershock data and the observed cumulative number of aftershocks (solid line), with the lowest RMS= 2.75.

Here is the magnitude-time form of the aftershock sequence.

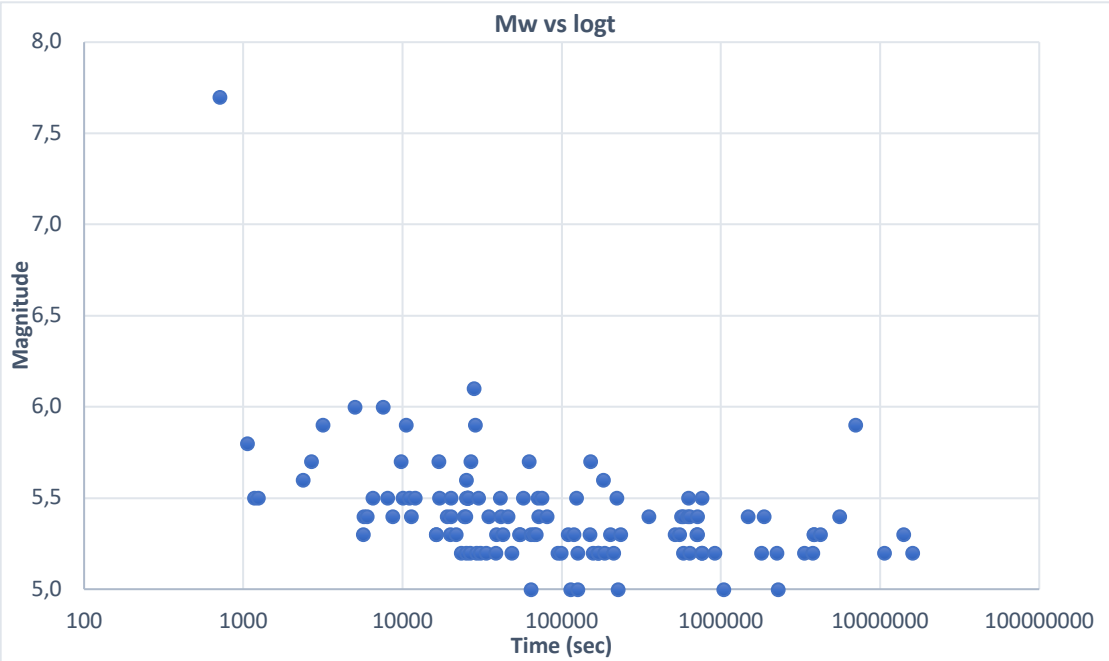

Figure 70. The magnitude-time pattern versus the logarithm of time of the mainshock M_w 7.7.

By the frequency-magnitude distribution for this earthquake, it is estimated a q_M= 1.06 with ci= 0.97-1.15.

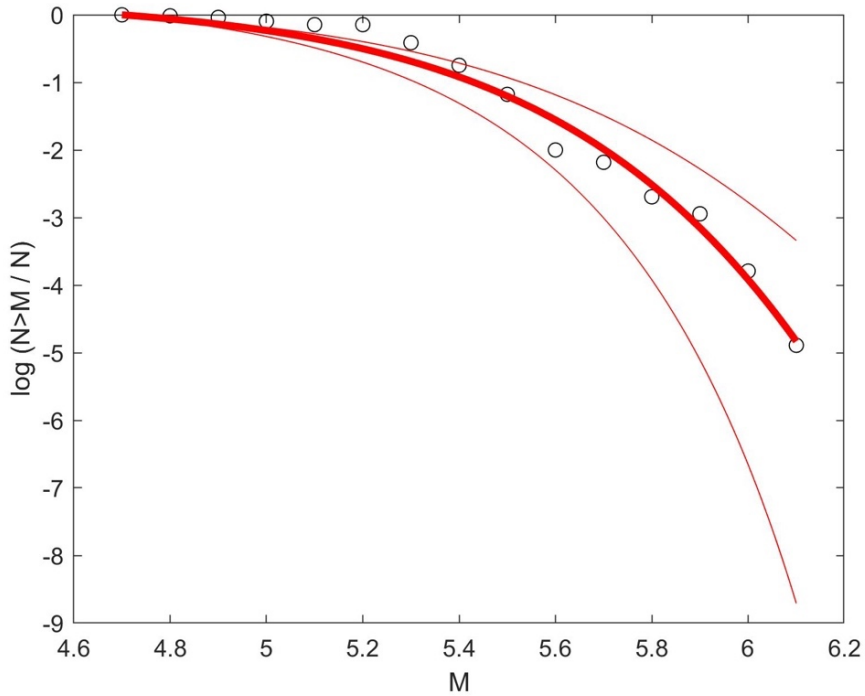

Figure 71. Frequency-magnitude distribution. The bold red line represents the model of equation (26) for qM= 1.06, while the other two lines present the corresponding 95% confidence intervals.

Figure 72 shows the typical Q-exponential pattern and Q-logarithmic function of the cumulative distribution function, P(>T) of the aftershocks interevent times and a q=1.67 is obtained.

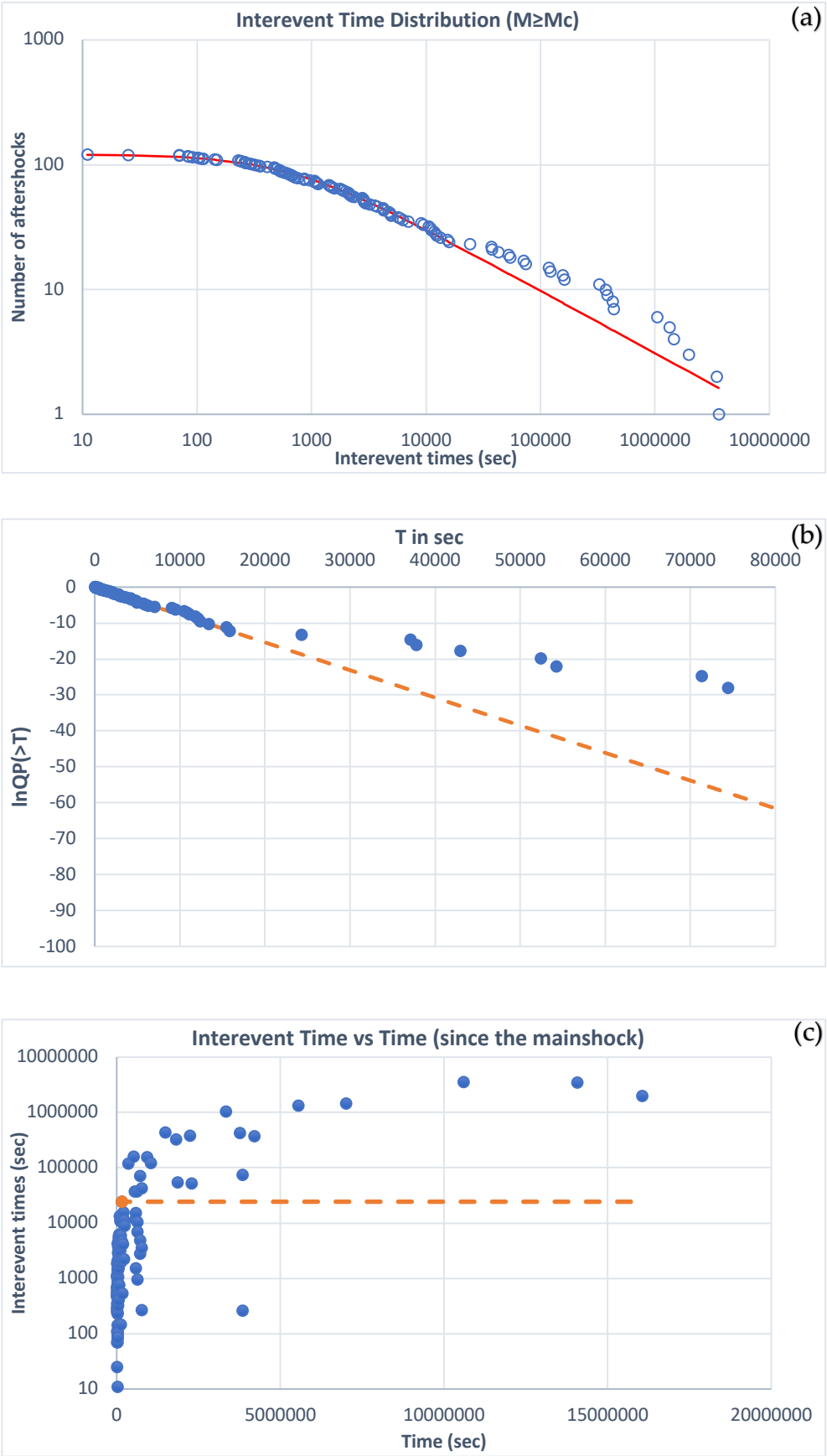

Figure 72. (a) The cumulative distribution function of the interevent times. The red line is the Q-exponential fitting with q = 1.67. **(b)** The Q-logarithmic function of the P(>T) as a function of the interevent times where the dashed line is the fitting with q=1.67. The deviation from the linearity suggests Tc values close to 15,000 s. **(c)** The evolution of interevent time T as a function of time t since the main event. The Tc value is indicated by the dashed line.

4.2.15 The 2007 Gizo Earthquake M_w=8.1 (Solomon Island)

The figure below shows Guttenberg-Richter distribution. The estimated parameters are Mc=5.0 and b=1.03 with a standard deviation of 0.06.

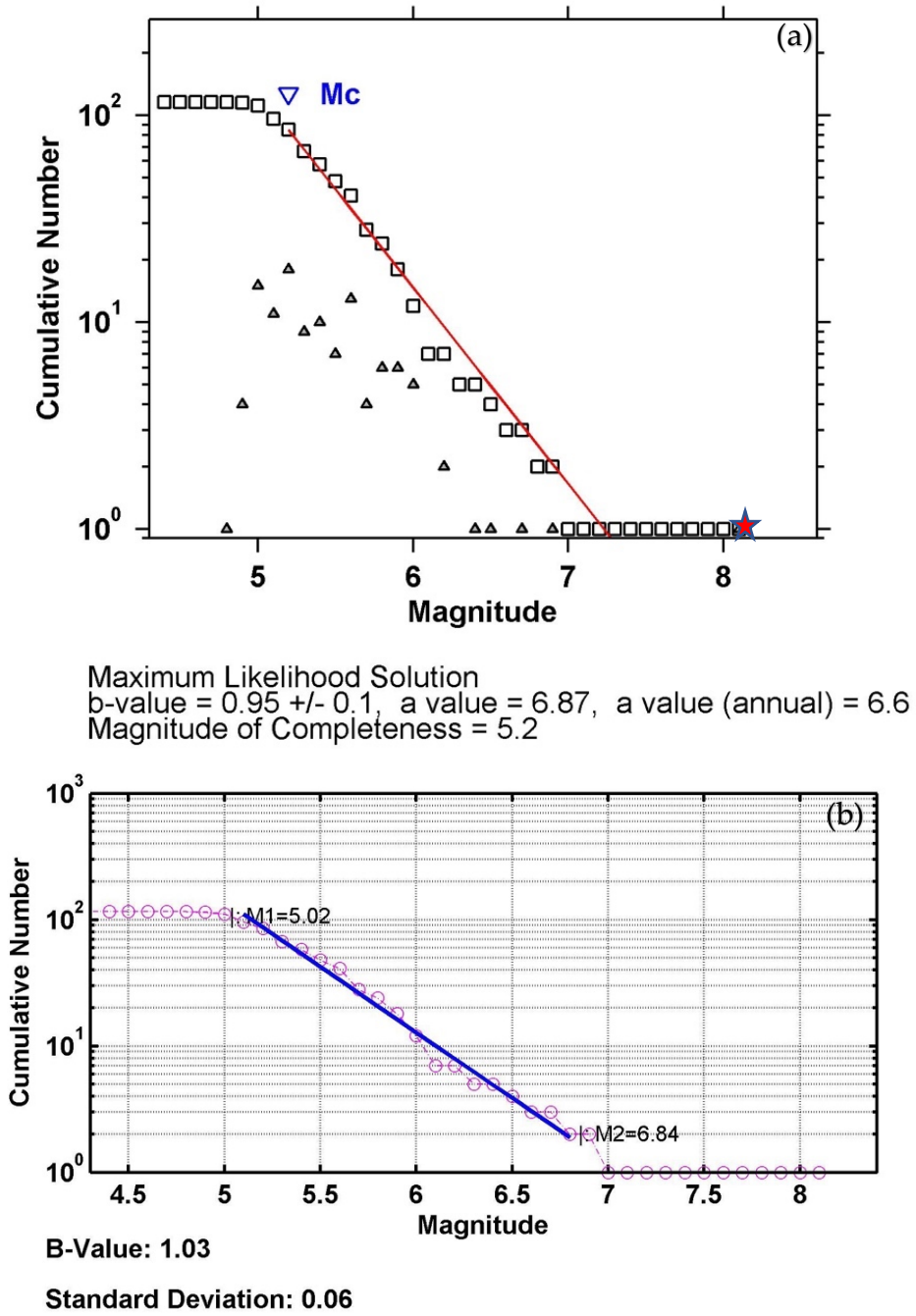

Figure 73. (a) The Guttenberg-Richter distribution using maximum likelihood method with the best combination of maximum curvature M_c 95% and M_c 90% probability. The red star shows the magnitude of the mainshock M_w 8.1. **(b)** The Guttenberg-Richter distribution using the manual method.

Next figure presents the model proposed by the AIC with p= 1.2, c= 0.46 and k= 18.6

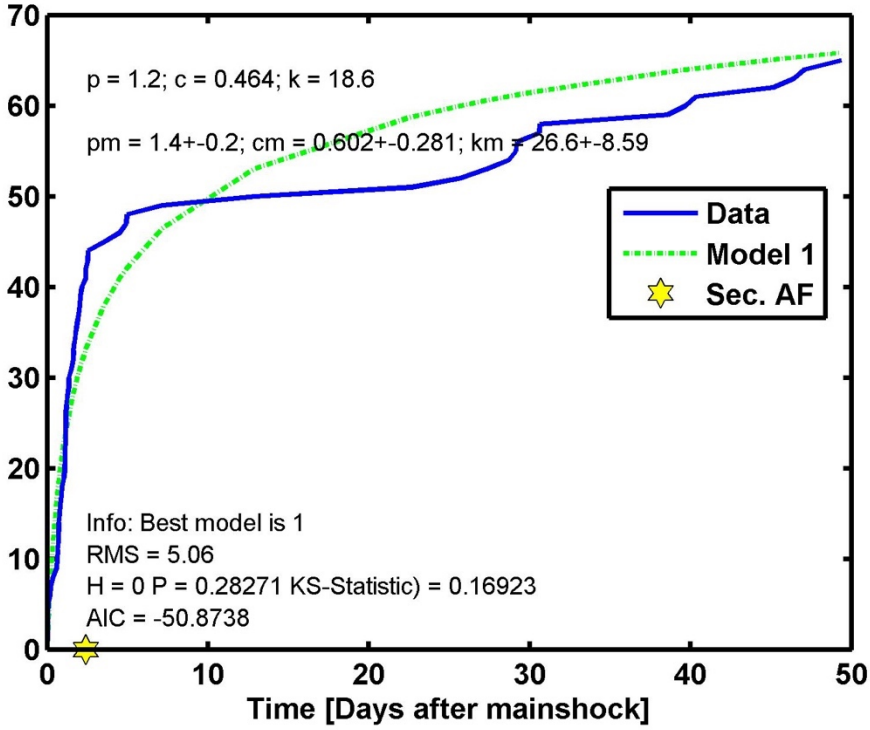

Figure 74. The best model (1) of the estimated curve of the modified Omori formula (dashed line) applied to the aftershock data and the observed cumulative number of aftershocks (solid line) based on the AIC with RMS= 5.06.

Here is the magnitude-time form of the aftershock sequence.

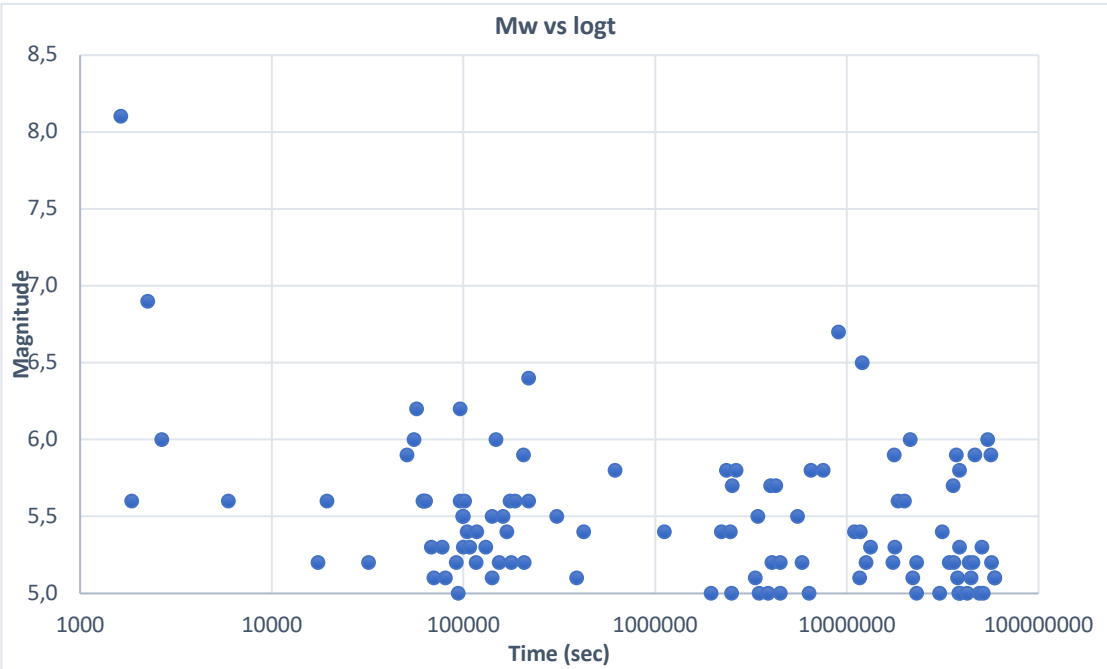

Figure 75. The magnitude-time pattern versus the logarithm of time of the mainshock M_w 8.1.

By the frequency-magnitude distribution for this earthquake, it is estimated a q_M= 1.42 with ci= 1.39-1.44.

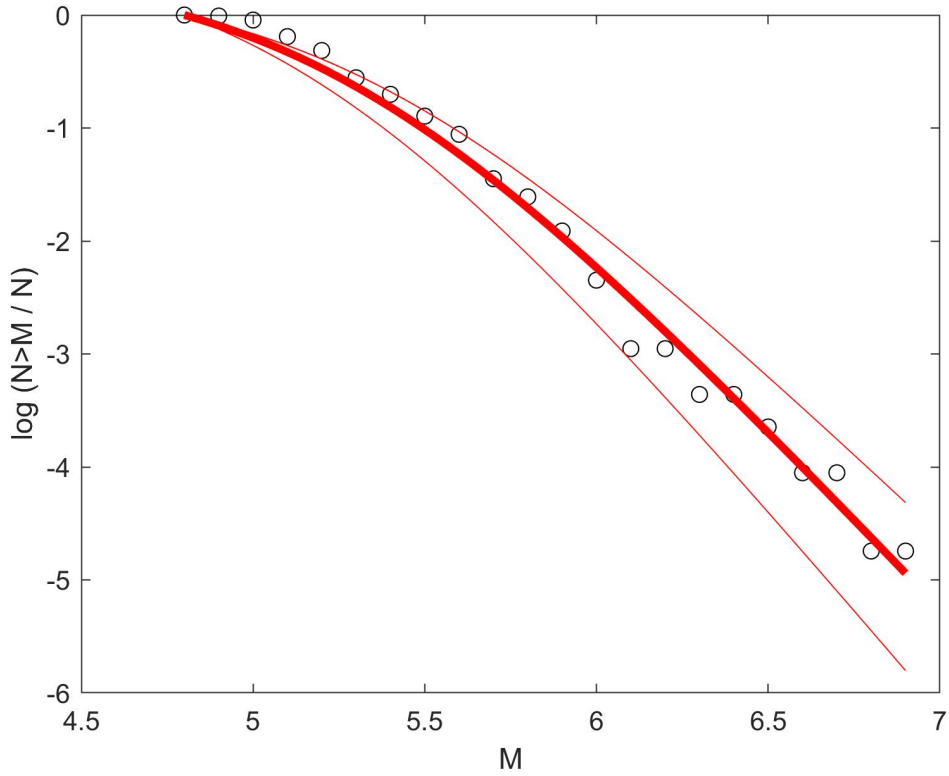

Figure 76. Frequency-magnitude distribution. The bold red line represents the model of equation (26) for qM= 1.42, while the other two lines present the corresponding 95% confidence intervals.

Figure 77 shows the typical Q-exponential pattern and Q-logarithmic function of the cumulative distribution function, P(>T) of the aftershocks interevent times and a q=1.80 is obtained.

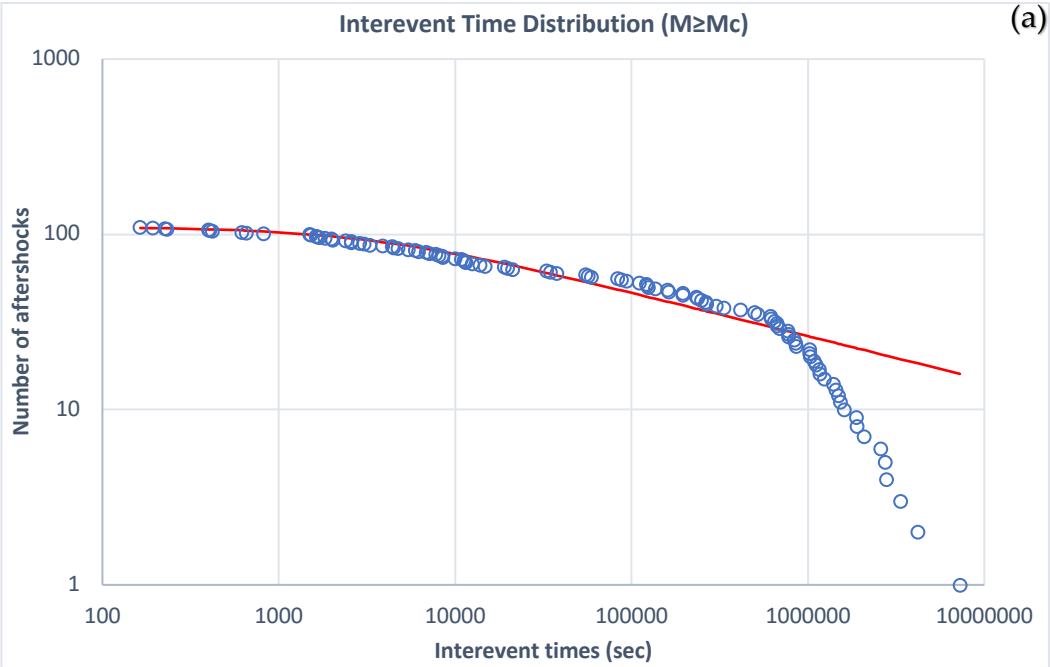

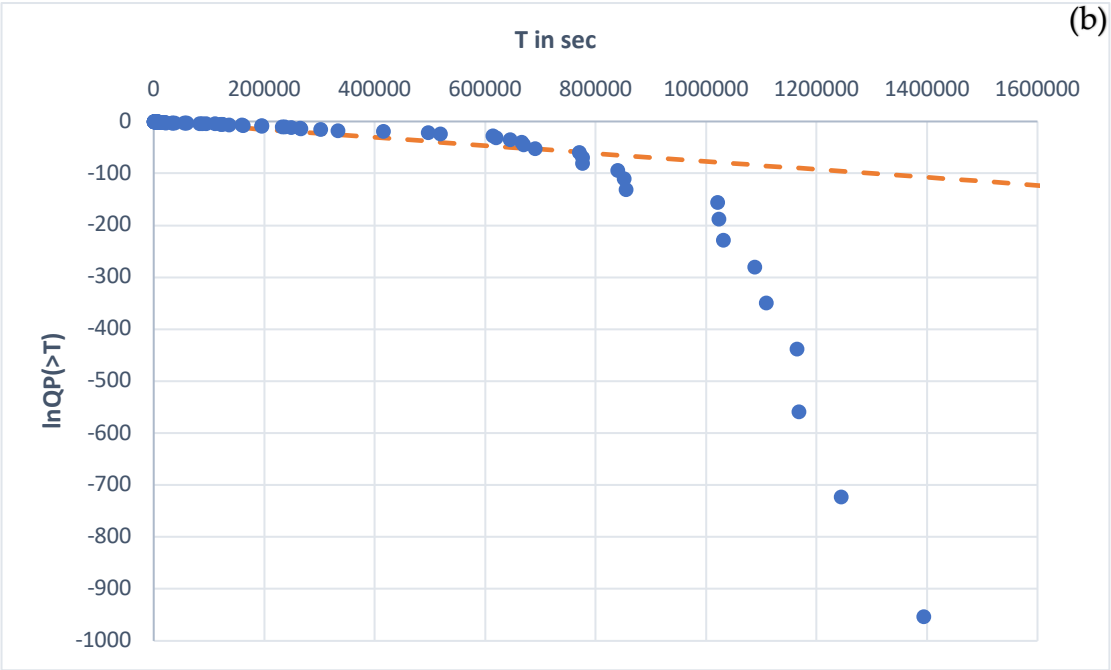

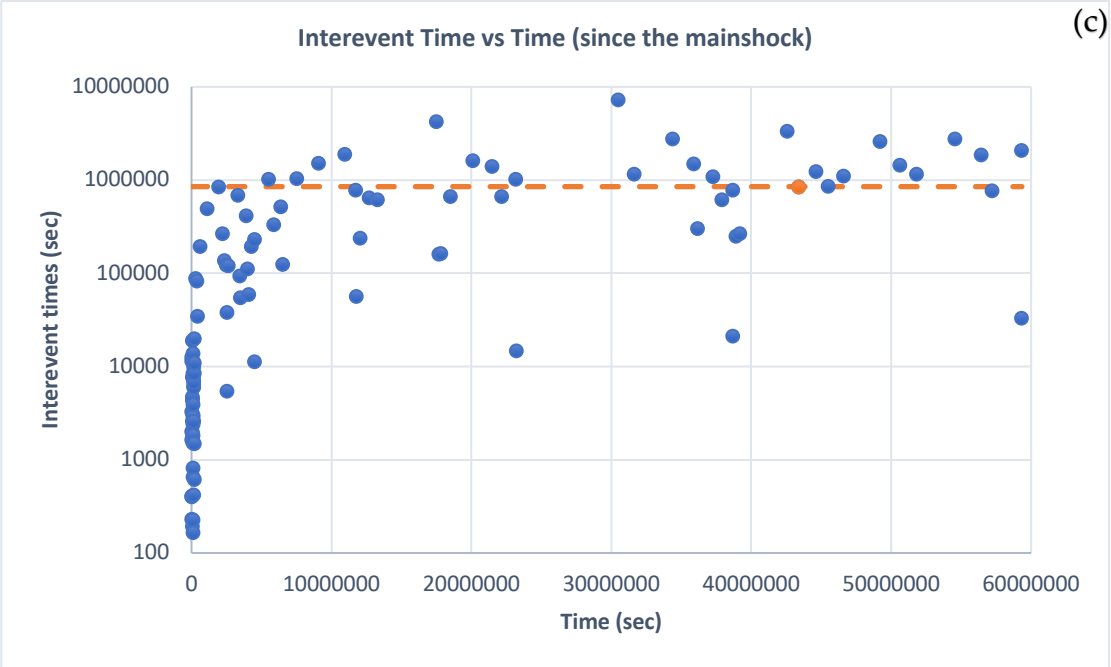

Figure 77. (a) The cumulative distribution function of the interevent times. The red line is the Q-exponential fitting with q = 1.80. **(b)** The Q-logarithmic function of the P(>T) as a function of the interevent times where the dashed line is the fitting with q=1.80. The deviation from the linearity suggests Tc values close to 800,000 s. **(c)** The evolution of interevent time T as a function of time t since the main event. The Tc value is indicated by the dashed line.

4.2.16 The 2007 Bengkulu Earthquake M_w=8.4 (Indonesia)

The figure below shows Guttenberg-Richter distribution. The estimated parameters are Mc=5.1, b=0.817 and a=6.36.

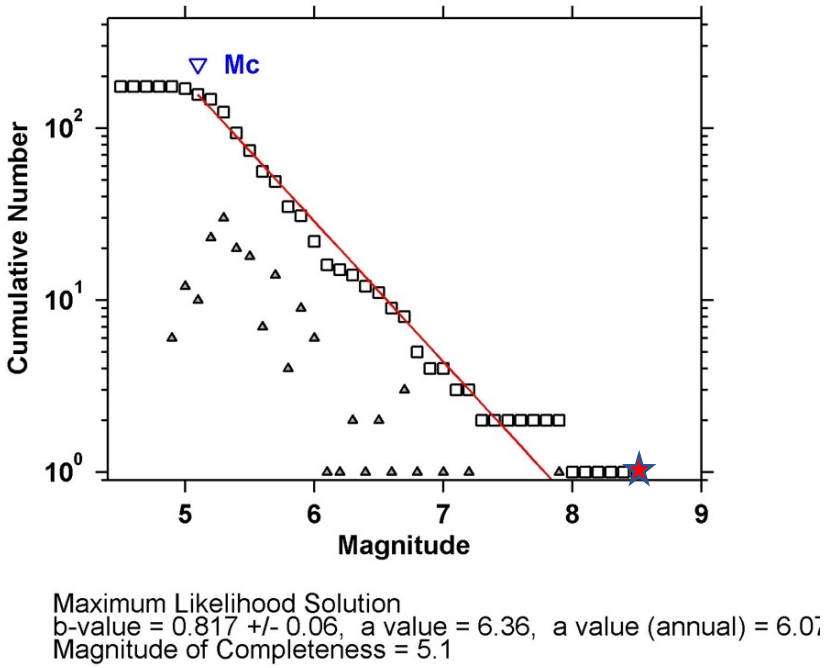

Figure 78. The Guttenberg-Richter distribution using maximum likelihood method with the best combination of maximum curvature M_c 95% and M_c 90% probability. The red star shows the magnitude of the mainshock M_w 8.4.

Next figure presents the model proposed by the AIC with p= 1.2, c= 0.24 and k= 20.2.

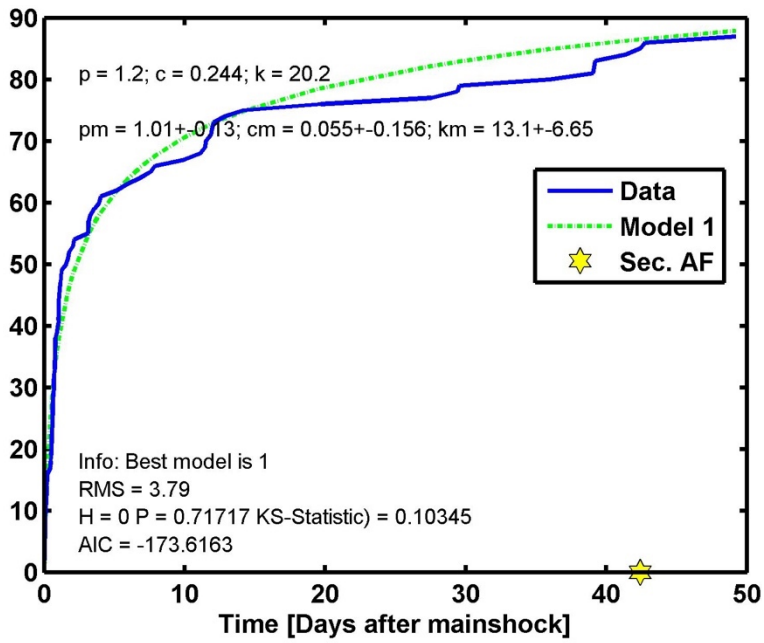

Figure 79. The best model (1) of the estimated curve of the modified Omori formula (dashed line) applied to the aftershock data and the observed cumulative number of aftershocks (solid line) based on the AIC with RMS=3.79.

Here is the magnitude-time form of the aftershock sequence.

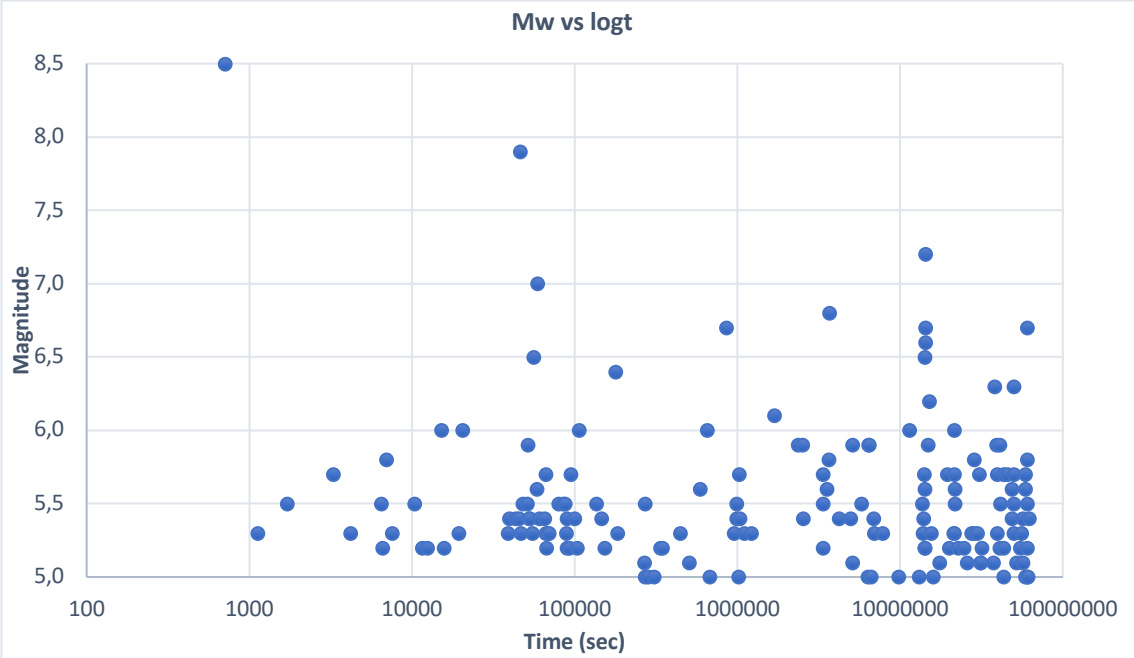

Figure 80. The magnitude-time pattern versus the logarithm of time of the mainshock M_w 8.4.

By the frequency-magnitude distribution for this earthquake, it is estimated a q_M= 1.58 with ci= 1.56-1.60.

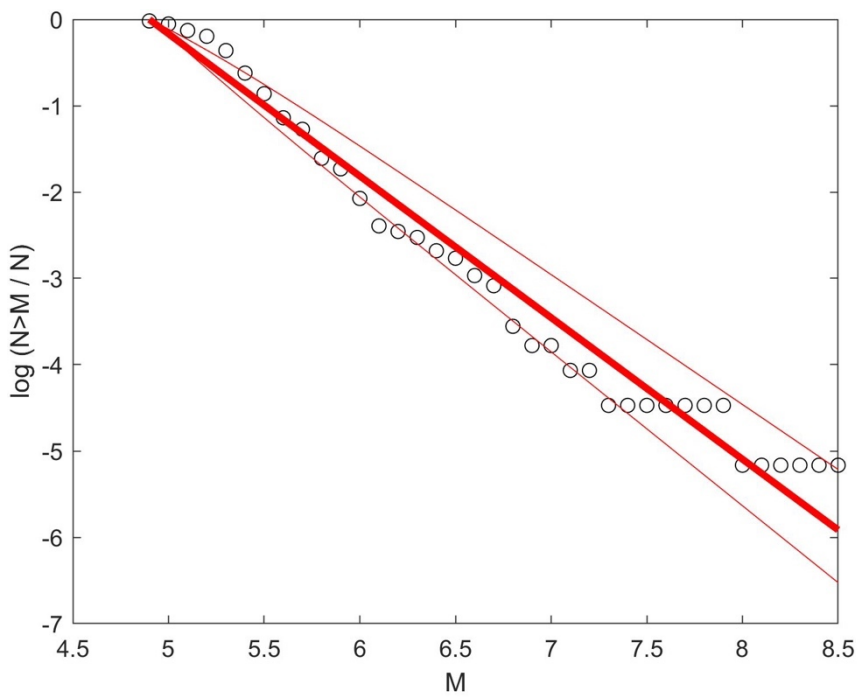

Figure 81. Frequency-magnitude distribution. The bold red line represents the model of equation (26) for qM= 1.58, while the other two lines present the corresponding 95% confidence intervals.

Figure 82 shows the typical Q-exponential pattern and Q-logarithmic function of the cumulative distribution function, P(>T) of the aftershocks interevent times and a q=1.83 is obtained.

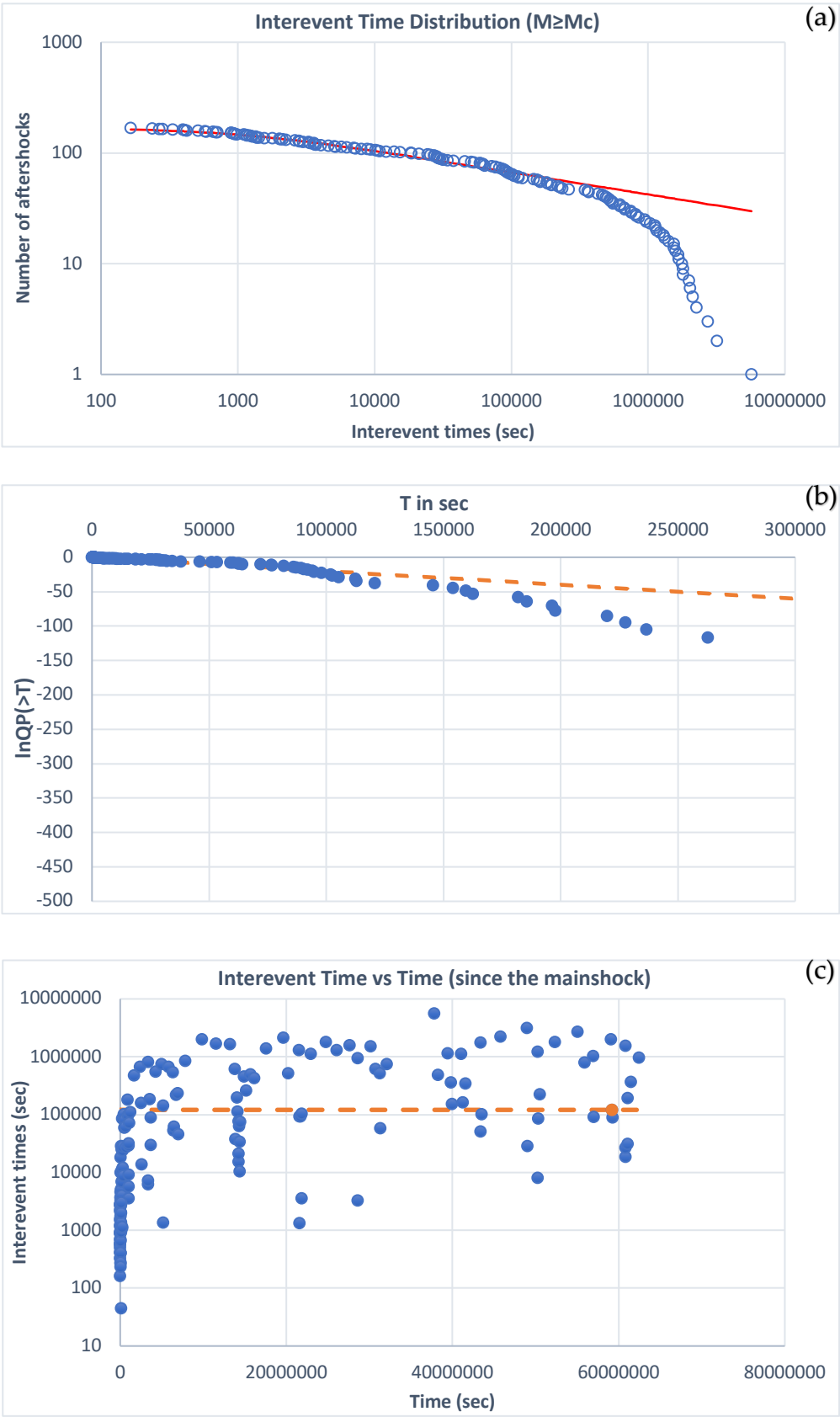

Figure 82. (a) The cumulative distribution function of the interevent times. The red line is the Q-exponential fitting with q = 1.83. **(b)** The Q-logarithmic function of the P(>T) as a function of the interevent times where the dashed line is the fitting with q=1.83. The deviation from the linearity suggests Tc values close to 150,000 s. **(c)** The evolution of interevent time T as a function of time t since the main event. The Tc value is indicated by the dashed line.

4.2.17 The 2009 Sarangani Earthquake M_w=7.2 (Philippines)

The figure below shows Guttenberg-Richter distribution. The estimated parameters are Mc=5.2, b=1.51 and a=9.91.

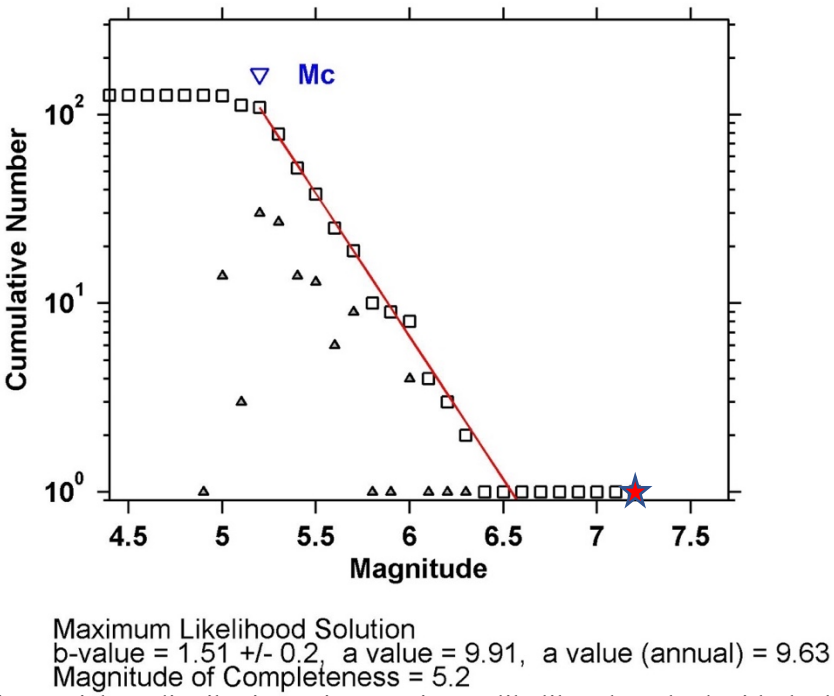

Figure 83. The Guttenberg-Richter distribution using maximum likelihood method with the best combination of maximum curvature M_c 95% and M_c 90% probability. The red star shows the magnitude of the mainshock M_w 7.2.

Next figure presents the model proposed by the AIC with p1= 1.31, p2=2.7, c1=0.09, c2=3.06, k1= 14.8 and k2=44.

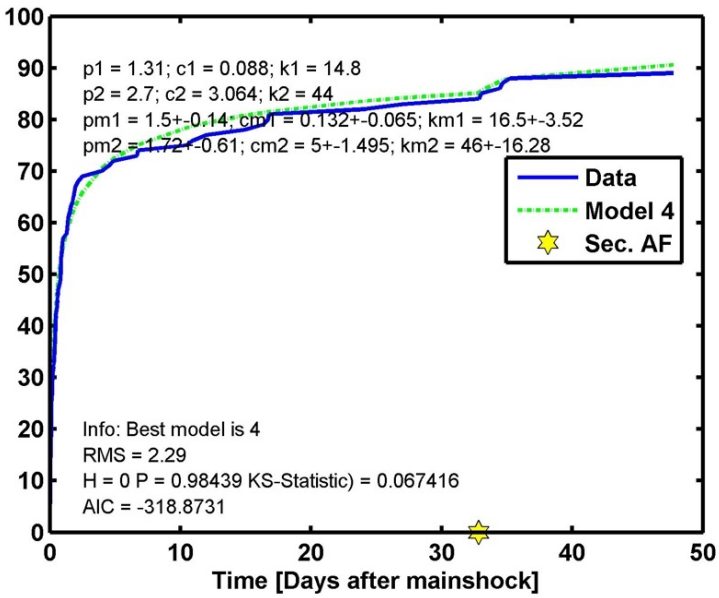

Figure 84. The best model (4) of the estimated curve of the modified Omori formula (dashed line) applied to the aftershock data and the observed cumulative number of aftershocks (solid line) based on the AIC with RMS= 2.29.

Here is the magnitude-time form of the aftershock sequence.

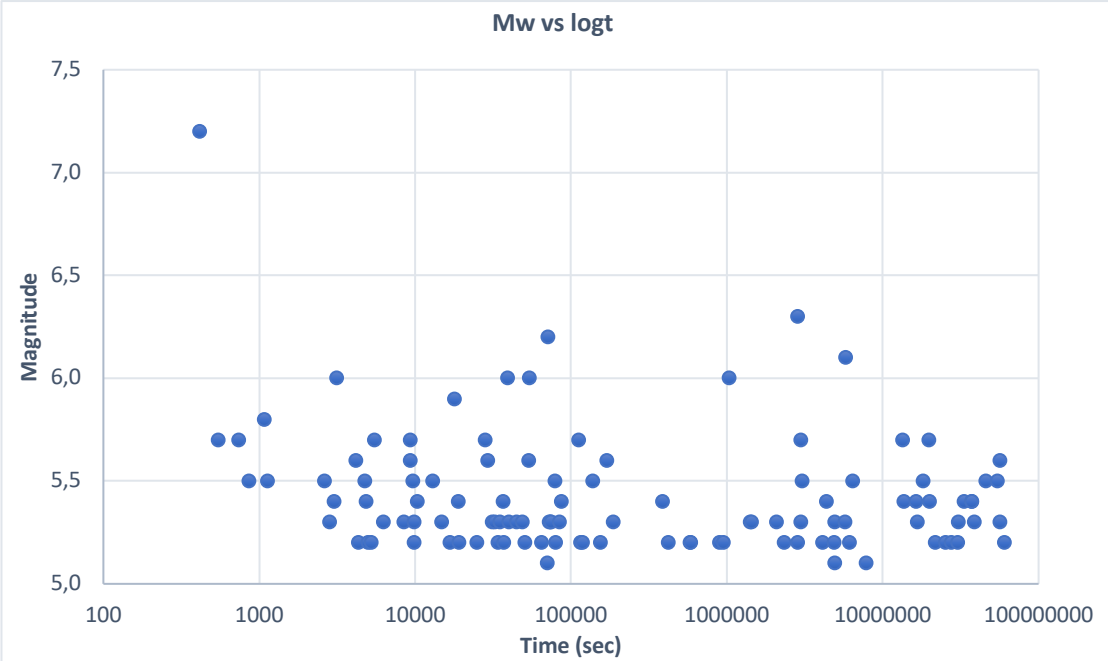

Figure 85. The magnitude-time pattern versus the logarithm of time of the mainshock M_w 7.2.

By the frequency-magnitude distribution for this earthquake, it is estimated a q_M= 1.48 with ci= 1.43-1.53.

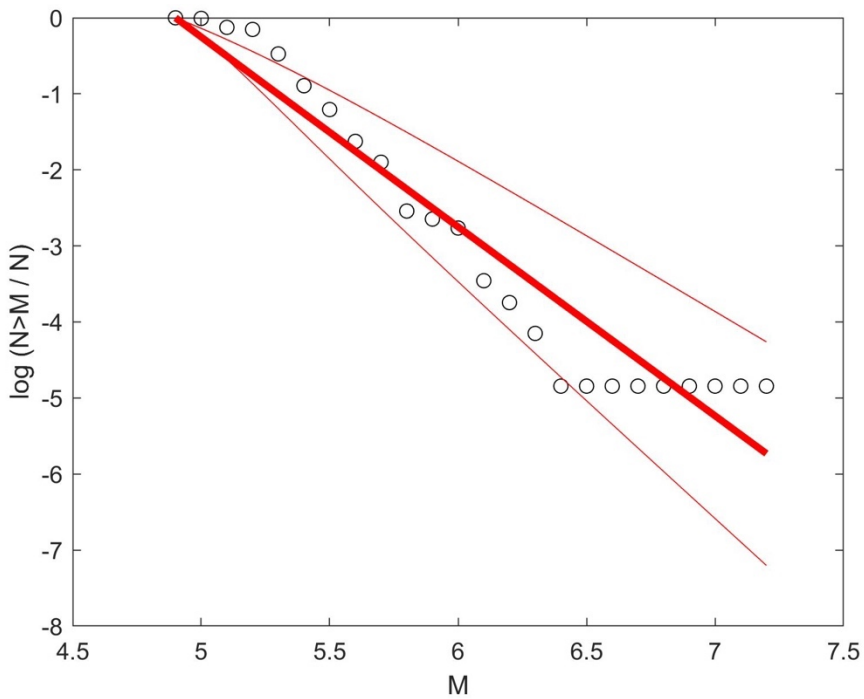

Figure 86. Frequency-magnitude distribution. The bold red line represents the model of equation (26) for qM= 1.48, while the other two lines present the corresponding 95% confidence intervals.

Figure 87 shows the typical Q-exponential pattern and Q-logarithmic function of the cumulative distribution function, P(>T) of the aftershocks interevent times and a q=1.80 is obtained.

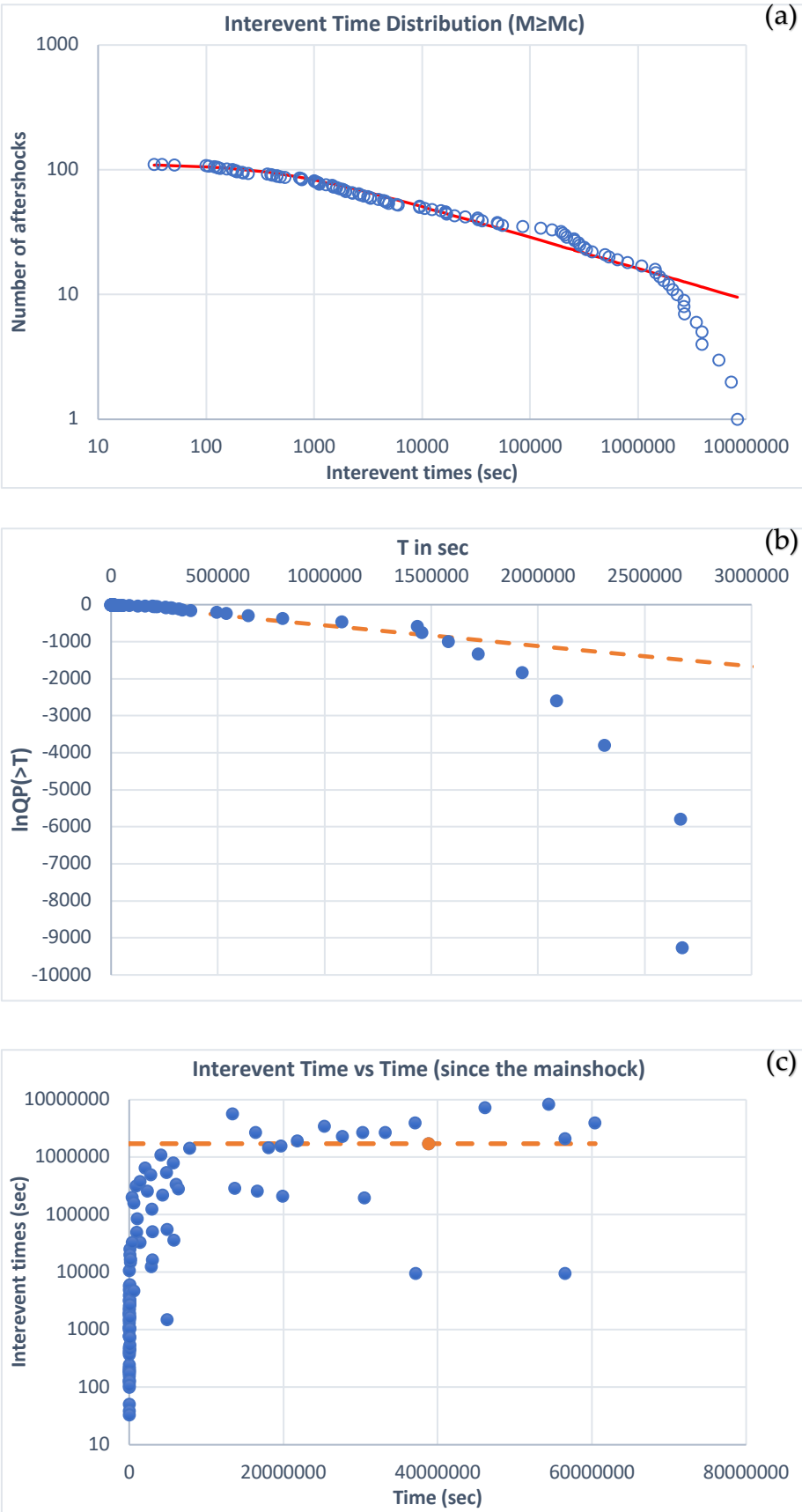

Figure 87. (a) The cumulative distribution function of the interevent times. The red line is the Q-exponential fitting with q = 1.80. **(b)** The Q-logarithmic function of the P(>T) as a function of the interevent times where the dashed line is the fitting with q=1.80. The deviation from the linearity suggests Tc values close to 1,500,000 s. **(c)** The evolution of interevent time T as a function of time t since the main event. The Tc value is indicated by the dashed line.

4.2.18 The 2009 Matavai Earthquake M_w=8.1 (Samoa)

The figure below shows Guttenberg-Richter distribution. The estimated parameters are Mc=5.0 and b=1.57 with a standard deviation of 0.09.

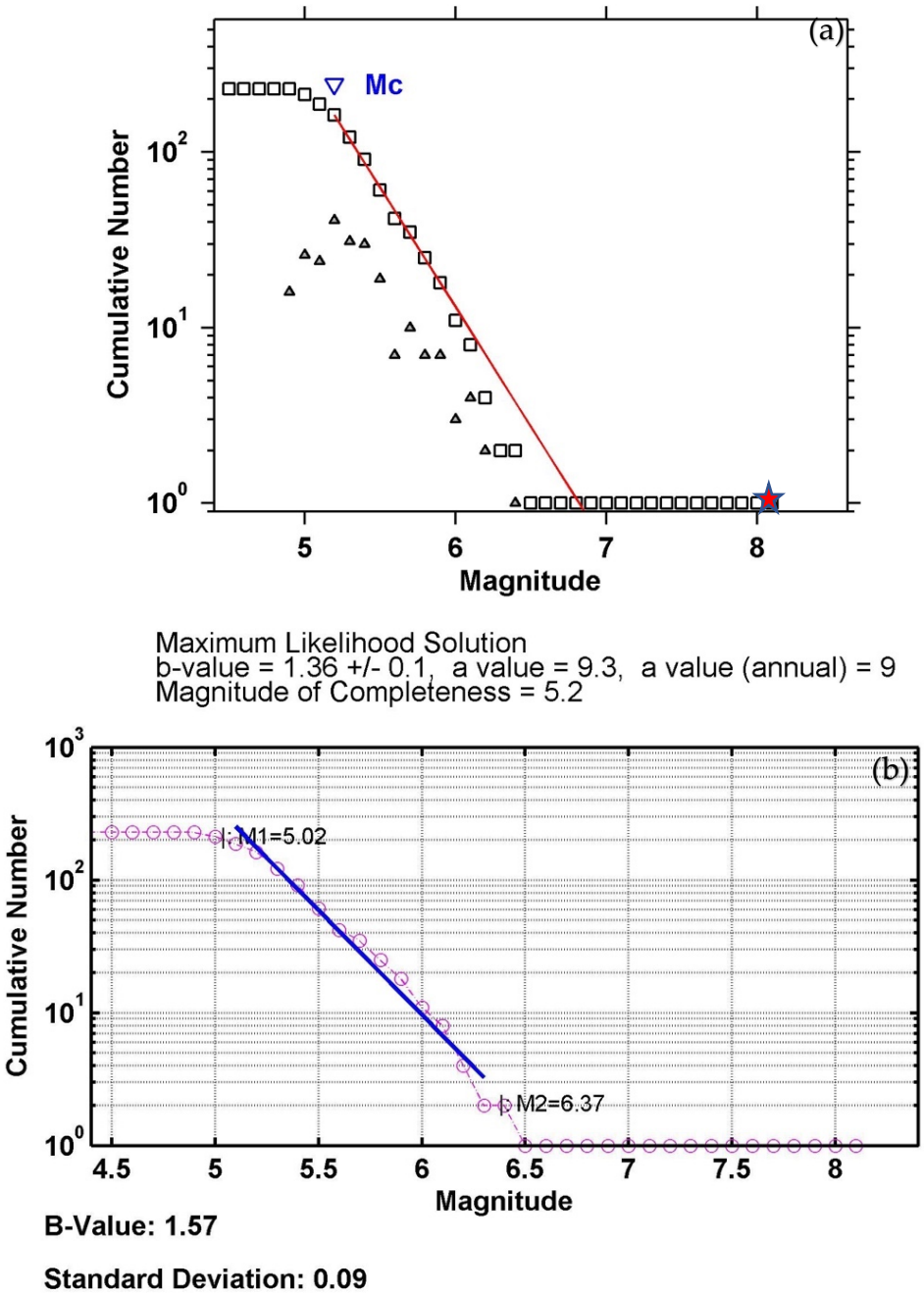

Figure 88. (a) The Guttenberg-Richter distribution using maximum likelihood method with the best combination of maximum curvature M_c 95% and M_c 90% probability. The red star shows the magnitude of the mainshock M_w 8.1. **(b)** The Guttenberg-Richter distribution using the manual method.

Next figure presents the model proposed by the AIC with p= 1.02, c= 0.01 and k= 14.4.

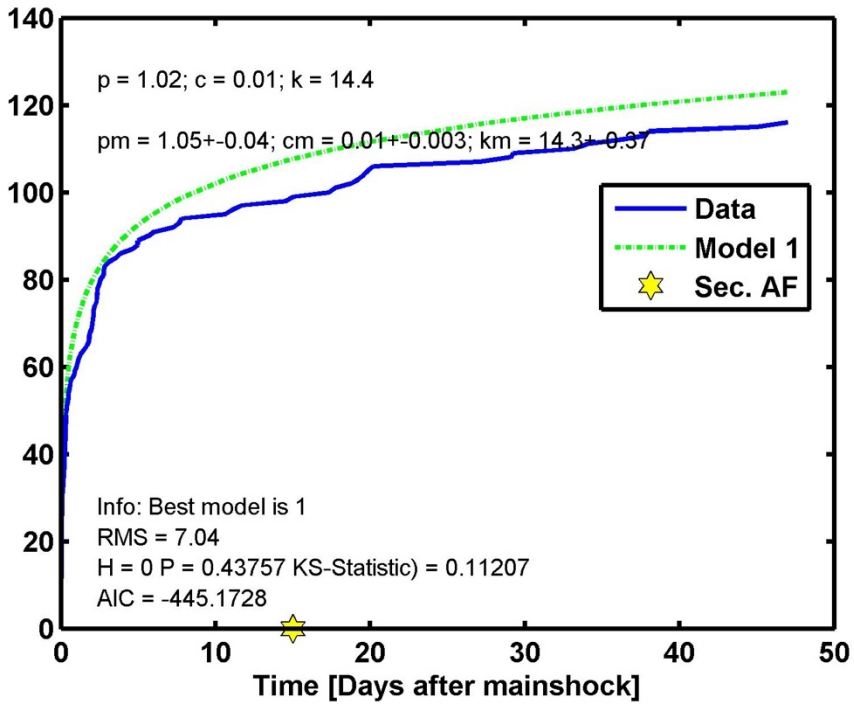

Figure 89. The best model (1) of the estimated curve of the modified Omori formula (dashed line) applied to the aftershock data and the observed cumulative number of aftershocks (solid line) based on the AIC with RMS= 7.04.

Here is the magnitude-time form of the aftershock sequence.

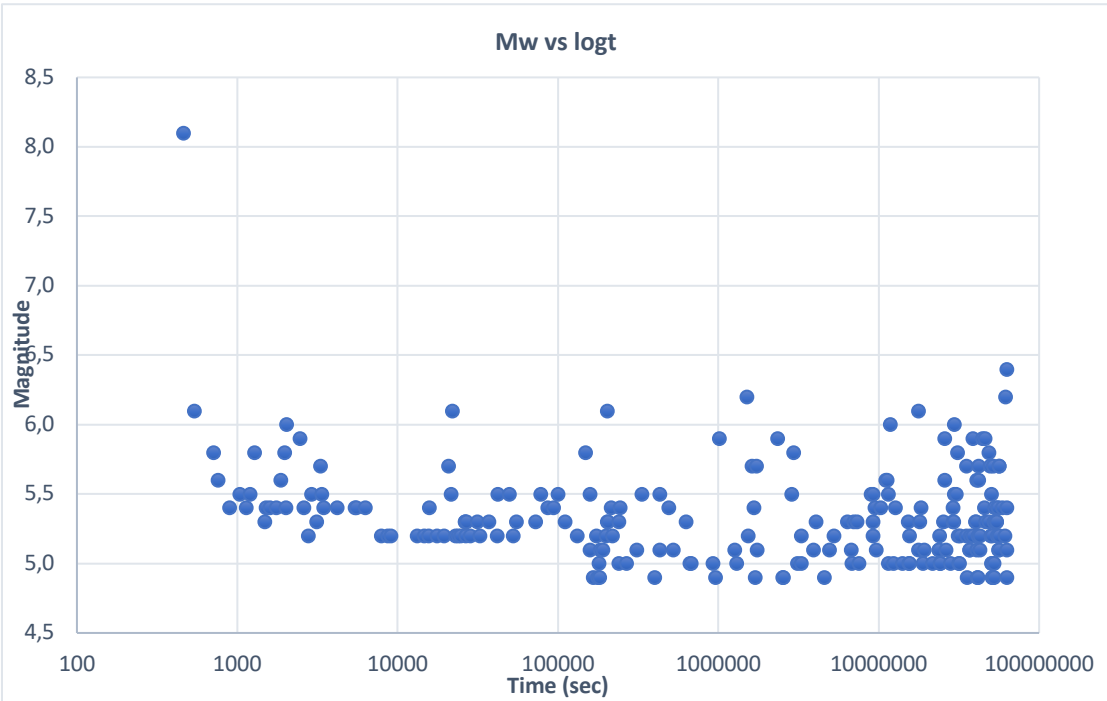

Figure 90. The magnitude-time pattern versus the logarithm of time of the mainshock M_w 8.1.

By the frequency-magnitude distribution for this earthquake, it is estimated a q_M= 1.23 with ci= 1.19-1.27.

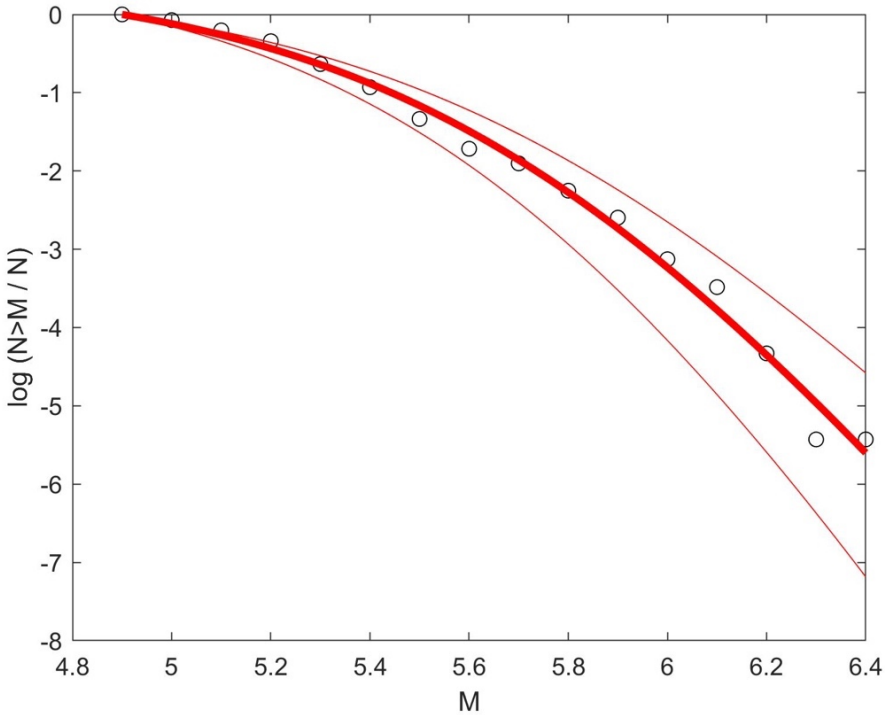

Figure 91. Frequency-magnitude distribution. The bold red line represents the model of equation (26) for qM= 1.23, while the other two lines present the corresponding 95% confidence intervals.

Figure 92 shows the typical Q-exponential pattern and Q-logarithmic function of the cumulative distribution function, P(>T) of the aftershocks interevent times and a q=1.83 is obtained.

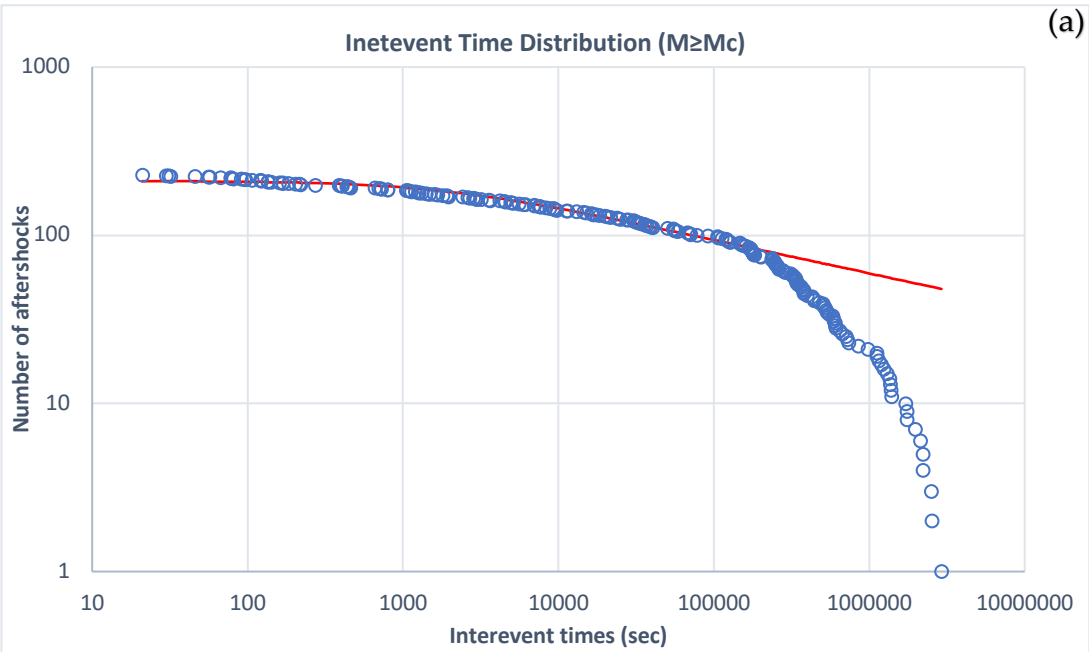

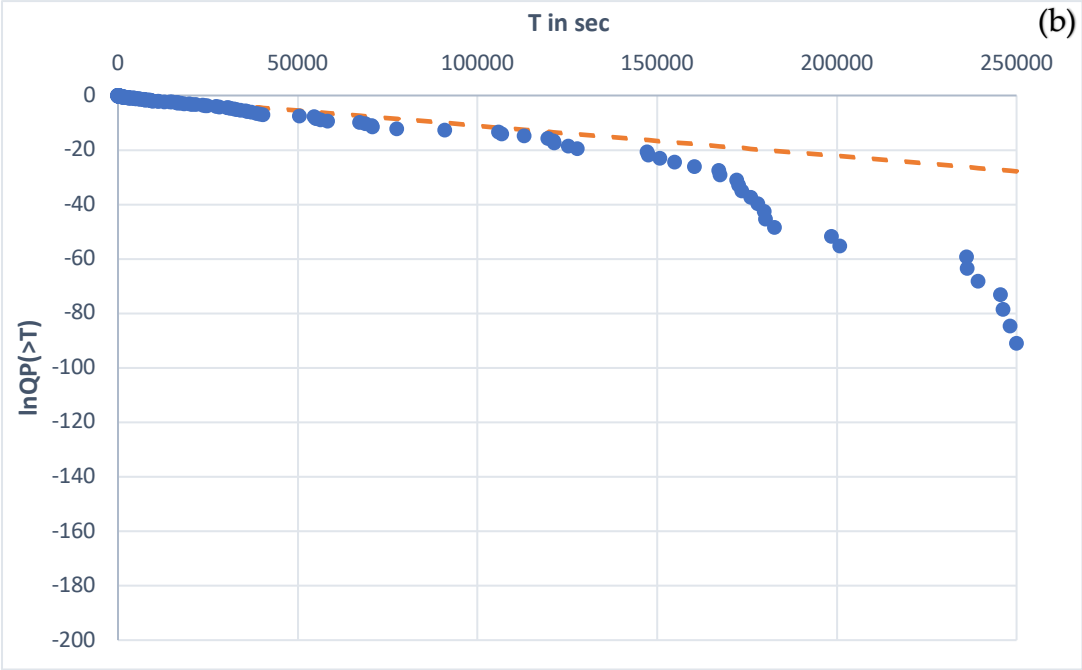

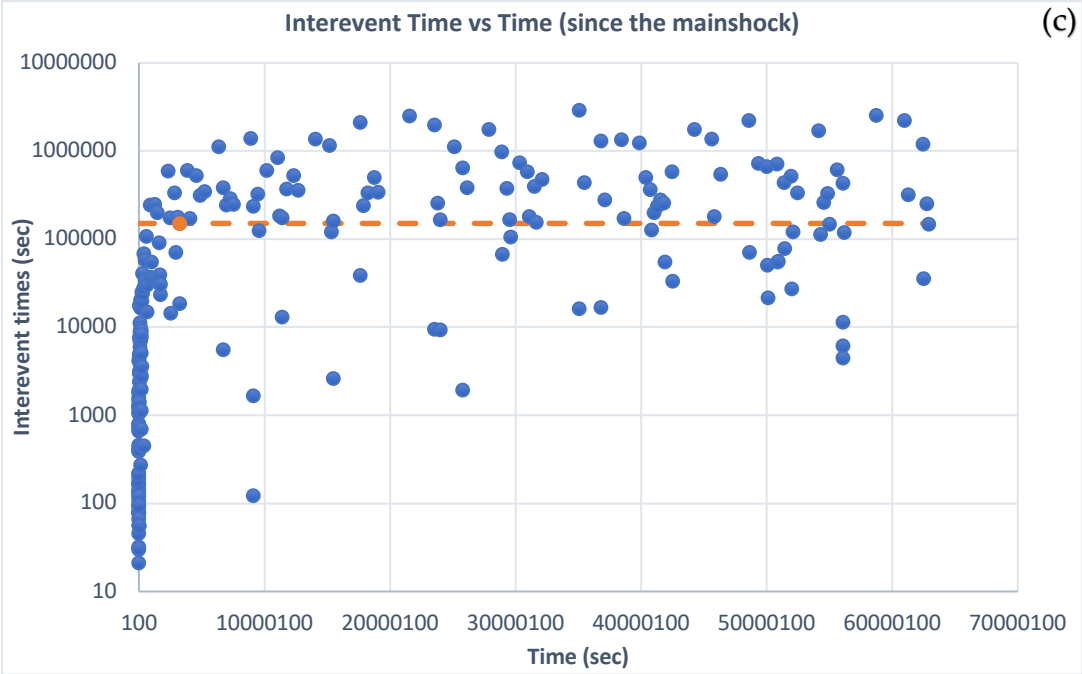

Figure 92. (a) The cumulative distribution function of the interevent times. The red line is the Q-exponential fitting with q = 1.83. **(b)** The Q-logarithmic function of the P(>T) as a function of the interevent times where the dashed line is the fitting with q=1.83. The deviation from the linearity suggests Tc values close to 150,000 s. **(c)** The evolution of interevent time T as a function of time t since the main event. The Tc value is indicated by the dashed line.

4.2.19 The 2009 Sola Earthquake M_w=7.8 (Vanuatu)

The figure below shows Guttenberg-Richter distribution. The estimated parameters are Mc=5.1, b=0.93 and a=6.83.

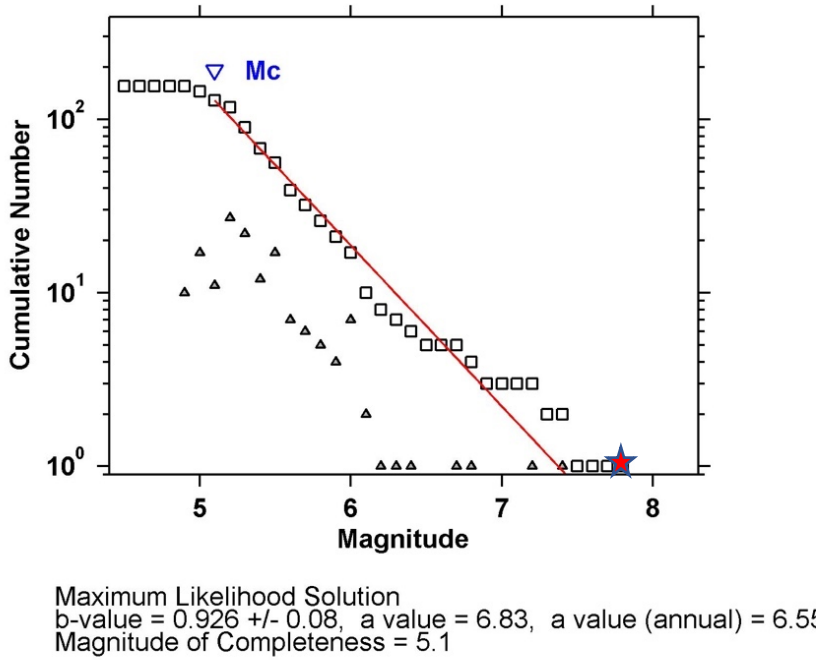

Figure 93. The Guttenberg-Richter distribution using maximum likelihood method with the best combination of maximum curvature M_c 95% and M_c 90% probability. The red star shows the magnitude of the mainshock M_w 7.8.

Next figure (94a) presents the model proposed by the AIC with p= 1, c= 0.02 and k= 12.6 while (84b) presents the model with the lowest RMS and p1= 1.01, p2=2.7, c1=0.02, c2=2.53, k1=12.2 and k2= 25.7.

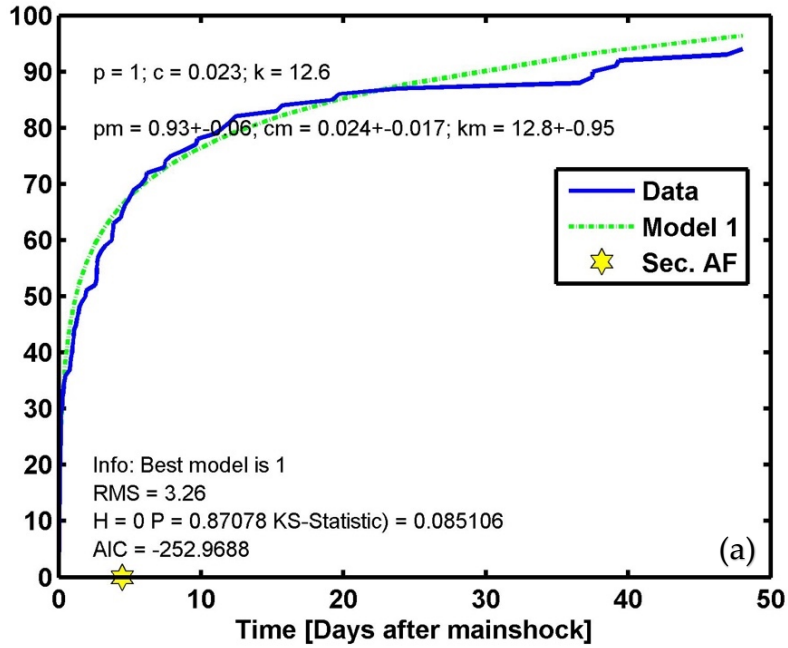

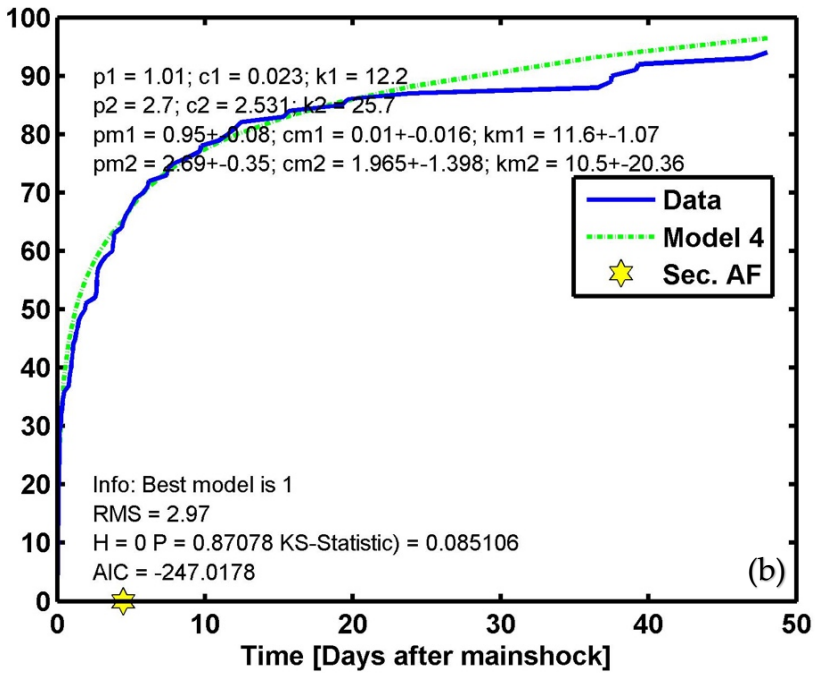

Figure 94. (a) The best model (1) of the estimated curve of the modified Omori formula (dashed line) applied to the aftershock data and the observed cumulative number of aftershocks (solid line) based on the AIC. **(b)** The model 4 of the estimated curve of the modified Omori formula (dashed line) applied to the aftershock data and the observed cumulative number of aftershocks (solid line), with the lowest RMS= 2.97.

Here is the magnitude-time form of the aftershock sequence.

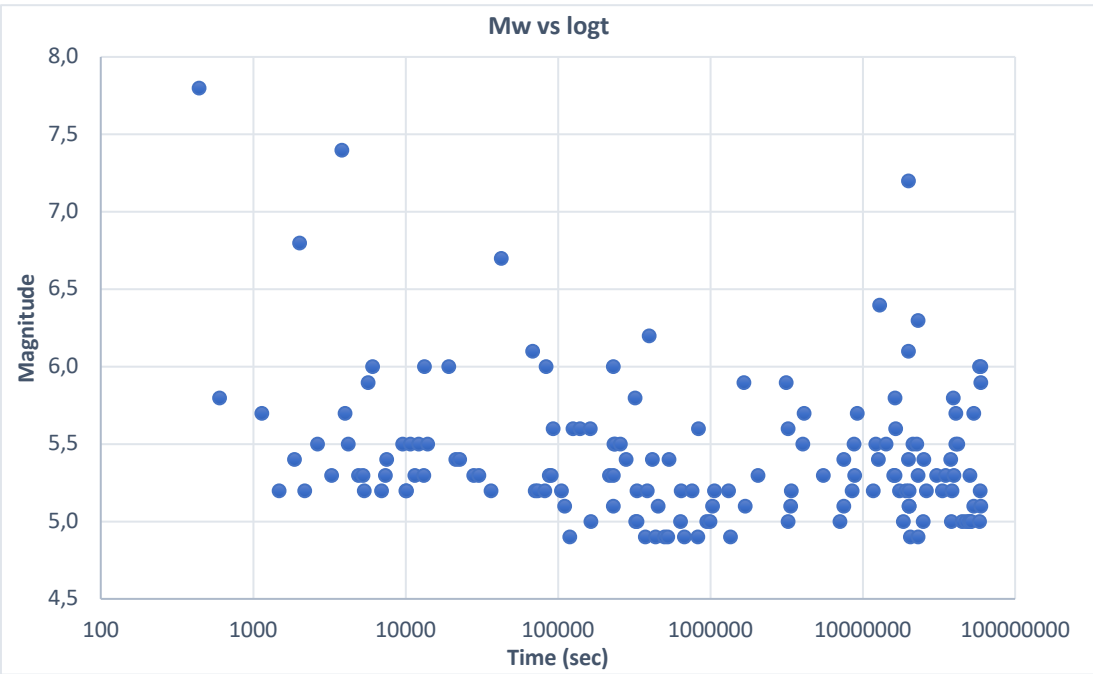

Figure 95. The magnitude-time pattern versus the logarithm of time of the mainshock M_w 7.8.

By the frequency-magnitude distribution for this earthquake, it is estimated a q_M= 1.56 with ci= 1.53-1.58.

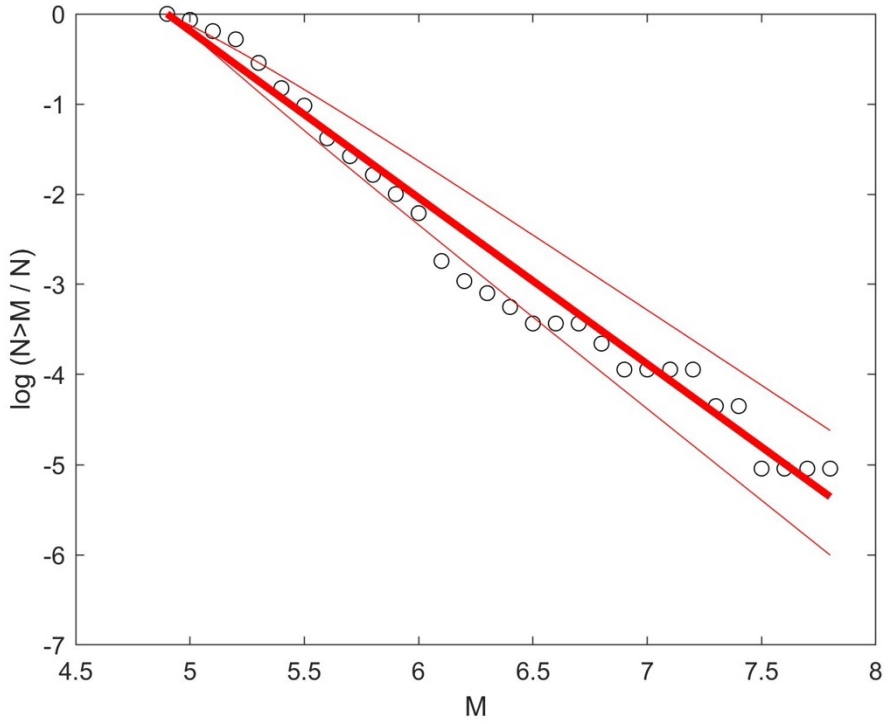

Figure 96. Frequency-magnitude distribution. The bold red line represents the model of equation (26) for qM= 1.56, while the other two lines present the corresponding 95% confidence intervals.

Figure 97 shows the typical Q-exponential pattern and Q-logarithmic function of the cumulative distribution function, P(>T) of the aftershocks interevent times and a q=1.80 is obtained.

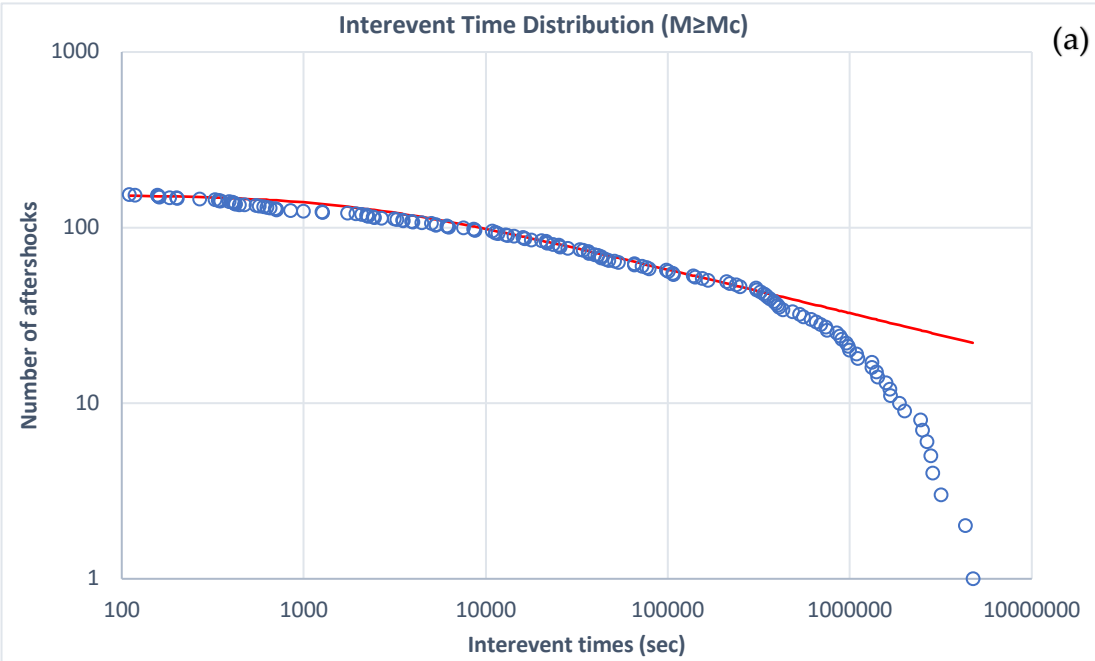

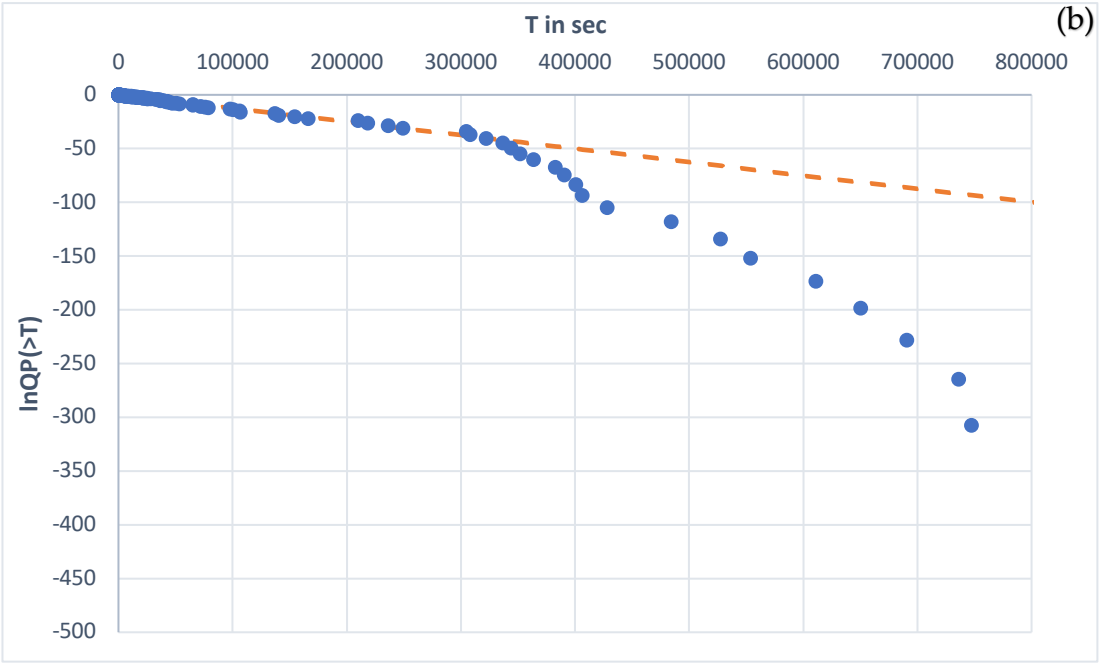

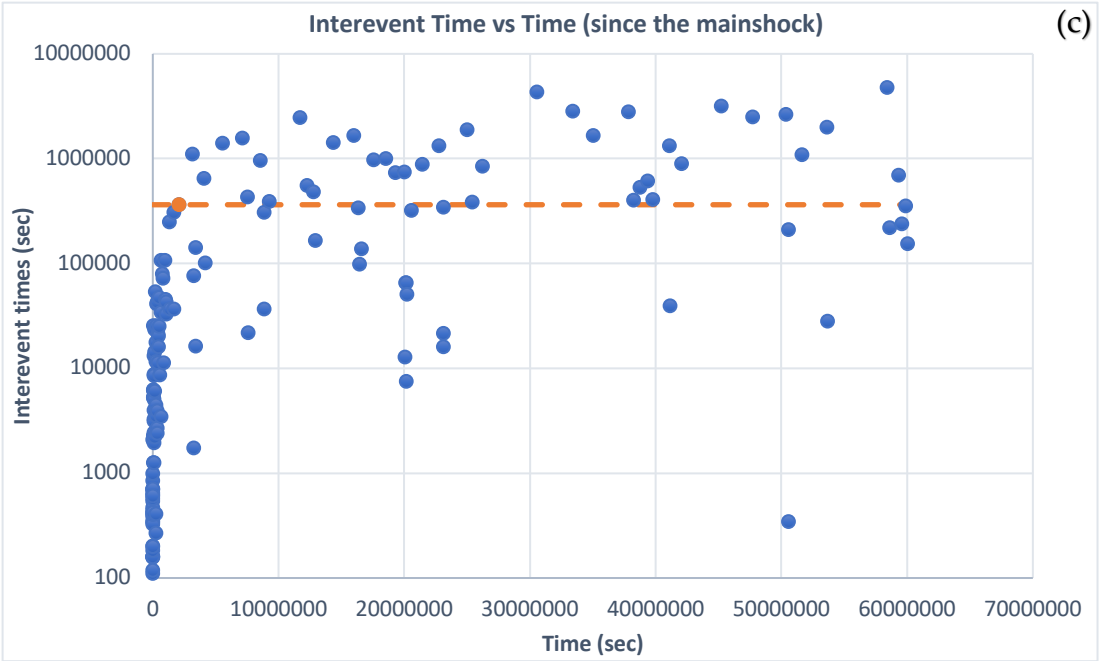

Figure 97. (a) The cumulative distribution function of the interevent times. The red line is the Q-exponential fitting with q = 1.80. **(b)** The Q-logarithmic function of the P(>T) as a function of the interevent times where the dashed line is the fitting with q=1.80. The deviation from the linearity suggests Tc values close to 400,000 s. **(c)** The evolution of interevent time T as a function of time t since the main event. The Tc value is indicated by the dashed line.

4.2.20 The 2010 Quirihue Earthquake M_w=8.8 (Chile)

The figure below shows Guttenberg-Richter distribution. The estimated parameters are Mc=5.0, b=0.85 and a=6.55.

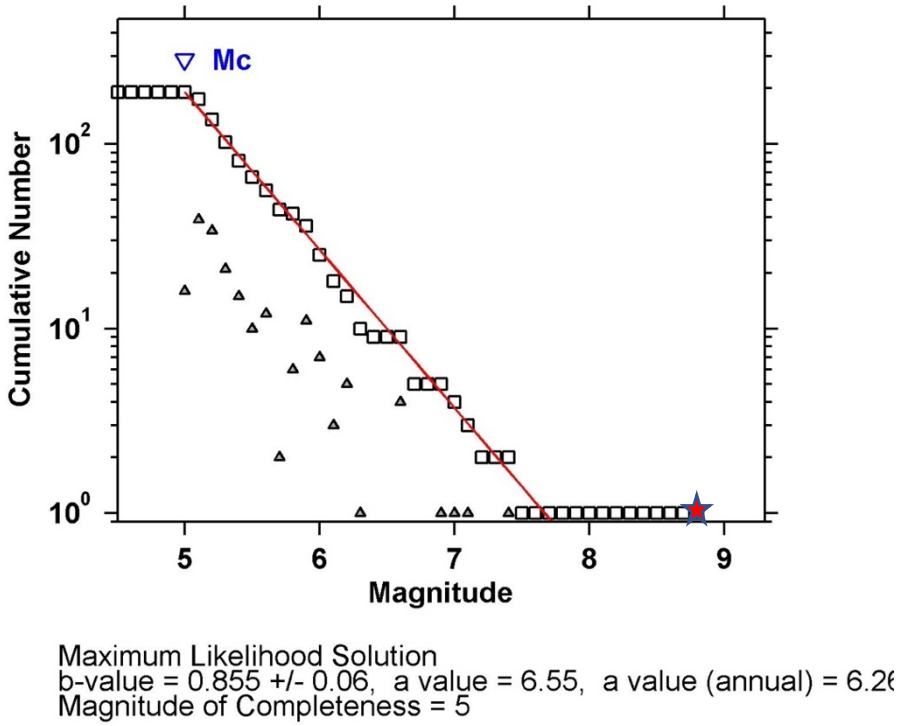

Figure 98. The Guttenberg-Richter distribution using maximum likelihood method with the best combination of maximum curvature M_c 95% and M_c 90% probability. The red star shows the magnitude of the mainshock M_w 8.8.

Next figure (99a) presents the model proposed by the AIC with p= 1.31, c=5, k=90.4 while (99b) presents the model with the lowest RMS and p1=1.39, p2=2.36 c1= 5, c2=3.28, k1=102.6 and k2=59.6.

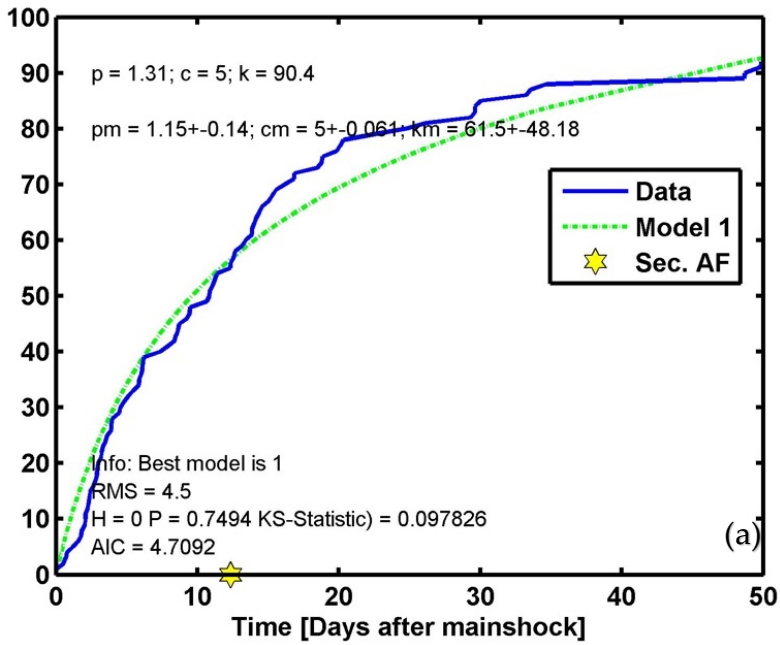

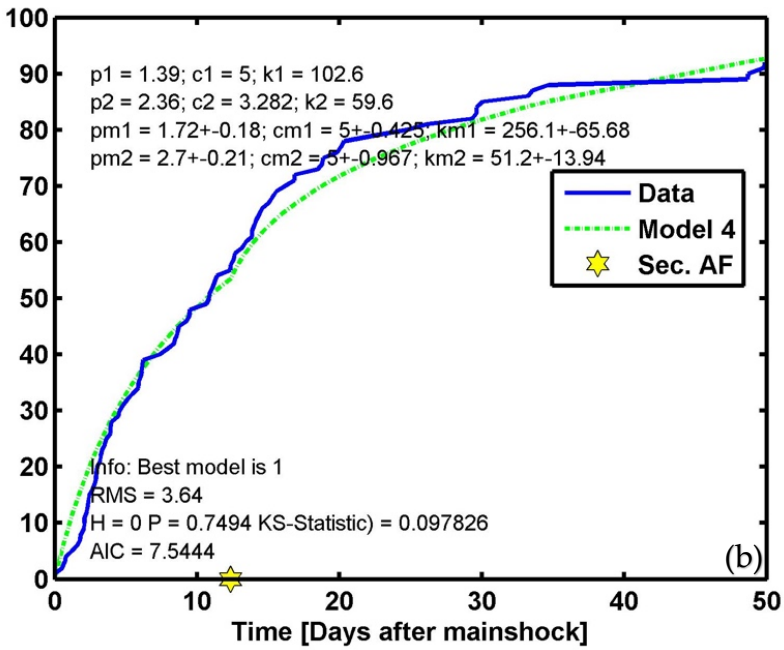

Figure 99. (a) The best model (1) of the estimated curve of the modified Omori formula (dashed line) applied to the aftershock data and the observed cumulative number of aftershocks (solid line) based on the AIC. **(b)** The model 4 of the estimated curve of the modified Omori formula (dashed line) applied to the aftershock data and the observed cumulative number of aftershocks (solid line), with the lowest RMS= 3.64.

Here is the magnitude-time form of the aftershock sequence.

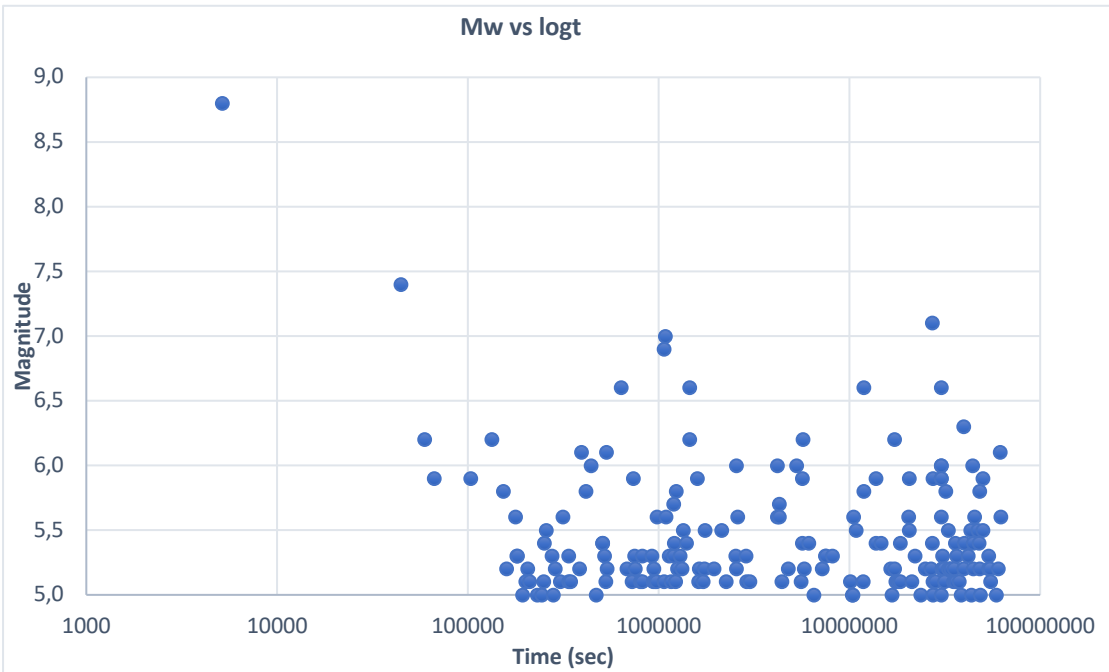

Figure 100. The magnitude-time pattern versus the logarithm of time of the mainshock M_w 8.8.

By the frequency-magnitude distribution for this earthquake, it is estimated a q_M= 1.50 with ci= 1.48-1.52.

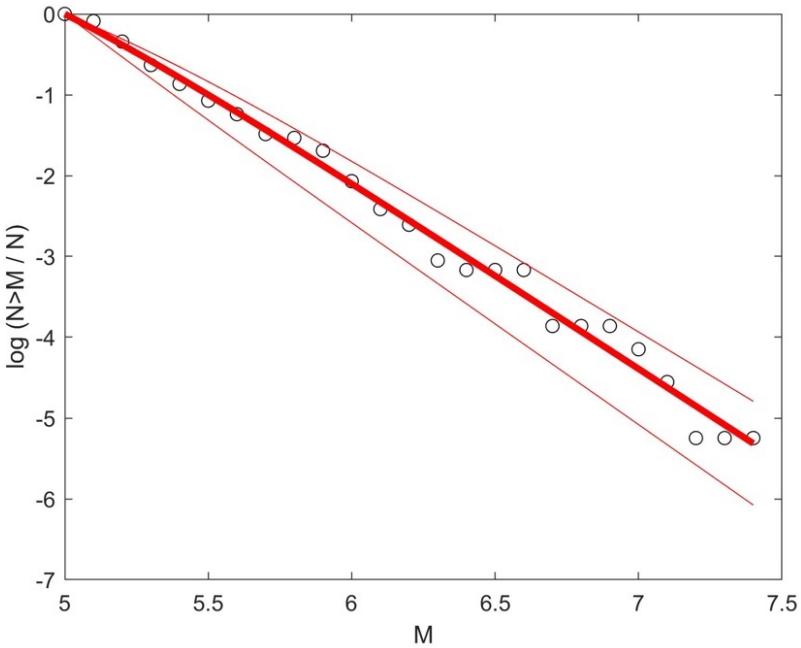

Figure 101. Frequency-magnitude distribution. The bold red line represents the model of equation (26) for qM= 1.50, while the other two lines present the corresponding 95% confidence intervals.

Figure 102 shows the typical Q-exponential pattern and Q-logarithmic function of the cumulative distribution function, P(>T) of the aftershocks interevent times and a q=1.67 is obtained.

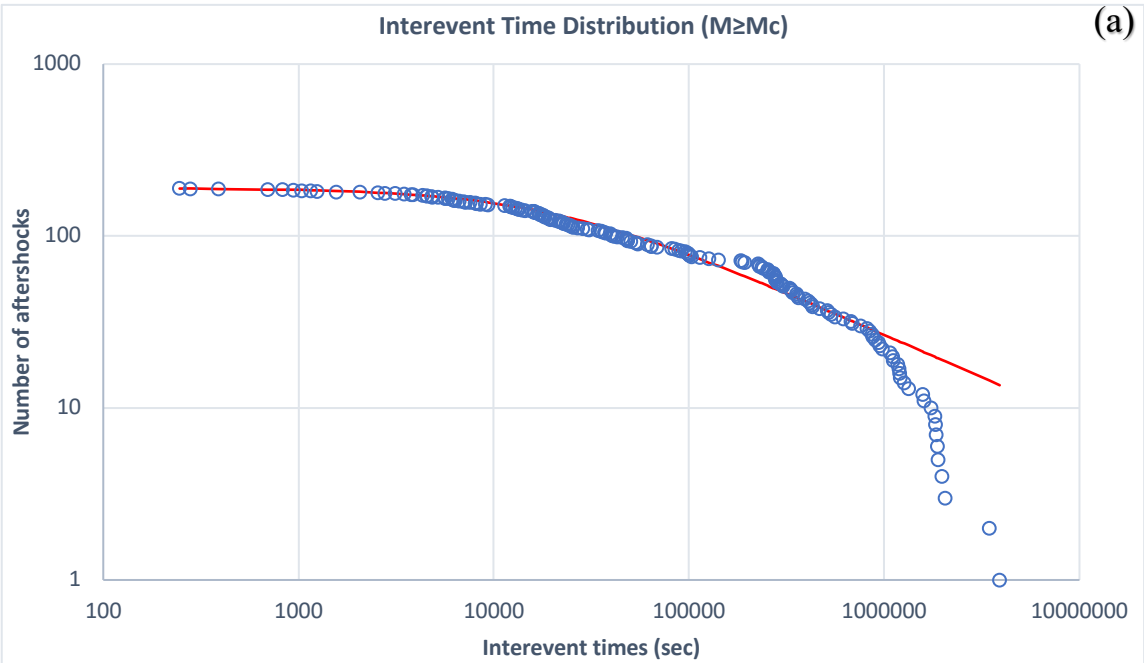

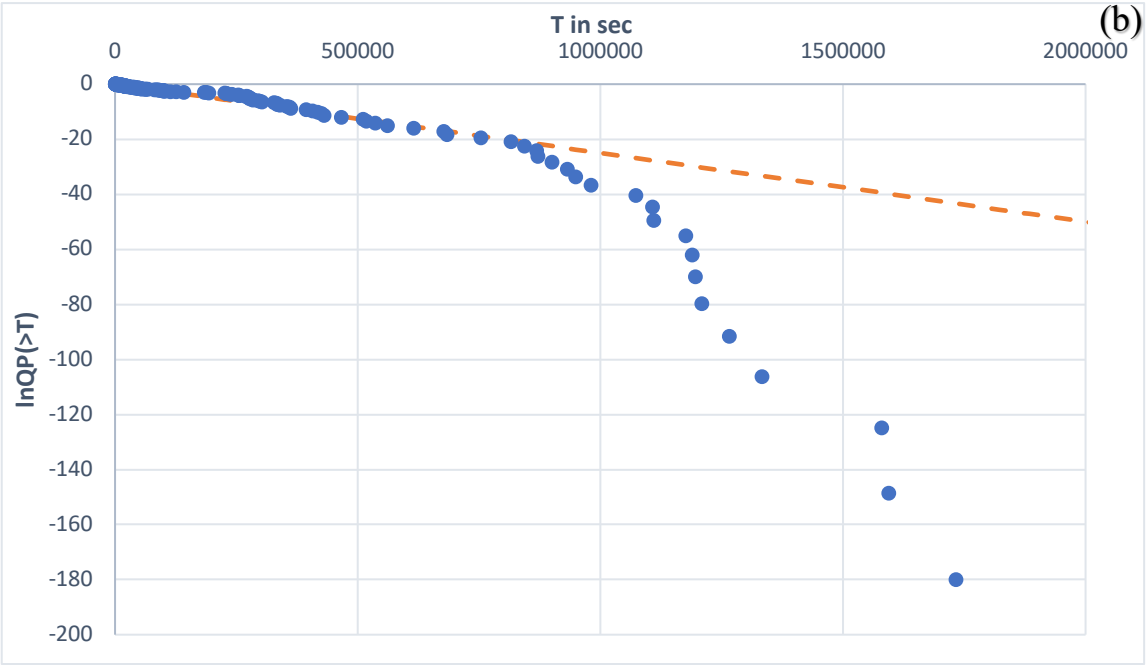

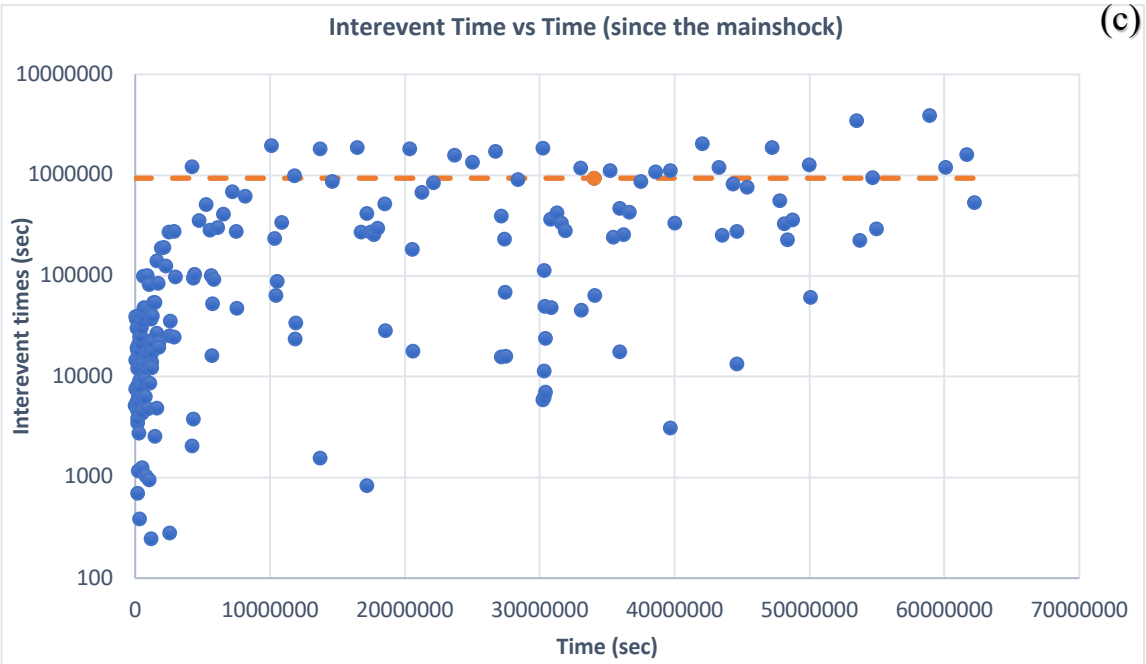

Figure 102. (a) The cumulative distribution function of the interevent times. The red line is the Q-exponential fitting with q = 1.67. **(b)** The Q-logarithmic function of the P(>T) as a function of the interevent times where the dashed line is the fitting with q=1.67. The deviation from the linearity suggests Tc values close to 1,000,000 s. **(c)** The evolution of interevent time T as a function of time t since the main event. The Tc value is indicated by the dashed line.

4.2.21 The 2011 Great Tohuko Earthquake M_w=9.1 (Japan)

The figure below shows Guttenberg-Richter distribution. The estimated parameters are Mc=5.0, b=0.93 and a=7.28.

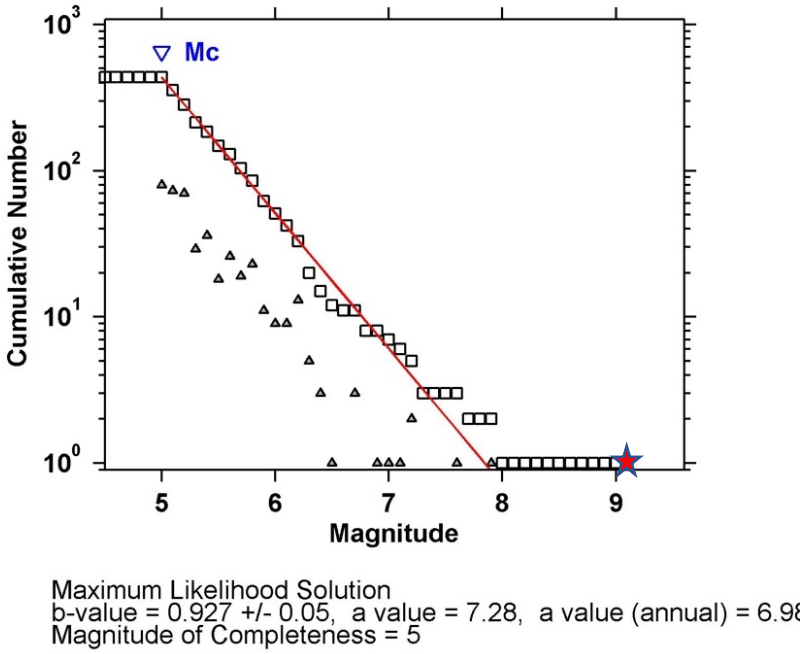

Figure 103. The Guttenberg-Richter distribution using maximum likelihood method with the best combination of maximum curvature M_c 95% and M_c 90% probability. The red star shows the magnitude of the mainshock M_w 9.1.

Next figure presents the model proposed by the AIC with p= 1.37, c= 5 and k= 265.1.

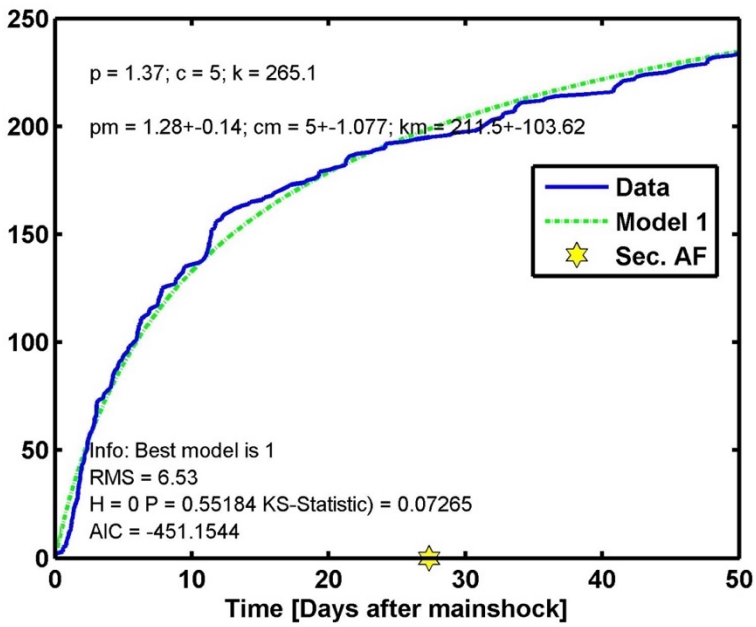

Figure 104. The best model (1) of the estimated curve of the modified Omori formula (dashed line) applied to the aftershock data and the observed cumulative number of aftershocks (solid line) based on the AIC with RMS= 6.53.

Here is the magnitude-time form of the aftershock sequence.

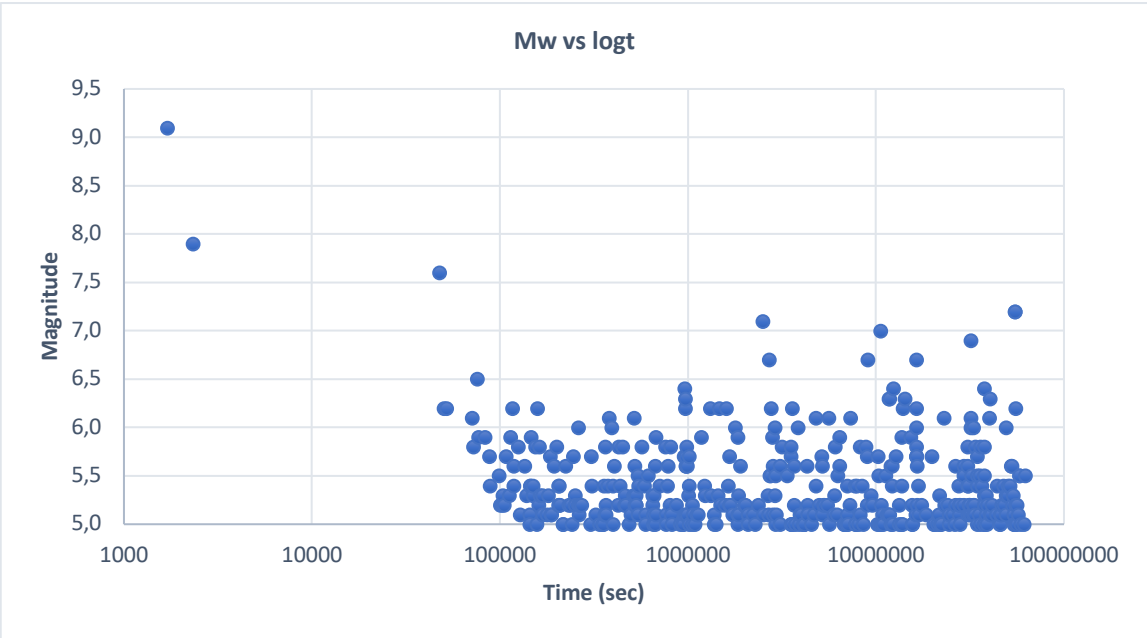

Figure 105. The magnitude-time pattern versus the logarithm of time of the mainshock M_w 9.1.

By the frequency-magnitude distribution for this earthquake, it is estimated a q_M= 1.51 with ci= 1.48-1.52.

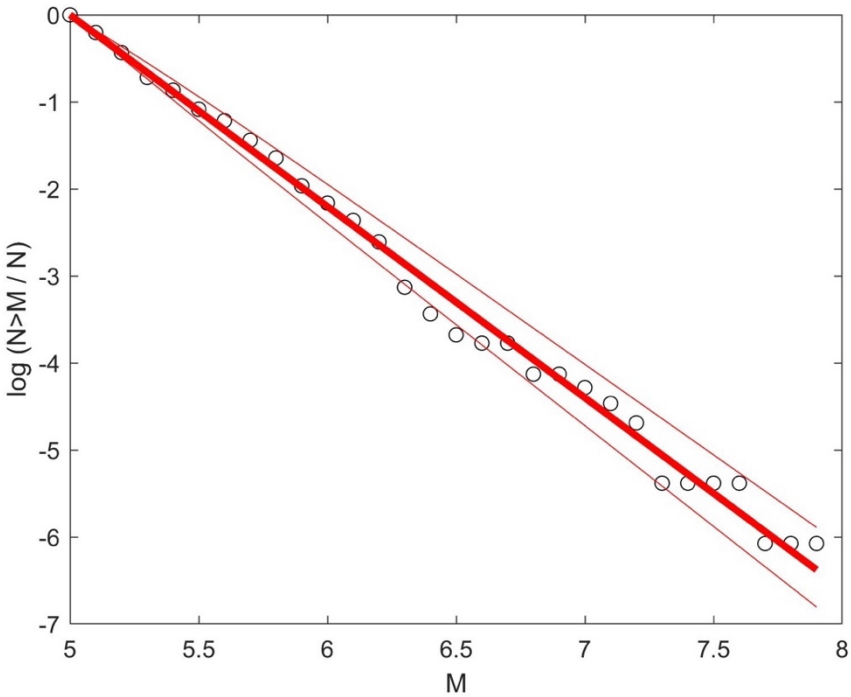

Figure 106. Frequency-magnitude distribution. The bold red line represents the model of equation (26) for qM= 1.51, while the other two lines present the corresponding 95% confidence intervals.

Figure 107 shows the typical Q-exponential pattern and Q-logarithmic function of the cumulative distribution function, P(>T) of the aftershocks interevent times and a q=1.67 is obtained.

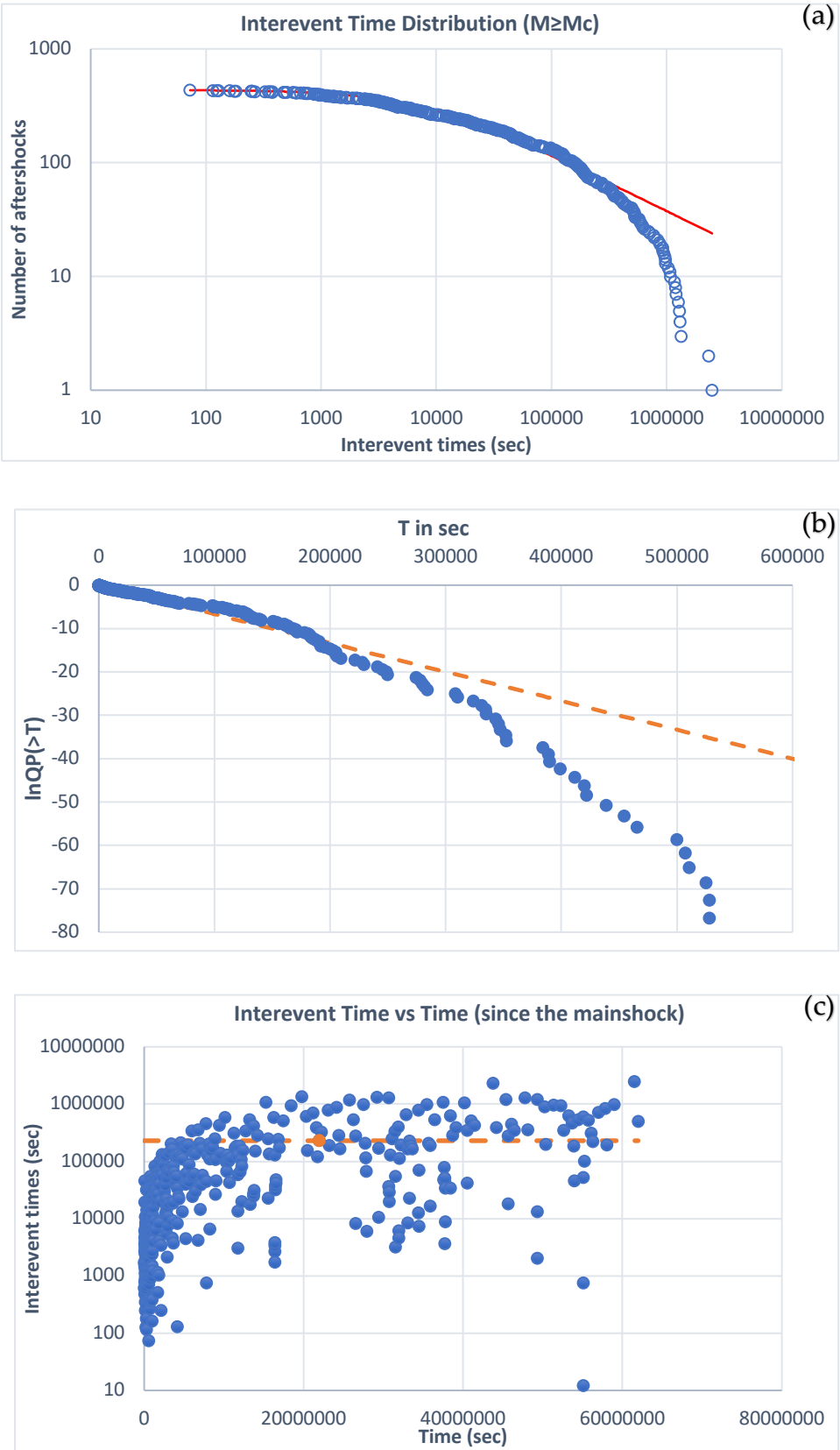

Figure 107. (a) The cumulative distribution function of the interevent times. The red line is the Q-exponential fitting with q = 1.67. **(b)** The Q-logarithmic function of the P(>T) as a function of the interevent times where the dashed line is the fitting with q=1.67. The deviation from the linearity suggests Tc values close to 300,000 s. **(c)** The evolution of interevent time T as a function of time t since the main event. The Tc value is indicated by the dashed line.

4.2.22 The 2011 Kermadec Island Earthquake M_w=7.6 (New Zealand)

The figure below shows Guttenberg-Richter distribution. The estimated parameters are Mc=5.1, b=1.35 and a=8.91.

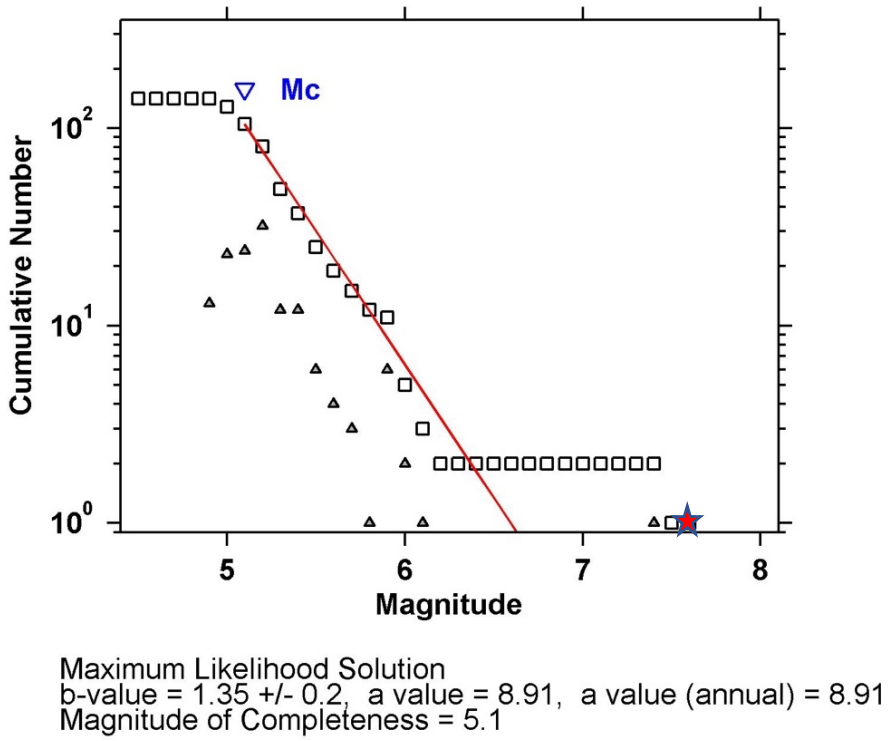

Figure 108. The Guttenberg-Richter distribution using maximum likelihood method with the best combination of maximum curvature M_c 95% and M_c 90% probability. The red star shows the magnitude of the mainshock M_w 7.6.

Next figure (109a) presents the model proposed by the AIC with p= 1.44, c= 2.29 and k= 48.9 while (109b) presents the model with the lowest RMS and p1= 1.8, p2=2.7, c1=4.46, k1=159.8 and k2= 89.1.

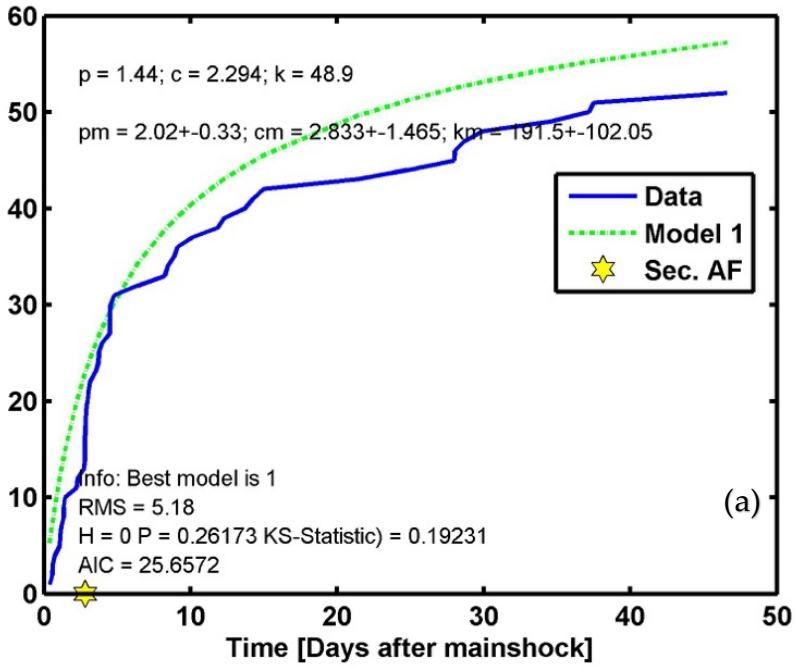

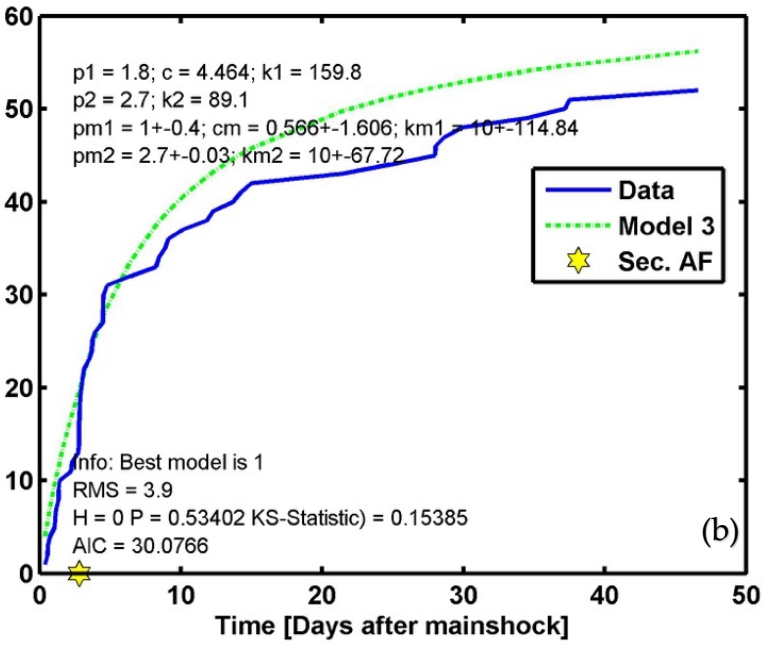

Figure 109. (a) The best model (1) of the estimated curve of the modified Omori formula (dashed line) applied to the aftershock data and the observed cumulative number of aftershocks (solid line) based on the AIC. **(b)** The model 3 of the estimated curve of the modified Omori formula (dashed line) applied to the aftershock data and the observed cumulative number of aftershocks (solid line), with the lowest RMS= 3.9.

Here is the magnitude-time form of the aftershock sequence.

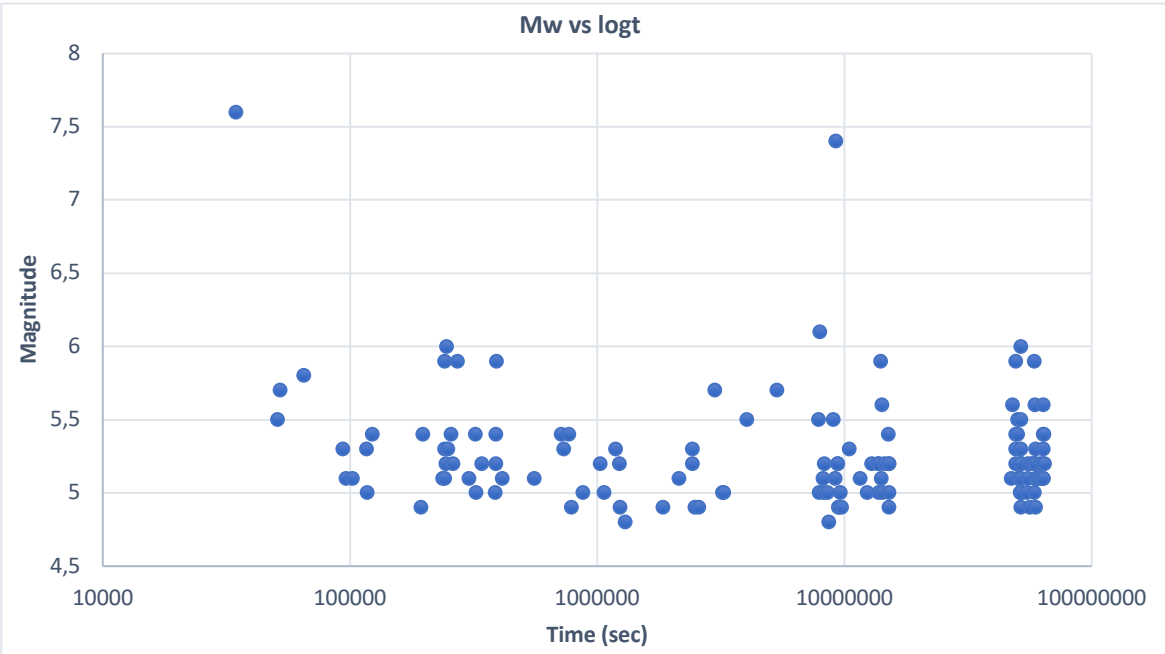

Figure 110. The magnitude-time pattern versus the logarithm of time of the mainshock M_w 7.6.

By the frequency-magnitude distribution for this earthquake, it is estimated a q_M= 1.51 with ci= 1.45-1.58.

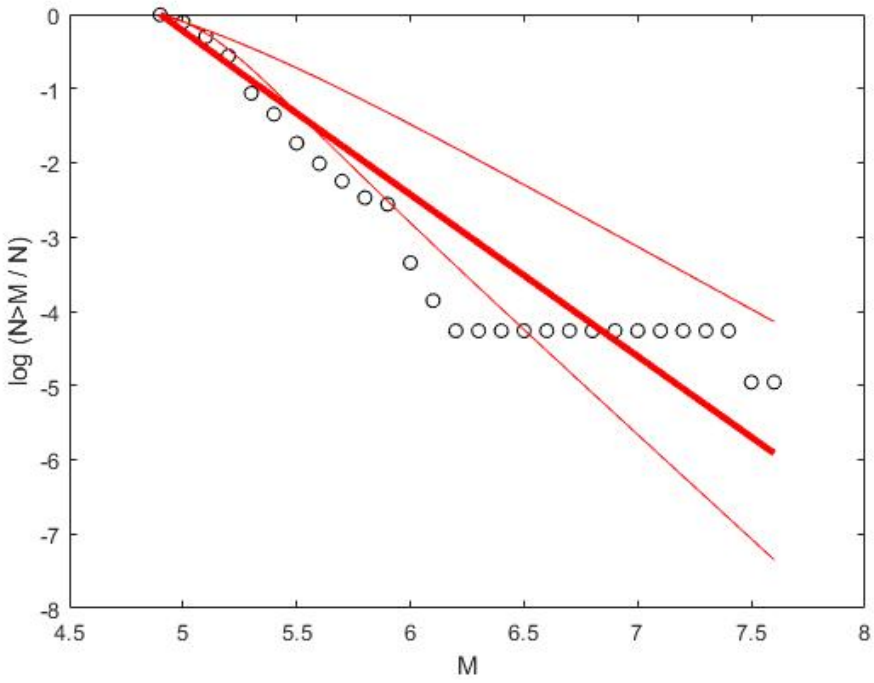

Figure 111. Frequency-magnitude distribution. The bold red line represents the model of equation (26) for qM= 1.51, while the other two lines present the corresponding 95% confidence intervals.

Figure 112 shows the typical Q-exponential pattern and Q-logarithmic function of the cumulative distribution function, P(>T) of the aftershocks interevent times and a q=1.74 is obtained.

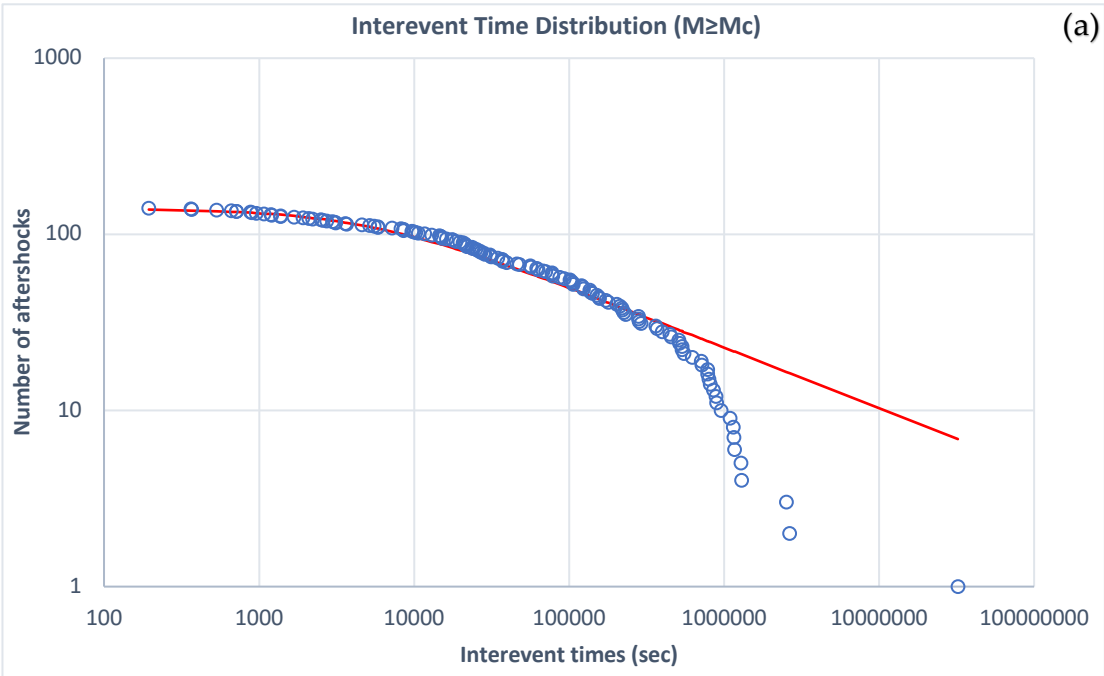

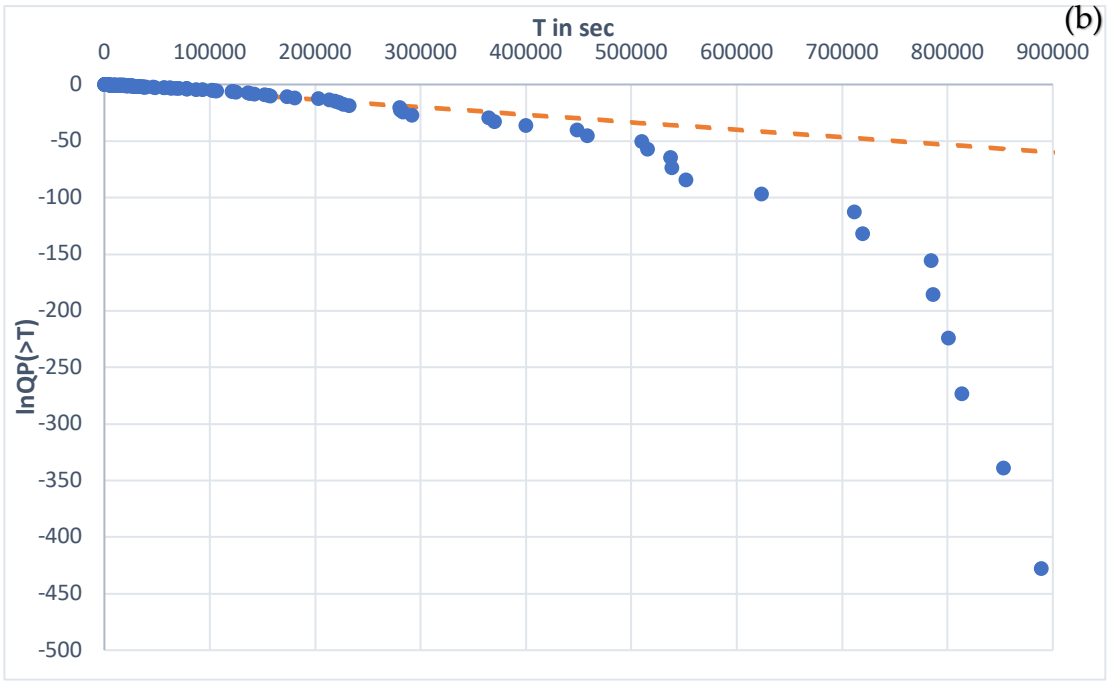

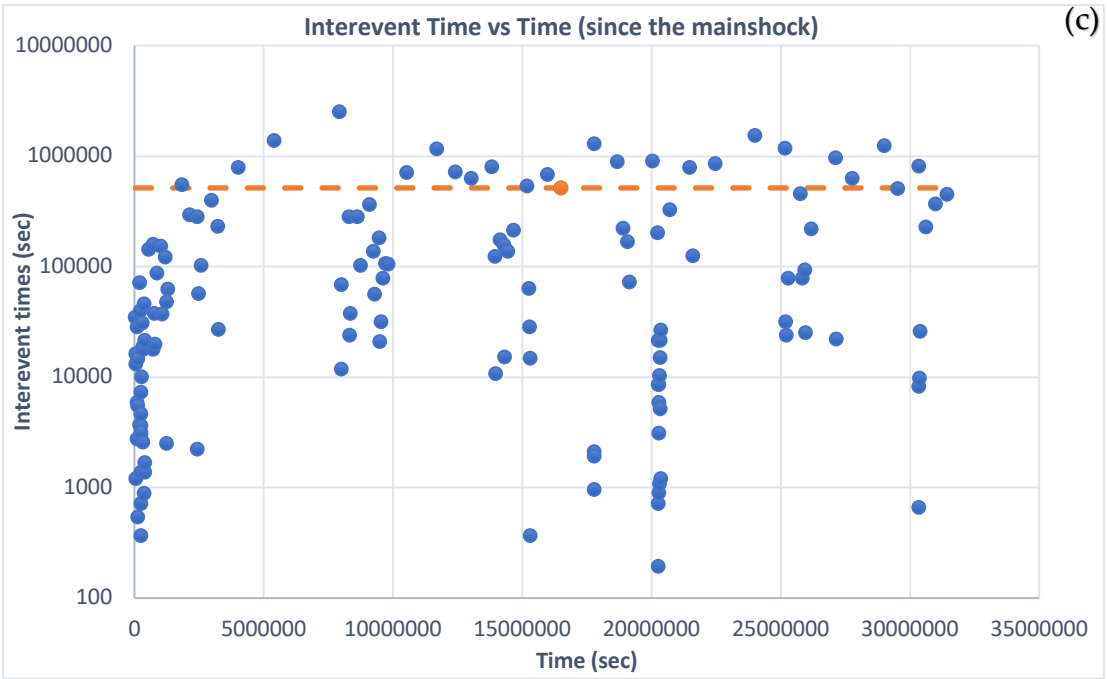

Figure 112. (a) The cumulative distribution function of the interevent times. The red line is the Q-exponential fitting with q = 1.74. **(b)** The Q-logarithmic function of the P(>T) as a function of the interevent times where the dashed line is the fitting with q=1.74. The deviation from the linearity suggests Tc values close to 500,000 s. **(c)** The evolution of interevent time T as a function of time t since the main event. The Tc value is indicated by the dashed line.

4.2.23 The 2012 West Coast of Northern Sumatra Earthquake M_w=8.6

The figure below shows Guttenberg-Richter distribution. The estimated parameters are Mc=5.0 and b=1.2 with a standard deviation of 0.05.

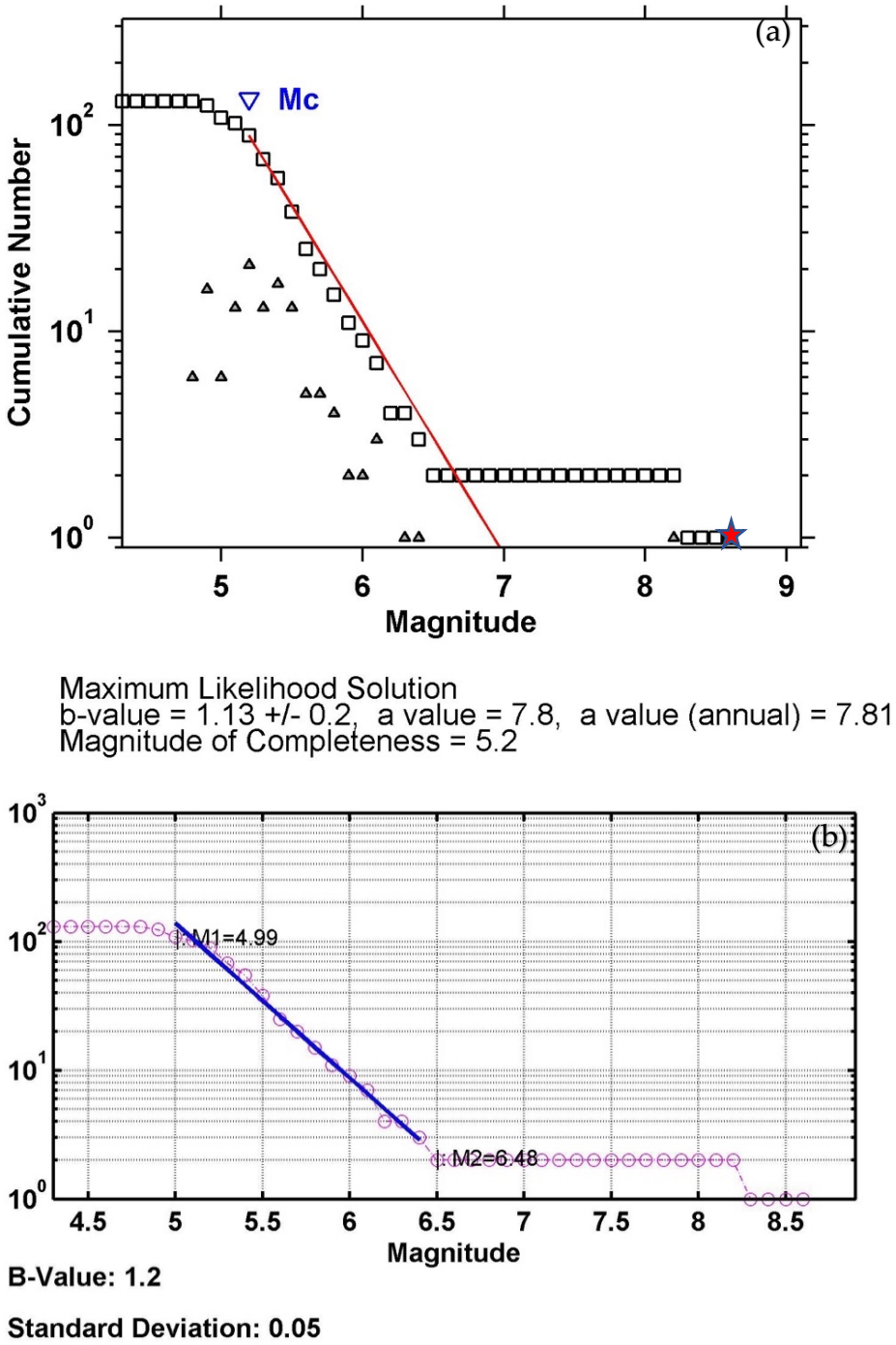

Figure 113. (a) The Guttenberg-Richter distribution using maximum likelihood method with the best combination of maximum curvature M_c 95% and M_c 90% probability. The red star shows the magnitude of the mainshock M_w 8.6. **(b)** The Guttenberg-Richter distribution using the manual method.

Next figure (114a) presents the model proposed by the AIC with p= 1.12, c= 0.04 and k= 15 while (114b) presents the model with the lowest RMS and p1= 2.12, p2=0.93, c1=0.31, c2=5, k1=22.8 and k2= 10.

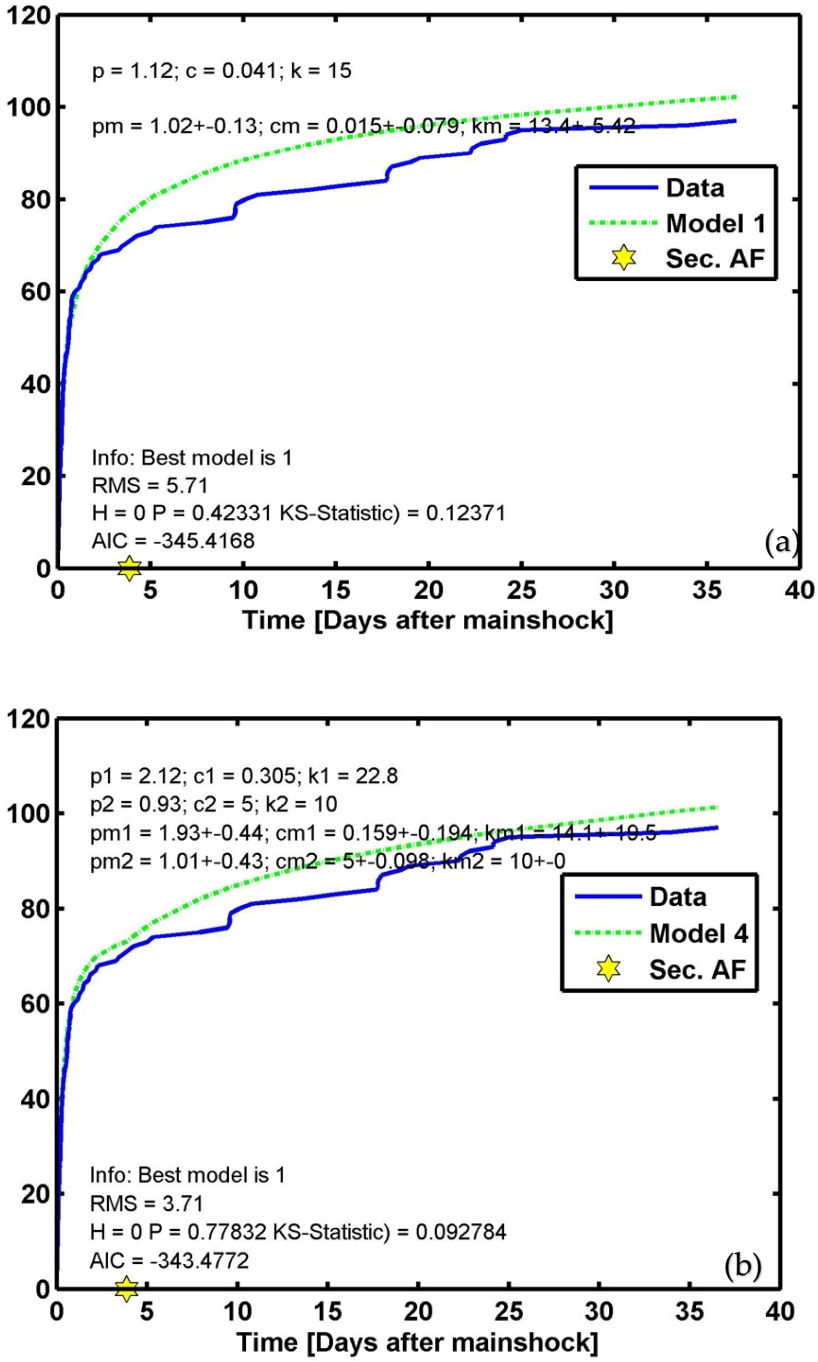

Figure 114. (a) The best model (1) of the estimated curve of the modified Omori formula (dashed line) applied to the aftershock data and the observed cumulative number of aftershocks (solid line) based on the AIC. **(b)** The model 4 of the estimated curve of the modified Omori formula (dashed line) applied to the aftershock data and the observed cumulative number of aftershocks (solid line), with the lowest RMS= 3.71.

Here is the magnitude-time form of the aftershock sequence.

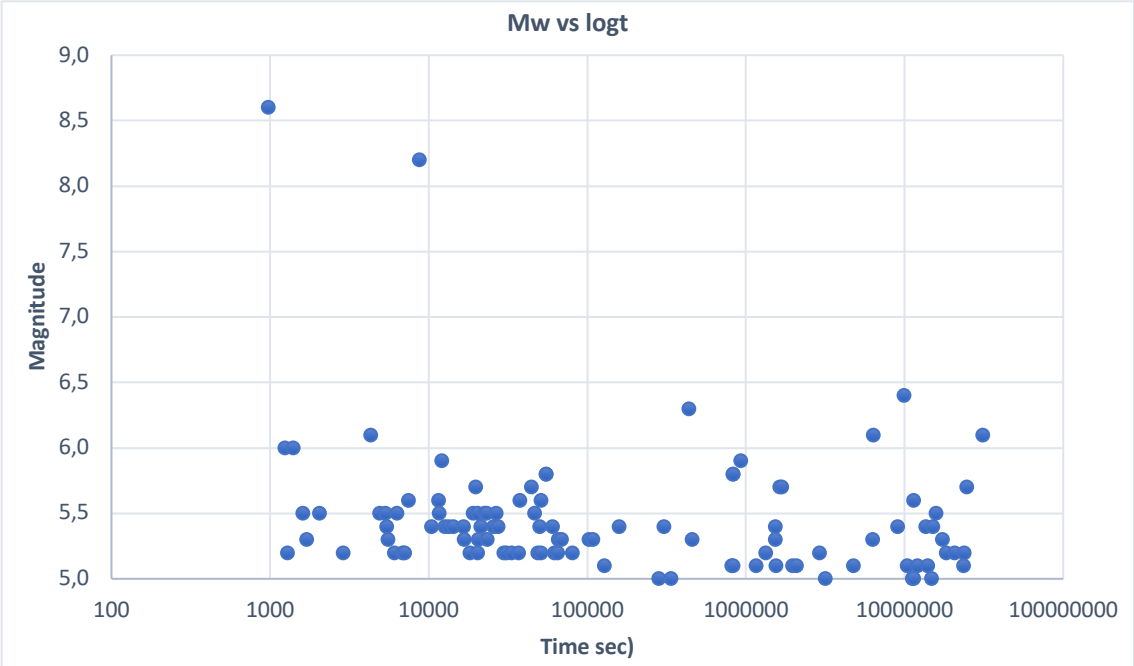

Figure 115. The magnitude-time pattern versus the logarithm of time of the mainshock M_w 8.6.

By the frequency-magnitude distribution for this earthquake, it is estimated a q_M= 1.30 with ci= 1.27-1.33.

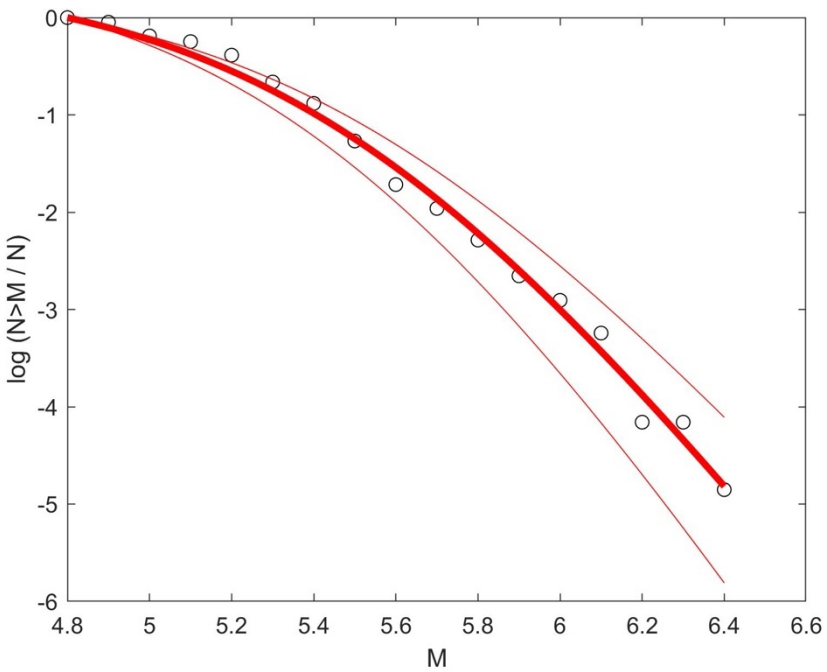

Figure 116. Frequency-magnitude distribution. The bold red line represents the model of equation (26) for qM= 1.30, while the other two lines present the corresponding 95% confidence intervals.

Figure 117 shows the typical Q-exponential pattern and Q-logarithmic function of the cumulative distribution function, P(>T) of the aftershocks interevent times and a q=1.83 is obtained.

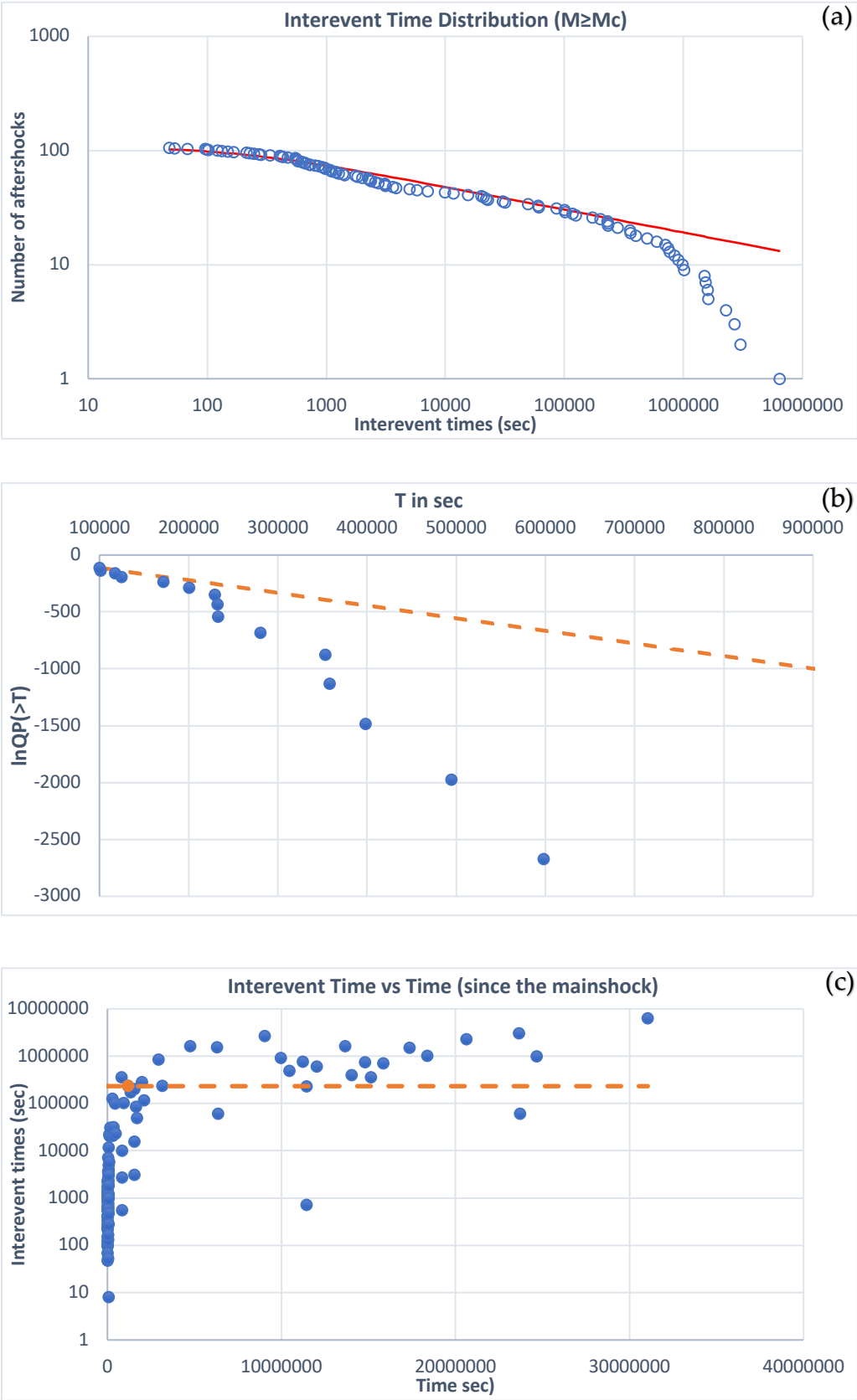

Figure 117. (a) The cumulative distribution function of the interevent times. The red line is the Q-exponential fitting with q = 1.83. **(b)** The Q-logarithmic function of the P(>T) as a function of the interevent times where the dashed line is the fitting with q=1.83. The deviation from the linearity suggests Tc values close to 250,000 s. **(c)** The evolution of interevent time T as a function of time t since the main event. The Tc value is indicated by the dashed line.

4.2.24 The 2013 Atka Earthquake M_w=7.0 (Alaska)

The figure below shows Guttenberg-Richter distribution. The estimated parameters are Mc=4.5 and b=1.03 with a standard deviation of 0.08.

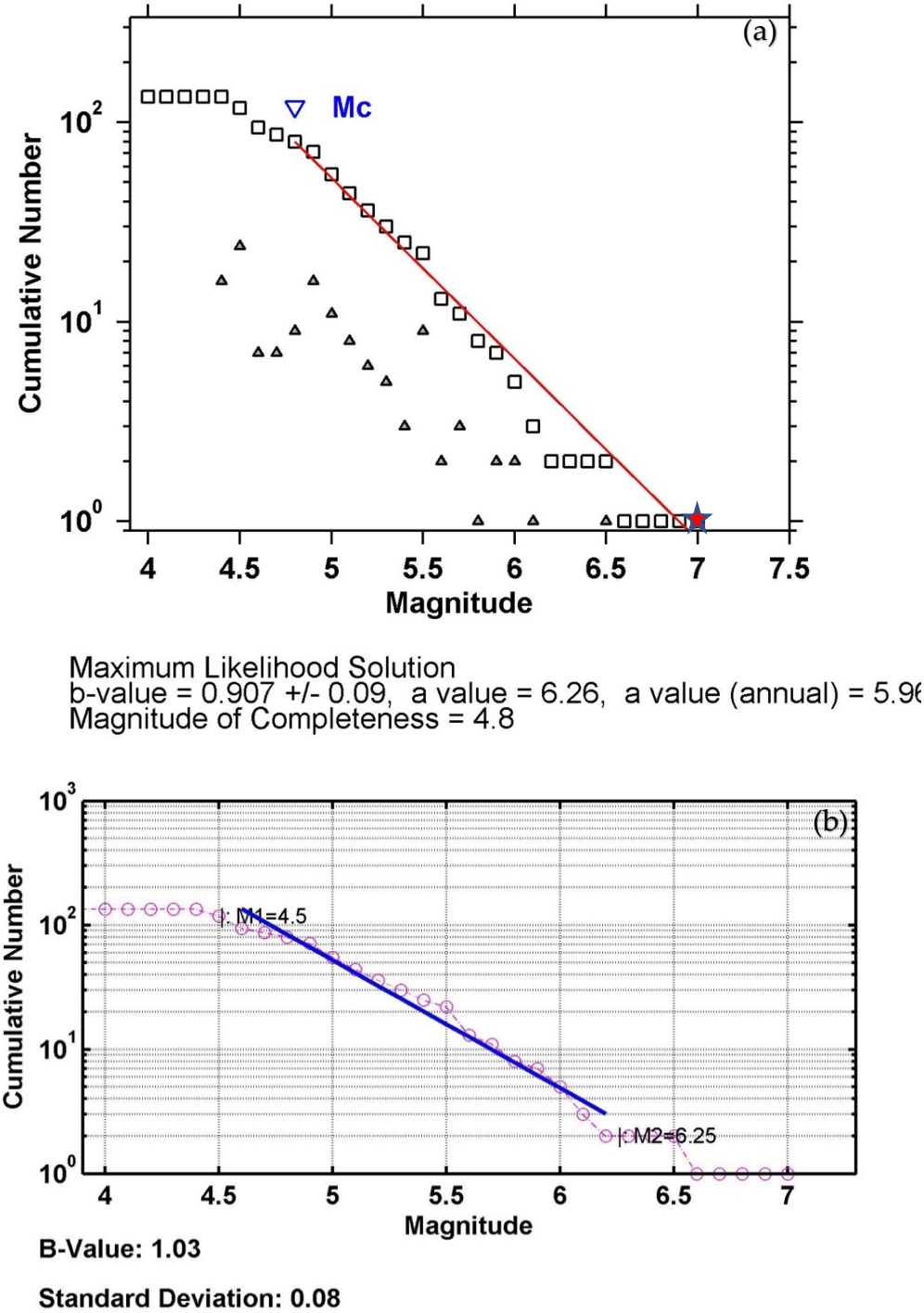

Figure 118. (a) The Guttenberg-Richter distribution using maximum likelihood method with the best combination of maximum curvature M_c 95% and M_c 90% probability. The red star shows the magnitude of the mainshock M_w 7.0. **(b)** The Guttenberg-Richter distribution using the manual method.

Next figure presents the model proposed by the AIC with p1= 1.28, p2=2.7, c= 0.44, k1= 24.9 and k2=10.

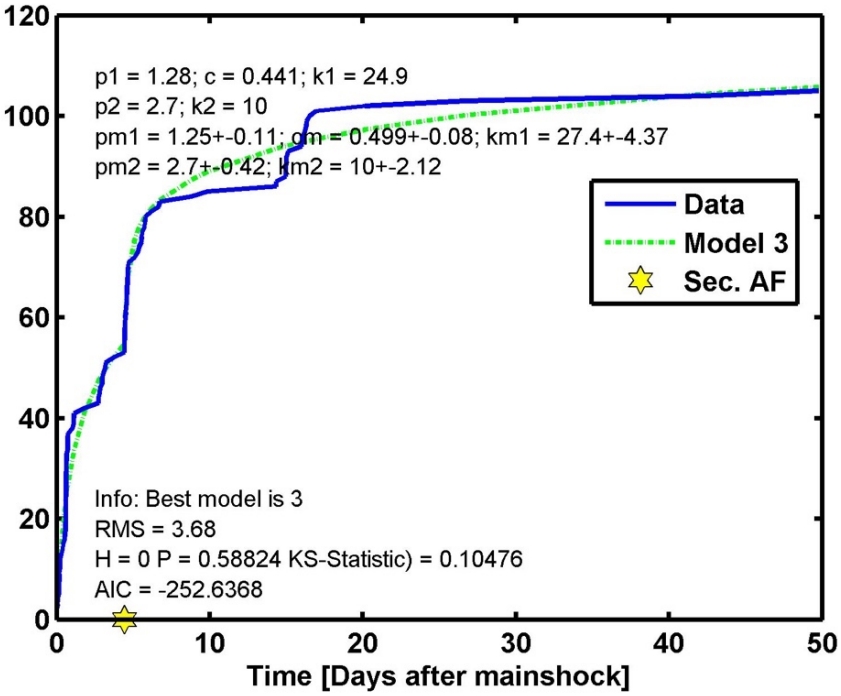

Figure 119. The best model (3) of the estimated curve of the modified Omori formula (dashed line) applied to the aftershock data and the observed cumulative number of aftershocks (solid line) based on the AIC with the lowest RMS= 3.68.

Here is the magnitude-time form of the aftershock sequence.

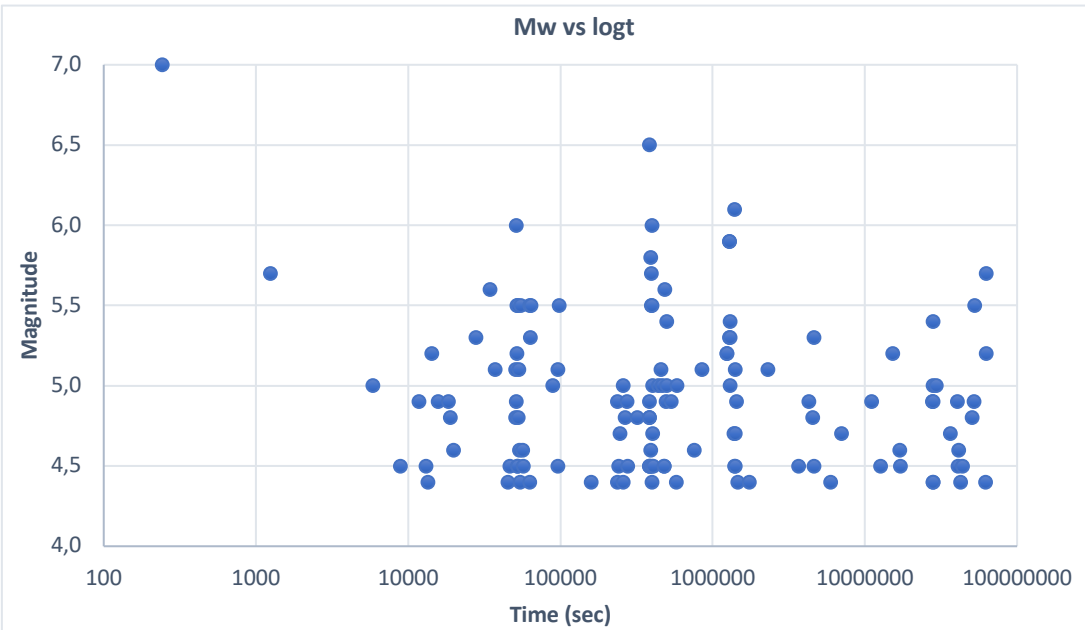

Figure 120. The magnitude-time pattern versus the logarithm of time of the mainshock M_w 7.0.

By the frequency-magnitude distribution for this earthquake, it is estimated a q_M= 1.50 with ci= 1.47-1.52.

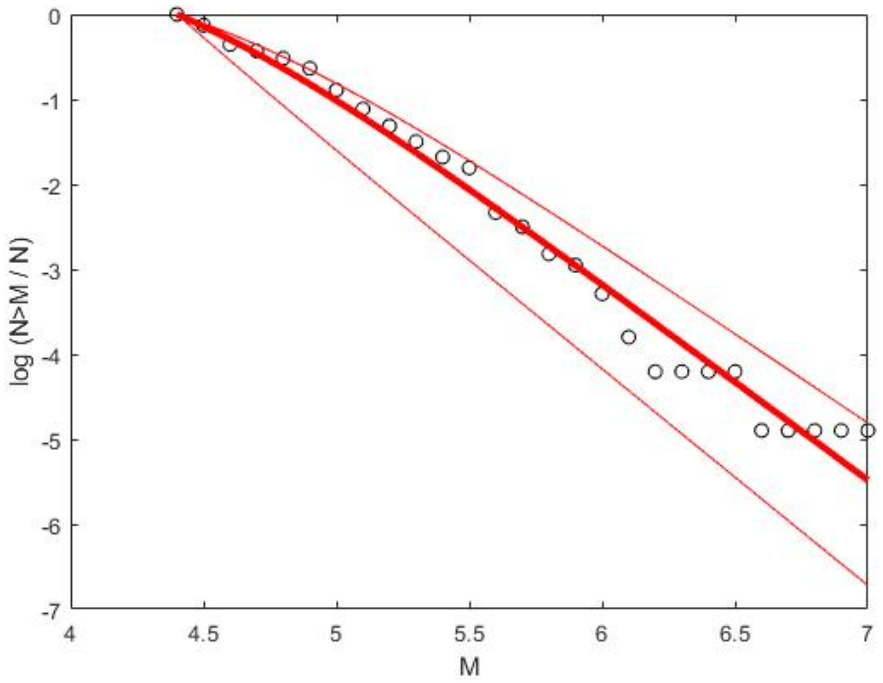

Figure 121. Frequency-magnitude distribution. The bold red line represents the model of equation (26) for qM= 1.50, while the other two lines present the corresponding 95% confidence intervals.

Figure 122 shows the typical Q-exponential pattern and Q-logarithmic function of the cumulative distribution function, P(>T) of the aftershocks interevent times and a q=1.77 is obtained.

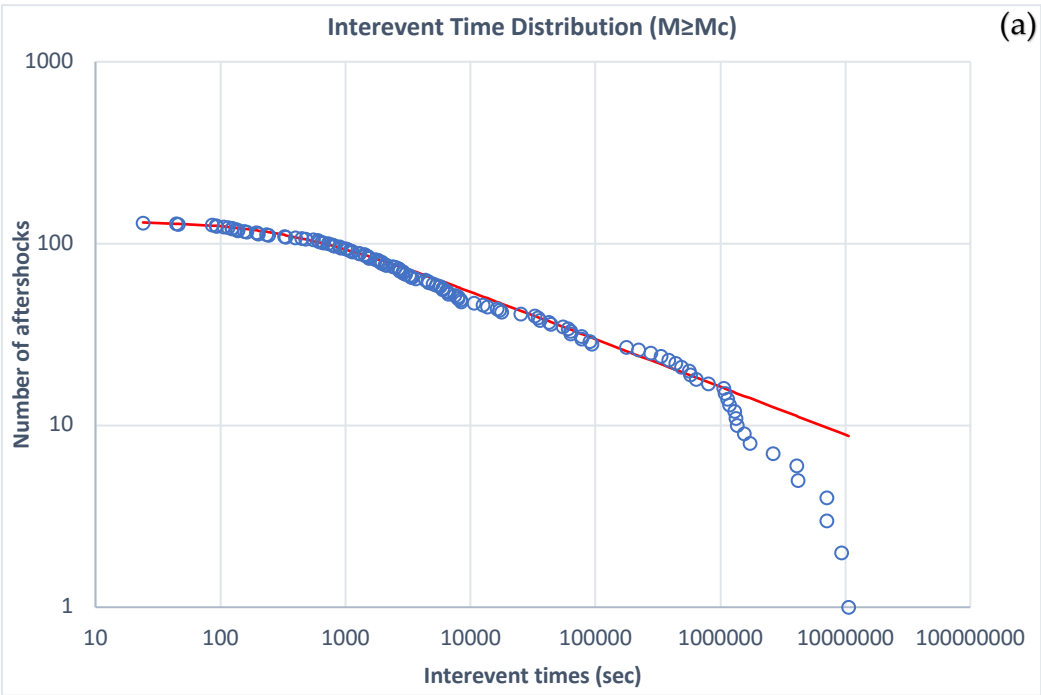

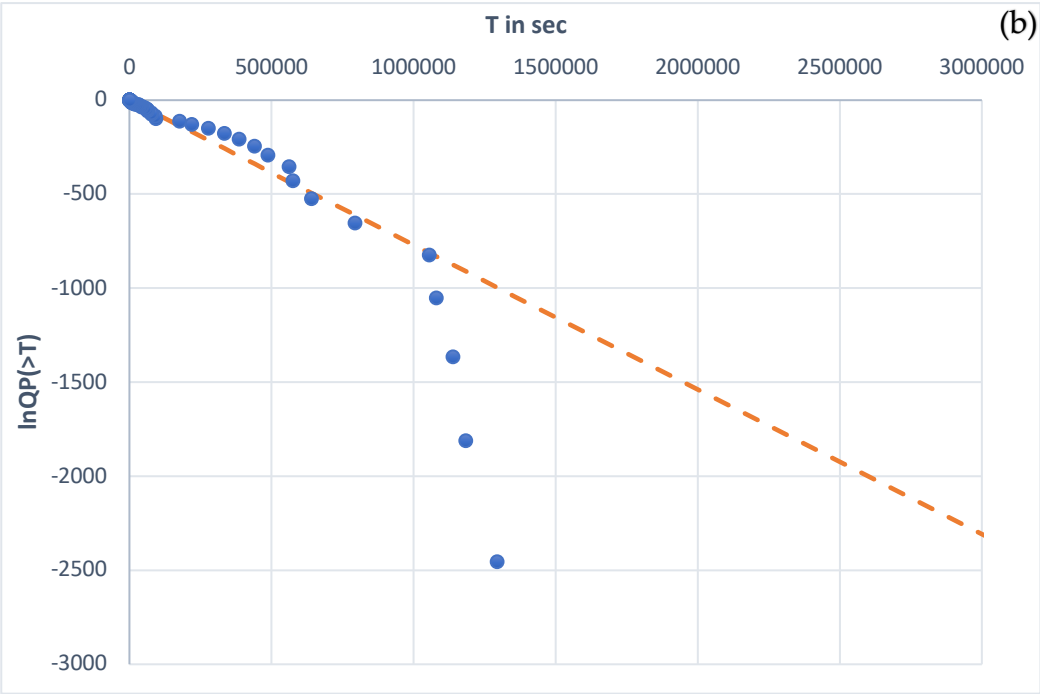

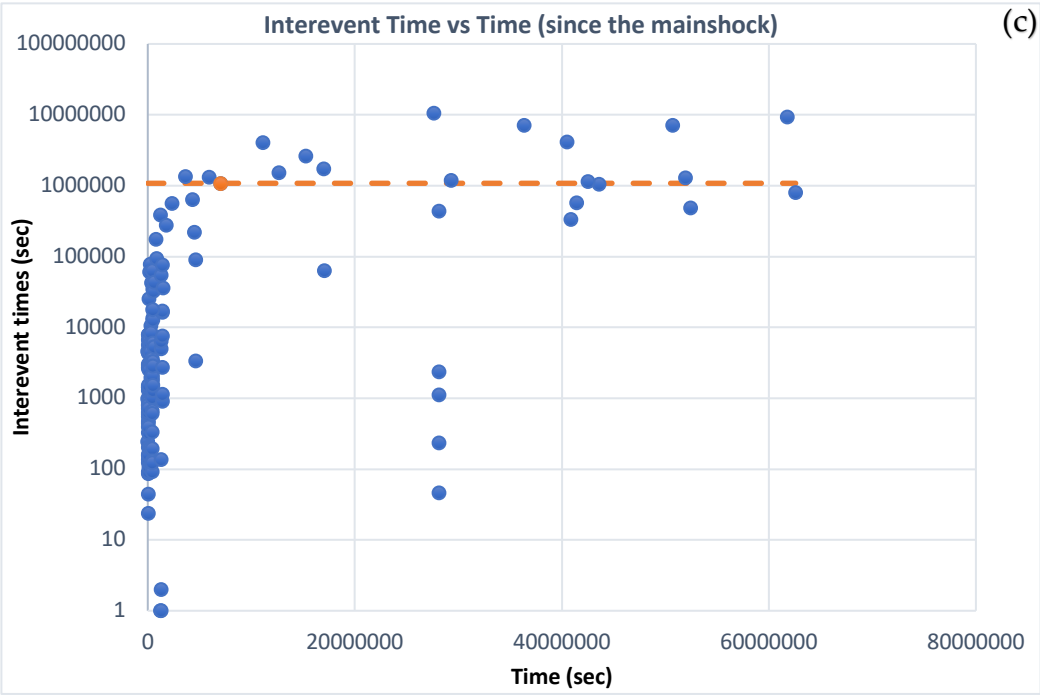

Figure 122. (a) The cumulative distribution function of the interevent times. The red line is the Q-exponential fitting with q = 1.77. **(b)** The Q-logarithmic function of the P(>T) as a function of the interevent times where the dashed line is the fitting with q=1.77. The deviation from the linearity suggests Tc values close to 1,000,000 s. **(c)** The evolution of interevent time T as a function of time t since the main event. The Tc value is indicated by the dashed line.

4.2.25 The 2014 Kirakira Earthquake M_w=7.6 (Solomon Island)

The figure below shows Guttenberg-Richter distribution. The estimated parameters are Mc=4.8 and b=1.32 with a standard deviation of 0.07.

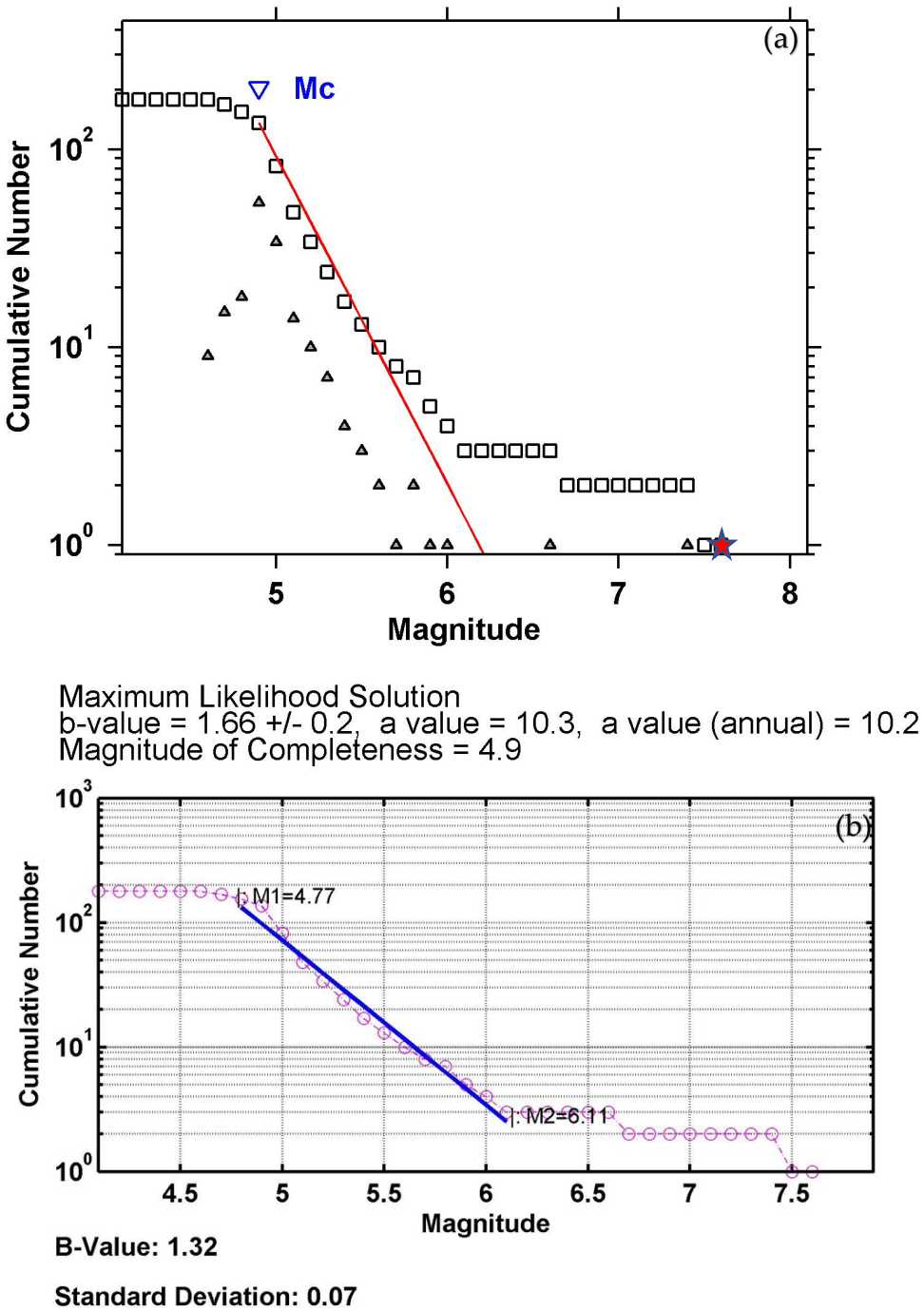

Figure 123. (a) The Guttenberg-Richter distribution using maximum likelihood method with the best combination of maximum curvature M_c 95% and M_c 90% probability. The red star shows the magnitude of the mainshock M_w 7.6. **(b)** The Guttenberg-Richter distribution using the manual method.

Next figure presents the model proposed by the AIC with p= 1.72, c= 0.63 and k= 86.4.

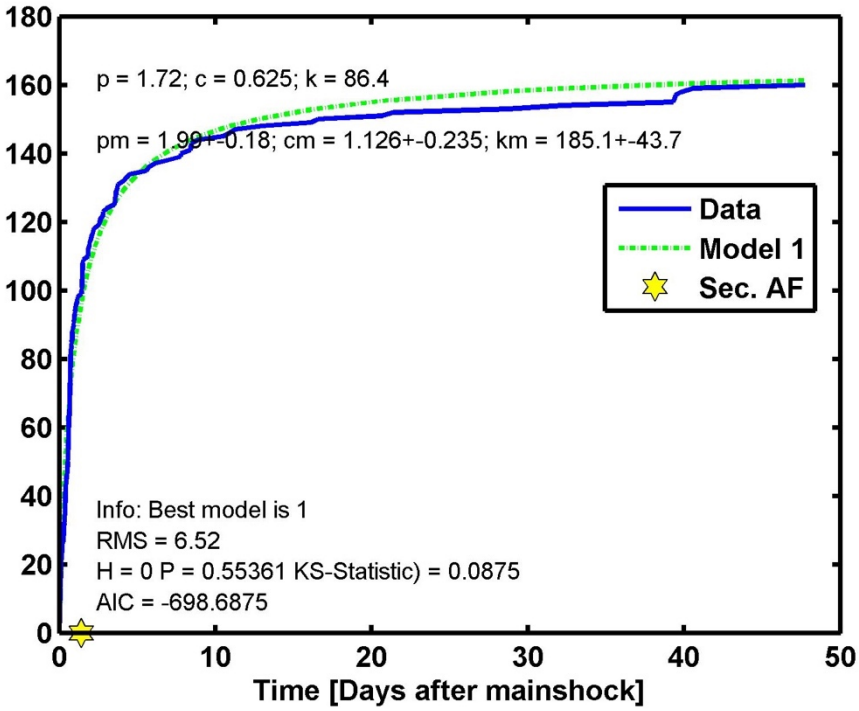

Figure 124. The best model (1) of the estimated curve of the modified Omori formula (dashed line) applied to the aftershock data and the observed cumulative number of aftershocks (solid line) based on the AIC with RMS= 6.52.

Here is the magnitude-time form of the aftershock sequence.

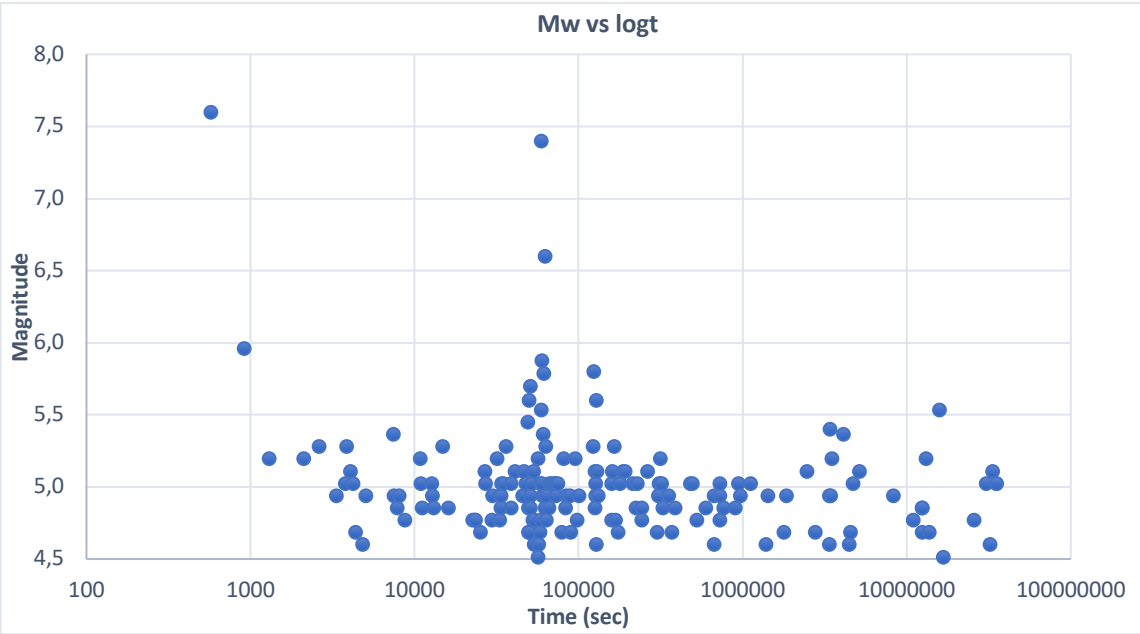

Figure 125. The magnitude-time pattern versus the logarithm of time of the mainshock M_w 7.6.

By the frequency-magnitude distribution for this earthquake, it is estimated a q_M= 1.55 with ci= 1.49-1.61.

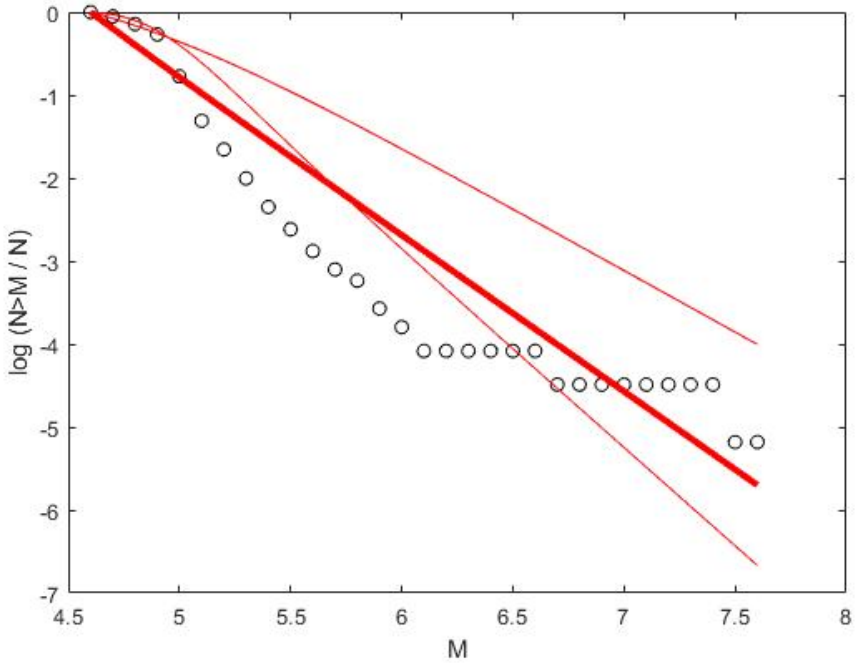

Figure 126. Frequency-magnitude distribution. The bold red line represents the model of equation (26) for qM= 1.55, while the other two lines present the corresponding 95% confidence intervals.

Figure 127 shows the typical Q-exponential pattern and Q-logarithmic function of the cumulative distribution function, P(>T) of the aftershocks interevent times and a q=1.74 is obtained.

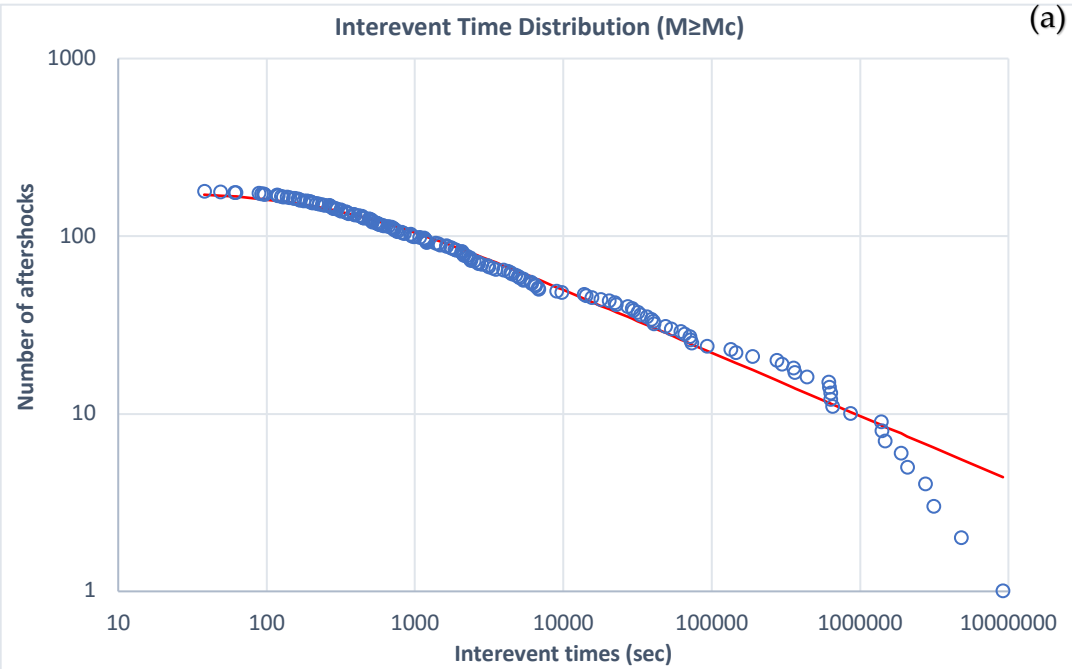

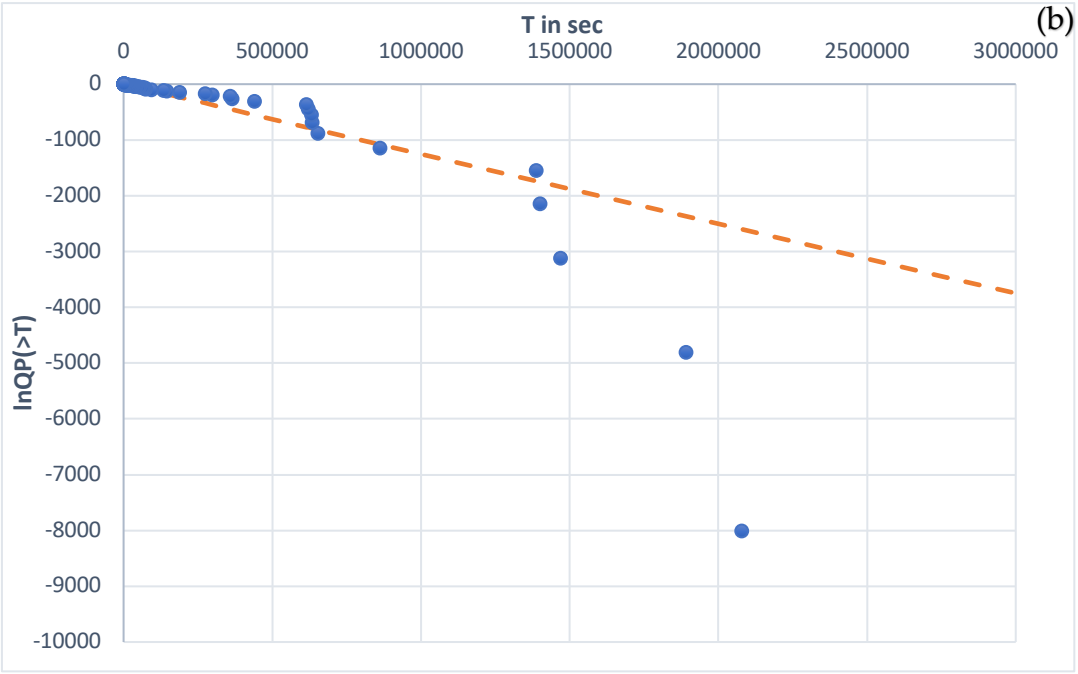

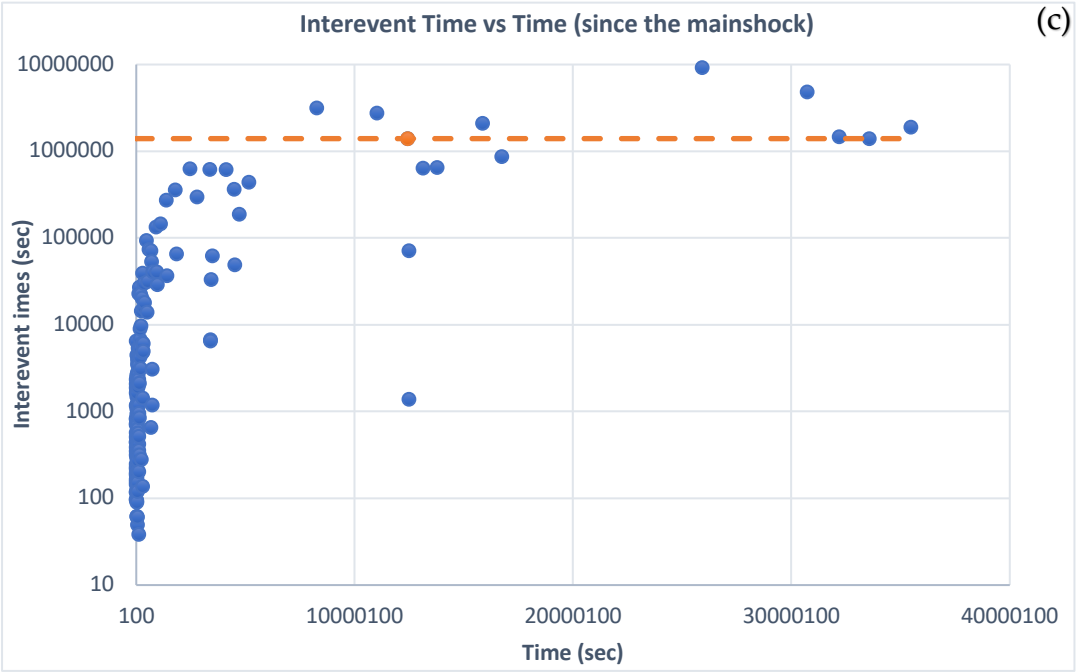

Figure 127. (a) The cumulative distribution function of the interevent times. The red line is the Q-exponential fitting with q = 1.74. **(b)** The Q-logarithmic function of the P(>T) as a function of the interevent times where the dashed line is the fitting with q=1.74. The deviation from the linearity suggests Tc values close to 1,000,000 s. **(c)** The evolution of interevent time T as a function of time t since the main event. The Tc value is indicated by the dashed line.

4.2.26 The 2014 Panguna Earthquake M_w=7.5 (Papua New Guinea)

The figure below shows Guttenberg-Richter distribution. The estimated parameters are Mc=4.7 and b=1.07 with a standard deviation of 0.03.

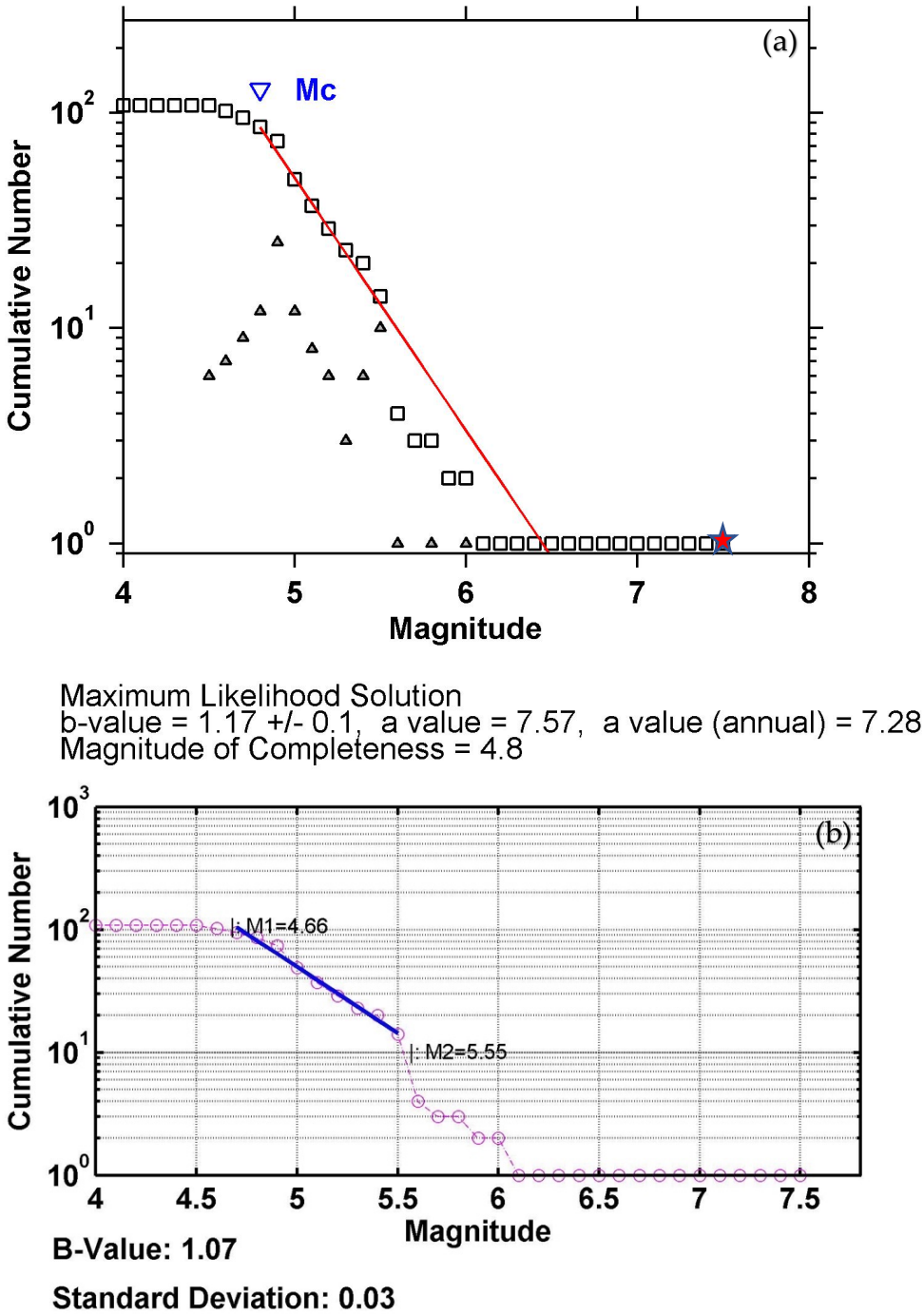

Figure 128. (a) The Guttenberg-Richter distribution using maximum likelihood method with the best combination of maximum curvature M_c 95% and M_c 90% probability. The red star shows the magnitude of the mainshock M_w 7.5. **(b)** The Guttenberg-Richter distribution using the manual method.

Next figure presents the model proposed by the AIC with p1= 1.05, p2=2.7, c1=0.03, c2=1.85, k1=10 and k2= 38.6.

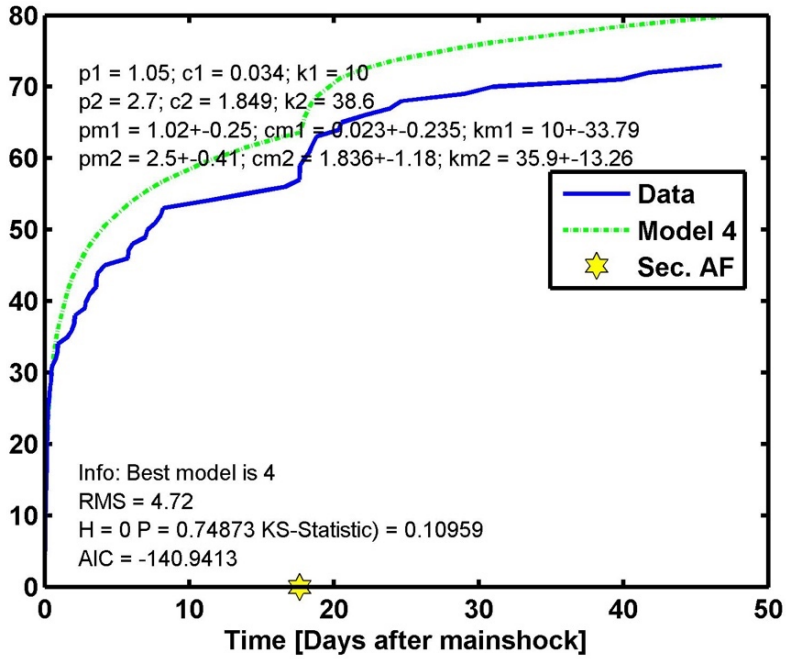

Figure 129. The best model (4) of the estimated curve of the modified Omori formula (dashed line) applied to the aftershock data and the observed cumulative number of aftershocks (solid line) based on the AIC with RMS= 4.72.

Here is the magnitude-time form of the aftershock sequence.

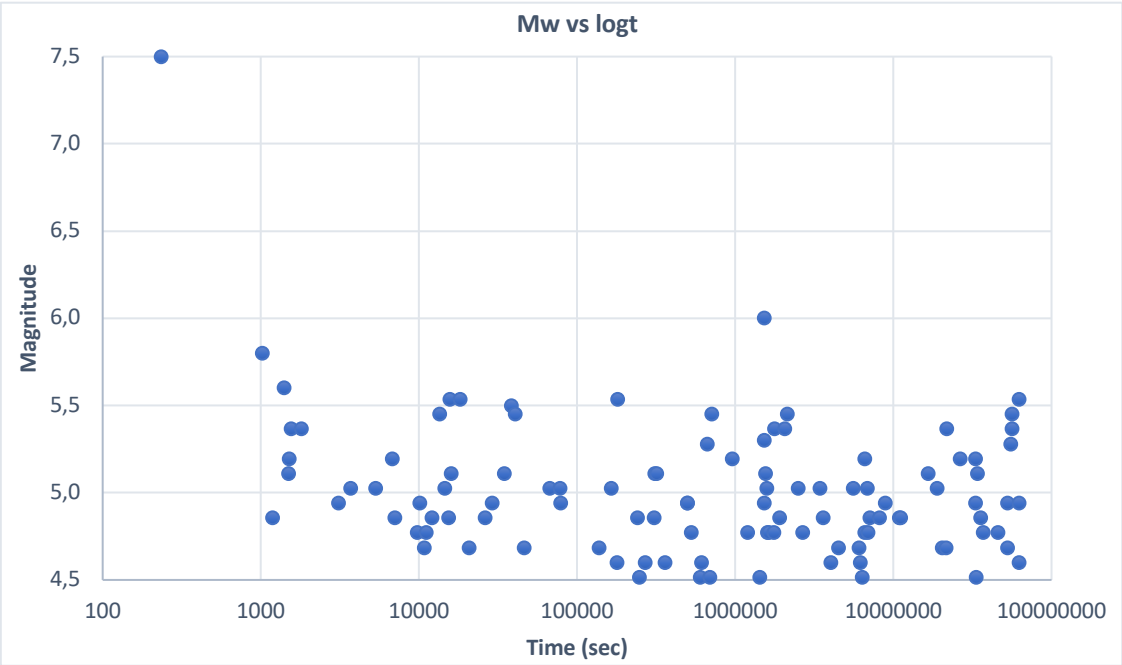

Figure 130. The magnitude-time pattern versus the logarithm of time of the mainshock M_w 7.5.

By the frequency-magnitude distribution for this earthquake, it is estimated a q_M= 1.21 with ci= 1.14-1.28.

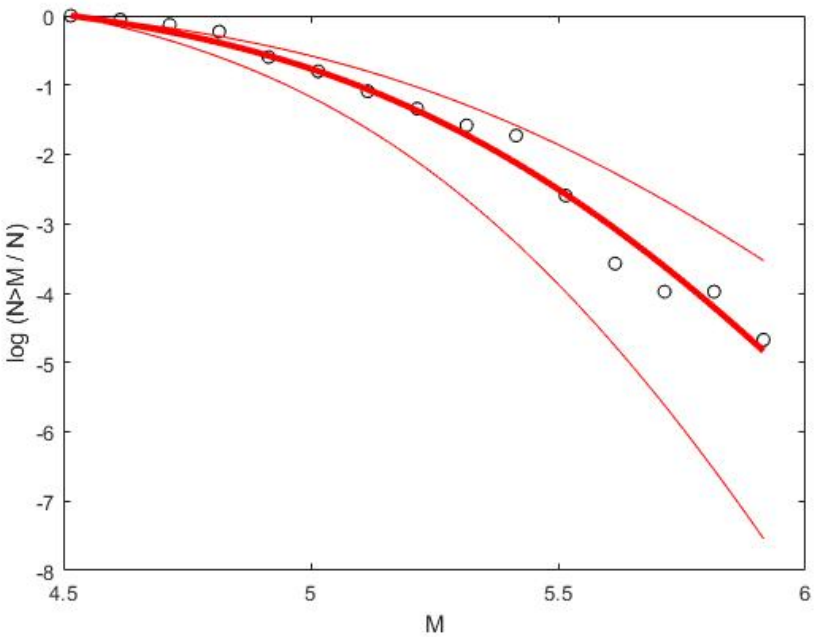

Figure 131. Frequency-magnitude distribution. The bold red line represents the model of equation (26) for qM= 1.21, while the other two lines present the corresponding 95% confidence intervals.

Figure 132 shows the typical Q-exponential pattern and Q-logarithmic function of the cumulative distribution function, P(>T) of the aftershocks interevent times and a q=1.78 is obtained.

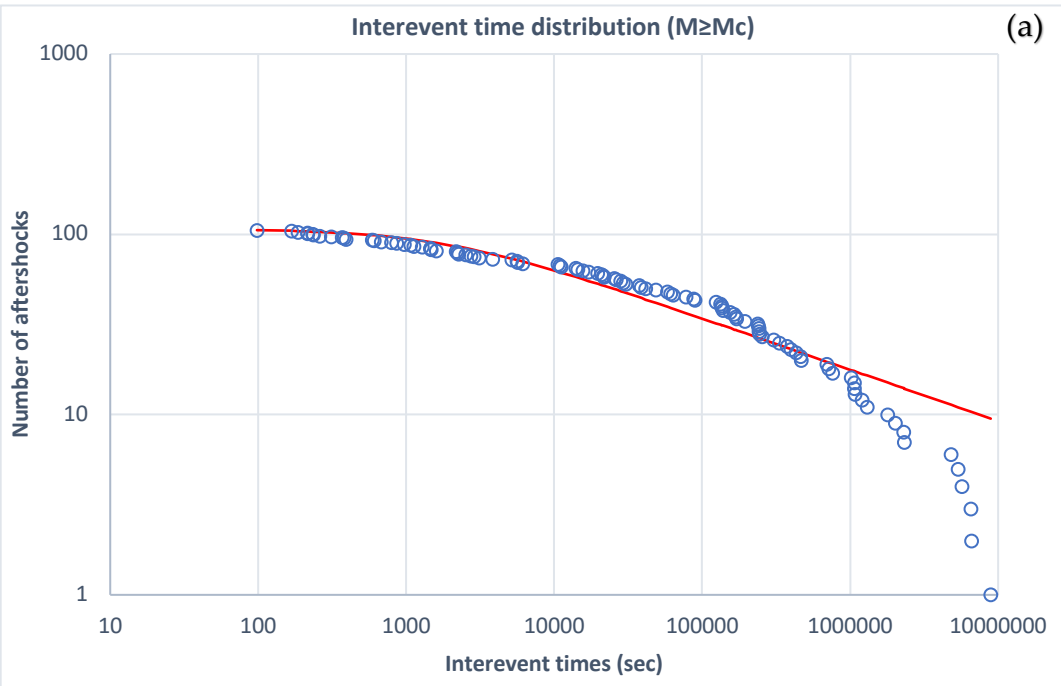

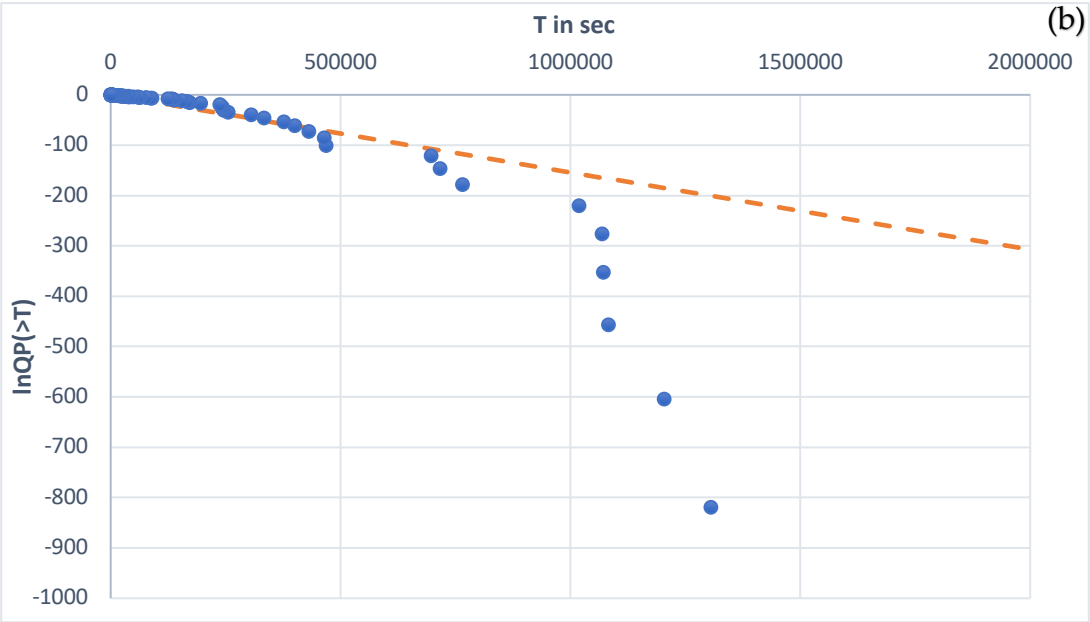

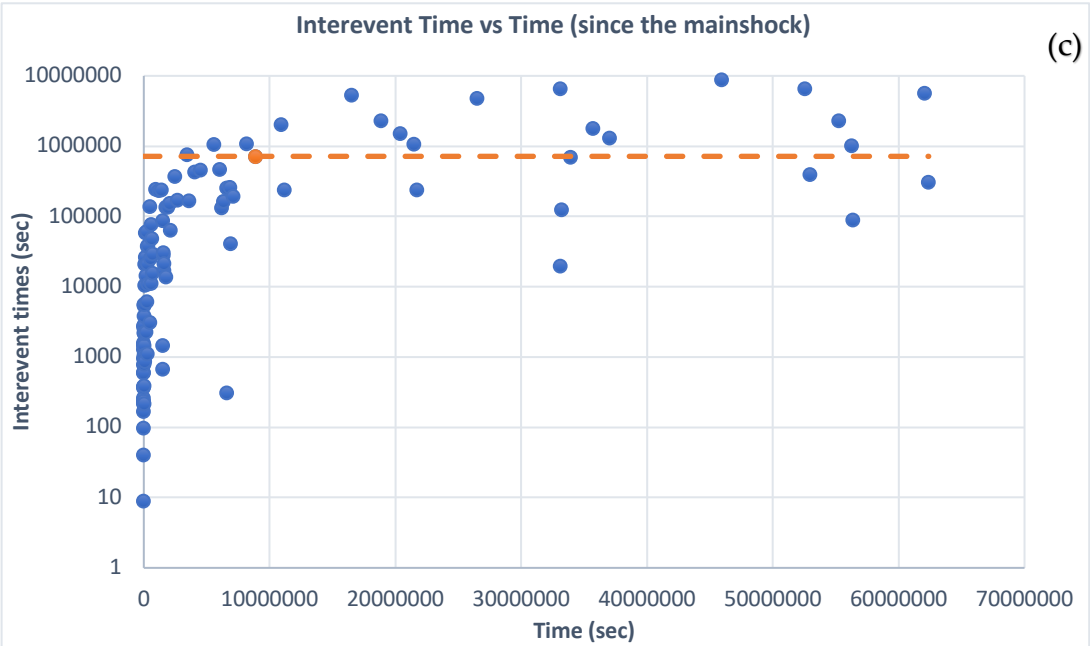

Figure 132. (a) The cumulative distribution function of the interevent times. The red line is the Q-exponential fitting with q = 1.78. **(b)** The Q-logarithmic function of the P(>T) as a function of the interevent times where the dashed line is the fitting with q=1.78. The deviation from the linearity suggests Tc values close to 1,000,000 s. **(c)** The evolution of interevent time T as a function of time t since the main event. The Tc value is indicated by the dashed line.

4.2.27 The 2014 Ternate Earthquake M_w=7.1 (Indonesia)

The figure below shows Guttenberg-Richter distribution. The estimated parameters are Mc=4.5 and b=1.96 with a standard deviation of 0.06.

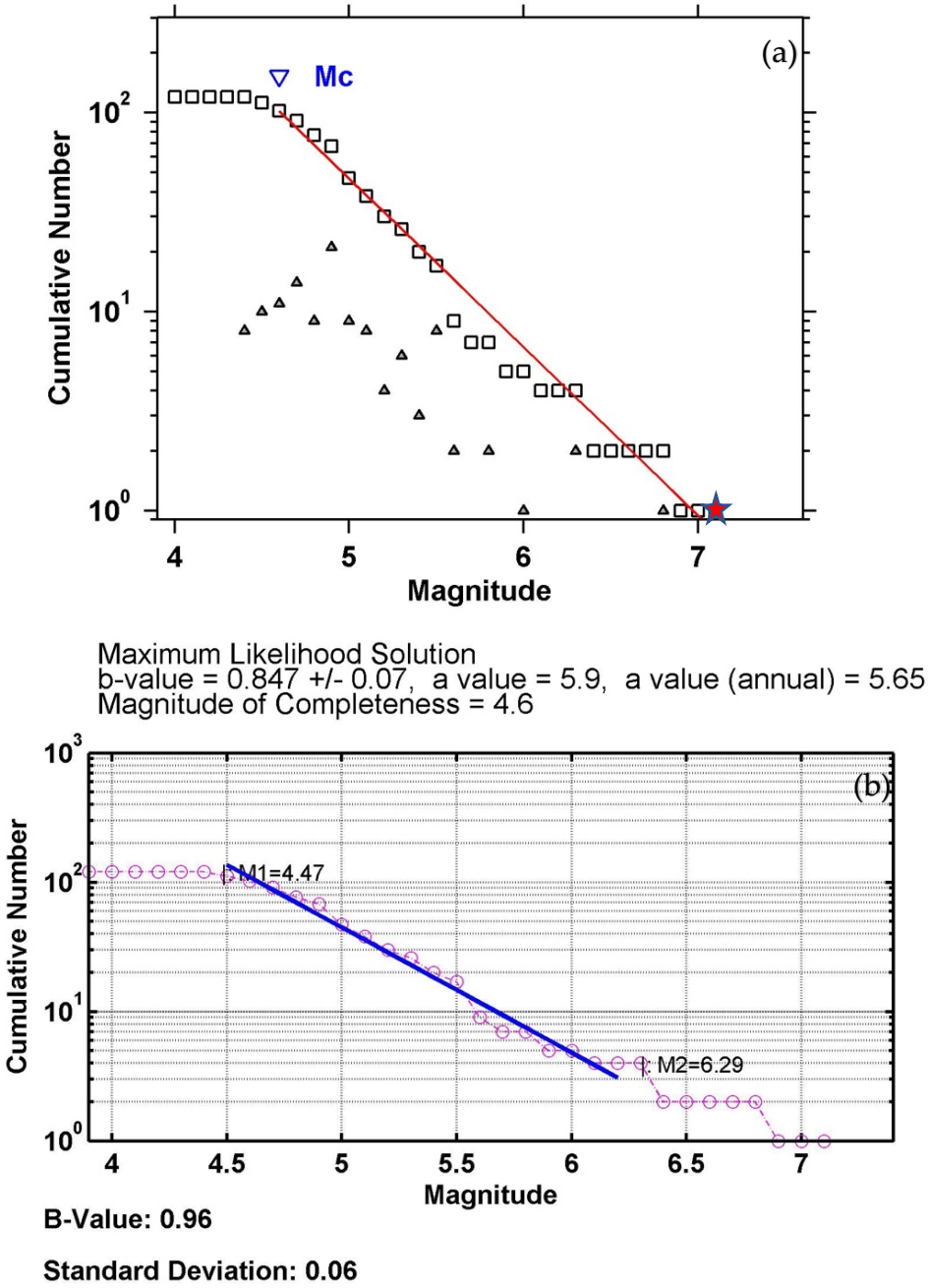

Figure 133. (a) The Guttenberg-Richter distribution using maximum likelihood method with the best combination of maximum curvature M_c 95% and M_c 90% probability. The red star shows the magnitude of the mainshock M_w 7.1. **(b)** The Guttenberg-Richter distribution using the manual method.

Next figure (134a) presents the model proposed by the AIC with p1= 0.83, p2=2.7, c1=0.01, c2=0.486, k1=10 and k2= 10, while (134b) presents the model with the lowest RMS and p= 0.74, c= 0.01 and k= 10.2.

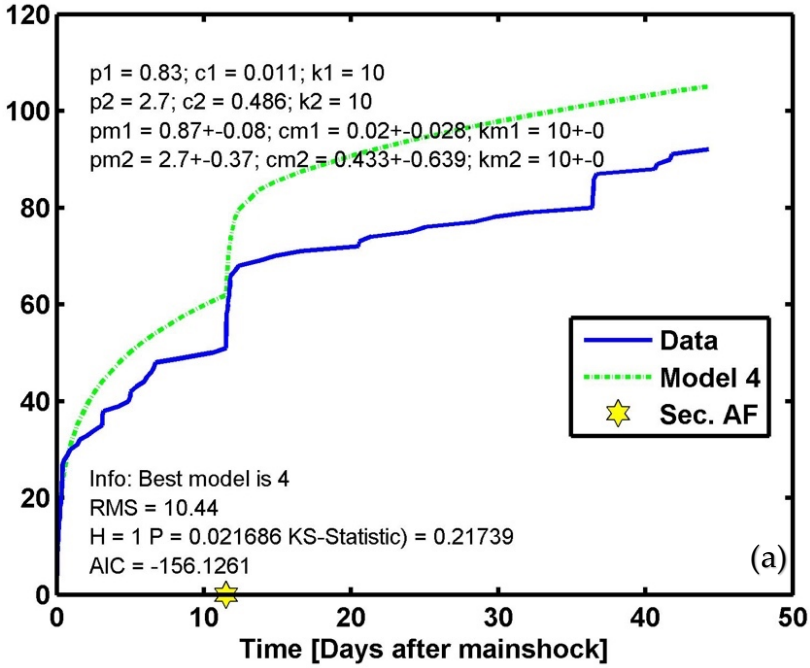

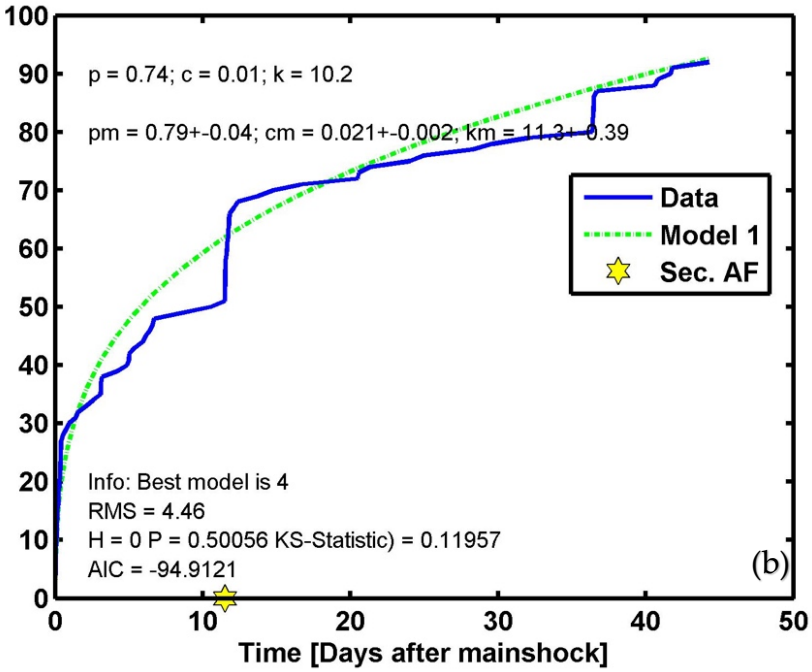

Figure 134. (a) The best model (4) of the estimated curve of the modified Omori formula (dashed line) applied to the aftershock data and the observed cumulative number of aftershocks (solid line) based on the AIC. **(b)** The model 1 of the estimated curve of the modified Omori formula (dashed line) applied to the aftershock data and the observed cumulative number of aftershocks (solid line), with the lowest RMS= 4.46.

Here is the magnitude-time form of the aftershock sequence.

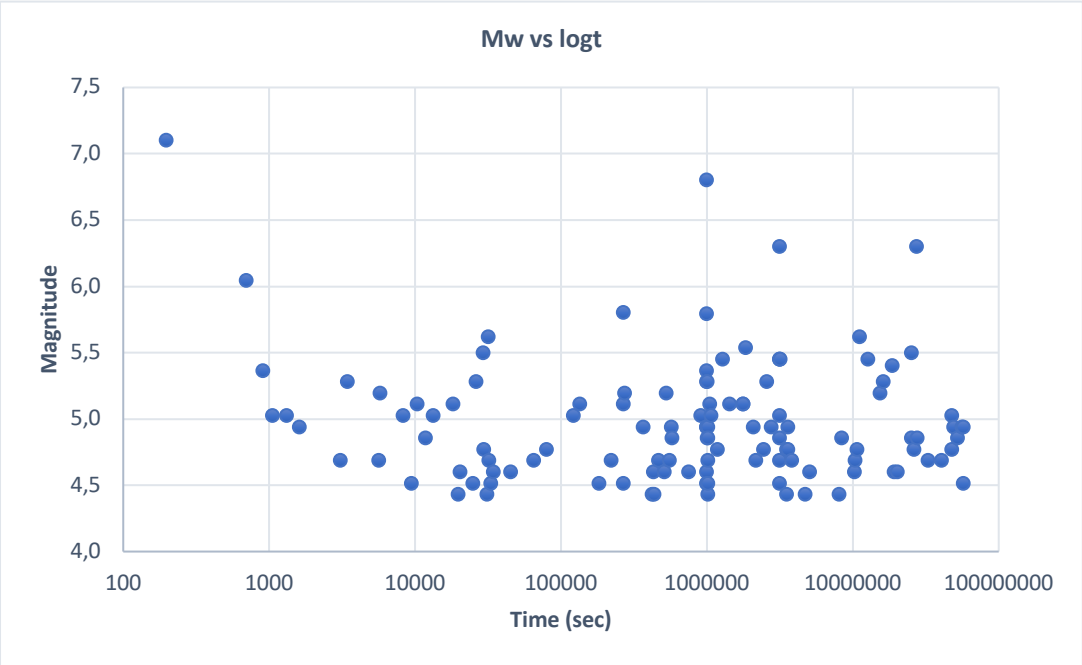

Figure 135. The magnitude-time pattern versus the logarithm of time of the mainshock M_w 7.1.

By the frequency-magnitude distribution for this earthquake, it is estimated a q_M= 1.55 with ci= 1.52-1.57.

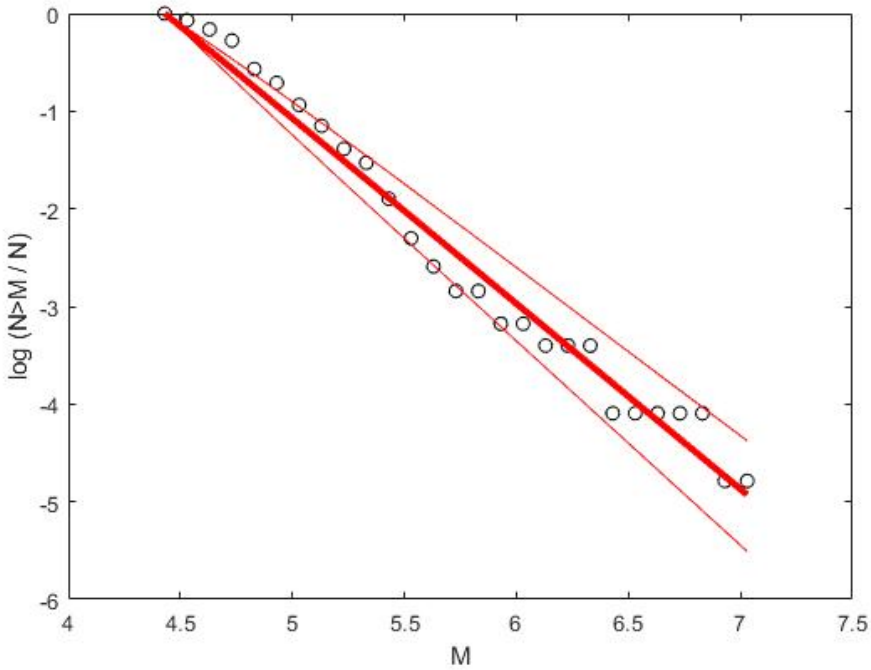

Figure 136. Frequency-magnitude distribution. The bold red line represents the model of equation (26) for qM= 1.55, while the other two lines present the corresponding 95% confidence intervals.

Figure 137 shows the typical Q-exponential pattern and Q-logarithmic function of the cumulative distribution function, P(>T) of the aftershocks interevent times and a q=1.77 is obtained.

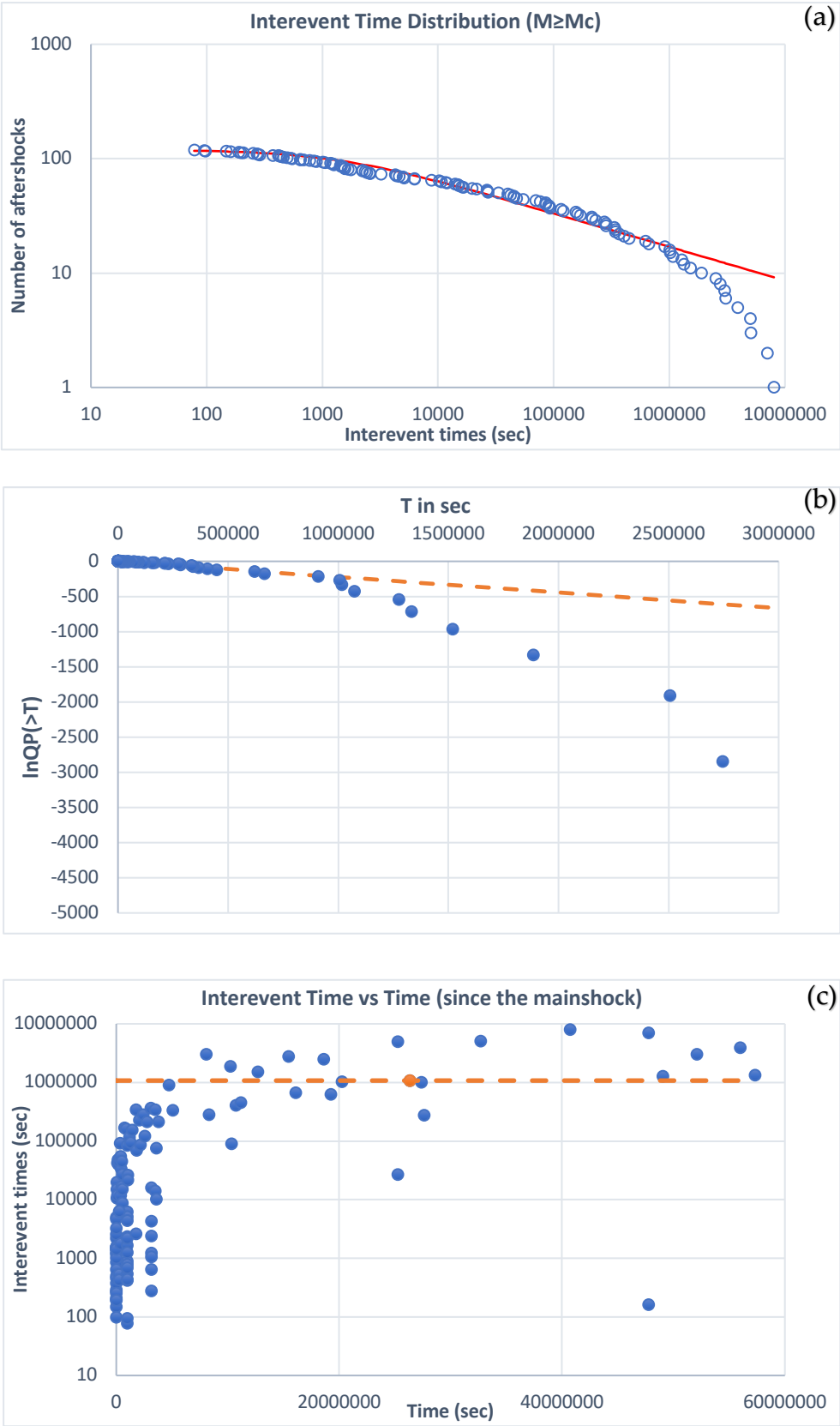

Figure 137. (a) The cumulative distribution function of the interevent times. The red line is the Q-exponential fitting with q = 1.77. **(b)** The Q-logarithmic function of the P(>T) as a function of the interevent times where the dashed line is the fitting with q=1.77. The deviation from the linearity suggests Tc values close to 1,000,000 s. **(c)** The evolution of interevent time T as a function of time t since the main event. The Tc value is indicated by the dashed line.

4.2.28 The 2015 Kokopo Earthquake M_w=7.5 (Papua New Guinea)

The figure below shows Guttenberg-Richter distribution. The estimated parameters are Mc=4.7 and b=1.15 with a standard deviation of 0.06.

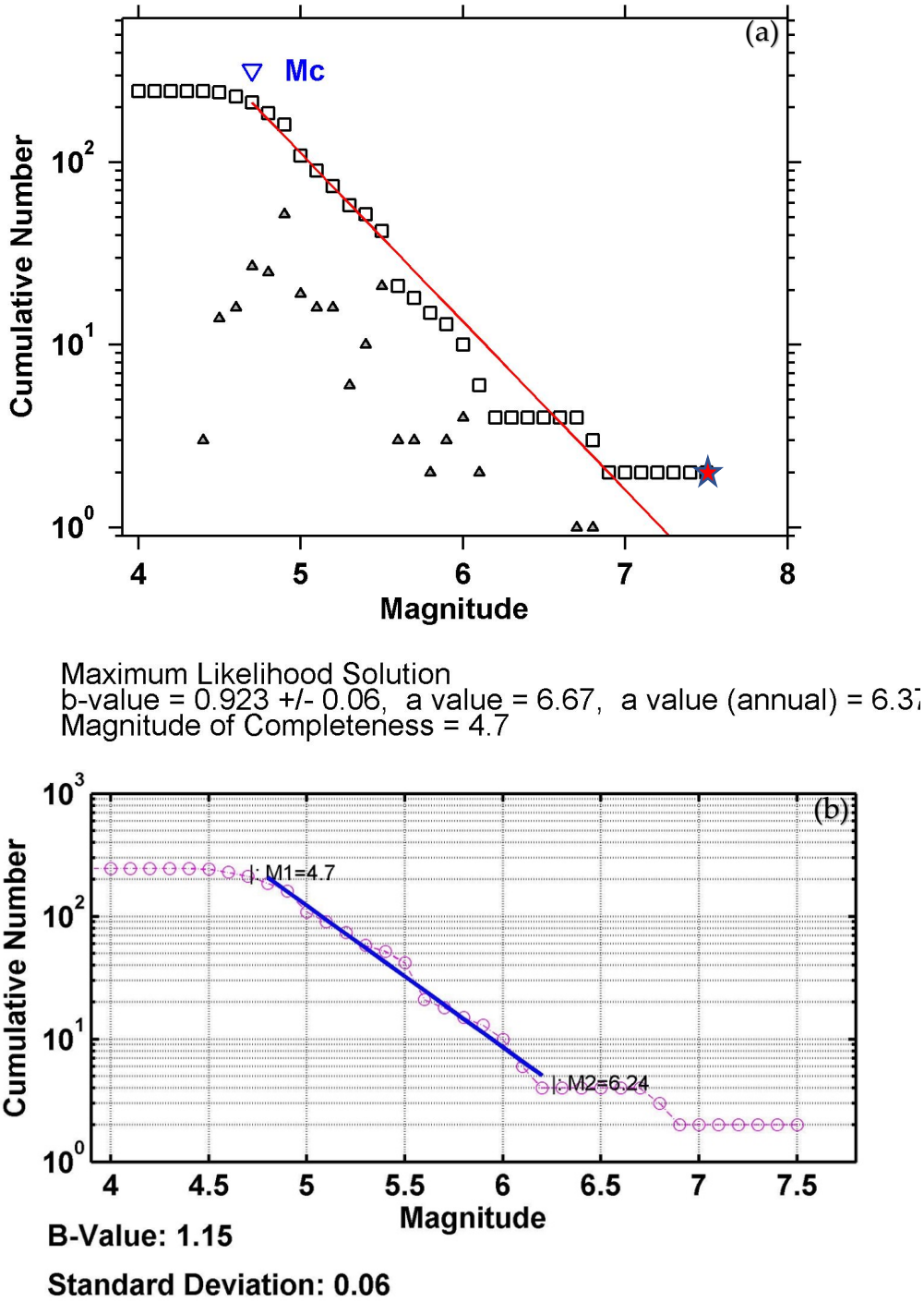

Figure 138. (a) The Guttenberg-Richter distribution using maximum likelihood method with the best combination of maximum curvature M_c 95% and M_c 90% probability. The red star shows the magnitude of the mainshock M_w 7.5. **(b)** The Guttenberg-Richter distribution using the manual method.

Next figure presents the model proposed by the AIC with p= 0.7, c= 0.01 and k= 10.9.

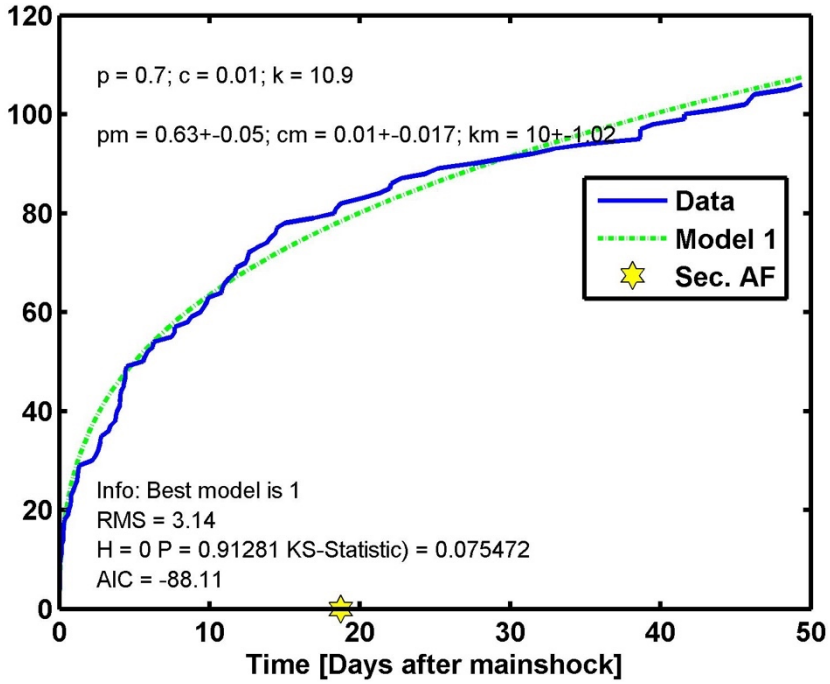

Figure 139. The best model (1) of the estimated curve of the modified Omori formula (dashed line) applied to the aftershock data and the observed cumulative number of aftershocks (solid line) based on the AIC with RMS= 3.14.

Here is the magnitude-time form of the aftershock sequence.

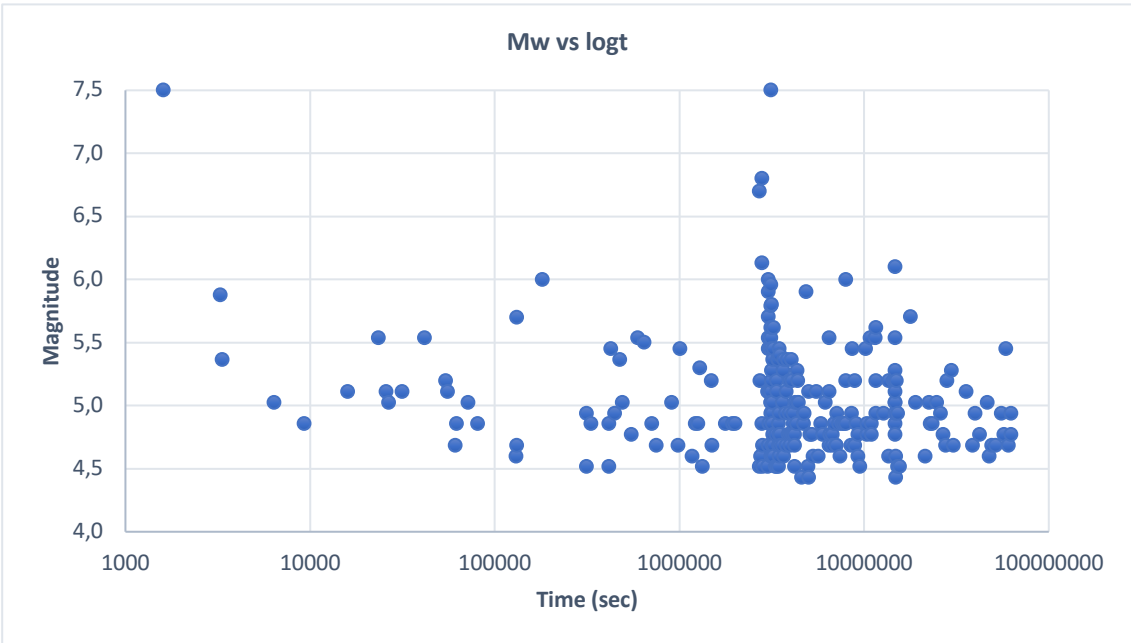

Figure 140. The magnitude-time pattern versus the logarithm of time of the mainshock M_w 7.5.

By the frequency-magnitude distribution for this earthquake, it is estimated a q_M= 1.56 with ci= 1.53-1.58.

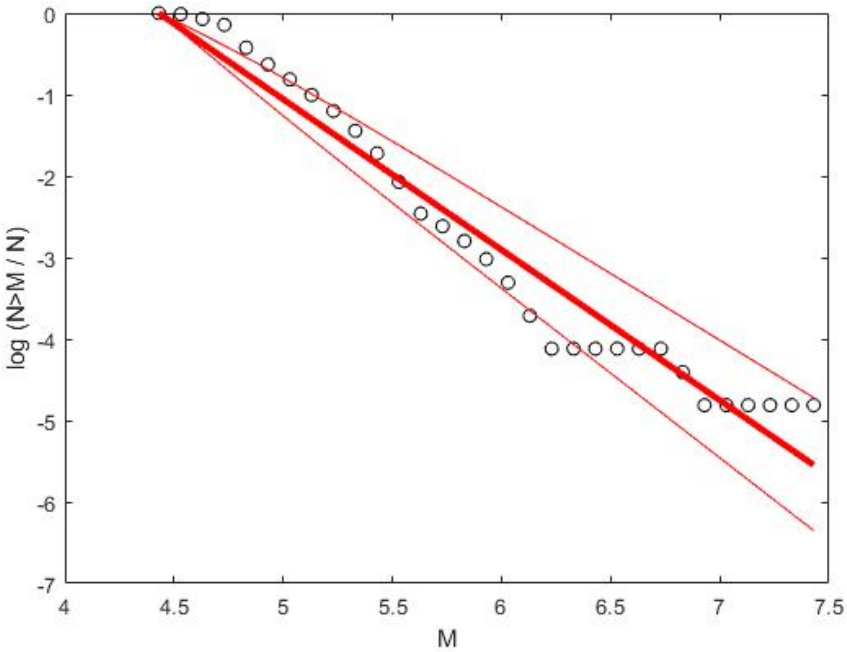

Figure 141. Frequency-magnitude distribution. The bold red line represents the model of equation (26) for qM= 1.56, while the other two lines present the corresponding 95% confidence intervals.

Figure 142 shows the typical Q-exponential pattern and Q-logarithmic function of the cumulative distribution function, P(>T) of the aftershocks interevent times and a q=1.71 is obtained.

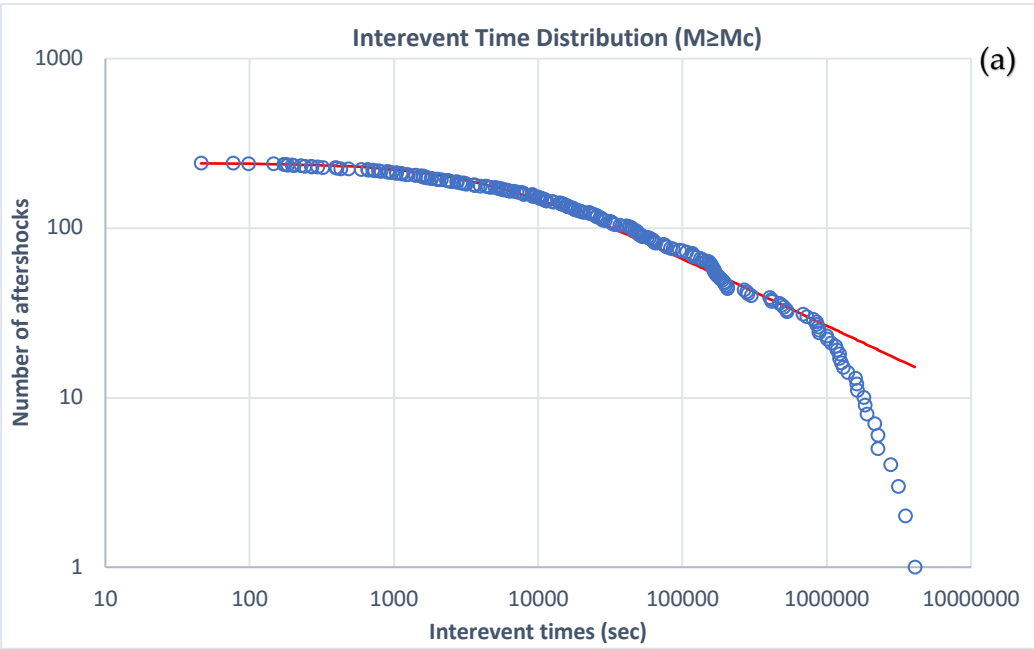

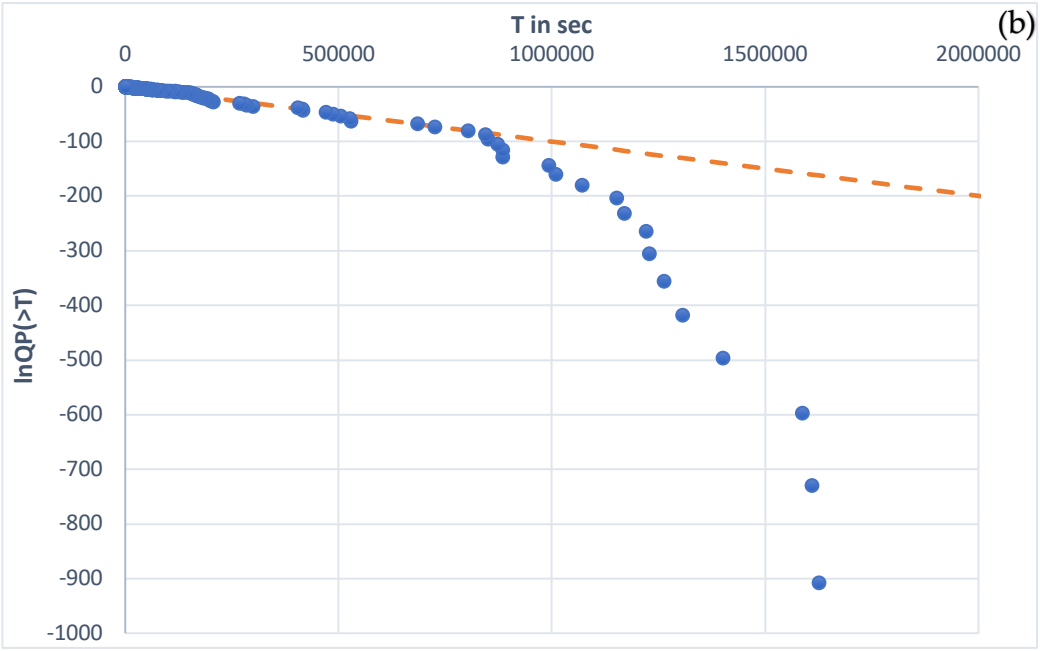

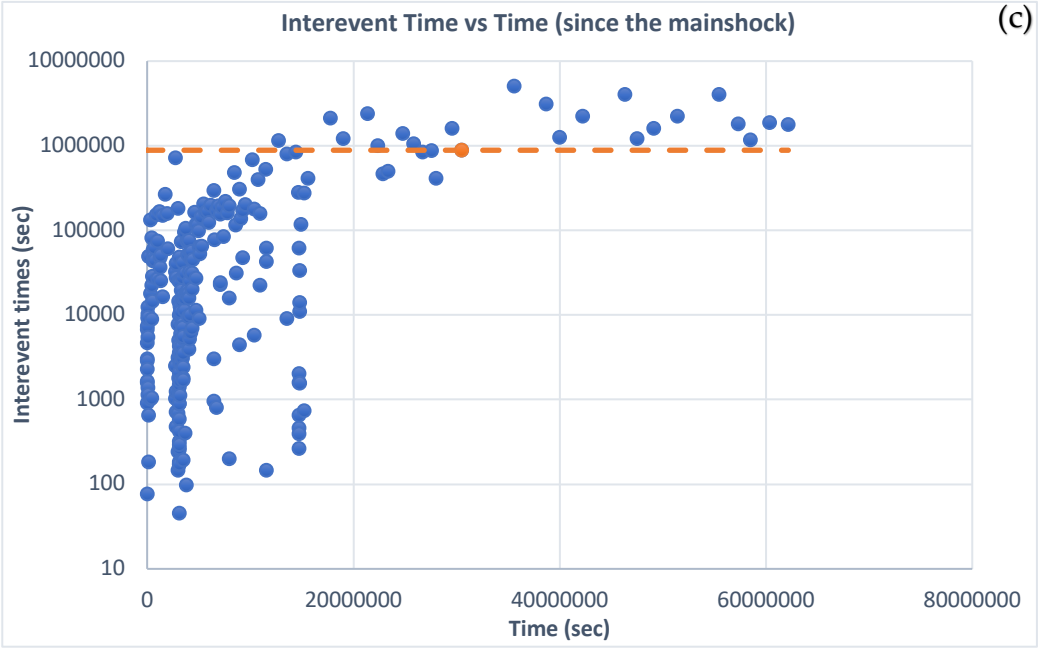

Figure 142. (a) The cumulative distribution function of the interevent times. The red line is the Q-exponential fitting with q = 1.71. **(b)** The Q-logarithmic function of the P(>T) as a function of the interevent times where the dashed line is the fitting with q=1.71. The deviation from the linearity suggests Tc values close to 1,000,000 s. **(c)** The evolution of interevent time T as a function of time t since the main event. The Tc value is indicated by the dashed line.

4.2.29 The 2015 Bharatpur Earthquake M_w=7.8 (Nepal)

The figure below shows Guttenberg-Richter distribution. The estimated parameters are Mc=4.5 and b=1.16 with a standard deviation of 0.05.

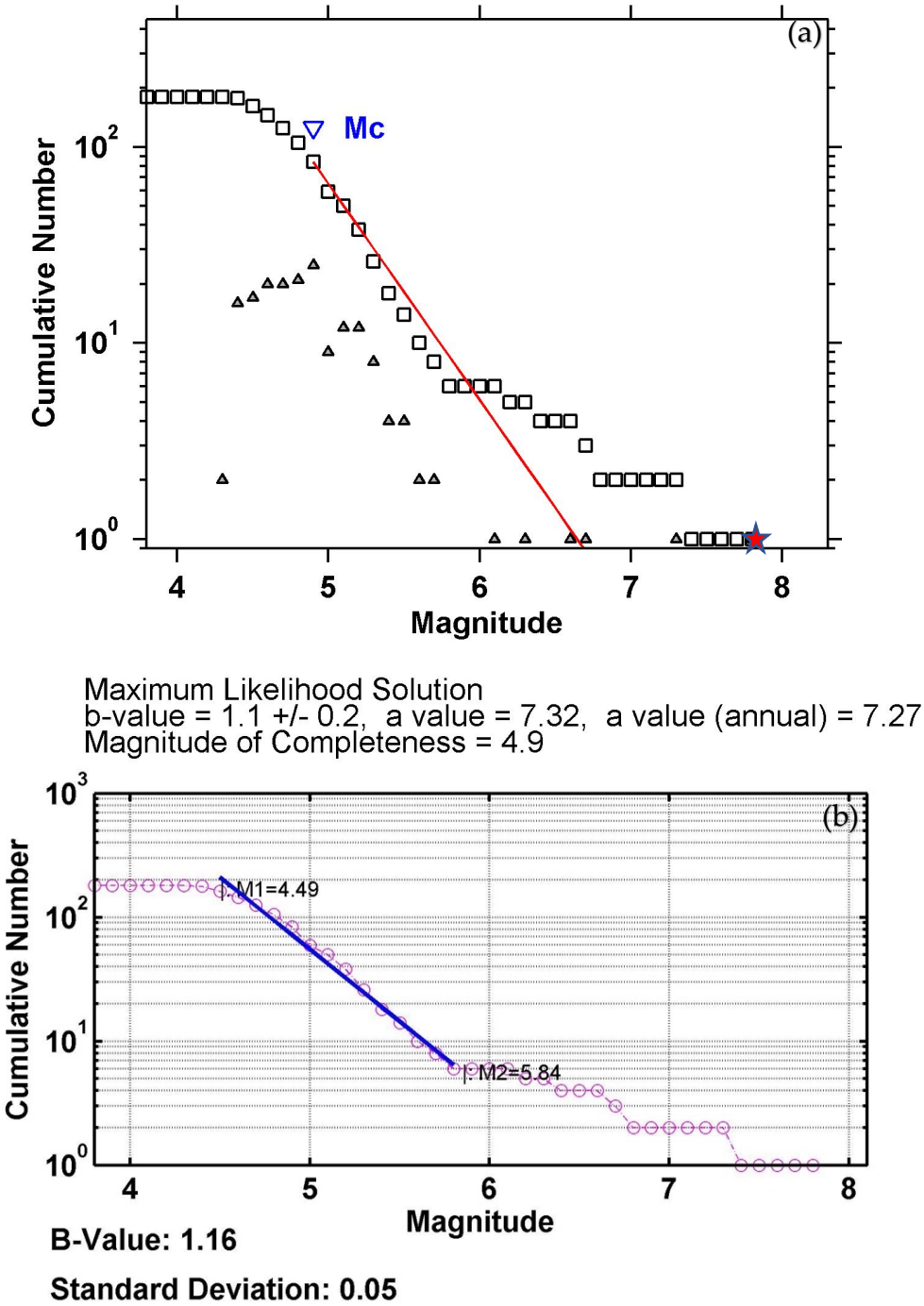

Figure 143. (a) The Guttenberg-Richter distribution using maximum likelihood method with the best combination of maximum curvature M_c 95% and M_c 90% probability. The red star shows the magnitude of the mainshock M_w 7.8. **(b)** The Guttenberg-Richter distribution using the manual method.

Next figure (144a) presents the model proposed by the AIC with p= 1.28, c= 0.07, k1= 16.5 and k2= 10 while (144b) presents the model with the lowest RMS and p1= 1.19, p2=1.51, c1=0.06, c2=0.1, k1=16.5 and k2= 10.

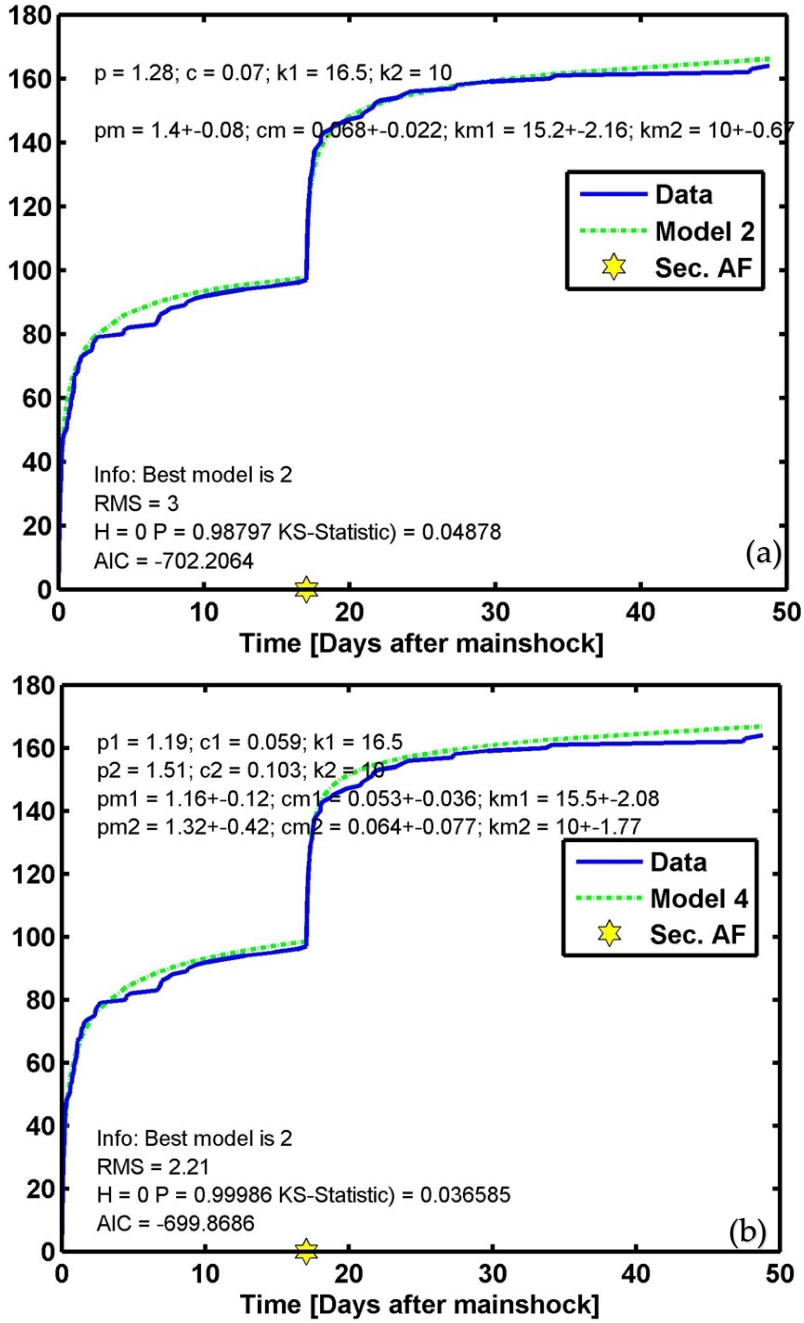

Figure 144. (a) The best model (2) of the estimated curve of the modified Omori formula (dashed line) applied to the aftershock data and the observed cumulative number of aftershocks (solid line) based on the AIC. **(b)** The model 4 of the estimated curve of the modified Omori formula (dashed line) applied to the aftershock data and the observed cumulative number of aftershocks (solid line), with the lowest RMS= 2.21.

Here is the magnitude-time form of the aftershock sequence.

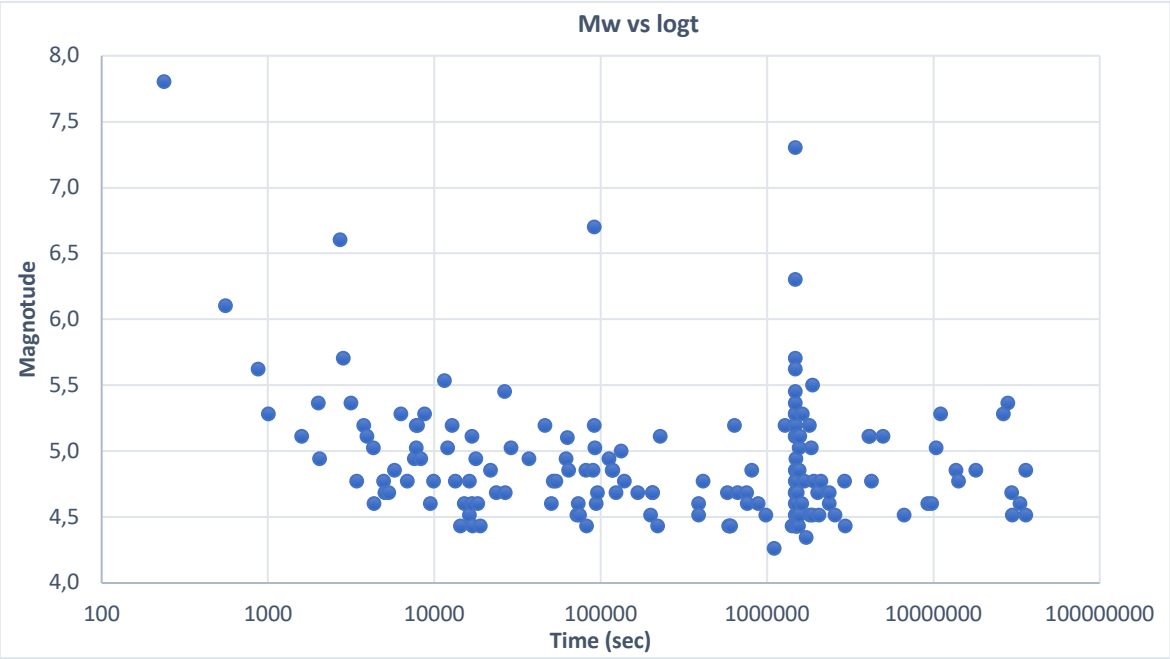

Figure 145. The magnitude-time pattern versus the logarithm of time of the mainshock M_w 7.8.

By the frequency-magnitude distribution for this earthquake, it is estimated a q_M= 1.54 with ci= 1.52-1.57

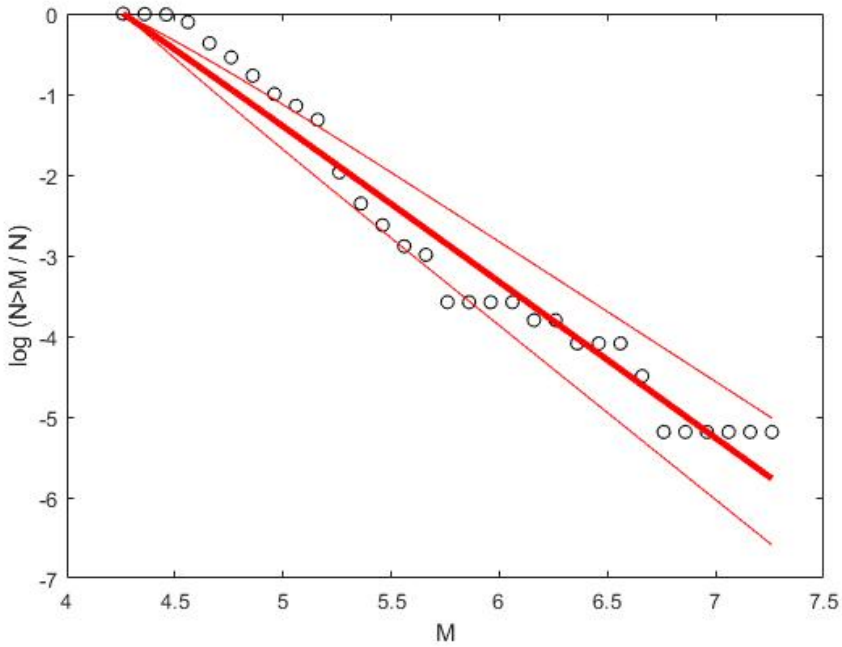

Figure 146. Frequency-magnitude distribution. The bold red line represents the model of equation (26) for qM= 1.54, while the other two lines present the corresponding 95% confidence intervals.

Figure 147 shows the typical Q-exponential pattern and Q-logarithmic function of the cumulative distribution function, P(>T) of the aftershocks interevent times and a q=1.71 is obtained.

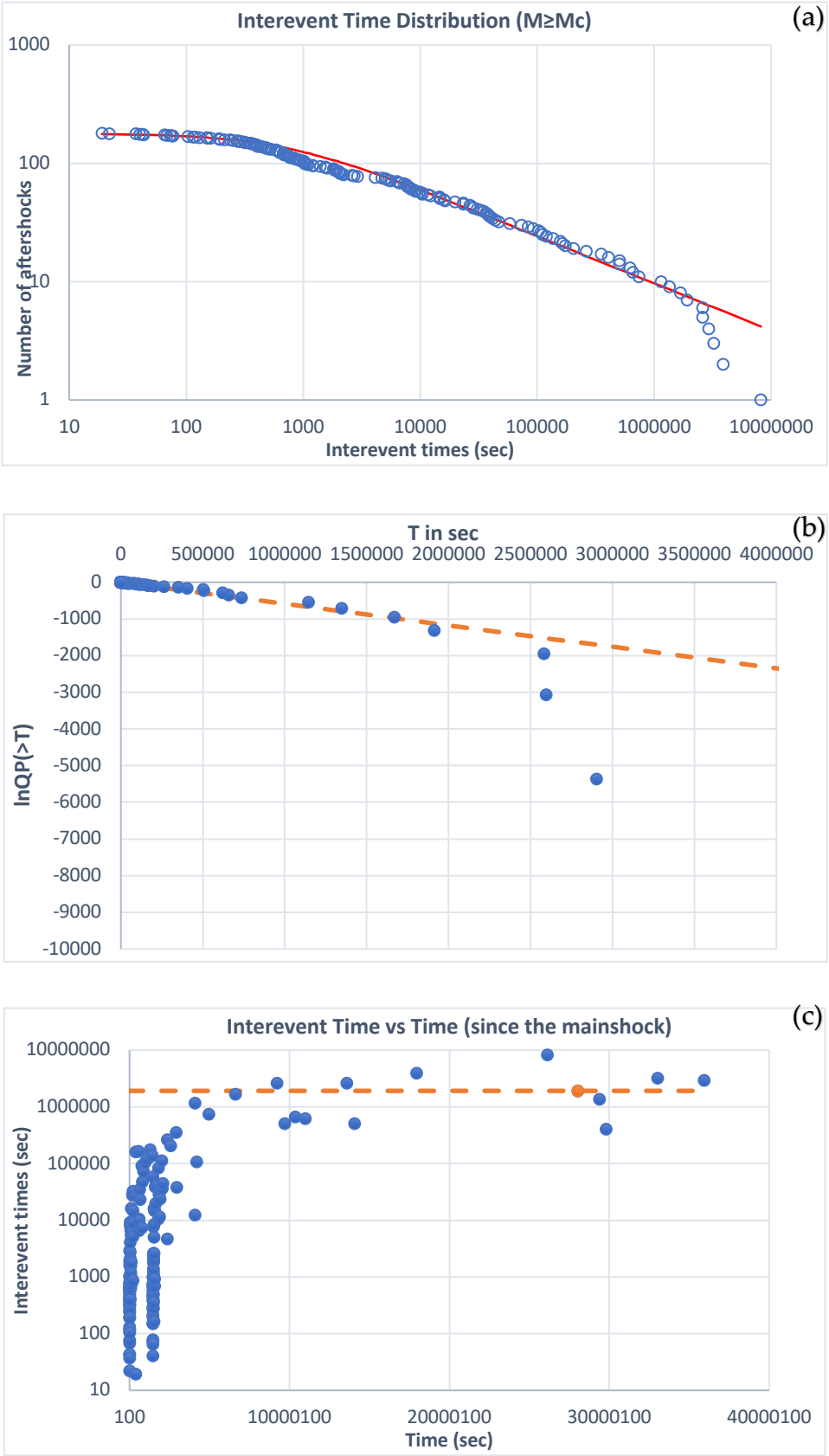

Figure 147. (a) The cumulative distribution function of the interevent times. The red line is the Q-exponential fitting with q = 1.71. **(b)** The Q-logarithmic function of the P(>T) as a function of the interevent times where the dashed line is the fitting with q=1.71. The deviation from the linearity suggests Tc values close to 2,500,000 s. **(c)** The evolution of interevent time T as a function of time t since the main event. The Tc value is indicated by the dashed line.

4.2.30 The 2015 Illapel Earthquake M_w=8.3 (Chile)

The figure below shows Guttenberg-Richter distribution. The estimated parameters are Mc=4.6, b=0.85 and a=6.2.

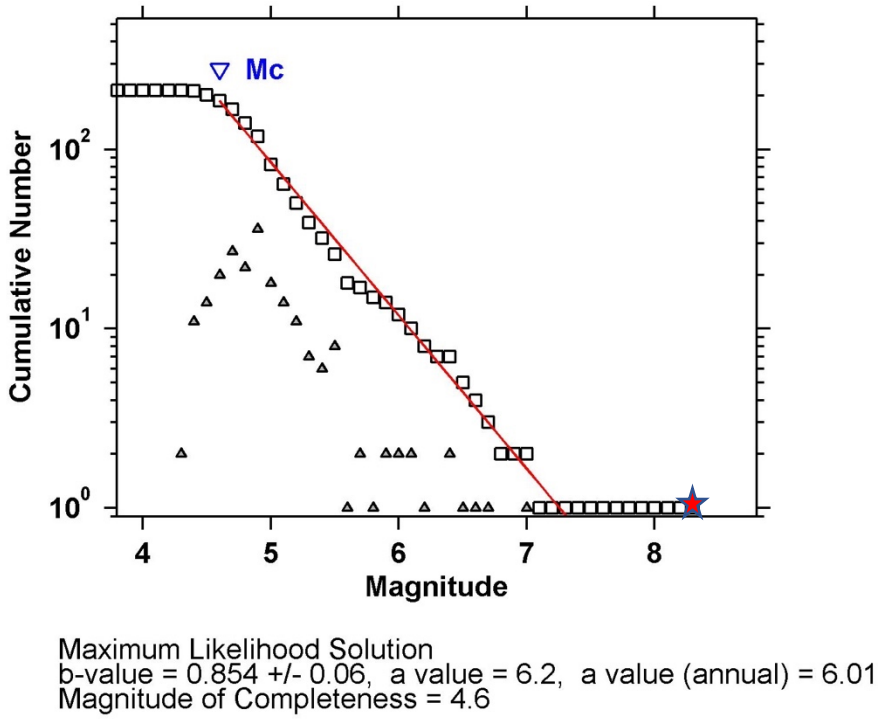

Figure 148. The Guttenberg-Richter distribution using maximum likelihood method with the best combination of maximum curvature M_c 95% and M_c 90% probability. The red star shows the magnitude of the mainshock M_w 8.3.

Next figure (149a) presents the model proposed by the AIC with p= 1.35, c= 0.13 and k= 35.2 while (149b) presents the model with the lowest RMS and p1= 1.59, p2=1.67, c1=0.2, c2=5, k1=38.1 and k2= 43.8.

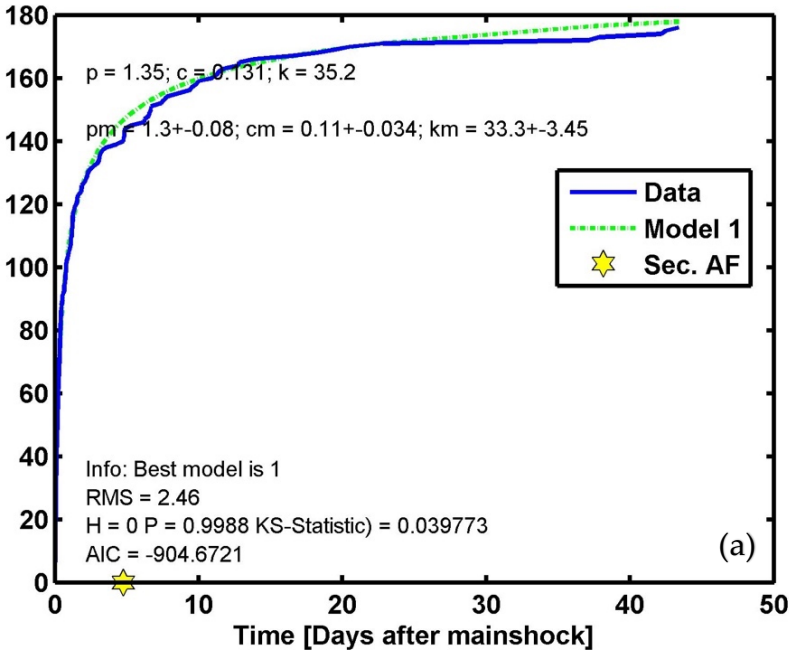

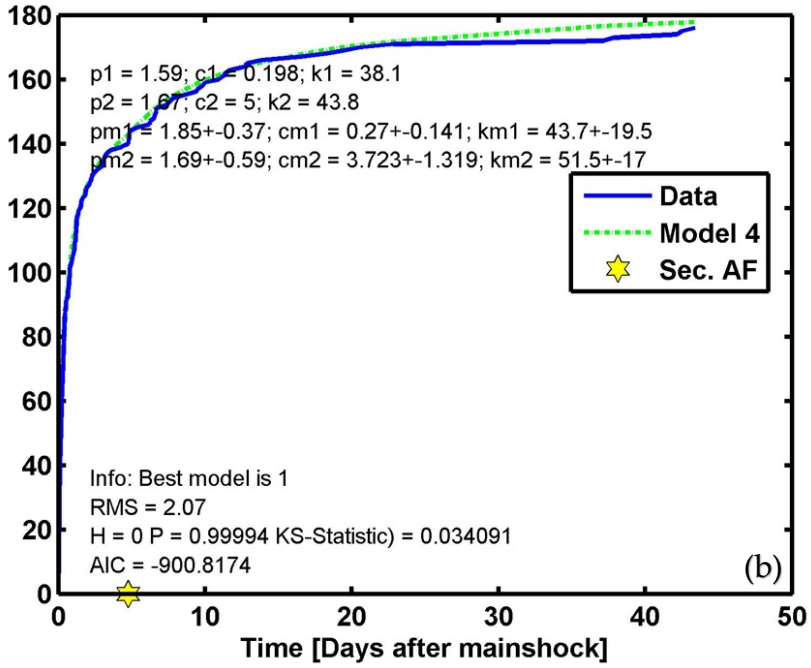

Figure 149. (a) The best model (1) of the estimated curve of the modified Omori formula (dashed line) applied to the aftershock data and the observed cumulative number of aftershocks (solid line) based on the AIC. **(b)** The model 4 of the estimated curve of the modified Omori formula (dashed line) applied to the aftershock data and the observed cumulative number of aftershocks (solid line), with the lowest RMS= 2.07.

Here is the magnitude-time form of the aftershock sequence.

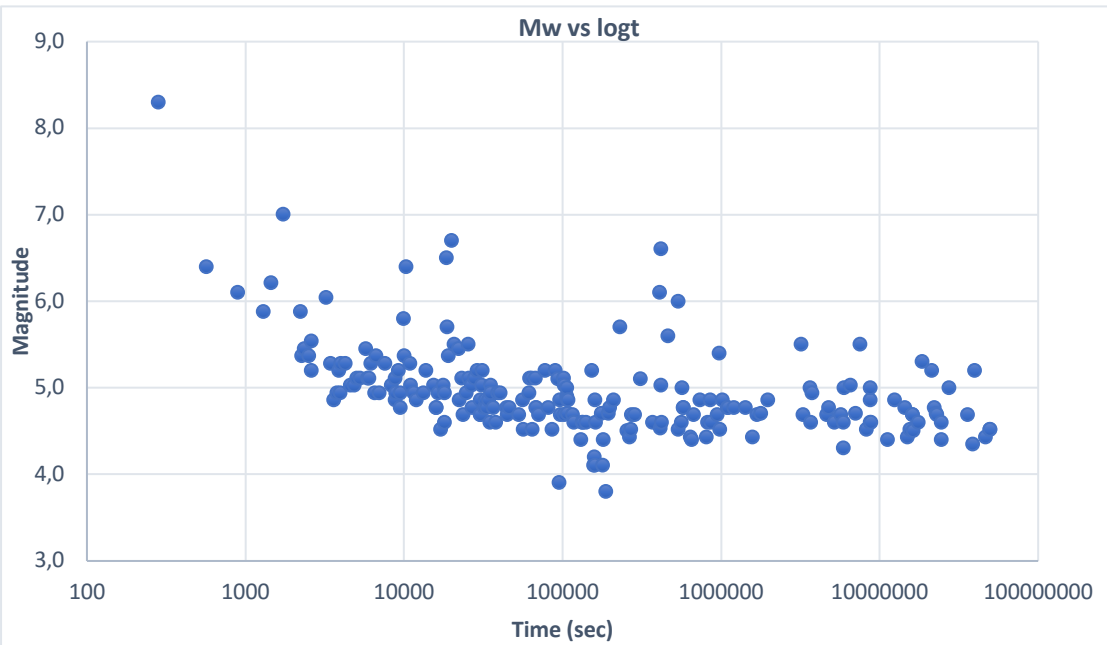

Figure 150. The magnitude-time pattern versus the logarithm of time of the mainshock M_w 8.3.

By the frequency-magnitude distribution for this earthquake, it is estimated a q_M= 1.50 with ci= 1.48-1.52.

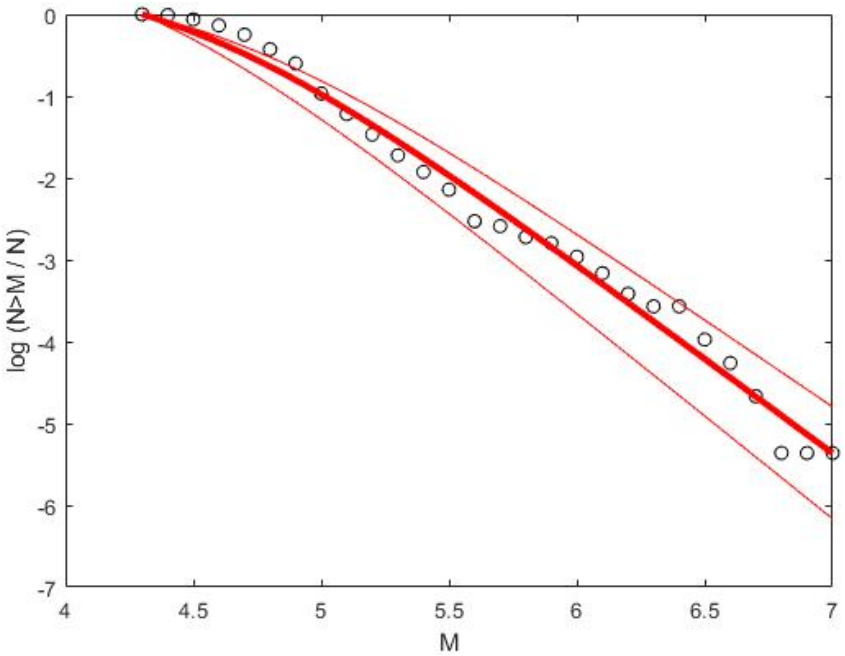

Figure 151. Frequency-magnitude distribution. The bold red line represents the model of equation (26) for qM= 1.50, while the other two lines present the corresponding 95% confidence intervals.

Figure 152 shows the typical Q-exponential pattern and Q-logarithmic function of the cumulative distribution function, P(>T) of the aftershocks interevent times and a q=1.78 is obtained.

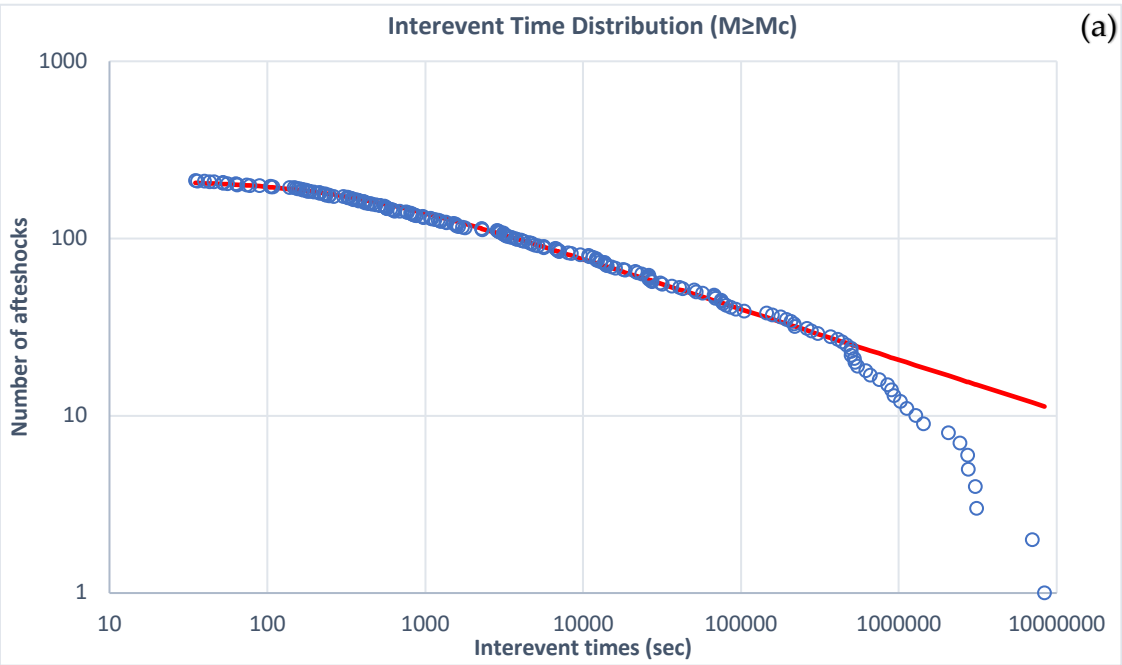

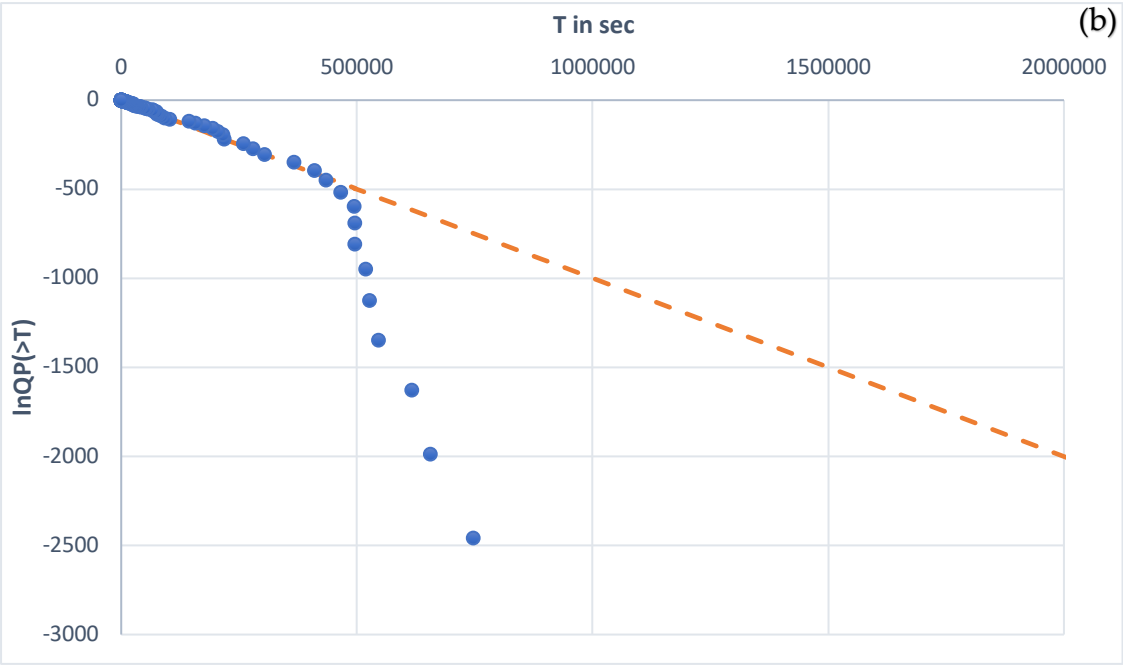

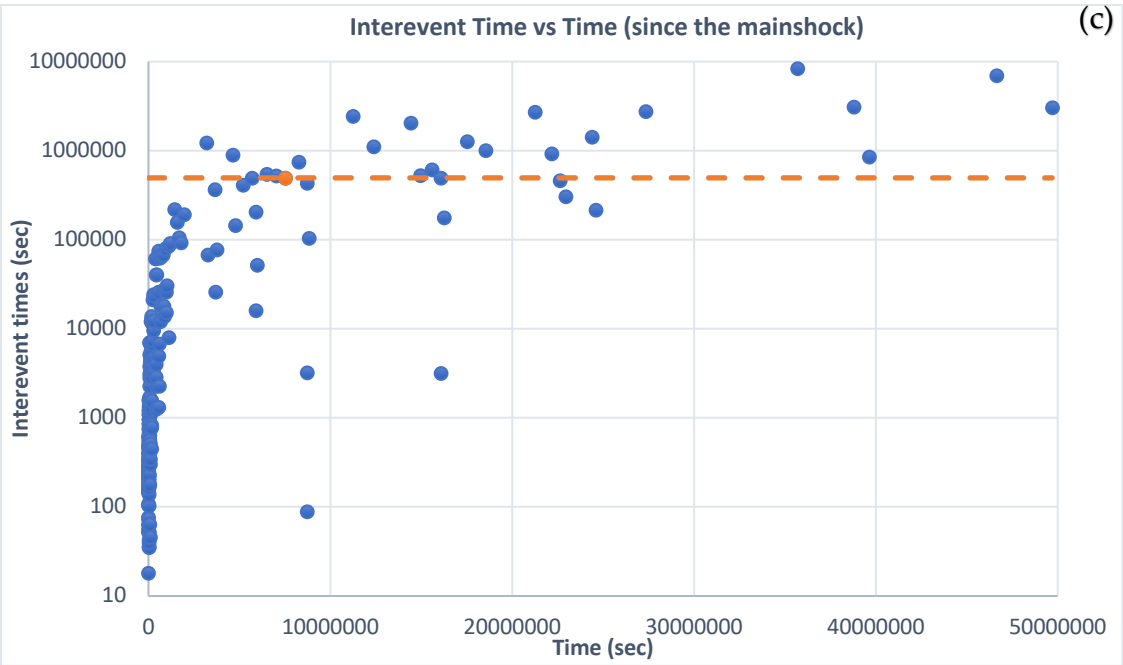

Figure 152. (a) The cumulative distribution function of the interevent times. The red line is the Q-exponential fitting with q = 1.78. **(b)** The Q-logarithmic function of the P(>T) as a function of the interevent times where the dashed line is the fitting with q=1.78. The deviation from the linearity suggests Tc values close to 500,000 s. **(c)** The evolution of interevent time T as a function of time t since the main event. The Tc value is indicated by the dashed line.

4.2.31 The 2016 South Sandwich Islands Earthquake M_w=7.2

The figure below shows Guttenberg-Richter distribution. The estimated parameters are Mc=4.9 and b=1.96 with a standard deviation of 0.15.

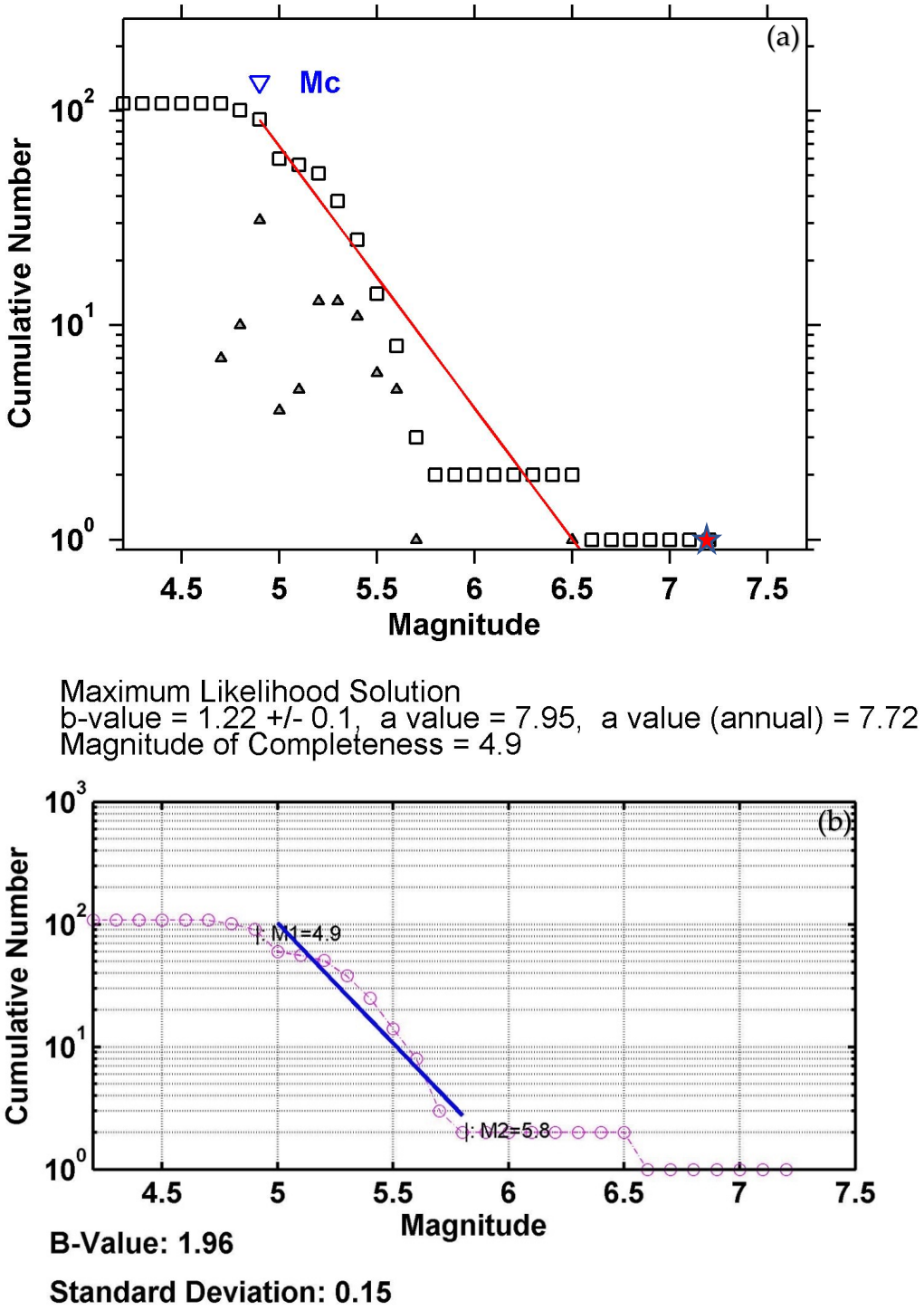

Figure 153. (a) The Guttenberg-Richter distribution using maximum likelihood method with the best combination of maximum curvature M_c 95% and M_c 90% probability. The red star shows the magnitude of the mainshock M_w 7.2. **(b)** The Guttenberg-Richter distribution using the manual method.

Next figure presents the model proposed by the AIC with p= 1.88, c= 3.55, k1= 60 and k2=35.3

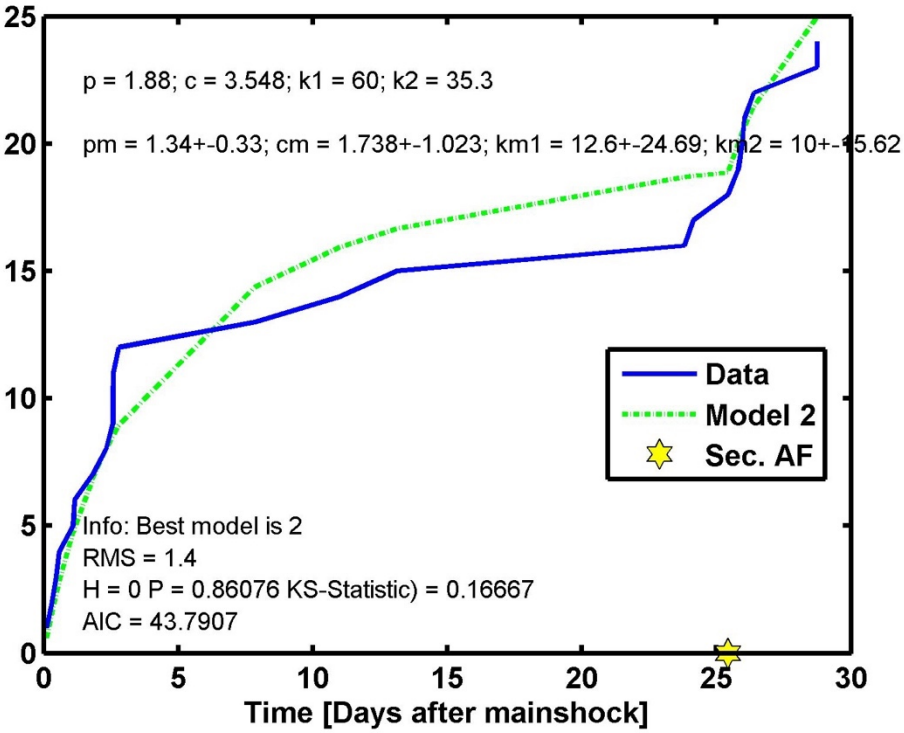

Figure 154. The best model (2) of the estimated curve of the modified Omori formula (dashed line) applied to the aftershock data and the observed cumulative number of aftershocks (solid line) based on the AIC with RMS= 1.4.

Here is the magnitude-time form of the aftershock sequence.

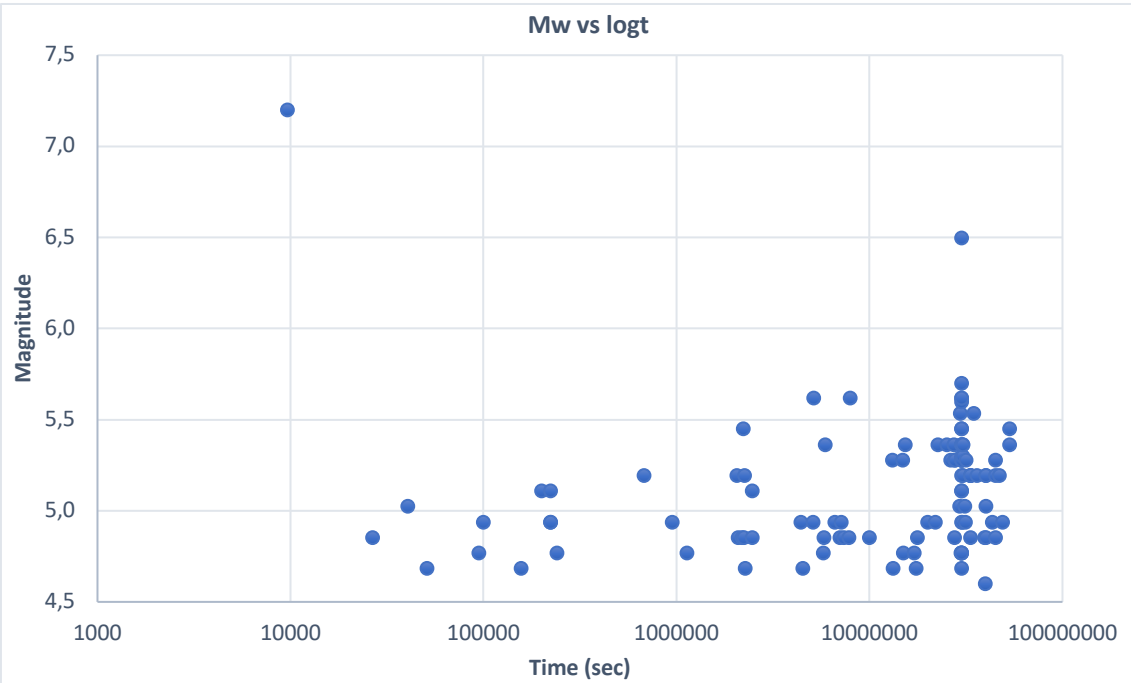

Figure 155. The magnitude-time pattern versus the logarithm of time of the mainshock M_w 7.2.

By the frequency-magnitude distribution for this earthquake, it is estimated a q_M= 1.41 with ci= 1.32-1.50.

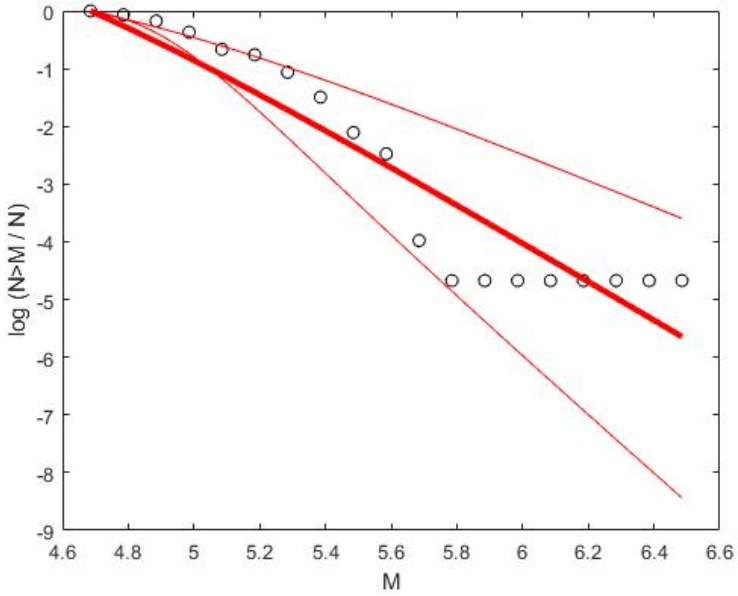

Figure 156. Frequency-magnitude distribution. The bold red line represents the model of equation (26) for qM= 1.41, while the other two lines present the corresponding 95% confidence intervals.

Figure 157 shows the typical Q-exponential pattern and Q-logarithmic function of the cumulative distribution function, P(>T) of the aftershocks interevent times and a q=1.78 is obtained.

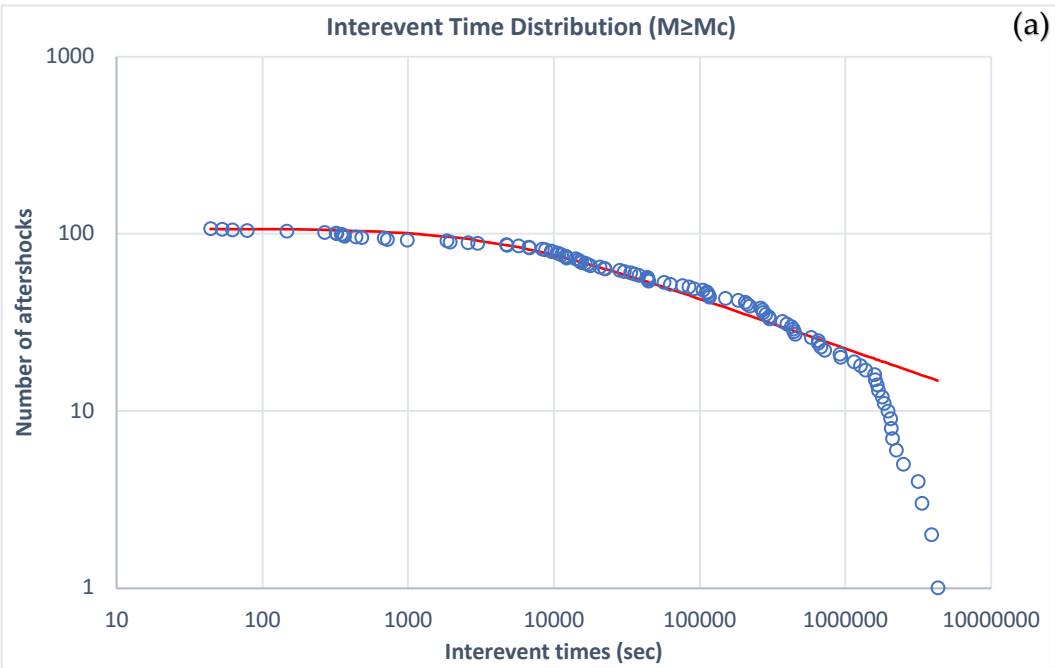

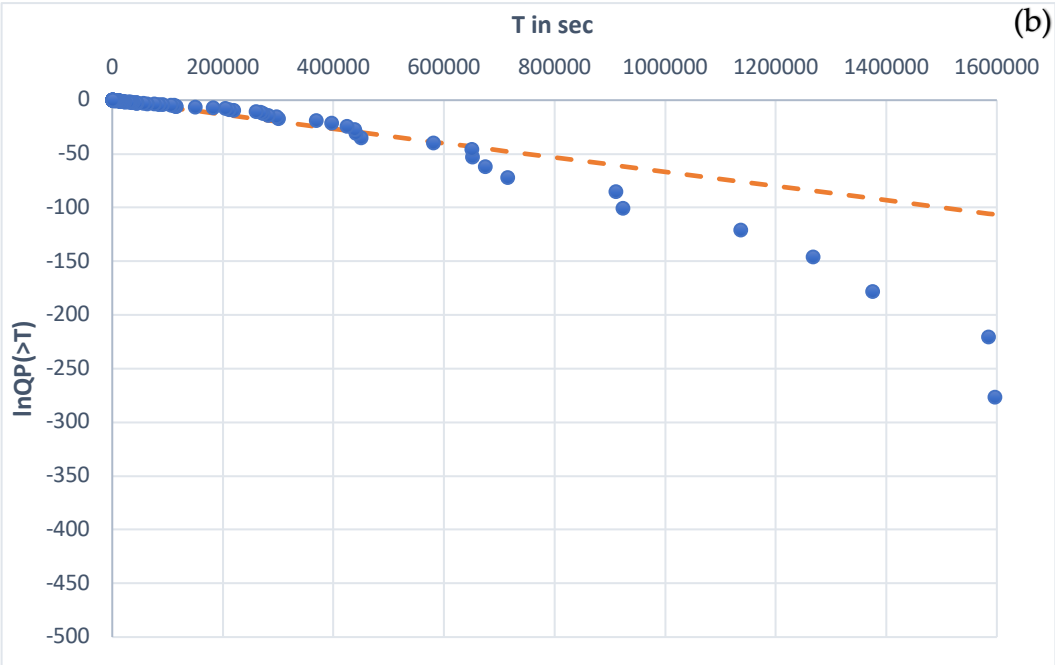

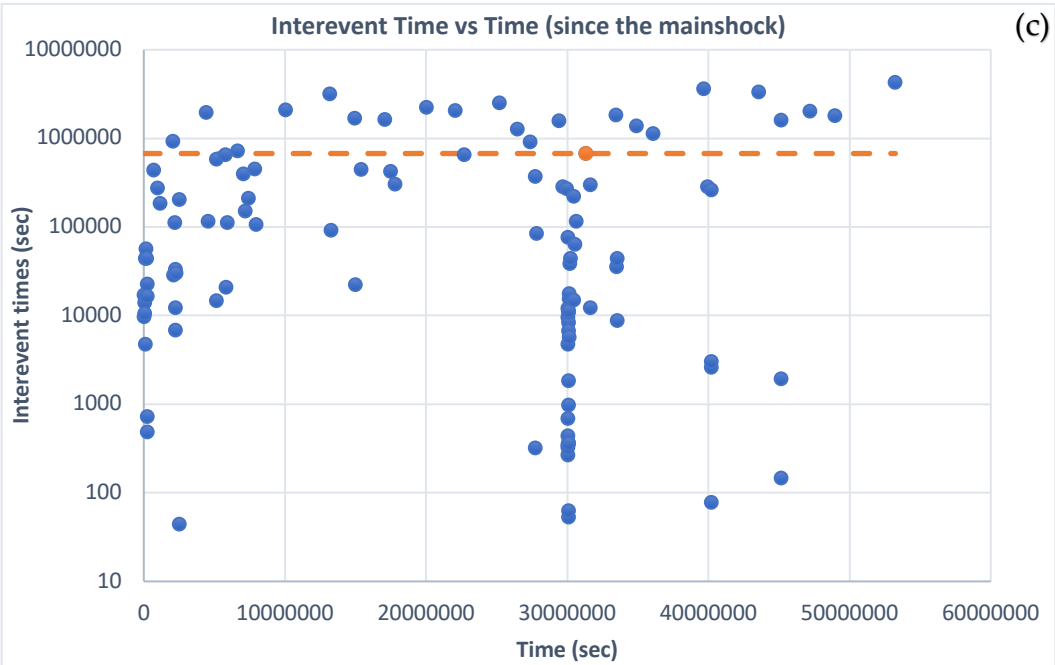

Figure 157. (a) The cumulative distribution function of the interevent times. The red line is the Q-exponential fitting with q = 1.78. **(b)** The Q-logarithmic function of the P(>T) as a function of the interevent times where the dashed line is the fitting with q=1.78. The deviation from the linearity suggests Tc values close to 700,000 s. **(c)** The evolution of interevent time T as a function of time t since the main event. The Tc value is indicated by the dashed line.

4.2.32 The 2016 Gisborne Earthquake M_w=7.0 (New Zealand)

The figure below shows Guttenberg-Richter distribution. The estimated parameters are Mc=4.7 and b=1.46 with a standard deviation of 0.08.

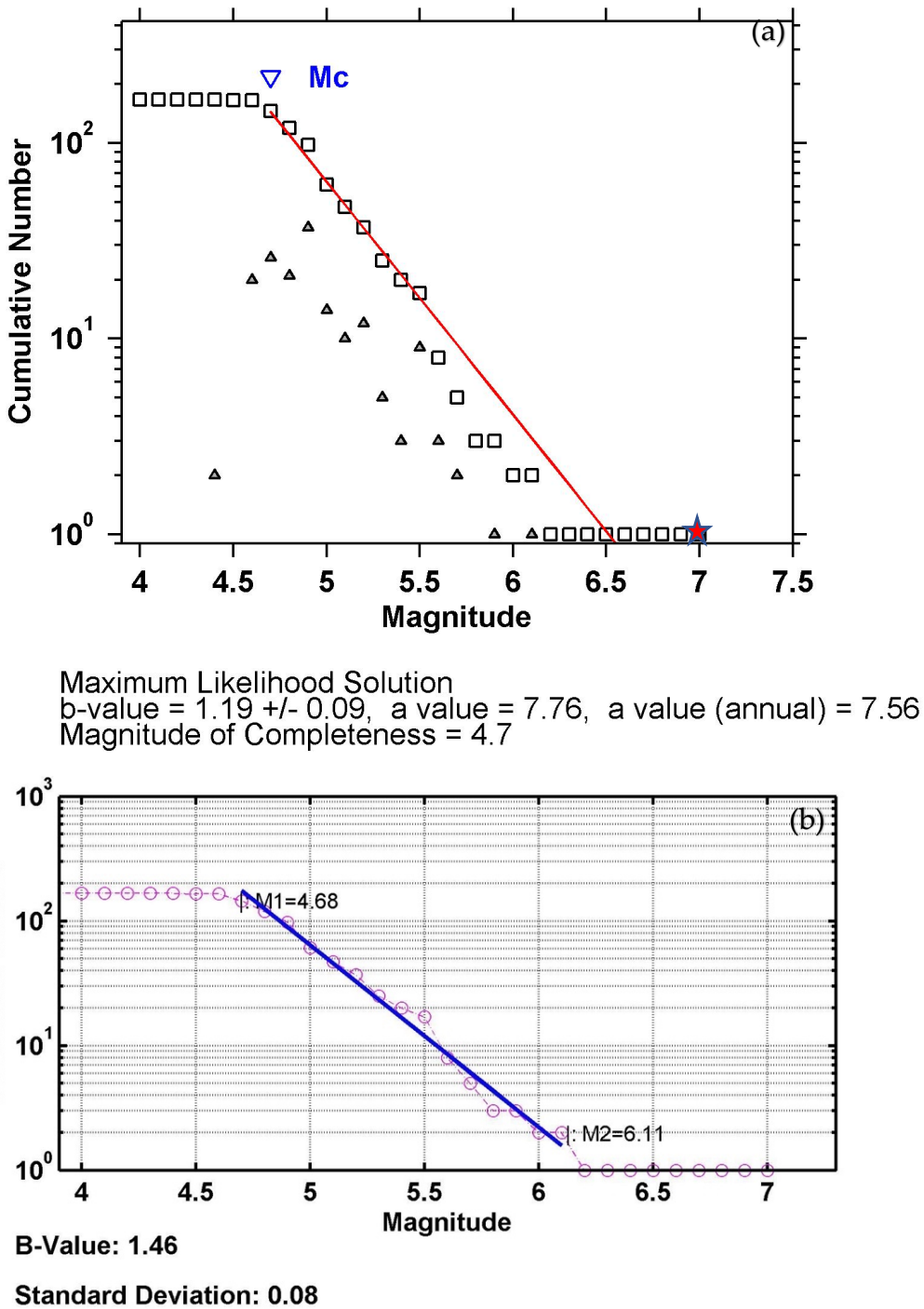

Figure 158. (a) The Guttenberg-Richter distribution using maximum likelihood method with the best combination of maximum curvature M_c 95% and M_c 90% probability. The red star shows the magnitude of the mainshock M_w 7.0. **(b)** The Guttenberg-Richter distribution using the manual method.

Next figure presents the model proposed by the AIC with p= 1.09, c= 0.03 and k= 21.2.

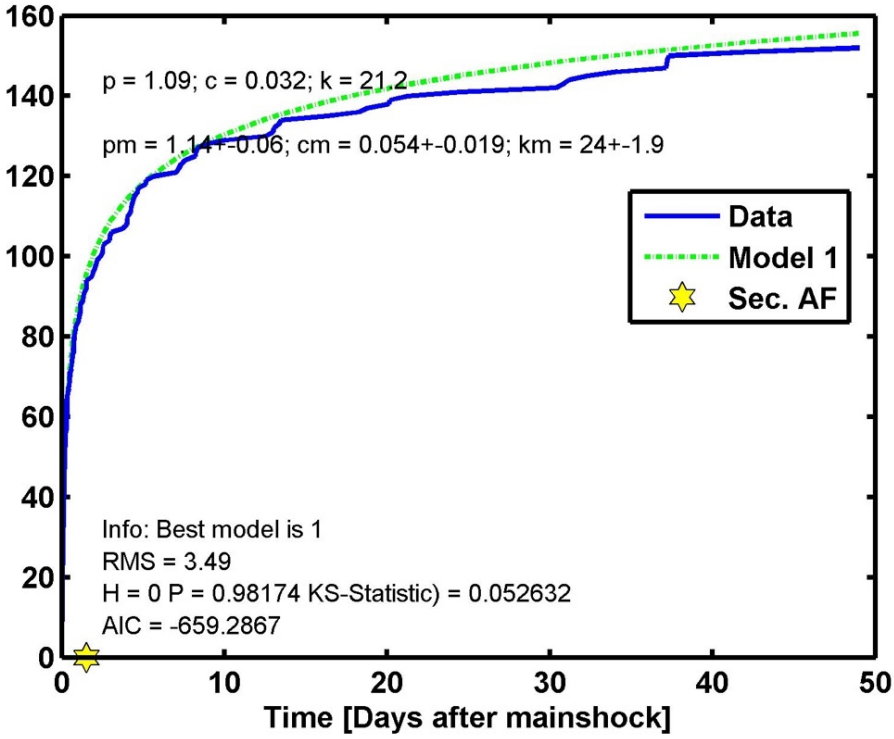

Figure 159. The best model (1) of the estimated curve of the modified Omori formula (dashed line) applied to the aftershock data and the observed cumulative number of aftershocks (solid line) based on the AIC with RMS= 3.49.

Here is the magnitude-time form of the aftershock sequence.

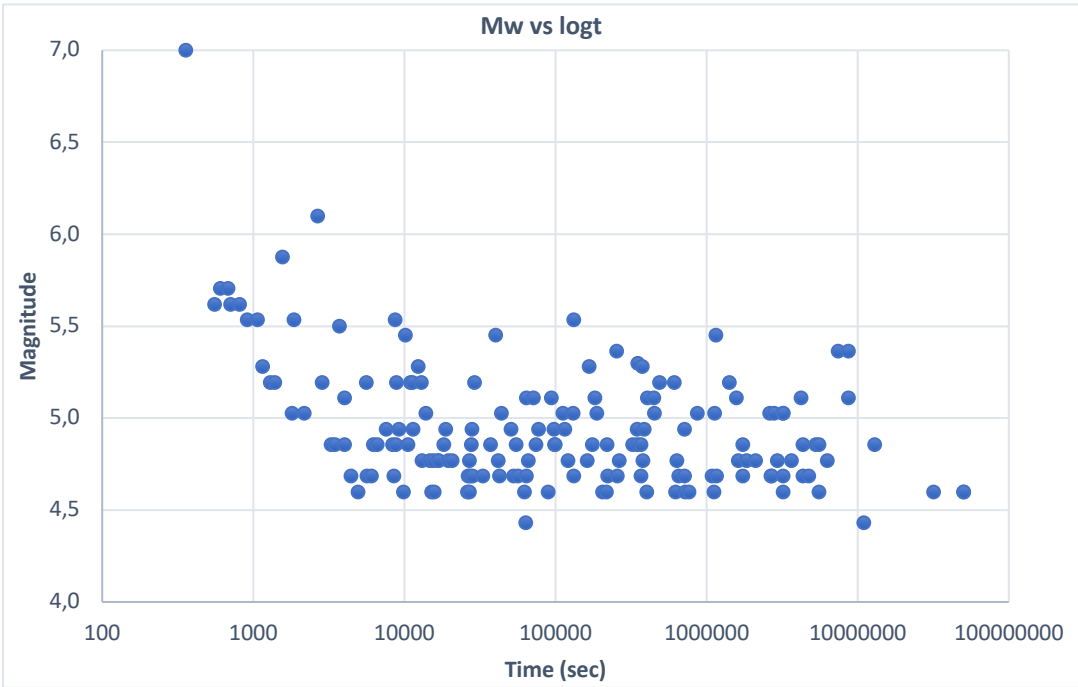

Figure 160. The magnitude-time pattern versus the logarithm of time of the mainshock M_w 7.0.

By the frequency-magnitude distribution for this earthquake, it is estimated a q_M= 1.25 with ci= 1.21-1.28.

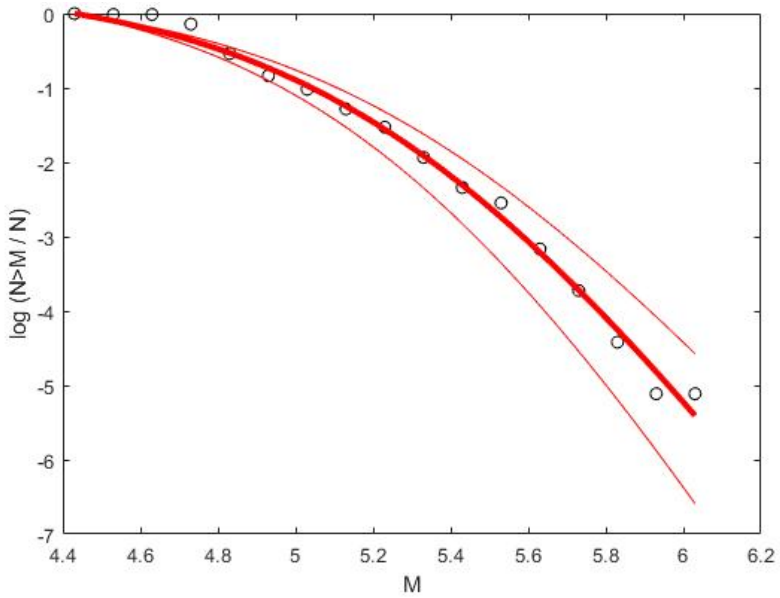

Figure 161. Frequency-magnitude distribution. The bold red line represents the model of equation (26) for qM= 1.25, while the other two lines present the corresponding 95% confidence intervals.

Figure 162 shows the typical Q-exponential pattern and Q-logarithmic function of the cumulative distribution function, P(>T) of the aftershocks interevent times and a q=1.74 is obtained.

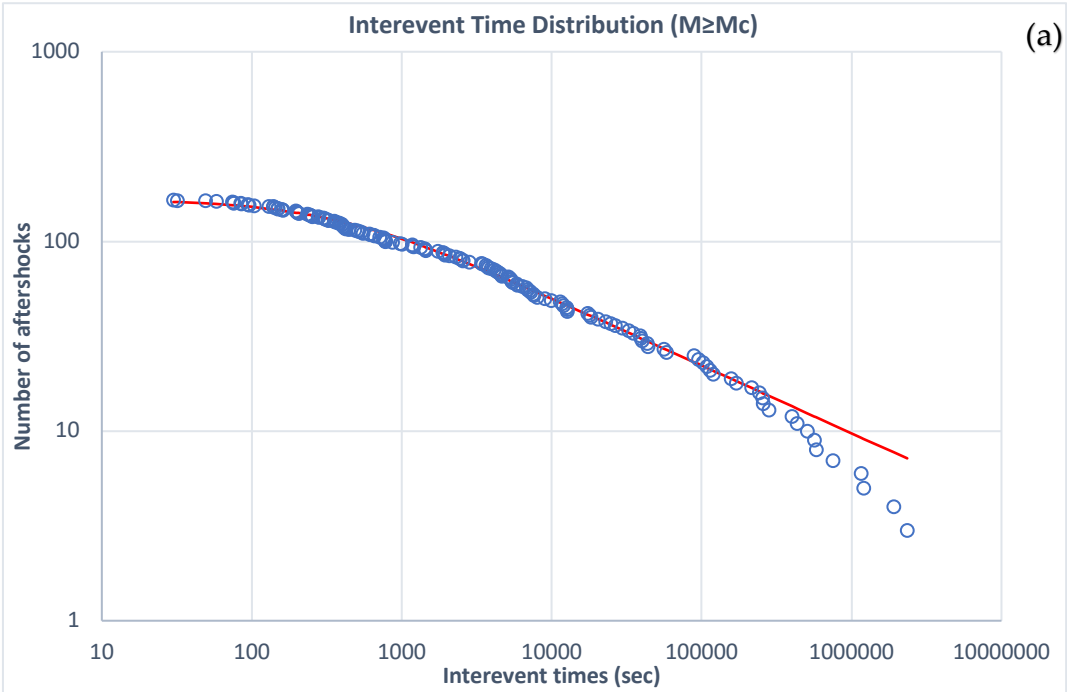

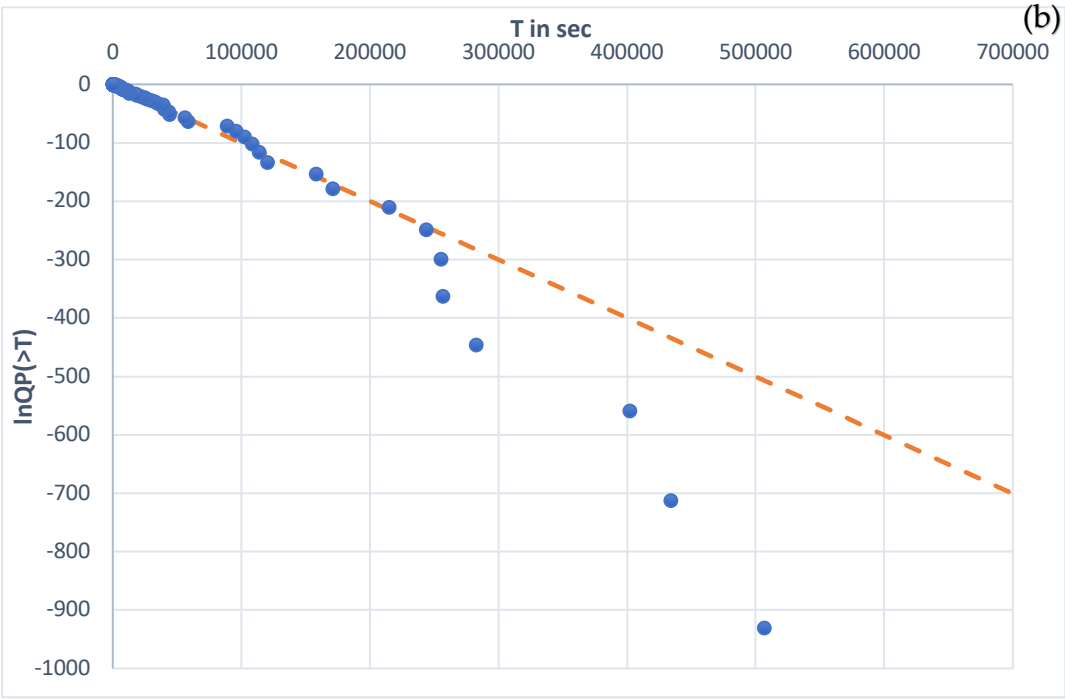

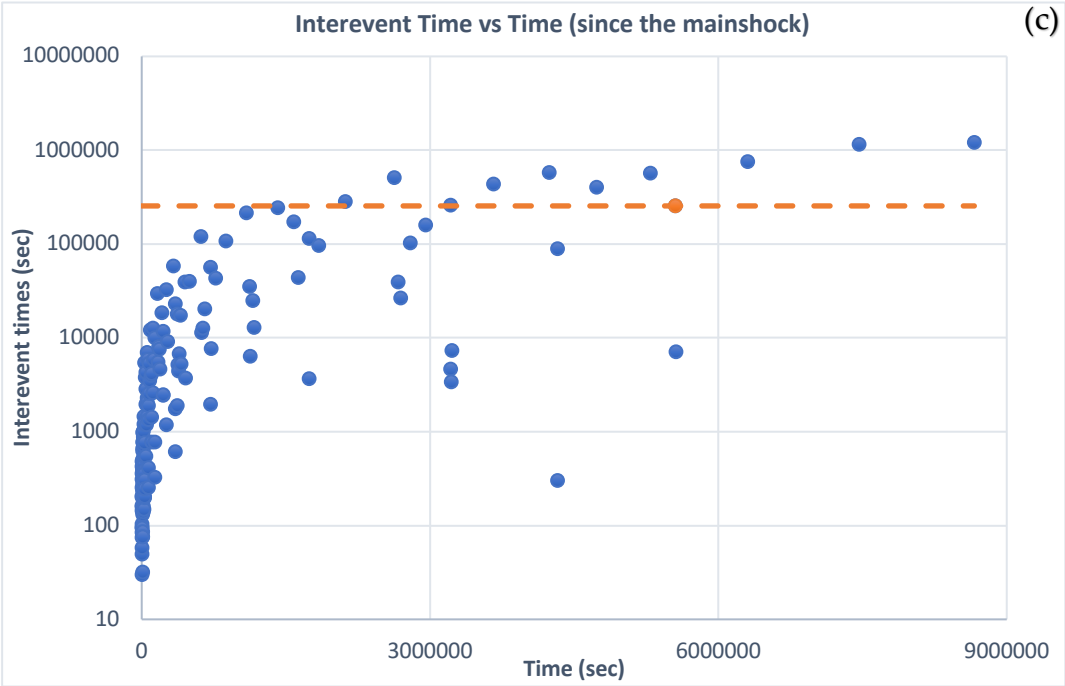

Figure 162. (a) The cumulative distribution function of the interevent times. The red line is the Q-exponential fitting with q = 1.74. **(b)** The Q-logarithmic function of the P(>T) as a function of the interevent times where the dashed line is the fitting with q=1.74. The deviation from the linearity suggests Tc values close to 250,000 s. **(c)** The evolution of interevent time T as a function of time t since the main event. The Tc value is indicated by the dashed line.

4.2.33 The 2016 Amberley Earthquake M_w=7.8 (New Zealand)

The figure below shows Guttenberg-Richter distribution. The estimated parameters are Mc=4.9, b=1.17 and a=7.74.

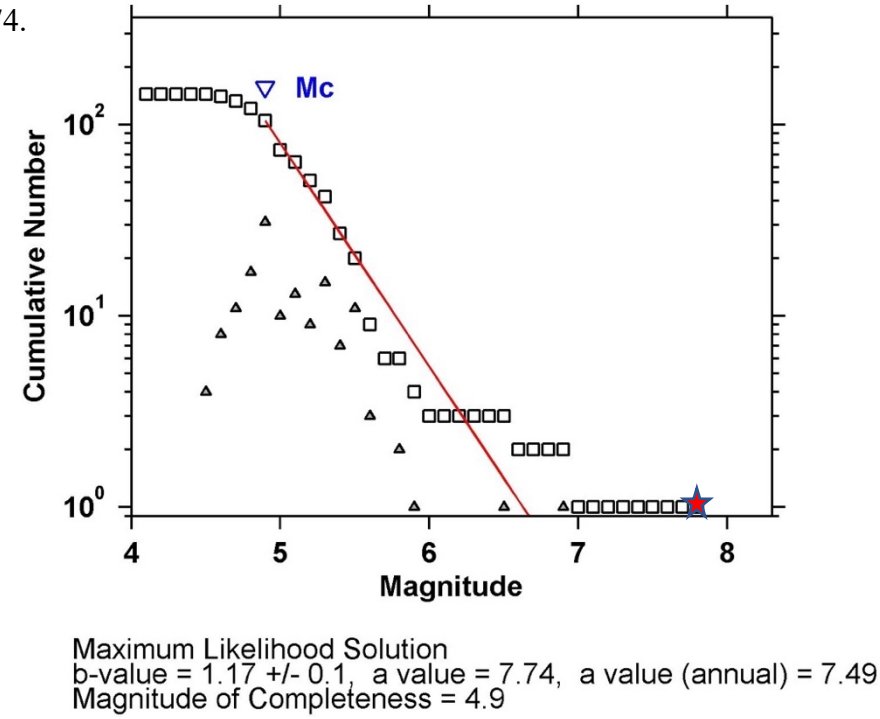

Figure 163. The Guttenberg-Richter distribution using maximum likelihood method with the best combination of maximum curvature M_c 95% and M_c 90% probability. The red star shows the magnitude of the mainshock M_w 7.8.

Next figure (164a) presents the model proposed by the AIC with p1= 1.52, p2=2.7, c1= 0.39, k1=37.9, k2=10 while (164b) presents the model with the lowest RMS and p1= 1.41, p2=2.7, c1=0.26, c2=0.393, k1=29.4 and k2= 10.

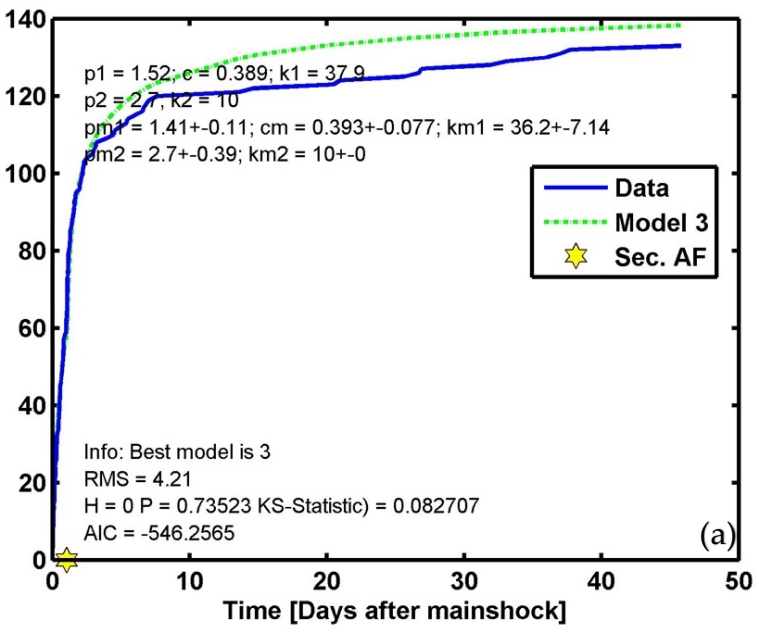

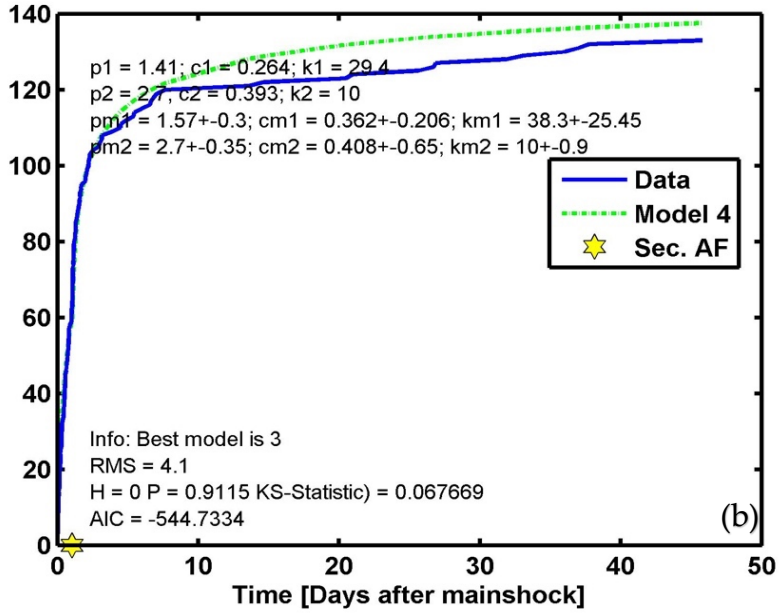

Figure 164. (a) The best model (3) of the estimated curve of the modified Omori formula (dashed line) applied to the aftershock data and the observed cumulative number of aftershocks (solid line) based on the AIC. **(b)** The model 4 of the estimated curve of the modified Omori formula (dashed line) applied to the aftershock data and the observed cumulative number of aftershocks (solid line), with the lowest RMS= 4.1.

Here is the magnitude-time form of the aftershock sequence.

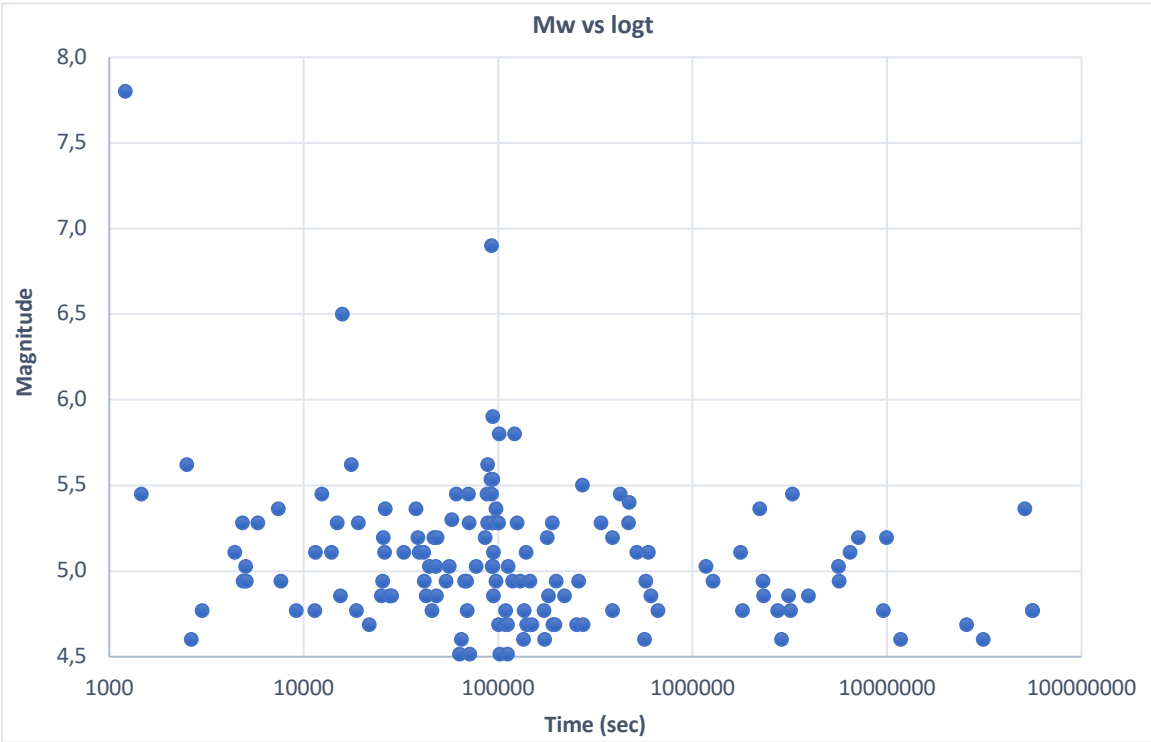

Figure 165. The magnitude-time pattern versus the logarithm of time of the mainshock M_w 7.8.

By the frequency-magnitude distribution for this earthquake, it is estimated a q_M= 1.47 with ci= 1.43-1.52.

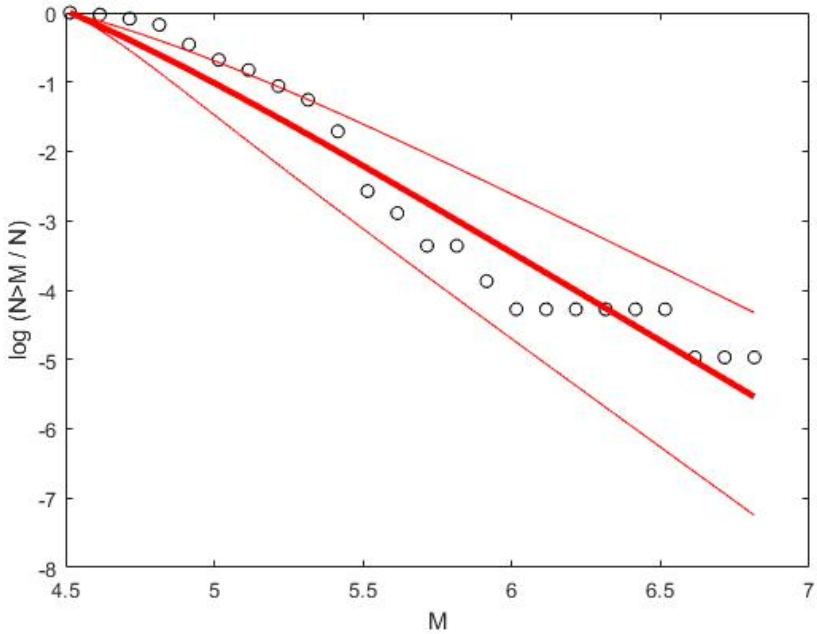

Figure 166. Frequency-magnitude distribution. The bold red line represents the model of equation (26) for qM= 1.47, while the other two lines present the corresponding 95% confidence intervals.

Figure 167 shows the typical Q-exponential pattern and Q-logarithmic function of the cumulative distribution function, P(>T) of the aftershocks interevent times and a q=1.73 is obtained.

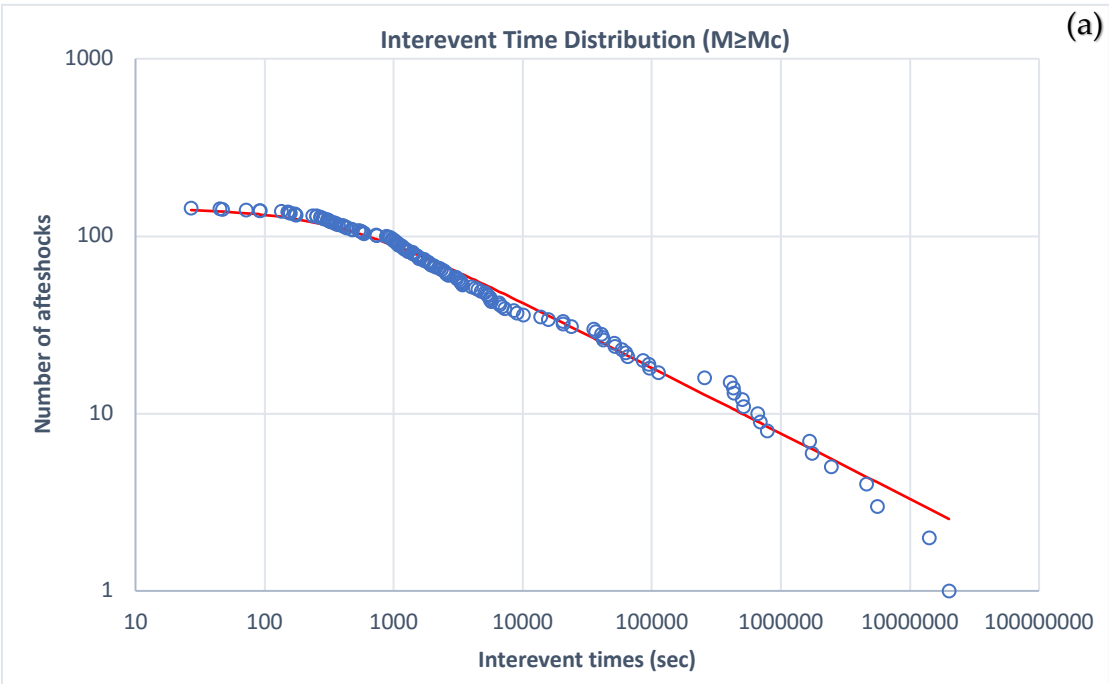

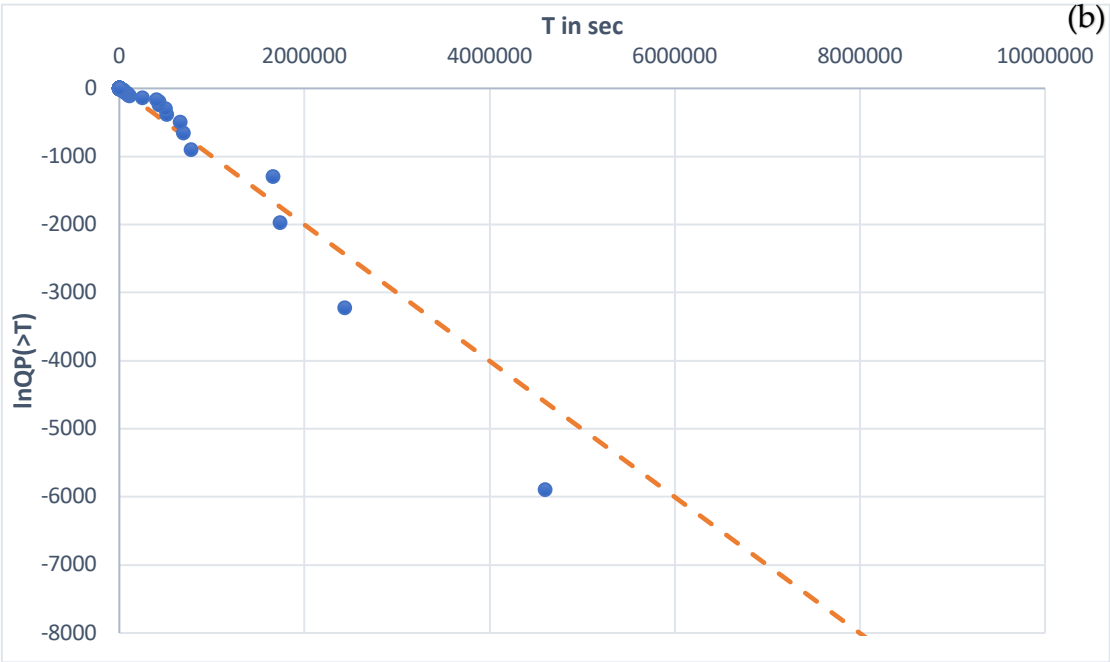

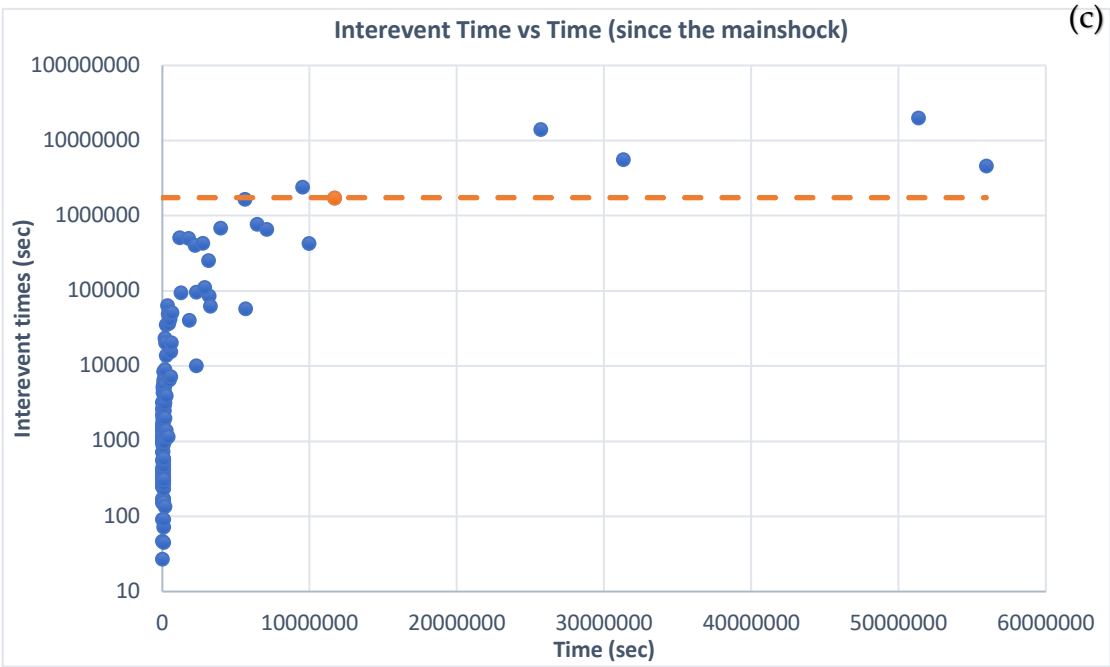

Figure 167. (a) The cumulative distribution function of the interevent times. The red line is the Q-exponential fitting with q = 1.73. **(b)** The Q-logarithmic function of the P(>T) as a function of the interevent times where the dashed line is the fitting with q=1.73. The deviation from the linearity suggests Tc values close to 2,000,000 s. **(c)** The evolution of interevent time T as a function of time t since the main event. The Tc value is indicated by the dashed line.

4.2.34 The 2016 Kirakira Earthquake M_w=7.8 (Solomon Islands)

The figure below shows Guttenberg-Richter distribution. The estimated parameters are Mc=5.0, b=0.87 and a=5.87.

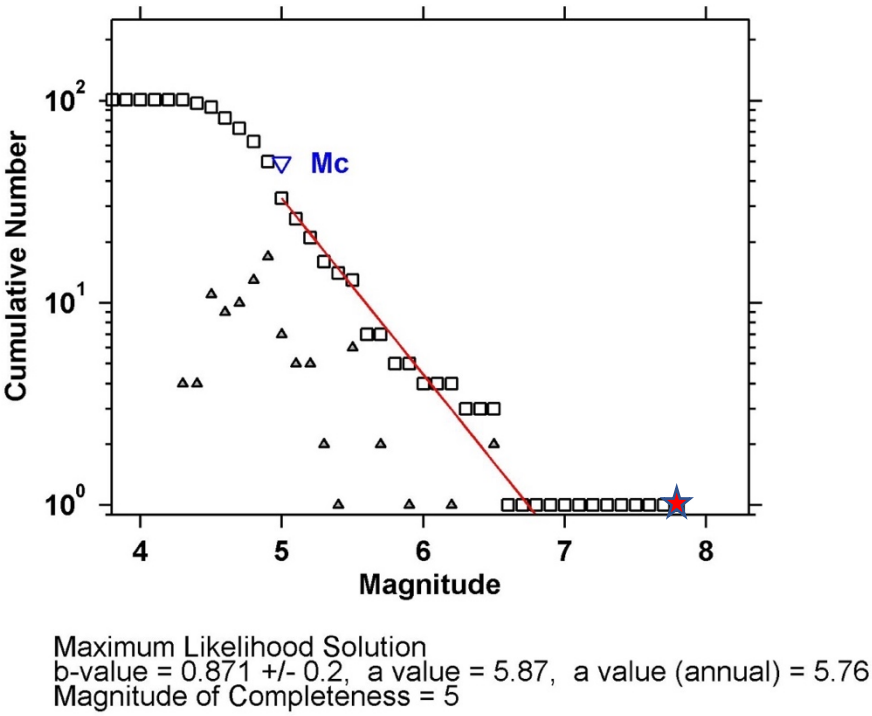

Figure 168. The Guttenberg-Richter distribution using maximum likelihood method with the best combination of maximum curvature M_c 95% and M_c 90% probability. The red star shows the magnitude of the mainshock M_w 7.8.

Next figure presents the model proposed by the AIC with p= 1.48, c= 0.29 and k= 27.2.

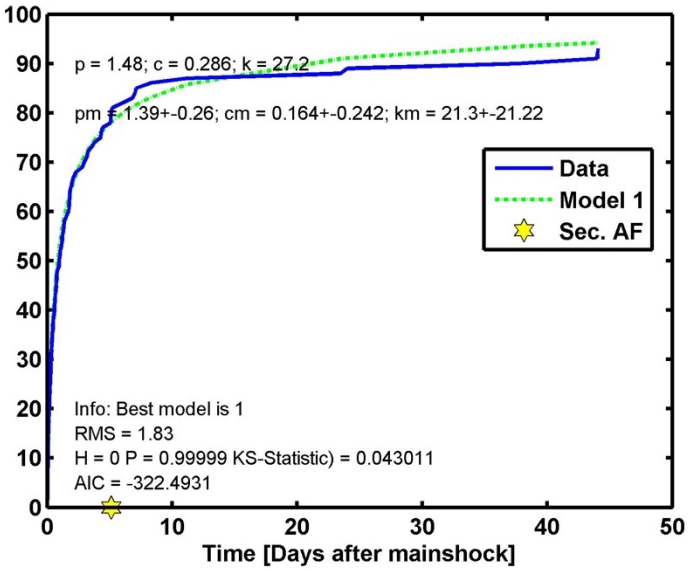

Figure 169. The best model (1) of the estimated curve of the modified Omori formula (dashed line) applied to the aftershock data and the observed cumulative number of aftershocks (solid line) based on the AIC with RMS= 1.83.

Here is the magnitude-time form of the aftershock sequence.

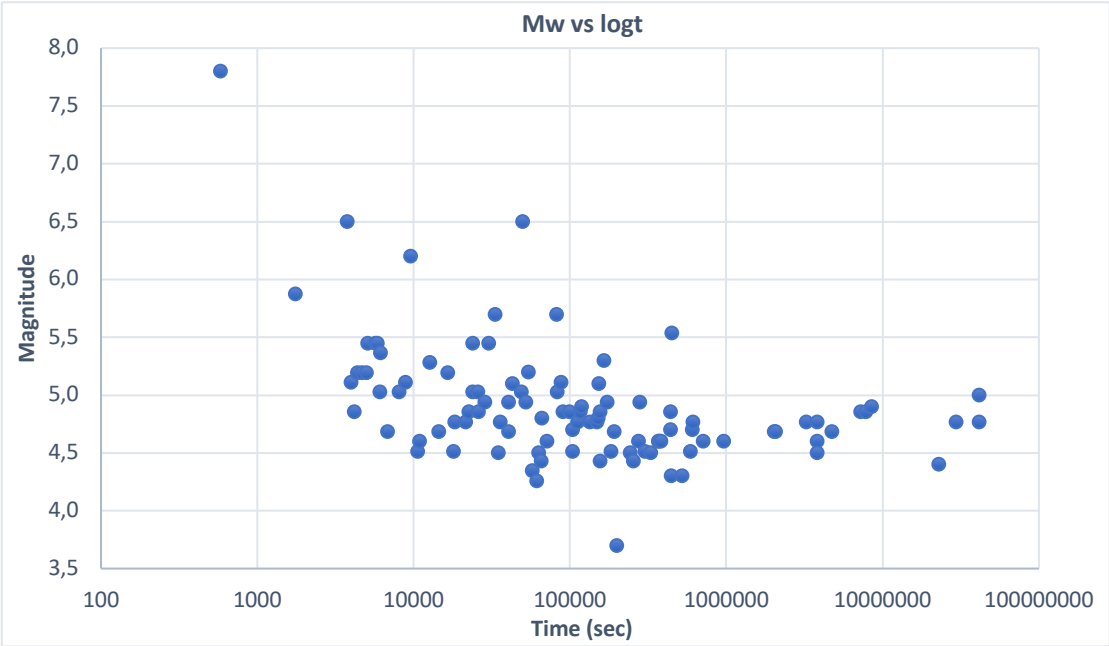

Figure 170. The magnitude-time pattern versus the logarithm of time of the mainshock M_w 7.8.

By the frequency-magnitude distribution for this earthquake, it is estimated a q_M= 1.51 with ci= 1.47-1.54.

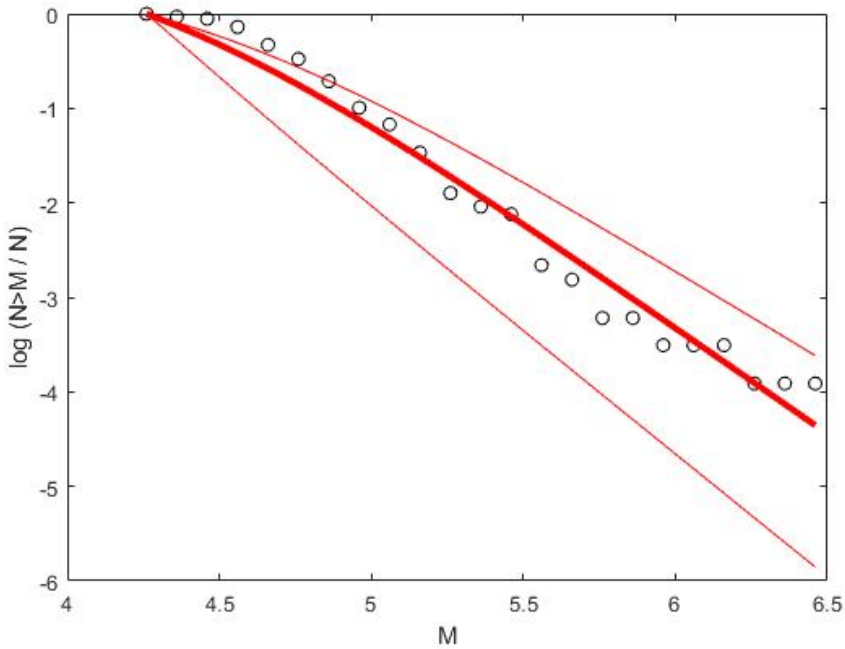

Figure 171. Frequency-magnitude distribution. The bold red line represents the model of equation (26) for qM= 1.51, while the other two lines present the corresponding 95% confidence intervals.

Figure 172 shows the typical Q-exponential pattern and Q-logarithmic function of the cumulative distribution function, P(>T) of the aftershocks interevent times and a q=1.71 is obtained.

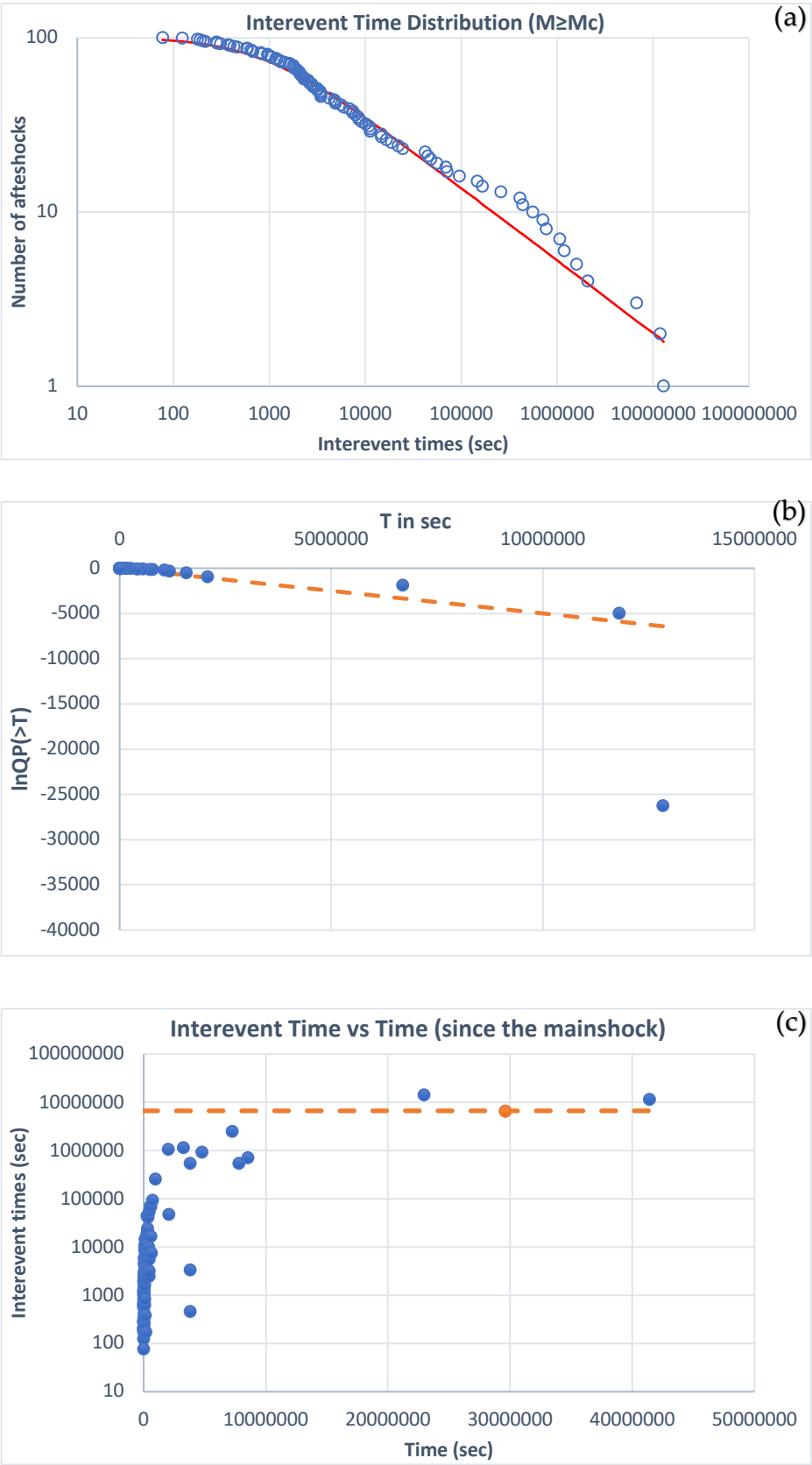

Figure 172. (a) The cumulative distribution function of the interevent times. The red line is the Q-exponential fitting with q = 1.71. **(b)** The Q-logarithmic function of the P(>T) as a function of the interevent times where the dashed line is the fitting with q=1.71. The deviation from the linearity suggests Tc values close to 10,000,000 s. **(c)** The evolution of interevent time T as a function of time t since the main event. The Tc value is indicated by the dashed line.

4.2.35 The 2017 Chiapas Earthquake M_w=8.2 (Mexico)

The figure below shows Guttenberg-Richter distribution. The estimated parameters are Mc=4.8, b=1.34 and a=8.55.

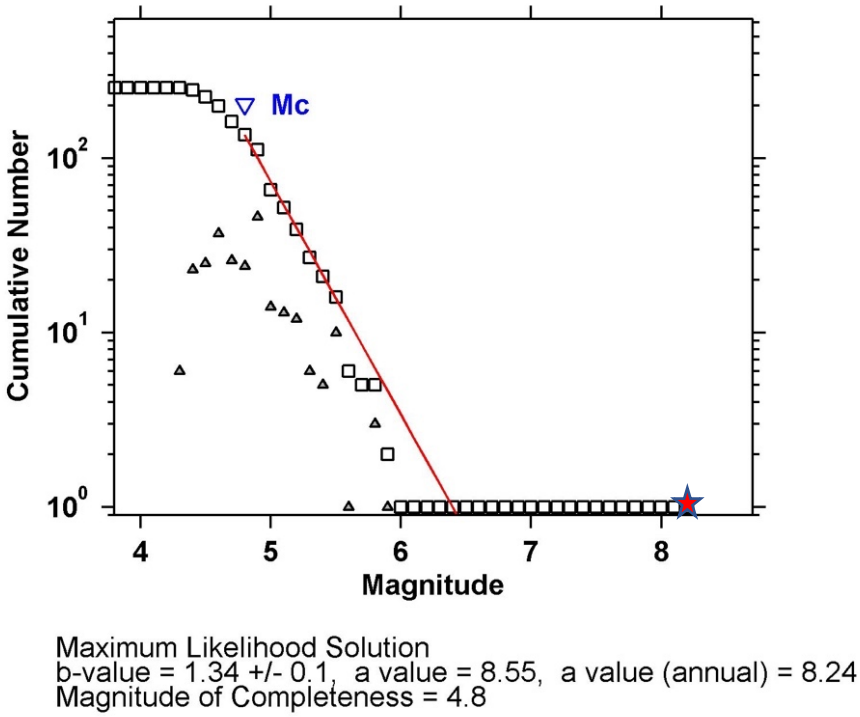

Figure 173. The Guttenberg-Richter distribution using maximum likelihood method with the best combination of maximum curvature M_c 95% and M_c 90% probability. The red star shows the magnitude of the mainshock M_w 8.2.

Next figure (174a) presents the model proposed by the AIC with p= 0.93, c= 0.12 and k= 31.5 while (174b) presents the model with the lowest RMS and p1= 0.96, p2=1.51, c1=0.11, c2=5, k1=29.2 and k2= 31.4.

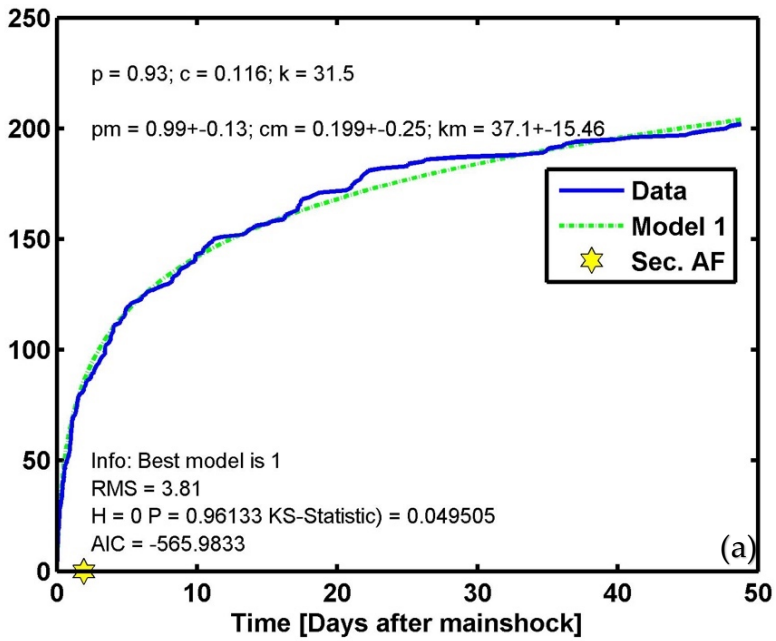

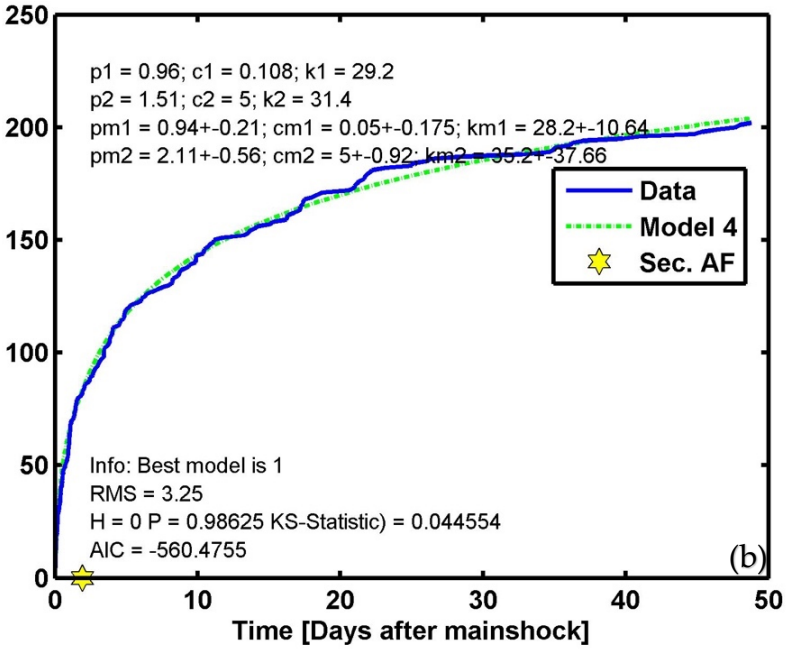

Figure 174. (a) The best model (1) of the estimated curve of the modified Omori formula (dashed line) applied to the aftershock data and the observed cumulative number of aftershocks (solid line) based on the AIC. **(b)** The model 4 of the estimated curve of the modified Omori formula (dashed line) applied to the aftershock data and the observed cumulative number of aftershocks (solid line), with the lowest RMS= 3.25.

Here is the magnitude-time form of the aftershock sequence.

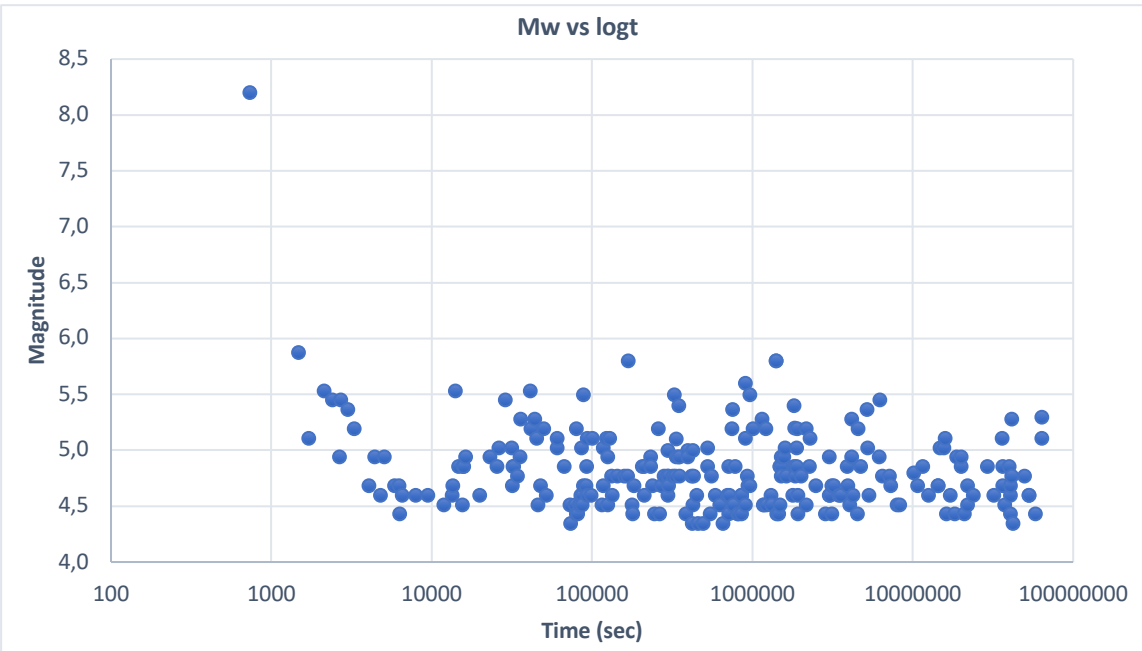

Figure 175. The magnitude-time pattern versus the logarithm of time of the mainshock M_w 8.2.

By the frequency-magnitude distribution for this earthquake, it is estimated a q_M= 1.31 with ci= 1.27-1.35.

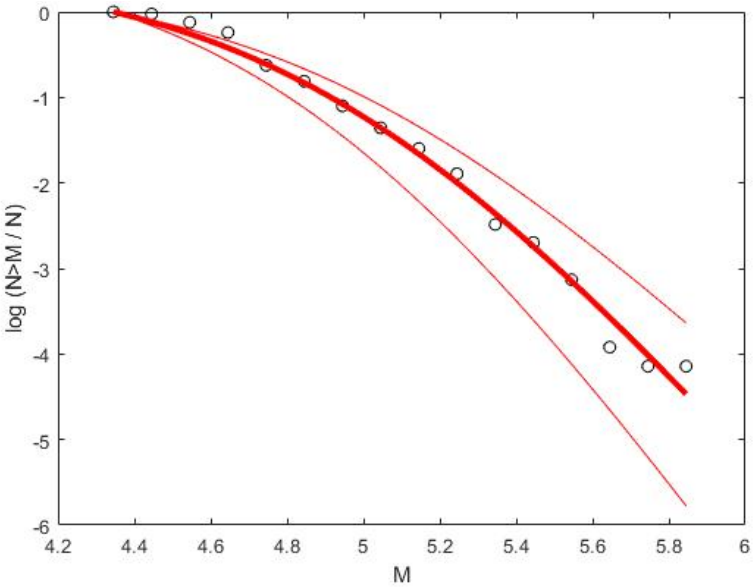

Figure 176. Frequency-magnitude distribution. The bold red line represents the model of equation (26) for qM= 1.31, while the other two lines present the corresponding 95% confidence intervals.

Figure 177 shows the typical Q-exponential pattern and Q-logarithmic function of the cumulative distribution function, P(>T) of the aftershocks interevent times and a q=1.74 is obtained.

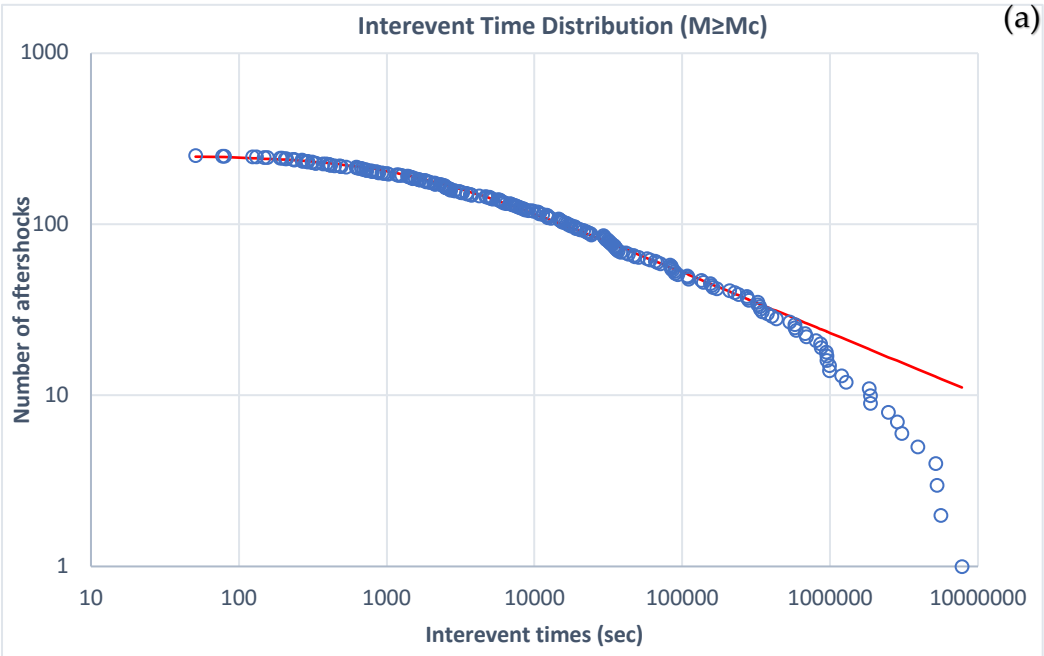

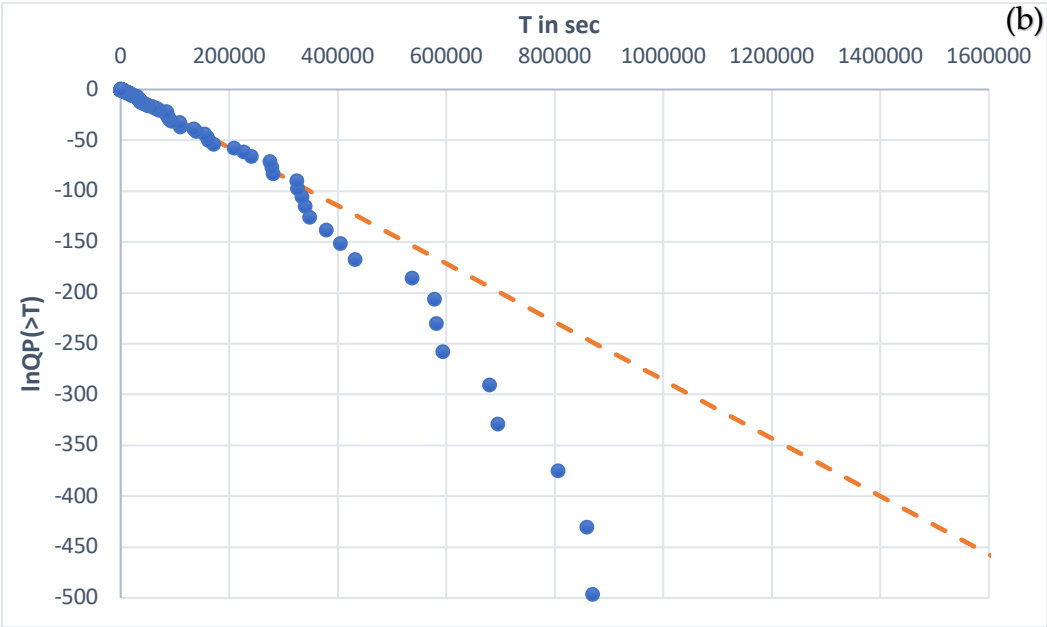

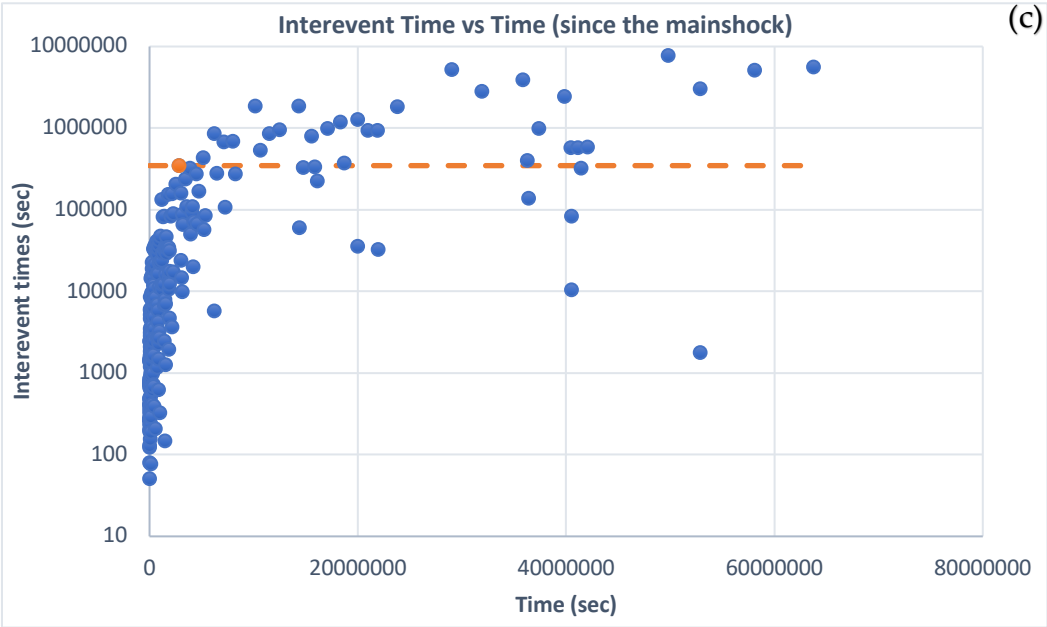

Figure 177. (a) The cumulative distribution function of the interevent times. The red line is the Q-exponential fitting with q = 1.74. **(b)** The Q-logarithmic function of the P(>T) as a function of the interevent times where the dashed line is the fitting with q=1.74. The deviation from the linearity suggests Tc values close to 400,000 s. **(c)** The evolution of interevent time T as a function of time t since the main event. The Tc value is indicated by the dashed line.

4.2.36 The 2017 Alabja Earthquake M_w=7.3 (Iraq)

The figure below shows Guttenberg-Richter distribution. The estimated parameters are Mc=4.7, b=1.33 and a=8.22.

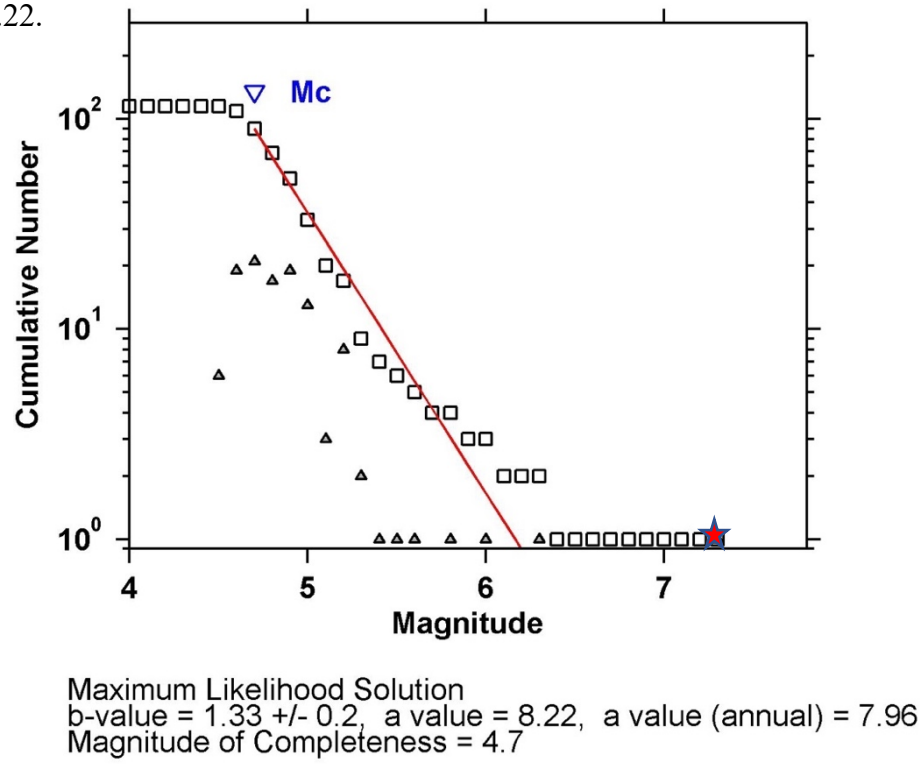

Figure 178. The Guttenberg-Richter distribution using maximum likelihood method with the best combination of maximum curvature M_c 95% and M_c 90% probability. The red star shows the magnitude of the mainshock M_w 7.3.

Next figure (179a) presents the model proposed by the AIC with p=1, c=0.32, and k= 10 while (179b) presents the model with the lowest RMS and p1= 1.05, p2=2.22, c1= 0.33, c2=5, k1=10 and k2=29.2.

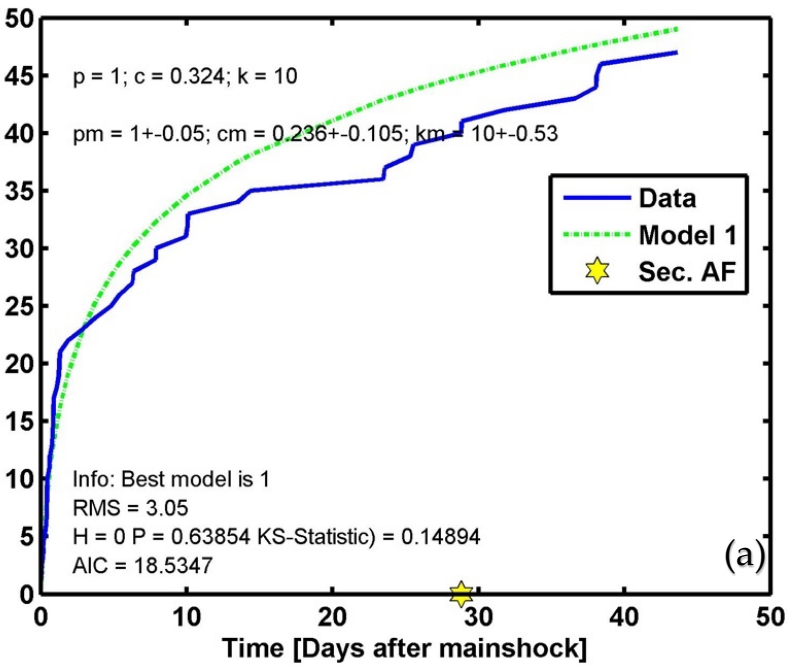

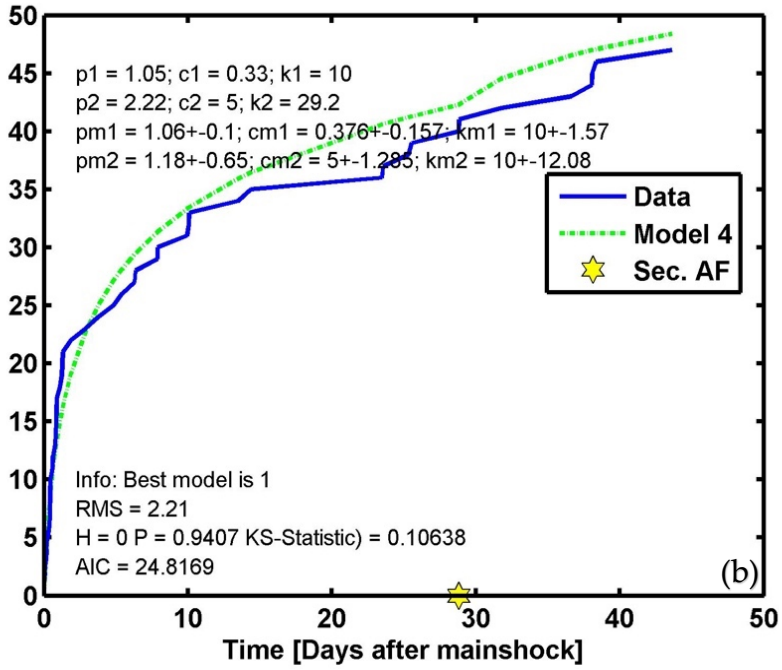

Figure 179. (a) The best model (1) of the estimated curve of the modified Omori formula (dashed line) applied to the aftershock data and the observed cumulative number of aftershocks (solid line) based on the AIC. **(b)** The model 4 of the estimated curve of the modified Omori formula (dashed line) applied to the aftershock data and the observed cumulative number of aftershocks (solid line), with the lowest RMS= 2.21.

Here is the magnitude-time form of the aftershock sequence.

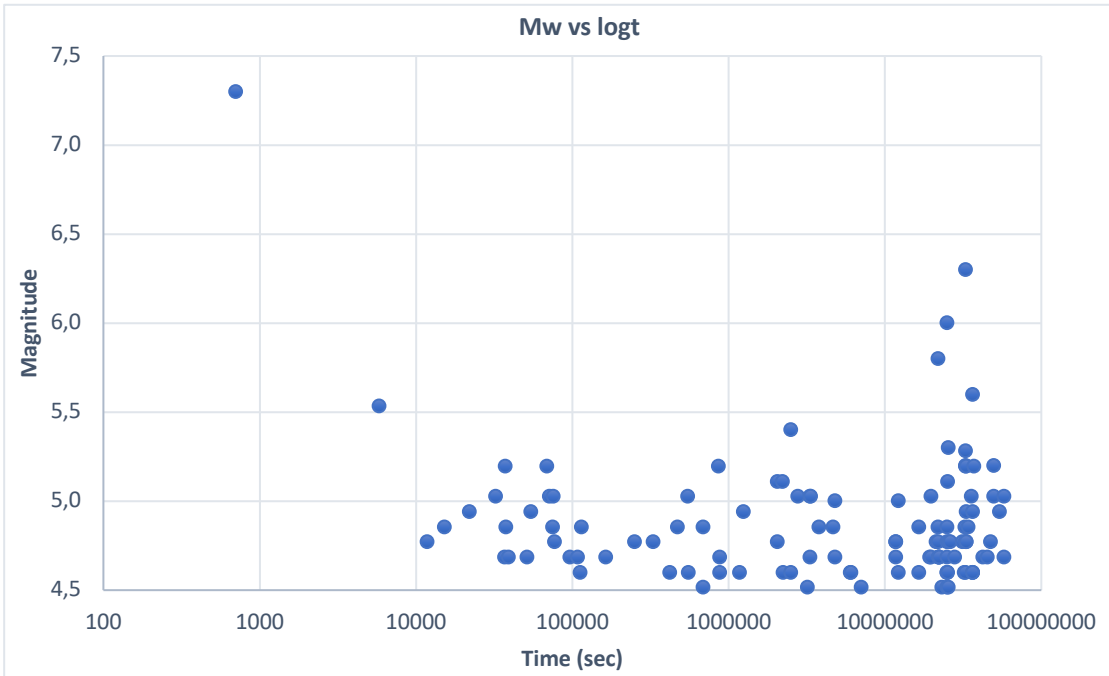

Figure 180. The magnitude-time pattern versus the logarithm of time of the mainshock M_w 7.3.

By the frequency-magnitude distribution for this earthquake, it is estimated a q_M= 1.44 with ci= 1.41-1.48.

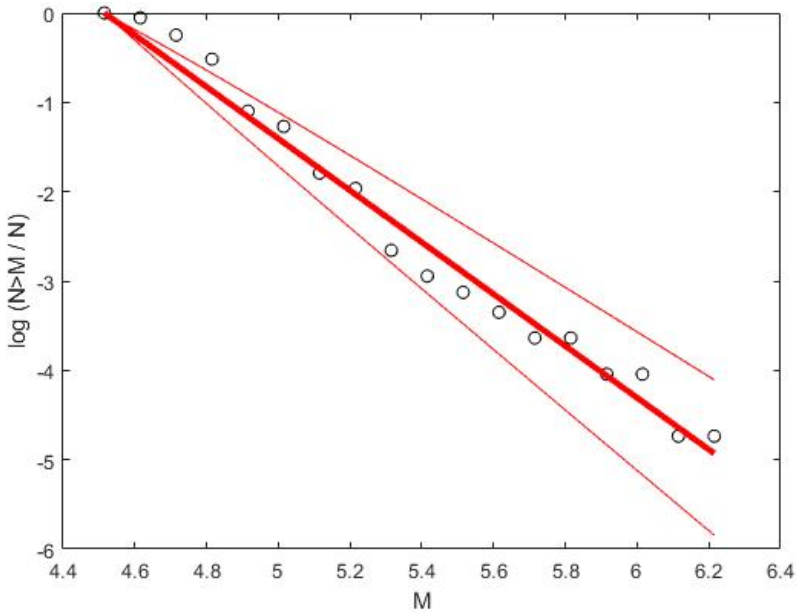

Figure 181. Frequency-magnitude distribution. The bold red line represents the model of equation (26) for qM= 1.44, while the other two lines present the corresponding 95% confidence intervals.

Figure 182 shows the typical Q-exponential pattern and Q-logarithmic function of the cumulative distribution function, P(>T) of the aftershocks interevent times and a q=1.80 is obtained.

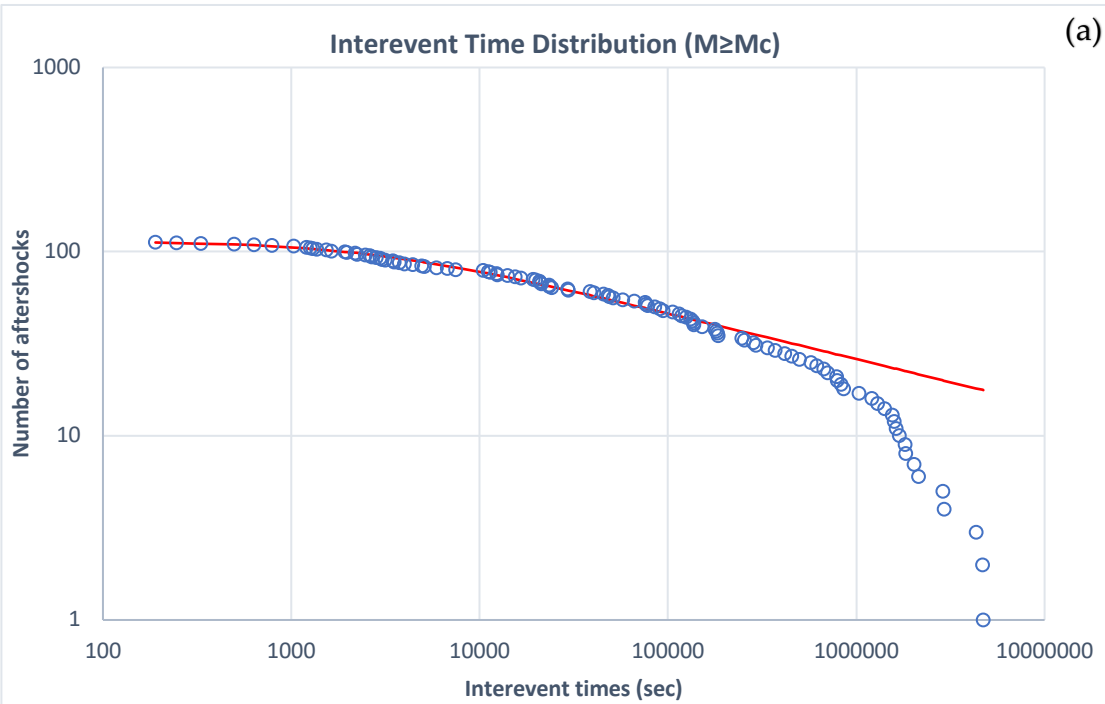

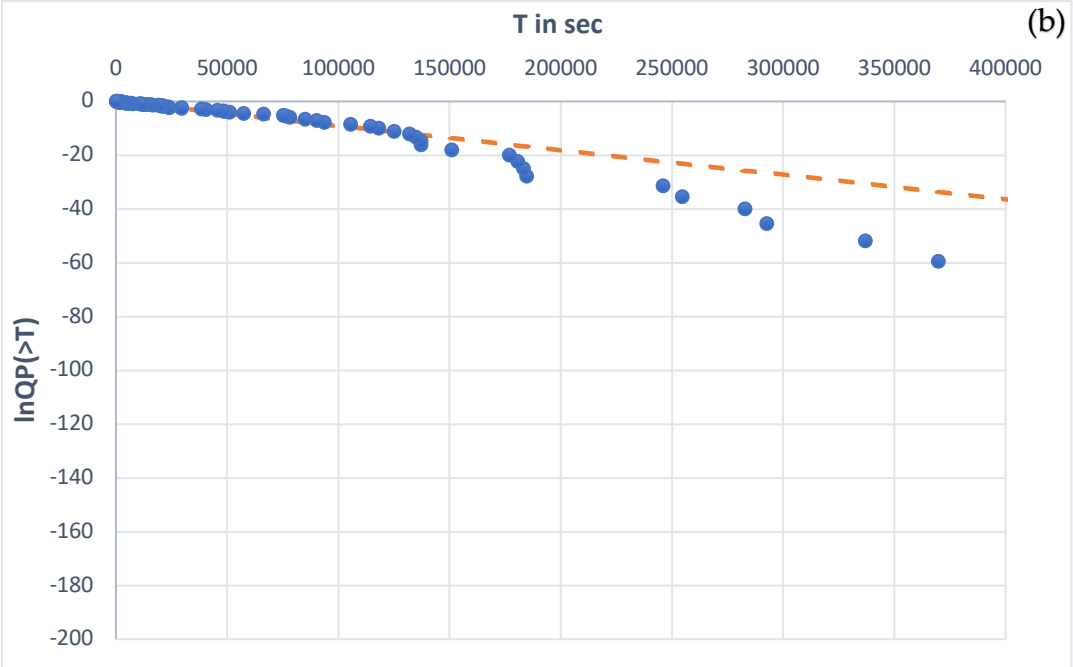

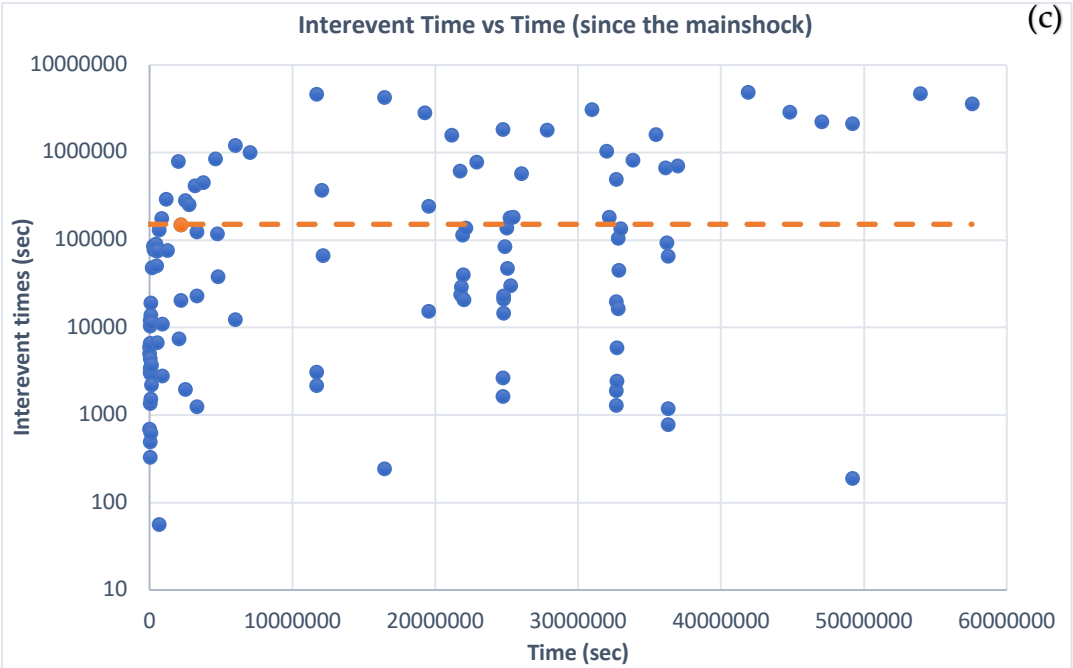

Figure 182. (a) The cumulative distribution function of the interevent times. The red line is the Q-exponential fitting with q = 1.80. **(b)** The Q-logarithmic function of the P(>T) as a function of the interevent times where the dashed line is the fitting with q=1.80. The deviation from the linearity suggests Tc values close to 150,000 s. **(c)** The evolution of interevent time T as a function of time t since the main event. The Tc value is indicated by the dashed line.

4.2.37 The 2018 Chiniak Earthquake M_w=7.9 (Alaska)

The figure below shows Guttenberg-Richter distribution. The estimated parameters are Mc=4.5, b=1.34 and a=7.92.

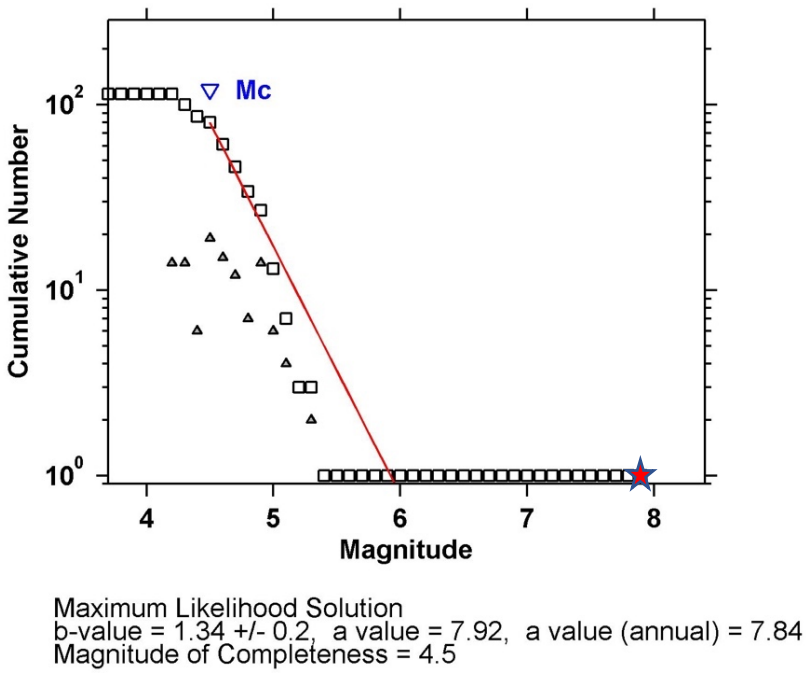

Figure 183. The Guttenberg-Richter distribution using maximum likelihood method with the best combination of maximum curvature M_c 95% and M_c 90% probability. The red star shows the magnitude of the mainshock M_w 7.9.

Next figure presents the model proposed by the AIC with p= 1.02, c= 0.02 and k= 13.

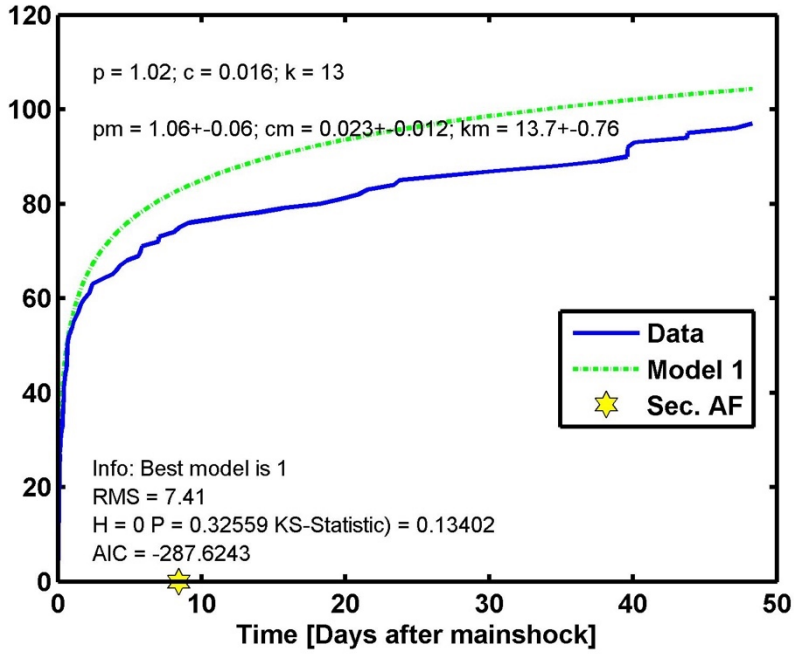

Figure 184. The best model (1) of the estimated curve of the modified Omori formula (dashed line) applied to the aftershock data and the observed cumulative number of aftershocks (solid line) based on the AIC with RMS= 7.41.

Here is the magnitude-time form of the aftershock sequence.

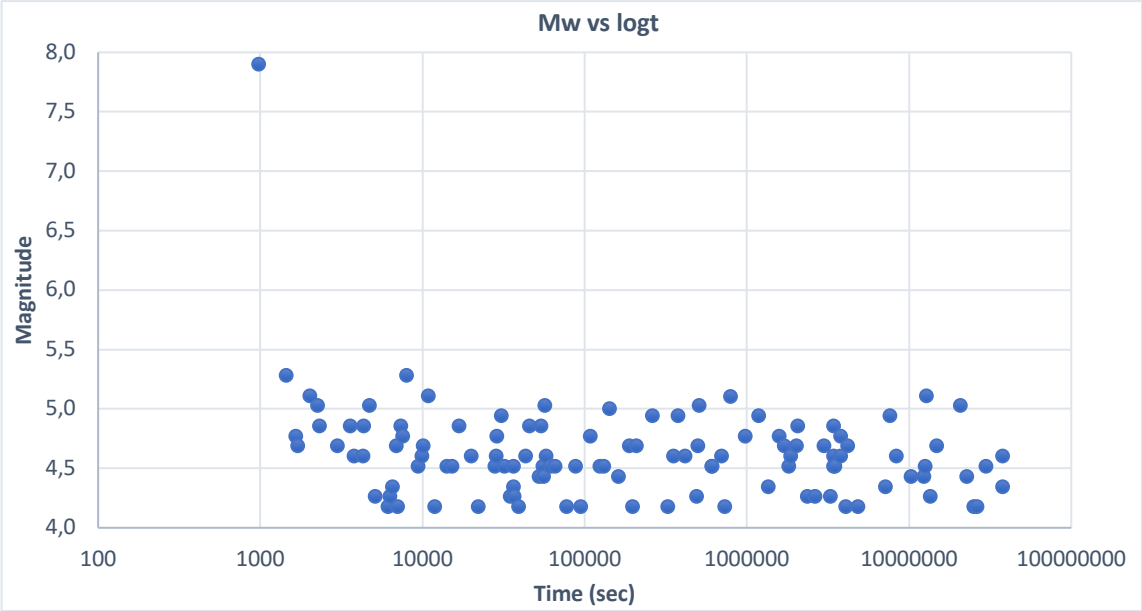

Figure 185. The magnitude-time pattern versus the logarithm of time of the mainshock M_w 7.9.

By the frequency-magnitude distribution for this earthquake, it is estimated a q_M= 1.03 with ci= 0.88-1.18.

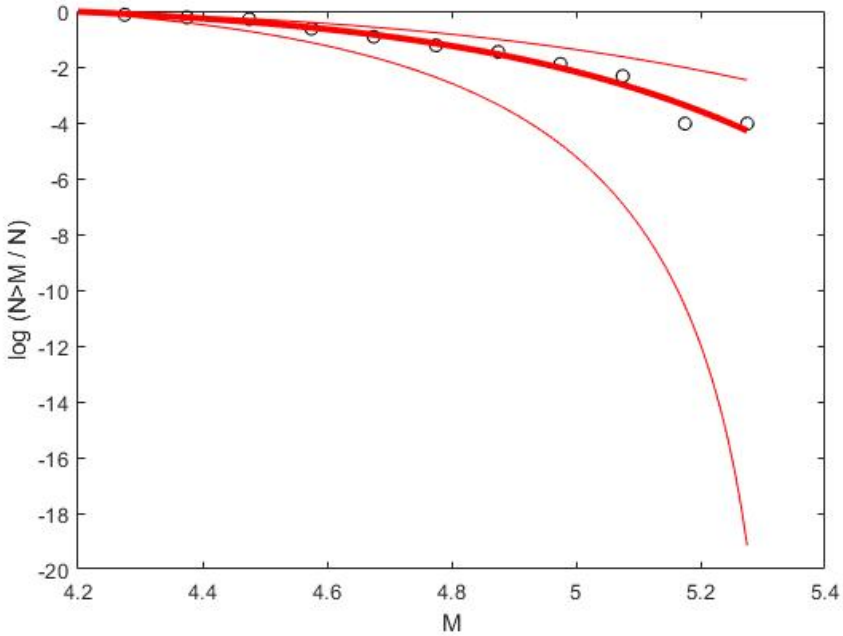

Figure 186. Frequency-magnitude distribution. The bold red line represents the model of equation (26) for qM= 1.03, while the other two lines present the corresponding 95% confidence intervals.

Figure 187 shows the typical Q-exponential pattern and Q-logarithmic function of the cumulative distribution function, P(>T) of the aftershocks interevent times and a q=1.80 is obtained.

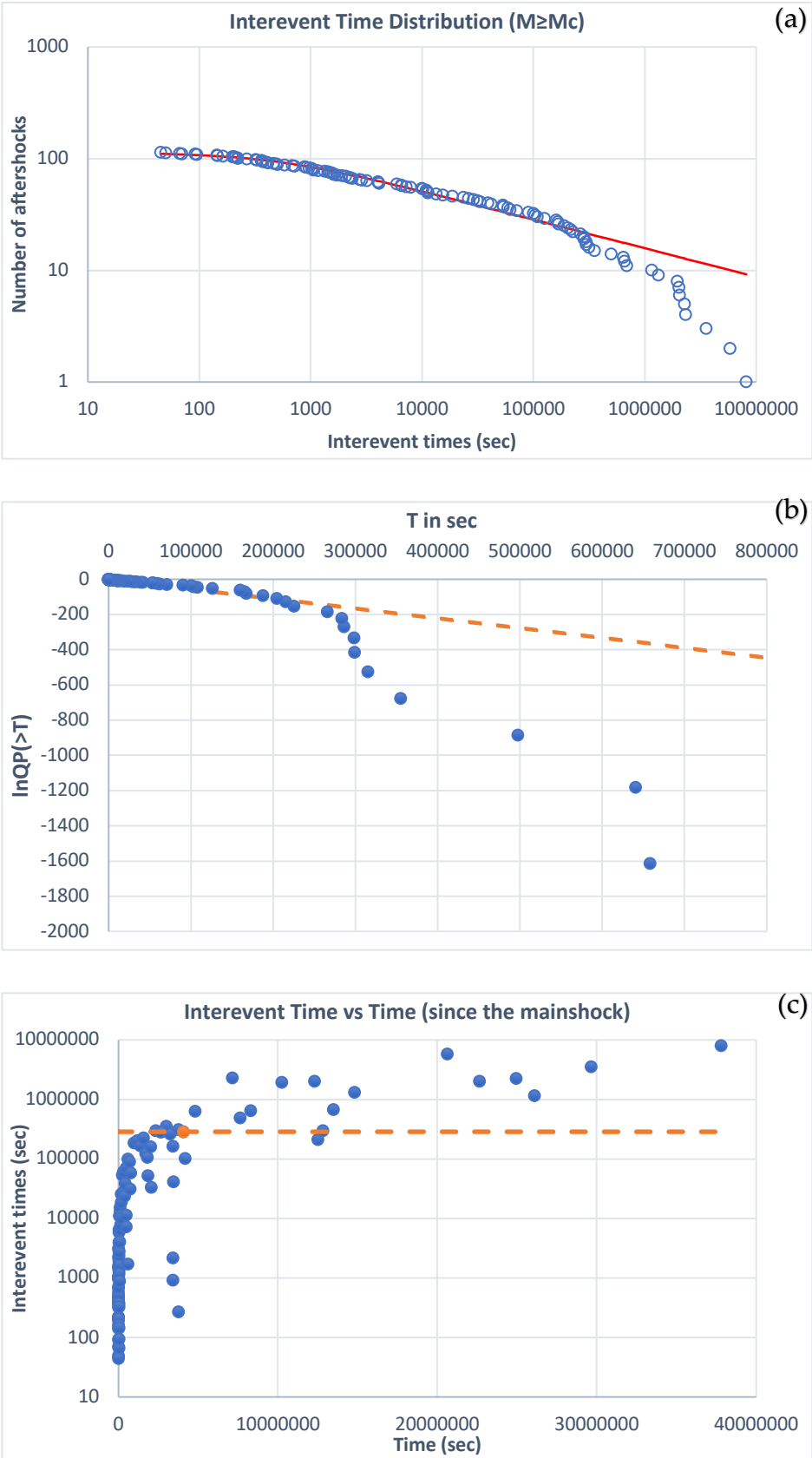

Figure 187. (a) The cumulative distribution function of the interevent times. The red line is the Q-exponential fitting with q = 1.80. **(b)** The Q-logarithmic function of the P(>T) as a function of the interevent times where the dashed line is the fitting with q=1.80. The deviation from the linearity suggests Tc values close to 300,000 s. **(c)** The evolution of interevent time T as a function of time t since the main event. The Tc value is indicated by the dashed line.

4.2.38 The 2018 Tadine Earthquake M_w=7.5 (New Caledonia)

The figure below shows Guttenberg-Richter distribution. The estimated parameters are Mc=4.8, b=1.07 and a= 7.32.

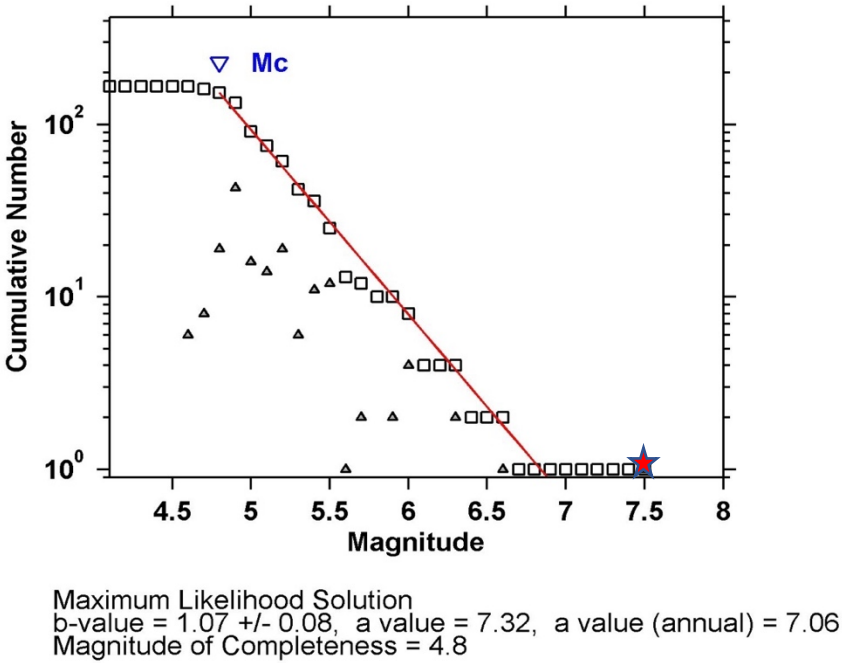

Figure 188. The Guttenberg-Richter distribution using maximum likelihood method with the best combination of maximum curvature M_c 95% and M_c 90% probability. The red star shows the magnitude of the mainshock M_w 7.5.

Next figure presents the model proposed by the AIC with p1= 2.7, p2=1.06, c=0.45, c2=5, k1=36.8 and k2= 10.

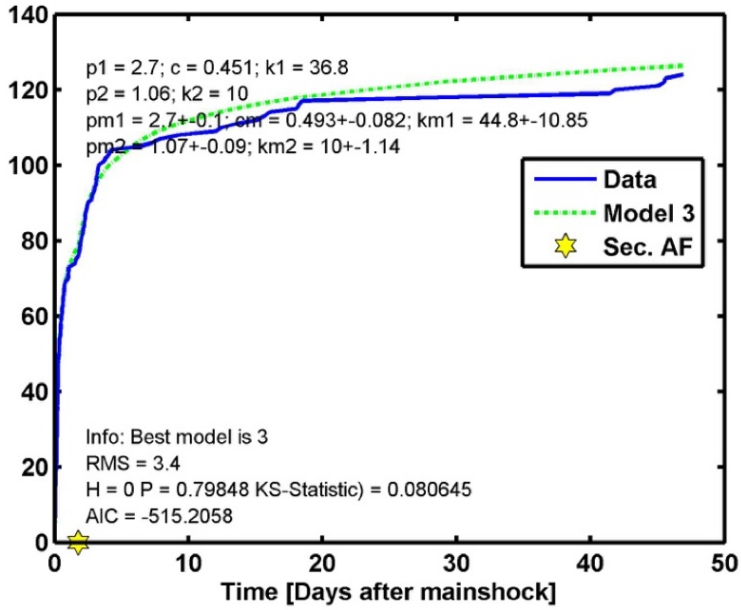

Figure 189. The best model (3) of the estimated curve of the modified Omori formula (dashed line) applied to the aftershock data and the observed cumulative number of aftershocks (solid line) based on the AIC with RMS= 3.4.

Here is the magnitude-time form of the aftershock sequence.

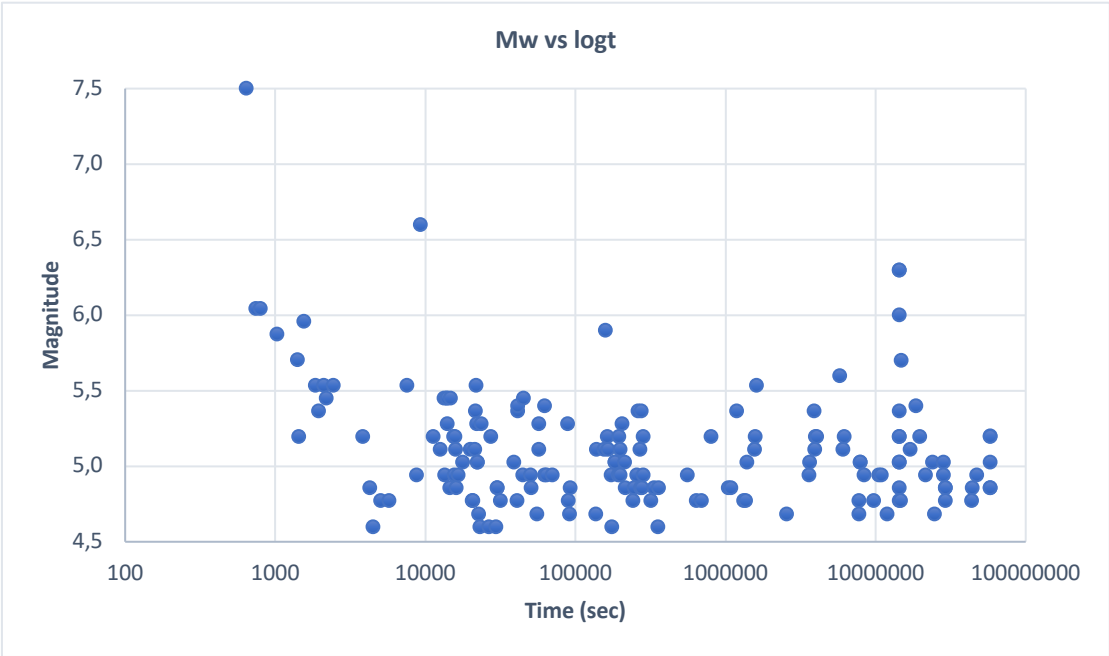

Figure 190. The magnitude-time pattern versus the logarithm of time of the mainshock M_w 7.5.

By the frequency-magnitude distribution for this earthquake, it is estimated a q_M= 1.52 with ci= 1.49-1.56.

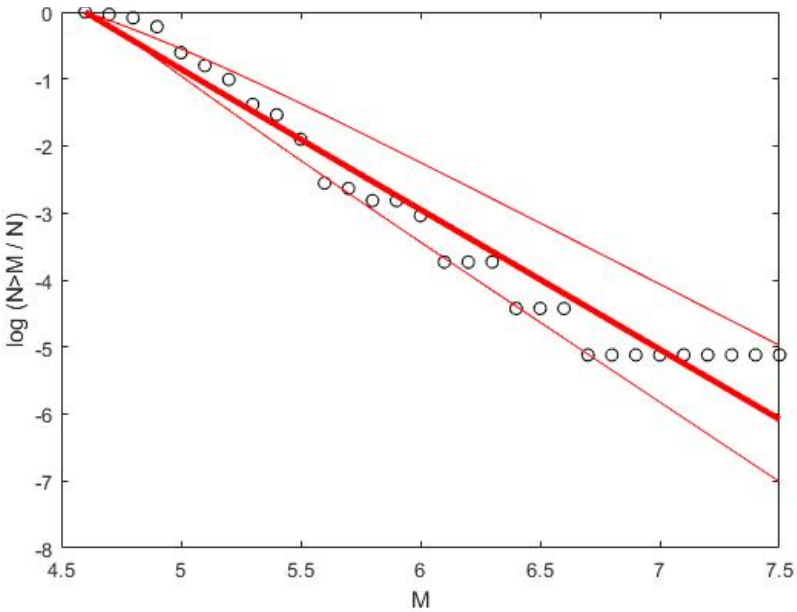

Figure 191. Frequency-magnitude distribution. The bold red line represents the model of equation (26) for qM= 1.52, while the other two lines present the corresponding 95% confidence intervals.

Figure 192 shows the typical Q-exponential pattern and Q-logarithmic function of the cumulative distribution function, P(>T) of the aftershocks interevent times and a q=1.78 is obtained.

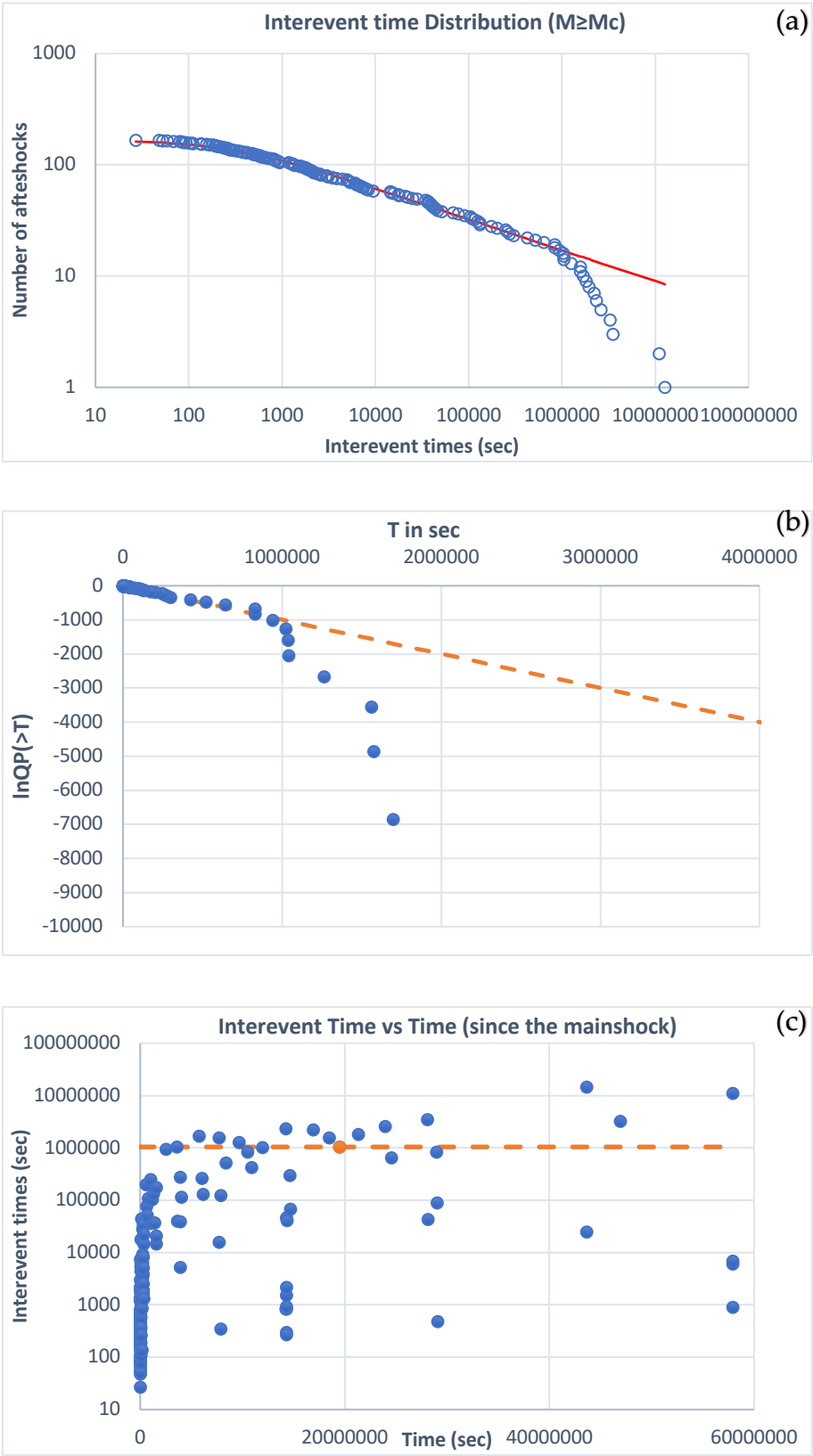

Figure 192. (a) The cumulative distribution function of the interevent times. The red line is the Q-exponential fitting with q = 1.78. **(b)** The Q-logarithmic function of the P(>T) as a function of the interevent times where the dashed line is the fitting with q=1.78. The deviation from the linearity suggests Tc values close to 1,000,000 s. **(c)** The evolution of interevent time T as a function of time t since the main event. The Tc value is indicated by the dashed line.

4.2.39 The 2018 Uts'-Kamchatsk Staryy Earthquake M_w=7.3 (Russia)

The figure below shows Guttenberg-Richter distribution. The estimated parameters are Mc=4.6, b=1.14 and a=7.31.

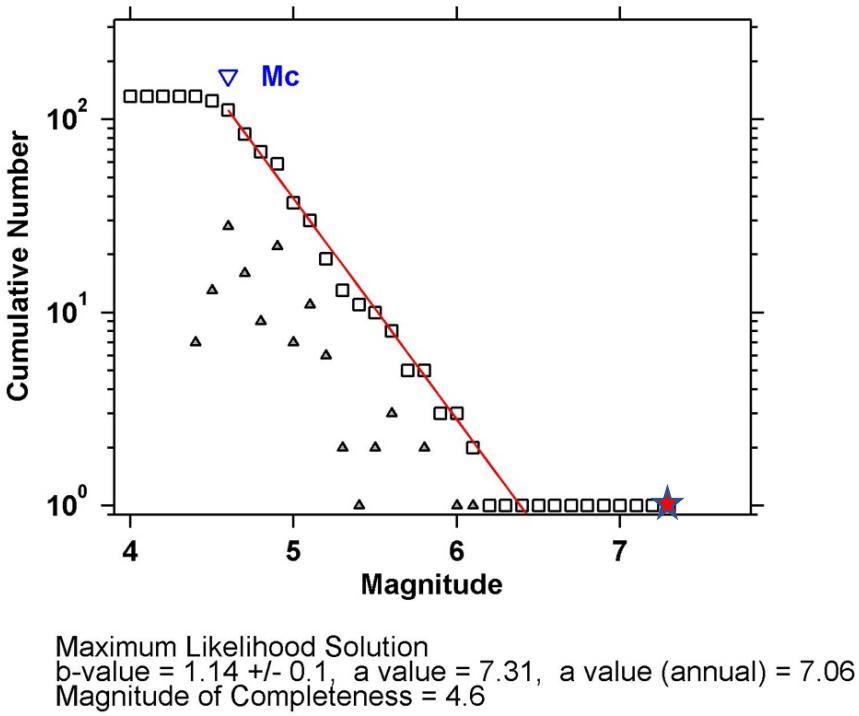

Figure 193. The Guttenberg-Richter distribution using maximum likelihood method with the best combination of maximum curvature M_c 95% and M_c 90% probability. The red star shows the magnitude of the mainshock M_w 7.3.

Next figure (194a) presents the model proposed by the AIC with p= 0.95, c= 0.01 and k= 12.8 while (194b) presents the model with the lowest RMS and p1= 0.97, p2=2.7, c1=0.01, c2=0.96, k1=12.1 and k2= 10.

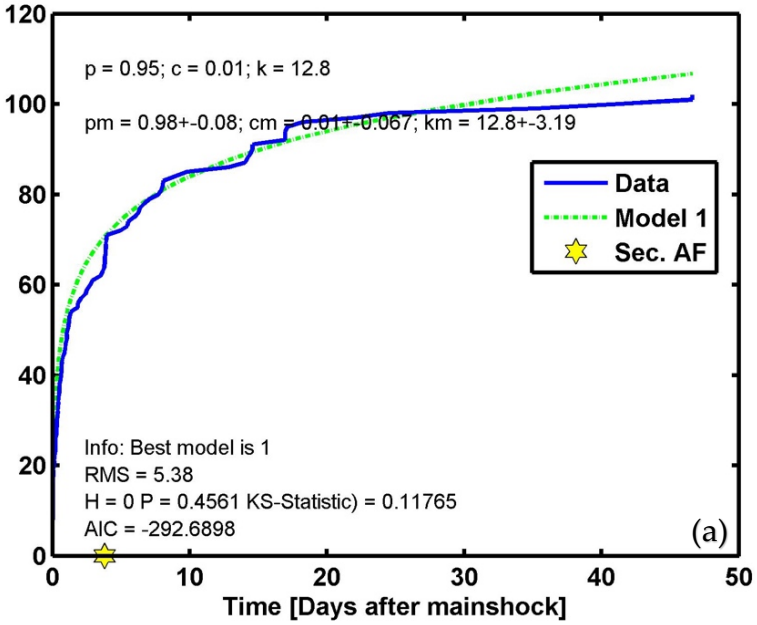

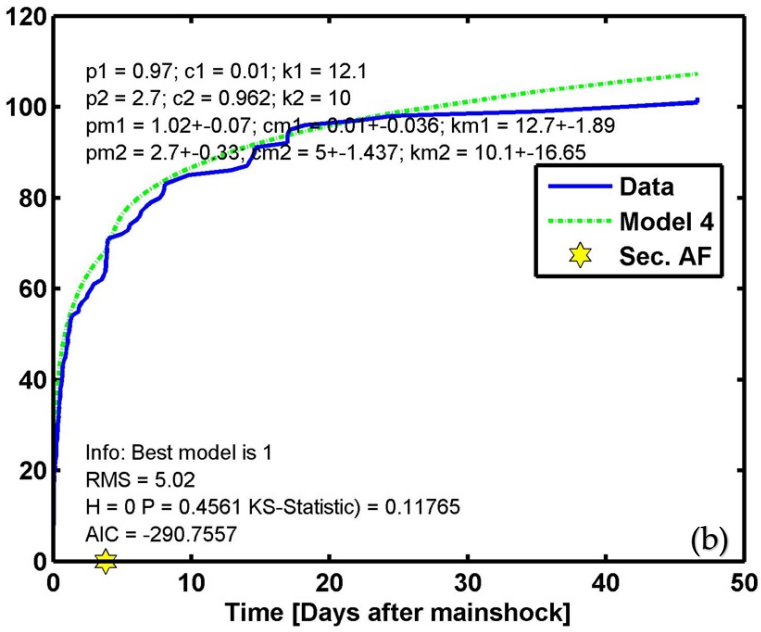

Figure 194. (a) The best model (1) of the estimated curve of the modified Omori formula (dashed line) applied to the aftershock data and the observed cumulative number of aftershocks (solid line) based on the AIC. **(b)** The model 4 of the estimated curve of the modified Omori formula (dashed line) applied to the aftershock data and the observed cumulative number of aftershocks (solid line), with the lowest RMS= 5.02.

Here is the magnitude-time form of the aftershock sequence.

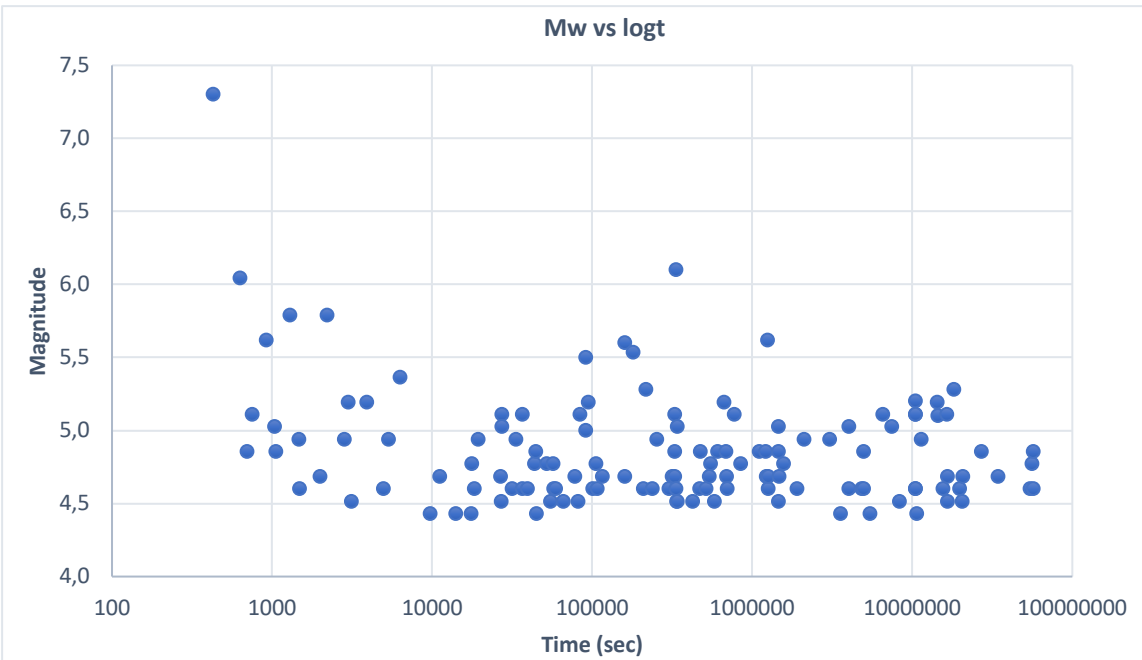

Figure 195. The magnitude-time pattern versus the logarithm of time of the mainshock M_w 7.3.

By the frequency-magnitude distribution for this earthquake, it is estimated a q_M= 1.42 with ci= 1.38-1.45.

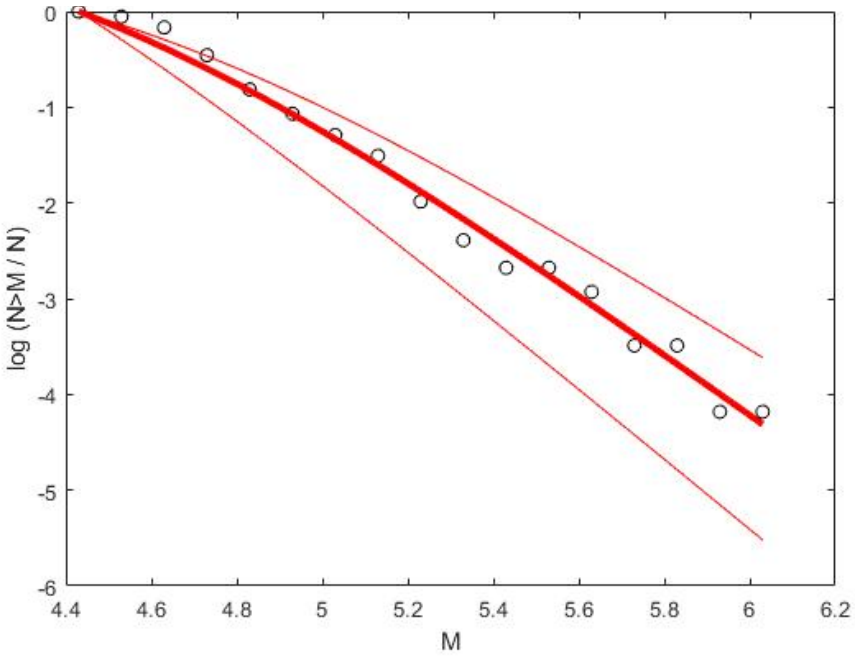

Figure 196. Frequency-magnitude distribution. The bold red line represents the model of equation (26) for qM= 1.42, while the other two lines present the corresponding 95% confidence intervals.

Figure 197 shows the typical Q-exponential pattern and Q-logarithmic function of the cumulative distribution function, P(>T) of the aftershocks interevent times and a q=1.78 is obtained.

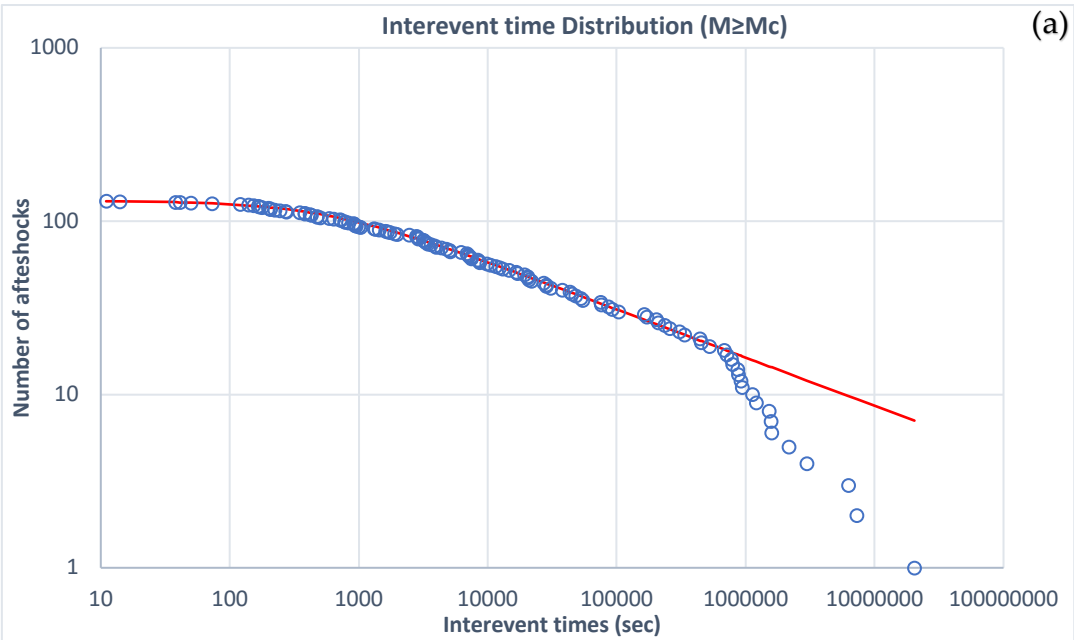

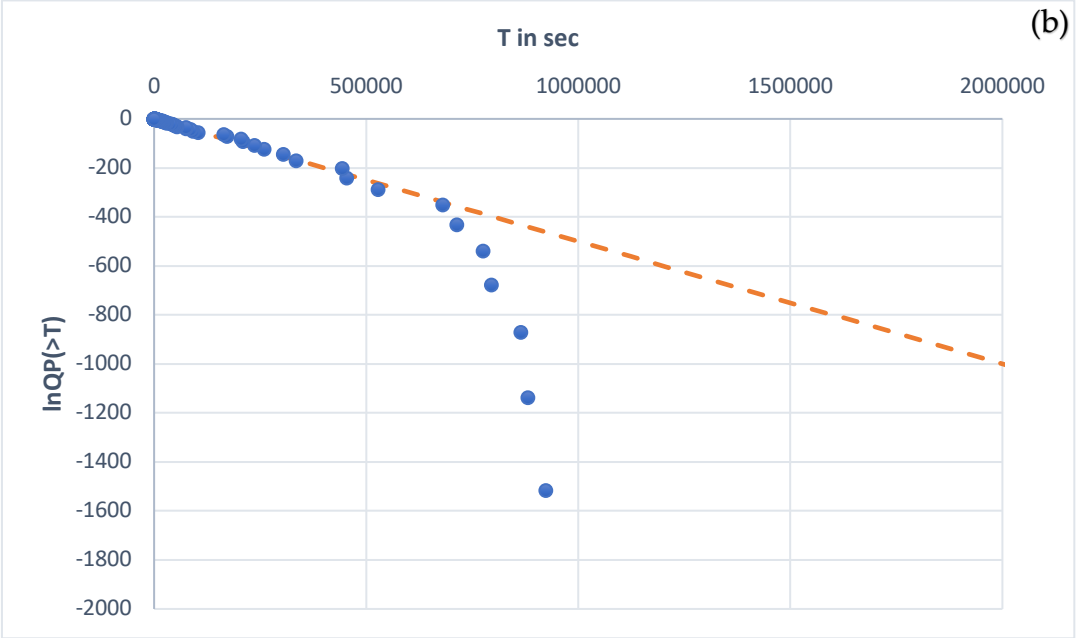

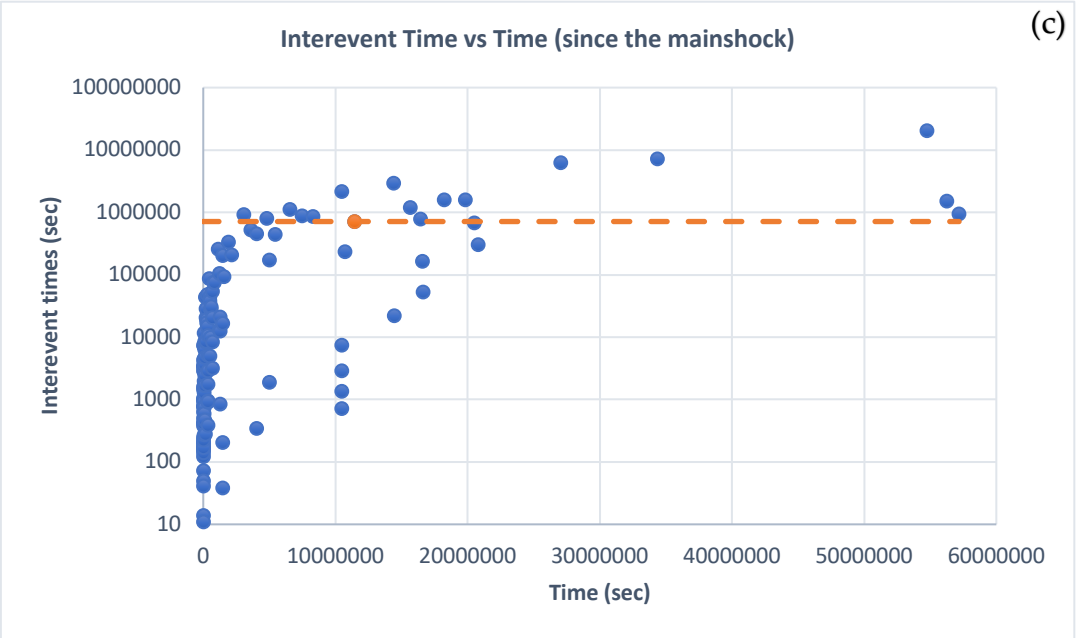

Figure 197. (a) The cumulative distribution function of the interevent times. The red line is the Q-exponential fitting with q = 1.78. **(b)** The Q-logarithmic function of the P(>T) as a function of the interevent times where the dashed line is the fitting with q=1.78. The deviation from the linearity suggests Tc values close to 750,000 s. **(c)** The evolution of interevent time T as a function of time t since the main event. The Tc value is indicated by the dashed line.

4.2.40 The 2019 Kokopo Earthquake M_w=7.6 (Papua New Guinea)

The figure below shows Guttenberg-Richter distribution. The estimated parameters are Mc=4.9, b=1.78 and a=10.6.

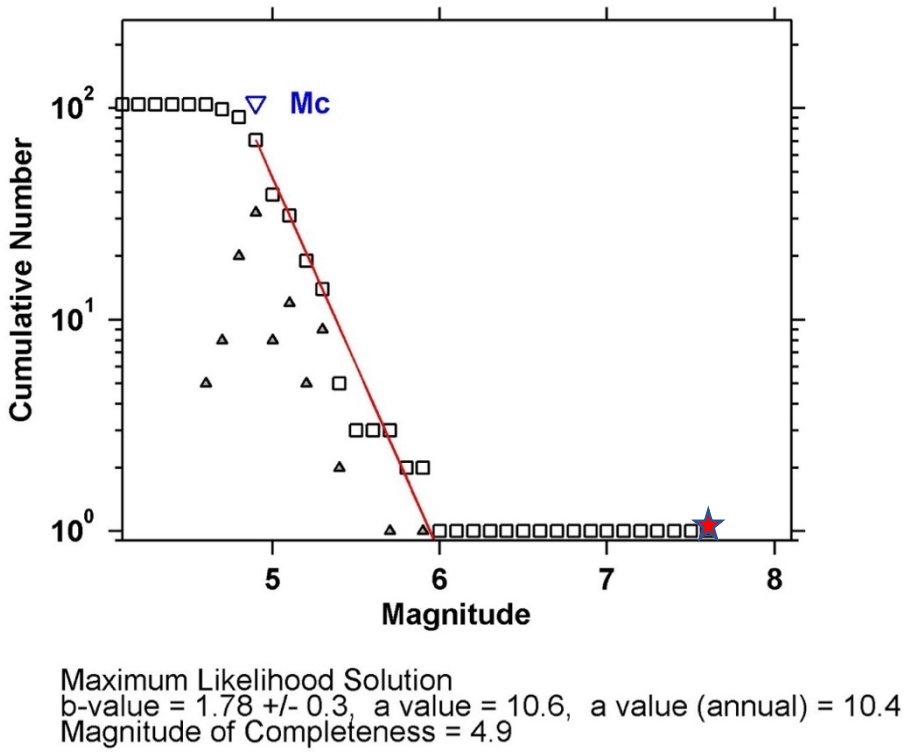

Figure 198. The Guttenberg-Richter distribution using maximum likelihood method with the best combination of maximum curvature M_c 95% and M_c 90% probability. The red star shows the magnitude of the mainshock M_w 7.6.

Next figure (199a) presents the model proposed by the AIC with p= 1.29, c= 0.06 and k= 10 while (199b) presents the model with the lowest RMS and p= 2.29, c=0.747, k1=39.6 and k2= 10.

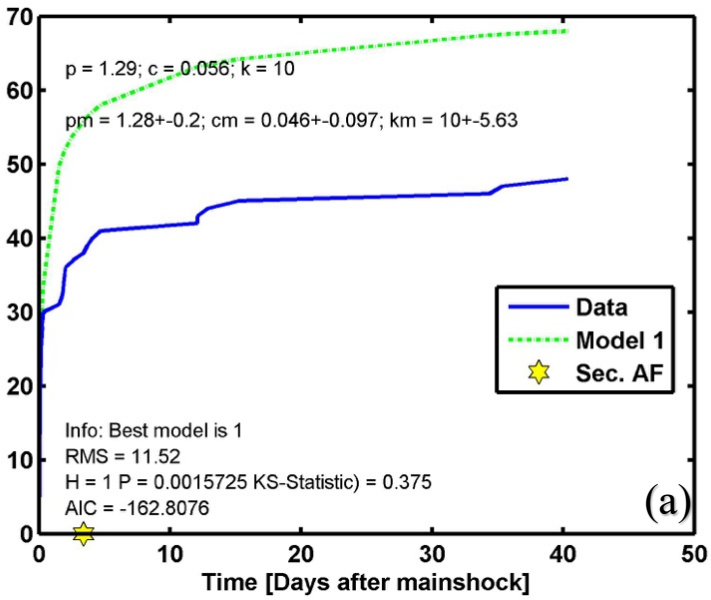

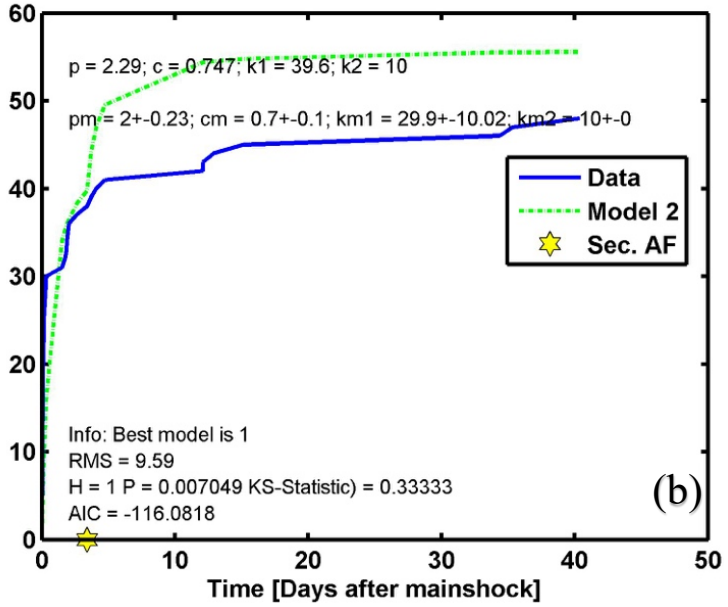

Figure 199. (a) The best model (1) of the estimated curve of the modified Omori formula (dashed line) applied to the aftershock data and the observed cumulative number of aftershocks (solid line) based on the AIC. **(b)** The model 2 of the estimated curve of the modified Omori formula (dashed line) applied to the aftershock data and the observed cumulative number of aftershocks (solid line), with the lowest RMS= 9.59.

Here is the magnitude-time form of the aftershock sequence.

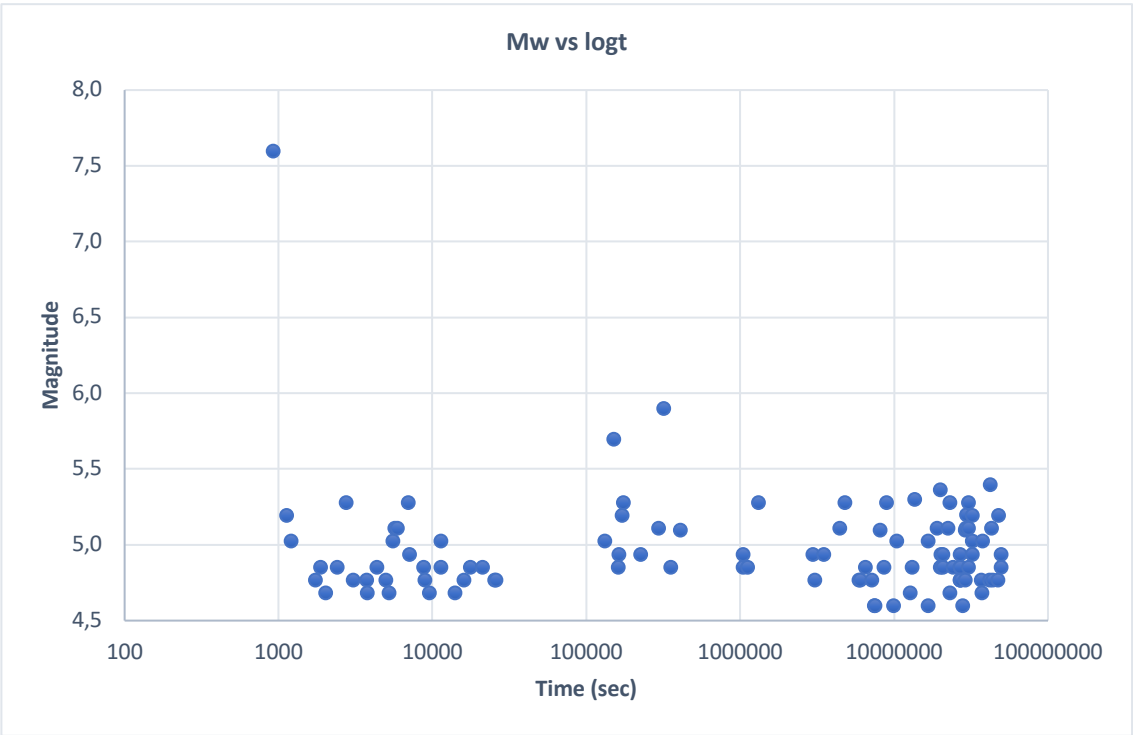

Figure 200. The magnitude-time pattern versus the logarithm of time of the mainshock M_w 7.6.

By the frequency-magnitude distribution for this earthquake, it is estimated a q_M= 1.30 with ci= 1.21-1.39.

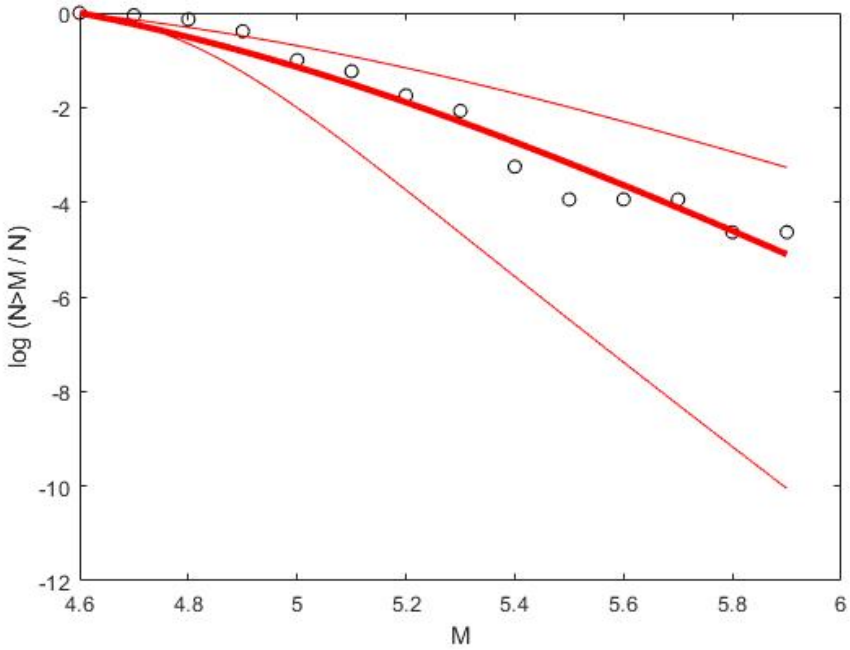

Figure 201. Frequency-magnitude distribution. The bold red line represents the model of equation (26) for qM= 1.30, while the other two lines present the corresponding 95% confidence intervals.

Figure 202 shows the typical Q-exponential pattern and Q-logarithmic function of the cumulative distribution function, P(>T) of the aftershocks interevent times and a q=1.87 is obtained.

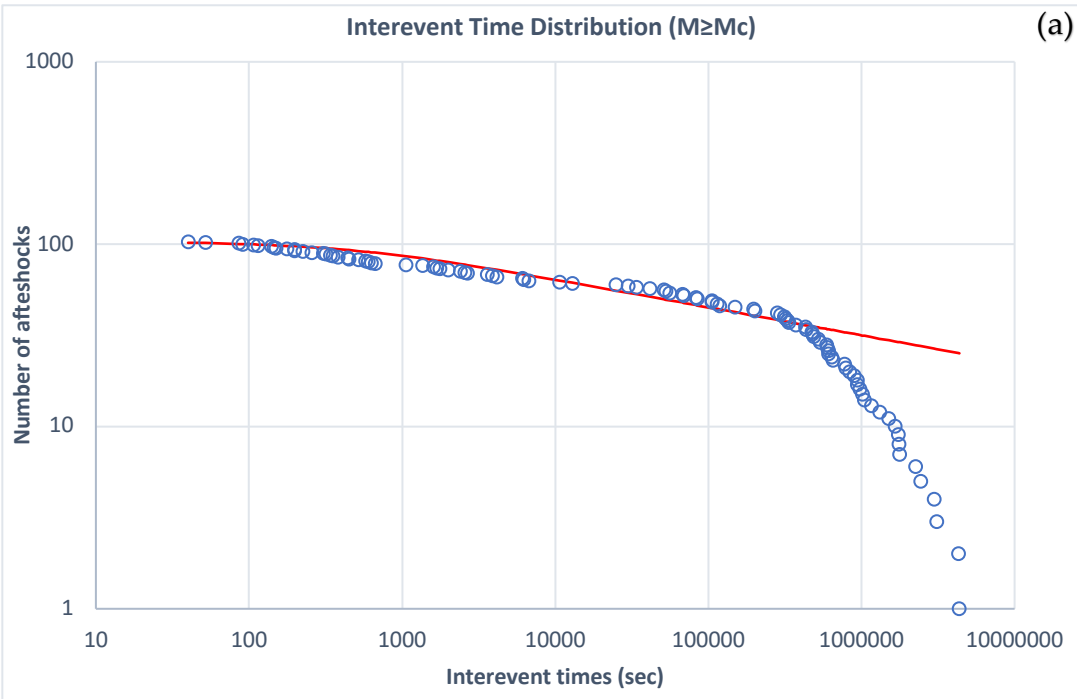

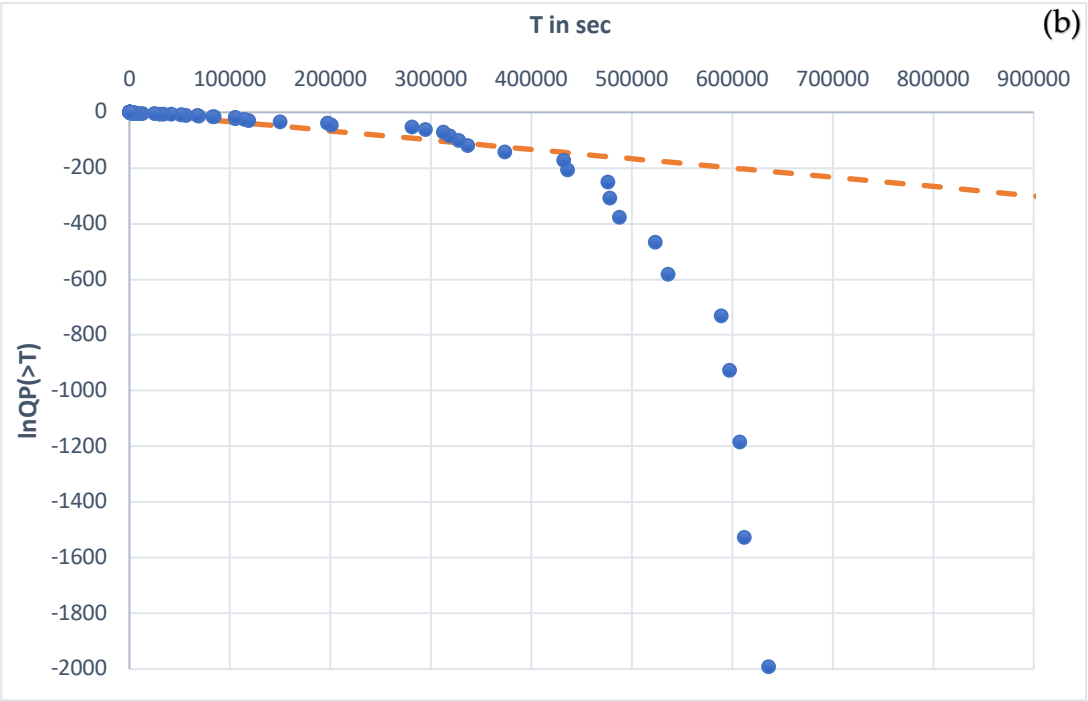

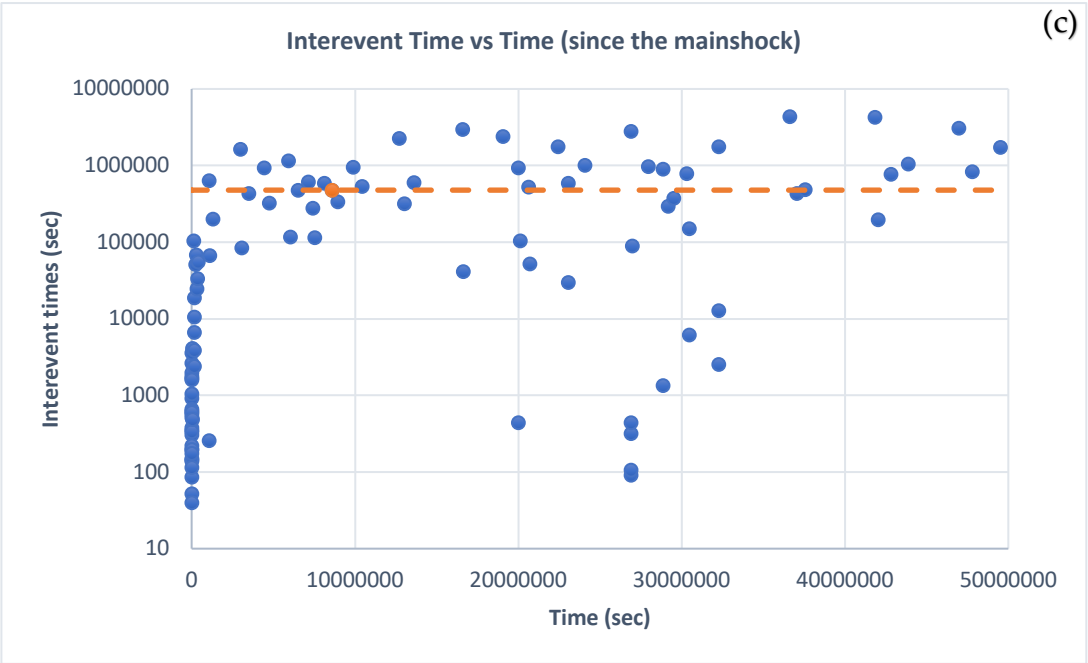

Figure 202. (a) The cumulative distribution function of the interevent times. The red line is the Q-exponential fitting with q = 1.87. **(b)** The Q-logarithmic function of the P(>T) as a function of the interevent times where the dashed line is the fitting with q=1.87. The deviation from the linearity suggests Tc values close to 500,000 s. **(c)** The evolution of interevent time T as a function of time t since the main event. The Tc value is indicated by the dashed line.

4.2.41 The 2019 Kermadec Islands Earthquake M_w=7.3 (New Zealand)

The figure below shows Guttenberg-Richter distribution. The estimated parameters are Mc=4.8, b=1.28 and a=8.44.

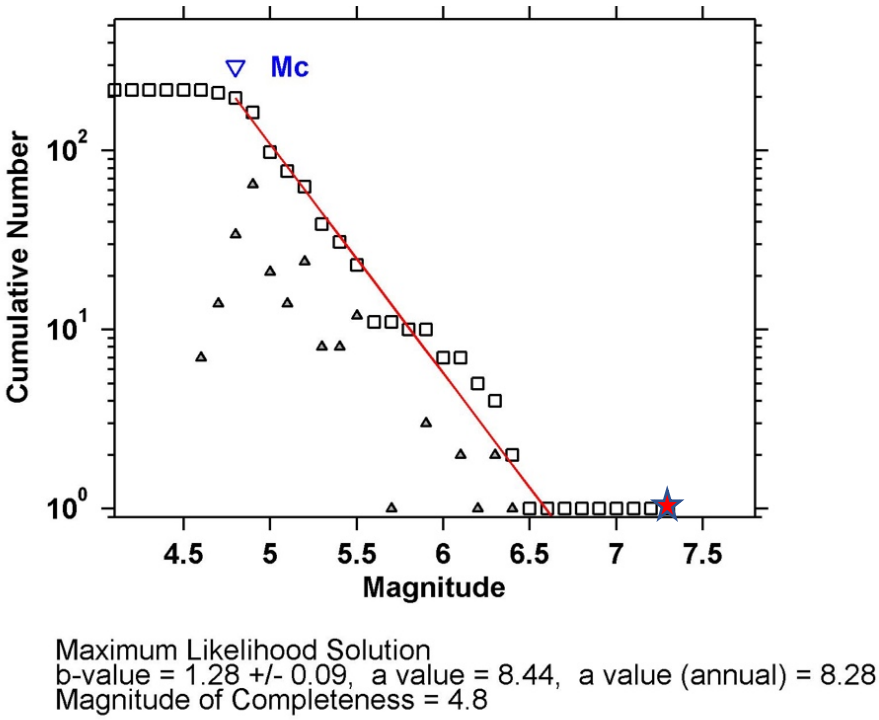

Figure 203. The Guttenberg-Richter distribution using maximum likelihood method with the best combination of maximum curvature M_c 95% and M_c 90% probability. The red star shows the magnitude of the mainshock M_w 7.3.

Next figure (204a) presents the model proposed by the AIC with p= 1.65, c= 3.67 and k= 228.3 while (204b) presents the model with the lowest RMS and p1= 1.47, p2=2.65, c1=2.62, c2=3.4, k1=117.8 and k2= 70.7.

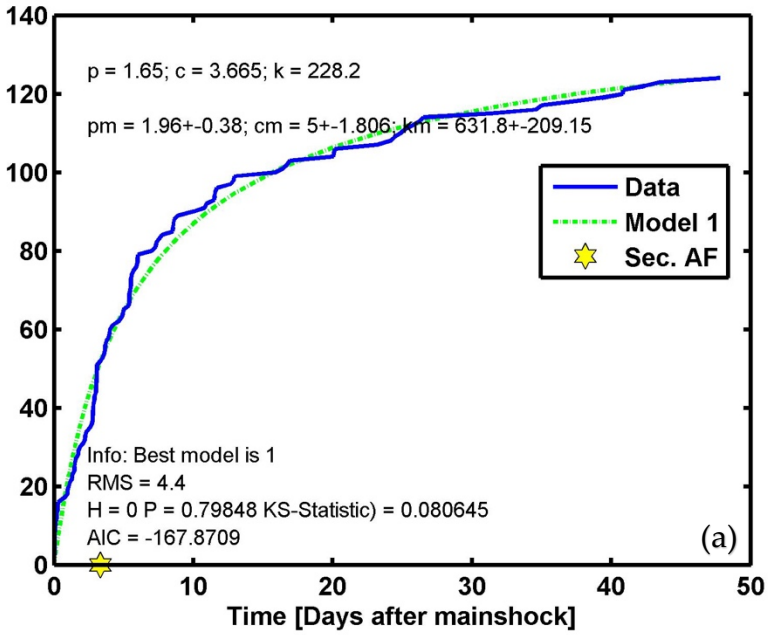

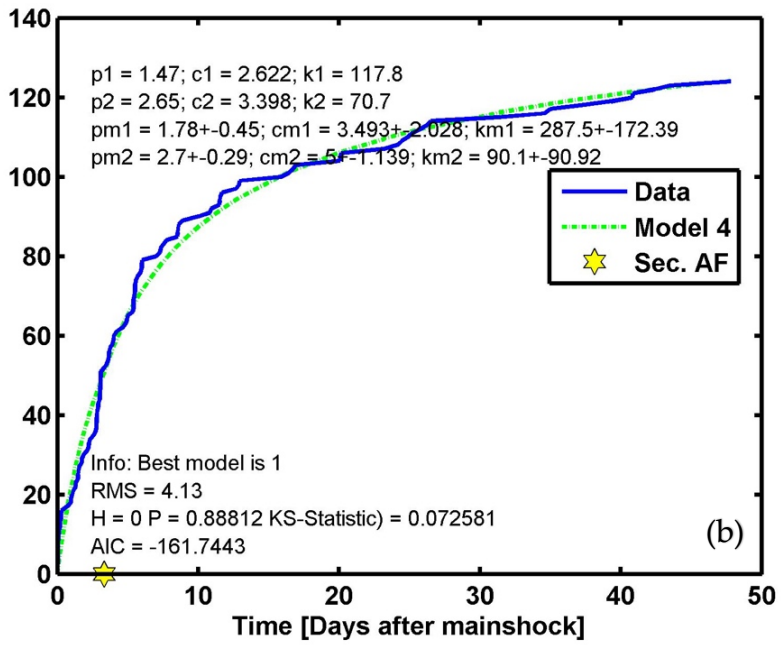

Figure 204. (a) The best model (1) of the estimated curve of the modified Omori formula (dashed line) applied to the aftershock data and the observed cumulative number of aftershocks (solid line) based on the AIC. **(b)** The model 4 of the estimated curve of the modified Omori formula (dashed line) applied to the aftershock data and the observed cumulative number of aftershocks (solid line), with the lowest RMS= 4.13.

Here is the magnitude-time form of the aftershock sequence.

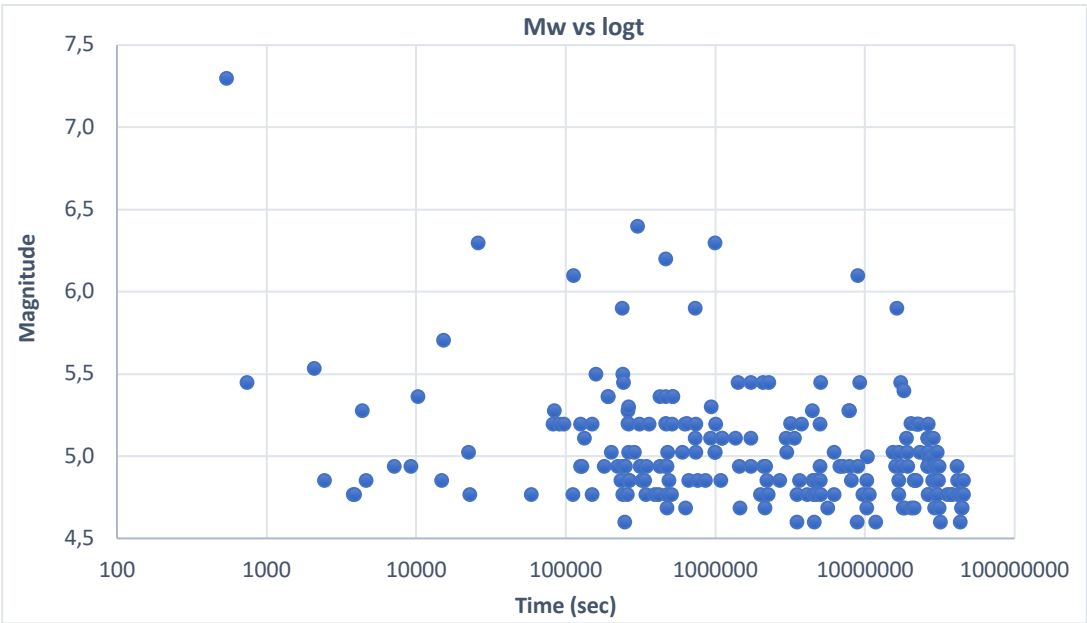

Figure 205. The magnitude-time pattern versus the logarithm of time of the mainshock M_w 7.3.

By the frequency-magnitude distribution for this earthquake, it is estimated a q_M= 1.43 with ci= 1.38-1.48.

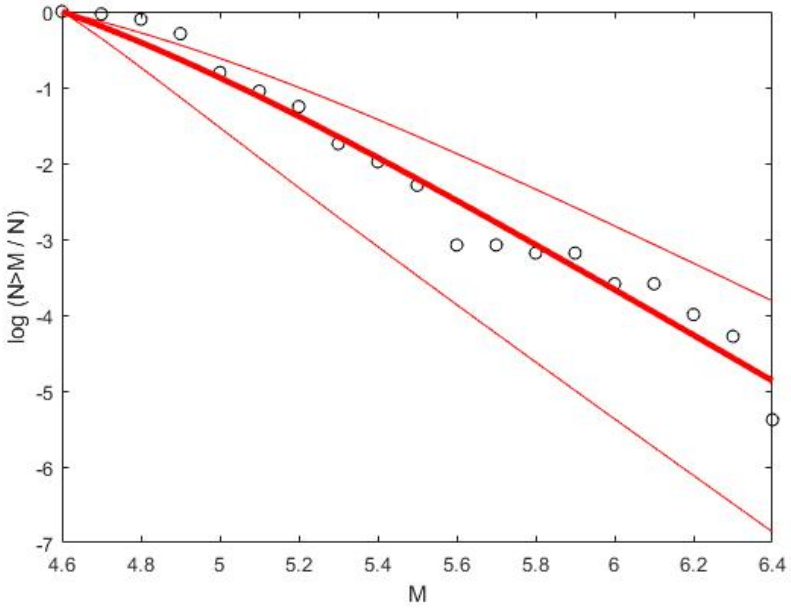

Figure 206. Frequency-magnitude distribution. The bold red line represents the model of equation (26) for qM= 1.43, while the other two lines present the corresponding 95% confidence intervals.

Figure 207 shows the typical Q-exponential pattern and Q-logarithmic function of the cumulative distribution function, P(>T) of the aftershocks interevent times and a q=1.75 is obtained.

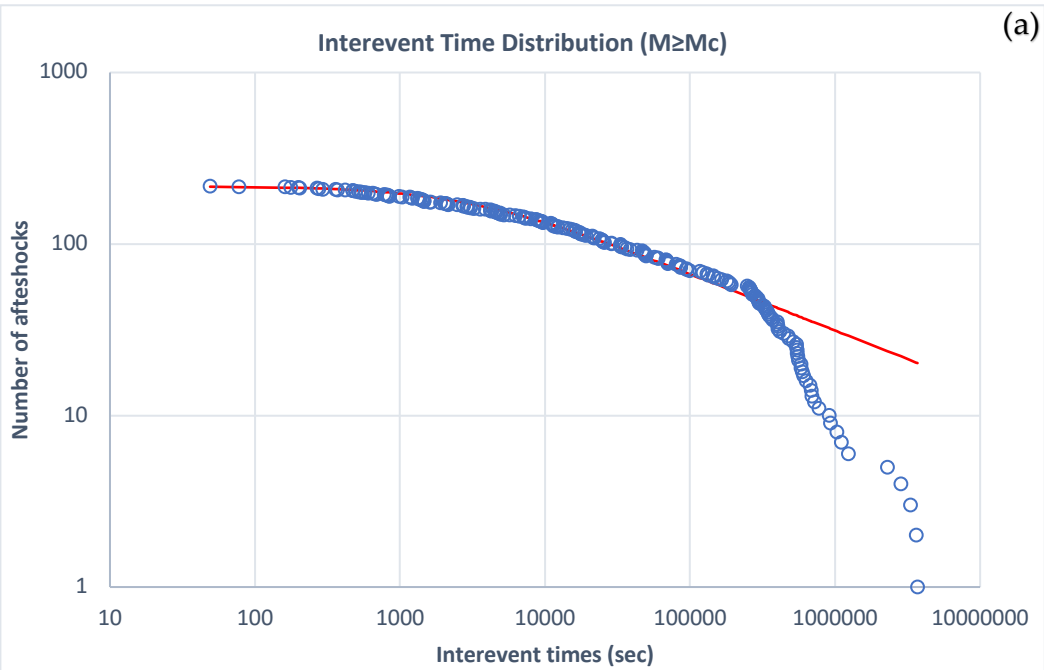

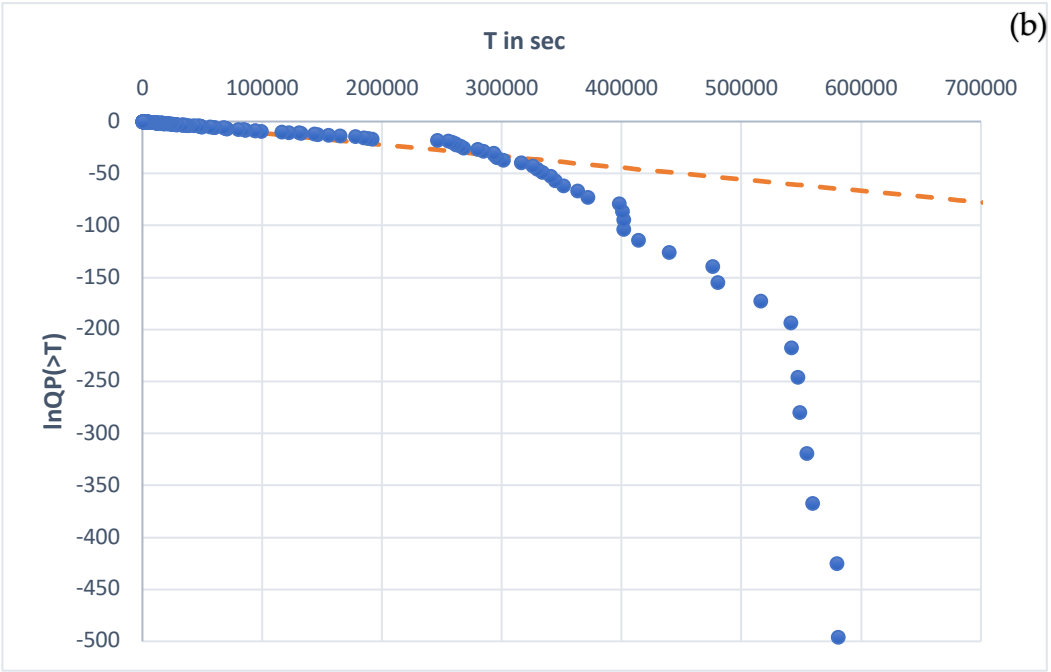

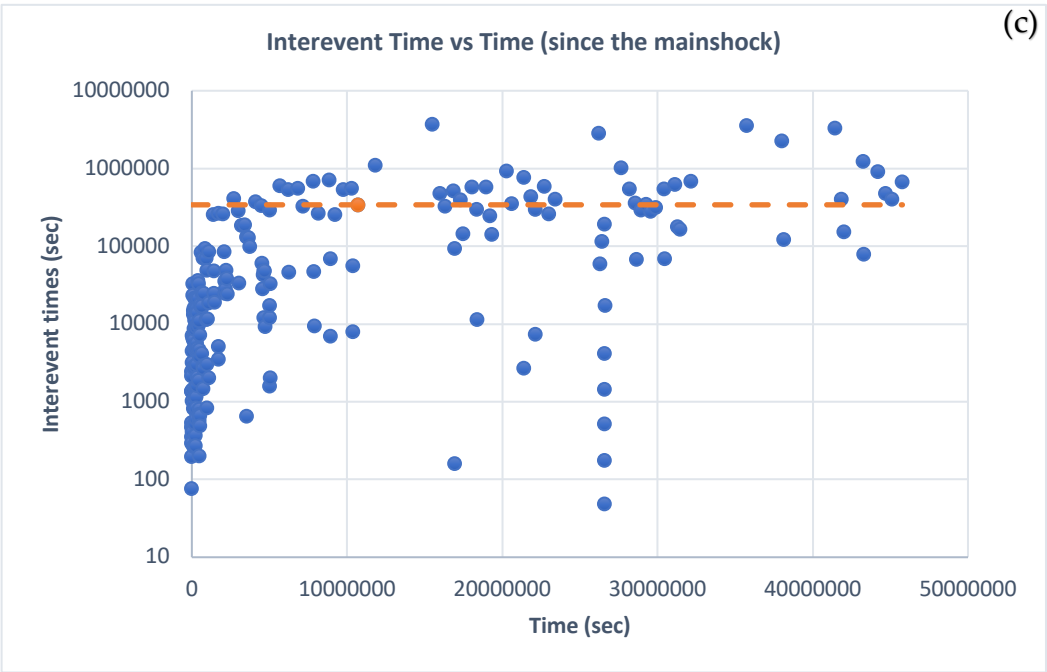

Figure 207. (a) The cumulative distribution function of the interevent times. The red line is the Q-exponential fitting with q = 1.75. **(b)** The Q-logarithmic function of the P(>T) as a function of the interevent times where the dashed line is the fitting with q=1.75. The deviation from the linearity suggests Tc values close to 400,000 s. **(c)** The evolution of interevent time T as a function of time t since the main event. The Tc value is indicated by the dashed line.

4.2.42 The 2019 Ternate Earthquake M_w=7.1 (Indonesia)

The figure below shows Guttenberg-Richter distribution. The estimated parameters are Mc=4.8, b=1.2 and a=7.89.

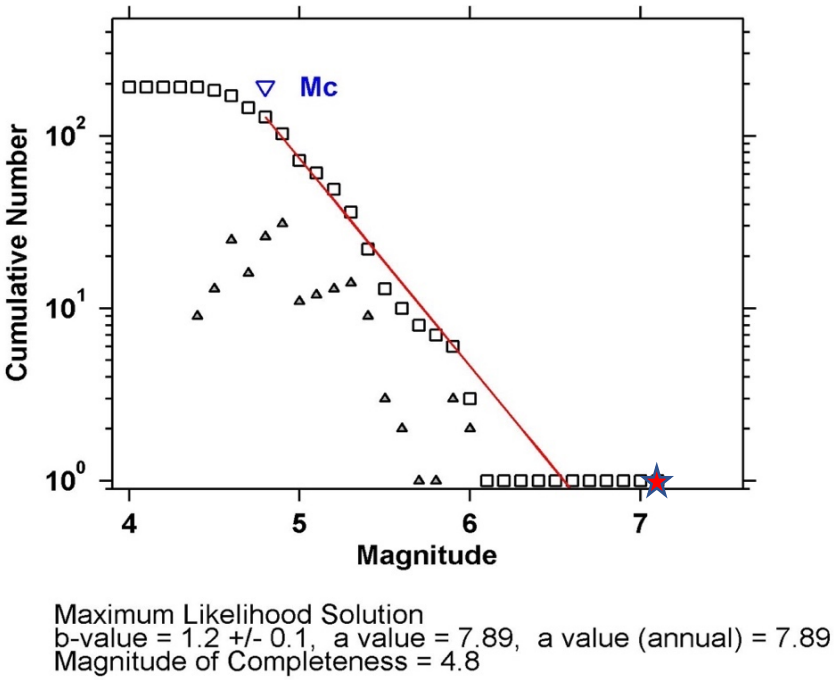

Figure 208. The Guttenberg-Richter distribution using maximum likelihood method with the best combination of maximum curvature M_c 95% and M_c 90% probability. The red star shows the magnitude of the mainshock M_w 7.1.

Next figure presents the model proposed by the AIC with p1= 2.7, p2=0.9, c1=0.63, c2=5, k1=88.6 and k2= 10.

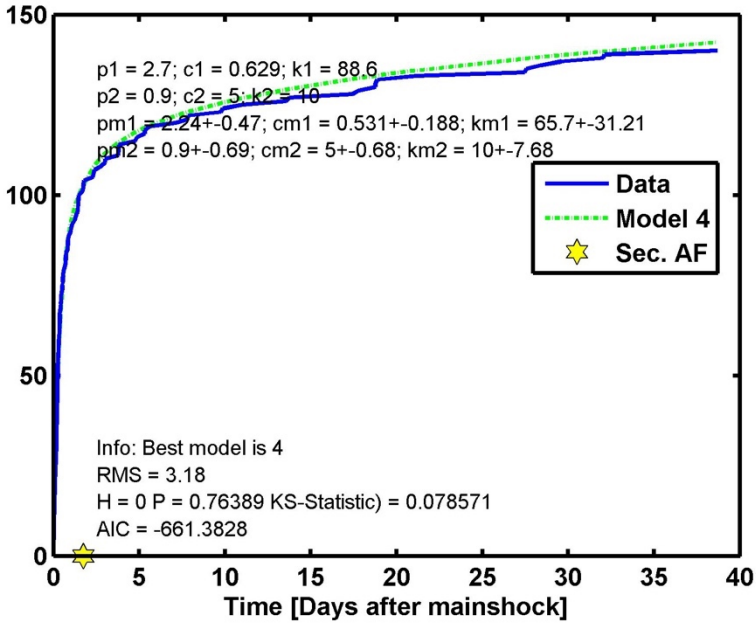

Figure 209. The best model (4) of the estimated curve of the modified Omori formula (dashed line) applied to the aftershock data and the observed cumulative number of aftershocks (solid line) based on the AIC with RMS= 3.18.

Here is the magnitude-time form of the aftershock sequence.

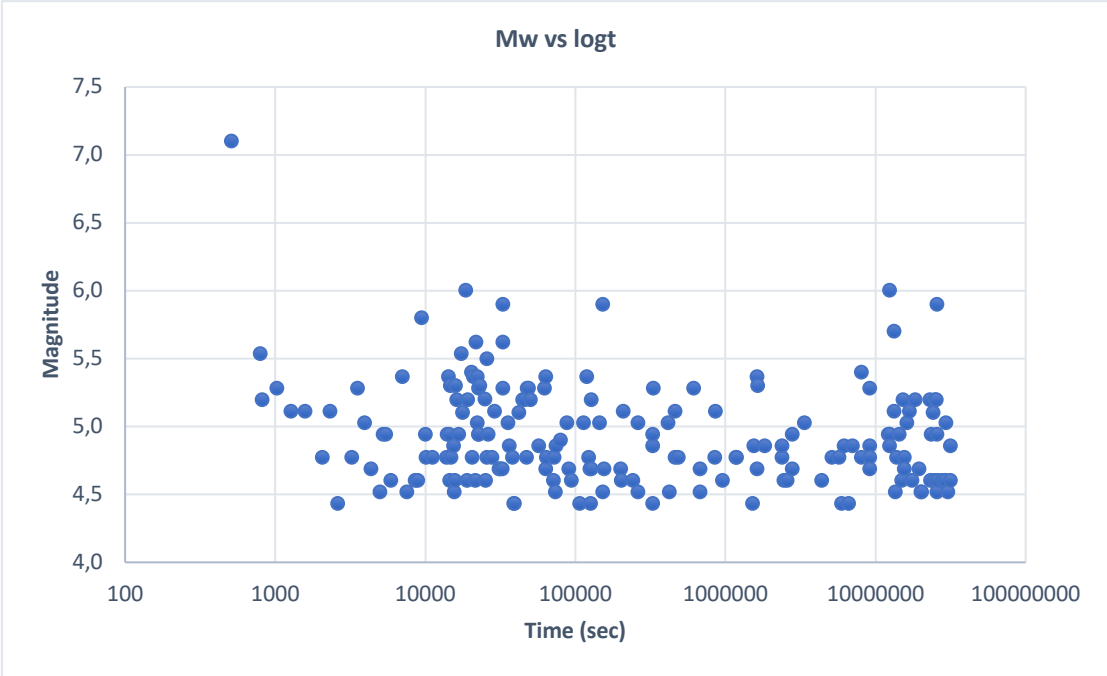

Figure 210. The magnitude-time pattern versus the logarithm of time of the mainshock M_w 7.1.

By the frequency-magnitude distribution for this earthquake, it is estimated a q_M= 1.37 with ci= 1.31-1.43.

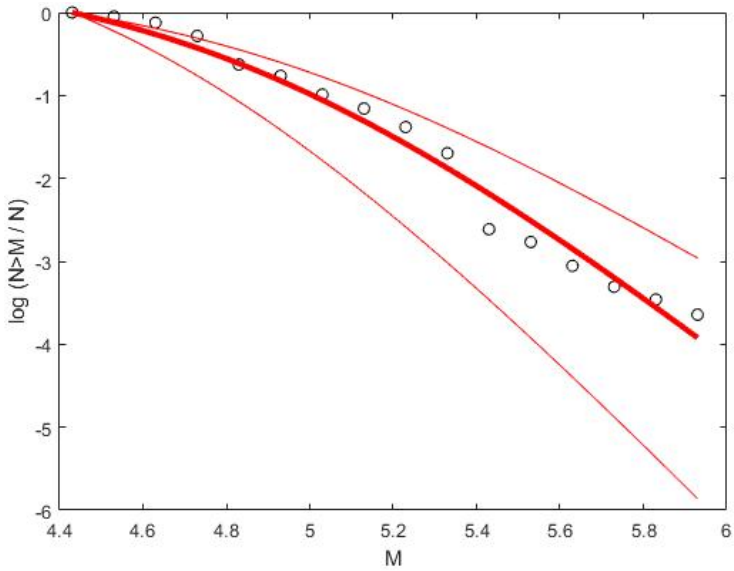

Figure 211. Frequency-magnitude distribution. The bold red line represents the model of equation (26) for qM= 1.37, while the other two lines present the corresponding 95% confidence intervals.

Figure 212 shows the typical Q-exponential pattern and Q-logarithmic function of the cumulative distribution function, P(>T) of the aftershocks interevent times and a q=1.74 is obtained.

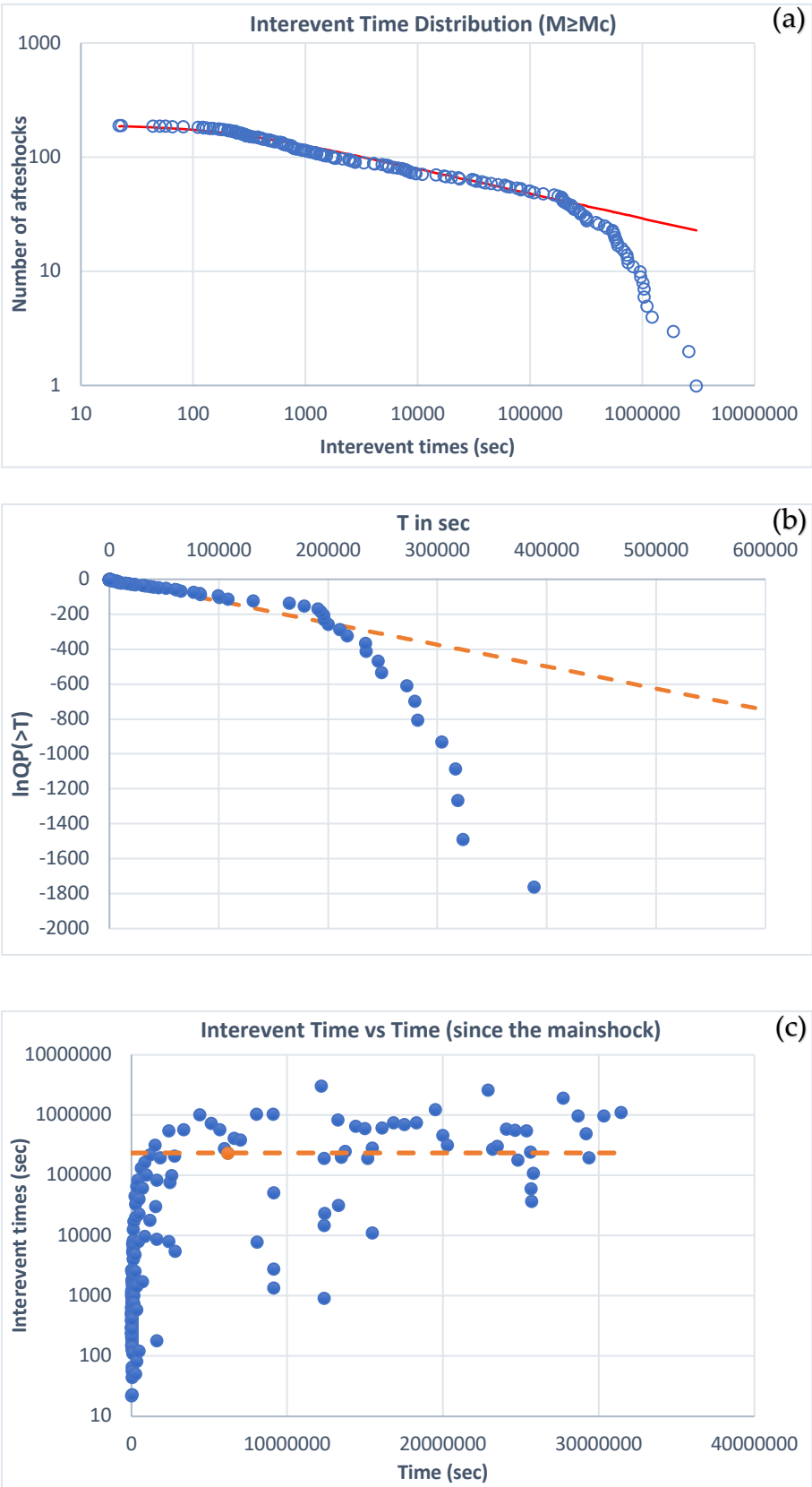

Figure 212. (a) The cumulative distribution function of the interevent times. The red line is the Q-exponential fitting with q = 1.74. **(b)** The Q-logarithmic function of the P(>T) as a function of the interevent times where the dashed line is the fitting with q=1.74. The deviation from the linearity suggests Tc values close to 250,000 s. **(c)** The evolution of interevent time T as a function of time t since the main event. The Tc value is indicated by the dashed line.

4.2.43 The 2020 Kermadec Islands Earthquake M_w=7.4 (New Zealand)

The figure below shows Guttenberg-Richter distribution. The estimated parameters are Mc=4.9, b=2.22 and a=12.8.

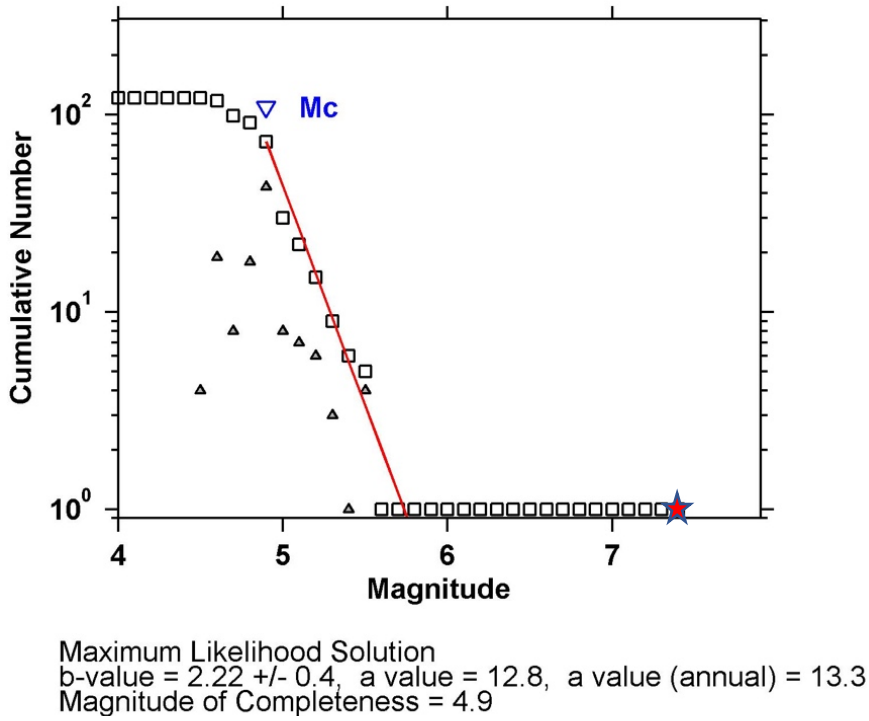

Figure 213. The Guttenberg-Richter distribution using maximum likelihood method with the best combination of maximum curvature M_c 95% and M_c 90% probability. The red star shows the magnitude of the mainshock M_w 7.4.

Next figure (214a) presents the model proposed by the AIC with p= 1.06, c= 0.2 and k= 22.4 while (214b) presents the model with the lowest RMS and p1= 1.06, p2=2.14, c1=0.13, c2=2.53, k1=18.2 and k2= 45.

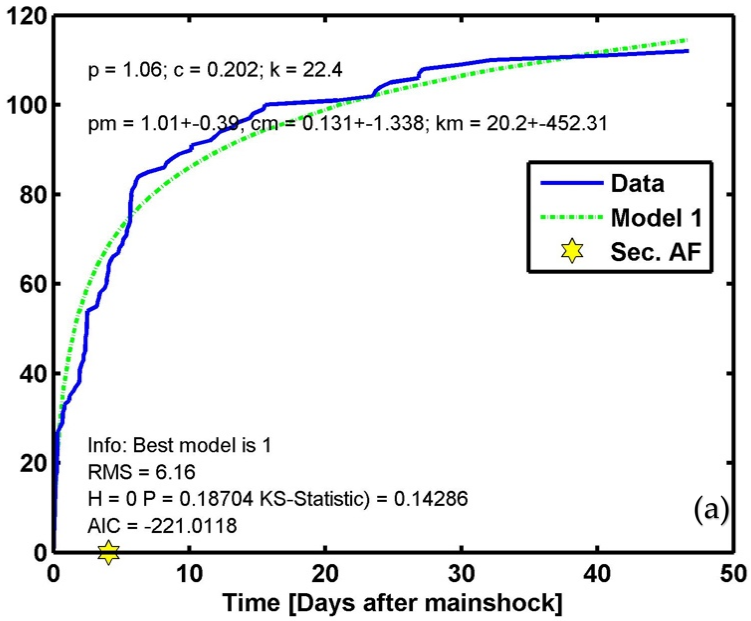

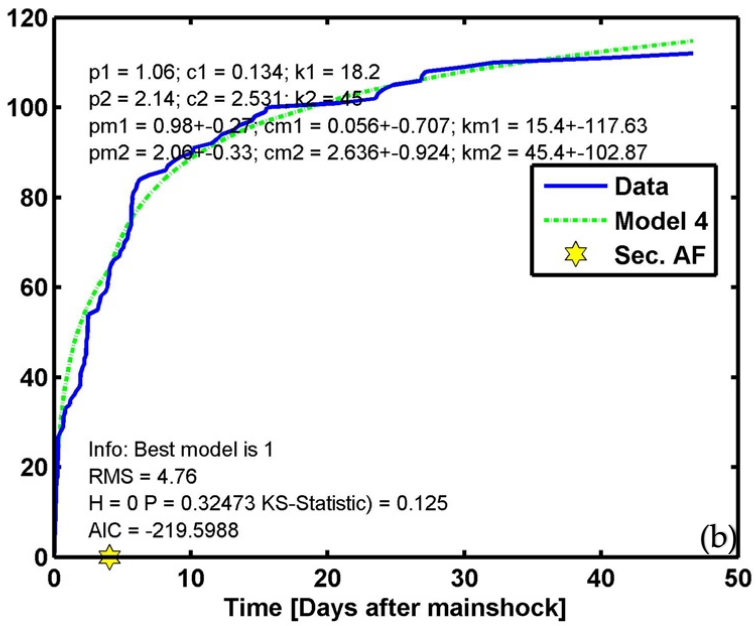

Figure 214. (a) The best model (1) of the estimated curve of the modified Omori formula (dashed line) applied to the aftershock data and the observed cumulative number of aftershocks (solid line) based on the AIC. **(b)** The model 4 of the estimated curve of the modified Omori formula (dashed line) applied to the aftershock data and the observed cumulative number of aftershocks (solid line), with the lowest RMS= 4.76.

Here is the magnitude-time form of the aftershock sequence.

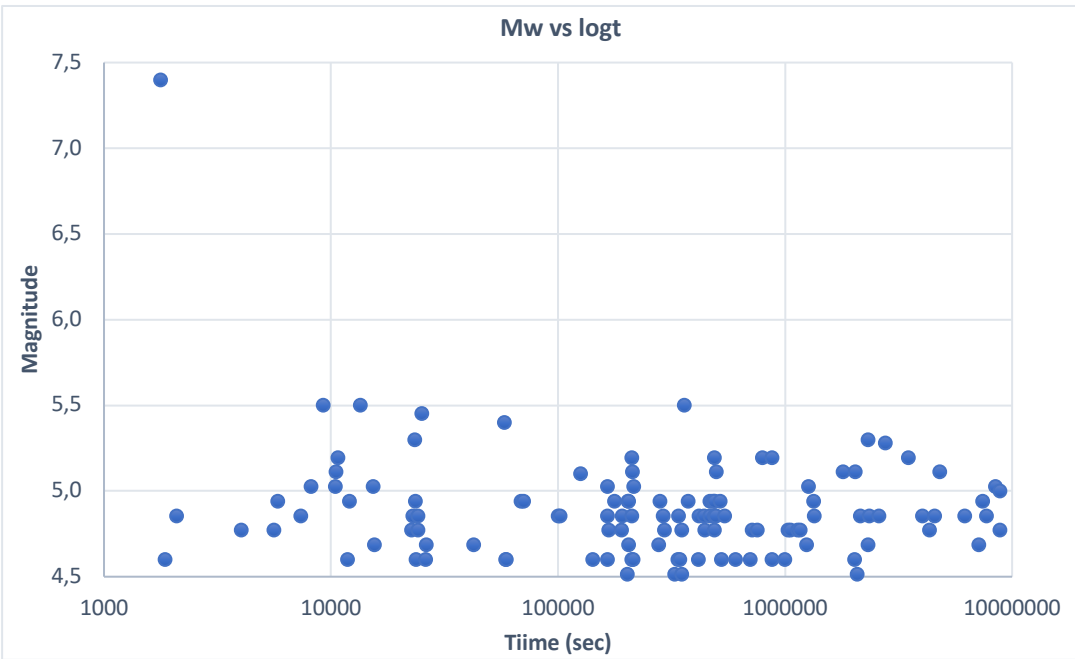

Figure 215. The magnitude-time pattern versus the logarithm of time of the mainshock M_w 7.4.

By the frequency-magnitude distribution for this earthquake, it is estimated a q_M= 1.17 with ci= 1.04-1.30.

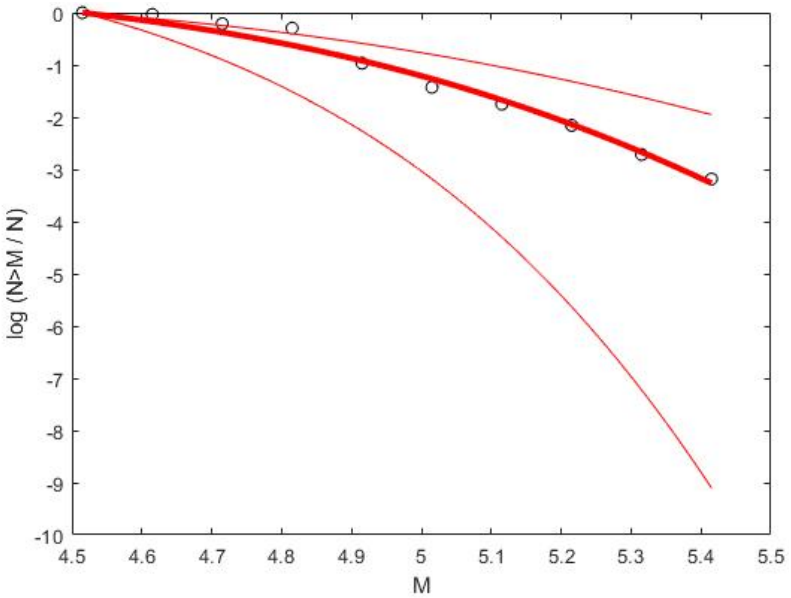

Figure 216. Frequency-magnitude distribution. The bold red line represents the model of equation (26) for qM= 1.17, while the other two lines present the corresponding 95% confidence intervals.

Figure 217 shows the typical Q-exponential pattern and Q-logarithmic function of the cumulative distribution function, P(>T) of the aftershocks interevent times and a q=1.72 is obtained.

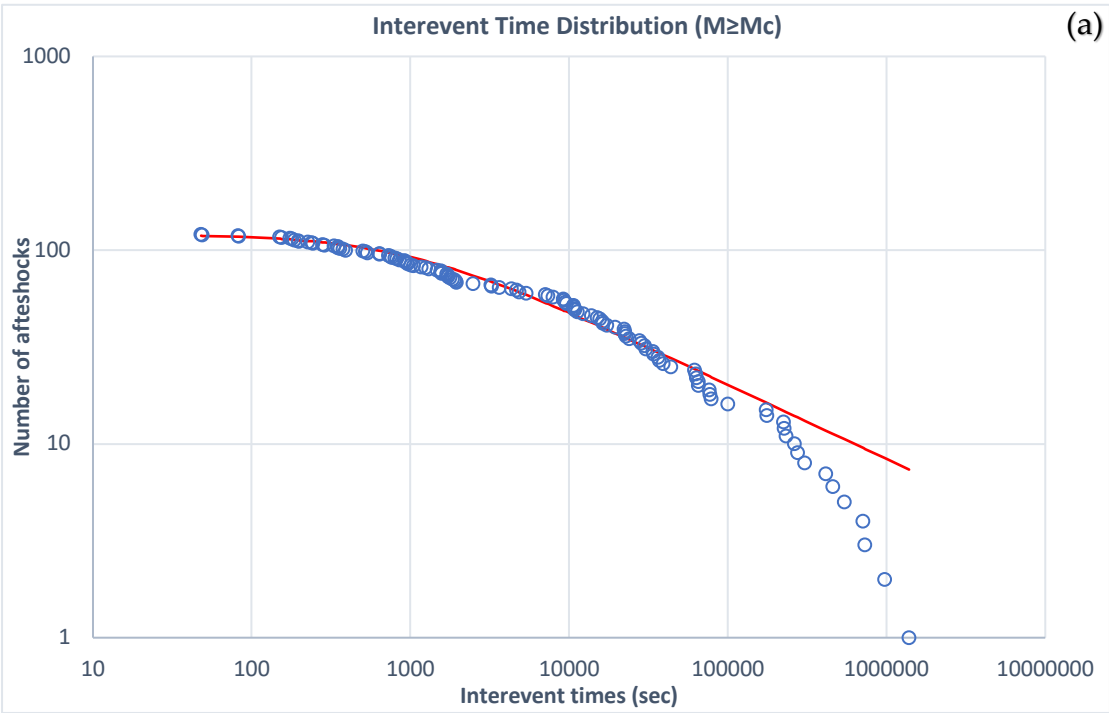

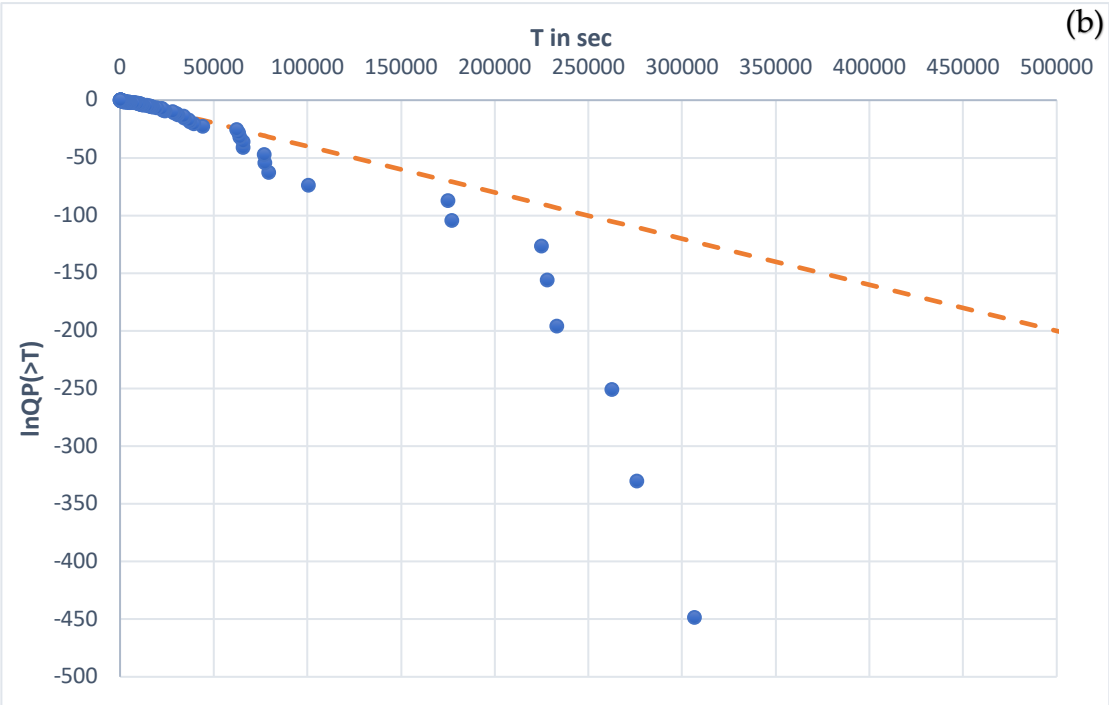

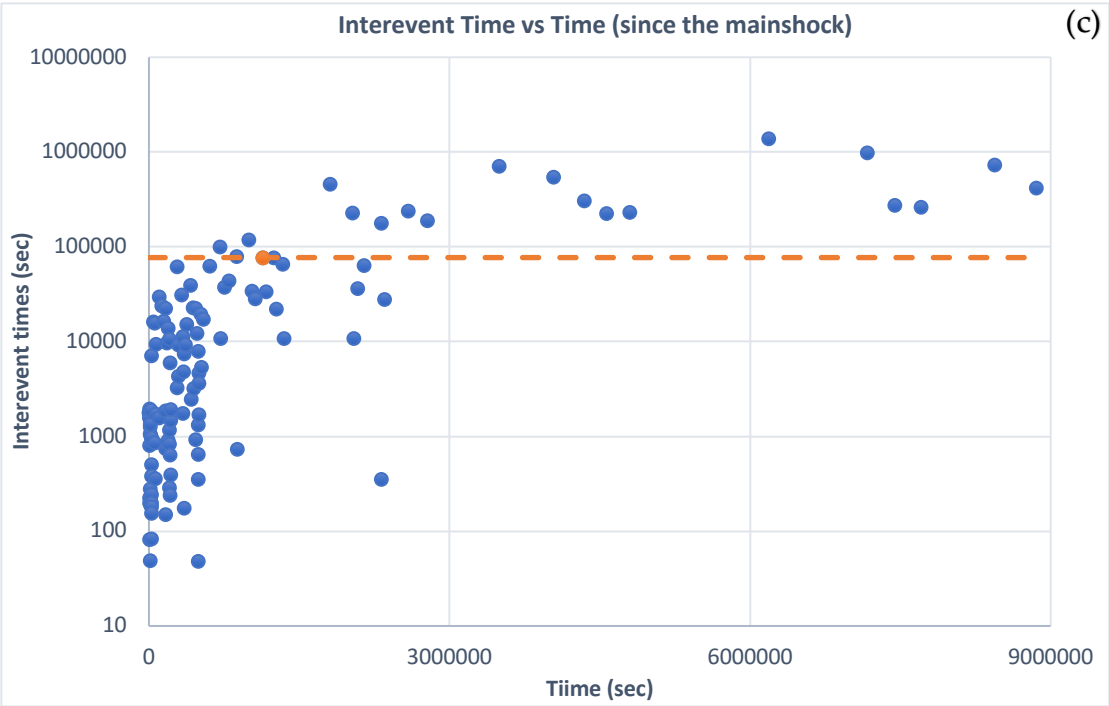

Figure 217. (a) The cumulative distribution function of the interevent times. The red line is the Q-exponential fitting with q = 1.72. **(b)** The Q-logarithmic function of the P(>T) as a function of the interevent times where the dashed line is the fitting with q=1.72. The deviation from the linearity suggests Tc values close to 100,000 s. **(c)** The evolution of interevent time T as a function of time t since the main event. The Tc value is indicated by the dashed line.

4.2.44 The 2020 Sand Point Earthquake M_w=7.6 (Alaska)

The figure below shows Guttenberg-Richter distribution. The estimated parameters are Mc=4.2 and b=0.97 with a standard deviation of 0.07.

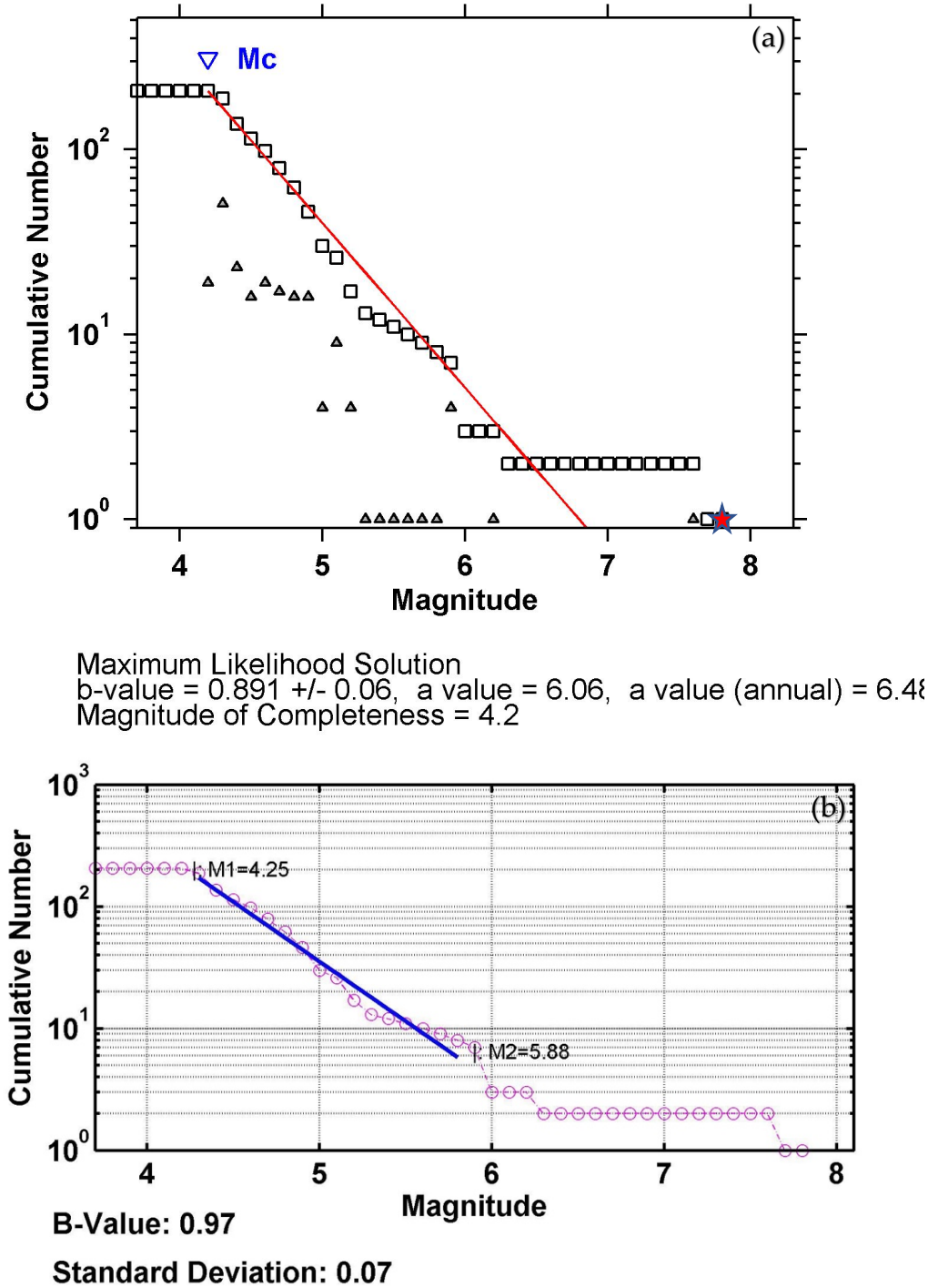

Figure 218. (a) The Guttenberg-Richter distribution using maximum likelihood method with the best combination of maximum curvature M_c 95% and M_c 90% probability. The red star shows the magnitude of the mainshock M_w 7.6. **(b)** The Guttenberg-Richter distribution using the manual method.

Next figure presents the model proposed by the AIC with p= 2.05, c= 0.64 and k= 10.

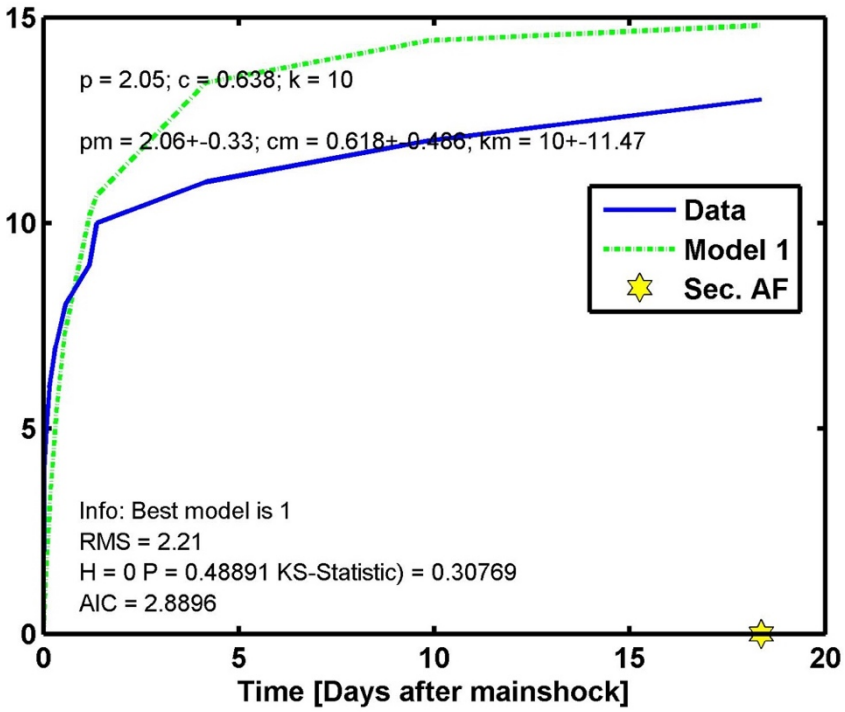

Figure 219. The best model (1) of the estimated curve of the modified Omori formula (dashed line) applied to the aftershock data and the observed cumulative number of aftershocks (solid line) based on the AIC with RMS= 2.21.

Here is the magnitude-time form of the aftershock sequence.

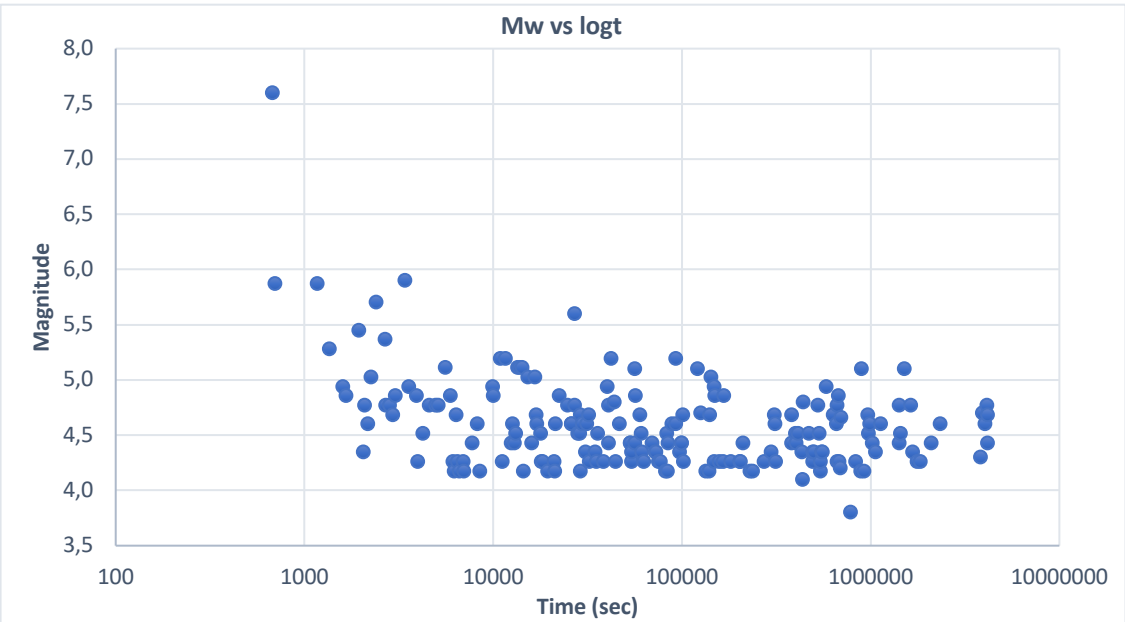

Figure 220. The magnitude-time pattern versus the logarithm of time of the mainshock M_w 7.6.

By the frequency-magnitude distribution for this earthquake, it is estimated a q_M= 1.43 with ci= 1.40-1.47.

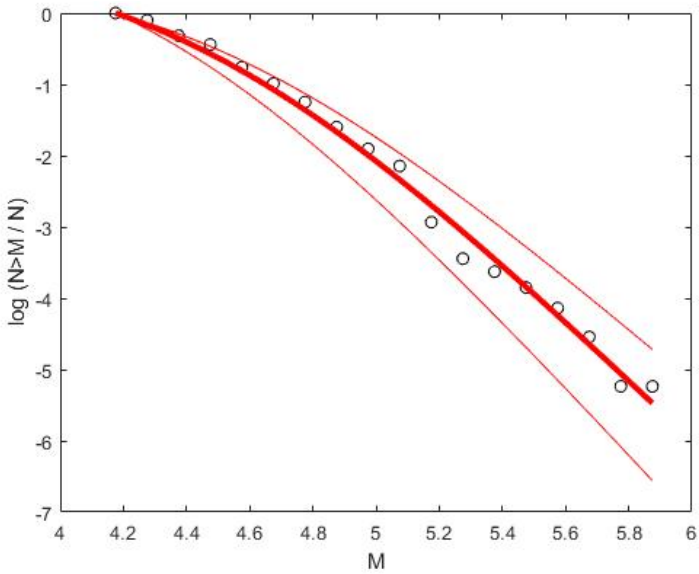

Figure 221. Frequency-magnitude distribution. The bold red line represents the model of equation (26) for qM= 1.43, while the other two lines present the corresponding 95% confidence intervals.

Figure 222 shows the typical Q-exponential pattern and Q-logarithmic function of the cumulative distribution function, P(>T) of the aftershocks interevent times and a q=1.71 is obtained.

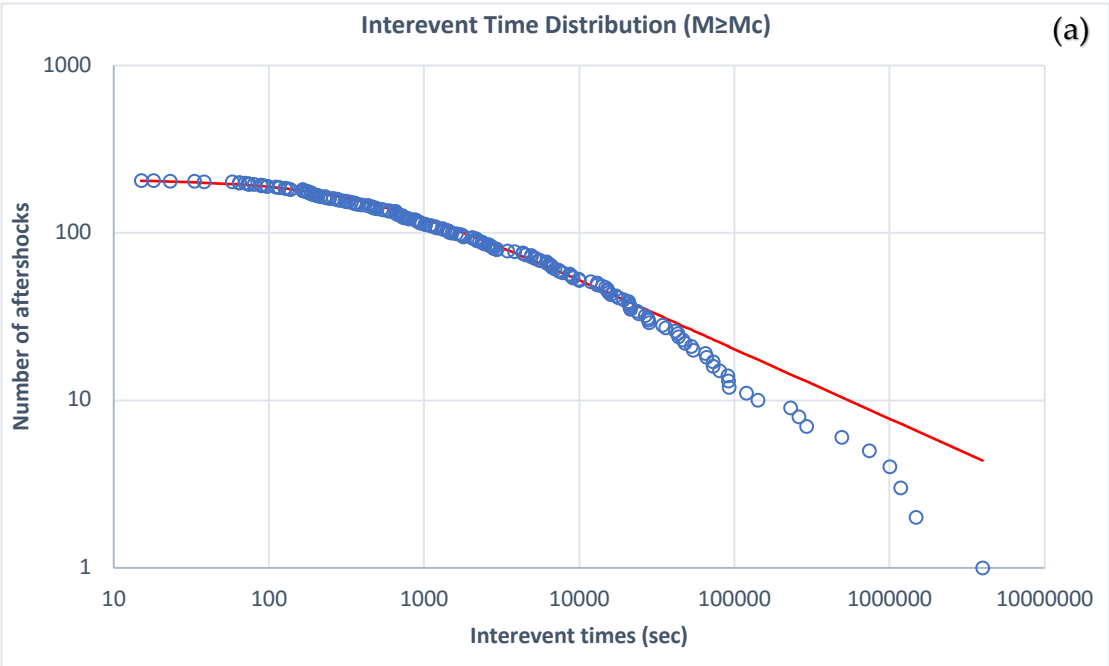

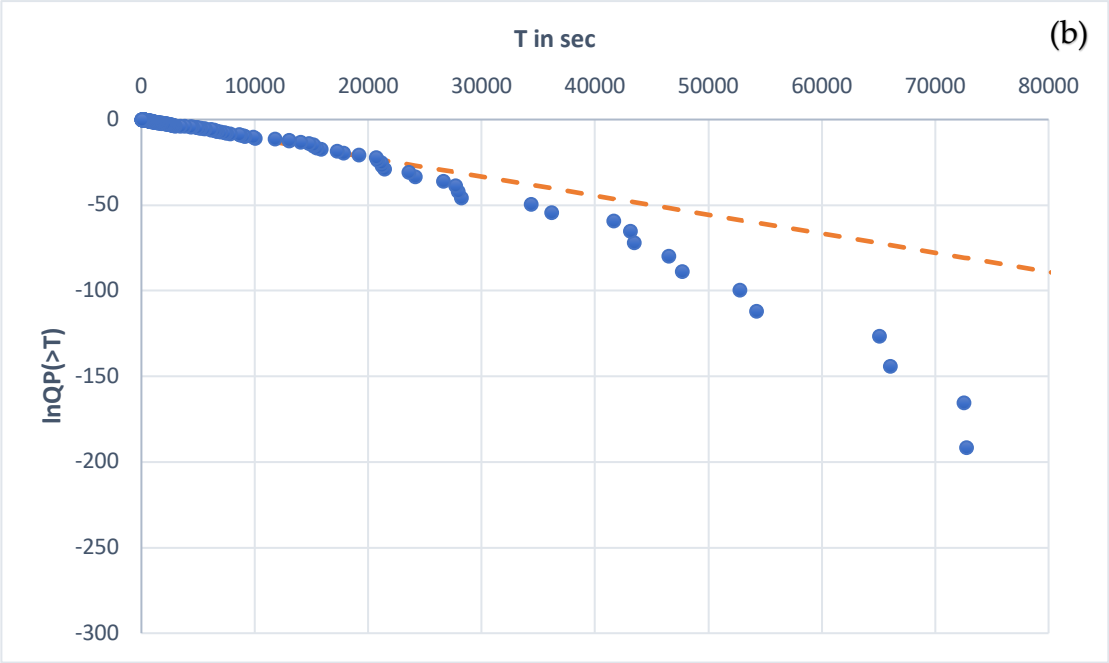

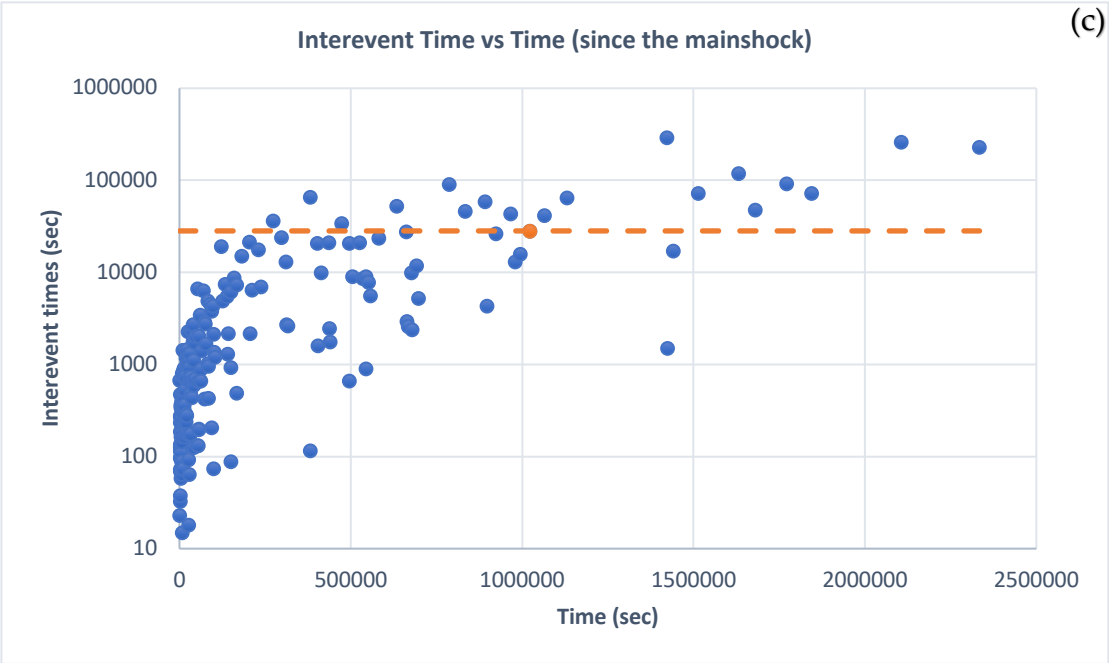

Figure 222. (a) The cumulative distribution function of the interevent times. The red line is the Q-exponential fitting with q = 1.71. **(b)** The Q-logarithmic function of the P(>T) as a function of the interevent times where the dashed line is the fitting with q=1.71. The deviation from the linearity suggests Tc values close to 40,000 s. **(c)** The evolution of interevent time T as a function of time t since the main event. The Tc value is indicated by the dashed line.

Chapter 5

DISCUSSION AND CONCLUSIONS

In this dissertation, the aftershock sequences of major earthquakes, occurred on subduction zones from 1973 to 2020, were statistically analyzed. Modeling these aftershocks sequences can provide useful data for seismic-hazard assessments and earthquake risk mitigation. For this reason, we conducted a thorough investigation of them, in order to derive parameters for several well-known empirical statistical laws. In particular, we examined the frequency– magnitude distribution of each sequence, using the Gutenberg–Richter scaling relationship to model them and concerning the temporal domain of this study, the decay rates of each sequence were modeled using the modified Omori law. The results of this research revealed that the parameters of the Gutenberg–Richter law and the modified Omori law are not affected by the magnitude of the mainshock that produced the aftershock sequences because no there is no correlation between the magnitude of earthquakes and the obtained parameters such as the b- and p- value. For instance, with an increase in the magnitude of the mainshocks there is no rising trend in the b-value. Nevertheless, the results indicate that there may be some changes among different regions, which can be attributed to various coupling regimes in the subduction zones under consideration.

This research is also linked with another case of study related to Non-Extensive Statistical Physics according to which the temporal scaling properties of aftershock sequences are further studied by looking into the probability distribution of the interevent times between the successive aftershocks. Furthermore, the cumulative distribution in terms of the earthquake magnitude is examined via NESP through which Telesca proposed a modified function taking into account the threshold magnitude Mc in a seismic region, which relates the cumulative number of earthquakes with the magnitude, normalized by the total number of earthquakes and we estimated the entropic index q_M with an average of 1.41 which informs us about the size of fault plane and fragment interactions (Matcharashvili et al. 2011; Papadakis et al. 2013; Telesca 2010; Valverde-Esparza et al. 2012). As a result, an increase in q_M indicates that the physical state of a seismic region is deteriorating but the estimated value is considered low and for this reason the system is moving close to equilibrium.

Finally, we demonstrated the applicability of non-extensive statistical physics in the cumulative distribution functions of interevent times and the presence of a crossover behavior from power-law ($q \neq 1$) to exponential ($q=1$) scaling for greater interevent times. We revealed that the interevent time distributions of the aftershock sequences of major earthquakes in subduction zones are described by non-extensive statistical mechanics, implying a sub-additive process with q-values greater than one, supporting the concept of long-range memory effects and scale-free nature and are well described by

the statistical physics method, suggesting the complexity of seismicity's temporal characteristics and the relevance of non-additivity in researching such complex phenomena. Furthermore, most of the estimated non-extensive q-values that characterize the observed distributions and are obtained using the NESP method are close to 1.76. Finally, we utilized superstatistics, which is based on a superposition of ordinary local equilibrium statistical mechanics with a suitable intensive parameter β that varies as a χ^2 distribution on a reasonably wide temporal scale and is supplementary to NESP. The superstatistical approach indicates the fact that the temporal evolution of the aftershocks sequences of earthquakes occurred on subduction zones have relatively low degrees of freedom which means that such systems follow a significant non-additive characteristic and have a strong organization and hierarchy.

BIBLIOGRAPHY

Books

Alejandro Ramírez-Rojas, Leonardo Di G. Sigalotti, Elsa Leticia Flores Márquez and Otto Rendón, *Time Series Analysis in Seismology*, Practical Applications, Elsevier, 2019.

Serge Lallemand and Francesca Funiciello (Eds.), Fronties in Earth Sciences, *Subduction Zone Geodynamics*, Springer-Verlag Berlin Heidelberg: Berlin, 2009.

Spyridon P. Lekkas, Stylianos G. Lozios and Emmanuel N. Skourtsos, *Introduction to Geodynamics*, National and Kapodistrian University of Athens, Department of Geology and Geoenvironment, Department of Dynamics, Tectonics & Applied Geology, Second Edition, Athens, December 2006.

Tamaz Chelidze, Filippos Vallianatos and Luciano Telesca, Andreas Tzanis and Angeliki Efstathiou, *Complexity of Seismic Time Series: Are Seismogenetic Systems Random or Organized? A Treatise of Their Statistical Nature Based on the Seismicity of the North-Northeast Pacific Rim*, Elsevier, 2018.

Articles

Armick Ivanian, *Studies of Aftershock Sequences of Large Subduction Zone Earthquakes*, The University of Western Ontario, School of Graduate and Postgraduate Studies, 2012.

A. Schmid and J.-R. Grasso, *Omori law for eruption foreshocks and aftershocks*, Journal of Geophysical Research, vol 117, B07302, 2012, doi:10.1029/2011JB008975.
Supra Note 29.

Andrzej Kijko and Asie Smit, *Estimation of the Frequency-Magnitude Gutenberg-Richter b-Value without Making Assumptions on Levels of Completeness*, Seismological Research Letters, Vol. 88, N. 2A, March/April 2017.

Bernice Bender, *Maximum Likelihood Estimation of b Values for Magnitude Grouped Data*, Bulletin of the Seismological Society of America, Vol 73, No 3, June 1983.

C. Godano, E. Lippiello and L. de Arcangelis, *Variability of the b valuein the Gutenberg-Richter distribution*, Geophysical Journal International, June 2014.

Chris G. Antonopoulos, George Michas, Filippos Vallianatos and Tassos Bountis, *Evidence of q-exponential statistics in Greek seismicity*, Physica A, 2014

C. Beck, *Superstatistics: theory and applications*, Continum Mech. Thermodyn, 2004, doi:10.1007/s00161-003-0145-1.

Denis Nikolaevich Sob'yanin, *Generalization of the Beck-Cohen superstatistics*, November 2011.

Elenora van Rijsingen, *Subduction interface roughness and megathrust earthquakes*: *Insights from natural data and analogue models*, Université Montpellier; Università degli studi Roma Tre, 2018.

E.M. Scordilis, *Emprirical global relations converting Ms and mb to moment magnitude*, Journal of Seismology, January 2006, doi:10.1007/s10950-006-9012-4.

F. A. Nava, V. H. Márquez-Ramírez, F. R. Zúñiga, L. Ávila-Barrientos and C. B. Quinteros, Gutenberg-Richter b-values maximum likelihood estimation and sample size, Springer Science and Business Media Dordrecht, June 2016.

F. Vallianatos, V. Karakostas and E. Papadimitriou, *A Non-Extensive Statistical Plhsics View in the Spatiotemporal Properties of the 2003 (Mw6.2) Lefkada, Ionian Island Greece, Aftershock Sequence*, Pure and Applied Geophysics, doi:10.1007/s00024-013-0706-6.

Filippos Vallianatos and Georgios Michas, *Complexity of Fracturing in Terms of Non-Extensive Statistical Physics: From Earthquake Faults to Arctic Sea Ice Fracturing*, Entropy, October 2020, doi:10.3390/e22111194.

Filippos Vallianatos, Giorgos Michas, Giorgos Papadakis and Peter Sammonds, *A Non-Extensive Statistical Physics View to the Spatiotemporal Properties of the June 1995, Aigion Earthquake (M6.2) Aftershock Sequence (West Corinth Rift, Greece)*, Acta Geophysica, vol. 60, no. 3, June 2012, doi:10.2478/s11600-012-0011-2.

F. Vallianatos, P. Benson, P. Meredith, P. Sammonds, *Experimental evidence of a non-extensive statistical physics behavior of fracture in triaxially deformed Etna basalt using acoustic emissions*, A Letters Jernal Exploring the Fronties of Physics, March 2012, doi:10.1209/0295-5075/97/58002.

Filippos Vallianatos, Ioannis Koutalonis, Georgios Chatzopoulos, *Evidence of Tsallis entropy signature on medicane induced ambient seismic signals*, Physica A: Statistical Mechanics and its Applications, Volume 520, 2019, doi: https://doi.org/10.1016/j.physa.2018.12.045.

Giorgos Papadakis, Filippos Vallianatos and Peter Sammonds, *A Nonextensive Statistical Physics Analysis of the 1995 Kobe, Japan Earthquake*, Pure and Appled Geophysics, 2014, doi:10.1007/s00024-014-0876-x.

Jiancang Zhuang, Statistical modeling of seismicity patterns before and after the Cape Palliser earthquake, Centre for Analysis and Prediction State Seismological Bureau Beijing, China, 2000.

Keiiti Aki, *Maximum Likelihood Estimate of b in the Formula logN= a -bm and its Confidence Limits*, Bulletin of the Earthquake Research Institute, Vol 43, March 1965.

L.I. Lobkovsky, V.I. Kerchman, B.V. Baranov and E.I. Pristavakina, *Analysis of Seismotectonic Processes in Subduction Zones from the Standpoint of a Keayboard Model of Great Earthquakes*, Tectonophysics, Volume 199, Issues 2-4, December 1991.

Lizhong Zhang, *Spatiotemporal Seismic Hazard and Risk Assessment of Global M9.0 Megathrust Earthquake Sequences*, University of Bristol, March 2020.

M. Holschneider, C. Narteau, P. Shebalin, Z. Peng and D. Schorlemmer, *Bayesian analysis of the modified Omori law*, Journal of Geophysical Research, vol. 17, B06317, 2012, doi:10.1029/2011JB009054.

Michas G., Papadakis G., Vallianatos F., *A Non-Extensive approach in investigating Greek seismicity, Bulletin of the Geological Society of Greece*, Volume XLVII, No3, 2016, doi: https://doi.org/10.12681/bgsg.10973.

P. Leary, P. Marlin and Tero Saarno, *A Physical Basis for Gutenberg-Richter Fractal Scaling*, Proceeding, 45th Workshop on Geothermal Reservoir Engineering Stanford University, California, February 2020.

Paul Nyffenegger and Cliff Frohlich, *Recommendations for Determining p Values for Aftershock Sequences and Catalogs*, Bulletin of the Seismological Society of America, Vol.88, No.5, October 1998.

Prasanta Chingtham, Babita Sharma, Sumer Chopra and Pareshnath SinghaRoy, *Statistical analysis of aftershock sequences related with two major Nepal earthquakes: April 25, 2015, M_w 7.8, and May 12, 2015, M_w 7.2*, Annals of Geophysics, doi:10.4401/ag-7025.

Prasanta Chingtham, Babita Sharma, Sumer Chopra and Pareshnath SinghaRoy, *Statistical analysis of aftershock sequences related with two major Nepal earthquakes: April 25, 2015, Mw 7.8 and May 12, 2015, Mw 7.2*, Annals of Geophysics, 59, 5, 2016, S0540; doi:10.4401/ag-7025.

Robert Shcherbakov, Donald L. Turcotte and John B. Rundle, *Aftershock Statistics*, Pure and Applied Geophysics, Birkhäuser Verlag, Basel, 2005.

Robert Shcherbakov, Katsuichiro Goda, Armick Ivanian and Gail M. Atkinson, *Aftershock Statistics of Major Subduction Earthquakes*, Bulletin of the Seismological Society of America, Vol. 103, No. 6, December 2013, doi:10.1785/0120120337.

Ranjit Das, H. R. Wason and M. L. Sharma, *Global regression relation for conversion of surface wave and body wave magnitudes to moment magnitude*, Nat Hazards, 2011, doi:10.1007/s11069-011-9796-6.

Susan L. Bilek and Thorne Lay, *Subduction Zone Megathrust Earthquakes*, The Geological Society of America, Geosphere, Volume 14, Number 4, 2018.

Serge A. Shapiro, *Fluid-Induced Seismicity*, Earth Science Department, Freie Universität Berlin, Cambridge Uneversity Press, United Kingdom, 2015.

Stephen A. Miller, *Aftershocks are fluid-driven and decay rates controlled by permeability dynamics*, Nature Communications, 2020.

Serkan Öztürk and Şakir Şahin, *A statistical space-time0magnitude analysis on the aftershocks occurrence of the July 21th, 2017 Mw=6.5 Bodrum-Kos, Turkey, earthquake*, Joyrnal of Asian Earth Sciences, October 2018, doi:10.1016/j.jseaes.2018.10.008.

Susanna J. Gross and Carl Kisslinger, *Tests of Models of Aftershock Rate Decay, Bulletin of the Seismological Society of America*, Vol. 84, No. 5, October 1994.

Tzanis A., Vallianatos F. and Efstathiou A. (2013), *Multidimensional earthquake frequency distributions consistent with Non-Extensive statistical physics: The interdependence of magnitude, interevent time and interevent distance in North California*, Bulletin of the Geological Society of Greece, Volume XLVII, No3, 1326-1337, doi: https://doi.org/10.12681/bgsg.10914.

Tokuji Utsu, Yosihiko Ogata and Ritsuko S. Matsu'ra, *The Centenary of the Omori Formula for a Decay Law of Aftershock Activity*, Institute of Statistical Mathematics, Minato-ku, Tokyo 106, Japan, J. Phys. Earth, Vol 43, No 1, 1995.

Warner Marzocchi and Laura Sandri, *A review and new insights on the estimation of the b-value and its uncertainty*, Istituto Nazionale di Geofisica e Vulcanologia, Bologna, Italy, Annals of Geophysics, Vol. 46, N. 6, December 2003.

Yosihiko Ogata and Ken'ichiro Yamashina, *Unbiased Estimate for b-Value of Magnitude Frequency*, J. Phys. Earth, 34, The Univeristy of Tokyo, Japan, 1986.

Online Resources

Brendan Sullivan, lecture of "Earthquake Physics*", Basic Statistical Seismology Tutorial*, Website link: http://geophysics.eas.gatech.edu/people/bsullivan/tutorial/StatisticalSeismology.htm#part1_

"NOAA Ocean Exploration - What are the different types of tectonic boundaries?", retrieved on 15 June 2021, https://oceanexplorer.noaa.gov/facts/plate-boundaries.html .